The Synthesis and Reactions of a Modified Cobalt Corrin

Monika Nowakowska

Supervised by H M Marques and A L Rousseau

A thesis submitted to the Faculty of Science, University of the Witwatersrand,

Johannesburg, in fulfilment of the requirements for the Degree of Doctor of Philosophy.

June 2018

DECLARATION

I declare that this is my own unaided work. It is being submitted for the Degree of Doctor of Philosophy at the University of the Witwatersrand, Johannesburg. It has not been submitted before for any degree or examination at any other university.

M Nowakowska

1 June 2018

ABSTRACT

The typically inert Co(III) ion exhibits remarkable lability when encapsulated in a corrin macrocycle such as in vitamin B_{12}. It has been postulated that this lability arises from a significant kinetic *cis*-effect through the delocalisation of electron density from the relatively electron-rich corrin to Co(III), thus conferring to it a degree of soft, labile Co(II)-like character. We suggest that structural and electronic modifications of the corrin should modulate the transfer of electron density to the central Co(III) ion, thus changing its electronic character. Another important feature of the corrin ring is the relatively small macrocyclic cavity. It appears that Co(III) may be compressed within the corrin macrocycle, which is likely to significantly impact its chemistry. To evaluate what effect these factors may have on the chemistry of Co(III), we prepared a vitamin B_{12} derivative, Co*α*,Co*β*-dicyano-5,6-dioxo-5,6-seco-heptamethylcob(III)yrinate, [DC-5-seco-Cbs], by perturbing the electronic structure of the dicyanocobyrinic acid heptamethyl ester, Co*α*,Co*β*-dicyano-heptamethylcob(III)yrinate ([DCCbs]) through a photosensitized oxygenation reaction. Not only does this disrupt the partially conjugated system of a normal corrin ring, but the bond between C5 and C6 has been cleaved such that the equatorial ligand of Co(III) is no longer macrocyclic, thereby relieving the steric constraints surrounding the axial coordination site of Co(III) corrins.

The secocobester was then converted to the aquacyano derivative, Coα,Coβ-aquacyano-5,6-dioxo-5,6-seco-heptamethylcob(III)yrinate, $[AC\text{-}5\text{-}seco\text{-}Cbs]^+$, in which a coordinated water could be readily displaced by an exogenous ligand in solution chemistry investigations.

The effect of these structural modifications was evaluated by comparing analogous thermodynamic and kinetic data for $[AC\text{-}5\text{-}seco\text{-}Cbs]^+$ with aquacyanocobyrinic acid heptamethyl ester (aquacyanocobester, $[ACCbs]^+$), a corrin with an intact delocalised system (the values were re-determined in this study), and aquacyano-stable yellow-cobester, ($[ACSYCbs]^+$), a corrin with a diminished delocalised π electron system, to observe the effect the nature of the corrin ring has on the properties of the Co(III) ion.

The pK_a for ionization of coordinated water decreases from 9.8 ± 0.3 in $[ACCbs]^+$ to 7.28 at 25 ^oC (ΔH = –88 ± 17 kJ mol^{-1} and ΔS = –434 ± 56 J K^{-1} mol^{-1}) in $[AC\text{-}5\text{-}seco\text{-}Cbs]^+$. The unusually low p$K_a$, confirmed by determining the pH-dependence of the coordination of SO_3^{2-} by $[AC\text{-}5\text{-}seco\text{-}Cbs]^+$, shows Co(III) in this complex behaves much more like Co(III) in simple hexacoordinate complexes than in intact cobalt corrins.

A comparison of log K values the for coordination of CN^-, SO_2^{2-}, NO_2^-, N_3^- and $S_2O_3^{2-}$ demonstrates that cleavage of the corrin ring significantly decreases the affinity of Co(III) for the softer ligands CN^-, SO_3^{2-} and, more marginally, NO_2^-. However, $[AC\text{-}5\text{-}seco\text{-}Cbs]^+$ has a higher affinity for N_3^- and $S_2O_3^{2-}$ than $[ACCbs]^+$. These trends correlate with the position of the ligands in the spectrochemical series ($N_3^- < S_2O_3^{2-} < NO_2^- < SO_3^{2-} < CN^-$); the first two behave as π donors towards metal ions, and the last three as π acceptors. Cleavage of the corrin, with a concomitant increase in hardness of the metal, decreases it affinity for π acceptors while the thermodynamic stability of its complexes with π donors increases as the metal ion becomes more Co(III)-like, and more capable of accepting electron density from the ligand. The temperature-dependence of log K values show very negative values for ΔH offset by ΔS values which are also large and negative. In the absence of crystal structures, DFT methods (BP86-D3/6-311G(d,p)) were used to assess the structural consequences of cleavage of the corrin. The topological properties of the electron density were assessed using Bader's Quantum Theory of Atoms in Molecules (QTAIM). The cleavage of the corrin does not unduly perturb the coordination sphere of the metal ion and the metal remains essentially octahedral. The sum of the partial charges on the metal and the entire coordination sphere, or the metal and the four equatorial donor N atoms, is less negative in the 5-seco-Cbs complexes than in the Cbs themselves and supports the supposition that cleavage of the corrin has made the metal and its immediate environment more positive.

A brief look into the binding of neutral N-donor ligands (N-MeIm, 4-MePy and NH_2EtOH) showed that the distinction between the softer Co(III) in $[ACCbs]^+$ and the harder Co(III) in $[AC\text{-}5\text{-}seco\text{-}Cbs]^+$ ($[ACCbs]^+ > [ACSYCbs]^+ > [AC\text{-}5\text{-}seco\text{-}Cbs]^+$) observed for the binding of anionic ligands was maintained for the neutral N-donor ligands. Furthermore, results also indicated

that relieving the steric hindrance surrounding the axial coordination site in $[AC\text{-}5\text{-}seco\text{-}Cbs]^+$ did enhance the metal's ability to bind larger neutral ligands.

To probe the *cis*-labilising effect of the corrins, kinetics data for the substitution of water *trans* to a cyanide moiety with a probe ligand, cyanide, were obtained under pseudo first-order conditions. The substitution of water coordinated to Co(III) by cyanide showed biphasic kinetics. The faster reaction was attributed to substitution of H_2O by CN^- *trans* to CN^-, and the slower phase to the reaction of the diaqua complex with CN^-, i.e., substitution of H_2O *trans* to H_2O. The rate of substitution of H_2O by CN^- in $[AC\text{-}5\text{-}seco\text{-}Cbs]^+$ is some two orders of magnitude slower than the substitution of H_2O by CN^- in $[ACCbs]^+$. Cleavage of the corrin together with the release of Co(III) from the small cavity of the corrin has therefore significantly decreased the lability of Co(III).

For interest, the data were compared to analogous data for aquacobalamin. In this way, the effect of the ligand *trans* to the axially coordinated water on its substitution could be elucidated. It was found that as the *trans* ligand varied from cyanide to dimethylbenzimidazole (DMBz) ($[AC\text{-}5\text{-}seco\text{-}Cbs]^+$ to aquacobalamin), the rate constant increased from $k^{II} \approx 10^2\ M^{-1}s^{-1}$ to $7.87 \times 10^2\ M^{-1}s^{-1}$; hence cracking of the corrin ring and the associated opening of the macrocyclic cavity results in an even more pronounced inert Co(III) character.

This study demonstrates how perturbation of the electronic structure of the corrin in cobalt corrin complexes significantly affects the coordination chemistry of the axial coordination sites and points to the importance of *cis* effects in cobalt corrin chemistry.

In memory of Dean, Babcia and Dziadek.

ACKNOWLEDGEMENTS

I would like to express my sincerest gratitude to my supervisor, Professor Helder Marques, for all his help, guidance, mentorship, support both professionally and personally, generosity of time and knowledge and for giving me the opportunity for so much growth.

Furthermore, I wish to thank

- Dr Susan Chemaly and Dr Chris Perry for the advice and assistance in characterising my compounds.
- Dr Amanda Rousseau and Dr Siya Ngubane for all the mentorship and guidance along the way.
- My Bioinorganic lab colleagues for all the assistance, friendships, laughs and for providing such a great work environment.
- Dr Richard Mampa and Dr Myron Johnson for collecting NMR data.
- Tapuwa Dzara for helping with any glassware requirements.
- Dr. Pradeep Varadwaj, Dr. Arpita Varadwaj and Prof. Koichi Yamashita for the DFT modeling work.
- My parents for the encouragement and the opportunity to receive the best education possible.
- Robyn, Amy, Jean and Bronwyn for the sisterhood in surviving a chemistry degree, and of course, all the cake and wine.
- Sam for being the greatest support system, believing in me and for all the snacks and late nights spent helping me through the tough times.
- The School of Chemistry for all the support.
- The University of the Witwatersrand and the NRF for financial support.

TABLE OF CONTENTS

CHAPTER 2

GENERAL MATERIALS, METHODS AND INSTRUMENTATION

CHAPTER 3

SYNTHESIS AND CHARACTERISATION

LIST OF FIGURES

List of Figures *(continued)*

List of Figures *(continued)*

List of Figures *(continued)*

List of Figures *(continued)*

List of Figures *(continued)*

List of Figures *(continued)*

List of Figures *(continued)*

List of Figures *(continued)*

List of Figures *(continued)*

List of Figures *(continued)*

LIST OF TABLES

List of Tables *(continued)*

LIST OF ABBREVIATIONS

$[AC\text{-}5\text{-}seco\text{-}Cbs]^+$	5-seco-aquacyanocobester
$[AC\text{-}15\text{-}seco\text{-}Cbs]^+$	15-seco-aquacyanocobester
ACCbi	Aquacobinamide
$[ACCbs]^+$	Aquacyanocobester
$[ACSYCbs]^+$	Aquacyano-stable yellow cobester
AdoCbl	Adenosylcobalamin
B_{12a}	Vitamin B_{12a} (aquacobalamin)
Cbl	Cobalamin
CNCbl	Cyanocobalamin
Co-A	Coenzyme-A
COSY	Homonuclear 2D shift correlation spectroscopy
[DC-5-seco-Cbs]	5-seco-dicyanocobester
[DC-15-seco-Cbs]	15-seco-dicyanocobester
[DCCbs]	Dicyanocobester
[DCSYCbs]	Dicyano-stable yellow cobester
DMBz	5,6-Dimethylbenzimidazole
ESI-MS	Electrospray ionisation-mass spectrometry
FTIR	Fourier Transform Infra-red
$[H_2OCbl]^+$	Aquacobalamin
HC	Haptocorrin
HC-Cbl	Haptocorrin-cobalamin complex
HMBC	Heteronuclear multiple bond correlation
HOMO	Highest occupied molecular orbital
HPLC	High performance liquid chromatography
HSQC	Heteronuclear single quantum coherence
IF	Intrinsic factor
IF-Cbl	Intrinsic factor-cobalamin complex

List of Abbreviations *(continued)*

MB	Methylene blue
MeCbl	Methylcobalamin
MMACHC	Methylmalonic aciduria and homocystinuria type C
MMCM	Methylmalonyl-CoA mutase
NMR	Nuclear magnetic resonance
pK_a	Acid dissociation constant
pK_{Co}	Acid dissociation constant of coordinated H_2O in corrin complexes
PTLC	Preparative thin layer chromatography
ppm	Parts per million
R_f	Retention factor
ROESY	Rotating frame Overhauser effect spectroscopy
RSE	Relative standard error
SeCNCbl	Selenocyanatocobalamin
Sen	Sensitizer
TC	Transcobalamin
TC-Cbl	Transcobalamin-cobalamin complex
TLC	Thin layer chromatography
TOCSY	Total correlation spectroscopy
UV-vis	Ultraviolet-visible
α ligand	The lower axial ligand coordinated to the Co ion in the corrins
β ligand	The upper axial ligand coordinated to the Co ion in the corrins

Buffers

CAPS	3-(Cyclohexylamino)-propanesulfonic acid
CHES	Cyclohexylaminoethanesulfonic acid
MES	3-(N-Morpholino)-ethanesulfonic acid
MOPS	3-(N-Morpholino)-propanesulfonic acid
Tris	Tris(hydroxymethyl)-aminoethane

† Sulfur rather than sulphur is the IUPAC-recommended spelling and will be used throughout this thesis for related words.

Symbols

μ	Ionic strength
A_∞	Final absorbance
A_0	Initial absorbance
A_1	Final absorbance
A_λ	Absorbance at monitored wavelength
K	Binding constant
K_a	Ionisation constant
k_l^{obs}	Experimentally determined pseudo first-order rate constant for the substitution of H_2O by exogenous ligand
k_l	pH-corrected pseudo first-order rate constant
k^{II}	Second-order rate constant
K_{obs}	Experimentally determined binding constant for coordination of exogenous ligand
λ	Wavelength

CHAPTER 1

INTRODUCTION

1.1 Vitamin B_{12}

In the early 19th century, Thomas Addison discovered a potentially life-threatening auto-immune disease subsequently known as pernicious anaemia, wherein patients succumbed to a characteristic decrease in the number of healthy red blood cells, coupled with the formation of excessively large red blood cells known as megaloblasts.[1,2] In 1926, physicians Whipple, Minot and Murphy discovered that patients with pernicious anaemia went into remission after treatment with a raw liver diet.[1,3] As such, raw liver had to contain some form of anti-pernicious anaemia factor.

1948 marked the beginning of vitamin B_{12} chemistry with the isolation of this anti-pernicious anaemia factor as dark red needle-like crystals, simultaneously discovered by Folkers and co-workers at the Merck laboratories (USA)[4,5] and Smith and associates at the Glaxo laboratories (UK).[6,7] The isolation of the crystalline factor, now known as vitamin B_{12} (or cyanocobalamin), was a momentous accomplishment as isolation of vitamin B_{12} was extremely difficult in large part due to the minute amount present in the liver (< 1 ppm).

Dorothy Hodgkin went on to elucidate the crystal structure of vitamin B_{12} using X-ray crystallographic techniques in 1955.[8-13] The crystal structure determination of a compound of this size and complexity was unprecedented at the time as X-ray crystallographic techniques and equipment were still only in the development stage.[14] The crystallographic data obtained from these vitamin B_{12} studies marked the first determination of a chemical formula by means of X-ray diffraction and was the first metalloenzyme structure to be deduced.[5,7] The first complete artificial synthesis of vitamin B_{12}, which can only be synthesised naturally by micro-organisms,[2,15,16] was performed by Woodward[17] and Eschenmoser[18,19] in 1973.

Once discovered, interest in the biological activity of vitamin B_{12} was enormous as a result of its purpose as a precursor for co-enzymes, which are small organic molecules essential for the

References on page 41

efficient enzymatic catalysis of oxidation-reduction and group transfer reactions.[20-22] In mammalian systems, the active cobalamin species is not vitamin B_{12} itself, but rather two vitamin B_{12} co-enzymes, methylcobalamin (MeCbl) and adenosylcobalamin (AdoCbl)[23], which reside in the active sites of enzymes[24] and are essential for two crucial enzyme-mediated processes. The first involves the methylcobalamin co-enzyme, which is required by the enzyme methionine synthase (also known as homocysteine methyl transferase) for the biosynthesis of the essential amino acid methionine, in which homocysteine is converted to methionine via a methyl group transfer reaction.[2,15,25-28] The second process involves the adenosylcobalamin co-enzyme, which is required by the enzyme methylmalonyl-CoA mutase (MMCM) to carry out the skeletal rearrangement involved in the conversion of methylmalonyl-CoA to succinyl-CoA during fatty acid oxidation.[2,15] As a result of its role in crucial enzymatic reactions, vitamin B_{12} is involved in many biochemical processes within the body, primarily in red blood cell formation, nucleic acid and lipid synthesis as well as the healthy functioning of the brain and central nervous system.[23,29] Vitamin B_{12} is also involved in many more biochemical processes in bacteria and is a crucial co-factor for a larger range of mutases, isomerases and dehalogenases.

Vitamin B_{12} is, however, commonly encountered as cyanocobalamin (CNCbl), in which a cyano group is coordinated to the central Co(III) ion.[30] It was found that cyanocobalamin is in fact an artefact from the methods utilised to isolate the vitamin after it has been synthesised by bacteria,[2] and thus needs to be converted into the physiologically-active forms methylcobalamin and adenosylcobalamin.

As previously mentioned, vitamin B_{12} can only be synthesised by bacteria; therefore, the body's requirements can only be fulfilled by the ingestion of animal products such as meat, poultry, milk and eggs or from fortified foods.[31] In such cases, cyanocobalamin is often found bound to proteins, and the human body requires three internal binding proteins to facilitate the efficient uptake and transport of the vitamin to the necessary cells (Figure 1.1).[23]

The first of these proteins is Haptocorrin (HC), which is released by the salivary glands and binds cobalamin, hence forming a HC-Cbl complex. The HC-Cbl complex is cleaved by pancreatic proteases, thereby releasing the cobalamin for complexing with the second binding protein, the

References on page 41

intrinsic factor, IF, which is secreted by gastric parietal cells. The resultant IF-Cbl complex is then absorbed through the intestinal tract into enterocytes via receptor-mediated endocytosis, where the complex is degraded. After lysosomal release, the cobalamin exits the enterocyte, facilitated by MDR1 (multi-drug resistance protein 1) and binds to the third binding protein, Transcobalamin (TC). The TC-Cbl complex is then released into plasma where it enters target cells via receptor-mediated endocytosis; here cyanocobalamin is liberated and reduced by the MMACHC protein (resulting in the loss of a cyanide ligand) and then converted enzymatically into its two coenzyme forms, MeCbl and AdoCbl. (Figure 1.1).[2,23,32,33]

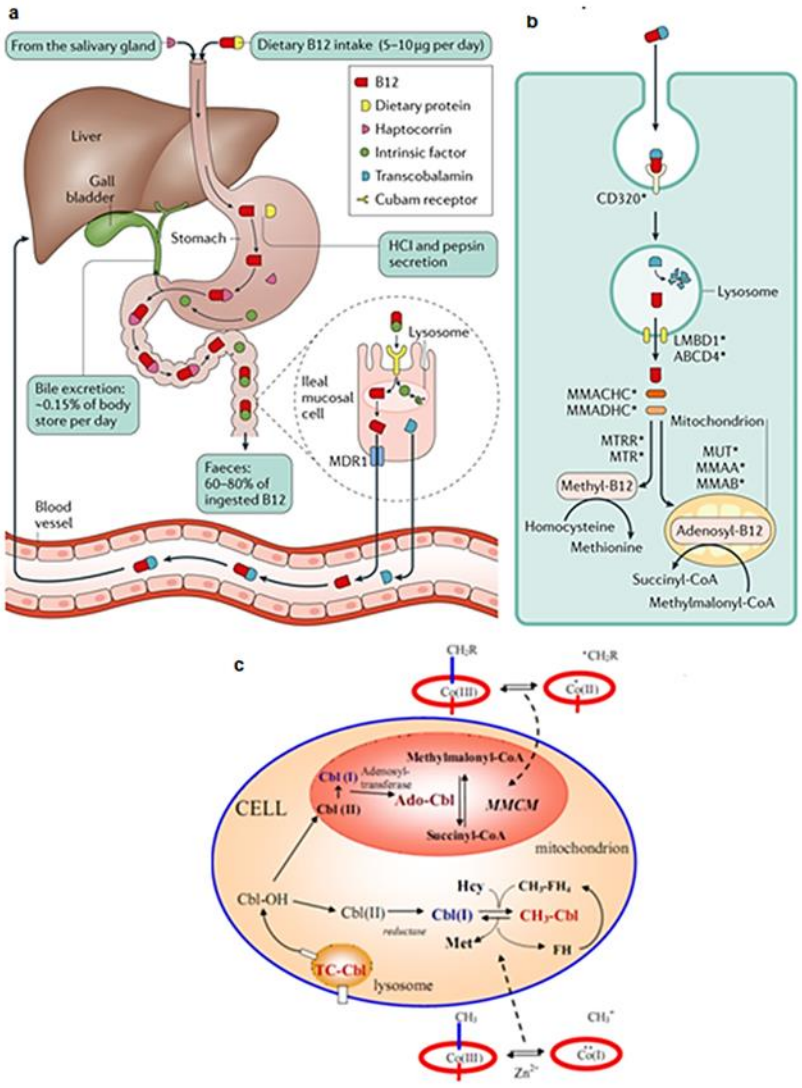

Figure 1.1 The transport (a) and intracellular uptake of cobalamin within the human body (b), indicating the formation and function of the co-factors MeCbl and AdoCbl (c).[2,33]

References on page 41

The structures of MeCbl and AdoCbl were determined by Galen Lenhert[34] and Marzilli and co-workers,[35] respectively, and the only significant difference between the two cobalamins is the nature of the axial organic ligand (Figure 1.2).

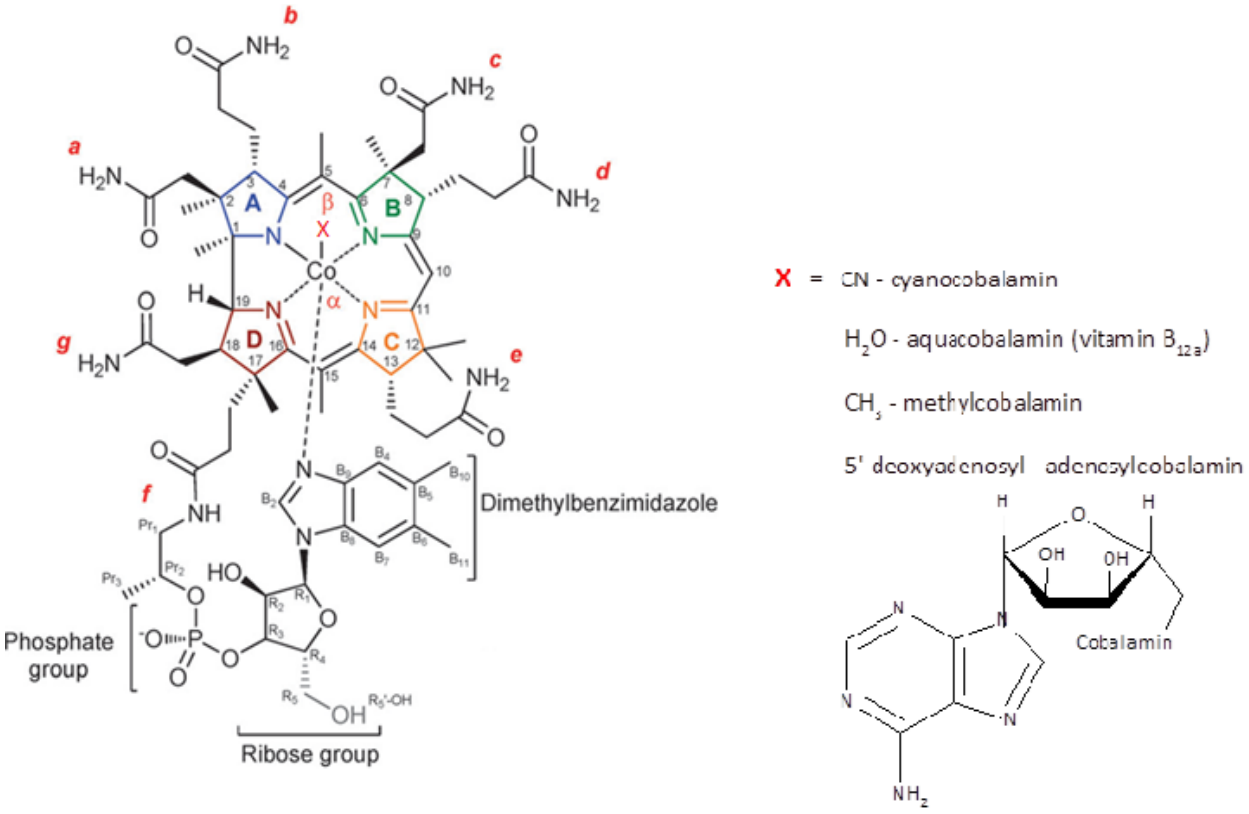

Figure 1.2 The structure of vitamin B_{12} and its derivatives.[23]

As enticing as the study of the biological activity of vitamin B_{12} was, the chemistry was even more so, as this complex vitamin contains a biologically rare metal cobalt(III) ion encased in a corrin ring. The Co(III) centre in the macrocyclic cavity has six coordination sites, four of which are occupied by the four equatorial pyrrole nitrogens of the corrin ring, and one axial ligand coordination site is occupied by the nitrogen atom of the 5,6-dimethylbenzimidazole nucleotide (DMBz) in the α (lower) face.[14,30,36-43] The second binding nitrogen in the nucleotide base is linked to a ribose, which is also bonded to a phosphate group. This in turn is connected to one of the amide side chains, thus forming a 'strap' back onto the corrin ring.[2,15] The remaining

References on page 41

axial ligand coordination site is the actual site of reactivity and the nature of this ligand varies between the different derivatives, thus forming an array of different cobalamins.[44] Hence cyanocobalamin arises if the sixth coordination site contains a cyano ligand (–CN), methylcobalamin if the site contains a methyl ligand ($–CH_3$), and 5'-deoxyadenosylcobalamin if the site contains a 5'-deoxyadenosyl group, all of which are located on the less sterically-hindered β (upper) face (Figure 1.2).[24]

1.2 Cobalt Corrinoids

Much of the chemistry discussed in this study pertains to the unusual chemistry of cobalt in the cobalt corrinoids. A corrinoid is a term used to define a group of compounds that are characterised by the presence of four reduced pyrrole rings joined together to form a macrocyclic ring by links between the α carbon atoms in each unit, three of which are formed by a methine bridge and one by a direct Cα-Cα bond.[14,36] The corrin structure closely resembles that of the biologically-widespread porphyrin; however, it is less extensively conjugated due to the additional methine bridge found in porphyrins in place of the direct Cα-Cα bond.[15,40] The corrin ring has a π-delocalised system involving N and sp^3 C atoms in which 14 π-electrons are spread across 13 atoms.[24,38,39,45,46] It is these features that make the corrin ring flexible and non-planar, and create a small macrocyclic central cavity that are all critical features in cobalt corrin chemistry.[47,48]

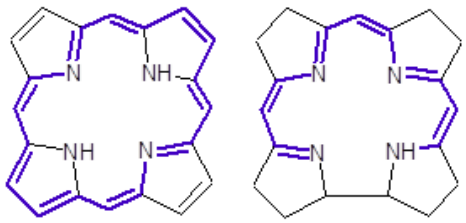

Figure 1.3 The structures of the porphyrin (left) and corrin (right) macrocycles showing the extent of delocalisation.

References on page 41

1.2.1 Cobalt

The most striking feature of the cobalt corrinoids is the inclusion of a biologically rare Co(III) metal ion. Cobalt(III), a classic example of an inert metal,[45,49] is a low spin, first row d^6 transition metal,[46,50,51] while it is the low spin d^7 cobalt(II) ion that is kinetically labile. The low spin pairing energy and remarkably high ligand field stabilisation energy of Co(III) make it highly unlikely for a spin crossover to the high spin configuration to occur.[29] Co(III) is therefore stable in a configuration with no unpaired electrons, rendering it kinetically inert because of the large contribution of the ligand field stabilisation energy to the activation energy for ligand substitution. As such, compounds containing Co(III) typically undergo very slow ligand substitution reactions; hence it is very unusual that Co(III) is found in a vitamin which is involved in fast, catalytic processes within the body. Surprisingly, however, the Co(III) centre of cobalt corrinoids exhibits remarkable lability towards axial ligand substitutions as evidenced in many reports.[41,45,46,52-66]

The unexpected lability of Co(III) when coordinated to a corrin macrocycle raises many questions, amongst which are: why has nature incorporated an inert metal into a crucial biological catalyst, and how is the structure manipulated to enhance the metal's inherent inertness?

A probable reason to rationalise why nature has preferentially selected cobalt is that the three oxidation states prevalent in cobalt chemistry, namely the +1, +2 and +3 oxidation states are all stable under physiological conditions.[30] This is imperative for cobalamins to perform their necessary biochemical functions, which involve the fission of the Co-C bond through either a homolytic **(a)** or one of two heterolytic **(b, c)** mechanisms.[2]

(a) RCo(III)alamin $\longrightarrow$ cob(II)alamin + $R^{\cdot}$

(b) RCo(III)alamin $\longrightarrow$ cob(III)alamin + R^{-}

(c) RCo(III)alamin $\longrightarrow$ cob(I)alamin + R^{+}

This is crucial during the various catalytic cycles of the cobalamins in which the cobalt ion is found in all three oxidation states, thus allowing for the necessary enzymatic functions to be

References on page 41

carried out (Figure 1.1).[2] This is also a property that other similar structures such as porphyrins do not possess, hence highlighting the preference of a cobalt corrin for vitamin B_{12} activities.

1.2.2 Axial Ligands

Over time, many vitamin B_{12} derivatives have been identified, and many of these have originated by varying the nature of the axial ligands coordinated at the α and β binding sites of the central Co(III) ion, thus affording a multitude of functions across the vitamin B_{12} group.[44] The β-axial ligand found on the upper face varies with each derivative and is the actual site of reactivity. For example, in cyanocobalamin, the β ligand is a cyano moiety, whereas in aquacobalamin (vitamin B_{12a}), the β ligand is a water molecule. The nature of the α-axial ligand found on the lower face determines whether the corrin is a 'complete corrinoid', also known as a cobalamin, in which case the α coordination site will be occupied by the dimethylbenzimidazole nucleotide base,[14,30,36,37] or an 'incomplete corrinoid', also known as a cobinamide, in which case the α axial ligand site can vary (a cyanide ligand in dicyano complexes or a water ligand in diaqua complexes, for example).

1.2.3 Side Chains

The corrin macrocycle is adorned with seven side chains on the periphery of the corrin skeleton, extending from the β position of each pyrrole ring (Figure 1.2). C12 however, does not possess a side chain. Three of these side chains, labelled *a, c* and *g* (Figure 1.2) are short acetamide side chains which extend above the plane of the corrin ring, and the remaining four side chains, *b, d, e* and *f*, are longer propionamide side chains extending below the plane of the corrin ring.[24] In 'complete corrinoids', side chain *f* is further connected to the dimethylbenzimidazole nucleotide base through an aminopropanol, phosphate and α-ribose.[36,37] In cases where the seven side chains have been hydrolysed, the corrin complexes are collectively referred to as a cobyric acids and the corresponding esters as cobesters; it is these complexes on which most of this study is focused.

References on page 41

1.2.4 Geometry and Crystal Packing

The corrinoids, which often crystallise in a $P2_12_12_1$space group,[14,25-27,46,67-69] do not have a planar geometry as a result of the direct link between the tetrahedral carbons of pyrrole rings A and D (Figure 1.2). The pyrrole rings are also puckered due to the β-substituents on the periphery of the corrin ring.

1.3 Coordination Chemistry of the Co(III) Corrins

The study of the coordination chemistry of vitamin B_{12} and its derivatives has been invaluable as the subsequent findings have led to the dismissal of several misconceptions such as the kinetic inertness of Co(III) complexes as well as the instability of the bond between a transition metal and alkyl ligand.[70] Hague and Halpern[71] undertook a study on the kinetics of the thiocyanate substitution reactions of $Co(DH)_2(NO_2)OH_2$ and $Co(DH)_2(I)OH_2$ where DH is a dimethylglyoximate ion (often used as a corrin model system) as described in the following reaction:

$$Co(DH)_2(X)OH_2 + Y^- \rightleftharpoons Co(DH)_2(X)Y + H_2O \qquad \text{where } X = NO_2^- \text{ or } I^-$$

[Equation 1.1]

The kinetic results obtained were similar to those obtained by Randall and Alberty[72] for the same reaction with aquacobalamin, although the rate constant was approximately 10^7 times larger for aquacobalamin than for the corresponding bisdimethylglyoximatocobalt(III) complexes, thus highlighting the unusual lability observed in the Co(III) corrins.[71]

In an attempt to further understand the lability of the Co(III) ion towards substitution reactions, Fleischer, Jacobs and Mestichelli[73] studied the ligand substitution reactions of a Co(III), Mn(II) and Fe(III) hematoporphyrin with a thiocyanate ligand. On comparison with Randall and Alberty's[72] kinetic studies on aquacobalamin, it was found that the reactions for aquacobalamin were faster (k^{II} = 5000 $M^{-1}s^{-1}$) than for the corresponding reaction with Co(III)HP (k^{II} = 1850 $M^{-1}s^{-1}$) and this was attributed to the labilizing effect of a nonaqua ligand in the fifth coordination site of Co(III). It is well known that the Co(III) ion found in the cobalamins is low

References on page 41

spin with 6 valence electrons occupying the d_{xz}, d_{yz} and d_{xy} orbitals. Surprisingly, the kinetic inertness towards substitution reactions typically associated with such an electronic arrangement is not observed in the cobalt corrinoids. Thus, it was rationalised that when Co(III) is coordinated to a macrocycle with a delocalised electronic structure, such as the corrin, the Co(III) complex could be kinetically labile following the breakdown of the Co(III) oxidation state formalism.[73,74]

1.4 *cis*- and *trans*-Effects in Co(III) Corrins

The corrinoids are exceptionally useful to coordination chemists as they afford the opportunity to study the *cis*- or *trans*-effect that one ligand has on another. The *cis*- and *trans*-effects are both mutual interactions occurring between two ligands through a central metal ion. The *trans*-effect is defined as the influence of ligand X on ligand Y directly opposite it, whereas the *cis*-effect is the influence of ligand X on ligand Y located directly next to it (Figure 1.4).[32,36,75] Pratt and Thorp[76] previously investigated Co(III) complexes and divided the *cis* and *trans* interactions into three levels: 'kinetic', 'thermodynamic' and 'ground state' *cis*- and *trans*-effects.[77,78] The 'kinetic' *cis*- and *trans*-effects describe the effect that a metal-bound ligand has on the rate of substitution reactions of ligands *cis* or *trans* to it, respectively. The 'ground state effect' is the effect that ligand X has on the properties of *cis* or *trans* ligand, Y, such as bond lengths and force constants. Lastly, the 'thermodynamic' effect (more correctly referred to as a '*trans* influence') is the effect that substitution of coordinated ligand X by incoming ligand L has on the equilibrium constant (*K*), as shown in Equation 1.2 below.

$$[\text{Co–X}] + \text{L}^- \overset{K}{\rightleftharpoons} [\text{Co–L}] + \text{X}^-$$

[Equation 1.2]

References on page 41

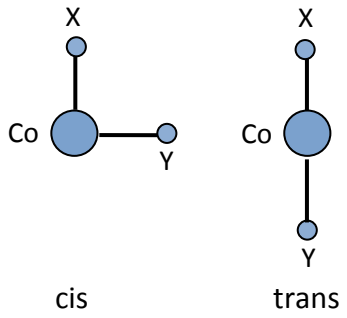

Figure 1.4 The *cis*-effect is defined as the influence Ligand X has on Ligand Y directly next to it, and the *trans*-effect is the influence of Ligand X on Ligand Y directly opposite it.

Pratt and Thorp[76] also revealed that a parallel exists between these *cis*- and *trans*-effects. The effect of an axial ligand on the electronic spectrum of the corrin complex (*cis*-effect) and on the equilibrium between water and the dimethylbenzimidazole nucleotide base (*trans*-effect) correlates with the position of the ligand in the nephelauxetic series in which ligands are ordered based on the amount of negative charge that they donate to a metal ion through σ-bonding. The general order, as identified by Pratt and Thorp[77] as well as Firth and co-workers,[78] is as follows: N, O, Cl, Br and C in CN^- < S, Se, I and C in the organo-ligands; and CN^- < ethinyl < vinyl < ethyl for the carbanions.

Hayward *et al*.[79] studied the 'thermodynamic' or *trans* influences for several ligand substitution reactions involving the cobalamins and cobinamides, and list the following reasons as to why the corrinoids were particularly useful for their study of the thermodynamic *trans* influence:

i) The octahedral coordination of the corrinoids eliminates the risk of binding further ligands that may occur with square-planar complexes;
ii) *Cis-trans* isomerisation is prevented by the equatorial corrin ring;
iii) The equilibria are generally rapidly established; and
iv) A wider range of ligands can be studied than in simpler cobalt(III) complexes.

References on page 41

The study demonstrated the thermodynamic *trans*-influence of ligand X on the equilibria for the substitution of another axial ligand Y by ligand Z. The results suggest that as the ligand changed in the following order: H_2O, NC^-, $HC{\equiv}C^-$, $H_2C{=}CH^-$ and CH_3^-, the *trans* cobalt-cyanide bond becomes less stable relative to the cobalt-dimethylbenzimidazole bond which subsequently becomes less stable relative to cobalt-water bond.

The kinetic *cis*-effect is very prominent in cobalt corrin chemistry. Table 1.1 shows some second-order rate constants for the substitution of a water molecule by various ligands in a few Co(III) complexes (each containing four N-donor ligands in the equatorial plane), as shown in the reaction below:[45]

$$[X{-}Co(III)(N_4){-}OH_2] + L \rightleftharpoons [X{-}Co(III)(N_4){-}L] + H_2O$$

[Equation 1.3]

Table 1.1 The rate constants for ligand substitution reactions in Co(III)(N_4) complexes.

X	N_4	L	$k^{II}/M^{-1}s^{-1}$	Reference
OH^-	Corrin	N_3^-	1.6×10^5	80
OH^-	Porphyrin	N_3^-	7.2×10^2	81
H_2O	Corrin	I^-	2.2×10^3	82
H_2O	Porphyrin	I^-	1.62	83
I^-	Corrin	SCN^-	1.5×10^2	82
I^-	Cobaloxime	SCN^-	1.2×10^{-3}	84
H_2O	Corrin	SCN^-	8.2×10^2	87
H_2O	$(NH_3)_4$	SCN^-	8.6×10^{-7}	85

References on page 41

The term k^{II} is the second-order rate constant for the substitution of coordinated H_2O by incoming ligand, L. Results from Table 1.1 indicate how the lability order increases as the corrinoid donor set varies from $(NH_3)_4$ to cobaloxime, to porphyrin and lastly to corrins. The study also revealed an increase in reaction rates with increasing degree of unsaturation of the equatorial ligands.[54,86] Therefore, labilisation of Co(III) in these macrocyclic complexes may arise from a significant structural and kinetic *cis*-effect of the equatorial ligand through to the axial coordination site.[45]

Hill *et. al.*[87] demonstrated the occurrence of a *cis*-effect in a study on the proton magnetic resonance spectra of some cobalamins, in which it was found that the chemical shift of the hydrogen at the C10 position of the corrin ring is dependent on the ligand that is attached to the cobalamin. The resonance belonging to the hydrogen at the C10 position was determined by comparing it with the spectrum of the chlorinated derivative wherein the corresponding resonance was absent. The study also revealed that keeping benzimidazole as the fixed ligand while the axial ligand in the β position varied in the order: $H_2O < OH^- < C_2H_3^- < CH_3^-$ resulted in the resonance of the C10 hydrogen shifting upfield. When water was the fixed ligand, the order became: $CH_3^- \sim C_2H_5^- < CN^-$. It was noted that the benzimidazole results were comparable with those expected when the cobalt atom experiences an increase in electron density, which in turn results in an increase of electron density at the C10 position. Furthermore, a correlation between the proton chemical shifts at the C10 position and the energies of the α and β bands in the UV-vis spectrum was also observed (Table 1.2). From the presented data, one can note that as the charge density at the C10 position increases, the shielding of the hydrogen at C10 position also increases and the ^1H NMR resonance occurs at a higher field. This correlation (R^2 = 0.97) can be seen in Figure 1.5 which is a plot of the β band wavelength against the δ value of H10.

References on page 41

Table 1.2 Correlation between the absorption bands and NMR spectra of various cobalamins and cobinamides.[36]

Compound	α Band / 10^{-3} cm^{-1}	β Band / 10^{-3} cm^{-1}	C10 Hydrogen chemical shift /ppm
Dicyanocobinamide	17.2	18.5	4.13
Ethylcobalamin	18.1	19.0	4.12
Methylcobalamin	18.2	19.1	4.12
Vinylcobalamin	18.2	19.2	4.05
Hydroxocobalamin	18.6	19.35	3.92
Aquacobalamin	19.0	20.05	3.72
Methylcobinamide	21.7	21.7	3.20

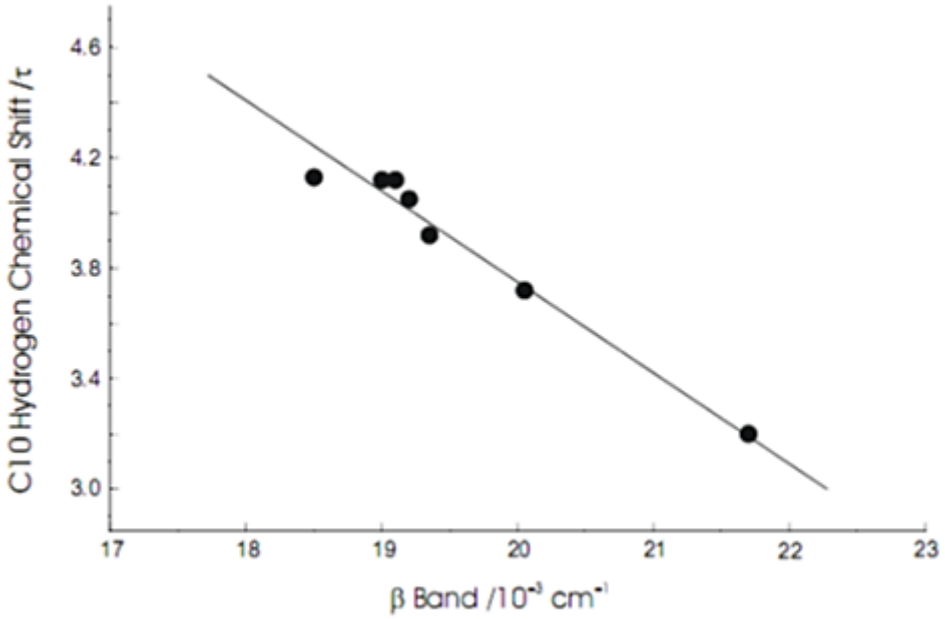

Figure 1.5 Correlation between the β band wavelength with the C10 proton chemical shift (R^2 = 0.97).[36]

References on page 41

Pratt elucidated the effect of varying the nature of ligand X in the β axial position on the Co–N bond lengths in the *cis* and *trans* positions for three cobalt(III) complexes.[75] The data presented in Table 1.3 suggests that varying ligand X generally affects the Co–N bond length in the *trans* position, and only methyl and dimethylphosphite lead to *cis* lengthening. The order of the observed *trans*-effect is the same across the three complexes, ie. ammonia < sulfite < methyl, which correlates with the position of the ligands in the nephelauxetic series. This is in agreement with what was previously mentioned regarding the *trans* effects and the nephelauxetic series.

Firth and co-workers[78] investigated the effect varying an axial ligand had on the stretching frequency of cyanide coordinated in the trans position in various Co(III) complexes. Pratt[75] has shown that cyanide is a convenient ligand for the study of the *cis*- and *trans*-effects of the cobalamins due to the minimal steric requirements of cyanide. The outcome of Firth's investigation is shown in Table 1.4. As the axial ligand X becomes more polarizable and the electron density on coordinated CN^- increases, CN^- becomes rather ionic and the stretching frequency decreases and approaches that of free CN^-.[78] This indicates that the negative charge donated from the axial ligand to the cobalt atom through the σ-bond is the main contribution to the *cis*- and *trans*-effects.

References on page 41

Table 1.3 The ground state *cis*- and *trans*-effects on the bond lengths of three Co(III) complexes.

	Co-N Bond Length (Å)						
X	**X-Co(NH_3)$_5$**		**X-Co(dmgH)$_2$$NH_3$**		**X-Co(corrin)(DMBz)**		**Reference**
	Co-N(cis)	**Co-N(trans)**	**Co-N(cis)**	**Co-N(trans)**	**Co-N(cis)**	**Co-N(trans)**	
H_2O					1.88–1.90	1.925	75
NH_3	1.966	1.966	1.893	1.960			75
HO^-						1.98	75
CN^-					1.88–1.92	2.01	75
-CF_3				2.030	1.87–1.95	2.05	75
SO_3^{2-}	1.966	2.055		2.053		2.17	75
-CH_3	1.973	2.105			1.88–1.97	2.19	75
$PF(OMe)O^-$					1.88–1.97	2.09	75
$P(OMe)O^-$					1.91–1.96	2.20	75
NO_2^-					1.87–1.92	1.99	88
$SeCN^-$					1.89–1.92	2.02	88
$S_2O_3^{2-}$					1.88–1.92	2.08	89
Isoamyl					1.86–1.91	2.27	90
i-Pr_2PO_3					1.88–1.92	2.19	91
Cl^-					1.88–1.92	1.99	69
SCN^-					1.89–1.92	1.99	88
$SC(NH_2)_2$					1.85–1.91	2.01	25

References on page 41

Table 1.4 The ground-state *cis*- and *trans*-effects of various coordinated ligands (X) on CN stretching frequencies in Co(III) complexes.[36]

	ν_{CN}/cm^{-1}		
X	**X–Co(corrin)CN**	**X–Co(CN)$_5$**	**X–Co(dmgH)$_2$CN**
H_2O	2.133	2.128	
DMBz	2.132		
–OH	2.131		
–CN	2.119	2.134	2.130
–C≡CH	2.110		~2.130
$-CH_2SO_3^-$	2.109	2.113	
$-CH=CH_2$	2.093		2.118
–Ado	2.091		
$-CH_2CO_2$	2.090	2.106	
–H		2.098	
–Me	2.088	2.094	2.112
–Et	2.082	2.094	2.109
(free CN^-)	(2.079)	(2.079)	(2.079)

1.5 Absorption Spectra of the Co(III) Corrins

Absorption spectroscopy has been extensively used to study the *cis*- and *trans*-effects in cobalt corrins, caused by modifying the nature of the axial ligands and substituents on the corrin periphery, for example.[32,40,66,70] Cobalt corrinoinds are intensely coloured, consequent on their extensively conjugated system.[38,92] Hence, corrin complexes can be found in a variety of colours ranging from yellow (MeCbl), to red (CNCbl) and purple as in selenocyanatocobalamin (SeCNCbl), depending on the extent of conjugation and the functional groups present.[32] This broad colour range allows various Co(III) complexes to be easily distinguishable from one another, as each complex will have a characteristic UV-vis spectrum. This allows UV-vis spectroscopy to be a highly attractive technique with which to

References on page 41

study Co(III) corrin reactions along with the high molar absorptivity of cobalt corrins which allows solution chemistry to be carried out at very dilute concentrations (ca. 50 μM).

Characteristic absorption spectra arise from numerous electronic transitions occurring within cobalt corrins. These include d-d transitions within the cobalt ion, internal transitions within the corrin ring and the axial ligands and charge transfer reactions between the cobalt ion and the corrin ring as well as the charge transfer reactions between the axial ligands and the cobalt ion.[32]

The six main bands observed in a Co(III) corrin spectrum above 300 nm (near UV-visible range) result from the spin-allowed π-π* transitions within the corrin ring,[24,32,36,38,42,65,66,70,75,93-95] which is an observation supported by calculations performed by Day (Figure 1.6).[96,97] The lowest intensity bands, labelled the D and E bands, occur near 400 nm. The σ band (low to medium intensity) is found in the 300 – 330 nm region. The αβ bands occur at around 500 nm and 550 nm, respectively, and are the second most intense bands observed in the spectrum (with the α band usually lower in intensity than the β band). The most intense band is known as the γ band and occurs around 350 nm. π-π* transitions occur when an electron moves from a filled molecular orbital to an empty orbital in the corrin ring. This electronic transition is often referred to as a HOMO-LUMO transition. Kuhn *et al.*[98] showed that since a corrin possesses 14 π-electrons delocalised over 13 atoms, the seven lowest energy molecular orbitals were already occupied. Hence, the lowest energy transition is from the highest occupied orbital to the lowest unoccupied orbital (level 7→8) and corresponds to the αβ bands, transitions 6→8 corresponds to the DE bands, and transition 7→9 corresponds to the γ band. No further transitions are expected at energies higher than those of the γ band.[70]

References on page 41

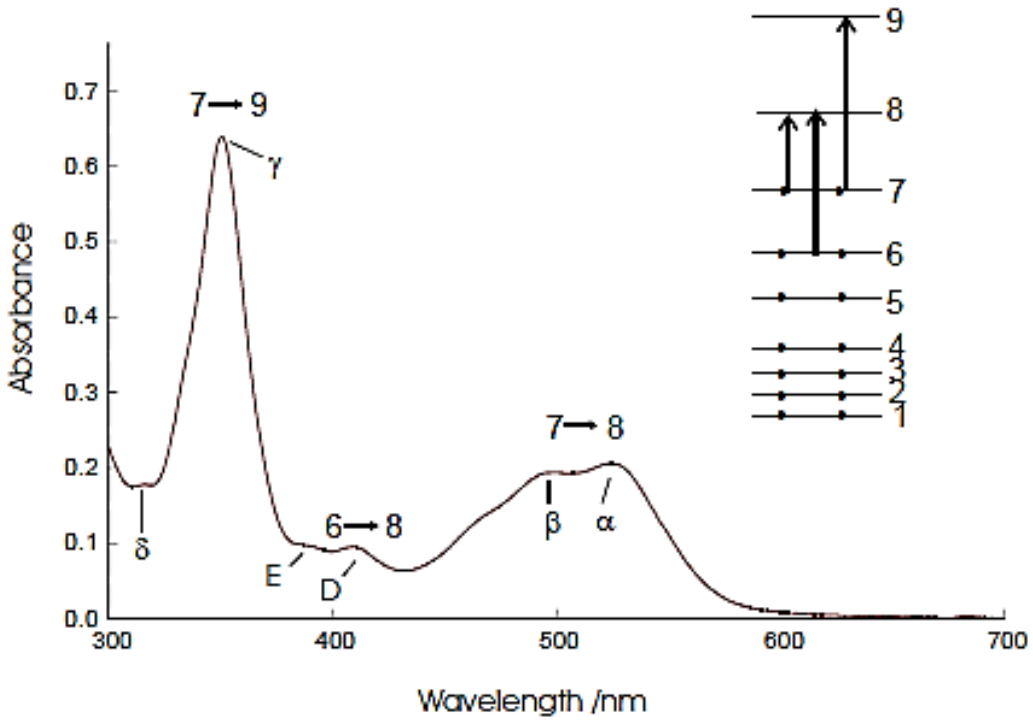

Figure 1.6 The energy levels of the π-electron system and the corresponding bands in the absorbance spectrum of a Co(III) corrin, aquacobalamin.[98]

The cobalt corrin spectrum seen in Figure 1.6 is known as a 'typical' spectrum; however, not all ligands will exhibit this type of spectrum. An 'atypical' spectrum is exhibited by the corrinoids with a soft axial ligand (for example, MeCbl and SeCNCbl (Figure 1.7)).[51,66,96,97] The remarkable difference generally observed from the transitions from levels 6→8 (DE bands) and 7→9 (γ band) can be attributed to the difference of the electron density on the nitrogen atoms of the corrin ring and the nature of the axial ligands.[70]

References on page 41

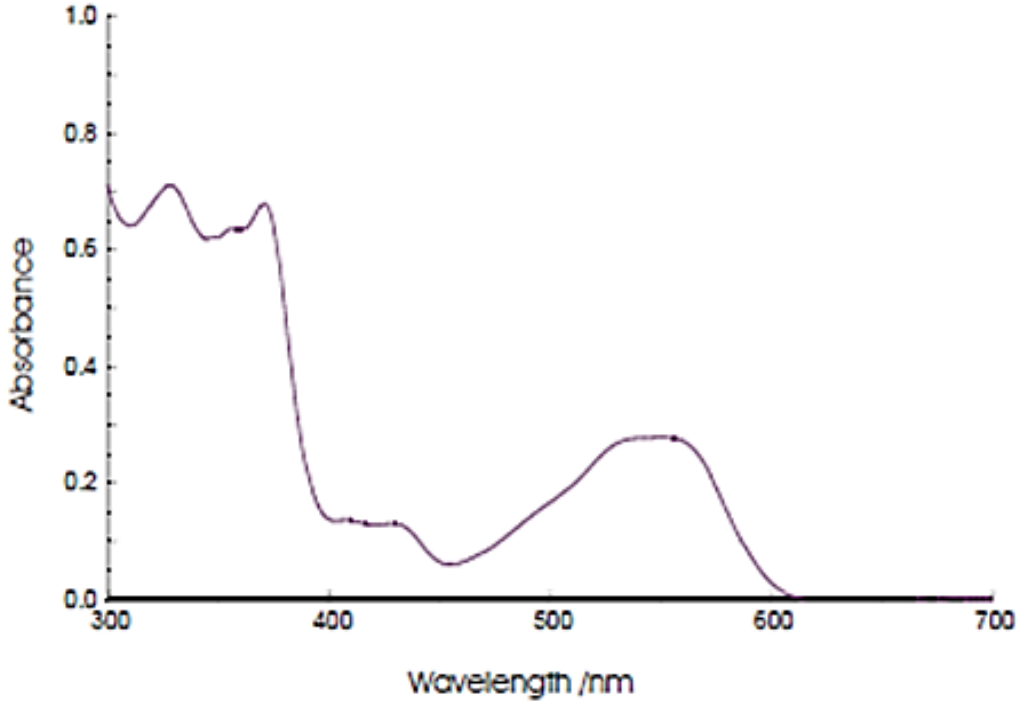

Figure 1.7 The 'atypical' spectrum of SeCNCbl with a reduced γ band occurring at 371 nm, along with more intense bands occurring in the region of 300 – 350 nm.[36]

In an 'atypical' spectrum, not only does the γ band undergo a bathochromic shift and decrease in intensity, but new, intense bands occur in the region of 300 – 350 nm. From these observations, it is noted that the number, positions and intensity of bands arising from π-π* transitions can be remarkably varied, in large part due to the nature of the axial ligands.[51,66,75] This is illustrated in Table 1.5 below, which lists the position of the γ band as a function of the β axial ligand. It can be seen that the γ band shifts in response to the electron donor ability of the axial ligand and undergoes a bathochromic shift when the β ligand has a high σ donor strength (S, Se, I and C), and a hypsochromic shift when the β ligand has a low σ donor strength (N, O, Cl, Br and C in CN^-).[45,76,80,93,99] These ligands exert a considerable influence on the *cis*- and *trans*- influences of the corrin ring.

References on page 41

Table 1.5 The effect on the position of the γ band due to the nature of the β ligand in various cobalamins (α ligand is DMBz).[70,99]

β Ligand	Donor Atom	λ /nm	β Ligand	Donor Atom	λ /nm
CN^-	C	360.5	NCS^-	S	357
$HC{\equiv}C^-$		367	SO_3^{2-}		364
$CH_2{=}CH^-$		372	Thiourea		366
			$S_2O_3^{2-}$		367
NH_3	N	356	Cysteine		370
NO_2^-		356			
NCO^-		357	H_2O	O	350
N_3^-		358	$CH_3CO_2^-$		352
Imidazole		358	HO^-		357
Pyridine		360			
			Halides	Cl^-	352
$NCSe^-$	Se	371		Br^-	353
				I^-	371

As the polarisability of the β ligand increases, the spectra of these substituted cobalamins become increasingly 'atypical'. Perry and Marques performed a Gaussian analysis on the absorption spectra of 11 cobalamin complexes and suggest that the model previously put forward by Kuhn is an over-simplification.[66] Their results correlated well with DFT calculation previously performed by Stich *et. al.*[94] which suggests that the γ band corresponds to at least three different electronic transitions. Perry and Marques also proposed that typical and 'atypical' spectra are not fundamentally different and that the 'atypical' spectrum arises from the separation of the components of the typical γ band as a result of an increase in electron density from the more electron donating, polarizable axial β ligands.[66]

In addition to the spectra mentioned above, there exists another set of compounds with a unique absorption spectrum. These compounds are generally yellow or brown in colour

References on page 41

with the main absorption band occurring between 400 – 500 nm (Figure 1.8). These are collectively referred to as the stable yellow corrinoids.

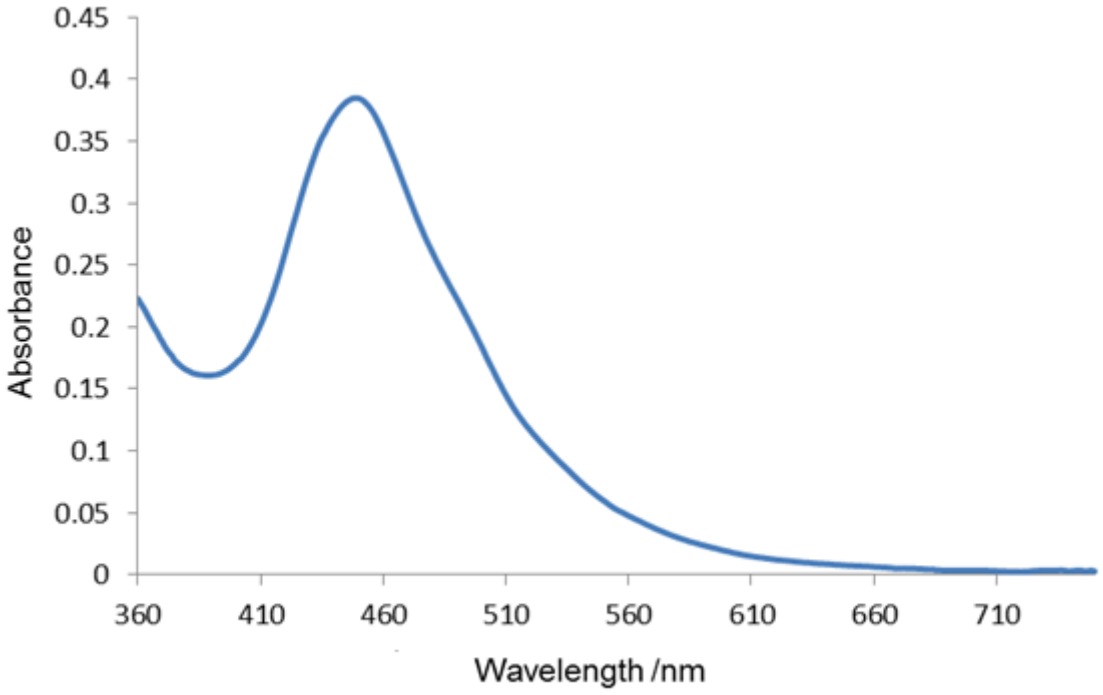

Figure 1.8 The absorption spectrum of aquacyano stable-yellow cobester ([ACSYCbs]$^{+}$).

The effect axial ligands have on the spectra of cobalt corrins has been succintly summarised by Pratt.[70] He pointed out that the axial ligand has a significant effect on the position and intensity of absorption bands and that the σ-donor strength of the ligands is the most influencing property. Hence, the broad range of spectra which are observed for Co(III) corrins can be explained by the change in the electronic distribution within the cobalt corrins as a result of the axial ligands. This is therefore one way of assessing the interaction between the cobalt ion and the axial ligands.

References on page 41

1.6 Background to this Study

Through the years, many studies have been undertaken in an attempt to understand how the structure of the corrin macrocycle affects the properties of the axial coordination site of Co(III). It is believed that the small cavity size of the corrin (compared to, for example, a porphyrin) and partial aromaticity of the corrin, in conjunction with various substituents on the corrin ring, are leading factors in the labilising of Co(III), by the manipulation of the charge density on the metal, increasing its electron density beyond that expected for a nominally 3+ ion. As such, this transfer of significant electron density will modify the characteristic inertness of Co(III) by imparting some partial, labile, d^7 Co(II) character to it.[45,46,51,62,66]

The origin of the labilising effect of cobalt in vitamin B_{12} is the subject of extensive research within the Bio-Inorganic Research group at the University of the Witwatersrand. Given that the nature of the environment surrounding the cobalt ion will affect the lability of the system, the electronic structure of the corrin ring has been perturbed in a variety of ways as shown in Figure 1.9 to test this hypothesis.[45,46,50,65,85,100-102]

Manipulation of the macrocycle can effect a change in the electronic structure (by substitution on the corrin periphery) as well as a change in the cavity size (comparing the properties of Co corrins and Co porphyrins, for example). These elements are thought to be leading contributors to the labilising of Co(III) in vitamin B_{12} and are the subject of an ongoing investigation.

References on page 41

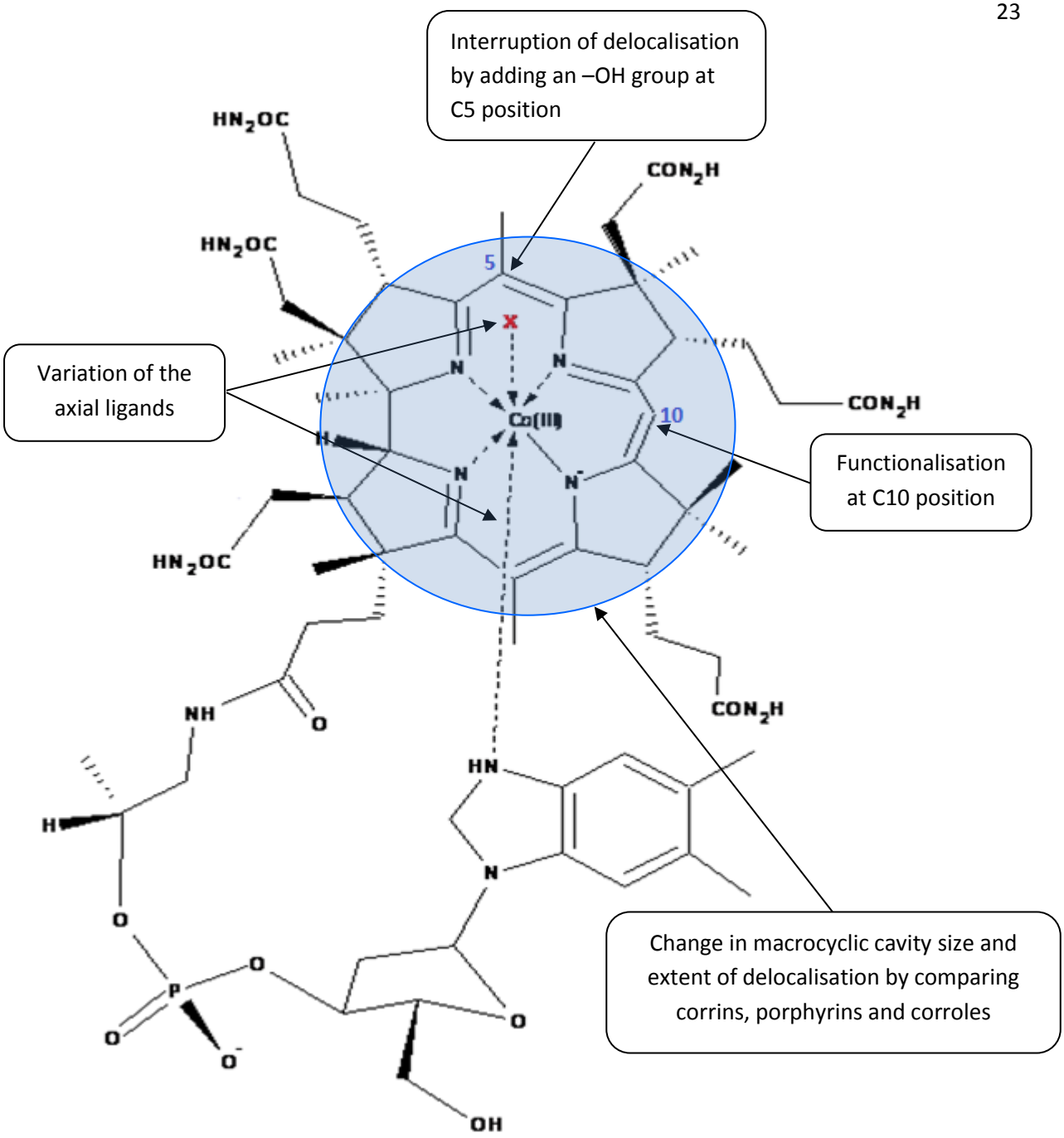

Figure 1.9 The structure of vitamin B_{12} illustrating areas of manipulation.

Cis-effects are crucial in cobalt corrin chemistry. As mentioned earlier, the absorption spectra of cobalt corrinoids are dominated by spin-allowed π → π* transitions, which are highly dependent on the nature of the axial ligand.[32,36,38,45,70,75,96,97] Therefore, as there is direct electronic communication between the axial ligands and the corrin ring itself, the lability of the axial ligands can be modified by perturbing the corrin ligand. This has been evidenced in a study performed by Knapton *et al.*[45] in which the C10–H of aquacobalamin

References on page 41

was substituted by a chlorine atom. Results showed that the length of the C10–Cl bond in the substituted corrin was highly dependent on the polarizability of the axial ligand. Although Cl is an electron-withdrawing group,[103] its resonance electron-donating effect towards the delocalised π-electron system of the macrocycle is far more notable, and as such, Cl competes with electron-donating axial ligands. It was found that when coupled to a neutral or electron-withdrawing axial ligand (H_2O, CN^-) as in the case of aquacobalamin and cyanocobalamin, respectively, the substitution of H by Cl caused an increase in the charge density at the cobalt ion, while the charge density at the equatorial ligand remained unchanged, however, when coupled to an electron-donating axial ligand such as a methyl group (methylcobalamin), the resonance donor ability of Cl decreases, resulting in a decrease in the charge density at the cobalt ion as well as at the equatorial ligand.[45]

To further investigate this *cis*-effect, C10–H was then substituted with a strong electron-withdrawing group, NO, and this was found to completely deactivate the axial ligand coordination site towards substitution reactions, as well as causing a significant increase in the acid dissociation constant of the complex (pK_a 10.71(6)).[100] This is evidence that the chemical properties of the Co(III) ion may be controlled by modifying the electronic properties of the corrin ring.

Ghadimi and co-workers[104,105] further explored the effect that functionalization at the C10–H position had on the activity of Co(III). A 10-nitro and 10-amino derivative of aquacyanocobester ($[ACCbs]^+$) were prepared, wherein the C10–H of $[ACCbs]^+$ was replaced by a strongly electron-withdrawing NO_2 group, or a strongly electron-donating NH_2 group, respectively. This resulted in a harder, less electron-rich cobalt centre in $[AC\text{-}(10\text{-}NO_2)Cbs]^+$ and a softer, more electron-rich cobalt centre in $[AC\text{-}(10\text{-}NH_2)Cbs]^+$, relative to $[ACCbs]^+$. It was found that the softer anionic ligands bound preferentially to the softer $[AC\text{-}(10\text{-}NH_2)Cbs]^+$ derivative, and the converse was true for $[AC\text{-}(10\text{-}NO_2)Cbs]^+$. This indicates the affinity of cobalt for an exogenous ligand depends on the electron density found at the metal centre, as a consequence of the *cis*- influence of the macrocyclic ligand.

References on page 41

In another study, the reaction represented by Equation 1.3 below, wherein an entering ligand, L, substitutes an axially coordinated water in various Co(III) complexes with four N-donor ligands (N_4) (see Table 1.1) was performed to determine the effect of equatorial ligands on axial ligand lability.

$$[X–Co(III)(N_4)–OH_2] + L \rightleftharpoons [X–Co(III)(N_4)–L] + H_2O$$

[Equation 1.3]

It was observed that the second-order rate constant, k^{II}, was largest for substitution reactions involving a corrin ring as the N_4 equatorial ligand, irrespective of the nature of the axial ligand L. For example, when X = H_2O and L = SCN^-, k^{II} was determined to be 8.6×10^{-7} $M^{-1}s^{-1}$ for $(NH_3)_4$,[85] but nine orders of magnitude larger at 8.2×10^2 $M^{-1}s^{-1}$ for the corrin ring.[82] The data suggests that the labilisation of axial ligands increases with increasing delocalisation of the *cis* π-electron system, ($(NH_3)_4$ < cobaloxime < porphyrin < corrin), and decreasing macrocyclic cavity size (porphyrin < corrin).[46] These observations led to the conclusion that labilisation of the Co(III) ion increased with increasing *cis* ligand polarizability and decreasing cavity size which would result in a larger overlap between the central metal ion and the equatorial ligand orbitals.

Mathura and co-workers[106,107] investigated the influence of the macrocycle on the chemistry of Co(III) by comparing a corrin (aquacobalamin) and a porphyrin based biomimetic model, N-acetyl-Co(III)microperoxidase-8 (NAcCoMP8). The coordination of anionic ligands to aquacobalamin was favoured over NAcCoMP8, while the converse was true for neutral N-donor ligands, thus indicating the effect altering the residual charge on the metal centre (+1 in corrin and +2 for the porphyrin) has on the chemistry of Co(III). The nature of the equatorial ligand was also found to affect the kinetics of the ligand substitution reactions as aquacobalamin was much more labile towards the substitution of anionic ligands than NAcCoMP8, but less labile towards the substitution by a neutral N-donor ligand. These thermodynamic and kinetic results highlight the profound effect the coordination environment of the metal ion has on the chemistry of Co(III).

Zipp *et. al*.[108-110] further investigated the effect of the coordinating macrocycle on Co(III) activity by comparing a corrin complex (aquacobalamin) with another biomimetic

References on page 41

tetrapyrrole complex, a corrole. A corrole also has a direct C1–C19 pyrrole-pyrrole bridge (Figure 1.3),[111] hence has a cavity topologically similar to that of a corrin,[112] but possesses a fully romatic 18 π-electron system similar to that of a porphyrin[113] and is subsequently more electron-rich than the corrin. Neutral N-donor ligands bound preferentially to the corrole, whereas anionic ligands bound preferentially to the corrin. Co(III) was also much more labile towards the coordination of cyanide by the corrole. It was argued that the residual charge on the metal centre (0 in corroles and +2 in the corrins) enhances the affinity of aqaucobalamin for the negatively charged ligands through an electrostatic interaction. This provided further evidence that the equatorial ligand of Co(III) complexes significantly affects the lability of the cobalt(III) ion.

Lastly, as it is believed that the extensive 13-atom, 14 π-electron conjugated system has an enormous impact on the lability of the cobalt ion, the connection between the electronic structure of the corrin and Co(III) lability was further examined by an in depth study into the stable yellow corrinoids, in which the delocalised system of the corrin was interrupted by oxidation at the C5 position, thus yielding an aquacyano-stable yellow cobester ($[ACSYCbs]^+$) with a diminished 10 π-electron conjugated system between N22–N24 and an isolated double bond between N21 and C4 (Figure 1.8).[46,65,101,102]

Chemaly *et al.*[46] prepared a vitamin B_{12} derivative, Coα,Coβ-dicyano-heptamethylcob(III)yrinate, (dicyanocobester, [DCCbs], **1**), by the hydrolysis and methanolysis of cyanocobalamin, followed by treatment with potassium cyanide. This resulted in the conversion of the amide side chains on the corrin periphery into ester moieties, as well as in the substitution of the nucleotide base coordinated at the α coordination site by a cyanide moiety. (5R-6R)-Coα,Coβ-dicyano-5,6-dihydro-5-hydroxy-heptamethylcob(III)yrinate-C,6-lactone (dicyano-stable yellow cobester, [DCSYCbs], **2**) was then synthesised by refluxing a solution of [DCCbs] with ascorbic acid, sodium bicarbonate, methanol, EDTA and phosphate buffer whilst being subjected to a slow stream of oxygen.

The corresponding aqua forms, aquacyanocobester ($[ACCbs]^+$, **1**) and aquacyano-stable yellow cobester ($[ACSYCbs]^+$, **2**), were then prepared by treating the cobesters with a solution of methanol and glacial acetic acid (pH 3) under a slow stream of nitrogen to remove HCN generated from the substitution of one of the cyanide ligands.[46,114]

References on page 41

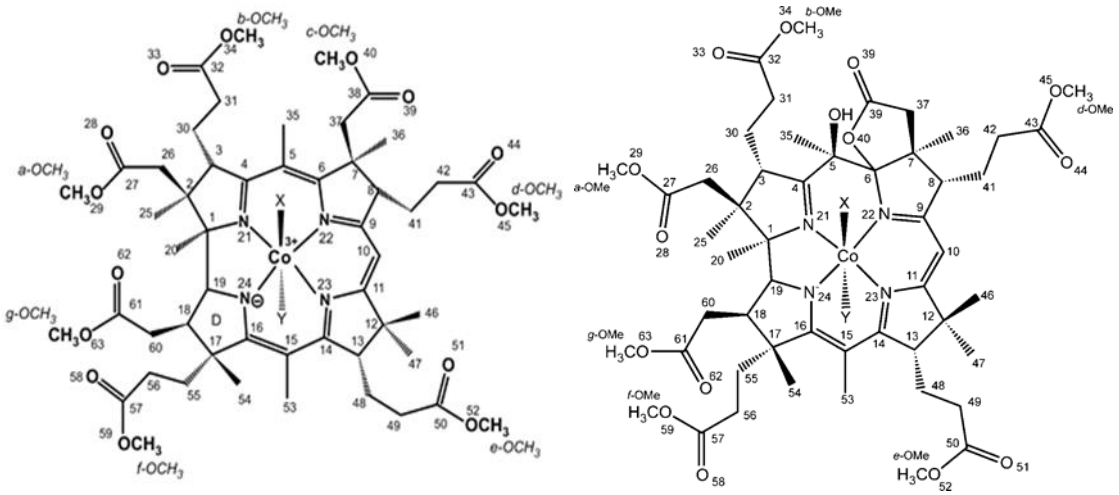

(1) **(2)**

Figure 1.10 The structures of [DCCbs] (X = CN) or $[ACCbs]^+$ (X = H_2O) **(1)**, and [DCSYCbs] (X = CN) or $[ACSYCbs]^+$ (X = H_2O) **(2)**.[46,50]

It was hypothesised that Co(III) in aquacyanocobester would be more electron rich than Co(III) in aquacyano-stable yellow cobester due to the disruption of the conjugated system in the stable yellow cobester. As such, Co(III) in $[ACCbs]^+$ should be 'softer' and exhibit a more Co(II)-like character than in $[ACSYCbs]^+$ and would be expected to thus bind better to soft donor atom ligands rather than the 'harder' Co(III) in $[ACSYCbs]^+$, which would conversely bind better to harder ligands.[50]

This hypothesis was tested by determining the equilibrium constants for the substitution of axially coordinated water with anionic ligands such as azide (N_3^-), nitrite (NO_2^-), cyanide (CN^-), thiosulfate ($S_2O_3^{2-}$) and sulfite (SO_3^{2-}) and neutral N-donor ligands including an imidazole (N-methylimidazole (N-MeIm)), pyridines (pyridine (Py), 4-methylpyridine (4-MePy), 4-methoxypyridine (4-MeOPy) and dimethylaminopyridine (DMAP)), and primary amines (ammonia (NH_3), ethanolamine (NH_2EtOH), methoxyethylamine (NH_2EtOMe) and 2,2,2-trifluoroethylamine ($CF_3CH_2NH_2$)).

References on page 41

Table 1.6 The equilibrium constants and thermodynamic parameters for the substitution of coordinated water in $[ACCbs]^+$ and $[ACSYCbs]^+$ by exogenous ligands.[50,65]

	$[ACCbs]^+$				$[ACSYCbs]^+$			
Ligand	**T / °C**	**log *K***	**ΔH / kJ mol^{-1}**	**ΔS / J K mol^{-1}**	**T / °C**	**log *K***	**ΔH / kJ mol^{-1}**	**ΔS / J K mol^{-1}**
N_3^-	9.6	2.662 (19)	–9.4 (7)	18(3)	9.9	2.80 (2)	–18.6(7)	–12(2)
	17.0	2.628 (6)			16.7	2.74 (3)		
	24.4	2.595 (10)			23.2	2.64(3)		
	31.8	2.550 (14)			29.9	2.57(4)		
	39.2	2.498 (12)			37.4	2.51(3)		
CN^-	9.6	8.19(11)	–23(2)	81(6)	9.9	7.20(5)	–17(1)	80(5)
	17.0	8.08(6)			16.7	7.13(5)		
	24.4	8.10(10)			23.2	7.10(5)		
	32.5	8.06(11)			29.9	7.00(5)		
	40.0	7.88(8)			37.4	6.93(7)		
NO_2^-	9.9	2.93(1)	–6.6(9)	33(3)	9.9	2.57(1)	–22.9(4)	–32(3)
	16.7	2.91(1)			16.7	2.46(2)		
	23.2	2.89(1)			23.2	2.38(1)		
	29.9	2.86(2)			29.9	2.28(1)		
	37.4	2.81(1)			34.7	2.20(2)		
SO_3^{2-}	9.9	4.70(3)	50(3)	265(9)	9.9	2.37(3)	59(1)	253(5)
	16.7	4.87(2)			16.7	2.56(5)		
	23.2	5.00(2)			20.5	2.83(3)		
	29.9	5.11(3)			23.2	3.06(2)		
	37.4	5.29(3)			29.2	3.31(1)		
$S_2O_3^{2-}$	9.9	0.33(2)	21(3)	80(10)	23.2	–0.2(1)		
	16.7	0.37(2)						
	23.2	0.51(4)						
	29.9	0.56(4)						
	37.4	0.7(2)						
NH_3	10.0	3.22(7)	–41(1)	–85(2)	10.0	3.30(4)	–46(2)	–98(7)
	15.0	3.08(5)			15.0	3.18(12)		
	20.0	2.95(7)			20.0	3.02(14)		
	25.0	2.84(6)			25.0	2.86(5)		
	30.0	2.71(3)			30.0	2.78(15)		

References on page 41

	[ACCbs]$^+$				[ACSYCbs]$^+$			
Ligand	**T / °C**	**log *K***	**ΔH / kJ mol^{-1}**	**ΔS / J K mol^{-1}**	**T / °C**	**log *K***	**ΔH / kJ mol^{-1}**	**ΔS / J K mol^{-1}**
NH_2EtOH	9.9	2.04(23)	–24(2)	–44(7)	10.0	2.18(7)	–79(3)	–23(9)
	16.7	2.00(13)			15.0	1.96(16)		
	23.2	1.89(13)			17.5	1.84(16)		
	32.0	1.74(16)			20.0	1.75(7)		
	37.4	1.69(10)			25.0	1.44(12)		
					30.0	1.24(10)		
					32.5	1.11(14)		
NH_2EtOMe	11.0	2.40(10)	–51(2)	–136(8)	10.0	2.28(35)	–53(4)	–145(15)
	17.5	2.15(8)			17.5	1.92(10)		
	25.0	1.89(9)			25.0	1.59(30)		
	32.5	1.68(10)			32.5	1.48(13)		
	40.0	1.52(7)			40.0	1.27(12)		
N-MeIm	9.9	4.43(4)	–23(1)	5(4)	9.9	1.31(29)	23(3)	107(11)
	16.7	4.32(3)			17.1	1.47(33)		
	23.2	4.21(3)			19.5	1.49(15)		
	32.0	4.16(6)			24.4	1.52(15)		
	37.4	4.05(4)			31.5	1.64(33)		
4-MePy	10.0	3.62(3)	–29(2)	-33(8)	10.0	0.37(16)	5(1)	24(2)
	17.5	3.53(2)			17.5	0.40(9)		
	25.0	3.41(3)			25.0	0.41(22)		
	32.5	3.22(2)			32.5	0.44(23)		
	40.0	3.14(2)						
4-MeOPy	10.0	3.54(4)	–25(1)	–19(3)				
	17.5	3.45(3)						
	25.0	3.32(3)						
	32.5	2.23(3)						
	40.0	3.11(3)						

Results from the coordination of anionic ligands indicated that the soft donor atom ligands (CN^-, SO_3^{2-}) did in fact bind better to softer [ACCbs]$^+$ than to [ACSYCbs]$^+$ (log *K* = 8.10(10) and 5.00(2)), respectively, in comparison to 7.10(5) and 2.83(2), respectively). Conversely, the hard donor atom ligands (NO_2^- and N_3^-) bound somewhat better to harder [ACSYCbs]$^+$ (log *K* = 2.89(1) and 2.595(10), respectively, for [ACCbs]$^+$ and 2.38(1) and 2.64(3) for

References on page 41

$[ACSYCbs]^+$).[50] At first glance, it may appear as if there was no significant difference between the two corrins as the log *K* values were somewhat similar. However, the corresponding thermodynamic parameters, namely enthalpy (ΔH) and entropy (ΔS), suggest otherwise. As ΔH values became more negative, the substitution reactions became more enthalpically driven, whereas the reactions became more entropically driven as ΔS becomes more positive. Thus, for example, ΔH for the substitution of coordinated water by azide in $[ACCbs]^+$ was – 9.4(7) kJ mol^{-1}, but for $[ACSYCbs]^+$, ΔH was determined to be – 18.6(7) kJ mol^{-1}. ΔS values on the other hand were 18(2) kJ mol^{-1} for $[ACCbs]^+$ and – 12(2) kJ mol^{-1} for $[ACSYCbs]^+$. In correlation with the spectroscopic evidence mentioned above, these parameters indicate how coordination of a hard donor atom ligand is much more thermodynamically favourable in harder $[ACSYCbs]^+$ than softer $[ACCbs]^+$, or conversely indicating how the softer cobalt ion in $[ACCbs]^+$ favoured softer ligands.

The neutral N-donor ligands were classed into 2 categories; the softer aromatic N-donor ligands (N-MeIm and the pyridines) and the harder aliphatic N-donor ligands (ammonia, ethanolamine and methoxyethylamine). Once again, the softer donor ligands bound preferentially to softer $[ACCbs]^+$, whereas the harder ligands bound preferentially to $[ACSYCbs]^+$. For the ligand substitution reactions of $[ACCbs]^+$, the binding of all ligands resulted in large and negative ΔH and ΔS values, with the exception of N-MeIm, where ΔS is nearly zero, thereby indicating that the substitution reactions are enthalpically driven. For ligand substitution reactions of $[ACSYCbs]^+$, the harder aliphatic N-donor ligands (NH_3, NH_2EtOH, NH_2EtOMe) also resulted in large and negative ΔH and ΔS values. In contrast, the softer aromatic N-donor ligands (N-MeIm and 4-MePy) yielded positive ΔH and ΔS values, and are thus entropically driven. Thus, based on the affinity of $[ACCbs]^+$ for the softer ligands, the distinction between the softer Co(III) in $[ACCbs]^+$ and the harder Co(III) in $[ACSYCbs]^+$ observed for the binding of anionic ligands is maintained for the neutral N-donor ligands.[65]

It was also observed that the equilibrium constants were generally found to be higher for $[ACCbs]^+$ than $[ACSYCbs]^+$, which was expected since the corrin in $[ACSYCbs]^+$ was disrupted thereby decreasing the thermodynamic stability of the system. It can therefore be concluded that the spectroscopic and thermodynamic results illustrate how the chemical

References on page 41

properties of the central Co(III) ion may be modified by perturbing the electronic structure of the *cis* equatorial corrin ligand.

It would be interesting to discover what effect fragmenting the corrin ring and the subsequent opening of the macrocyclic cavity would have on the labilising effect of the macrocycle on the Co(III) ion. In this study a different approach was taken by using photo-oxidation reactions to exploit the photochemical reactivity of cobalt corrins[92] with electrophilic singlet oxygen,[115] so as to cleave a part of the corrin ring and open the macrocyclic cavity up, resulting in the formation of a secocobester.[116]

Furthermore, as it is now well known that diminishing the extent of delocalisation in the corrin π-electron system inhibits the ability of the system to impart electron density onto the cobalt ion, it would also be of interest to take the opposite approach in the second part of this study and increase the extent of delocalisation beyond that typically observed in a corrin ring. This will be achieved by synthesising another vitamin B_{12} derivative, hexamethyl Coα,Coβ-dicyano-7-de-(carboxymethyl)-7-8-didehydro-cobyrinate ('pyrocobester')[117,118] in which the length of the corrin chromophore has been increased but the macrocyclic cavity remains intact, to determine whether the resulting increased electron density of the corrin ring will further increase the lability of the Co(III) ion.

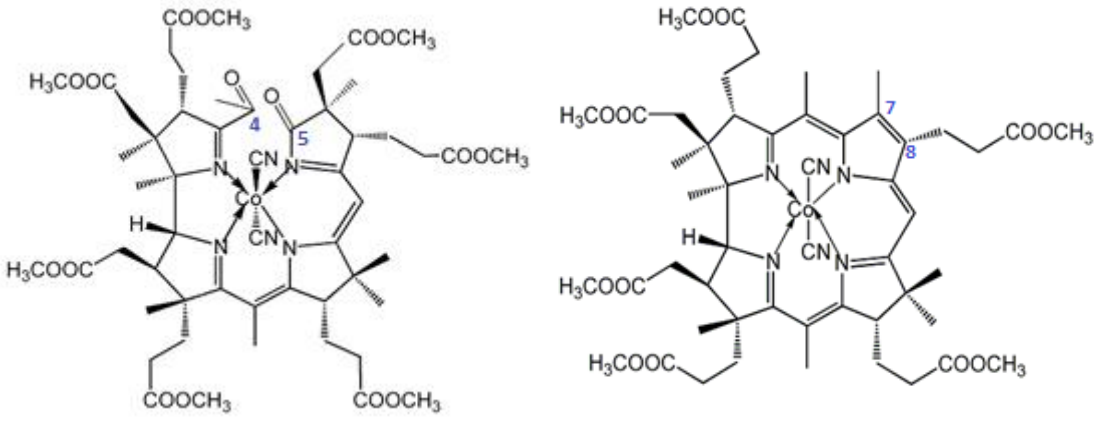

Figure 1.11 The structures of 5-seco-dicyanocobester ([DC-5-seco-Cbs]) wherein the corrin has been cleaved at the C5 position (left) and dicyanopyrocobester with an additional double bond between C7 and C8 (right).

References on page 41

1.7 Photochemistry

Electromagnetic radiation, when absorbed at a wavelength corresponding to an electronic transition within a molecule, can provide enough activation energy to initiate a chemical reaction.[119] Photochemistry is concerned with the chemical reactions that proceed as a result of the absorbance of UV-vis light by molecules.[120]

Photochemistry is governed by two main principles, the Grotthus-Draper law and the Stark-Einstein law.[121] The Grotthus-Draper law is the first law of photochemistry and states that light must be absorbed by a compound for a photochemical reaction to take place. The second law of photochemistry, the Stark-Einstein law, is also known as the photo-equivalence law, and states that for each photon absorbed by a chemical system, only one molecule is activated for subsequent reaction.[119]

Absorption of light may initiate a chemical reaction by altering the symmetry of the electronic configuration of a molecule, thus enabling a previously inaccessible reaction pathway; more commonly, light may be absorbed by a reactant molecule or photosensitizer, leading to excitation of the reactant molecule.[119] Excitation induces a change in the molecular orbital occupancy of the molecule, resulting in an increase in the internal energy, a change in the local bonding as well as in the charge distribution. The excited states are classified as either a singlet or triplet state depending on the spin angular momentum, and photo-induced reactions always lead to a state with the same multiplicity.[119]

There are three main reactions that may occur when light interacts with coordination compounds: intra- and intermolecular photo oxidation-reduction reactions involving ligands and the central metal atom, photo-substitution reactions, and photo-isomerisation reactions.[120]

1.7.1 Singlet Oxygen Formation

In a photosensitized oxidation-reduction reaction, a sensitizer molecule that absorbs radiation, transfers energy to molecular oxygen ($^3\sum_g$) thus forming a diamagnetic oxygen species in a high-energy singlet state, known as singlet oxygen (O_2 ($^1\Delta_g$)).[122-124]

References on page 41

The photochemical approach of singlet oxygen formation incorporates the use of photosensitizers such as porphyrins or synthetic dyes, which absorb energy from light to form an excited, unstable singlet state molecule (^{1}Sen*).[115] The sensitizer then reaches an excited triplet state (^{3}Sen*) via inter-system crossing. The triplet state sensitizer can now undertake one of two possible reaction pathways (Figure 1.12).[115] The first possible reaction pathway is the direct reaction of (^{3}Sen*) with a substrate, which involves the transfer of a hydrogen atom or electron to generate radicals which will react with oxygen to form superoxide radical anions (Type I).[125] The more common reaction though, involves the excited triplet state sensitizer reacting with triplet oxygen,[115] thus generating singlet oxygen in an energy transfer reaction as the sensitizer returns to the ground state to be available for the next cycle (Type II).[125]

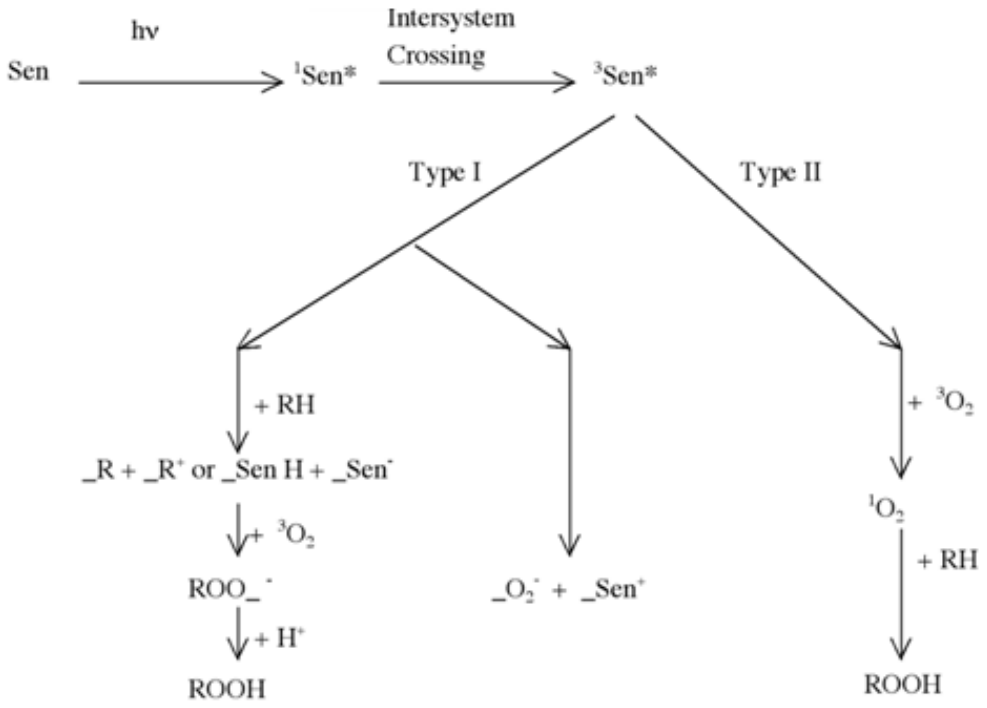

Figure 1.12 The possible reactions involving excited state sensitizer molecules.[115]

Singlet oxygen is receiving increasing interest as a reactive species in many chemical and biological systems.[126] It is one of the most active intermediates[125] because of its unusual properties arising from its open shell electronic structure, in which the outer shell electrons

References on page 41

are paired in anti-parallel spins.[115] As there are no unpaired electrons, spin restriction is removed, thus increasing the oxidizing ability of the oxygen molecule.[125]

In triplet oxygen the two most energetic electrons are distributed between the two degenerate π anti-bonding orbitals[123] with identical spins ($^3\sum$ state) giving rise to a diradical nature,[123] and as such can only react with radicals; electrophilic singlet oxygen molecular orbitals are doubly occupied and the two most energetic electrons are located in a single π anti-bonding orbital, as shown in Figure 1.13. The paired electrons have opposite spins ($^1\Delta$),[123] giving rise to the diamagnetic non-radical nature.[115] This allows singlet oxygen to react with electron rich compounds making it a very useful reactant in medicine, biochemistry, organic, food and environmental chemistry.[115]

Singlet oxygen has a multiplicity of 1 and is thus a violation of Hund's rule,[115] making the molecule extremely energetic (the ground state is 94.20 kJ above that of triplet oxygen),[123,126] and consequently, highly reactive. The non-radical, electrophilic nature allows the molecule to react with non-radical, singlet-state, electron rich compounds with double bonds, such as bio-inorganic compounds.[123] As singlet oxygen is an electrophile, it seeks electrons to fill the highest degenerate vacant molecular orbital,[115] and is known to electronically resemble the reactivity of ethylene.[118] Reactions involving singlet oxygen are much faster than that involving triplet oxygen, and this is attributed to the lower activation energy of singlet oxygen.[115]

References on page 41

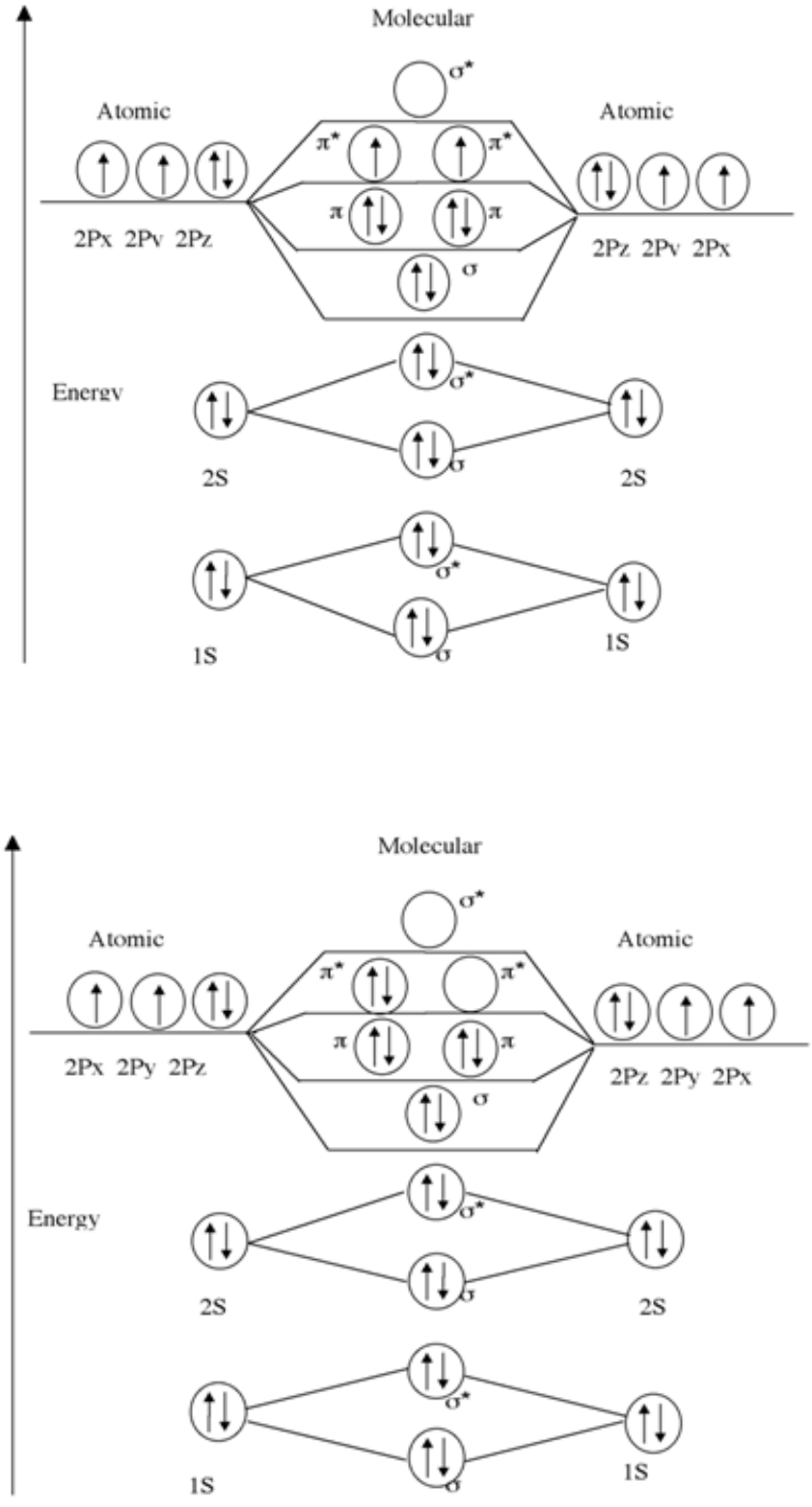

Figure 1.13 The molecular orbital diagrams of triplet oxygen (above) and singlet oxygen (below).[115]

References on page 41

1.7.2 Photosensitized Oxygenation in Vitamin B_{12}

Cobalt corrins are intensely coloured compounds[42,92] and may undergo two main types of light-induced reactions: the light induced loss of an axial ligand or the sensitization of reactions with singlet oxygen.[92] The methylene blue (MB)-sensitized photo-oxygenation reactions of corrinoid Co(III) complexes result in the cleaving of a double bond within the corrinoid macrocycle, thus providing an efficient method for the mild and specific homolytic dissociation of the corrinoid.[116,122,124,128,129]

The vitamin B_{12} derivative heptamethyl Coα,Coβ-dicyanocobyrinate[116,129] **(1)**, is one such cobalt corrin on which much photo-oxygenation research has been conducted.[122] It has been observed that MB-sensitized light-induced oxygenation reactions involving singlet oxygen cleave the corrin at the northern or southern meso positions,[116,129] namely the 5,6 or 14,15 positions, yielding a heptamethyl Coα,Coβ-dicyano-5,6-dioxo-5,6-secocobyrinate **(3a)** and heptamethyl Coα,Coβ-dicyano-14,15-dioxo-14,15-secocobyrinate **(3b)**, respectively.[116,129] Upon further oxidation, the isomers undergo a sequential breakage of bonds to form a tetraoxodisecocobester, heptamethyl Coα,Coβ-dicyano-5,6:14,15-tetraoxo-5,6:14,15-disecocobyrinate **(4)** (Figure 1.14).[128]

References on page 41

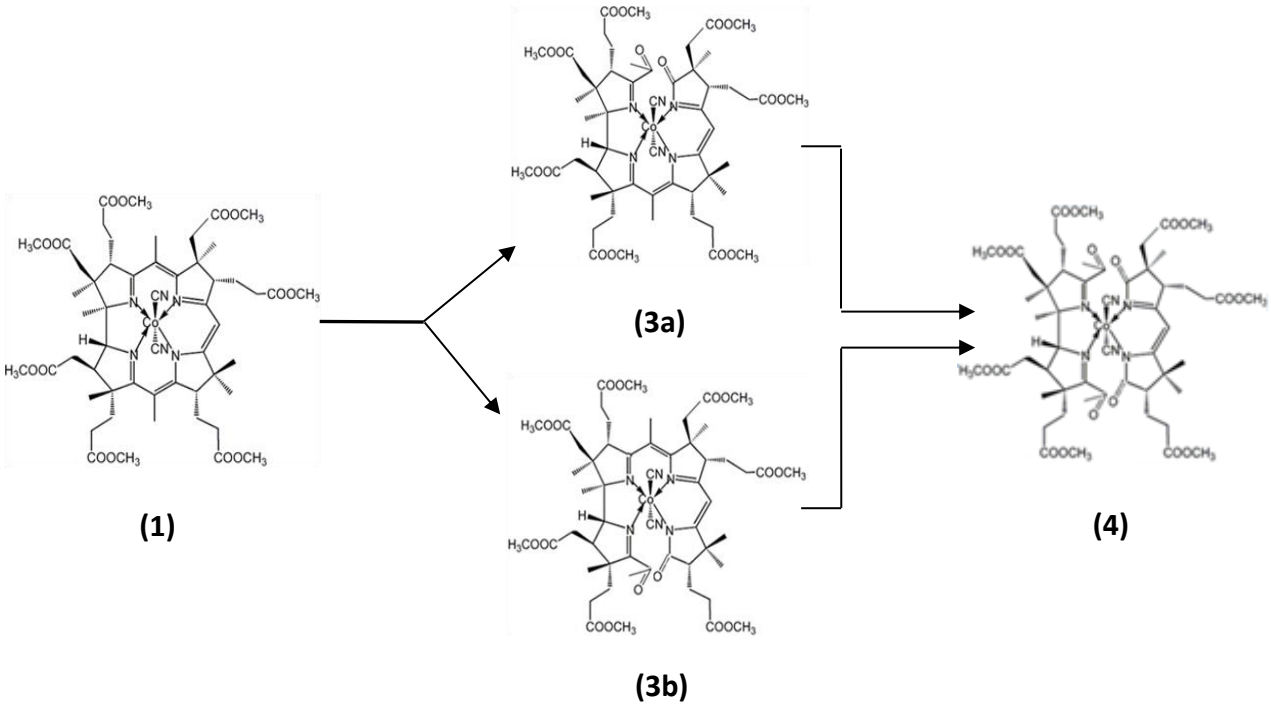

Figure 1.14 The photo-oxidation reaction of heptamethyl Coα,Coβ-dicyanocobyrinate.[128]

The photochemical reactivity of vitamin B_{12} derivatives is primarily a result of the intramolecular interactions between Co(III) and the π-system of the corrin ligand.[116] The selectivity of the attack by electrophilic singlet oxygen suggests strong local enhancement of the reactivity of the corrin macrocycle by the chromophore-bound methyl groups. The regioselectivity of the reaction at the 5,6 position[129] is associated with the minimal HOMO localisation energy for the ligand π-system of the cobester; as such, it has been calculated that the smallest decrease in the π-electronic energy of the conjugation system occurs at the C5 position upon interruption.[129] The cleavage sites are also estimated to be the sites of highest nucleophilic reactivity in the corrinoid π-system.[128]

References on page 41

1.8 Aims

The general aim of this study was to continue the ongoing research performed at the University of the Witwatersrand focusing on the origin of the labilising effect of Co(III). It is well known that the typically inert Co(III) ion is labile when coordinated to a corrin ligand[41,45,46,52-66] and it is hypothesised that kinetic lability increases with an increase in the degree of unsaturation within the *cis* π-electron system and decreasing macrocyclic cavity size.[46,66]

In several previous studies,[36,46,50,65,70,104-110] thermodynamic and kinetic investigations have suggested that modifying the electronic structure of the equatorial ligand in cobalt corrins affects axial ligand chemistry. The main objective of this study was to further examine the correlation between the electronic structure of the corrin ring and cobalt corrin chemistry by perturbing the electronic structure of Coα,Coβ-dicyano-heptamethylcob(III)yrinate, (dicyanocobester, [DCCbs]), by cleaving the corrin at the C5 (or C15) position and observing the effect this has on the chemical properties of the central Co(III) ion. This was to be achieved by photosensitized oxygenation, which would selectively cleave C=C bonds at the C5 or C15 position.

The second objective of this study was to investigate the effect lengthening of the corrin chromophore (thereby increasing the electron density beyond that typically observed in a cobalt corrin) has on the activity of the central Co(III) ion. This was to be achieved by the pyrolysis of [DCCbs], resulting in the synthesis of Coα,Coβ-dicyano-7-de-(carboxymethyl)-7-8-didehydro-cobyrinate ('pyrocobester'),[117,118] in which an additional double bond was formed between C7 and C8 accompanied by the formal elimination of a methyl acetate side chain.

Disruption of the corrin ring and subsequent opening of the macrocyclic cavity through the cleaving of the corrin at the C5 or C15 position, as in the case of $[AC\text{-}5\text{-}seco\text{-}Cbs]^+$ or $[AC\text{-}15\text{-}seco\text{-}Cbs]^+$, as well as extending the chromophore in the pyrocobester and observing the effect these modifications have on the chemical properties of the central Co(III) ion can provide further insight into the *cis*-labilising effect of the corrin ligand. Thus, once isolated, the cleaved [DC-5-seco-Cbs], [DC-15-seco-Cbs] and dicyanopyrocobester were to be converted to the corresponding aquacyano derivatives for solution chemistry investigations.

References on page 41

The acid dissociation constant (pK_a) for $[AC\text{-}5\text{-}seco\text{-}Cbs]^+$, $[AC\text{-}15\text{-}seco\text{-}Cbs]^+$, $[ACCbs]^+$ and aquacyanopyrocobester were to be determined as a function of temperature so as to allow for corrections for the aqua ⇌ hydroxo equilibrium at the pH at which the ligand substitution reactions were to be performed. It would be interesting to investigate the equilibrium constants for complexes formed with a variety of ligands and compare these results with those available for $[ACCbs]^+$ (re-measured in this study) and $[ACSYCbs]^+$, to observe whether modifying the electronic structure and cavity size of the corrin had any effect on the stability of the secocobester-ligand complexes. The equilibrium constants were to be determined for the substitution of axially coordinated water by the anions: sulfite, cyanide, nitrite, azide and thiosulfate. As an aside, the binding of neutral *N*-donor ligands N-methylimidazole, ethanolamine and 4-methylpyridine were briefly studied.

The kinetics of the rate of reaction of cyanide with $[AC\text{-}5\text{-}seco\text{-}Cbs]^+$, $[AC\text{-}15\text{-}seco\text{-}Cbs]^+$ and aquacyanopyrocobester were to be investigated to elucidate the kinetic behaviour of the cleaved corrin ring in solution. Results would be compared to rate constants obtained for $[ACCbs]^+$ and $[ACSYCbs]^+$ to determine the *cis*-effect the corrin ligand has on cobalt lability, as well as to vitamin B_{12a} (aquacobalamin) which has a dimethylbenzimidazole base in the α ligand site instead of a cyanide ligand, to observe what *trans*-effect the α ligand has on cobalt lability.

Techniques utilised in the determination of the effect of perturbing the corrin ring on Co(III) lability and structure characterisation include UV-vis spectroscopy (the principal technique to monitor the conversion of [DCCbs] to [DC-5-seco-Cbs], [DC-15-seco-Cbs] and dicyanopyrocobester, and of [DCCbs], [DC-5-seco-Cbs], [DC-15-seco-Cbs] and dicyanopyrocobester to their aquacyano derivatives, $[ACCbs]^+$, $[AC\text{-}5\text{-}seco\text{-}Cbs]^+$, $[AC\text{-}15\text{-}seco\text{-}Cbs]^+$ and aquacyanopyrocobester); ^1H NMR, ^{13}C NMR, IR and mass spectrometry (to verify the structure of the target molecule); HPLC (to verify the purity of the preparations); and where possible, single-crystal X-ray diffraction presuming that we are able to produce diffraction-quality crystals of the target molecule.

In this report, the experimental work is separated into the synthesis and characterisation of [DCCbs], [DC-5-seco-Cbs], [DC-15-seco-Cbs] and dicyanopyrocobester, and the aquacyano derivatives; $[ACCbs]^+$ and $[AC\text{-}5\text{-}seco\text{-}Cbs]^+$, the determination of the acid dissociation

References on page 41

constants, the determination of the equilibrium constants and an investigation into the kinetics of [AC-5-seco-Cbs]$^{+}$. Difficulties encountered with working with the pyrocobester are also described. Each of the subsequent chapters is divided into an introductory section in which a brief summary of the relevant literature and specific aims of the work are presented; a discussion into the results obtained; and a concluding statement in which the main findings and conclusion are outlined. The final chapter, Chapter 7, contains a summary of the general conclusions reached in the abovementioned investigations, together with concluding remarks on the contribution of this study to the ongoing investigation of the *cis*-labilising effect on cobalt corrins.

References on page 41

REFERENCES FOR CHAPTER 1

1. Okuda, K. *J. Gastroenterol. Hepatol.* **1999**, 14, 301-308.
2. Randaccio, L.; Geremia, S.; Demitri, N.; Wuerges, J. *Molecules* **2010**, 15, 3228-3259.
3. Minot, G. R.; Murphy, W. P. *J. Am. Med. Assoc*. **1926**, 87, 470-476.
4. Smith, E. L.; Fantes, K. H.; Ball, S.; Waller, J. G.; Emery, W. B.; Anslow, W. K.; Walker, A. D. *Biochem. J.* **1952**, 52, 389-395.
5. Rickes, E. L.; Brink, N. G.; Koniuszy, F. R.; Wood, T. R.; Folkers, K. *Science* **1948**, 107, 396-397.
6. Smith, E. L. *Nature* **1948**, 162, 144-145.
7. Smith, E. L.; Parker, L. F. J. *Biochem. J.* **1948**, 43, viii.
8. Hodgkin, D. C.; Pickworth, J.; Robertson, J. H.; Trueblood, K. N.; Prosen, R. J. *Nature* **1955**, 176, 325-328.
9. Hodgkin, D. C.; Porter, M. W.; Spiller, R. C. *Proc. Roy. Soc. B* **1950**, 136, 609-613.
10. Brink, C.; Hodgkin, D. C.; Lindsey, J.; Pickworth, J.; Robertson, J. H.; White, J. G. *Nature* **1954**, 174, 1169-1171.
11. Hodgkin, D. C. *Proc. Roy. Soc. A* **1965**, 228, 294-305.
12. Hodgkin, D. C.; Kamper, J.; Lindsey, J.; McKay, M.; Pickworth, J.; Robertson, J. H.; Shoemaker, C. B.; White, J. G.; Prosen, R. J.; Trueblood, K. N. *Proc. Roy. Soc. A* **1957**, 242, 228-263.
13. Hodgkin, D. C.; Pickworth, J.; Robertson, J. H.; Prosen, R. J.; Sparks, R. A.; Trueblood, K. N. *Proc. Roy. Soc. A* **1959**, 251, 306-352.
14. Sannasy, D. MSc Dissertation, University of the Witwatersrand, Johannesburg, 2006.
15. Gruber, K.; Puffer, B.; Kräutler, B. *Chem. Soc. Rev.* **2011**, 40, 4346-4363.
16. Fang, H.; Kang, J.; Zhang, D. *Microb. Cell. Fact.* **2017**, 16 (15), 1-14.
17. Woodward, R. B. *Pure Appl. Chem.* **1973**, 33, 145-177.
18. Eschenmoser, A. *Pure Appl. Chem.* **1963**, 7, 297-316.
19. Eschenmoser, A.; Scheffold, R.; Bertele, E.; Pesaro, M.; Gschwend, H. *Proc. Roy. Soc. A* **1965**, 288, 306-323.
20. Voet, D.; Voet, J. G. In *Biochemistry*, Third (Wiley International Edition) edn., John Wiley & Sons, Inc., 2004.
21. Giedyk, M.; Goliszewska, K.; Gryko, D. *Chem. Soc. Rev.* **2015**, 44, 3391-3404.

22. Karczewski, M.; Ociepa, M.; Pluta, K.; Proinsias, K.; Gryko, D. *Chem. Eur. J.* **2017**, 23, 7024-7030.
23. Pettenuzzo, A.; Pigot, R.; Ronconi, L. *Eur. J. Inorg. Chem.* **2017**, 1625-1638.
24. Hamza, M. S. A. *J. Inorg. Biochem.* **1998**, 69, 269-274.
25. Randaccio, L.; Geremia, S.; Nardin, G.; Slouf, M.; Srnova, I. *Inorg. Chem.* **1999**, 38, 4087-4092.
26. Randaccio, L.; Furlan, M.; Geremia, S.; Slouf, M.; Srnova, I.; Toffoli, D. *Inorg. Chem.* **2000**, 39, 3403-3413.
27. Randaccio, L.; Geremia, S.; Stener, M.; Toffoli, D.; Zangrando, E. *Eur. J. Inorg. Chem.* **2002**, 93-103.
28. Kung, Y.; Ando, N.; Doukov, T. I.; Blasiak, L. C.; Bender, G.; Seravalli, J.; Ragsdale, S. W.; Drennan, C. L. *Nature* **2012**, 1-5.
29. Medek, A.; Frydman, V.; Frydman, L. *Proc. Natl. Acad. Sci. USA* **1997**, 94, 14237-14242.
30. Shriver, D. F.; Atkins, P. W.; Overton, T. L.; Rourke, J. P.; Weller, M. T.; Armstrong, F. A. In *Inorganic Chemistry,* Fourth edn., W. H. Freedman and Company, New York, 2006.
31. Moll, R.; Davis, B. *Clinical Sciences **2017**, 45(4), 198-203.*
32. Perry, C. B. Ph.D. Thesis, University of the Witwatersrand, Johannesburg, 2004.
33. Green, R.; Allen, L. H.; Bjørke-Monsen, A. B.; Brito, A.; Guéant, J.; Miller, J. W.; Mollay, A. M.; Nexø, E.; Stabler, S.; Toh, B.; Ueland, P. M.; Yajnik, C. *Nat. Rev. Dis. Primers* **2017**, 3, 17040.
34. Lenhert, P. G.; Hodgkin, D. C. *Nature* **1961**, 192, 937-938.
35. Rossi, M.; Glusker, J. P.; Randaccio, L.; Summers, M. F.; Toscano, P. J.; Marzilli, L. G. *J. Am. Chem. Soc.* **1985**, 107, 1729-1738.
36. Knapton, L. Ph.D. Thesis, University of the Witwatersrand, Johannesburg, 2005.
37. Pratt, J. M. In B_{12}; Volumes 1-2, Dolphin, D., Ed; Wiley, New York, 1982.
38. Andruniow, T.; Kozlowski, P. M.; Zgierski, M. Z. *J. Chem. Phys.* **2001**, 115, 7522-7533.
39. Marques, H. M. Ph.D Thesis, University of the Witwatersrand, Johannesburg, 1986.
40. Chemaly, S. M. Ph.D Thesis, University of the Witwatersrand, Johannesburg, 1980.
41. Marques, H. M.; Egan, T. J.; Marsh, J. H.; Mellor, J. R.; Munro, O. Q. *Inorg. Chim. Acta.* **1989**, 166, 249-255.

42. Proinsias, K.; Giedyk, M.; Gryko, D. *Chem. Soc. Rev.* **2013**, 42, 6605-6619.
43. Dereven'kov, I. A.; Salnikov, D. S.; Silaghi-Dumitrescu, R.; Makarov, S. V.; Kaifman, O. I. *Coord. Chem. Rev.* **2016**, 309, 68-83.
44. Bridwell-Rabb, J.; Drennan, C. L. *Current Opinion on Chemical Biology* **2017**, 37, 63-70.
45. Brown, K. L.; Cheng, S.; Zou, X.; Zubkowski, J. D.; Valente, E. J.; Knapton, L.; Marques, H. M. *Inorg. Chem*. **1997**, 36, 3666-3675.
46. Chemaly, S. M.; Brown, K. L.; Fernandes, M. A.; Munro, O. Q.; Grimmer, C.; Marques, H. M. *Inorg. Chem.* **2011**, 50, 8700-8718.
47. Geno, M. K.; Halpern, J. *J. Am. Chem. Soc.* **1987**, 109, 1238-1240.
48. Halpern, J. *Science* **1985**, 227, 869-875.
49. Gütlich, P.; Goodwin, H. A. *Top. Curr. Chem.* **2004**, 233, 1-47.
50. Chemaly, S. M.; Florczak, M.; Dirr, H.; Marques, H. M. *Inorg. Chem.* **2011**, 50, 8719-8727.
51. Perry, C. B.; Fernandes, M. A.; Brown, K. L; Valente, E. J.; Marques, H. M. *Eur. J. Inorg. Chem.* **2003**, 136, 2095-2107.
52. Randall, W. C.; Alberty, R. A. *Biochemistry* **1967**, 6, 1520-1525.
53. Reenstra, W. W.; Jencks, W. P. *J. Am. Chem. Soc*. **1979**, 101, 5780-5791.
54. Balt, S.; van Herk, A. M. *Transition Met. Chem*. **1983**, 8, 152-154.
55. Baldwin, D. A.; Betterton, E. A.; Pratt, J. M. *J. Chem. Soc., Dalton Trans.* **1983**, 2217-2222.
56. Marques, H. M.; Brown, K. L.; Jacobsen, D. W. *J. Biol. Chem*. **1988**, 263, 12378-12383.
57. Stochel, G.; van Eldik, R.; Kunkely, H.; Vogler, A. *Inorg. Chem*. **1989**, 28, 4314-4318.
58. Stochel, G.; van Eldik, R. *Inorg. Chem.* **1990**, 29, 2075-2077.
59. Marques, H. M. *J. Chem. Soc., Dalton Trans.* **1991**, 1437-1442.
60. Marques, H. M.; Bradley, J. C.; Campbell, L. A. *J. Chem. Soc., Dalton Trans*. **1992**, 2019-2027.
61. Waddington, M. D.; Finke, R. G. *J. Am. Chem. Soc*. **1993**, 115, 4629-4640.
62. Marques, H. M.; Knapton, L. *J. Chem. Soc., Dalton Trans.* **1997**, 3827-3833.
63. Hamza, M. S. A.; Zou, X.; Brown, K. L.; van Eldik, R. *Inorg. Chem*. **2001**, 40, 5440-5447.

64. Hamza, M. S. A.; Elawady, M. A.; Marques, H. M. *S. Afr. J. Chem*. **2008**, 61, 68-73.

65. Chemaly, S. M.; Kendall, L.; Nowakowska, M.; Pon, D.; Perry, C. B.; Marques, H. M. *Inorg. Chem*. **2013**, 52, 1077-1083.

66. Perry, C. B.; Marques, H. M. *S. Afr. J. Chem.* **2005**, 58, 9-15.

67. Brink-Shoemaker, C.; Cruickshank, D. W. J.; Hodgkin, D. C.; Kamper, J.; Pilling, D. *Proc. Roy. Soc. A* **1964**, 278, 1-26.

68. Gruber, K.; Jogl, G.; Klintschar, G.; Kratky, C. In *Vitamin B_{12} and B_{12}-Proteins*; Kräutler, B.; Arigoni, D.; Golding, B. J. Eds.; Wiley-VCH, Weinheim, 1998, pp 335-347.

69. Randaccio, L.; Furlan, M.; Geremia, S.; Slouf, M. *Inorg. Chem.* **1998**, 37, 5390-5393.

70. Pratt, J. M. In *The Inorganic Chemistry of Vitamin B_{12}*; Academic Press, London, 1972.

71. Hague, D. N.; Halpern, H. *Inorg. Chem*. **1967**, 6, 2059-2063.

72. Randall, W. C.; Alberty, R. A.; *Biochemistry* **1966**, 5, 3189-3193.

73. Fleischer, E. B.; Jacobs, S.; Mestichelli, L. *J. Am. Chem. S*oc. **1968**, 90, 2527-2531.

74. Kernohan, J. A.; Endicott, J. F. *Inorg. Chem*. **1970**, 9, 1504-1512.

75. Pratt, J. M. In *Chemistry and Biochemistry of B_{12}*; Banerjee, R. Eds.; John Wiley & Sons, Inc., New York, 1999.

76. Pratt, J. M.; Thorp, R. G. *Adv. Inorg. Chem. Radiochem*. **1969**, 12, 375-427.

77. Pratt, J. M.; Thorp, R. G. *J. Chem. Soc*. *A* **1966**, 187-191.

78. Firth, R. A.; Hill, H. A. O.; Pratt, J. M.; Thorp, R. G.; Williams, R. J. P. *J. Chem. Soc. A* **1968**, 2428-2433.

79. Hayward, G. C.; Hill, H. A. O.; Pratt, J. M.; Vanston, N. J.; Williams, R. J. P. *J. Chem. Soc. A*, **1965**, 6485-6493.

80. Marques, H. M.; Bradley, J. C.; Brown, K. L.; Brooks, H. *J. Chem. Soc., Dalton Trans.* **1993**, 3475-3478.

81. Pasternack, R. F.; Gillies, B. S.; Stromsted, J. P. *Bioinorg. Chem.* **1978**, 8, 33-44.

82. Betterton, E. A. Ph.D. Thesis, University of the Witwatersrand, Johannesburg, 1982.

83. Ashley, K. R.; Berggren, M.; Cheng, M. *J. Am. Chem. Soc.* **1975**, 97, 1422-1426.

84. Hague, D. N.; Halpern, J. *Inorg. Chem.* **1967**, 6, 2059-2063.

85. Jackson, W. G.; Jurisson, S. S.; McGregor, B. C. *Inorg. Chem.* **1985**, 24, 1788-1790.

86. Poon, C. K.; *Coord. Chem. Rev.* **1973**, 10, 1-35.

87. Hill, H. A. O.; Mann, B. E.; Pratt, J. M.; Williams, R. J. P. J. *Chem. Soc. A* **1968**, 564-567.
88. Gardu, G.; Geremia, S.; Marzili, L. G.; Nardin, G.; Randaccio, L.; Tauzher, G. *Acta. Cryst*. **2003**, B59, 51.
89. Finke, R. G.; Hay, B. P. *Inorg. Chem*. **1984**, 23, 3041-3043.
90. Perry, C. B.; Fernandes, M. A.; Marques, H. M. *Acta. Cryst*. **2004**, C60, 165-167.
91. Chemaly, S. M.; Marques, H. M.; Perry, C. B. *Acta. Cryst*. **2004,** C60, 88-90.
92. Kräutler, B. *Coord. Chem. Rev.* **1991**, 111, 215-220.
93. Giannotti, C. In B_{12}; Dolphin, D., Ed., Wiley, New York, 1982, pp 393-430.
94. Stich, T. A.; Brooks, A. J.; Buan, N. R.; Brunold, T. C. *J. Am. Chem. Soc*. **2003**, 125, 5897-5914.
95. Salama, S.; Spiro, T. G. *J. Raman Spectrosc*. **1997**, 6, 57-60.
96. Day, P. *Theor. Chim. Acta.* **1967**, 7, 328-341.
97. Day, P. *Coord. Chem. Rev*. **1967**, 2, 99-108.
98. Kuhn, H.; Drexhage, K. H.; Martin, H. *Proc. Roy. Soc. A* **1965**, 288, 348-351.
99. Firth, R. A.; Hill, H. A. O.; Pratt, J. M.; Thorp, R. G.; Williams, R. J. P. *J. Chem. Soc. A* **1969**, 381-386.
100. Marques, H. M.; Knapton, L.; Zou, X.; Brown, K. L. *J. Chem. Soc., Dalton Trans*. **2002**, 3195-3200.
101. Grüning, B.; Holze, G.; Jenny, T. A.; Nesvadba, P.; Gossauer, A.; Ernst, L.; Sheldrick, W. S. *Helv. Chim. Acta.* **1985**, 68, 1754-1770.
102. Gossauer, A.; Grüning, B.; Ernst, L.; Becker, W.; Sheldrick, W. S. *Angew. Chem. Int. Ed.* **1977**, 16, 481-482.
103. Ehrenson, S.; Brownlee, R. T. C.; Taft, R. W. *Prog. Phys. Org. Chem*. **1973**, 10, 1-80.
104. Ghadimi, N.; Perry, C. B.; Govender, P. P.; Marques, H. M. *Inorg. Chim. Acta.* **2016**, 450, 269-278.
105. Ghadimi, N. Ph.D Thesis, University of the Witwatersrand, Johannesburg, 2016.
106. Mathura, S.; Sanassy, D.; de Sousa, A. S.; Perry, C. B.; Navizet, I.; Marques, H. M. *J. Inorg. Biochem*. **2013**, 123, 66-79.
107. Mathura, S. Ph.D Thesis, University of the Witwatersrand, Johannesburg, 2014.
108. Zipp, C. F.; Michael, J. P.; Fernandes, M. A.; Nowakowska, M.; Dirr, H. W.; Marques, H. M. *Inorg. Chem. Comm*. **2015**, 57, 15-17.

109. Zipp, C. F.; Michael, J. P.; Fernandes, M. A.; Mathura, S.; Perry, C. B.; Navizet, I.; Govender, P. P.; Marques, H. M. *Inorg. Chem*. **53**, 4418-4429.
110. Zipp, C. F. Ph.D Thesis, University of the Witwatersrand, Johannesburg, 2014.
111. Gross, Z. *J. Biol. Inorg. Chem*. **2001**, 6, 733-738.
112. Gryko, D. T. *Eur. J. Org. Chem*. **2002**, 1735-1743.
113. Aviv-Hard, I.; Gross, Z. *Chem. Eur. J.* **2009**, 15, 8382-8394.
114. Markwell, A. J.; Pratt, J. M.; Shaikjee, M. S.; Toerien, J. G. *J. Chem. Soc., Dalton Trans.* **1987**, 1349-1357.
115. Min, D. B.; Boff, J. M. *Comp. Rev. Food Sci. Food Safety* **2002**, 1, 58-72.
116. Kräutler, B. *Helv. Chim. Acta.* **1982**, 65, 1941-1948.
117. Ernst, L.; Holze, G.; Inhoffen, H. H. *Liebigs Ann. Chem*. **1981**, 198-201.
118. Kräutler, B.; Stepanek, R.; Holze, G. *Helv. Chim. Acta.* **1983**, 66, 44-49.
119. Cundall, R. B.; Gilbert, A. In *Photochemistry: Studies in Modern Chemistry,* Thomas Nelson & Sons Ltd, London, 1970.
120. Balzani, V.; Carassiti, V. In *Photochemistry of Coordination Compounds*; Academic Press, London, 1970.
121. Okabe, H. In *Photochemistry of small molecules;* John Wiley & Sons, Inc., New York, 1978.
122. Oliveros, E.; Besancon, F.; Boneva, M.; Kräutler, B.; Braun, A. M. *J. Photochem. Photobiol. B: Biol.* **1995**, 29, 37-44.
123. Bland, J. *J. Chem. Educ.* **1976**, 53, 274-279.
124. Kräutler, B.; Stepanek, R. *Photochem. & Photobiol*. **1991**, 54, 585-592.
125. http://www.healthcare.uiowa.edu/corefacilities/esr/education/.../1/zhao-paper1.pdf (accessed 26 December 2017).
126. Miyamoto, S.; Ronsein, G. E.; Prado, F. M.; Vemi, M.; Correa, T. C.; Toma, I. N.; Bertolucci, A.; Oliveira, M. C. B.; Motta, F. F.; Medeiros, M. H. G.; Di Mascio, P. *Life* **2007**, 59, 322-331.
127. Schweitzer, C.; Schmidt, R. *Chem. Rev.* **2003**, 103, 1685-1757.
128. Kräutler, B.; Stepanek, R. *Helv. Chim. Acta.* **1985**, 68, 1079-1088
129. Kräutler, B.; Stepanek, R.; Holze, G. *Helv. Chim. Acta.* **1983**, 66, 44-49.

CHAPTER 2

GENERAL MATERIALS, METHODS AND INSTRUMENTATION

2.1 General Materials

Reagents and solvents used in this work are reported in **Appendix A.1**. All reagents and solvents were commercially available and used without further purification. De-ionised water, produced by a Millipore DirectQ UV3 system and further purified using a Millipore MilliQ unit (18 MΩ.cm), was used throughout this work.

2.2 General Laboratory Techniques and Instrumentation

All laboratory equipment and relevant software used in this work are reported in **Appendix A.2**.

2.2.1 Evaporation *in vacuo*

Solvents were evaporated under reduced pressure using a Buchi R-100 rotavapor in conjunction with a Buchi B-100 heating bath set at 40.0 ^{o}C.

2.2.2 pH Measurements

pH measurements were performed using either a Metrohm 780 pH meter with a Metrohm LL UnitrodePt 1000 glass electrode or an Ohaus Starter 3100 pH metre with an Ohaus ST310 electrode. Metrohm Ion analysis standard buffer solutions (pH 4.0, 7.0 and 9.0) were used to calibrate the electrode using a 3 buffer calibration an hour prior to use, at a temperature specific to the experiment being performed using a water-circulating bath. Care was taken to ensure thermal equilibrium was reached.

References on page 64

2.2.3 Buffers

The buffers used throughout the study are tabulated in Table 2.1. In cases where the pH of buffers needed to be adjusted, NaOH and H_2SO_4 were used to increase and decrease the pH, respectively. A multi-component buffer required for pK_a studies was made up to an overall ionic strength of 0.1 M. Determination of the multi-component buffer quantities can be found in **Appendix B.1**.

Table 2.1 Summary of buffers used in this study.

Buffers	μ /M	pK_a (25.0 °C)	pH range[1]
CAPS	0.1	10.40	9.7 – 11.1
CHES	0.1	9.50	8.6 – 10.0
MES	0.1	6.10	5.5 – 6.7
MOPS	0.1	7.14	6.5 – 7.9
Tris/HCl	0.1	8.06	7.0 – 9.0
Multi-component buffer (CHES, MES, MOPS, Tris/HCl, Potassium hydrogen phthalate, Sodium sulfate)*	0.1	–	4.0 – 10.0

*Sodium sulfate was used to adjust the ionic strength; it itself has little buffer capacity above pH 2.

2.2.3.1 Ammonium Phosphate Buffer

A phosphate buffer (0.025 M, pH 3.0) required for HPLC analysis, was prepared by dissolving concentrated phosphoric acid (1.67 ml) in de-ionised water (1.0 L). The pH was adjusted with ammonia.

References on page 64

2.2.4 Thin Layer Chromatography (TLC)

Thin layer chromatography is an analytical chromatographic technique used to separate the components of a reaction mixture on a thin stationary phase (TLC plates) to monitor the progress of a reaction.[2] TLC plates are comprised of a thin layer of silica gel or alumina coated onto a glass or aluminium foil plate.[3] Small drops of sample were applied to a pencil line drawn horizontally 10.0 mm from the bottom edge of the plate and once the sample solvent had evaporated, the plates were placed in a closed container saturated with the vapours of the developing solvent found at the bottom of the container.[4] The chromatogram develops by the capillary movement of solvent up the plate and separation of compound bands is based on the affinity of the compounds for the mobile phase relative to the polar stationary phase.[5] Once the solvent front reached a line drawn 10.0 mm from the top of the plate, the plate was removed from the container and the solvent was allowed to evaporate.[2] Corrins are intensely coloured,[6,7] hence the resulting spots were easy to detect visually; however, the plates were still exposed to UV light ("black light") to detect any UV-only absorbing bands. Compounds can be differentiated by determining the retention factor (R_f) which is unique to each compound. All R_f data can be found in **Appendix C**.

2.2.5 Column Chromatography

Column chromatography is a purification technique for the separation of individual constituents from a mixture of compounds. The compounds to be separated were dissolved in a minimum amount of solvent (mobile phase) which carried the compounds through a stationary phase comprised of either silica or alumina particles packed in a column, as it percolated through the particles. Individual components were retained by the stationary phase differently as each component contains varying functionalities. The compounds will therefore have distinctly different affinities for the stationary phase, resulting in varying retention times. On this account, individual components will separate while eluting at different rates based on the partitioning between the stationary and mobile phase as each compound has a different partition coefficient between the mobile and stationary phase.[5]

References on page 64

Flash column chromatography, although relying on the same principles as the more frequently-used gravity column chromatography, differs in the sense that the elution solvent is driven through a column containing finer silica particles (40 – 63 μm as opposed to normal 63 – 200 μm) by applying external pressure at an inlet as opposed to allowing the solvents to percolate through by gravity.[4] This increases the speed at which the solvent flows through the finer particles with a larger surface area, therefore decreasing the time required to elute compounds as well as affording increased separation.

The compounds eluted in ascending order of polarity as the most polar compounds were adsorbed more strongly to the polar silica particles. The compounds were collected in a series of fractions and analysed by UV-vis spectroscopy using a CARY 300 BIO UV-vis spectrophotometer to determine the identity of the compounds, as well as HPLC to assess the purity of the compounds.

2.2.6 Preparative Thin Layer Chromatography (PTLC)

Preparative thin layer chromatography is an analytical purification tool for the separation of large quantities of material. The compounds to be separated were applied as long, narrow, concentrated bands to a 200 × 200 mm, 2000 micron thick silica plate. The plate was developed in a glass tank (29.0 × 9.5 × 27.0 cm) saturated with a polar mobile phase which drew the compounds up the silica plate via capillary action. An increase in separation was afforded by repeating the development stage multiple times, drying the plate in between repetitions. The various analytes which constitute the compounds ascend at different rates as their affinity for the mobile phase varies, thus enabling separation.[8] The desired products were recovered by scraping the adsorbent layer off the plate with a scalpel, and eluted with the least polar solvent possible to extract adsorbed analytes from the silica particles; [8] this was followed by filtration through a cotton wool plug to remove any remaining silica particles. Purity was assessed by HPLC and UV-vis spectroscopy.

References on page 64

2.3 Physical Techniques of Characterisation

2.3.1 UV-vis Spectrophotometry

Different spectrophotometers were used for different studies throughout the project. The UV-vis spectra for pK_a, ligand binding and [AC-5-seco-Cbs]$^+$ kinetic studies were recorded on Cary 300 BIO UV-vis spectrophotometers fitted with water-circulating baths to maintain the temperature of the system at a temperature applicable to that experiment. The spectrophotometers were fitted with multi-cell cuvette holders for 1 cm pathlength quartz cuvettes. Matched standard quartz cuvettes with Teflon stoppers were used for ligand binding and kinetic studies. A 1 cm pathlength quartz flow cell together with a standard quartz cuvette reference cell were used for pK_a studies. To ensure optimum performance, the instruments were allowed to warm up for 30 minutes prior to usage. Spectra were collected using the Scan application within the Cary WinUV software suite.[9] The instrument parameters are outlined in Table 2.2 below.

Samples were run against a reference background relevant to the experiment (i.e. the buffer or solvent system used). The resultant spectra were exported as comma-delimited text files (*.csv) so that they could be opened in a Microsoft Excel spreadsheet for further analysis using SigmaPlot.[10]

Table 2.2 Instrument settings for recording UV-vis spectra on Cary spectrophotometers.

Parameters	Settings
Range	300 – 750 nm
Signal averaging time	0.5 s
Data interval	1.0 nm
Scan rate	120.0 nm min^{-1}
Spectral band width	2.0 nm
Double beam mode	Source changeover at 350 nm

References on page 64

For $[H_2OCbl]^+$ kinetic studies, UV-vis spectra were recorded on an Agilent diode array spectrometer using a single 1.0 cm quartz cuvette. The temperature was maintained at a temperature applicable to that experiment using a thermostatted cell-holder attached to an Agilent Peltier temperature controller unit. To ensure optimum performance, the instrument was allowed to warm up for 30 minutes prior to usage. Samples were run using the kinetics mode in the UV-visible ChemStation onboard the Agilent software suite.[11] The instrument parameters are outlined in Table 2.3.

The monitoring wavelength and run times were experiment-specific and these were set up as required. The spectrum of a blank sample containing only the buffer solution used in the experiment was first recorded, followed by the sample to be run. In each case, the samples were allowed to reach thermal equilibrium (ca. 15 minutes) prior to time based measurements. The resultant spectra were exported as *.csv files so that they could be opened in a Microsoft Excel spreadsheet for further analysis using SigmaPlot.[10]

Table 2.3 Instrument settings for recording UV-vis spectra on the Agilent photodiode array spectrometer.

Parameters	Settings
Range	300 – 750 nm
Signal averaging time	1.0 s
Data interval	1.0 nm
Cycle time	1.0 s
Light source	Tungsten and deuterium lamps

2.3.2 High Performance Liquid Chromatography (HPLC)

HPLC analyses were performed to assess the purity of products using a reverse phase C18 column (Supelco Analytical 5µm, 250.0 × 4.6 mm) coupled with a Supelco guard column using a Dionex UltiMate 3000 pump and an UltiMate 3000 Photodiode Array Detector with

References on page 64

Chromeleon Chromatographic Management System software.[12] All solutions were freshly prepared and filtered (0.47 µm) under vacuum prior to use. All solvents were HPLC grade.

The HPLC column was first flushed with de-ionised water for 10 minutes followed by an acetonitrile/water (1:1) solution or phosphate buffer/methanol (98:2) solution[13] (Table 2.4) for a further 10 minutes. A Hamilton syringe was used to inject 20.0 µl aliquots of sample onto the silica column using a Rheodyne valve and the sample was separated using either an isocratic elution (acetonitrile:water, 1:1) at a flow rate of 1 ml min^{-1} or multi-step gradient elution program (Table 2.4) as required. Blanks (de-ionised water) were run between samples. Once an analysis was complete, the column was flushed with either acetonitrile/water or phosphate buffer/methanol as before, followed by water.

Table 2.4 Multi-step gradient HPLC elution program.

Time /min	**% 0.025M Ammonium phosphate buffer**	**% Methanol**	**Flow rate /ml min^{-1}**
0.0	98.0	2.0	1
0.2	98.0	2.0	1
3.0	35.0	65.0	1
8.0	35.0	65.0	1
13.0	98.0	2.0	1
15.0	98.0	2.0	1

2.3.3 Electrospray Ionisation (ESI) Mass Spectrometry

High resolution mass spectra were recorded on a Bruker Compact Q-TOF high resolution mass spectrometer equipped with Bruker otofControl software[14] and processed using the Bruker Compass DataAnalysis software suite.[15] Dicyano samples were prepared in

References on page 64

acetonitrile whereas aquacyano samples were prepared in methanol and exposed to an ESI source in the positive mode. Data are reported as mass to charge ratios (m/z).

Mass spectrometry data were collected and analysed by the author. Selected mass spectra can be found in **Appendix D**.

2.3.4 Fourier-Transform Infra-Red Spectroscopy (FTIR)

Solid state infra-red spectra were recorded on a Bruker Alpha FTIR Spectrometer fitted with a Platinum ATR diamond accessory. Spectra acquisition was facilitated by OPUS software.[16] The instrument parameters are outlined in Table 2.5 below. Selected FTIR spectra can be found in **Appendix E**.

Table 2.5 Instrument settings for FTIR Spectra.

Parameters	Settings
Range	4000 – 375 cm^{-1}
Resolution	2 cm^{-1}
Sample scan time	32 scans
Background scan time	32 scans

2.3.5 Nuclear Magnetic Resonance Spectroscopy (NMR)

One-dimensional ^{1}H, ^{13}C and DEPT135, two-dimensional proton homonuclear (COSY, TOCSY, and ROESY) and two-dimensional heteronuclear (^{1}H-^{13}C) (HSQC, HMBC) measurements were recorded on a Bruker Avance 500 III Ultra Shield Plus spectrometer operating at 500.133 MHz (^{1}H) and 125.770 (^{13}C) equipped with a 5.0 mm PABBO broadband probe. All NMR data were collected at 25.0 ^{o}C using 5.0 mm NMR tubes on 20.0 mg samples dissolved in 600.0 µl CD_3OD (99.8% deuteration). Chemical shifts on the δ scale (parts per million

References on page 64

(ppm)) are reported relative to the signal obtained from deuterated methanol taken at δ 49.00 ppm for ^{13}C NMR or at δ 3.31 ppm for ^{1}H NMR.

NMR spectra were collected by Dr Richard Mampa and Dr Myron Johnson at the University of the Witwatersrand, and processed by the author using the MestReNova software suite.[17] Selected NMR spectra can be found in **Appendix F**.

2.3.6 DFT Calculations

Density functional theory (DFT) calculations were performed using the BP86 functional[18,19] with a 6-311G(d,p) basis set applied to all atoms as implemented in the Gaussian 09[20] suite of programs. An empirical correction was incorporated to this functional to account for the D3 version of Grimme's dispersion with the original D3 damping function.[21] [DCCbs] was modelled starting from its crystal structure[22] but all corrin side chains were truncated to ethyl groups. The starting point for the model of [DC-5-seco-Cbs] was the energy-minimized structure of [DCCbs], which was edited to incorporate the oxidation at C5 and C6, and the cleavage of the C5–C6 bond. This was then initially energy-minimized using a 3-21G basis set before changing the basis set to 6-311G(d,p). All geometry optimizations were followed by a frequency calculation to ensure that the structures were completely minimized to a stable ground state. The topological properties of the electron density of the modelled structures were explored by generating wavefunction files with Gaussian 09 and analysed using Bader's Quantum Theory of Atoms in Molecules (QTAIM)[23,24] as implemented in AIMAll.[25]

2.4 Investigating the Solution Chemistry of Modified Cobalt Corrins

2.4.1 Data Analysis

All results were analysed with the computer program SigmaPlot,[10] which employs Marquardt's algorithm[26] and a Newton-Raphson procedure.

References on page 64

2.4.2 Spectroscopic pK_a Investigations as a function of pH

The titration procedure for the determination of the spectroscopic pK_a of [AC-5-seco-Cbs]$^+$ (and [ACCbs]$^+$ for comparative purposes) was adapted from a method previously published by Munro[27] and Sanassy.[28] The relevant compound was dissolved in methanol (100.0 µl) and diffused into an aqueous multi-component buffer (35.0 ml) consisting of 0.001 M solutions of non-coordinating buffers MES, MOPS, Tris/HCl, CHES and potassium hydrogen phthalate, coupled with a 0.10 M solution of Na_2SO_4 to adjust the total ionic strength of the buffer system at 0.10 M. The buffered solution was then transferred to an external 50.0 ml double-walled glass cell, which was connected to a water-circulating bath, thus allowing the temperature of the cell to be maintained at a temperature relevant to a particular experiment. A magnetic stirrer bar was placed into the cell, which was then placed on a stirring mantle to allow for constant stirring and to provide a homogenous solution. The pH of the sample solutions was adjusted in approximately 0.5 pH unit increments from approximately pH 5.0 to 11.5 by diffusing negligible quantities of 8 M NaOH with a drawn-out capillary tube, after which the pH was recorded. Subsequent to each pH adjustment, the sample was allowed to attain thermal equilibrium and a Watson-Marlow 101U peristaltic pump set at a rate of 90 revolutions per minute was used to circulate the sample solution through the system into a 1.5 ml volume quartz flow cell housed within the thermostatted cell block of a CARY 300 BIO UV-vis spectrophotometer, where a full spectrum was recorded before returning the sample to the external cell.

The absorbance changes as a function of pH were analysed at multiple wavelengths at which large spectroscopic changes were observed. The pK_a was calculated by fitting the experimental data to an ionisation isotherm (Equation 2.1), which is relevant when an acid/base equilibrium is present.[29-32]

$$A = \frac{[H^+]A_0 + K_a A_1}{[H^+] + K_a}$$

[Equation 2.1]

In Equation 2.1, A_0 and A_1 are the limiting values of absorbance at the monitoring wavelength, λ; at low and high pH, respectively, and K_a is the equilibrium constant for the

References on page 64

dissociation of H^+ from coordinated H_2O. The equation was fitted by standard non-linear least squares methods using SigmaPlot[10] with *A* as the dependent variable, $[H^+]$ as the independent variable and with A_0, A_1 and K_a as variables in the fitting procedure. The reported pK_a was calculated by averaging the pK_a values at these wavelengths, so as to average out the wavelength dependence found in the determination of pK_a values.

These investigations were carried out at seven temperatures ranging between 10 – 40 ^oC for $[ACCbs]^+$ pK_a determinations, and at four temperatures ranging between 15 – 40 ^oC for [AC-5-seco-Cbs]$^+$ investigations. The thermodynamic parameters, ΔH and ΔS, were then determined from the slope and intercept, respectively, from the plot of ln *K* against T^{-1}. An example of a pK_a determination can be found in **Appendix G**. The raw spectroscopic data and accompanying pK_a calculations can be found on the accompanying CD **(Digital Appendix A)**.

2.4.3 Investigations into the Thermodynamics of Ligand Substitution Reactions

The equilibrium constants (log *K*) for the substitution of axially coordinated water in $[ACCbs]^+$ and [AC-5-seco-Cbs]$^+$ by a range of anionic (SO_3^{2-}, CN^-, NO_2^-, N_3^- and $S_2O_3^{2-}$) and neutral N-donor (N-MeIm, 4-MePy and NH_2EtOH) ligands, L, (Equation 2.2) were determined spectrophotometrically as a function of temperature.

$$[CN–Co–H_2O] + L \overset{K}{\rightleftharpoons} [CN–Co–L] + H_2O$$

[Equation 2.2]

The equilibrium constants were determined by the addition of aliquots of stock solutions of the relevant ligand to a solution of $[ACCbs]^+$ or [AC-5-seco-Cbs]$^+$ (2.3 ml) contained in a 1.0 cm pathlength standard quartz cuvette housed within the thermostatted cell block of a CARY 300 BIO spectrophotometer. The temperature of the cell block was maintained by a water-circulating bath set at a temperature relevant to the study being undertaken. Initial spectra of either $[ACCbs]^+$ or [AC-5-seco-Cbs]$^+$ with no ligand present were first recorded. Typically, between 12 and 20 aliquot additions were then added in each titration using a 10,

References on page 64

50, 100 or 250 µl microsyringe. A micro-stirrer bar was placed into the cuvette and placed on a stirring mantle to ensure homogenous mixing. The UV-vis spectrum was then recorded after allowing for equilibration. Ligand additions were made until no further change in the spectrum was observed, after which the final pH of the solution was recorded. All absorbance readings were corrected for dilution by multiplying the experimentally obtained absorbance reading by the ratio of the total and initial solution volumes.

The corrin solutions were buffered at an appropriate pH which is dependent on the pK_a of the ligand so as to ensure maximum complex formation is obtained (i.e., the ligand needs to occur as an anion or free base in solution). Therefore, $[ACCbs]^+$ solutions were buffered with MES (for titrations performed at pH 6 with N_3^- and $S_2O_3^{2-}$), MOPS (for titrations performed at pH 7 with CN^-, NO_2^- and SO_3^{2-}) and CHES (for titrations performed at pH 9 with N-MeIm, 4-MePy and NH_2EtOH) at an ionic strength of µ = 0.1 M. $[AC\text{-}5\text{-}seco\text{-}Cbs]^+$ solutions were buffered with MES (for titrations performed at pH 6 with N_3^- and $S_2O_3^{2-}$), MOPS (for titrations performed at pH 7 with SO_3^{2-} and NO_2^-), Tris/HCl (for titrations performed at pH 7.5, 8 and 8.5 with CN^-, SO_3^{2-}, N-MeIm and 4-MePy) and CHES (for titrations performed at pH 9 and 9.5 with SO_3^{2-}) at an ionic strength of µ = 0.1 M.

Ligand stock solutions were prepared by dissolving the ligand in an appropriate buffer, and the pH was adjusted to the required pH by the addition of NaOH or H_2SO_4 to increase or decrease the pH, respectively.

By analogy with $[ACCbs]^+$ and $[ACSYCbs]^+$ amongst other aquacyano derivatives of vitamin B_{12},[33-38] $[AC\text{-}5\text{-}seco\text{-}Cbs]^+$ also exists as an equilibrium of two diastereomers in solution (i.e., the α-cyano, β-aqua and α-aqua, β-cyano isomers). The diastereomers are expected to have a very similar equilibrium constant for the substitution of axially coordinated water by an exogenous ligand, L.[33] In such circumstances, the spectrophotometric determination of log *K* will exhibit a wavelength dependence which is attributed to the relative extinction co-efficients of the diastereomers at the monitored wavelengths.[39] As such, log *K* was determined at every 1 nm in ranges on either side of the isosbestic points at which a large change in absorbance was observed, excluding wavelengths where the change in absorbance was small (such as near the isosbestic point) or where the data was deemed unreliable.

References on page 64

In cases where log *K* values were relatively small (log *K* < 4), it is assumed that $[L]_{free} = [L]_{total}$, thus the absorbance data at each monitored wavelength were fitted to a simple binding isotherm (Equation 2.3) using non-linear least squares methods[30-33,38,40,41] where A_λ is the absorbance measurement at the monitored wavelength, λ. A_0, A_1 and *K* were the parameters to be optimized. A_0 and A_1 are the absorbance values corresponding to 0 and 100% cobalt-ligand complex formation at a particular ligand concentration [*L*], respectively. *K* corresponds to the binding constant determined at each wavelength. The derivation of Equation 2.3 can be found in **Appendix B.2.1.**

$$A_\lambda = \frac{A_0 + A_1 K[\mathrm{L}]}{1 + K[\mathrm{L}]}$$

[Equation 2.3]

In cases where log *K* is large (log *K* > 4), the assumption that the concentration of free ligand $[L]_{free}$ is the same as the total concentration of ligand $[L]_{total}$ added is invalid, as a significant fraction of the total amount of ligand added will be complexed to the metal ion. It is therefore necessary to replace [*L*] in Equation 2.3 with $[L]_{free}$ which is determined by using Equation 2.4 below, where $[M]_{total}$ is the total metal ion concentration.[31-33,38,40-42]

$$[L]_{\mathrm{free}} = \frac{-a_2 \pm \sqrt{a_2^2 - 4a_1a_3}}{2a_1}$$
$$a_1 = K; \quad a_2 = 1 + K[\mathrm{M}]_{\mathrm{total}} - K[\mathrm{L}]_{\mathrm{total}}; \quad a_3 = -[\mathrm{L}]_{\mathrm{total}}$$

[Equation 2.4]

Equation 2.4 could then be substituted into Equation 2.3 by replacing [*L*], resulting in a new equation to compensate for the amount of free ligand in solution. The derivation of Equation 2.5 can be found in **Appendix B.2.2**.

$$A_\lambda = \frac{A_0 + A_1 K[L]_{\mathrm{free}}}{1 + K[L]_{\mathrm{free}}}$$

[Equation 2.5]

References on page 64

It is well established in cobalt-corrin chemistry that hydroxide in hydroxocyano complexes will not be displaced by exogenous ligands.[29-33,38,40,41] Furthermore, the protonated form of a ligand will not coordinate to a metal ion. Hence the observed equilibrium constants (log *K* values) were corrected for the pK_a of $[ACCbs]^+$ or $[AC\text{-}5\text{-}seco\text{-}Cbs]^+$ and the pK_a of the ligands to obtain pH-independent *K* values using Equation 2.6 where pK_{Co} is the acid dissociation constant for coordinated water in $[ACCbs]^+$ or $[AC\text{-}5\text{-}seco\text{-}Cbs]^+$ and pK_{aL} refers to the conjugate acid of a ligand.

$$K = K_{(obs)}(1+10^{(pKaL-pH)})(1+10^{(pH-pKCo)})$$

[Equation 2.6]

The final equilibrium constants were found from a weighted average, weighted by the reciprocal of the relative percentage error. The log *K* was determined by simply taking the log of the final weighted *K* value, and the error was determined using the following equation:

$$\log K \text{ error} = \log(\text{Final weighted } K + \text{error}) - \log K$$

[Equation 2.7]

Equilibrium constants for the coordination of CN^- and SO_3^{2-} by ACCbs were expected to be large and were therefore determined in a competition reaction in the presence of 0.20 M N_3^-. Under these experimental conditions, > 99% of the cobester solution is present as an azidocyano complex. *K* values for the binding of CN^- and SO_3^{2-} were determined from $K_{cyanide/sulfite} = K_{obs}K_{azide}$, wherein K_{obs} is the observed equilibrium constant for the binding of CN^- or SO_3^{2-} in the presence of excess N_3^-.

Equilibrium constants were determined as a function of the temperature hence all log *K* values were determined at seven temperatures ranging between 10 – 40 ^oC. Values of Δ*H* and Δ*S* were determined from the slope and intercept, respectively, of weighted linear least-squares van't Hoff plots of ln *K* against 1/*T*. An example of a log *K* determination can be found in **Appendix H**. The raw spectroscopic data and determination of log *K* values can be found on the accompanying CD **(Digital Appendix B)**.

References on page 64

2.4.4 Investigations into the Kinetics of Ligand Substitution Reactions of [AC-5-seco-Cbs]$^+$

The kinetics of substitution reactions of [AC-5-seco-Cbs]$^+$ (and vitamin B_{12a} for comparative purposes) with a probe ligand (cyanide) can be described by Equation 2.8.

$$[CN–Co–H_2O] + CN \overset{k^{II}}{\rightleftharpoons} [CN–Co–CN] + H_2O$$

[Equation 2.8]

The second-order rate constants, k^{II}, were determined spectrophotometrically under pseudo first-order conditions where [L] ›› [cobester].[33]

A freshly prepared solution of [AC-5-seco-Cbs]$^+$ (ca. 50 µM) or vitamin B_{12a} (ca. 30 µM) was buffered with CAPS (µ = 0.1 M, pH = 10.5) and added to a 1.0 cm pathlength cuvette housed in the thermostatted cell block of a spectrophotometer. To this an aliquot of a known concentration of cyanide which was also freshly prepared and buffered with CAPS and adjusted with either H_2SO_4 or NaOH to obtain a similar pH value as that of the secocobester or B_{12a}[43] solutions was added, and the rate of the reaction was monitored by recording the increase or decrease of the absorbance over time at 400 nm or 362.1 nm for [AC-5-seco-Cbs]$^+$ and vitamin B_{12a},[43] respectively. Between five and seven ligand concentrations were used, each differing in concentration by approximately a factor of ten. Each ligand concentration was then repeated a minimum of five times.

The pseudo first-order rate constants, k_l^{obs}, were obtained by fitting a double exponential (Equation 2.9 for [AC-5-seco-Cbs]$^+$)[33] or a standard exponential function (Equation 2.10 for aquacobalamin) employing a Newton-Raphson procedure using SigmaPlot to the absorbance vs time plots obtained for each titration.

$$A_\lambda = A_\infty + (A_0 - A_1)e^{-k_1^{obs}t} + (A_1 - A_\infty)e^{-k_2^{obs}t}$$

[Equation 2.9]

References on page 64

$$A_\lambda = A_0 + (A_1\text{-}A_0)e^{-k1t}$$

[Equation 2.10]

In Equation 2.9, k_1 and k_2 are the pseudo first-order rate constants for the faster and slower phases, respectively, A_∞ is the absorbance at the end of the reaction, $|A_0 - A_1|$ the absorbance change associated with the faster phase and $|A_1 - A_\infty|$ that associated with the slower phase. Thereafter, the observed first order rate constants were corrected for the pK_a of [AC-5-seco-Cbs]$^+$. The second order rate constant, k_i^{II} (i = f (fast), s (slow)), was then obtained from the slope of a plot of k_i against [CN^-].

The reason for using a double exponential function for the kinetics of the reaction of [AC-5-seco-Cbs]$^+$ will be discussed in Chapter 6. An example of the determination of the rate constant can be found in **Appendix I**. The raw spectroscopic data and determination of rate constants can be found on the accompanying CD **(Digital Appendix C)**.

2.5 Crystal Structure Determination

Two methods were investigated in attempts to crystallise [DC-5-seco-Cbs]. Firstly, we attempted to grow crystals by the slow evaporation of acetonitrile, methanol, chloroform, ethyl acetate and hexane at room temperature. We also attempted to grow crystals in an H-tube in a refrigerator by the vapour diffusion of either hexane, toluene, chloroform or diethyl ether into a solution of [DC-5-seco-Cbs] in ethyl acetate as well as by the vapour diffusion of diethyl ether into a solution of [DC-5-seco-Cbs] in methanol.

Unfortunately, no suitable crystals were obtained as [DC-5-seco-Cbs] formed a ‘gel’ in slow evaporation attempts and amorphous masses in H-tube attempts (Figure 2.1).

References on page 64

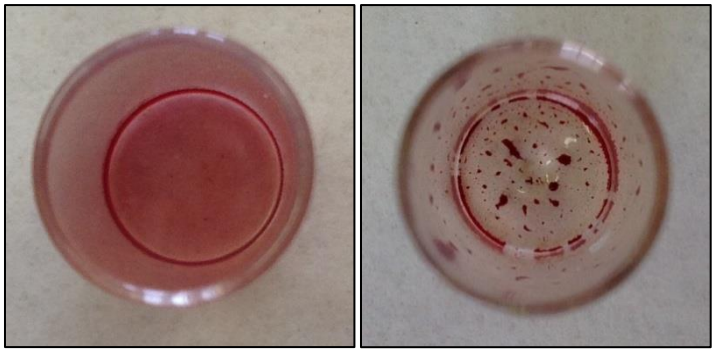

Figure 2.1 Crystallisation attempts of [DC-5-seco-Cbs] resulting in the formation of a ‘gel’ by slow evaporation (left) and the formation of amorphous masses by H-tube attempts (right).

References on page 64

REFERENCES FOR CHAPTER 2

1. https://www.applichem.com/fileadmin/Broschueren/BioBuffer.pdf (Accessed 25 January 2018)
2. https://chem.libretexts.org/Demonstrations_and_Experiments_Basic_Lab_ Techniques/Thin_Layer_Chromatography (Accessed 30 November 2017).
3. Pietrzyk, D. J.; Frank, C. W. In *Analytical Chemistry*; Academic Press Inc., New York, 1979, pp 540-552.
4. Skoog, D. A.; West, D. M. In *Fundamentals of Analytical Chemistry*; Thomson Learning Inc., Belmont, 1982, pp 482, 680-682.
5. Pasto, D. J.; Johnson, C. R.; Miller, M. J. In *Experiments and Techniques in Organic Chemistry*; Prentice-Hall Inc., New Jersey, 1992, pp 60, 69-73.
6. Kräutler, B. *Coord. Chem. Rev.* **1991**, 111, 215-220.
7. Andruniow, T.; Kozlowski, P. M.; Zgierski, M. Z. *J. Chem. Phys.* **2001**, 115, 7522-7533.
8. Marston, A.; Hostettman, M. In *Preparative Thin Layer Chromatography Techniques: Applications in natural product isolation*; Fourth edn., Springer, Germany, 1998.
9. CARY WinUV; 4.20(470) ed.; Agilent Technologies, 2017.
10. SigmaPlot, v. 14, Systat Software, 2017.
11. UV-Visible ChemStation; B.04.01 (61) ed.; Agilent Technologies, 2011.
12. Chromeleon; 6.80 SR7 Build 2528 (1483691) ed.; Dionex Corporation, 2005.
13. Chemaly, S. M.; Brown, K. L.; Fernandes, M. A.; Munro, O. Q.; Grimmer, C.; Marques, H. M. *Inorg. Chem.* **2011**, 50, 8700-8718.
14. otofControl; 4.0 Build 60.11 ed.; Bruker Daltonik GmbH, 2015.
15. Compass DataAnalysis; 4.3 Build 110.102.1532 ed.; Bruker Daltonik GmbH, 2014.
16. OPUS; 7.5 Build 7.5.18 ed.; Bruker OptikGmbH, 2014.
17. MestReNova; 9.0.1-13254 ed.; Mestrelab Research S. L., 2014.
18. Perdew, J. P. *Phys. Rev. B* **1986**, 33, 8822-8824.
19. Becke, A. D. *Phys. Rev. A* **1988**, 38, 3098-3100.
20. Frisch, M. J. T., G. W.; Schlegel, H. B.; Scuseria, G. E.; Robb, M. A.; Cheeseman, J. R.; Scalmani, G.; Barone, V.; Mennucci, B.; Petersson, G. A.; Nakatsuji, H.; Caricato, M.; Li, X.; Hratchian, H. P.; Izmaylov, A. F.; Bloino, J.; Zheng, G.; Sonnenberg, J. L.; Hada, M.; Ehara, M.; Toyota, K.; Fukuda, R.; Hasegawa, J.; Ishida, M.; Nakajima, T.; Honda,

Y.; Kitao, O.; Nakai, H.; Vreven, T.; Montgomery, J., J. A.; Peralta, J. E.; Ogliaro, F.; Bearpark, M.; Heyd, J. J.; Brothers, E.; Kudin, K. N.; Staroverov, V. N.; Kobayashi, R.; Normand, J.; Raghavachari, K.; Rendell, A.; Burant, J. C.; Iyengar, S. S.; Tomasi, J.; Cossi, M.; Rega, N.; Millam, N. J.; Klene, M.; Knox, J. E.; Cross, J. B.; Bakken, V.; Adamo, C.; Jaramillo, J.; Gomperts, R.; Stratmann, R. E.; Yazyev, O.; Austin, A. J.; Cammi, R.; Pomelli, C.; Ochterski, J. W.; Martin, R. L.; Morokuma, K.; Zakrzewski, V. G.; Voth, G. A.; Salvador, P.; Dannenberg, J. J.; Dapprich, S.; Daniels, A. D.; Farkas, Ö.; Foresman, J. B.; Ortiz, J. V.; Cioslowski, J.; Fox, D. J. Gaussian 09; Revision C.01, v. Gaussian, Inc: Wallingford C, 2009.

21. Grimme, S.; Antony, J.; Ehrlich, S.; Krieg, H. *J. Chem. Phys*. **2010**, 132, 154104-154119.
22. Markwell, A. J.; Pratt, J. M.; Shaikjee, S. S.; Toerien, J. G. *J. Chem. Soc., Dalton Trans*. **1987**, 1349-1357.
23. Bader, R. F. W. *Acc. Chem. Res*. **1985**, 18, 9-15.
24. Bader, R. F. Atoms in Molecules: A Quantum Theory. Oxford University Press: Oxford, 1990.
25. Keith, T. A. AIMAll (version 17.01.25), v. TK Gristmill Software, http://aim.tkgristmill.com: Overland Park, KS, 2016.
26. http://www.mathfinance.cm/Levenberg-Marquardt-non-linear-least-squares (accessed 20 October 2015).
27. Munro, O. Q.; Marques, H. M. *Inorg. Chem*. **1996**, 35, 3752-3767.
28. Sannasy, D. MSc Dissertation, University of the Witwatersrand, Johannesburg, 2006.
29. Knapton, L. Ph.D. Thesis, University of the Witwatersrand, Johannesburg, 2005.
30. Zipp, C. F. Ph.D Thesis, University of the Witwatersrand, Johannesburg, 2014.
31. Ghadimi, N. Ph.D Thesis, University of the Witwatersrand, Johannesburg, 2016.
32. Ghadimi, N.; Perry, C. B.; Fernandes, M. A.; Govender, P. P.; Marques, H. M. *Inorg. Chim. Acta.* **2015**, 436, 29-38.
33. Chemaly, S. M.; Florczak, M.; Dirr, H.; Marques, H. M. *Inorg. Chem.* **2011**, 50, 8719-8727.
34. Friedrich, W. Z. *Naturforsch. B* **1966**, 21, 595-596.
35. Pratt, J. M. In *Inorganic Chemistry of Vitamin B_{12};* Academic Press, London, 1972.
36. Friedrich, W. Z.; Bieganowski, R. Z. *Naturforsch*. B **1967**, 22, 741-747.

37. Friedrich, W. Z.; Ohlms, H.; Sandeck, W.; Bieganowski, R. Z. *Naturforsch. B* **1967**, 22, 839-850.
38. Chemaly, S. M.; Kendall, L.; Nowakowska, M.; Pon, D.; Perry, C. B.; Marques, H. M. *Inorg. Chem*. **2013**, 52, 1077-1083.
39. Johnson, G. D.; Bowen, R. E. *J. Am. Chem. Soc.* **1965**, 87, 1655-1660.
40. Zipp, C. F.; Michael, J. P.; Fernandes, M. A.; Nowakowska, M.; Dirr, H. W.; Marques, H. M. *Inorg. Chem. Comm*. **2015**, 57, 15-17.
41. Ghadimi, N.; Perry, C. B.; Govender, P. P.; Marques, H. M. *Inorg. Chim. Acta.* **2016**, 450, 269-278.
42. Marques, H. M.; Munro, O. Q.; Crawcour, M. L. *Inorg. Chim. Acta.* **1992**, 196, 221-229.
43. Reenstra, W. W.; Jencks, W. P. *J. Am. Chem. Soc*. **1979**, 101, 5780-5791.

CHAPTER 3

SYNTHESIS AND CHARACTERISATION

3.1 Introduction

The consequence of cleaving the corrin ring and subsequent opening of the macrocyclic cavity as well as the consequence of extending the corrin chromophore beyond that typically observed in a corrin ring, which ultimately addresses the effect the corrin ring has on the chemistry of the central Co(III) ion, is explored in this study. The aim of this chapter is to describe the synthesis of the starting material dicyanocobester ([DCCbs]); how the electronic structure of an intact corrin ring, as present in [DCCbs], was perturbed by selectively cleaving the corrin ring at the C5 or C15 position by photosensitized oxygenation, followed by an in depth account of the two alternative techniques attempted for the separation and isolation of the secocobester isomers. Thereafter, the pyrolysis of [DCCbs] for the synthesis of dicyanopyrocobester is explored. The conversion of dicyano complexes to the aquacyano forms wherein a coordinated cyanide ligand is substituted by a water molecule, which is essential for solution chemistry investigations, is also discussed. This chapter also presents all relevant characterisation work for the identification and assessment of purity of synthesised compounds.

3.2 Synthesis and Characterisation of Modified Cobalt Corrins

3.2.1.1 Synthesis and Characterisation of Heptamethyl Coα,Coβ-dicyano-cob(III)yrinate (Dicyanocobester, [DCCbs])

Dicyanocobester was prepared according to the procedure reported by Chemaly *et. al.*[1] which was adapted from a method originally developed by Werthermann.[2] Cyanocobalamin (1.3 g, 959 µmol) was dissolved in a solution of 1.0 M sulfuric acid in methanol (160.0 ml) and refluxed at 65 ^{o}C for four days under a slow stream of nitrogen. Thereafter, the reaction mixture was concentrated *in vacuo* to approximately 50 ml and then diluted with water (ca. 200 ml). The acidic solution was neutralised by the addition of sodium carbonate resulting in a deep red solution. Sodium cyanide (0.71 g, 14.49 mmol) was then added to

References on page 103

produce a purple solution. The product mixture was first extracted with trichloroethylene (3 × 200 ml), followed by dichloromethane (3 × 200 ml). The trichloroethylene extract was rotary evaporated to dryness. The dichloromethane extract was first rotary evaporated to dryness and then re-dissolved in a solution of 1.0 M sulfuric acid in methanol and refluxed again. Once the entire procedure was repeated, the trichloroethylene extracts from both reflux steps were combined, dried *in vacuo* and separated by column chromatography on a mixture of silica gel (75.0 g) and sodium cyanide (2.0 g) with a toluene:methyl acetate (2:3 v/v) eluent.[3] Fractions containing [DCCbs], as determined by UV-vis spectroscopy and TLC, were concentrated *in vacuo*, yielding a purple solid. Purity was assessed by HPLC (acetonitrile/water) (Figure 3.1) which indicated a single peak at a retention time of 9.42 minutes. [DCCbs] was prepared in a 55% yield, which compares favourably with a 57% yieldreported by Chemaly for the same synthesis. [1]

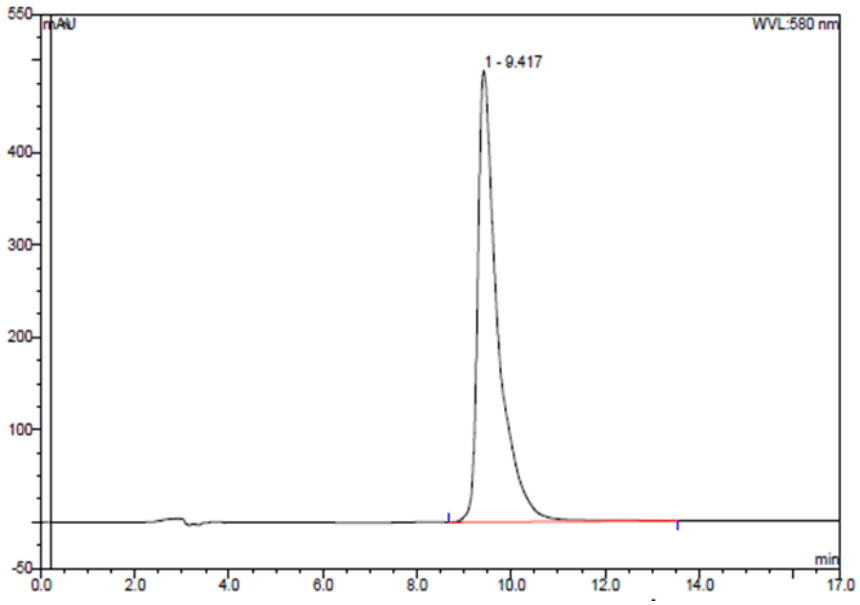

Figure 3.1 HPLC chromatogram of purified [DCCbs] with a retention time of 9.42 minutes, indicating 100% purity.

ESI-MS in the positive mode was used to verify the molecular mass of [DCCbs]. The molecular ion peak ($C_{54}H_{73}CoN_6O_{14}$) expected at 1089.12 was observed at very low intensity. Peaks observed at 1062.45 and 1036.45 were attributed to the loss of one or both axial cyanide ligands ($(M–CN)^+$, $C_{53}H_{73}CoN_5O_{14}$; (calc. 1063.09) and $(M–2CN+H)^+$, $C_{52}H_{73}CoN_4O_{16}$;

References on page 103

(calc. 1037.07)) which is consistent with the observations recorded by Chemaly.[1] Selected mass spectra can be found in **Appendix D.1**.

FTIR was also used to verify the nature of the synthesised cobester. A small amount of water was observed at 3448 cm^{-1} which is consistent with the water of crystallisation observed in literature. Other characteristic peaks such as the C≡N stretch (2122 cm^{-1}), C=O ester stretch (1726 cm^{-1}), aliphatic and aromatic C–H stretches were all consistent with literature for [DCCbs].[1] Selected FTIR spectra can be found in **Appendix E.1**.

3.2.1.2 Synthesis and Characterisation of Heptamethyl Coα,Coβ-aquacyano-cob(III)yrinate (Aquacyanocobester, $[ACCbs]^+$)

The synthesis of $[ACCbs]^+$ was previously reported by Chemaly *et. al.*[1] In a typical experiment, dicyanocobester (39 mg, 35 μmol) was dissolved in methanol (25.0 ml), to which glacial acetic acid was added to lower the pH of the solution to 3. The acidic solution was then stirred for 24 hours during which a constant, slow stream of nitrogen gas was passed through the solution to remove any HCN gas generated.[3-5] The reaction was monitored by UV-vis spectroscopy. As the conversion proceeded, the principal bands blue shifted from 313, 368, 544 and 583 nm to 322, 354, 404, 495 and 527 nm, respectively, as the colour of the solution changed from purple to red (Figure 3.2). Once conversion was complete, the reaction mixture was dried *in vacuo*, after which the flask containing the newly-generated $[ACCbs]^+$ was attached to a Schlenk apparatus which in turn was connected to a high-vacuum line powered by a KNF Laboport Diaphragm vacuum pump for the removal of any residual acetic acid. Purity was assessed by HPLC (phosphate buffer/methanol). Figure 3.3 indicated two peaks with a retention time of 8.33 minutes (56%) and 8.76 minutes (43%), attributed to the presence of the two diastereomers (α- H_2O, β-CN and α-CN, β-H_2O).

References on page 103

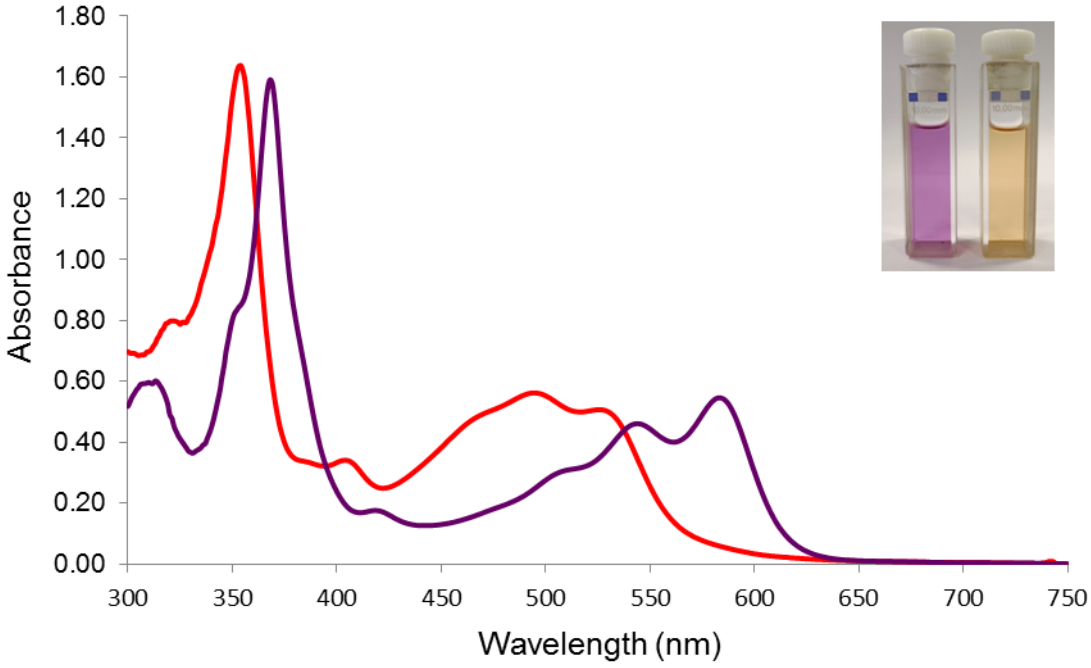

Figure 3.2 UV-vis spectra of [DCCbs] (purple) and $[ACCbs]^+$ (red) in methanol.

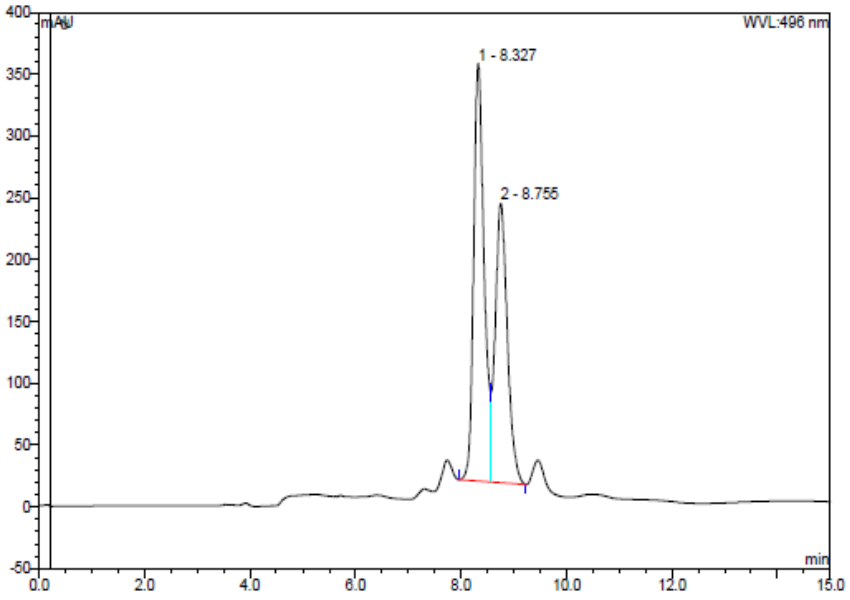

Figure 3.3 HPLC chromatogram of $[ACCbs]^+$ with two peaks at a retention time of 8.33 (57%) and 8.76 (43%) minutes, together with two small peaks occurring at 7.8 and 9.0 minutes, corresponding to the spontaneous formation of the diaqua and dicyano species, respectively, in solution.

References on page 103

The molecular mass of $[ACCbs]^+$ was verified by ESI-MS in the positive mode. The molecular ion peak ($C_{53}H_{75}CoN_5O_{15}$) was detected at 1082.48 at very low intensity. Characteristic peaks attributed to the loss of axial ligands (1062.49 $(M–H_2O)^+$, $C_{53}H_{73}CoN_5O_{14}$; (calc. 1063.09) and 1036.48 $(M–H_2O\text{-}CN+H)^+$, $C_{52}H_{73}CoN_4O_{14}$; (calc. 1063.09)) were also observed and consistent with literature.[1] Selected mass spectra can be found in **Appendix D.2**.

FTIR was also performed to verify the nature of the cobester formed. Once again, characteristic peaks such as the O–H stretch (3435 cm^{-1}) C≡N stretch (2128 cm^{-1}) and C=O ester stretch (1727 cm^{-1}) were all observed and consistent with literature.[1] Selected FTIR spectra can be found in **Appendix E.2**.

3.2.2.1 Synthesis and Characterisation of Heptamethyl Coα,Coβ-dicyano-5,6-dioxo-5,6-secocob(III)yrinate (5-seco-Dicyanocobester, [DC-5-seco-Cbs]) and Heptamethyl Coα,Coβ-dicyano-14,15-dioxo-14,15-secocob(III)yrinate (15-seco-Dicyanocobester, [DC-15-seco-Cbs])

The photo-oxygenolysis procedure was adapted from a previously published method developed by Kräutler for the photo-oxygenation of heptamethyl Coα,Coβ-dicyano-cob(III)yrinate (dicyanocobester, [DCCbs]) and involved preparing a solution of [DCCbs] (354 mg, 324 µmol) and methylene blue (0.33 mg, 1.02 µmol) in deuterated methanol (CH_3OD) (9.3 ml).[6]

This solution was then introduced into a photolysis cell which was constructed as a nearly flat cell (45.0 × 5.0 × 40.0 mm) designed specifically for the maximum exposure of incident light for the irradiation of small sample volumes, coupled with an inlet and outlet passage (8.0 mm in diameter) to allow for a constant, slow stream of oxygen. The photolysis cell was then immersed into a concentric arrangement consisting of a beaker (100.0 × 100.0 mm) containing water maintained at 15.0 ^oC, into which was immersed a double-walled cylinder with a 3.0 mm gap. A 0.5 M sodium dichromate solution was placed into the compartment of the cylinder to filter out radiation with a wavelength of less than 550 nm. Once immersed, the photolysis cell was purged with oxygen for several minutes, after which a slow and constant stream of oxygen was maintained whilst the cell was exposed to

References on page 103

homogeneous illumination from an external 15 V/150 W halogen lamp light source placed 5.0 cm away from the cell.

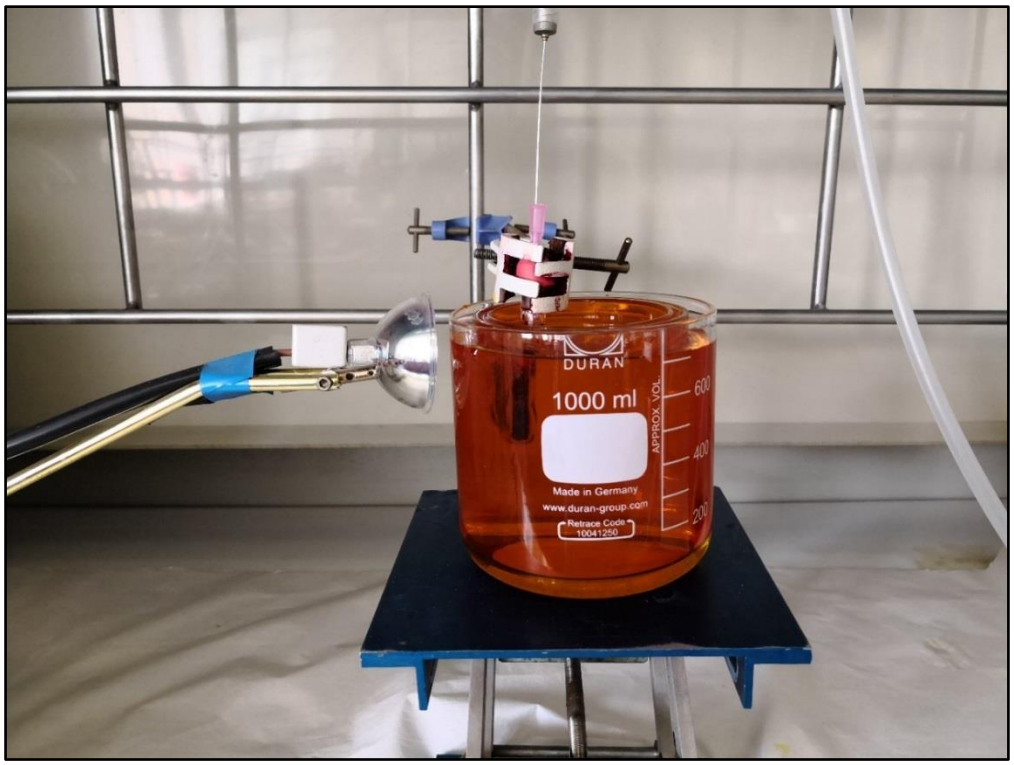

Figure 3.4 A photograph showing the typical photo-oxygenolysis set-up.

The reaction was monitored by withdrawing an aliquot of solution at 45 minute intervals and recording the UV-vis spectrum. As the reaction proceeded, one could observe a steady decrease in the intensity of the characteristic α, β and γ bands of [DCCbs] coupled with the emergence of a new product peak at 480 nm (Figure 3.5). The insert in Figure 3.5 illustrates the vivid colour change observed during the photolysis reaction; this allows UV-vis spectrophotometry to be an excellent tool for the monitoring of this reaction. The study performed by Kräutler suggested that the irradiation procedure be continued for 90 minutes,[6] however, it was found that an additional 45 minutes afforded a better conversion of starting material, [DCCbs], to [DC-5-seco-Cbs], with the observation of a further decrease in the intensity of the α, β and γ bands of [DCCbs]. Hence, after 135 minutes of irradiation, photolysis was discontinued after which no further change in the electronic spectrum was observed. The photolysis cell contents were then transferred to a round bottom flask and dried *in vacuo*.

References on page 103

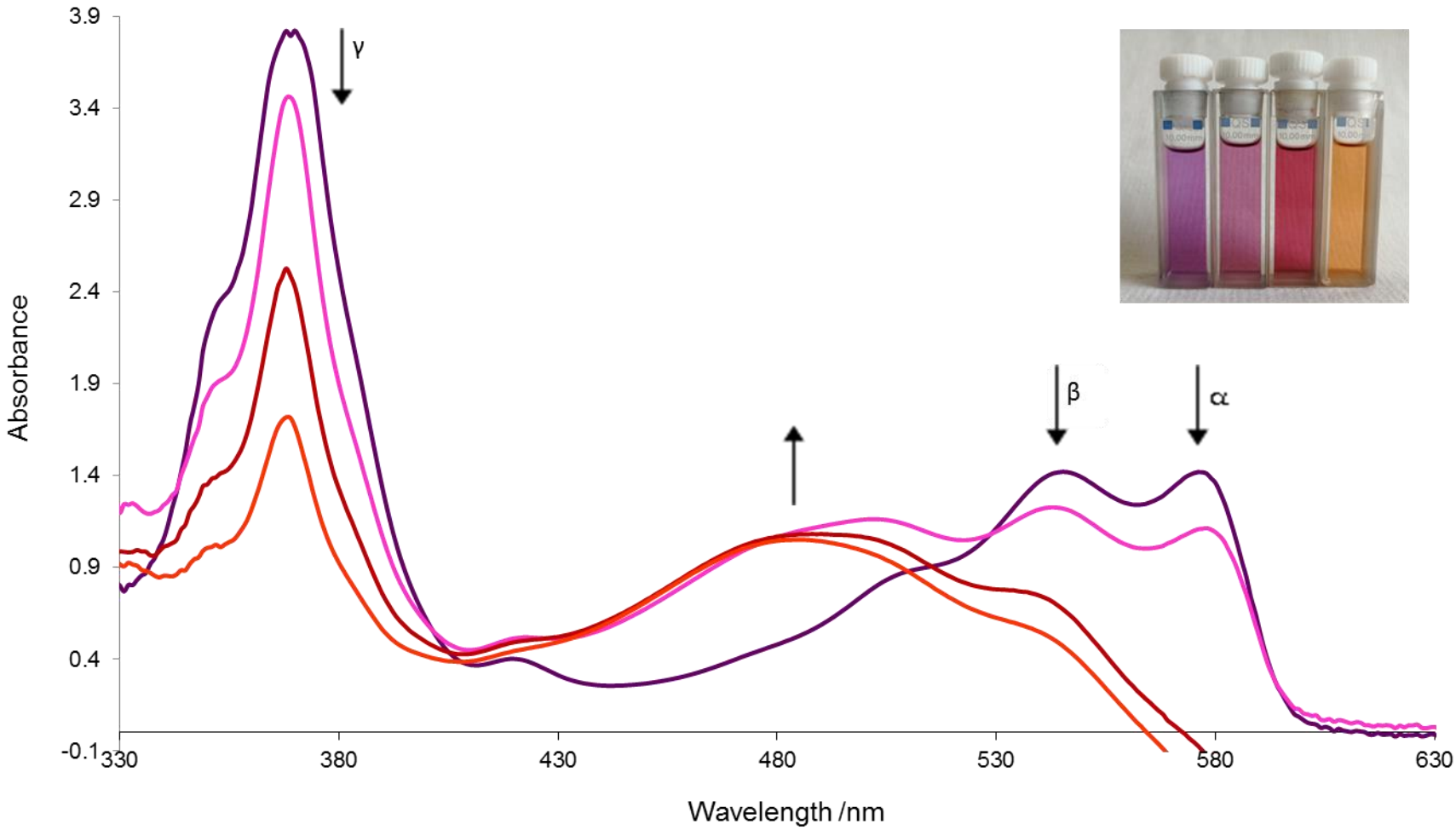

Figure 3.5 UV-vis spectral changes illustrating the progress of the photo-oxygenation procedure starting with [DCCbs] at t = 0.0 minutes (purple) to t = 45.0 minutes (pink), t = 90.0 minutes (red) and at the end of the reaction at t = 135.0 minutes (orange).

References on page 103

The broadened shoulder observed in the product peak at 480 nm (Figure 3.5, red curve) is indicative of the presence of small amounts of unreacted starting material, suggesting the reaction does not go to completion. Furthermore, not only is the reaction solution a mixture of unreacted starting material and [DC-5-seco-Cbs], but the reaction also generates the isomer, [DC-15-seco-Cbs], in which the bond between C14 and C15 has been cleaved (Figure 3.6).[6]

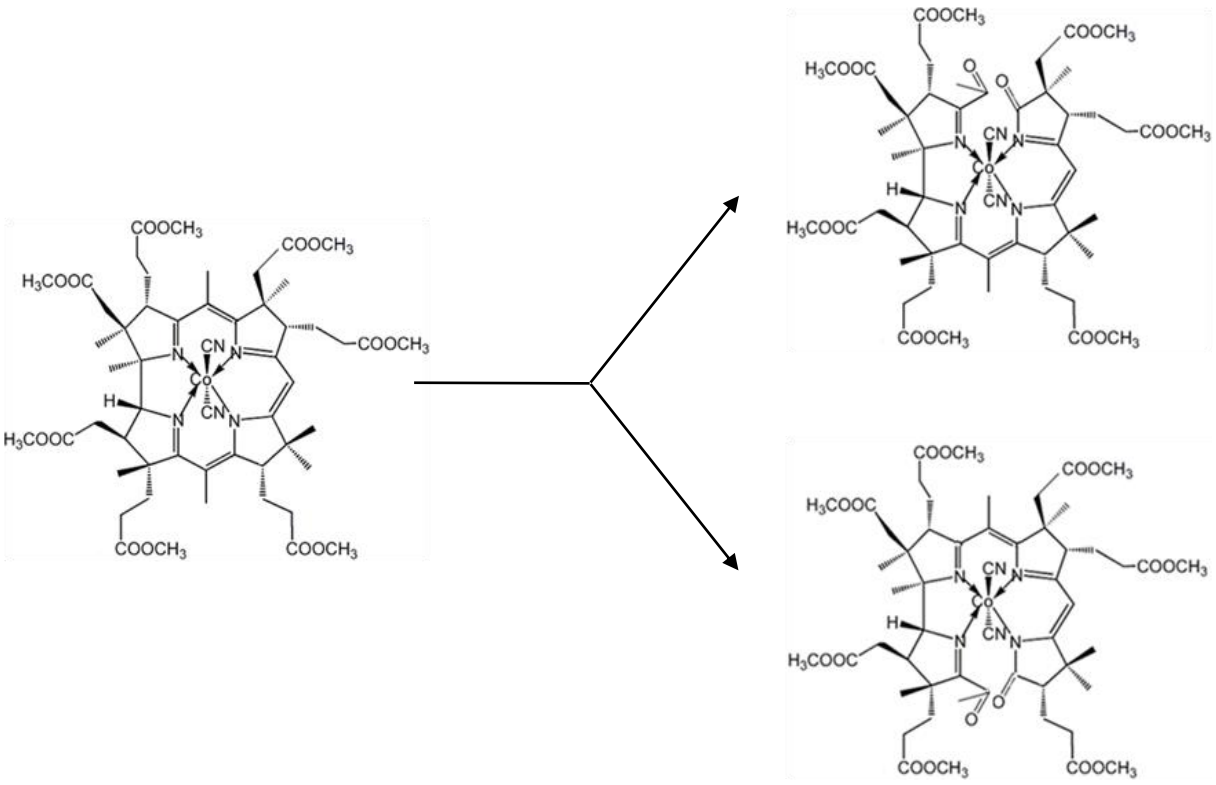

Figure 3.6 The structures of the starting material, [DCCbs] (left) and the two photo-oxygenation products synthesised, [DC-5-seco-Cbs] (top) and [DC-15-seco-Cbs] (bottom).[6]

Two separation routes (Route A and Route B) were explored to optimize the isolation and purification of the three compounds. Separation Route A describes the development of a novel method for the separation of the three compounds by column chromatography, whereas Route B represents a modified version of the original method as described by Kräutler using a combination of column and preparative thin layer chromatography (PTLC).[6]

References on page 103

3.2.2.2 Separation Route A

In order to chromatograph the photo-oxidation products, two solvent systems (Table 3.1) were investigated to determine the optimum conditions for the separation of unreacted starting material, [DCCbs] (purple), [DC-5-seco-Cbs] and [DC-15-seco-Cbs] (both orange).

Table 3.1 Solvent systems investigated for the isolation of [DCCbs], [DC-5-seco-Cbs] and [DC-15-seco-Cbs].

	System	Ratio
Method 1	EtOAc:toluene:acetone	4:1:0.01
Method 2	EtOAc:methanol:toluene	9.5:1:0.5

Method 1 is a modified version of the procedure developed by Kräutler for the purification of heptamethyl Coα,Coβ-dicyano-5,6-dioxo-5,6-secocobyrinate and heptamethyl Coα,Coβ-dicyano-14,15-dioxo-14,15-secocobyrinate,[6] whereas method 2 is adapted from the procedure used by Chemaly and co-workers for the synthesis of heptamethyl Coα,Coβ-dicyanocobyrinate.[1]

TLC analysis (silica gel, Method 1) of the photo-oxygenation product shows the presence of two very poorly separated bands (R_f = 0.17 and 0.10, respectively) (Figure 3.7). There also appeared to be no separation of unreacted starting material from the secocobester isomers. Furthermore, the compounds did not migrate far enough up the silica plate for the solvent system to be suitable for column chromatography. Conversely, TLC analysis (silica gel, Method 2) of the photo-oxygenation mixture showed somewhat improved separation of bands as opposed to the method developed by Kräutler, with the evident distinction between a red-purple band (starting material) and an orange band (secocobester) (R_f = 0.69 and 0.61, respectively). However, the orange band exhibited severe streaking (i.e. tailing) and appeared to merge with the top red-purple spot.

References on page 103

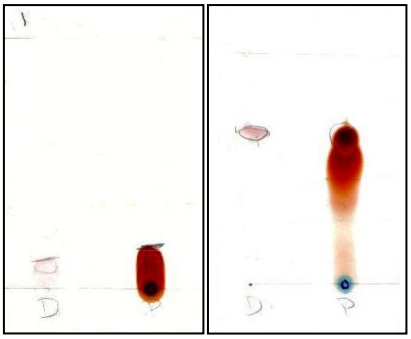

Figure 3.7 Silica TLC plates from investigations of solvent systems employed in method 1 (left) and method 2 (right). D = [DCCbs] and P= photo-oxygenation products.

The extent of separation was however, insufficient, and was further complicated by the observation that purple [DCCbs] (unreacted starting material) has a similar R_f value to one of the orange isomers, thus co-eluting with the secocobester and appearing as a red band. Nevertheless, these observations provided a starting point from which to determine the conditions for optimal separation. The ensuing attempts were variations of Method 2, whereby the polarity of the EtOAc:MeOH:toluene system was altered by adjusting the ratio of ethyl acetate to methanol and toluene (Table 3.2). Care was taken not to allow the percentage of methanol in the system to exceed 20% (v/v), as methanol dissolves silica particles.

Table 3.2 A variety of solvent ratios for the determination of an EtOAc:MeOH:toluene solvent system.

Sample	EtOAc	MeOH	Toluene
a	9	1.5	0.5
b	8	2.5	0.5
c	10	0.5	0.5
d	10	0.25	0.25
e	10	0	0.25
f	10	0.1	0.25

References on page 103

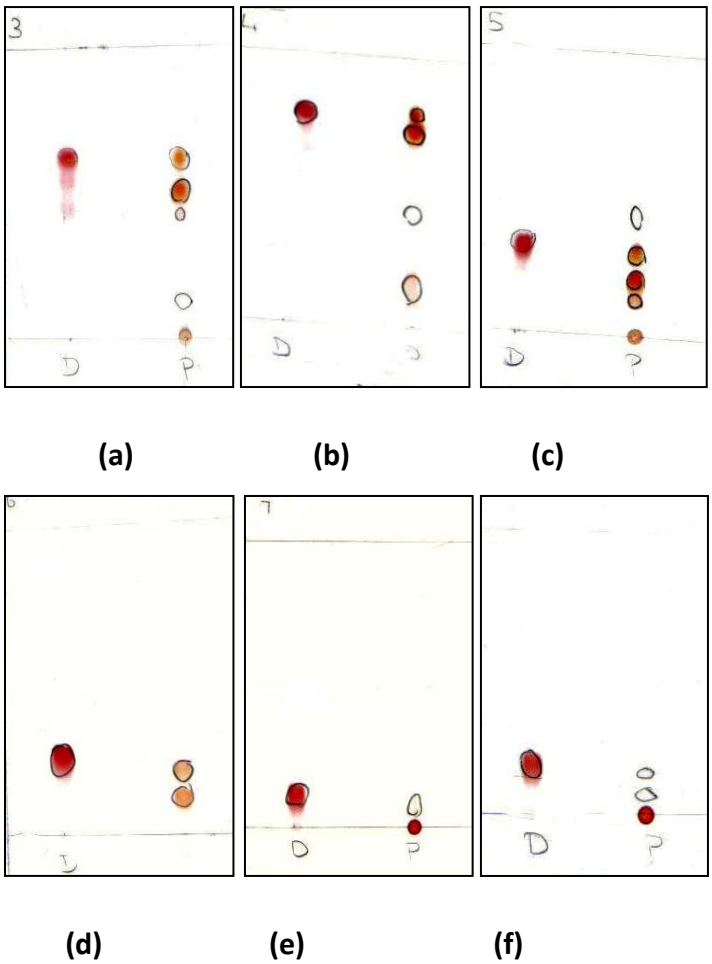

Figure 3.8 Silica TLC plates from the determination of a suitable ratio within an EtOAc:MeOH:toluene solvent system. D = [DCCbs], P = photo-oxygenation products and (a)-(f) are the samples referred to in Table 3.2.

Analysis of the various TLC plates showed varying degrees of separation. Investigations also showed that methanol was required in the system as its absence resulted in minimal migration of bands, resulting in very poor separation. On the contrary, in cases where methanol constituted approximately 20% (v/v) of the solvent system, the bands travelled too far up the silica plate for efficient separation by column chromatography.

It was found that an EtOAc:MeOH:toluene (10:0.25:0.25) (Figure 3.8, TLC (d)) system afforded the best separation of compounds and was suitable for flash silica column chromatography (which requires an R_f of approximately 0.2 for efficient separation). The photo-oxygenation products were then transferred to a column (28.0 × 2.0 cm) containing

References on page 103

flash silica gel (30.0 g) and sodium cyanide (0.750 g) to ensure all constituents remain in the dicyano form, and were separated using the EtOAc:MeOH:toluene (10:0.25:0.25) eluent system. Column chromatography revealed three bands: a distinct purple band (starting material), followed by a red and orange band from the photo-oxygenation products (Figure 3.9).

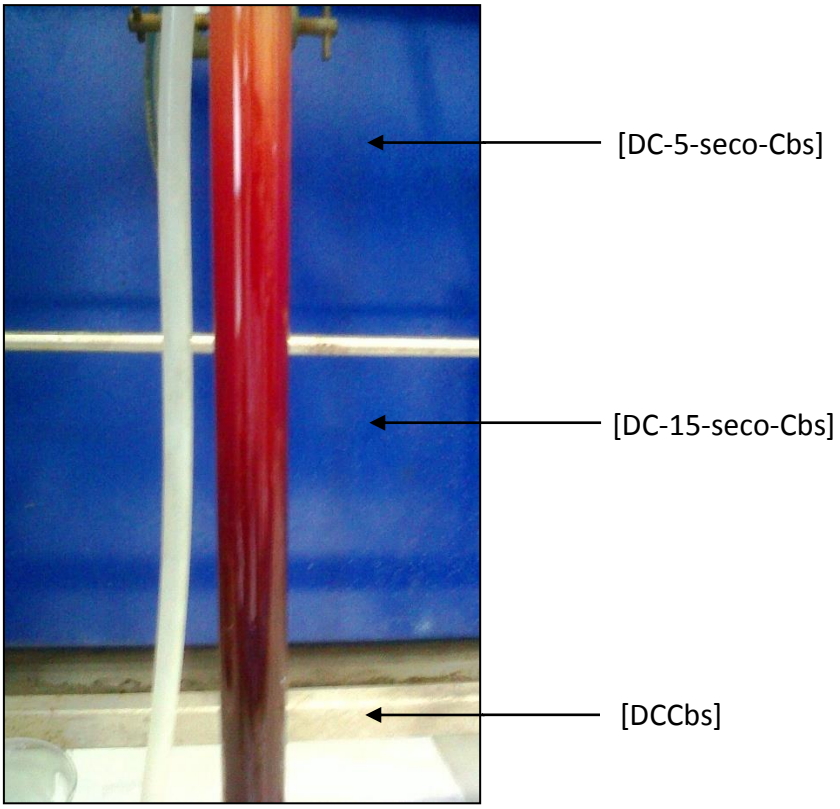

Figure 3.9 A typical column obtained for the separation of [DCCbs], [DC-15-seco-Cbs] and [DC-5-seco-Cbs].

TLC and UV-vis spectroscopy allowed for the differentiation of products as the starting material has a very different UV-vis spectrum compared to the virtually identical spectra obtained for the isomers (Figure 3.10), whereas [DC-5-seco-Cbs] and [DC-15-seco-Cbs] have different R_f values.[6] Of the three constituents within the photolysis product mixture, [DCCbs] is the least polar compound as the two oxygen-containing groups introduced at the

References on page 103

C5 and C15 position in [DC-5-seco-Cbs] and [DC-15-seco-Cbs], respectively, make these compounds more polar. As such, [DCCbs] would elute first in a silica column as a result of a lower affinity for the polar stationary phase, or conversely travel further up a silica TLC plate by virtue of its affinity for the less polar mobile phase. Therefore, the remaining two bands were attributed to the secocobester isomers. In the aforementioned procedure by Kräutler,[6] it was stated that [DC-15-seco-Cbs] was in actual fact less polar than the [DC-5-seco-Cbs] isomer, that is to say, [DC-15-seco-Cbs] would elute before [DC-5-seco-Cbs] during column chromatography, or travel further up a silica TLC plate than [DC-5-seco-Cbs]. This allows the bands at R_f 0.19 and 0.25 to be attributed to [DC-5-seco-Cbs] and [DC-15-seco-Cbs], respectively (Figure 3.8, TLC (d)). The experimentally obtained R_f values differ in comparison to the R_f values of [DC-5-seco-Cbs] and [DC-15-seco-Cbs] obtained by Kräutler (0.18 and 0.28, respectively),[6] as different solvent systems were used as were silica plates of different grades.

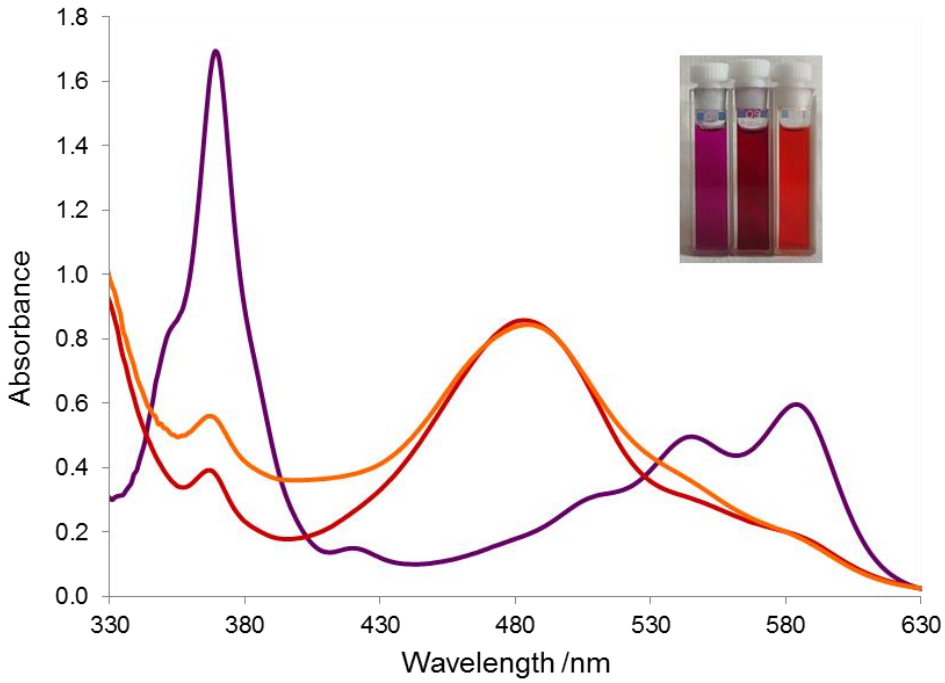

Figure 3.10 UV-vis spectra of [DCCbs] (purple), [DC-15-seco-Cbs] (red) and [DC-5-seco-Cbs] (orange).

References on page 103

Although it appeared that [DC-5-seco-Cbs] and [DC-15-seco-Cbs] were successfully separated, HPLC analysis (Figure 3.11) revealed traces of starting material in the secocobester fractions as well as only partial separation of the two isomers. Thus the EtOAc:MeOH:toluene system was unsuccessful in isolating the three constituents.

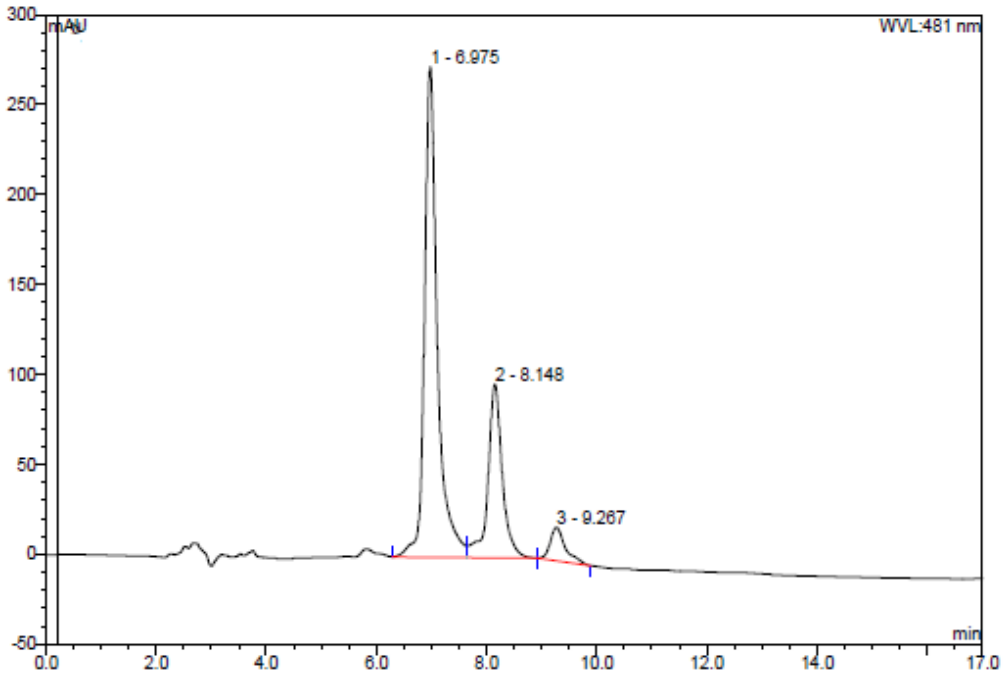

Figure 3.11 HPLC chromatogram illustrating lack of separation after column chromatography. Peak 1 = [DC-5-seco-Cbs], peak 2 = [DC-15-seco-Cbs] and peak 3 = [DCCbs].

It was then decided to revert back to the original Kräutler method involving an EtOAc:toluene:acetone (4:1:0.01) system.[6] As previously discussed, the given ratio was inappropriate for the separation required, so further attempts were made to alter the polarity of the system. A variety of ratios ranging from EtOAc:toluene:acetone (4:1:0) to EtOAc:toluene:acetone (4:1:4) were investigated as shown in Table 3.3; testing the fractions separated in previous column attempts all gave poor results.

References on page 103

Table 3.3 Ratios for the determination of an EtOAc:toluene:acetone solvent system.

Sample	EtOAc	Toluene	Acetone
a	4	1	0
b	4	1	0.01
c	4	1	0.1
d	4	1	0.5
e	4	1	1
f	4	1	2
g	4	1	3
h	4	1	4

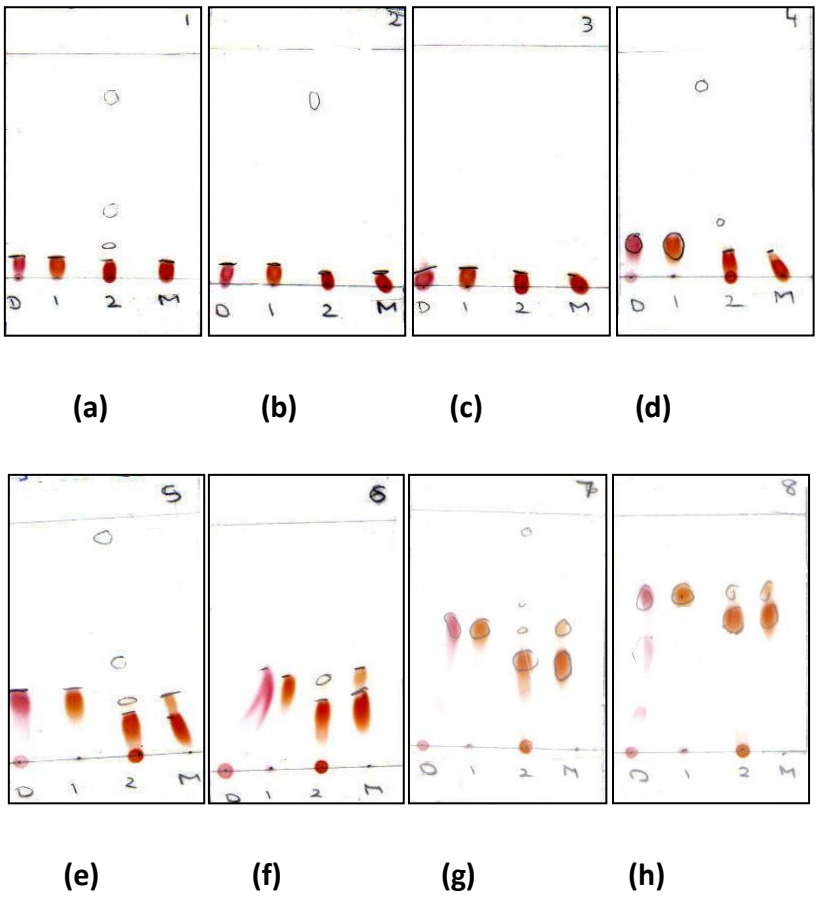

Figure 3.12 Silica TLC plates from the determination of a suitable EtOAc:toluene:acetone solvent system. D = [DCCbs], 1 = [DC-15-seco-Cbs], 2 = [DC-5-seco-Cbs], M = fractions obtained between the clearly defined isomer bands and (a)-(h) are the samples referred to in Table 3.3.

References on page 103

It was concluded that the system needs to be quite polar to observe any migration of bands. In cases where the percentage of acetone was less than that of toluene in the system, minimal migration was observed (Figure 3.12 (a)-(d)). In cases where acetone constituted more than 20% (v/v) of the solvent system, the migration of the bands was significant, and in some examples good separation of the isomers occurred (Figure 3.12 (e)-(h)); however, there was no evident isolation of unreacted starting material.

A new strategy was then pursued and the TLC procedure was repeated but now on a different stationary phase, alumina. Alumina is known to have increased adsorption power in comparison to silica gel and is better suited for the separation of basic compounds whereas silica is better suited for the separation of acidic and neutral compounds.[7,8] Silica gel particles may also occasionally swell as a result of the solvent system which would decrease the efficiency of separation.[7] TLC analysis using the same ratios of solvents in the mobile phase revealed that the use of alumina plates afforded considerably improved separation.

TLC chromatography on alumina (Figure 3.13) show that the bands migrated up the plate even in the absence of acetone, and in many cases there appeared to be excellent separation of the two isomers (Figure 3.13 (d)-(h)). Once again, however, [DCCbs] continued to co-elute with [DC-15-seco-Cbs], dismissing this solvent system as a potential system for column chromatography. However, a system to successfully separate the secocobester isomers was now known and further work was required for the separation of [DCCbs] and [DC-15-seco-Cbs]. Thus an entirely new system had to be developed and an array of solvents was tested to observe the effect each individual solvent had on the separation of the compounds using both silica and alumina stationary phases.

References on page 103

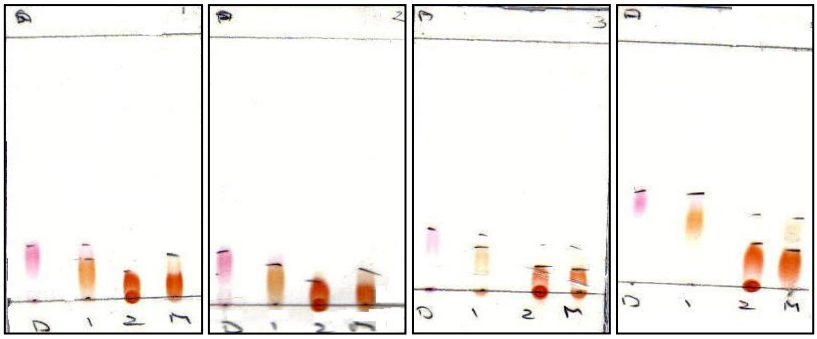

(a) (b) (c) (d)

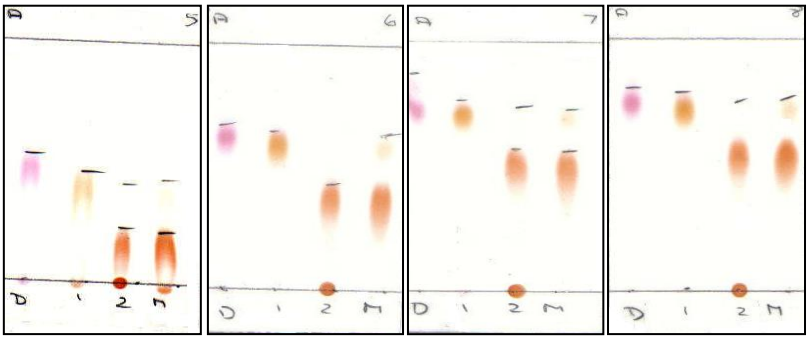

(e) (f) (g) (h)

Figure 3.13 Alumina TLC plates from the investigations of an EtOAc:toluene:acetone solvent system for comparison with silica as a stationary phase. D = [DCCbs], 1 = [DC-15-seco-Cbs], 2 = [DC-5-seco-Cbs], M = fractions obtained between the clearly defined isomer bands and (a)-(h) are the samples referred to in Table 3.3.

Table 3.4 Effect of isocratic solvent systems on the separation of products.

Effect	Solvent
No separation	Toluene, cyclohexane, diethyl ether, Dichloromethane
Good separation	Ethyl acetate, acetonitrile, acetone

Toluene, cyclohexane, diethyl ether and dichloromethane effected no separation and no movement of bands was observed. Ethyl acetate, acetonitrile and acetone showed potential separation of a pink ([DCCbs]) and orange ([DC-15-seco-Cbs]) band, specifically on

References on page 103

alumina plates; however, significant streaking of the bands on both silica and alumina plates was observed, hence a drop of triethylamine (Et_3N) was added to make the bands more compact (Figure 3.14).

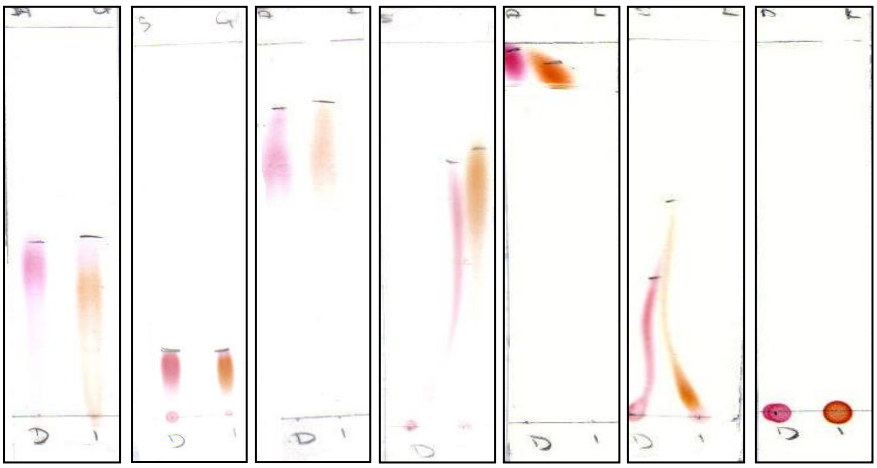

(a.1) **(a.2)** **(b.1)** **(b.2)** **(c.1)** **(c.2)** **(d)**

Figure 3.14 TLC plates from the investigations on the effect of isocratic solvent systems on the separation of products performed on both silica *(marked* .1*)* and alumina *(marked* .2*)* a = ethyl acetate, b = acetone, c = acetonitrile and d = an example of the result obtained from toluene, cyclohexane, diethyl ether and dichloromethane on both alumina and silica. D = [DCCbs] and 1 = [DC-15-seco-Cbs].

Various combinations of solvents were then randomly selected and investigated to optimize the separation afforded by ethyl acetate, acetonitrile and acetone as shown in Table 3.5. Investigations were performed on both silica and alumina TLC plates for comparison.

References on page 103

Table 3.5 Various combinations of solvents investigated.

Sample	Solvent System	Ratio
a	Hexane:toluene:acetone	8:1:3
b	Dichloromethane:toluene:methanol	8:1:2
c	EtOAc:hexane:acetonitrile	10:1:0.5
d	Diethyl ether:EtOAc:methanol	10:2:0.5
e	Hexane:EtOAc	1:1
f	Dichloromethane:hexane	1:1

In cases where the majority of the solvent system was non-polar (example hexane, (3.15 (a))) no movement of bands was observed thus indicating a need for a more polar solvent system. Once again, an alumina stationary phase provided improved separation. Of the six methods attempted, the system comprised of EtOAc:hexane:acetonitrile (10:1:0.5) (Figure 3.15 (c.1)) with a drop of triethylamine was most promising.

References on page 103

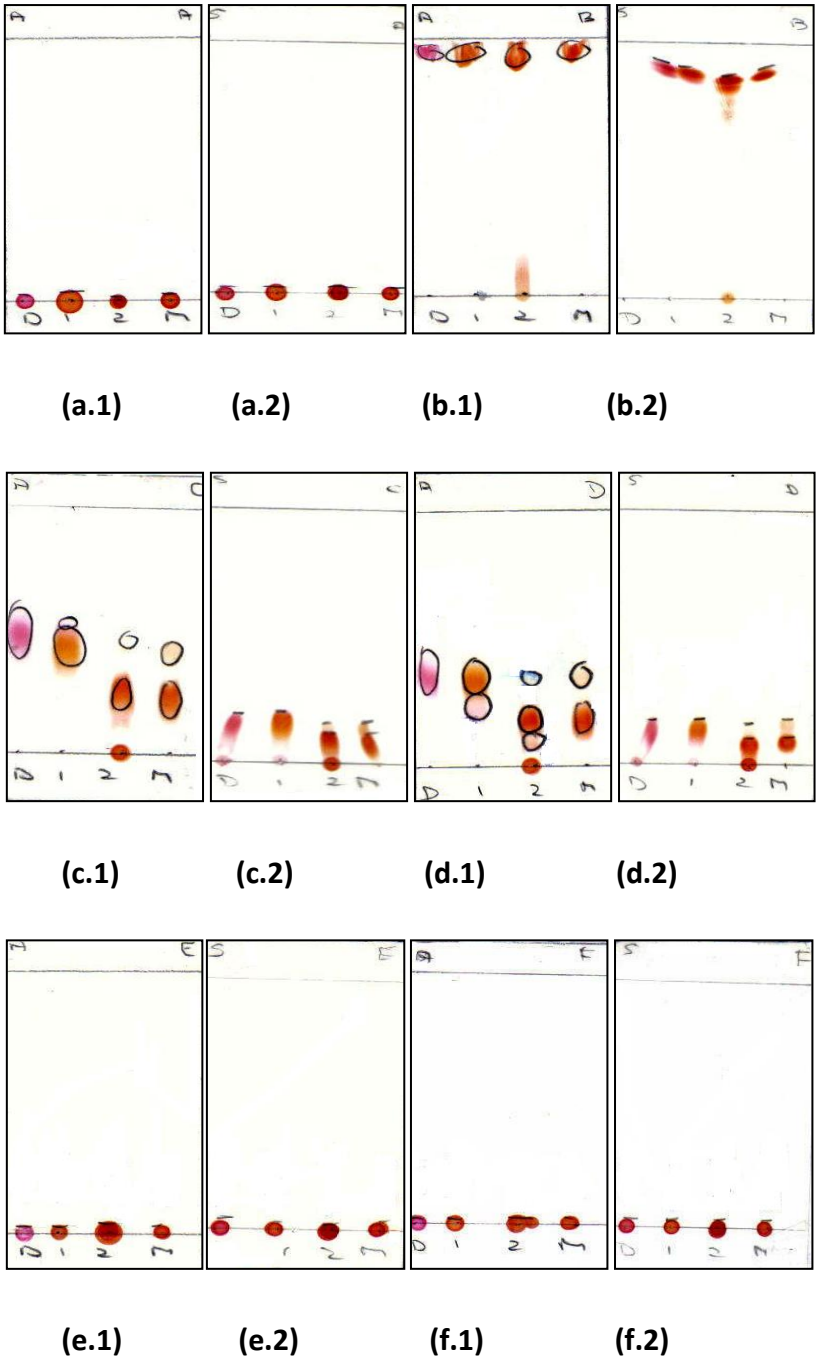

(a.1) **(a.2)** **(b.1)** **(b.2)**

(c.1) **(c.2)** **(d.1)** **(d.2)**

(e.1) **(e.2)** **(f.1)** **(f.2)**

Figure 3.15 TLC plates from investigations into various combinations of solvents performed on both alumina *(marked .1)* and silica *(marked .2)* stationary phases. D = [DCCbs], 1 = [DC-15-seco-Cbs], 2 = [DC-5-seco-Cbs], M = fractions obtained between the clearly defined isomer bands and (a)-(f) are the samples referred to in Table 3.5.

Further work was done to determine the optimum polarity of the system, first by determining the ratio of ethyl acetate to hexane that provided the best separation, followed

References on page 103

by the amount of acetonitrile required to maximize this separation. All investigations were performed on alumina TLC plates.

Table 3.6 Ratios of ethyl acetate to hexane investigated.

Sample	EtOAc	Hexane
a	10	0.01
b	10	0.10
c	10	0.5
d	10	1
e	10	2
f	10	3
g	10	4
h	10	5
i	10	6
j	10	7
k	10	8
l	10	9

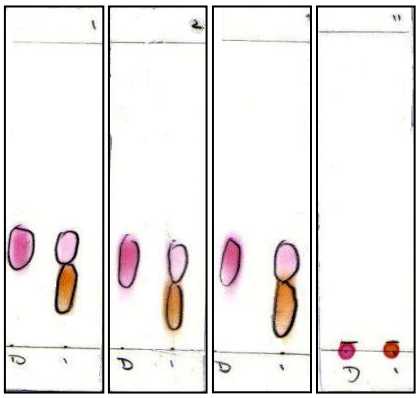

(a) **(b)** **(c)** **(d)**

Figure 3.16 Alumina TLC plates from the investigations of a suitable EtOAc:hexane solvent system. Plates (a), (b) and (c) illustrate examples of the best separation attained. Plate (d) illustrates the general lack of separation when hexane constitutes more than 5% (v/v) of the solvent system.

References on page 103

Investigations showed very good separation between a pink and an orange band in cases where hexane constituted up to 5% (v/v) of the solvent system. Any quantity above 5% (v/v) resulted in minimal migration and subsequent poor separation of bands. As plates (a), (b) and (c) showed good separation, all three solvent systems were then tested further with a variety of ratios of acetonitrile (Table 3.7).

Table 3.7 Ratios of ethyl acetate, hexane and acetonitrile investigated.

Sample	EtOAc	Hexane	MeCN
a	10	0.01/0.10/0.50	0.01
b	10	0.01/0.10/0.50	0.1
c	10	0.01/0.10/0.50	0.5
d	10	0.01/0.10/0.50	1
e	10	0.01/0.10/0.50	2
f	10	0.01/0.10/0.50	5
g	10	0.01/0.10/0.50	8
h	10	0.01/0.10/0.50	10

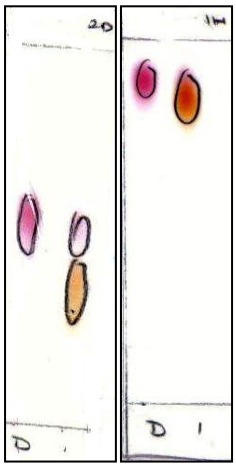

(d) (h)

Figure 3.17 Alumina TLC plates illustrating examples of good separation (d-10:0.1:1.0) and poor separation (h-10:0.1:10) obtained between [DCCbs] (pink) and [DC-15-seco-Cbs] (orange).

References on page 103

In all cases, good separation of the bands was observed when acetonitrile constituted up to 10% (v/v) of the solvent system (Table 3.7 (a), (b), (c) and (d)), after which the degree of separation decreased significantly.

A solvent system comprising of EtOAc:hexane:MeCN (10:0.10:1.0) (Figure 3.17 (d)) showed the highest degree of separation, as one can see a distinct separation between [DCCbs] and [DC-15-seco-Cbs]. Several of the TLC plates were then re-run, each with an increasing volume of triethylamine in an attempt to minimize streaking and subsequently improve separation.

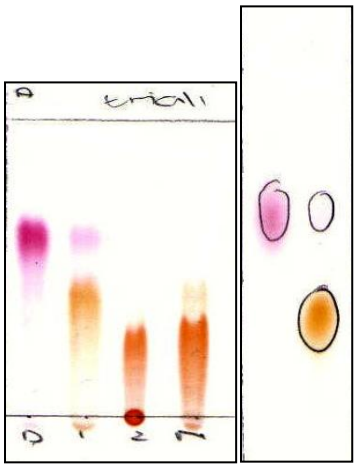

Figure 3.18 Alumina TLC plates indicating the effect of triethylamine (5% (left) and 10% (right) of the entire volume of the solvent system) on the streaking of bands observed when an EtOAc:hexane:MeCN (10:0.1:1.0) system was used.

Thus a quartenary system of EtOAc:hexane:MeCN+Et_3N (10:0.1:1+10%) was established for column chromatography. The photo-oxygenation products were then transferred to a column (23.0 × 2.0 cm) containing aluminium oxide (25.0 g). The compounds were separated using the quartenary solvent system; however, HPLC analysis of the fractions showed that traces of [DCCbs] were still present in most fractions, and that there has been only partial separation of the secocobester isomers (Figure 3.19). Therefore all attempts to separate the compounds by column chromatography proved unsuccessful.

References on page 103

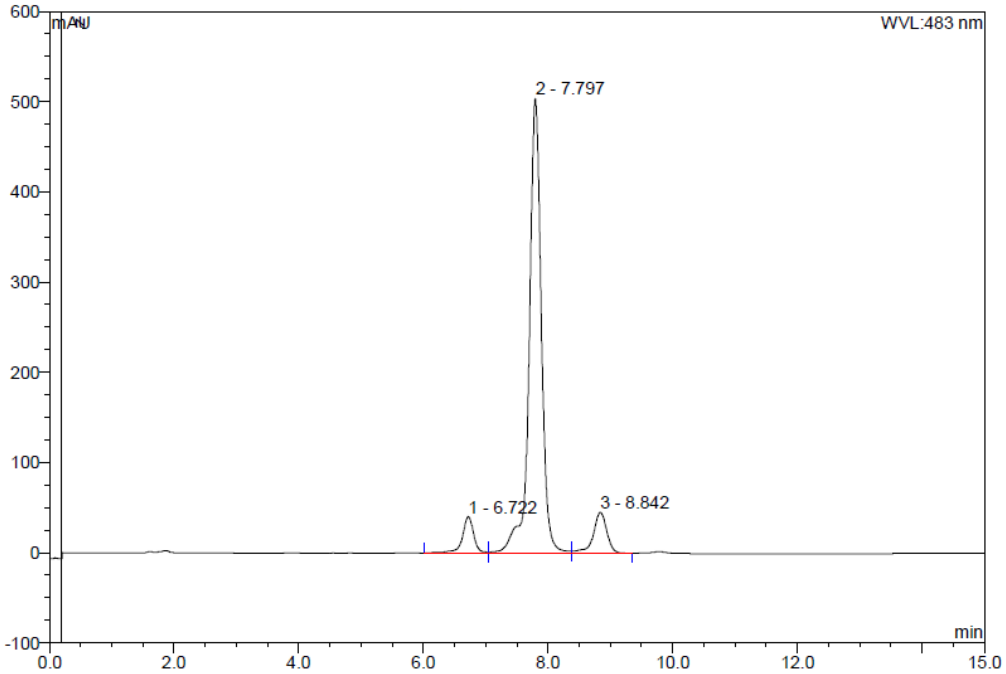

Figure 3.19 HPLC chromatogram illustrating the inefficient separation of compounds after column chromatography. Peak 1 = [DC-5-seco-Cbs] (6.4%), peak 2 = [DC-15-seco-Cbs] (85.1%) and peak 3 = [DCCbs] (8.5%).

3.2.2.3 Separation Route B

In a different approach, we attempted to separate the photolysis mixture using a modified version of the procedure developed by Kräutler for the separation of the photo-oxidation products.[6] Following photo-oxidation, the contents of the photolysis cell were dried *in vacuo*, transferred to a column and separated according to the flash column chromatography method developed in Separation Route A involving an EtOAc:MeOH:toluene (10:0.25:0.25) eluent system. Each fraction was analysed according to colour by UV-vis spectroscopy as well as by TLC. This allowed the fractions to be categorised into three groups: the purple fractions containing mostly [DCCbs], red fractions containing mostly [DC-15-seco-Cbs] and orange fractions containing mostly [DC-5-seco-Cbs]. The pooled fractions were applied onto individual preparative thin layer chromatography silica plates and separated using a methyl acetate:benzene (4:1) mobile phase.

References on page 103

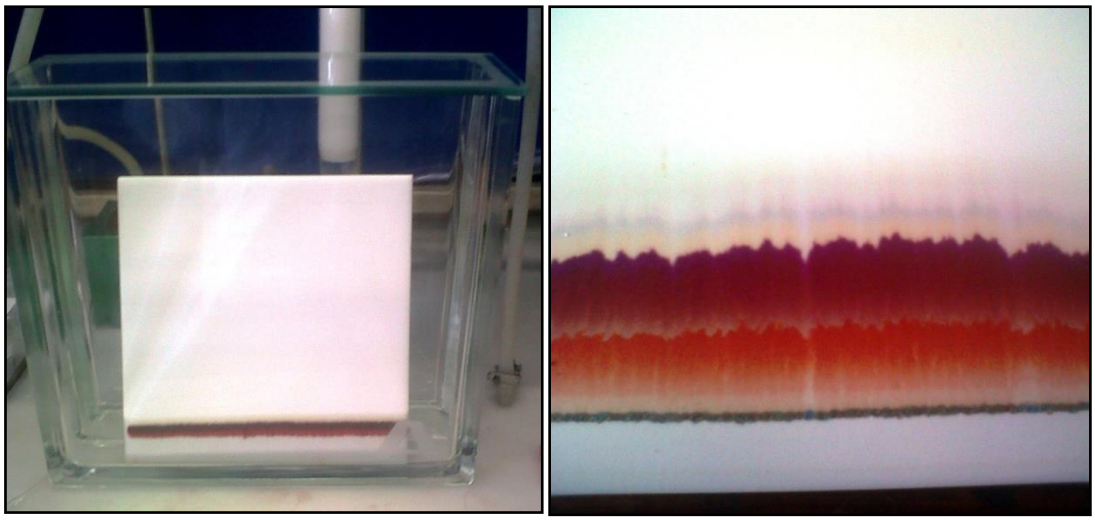

Figure 3.20 The development of a preparative thin layer chromatography silica plate in a tank containing a methyl acetate:benzene (4:1) solvent system. Evident separation of an orange, red and purple band can be observed (right).

Once separated, each individual band was scraped off and eluted with a dichloromethane:methanol (10:1) solvent system by continuously washing the silica particles with the solvent mixture until the silica particles were white again. The residues were then dried under vacuum and re-dissolved in dichloromethane and filtered through a cotton wool plug to remove any silica particles that may have previously dissolved in methanol. To remove any possible impurities, the compounds (still dissolved in approximately 20.0 ml dichloromethane) were shaken with a solution of $NaHCO_3$ (20.0 ml) containing NaCN (20.0 mg, 0.408 mmol); the organic layer was separated and the solvent was evaporated.

The remaining [DCCbs] was therefore re-isolated but the [DC-5-seco-Cbs] required a final purification step. [DC-5-seco-Cbs] was dissolved in a solution of dichloromethane (0.5 ml) and benzene (1.0 ml) and precipitated by adding the solution to a beaker containing cyclohexane (25.0 ml). The precipitate formed was too fine to be filtered and as a result the solution was centrifuged at 4000 revolutions per minute for 10 minutes to isolate the precipitate particles. The secocobester settled as a red film along the bottom of the centrifuge tubes. The supernatant was then centrifuged again to ensure all products have been removed. The precipitate, which was scraped out as a fine orange powder was then

References on page 103

dried on a high-vacuum line. The UV-vis spectrum recorded in methanol indicated that the principal bands in [DC-5-seco-Cbs] occur at 326 and 480 nm, which is in agreement with the observations recorded by Kräutler.[6] Purity was assessed by HPLC (acetonitrile/water) (Figure 3.21) which indicated a single peak at a retention time of 6.84 minutes, hence proving the combination of column and preparative thin layer chromatography was successful for the isolation and purification of [DC-5-seco-Cbs]. [DC-5-seco-Cbs] was prepared in a 42% yield, which compares favourably to a 47% yield reported by Kräutler for the same reaction.[6]

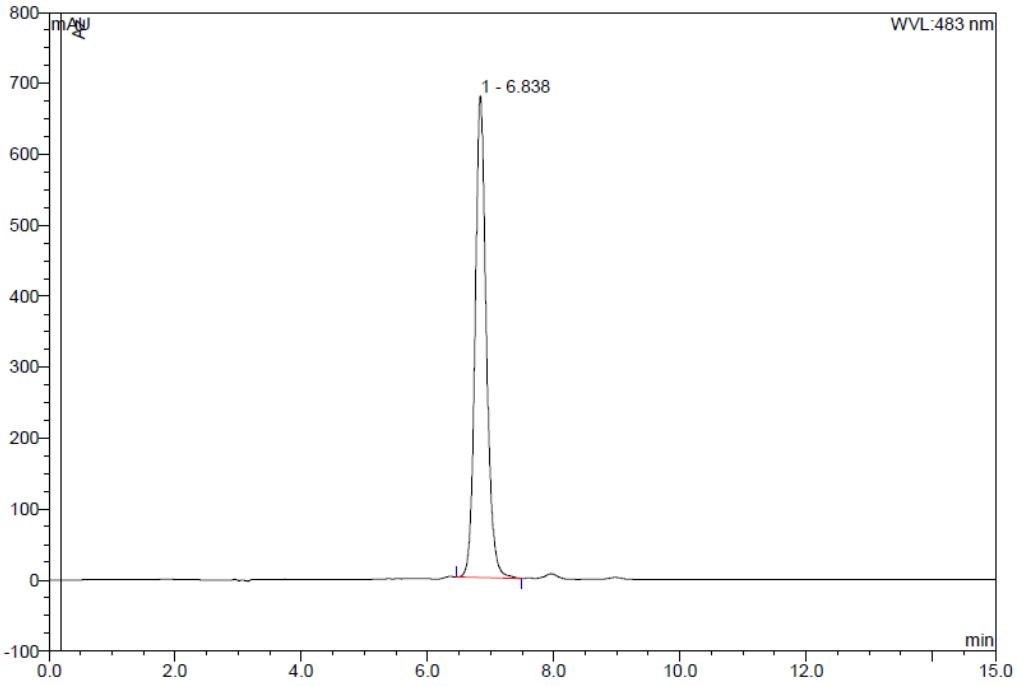

Figure 3.21 HPLC chromatogram of purified [DC-5-seco-Cbs] with a retention time of 6.84 minutes indicating 100% purity.

Positive mode ESI-MS was used to verify the molecular mass of [DC-5-seco-Cbs]. The molecular ion ($C_{54}H_{73}CoN_6O_{16}$) was expected at 1120.65 and was detected at 1120.45 at very low intensity. The secocobester also showed peaks that are consistent with the loss of one or both axial cyanide ligands, the facile loss of which is observed in many cobesters (1094.44 – $(M–CN)^+$, $C_{53}H_{73}CoN_5O_{16}$; (calc. 1095.09) and 1068.43 – $(M–2CN+H)^+$, $C_{52}H_{73}CoN_4O_{16}$; (calc. 1069.07)).[1,9] This observation indicated that [DC-5-seco-Cbs] was successfully synthesised, as these are the same values obtained by Kräutler for the loss of one or both axial cyanides.[6] This is also very similar to Inhoffen's work on [DC-5-seco-Cbs] in

References on page 103

which peaks at 1068 $(M–2CN+H)^+$ and 1094 $(M–CN)^+$ were obtained.[10] The characteristic $(M + Na)^+$ peak typically observed in positive mode spectra was also detected (1143.44). Selected mass spectra can be found in **Appendix D.3**.

The FTIR spectrum of a solid sample of [DC-5-seco-Cbs] was obtained and compared to literature values as well as to other similar structures, [DCCbs] and [DCSYCbs].[1]

A small amount of water was observed at 3442 cm^{-1} which is consistent with the water of crystallisation observed with [DCCbs] and [DCSYCbs].

The C≡N stretch detected at 2124 cm^{-1} is invaluable for information on the corrin macrocycle. Cyanide is an unusual ligand in that the frequency of the stretch increases on coordination to the cobalt ion, compared to free cyanide ligand (2078 or 2080 cm^{-1}).[11,12] Based on ^{59}Co data, it has been suggested that an increase in the extent of electron delocalisation within the corrin ring causes a stronger *cis* interaction between cobalt and the corrin macrocycle; in other words, increasing π-electron density in the corrin improves Co-corrin orbital overlap and strengthens the bonding between the metal and the macrocycle. As a result, the frequency of coordinated cyanide shifts to a lower frequency, i.e. begins to approach the stretching frequency of free cyanide (for example, ν_{CN} = 2122 cm^{-1} for the more delocalised [DCCbs] but 2138 cm^{-1} for [DCSYCbs]). The stretch observed for [DC-5-seco-Cbs] at 2124 cm^{-1} (cf. 2122 cm^{-1} for [DCCbs]) shows only a minimal downfield shift on cracking of the corrin ring, indicative of a decrease in the strength of the interaction between the cobalt ion and the corrin ring. Surprisingly, the effect on this interaction is however very much smaller than in [DCSYCbs].

Other characteristic peaks such as the C=O ester stretch, and aliphatic and aromatic C-H stretches are all consistent with literature for [DC-5-seco-Cbs].[6] The signal for the C=O stretch at C5 would occur at a lower frequency than the ester signals, but it is obscured by them. Selected FTIR spectra and assignments can be found in **Appendix E.3**.

Using a combination of one-dimensional and two-dimensional experiments, the ^1H and ^{13}C NMR assignments were possible using a previously published strategy.[13] The signals corresponding to the axial cyanide ligands were detected at 131.79 and 135.43 ppm. The small difference between the two cyanide ligands is because each cyanide has a unique

References on page 103

magnetic resonance due to the different chemical environments in which they are located. By analogy with reports on [DCSYCbs], the cyanide in the β position will experience a higher degree of steric hindrance than the cyanide in the α position, hence it is more shielded.[1] Thus the signal at 131.79 ppm is tentatively attributed to the β cyanide and the signal at 135.43 ppm to the α cyanide.

Numerous characteristic signals were compared to data obtained by Inhoffen to assess the identity of the secocobester synthesised.[10] The C signals for the carbons bonded to the nitrogen atoms of the corrin ring occurred between 161 – 188 ppm, and the methyl groups bound to C5 and C15 were detected at 21 and 15.2 ppm, respectively. Spectral crowding due to the numerous methylene and ester groups was observed in the region between 20 – 40 ppm and 50 ppm, respectively. The C10–H signal was detected 94.04 ppm. C5 and C15 gave signals at 196 and 106 ppm, respectively. The data corresponds well with that reported by Inhoffen with some minor shifts observed due to the varying solvent magnetic susceptibility. The NMR data provides good evidence that the product produced was indeed [DC-5-seco-Cbs].

The data also corresponds well to the data for [DCSYCbs]. However, it is worth noting that the C5 and C15 signals were detected at 79.04 and 100.74 ppm, respectively. As the C15 signals in both corrins range between 100 – 106 ppm, this provides conclusive evidence that it is indeed the [DC-5-seco-Cbs] isomer and not the [DC-15-seco-Cbs] isomer, because if this was the case, the C5 signal would not have shifted significantly downfield. The NMR spectra and assignments can be found in **Appendix F**.

3.2.2.4 15-Seco-Dicyanocobester

The [DC-15-seco-Cbs] isomer proved far more problematic in terms of isolation. After separation by column chromatography followed by preparative thin layer chromatography as done with [DC-5-seco-Cbs], HPLC analysis showed that [DCCbs] was still present. Therefore, [DC-15-seco-Cbs] could not be fully isolated even after multiple repetitions of preparative thin layer chromatography and because of this, work in this project was focused on the [DC-5-seco-Cbs] only.

References on page 103

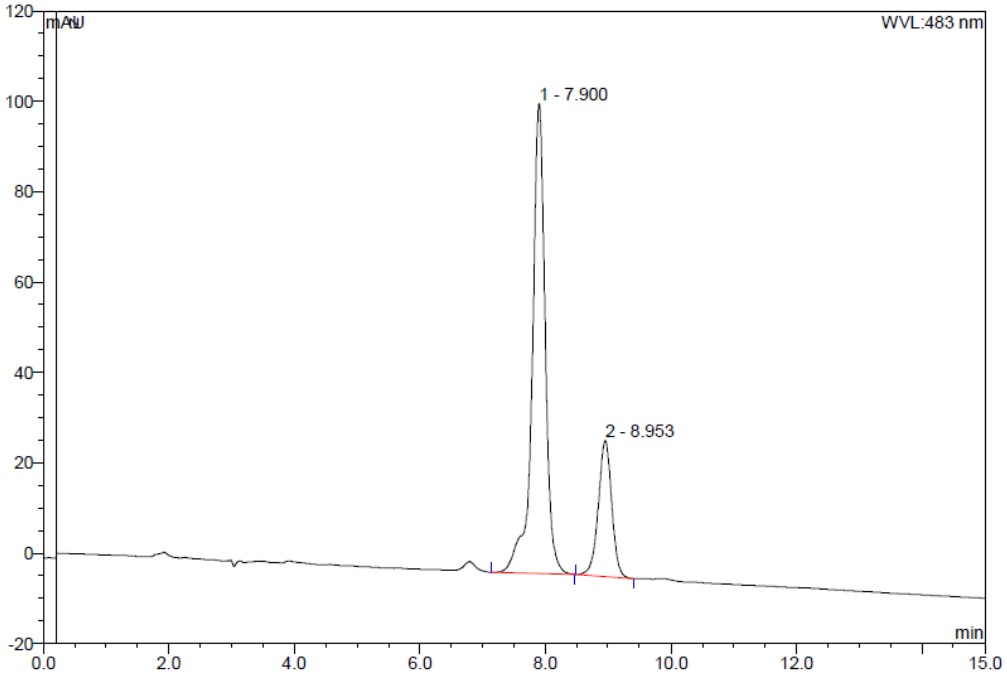

Figure 3.22 HPLC chromatogram of [DC-15-seco-Cbs] (peak 1, 77.0%) contaminated with [DCCbs] (peak 2, 23.0%).

3.2.2.5 Synthesis of Heptamethyl Coα,Coβ-aquacyano-5,6-dioxo-5,6-secocob(III)yrinate (5-seco-Aquacyanocobester, [AC-5-seco-Cbs]$^{+}$)

Two methods were investigated for the conversion of [DC-5-seco-Cbs] to the aquacyano form, [AC-5-seco-Cbs]$^{+}$.

The first attempt was based on the procedure described by Chemaly *et al.*[1] (Chapter 3.2.1.2) in which the dicyanosecocobester was dissolved in methanol, to which glacial acetic acid was added to lower the pH of the solution to 3. The acidic solution was then subjected to a slow stream of nitrogen and stirred for 24 hours. The attempt, however, proved unsuccessful. The conversion procedure was monitored by UV-vis spectroscopy and after 24 hours only a 3 nm shift in the absorption wavelength was observed. The reaction was then allowed to continue for a further 24 hours which afforded no further change in the absorption spectrum. This aquacyano preparation procedure is therefore unsuitable for cleaved corrin rings.

References on page 103

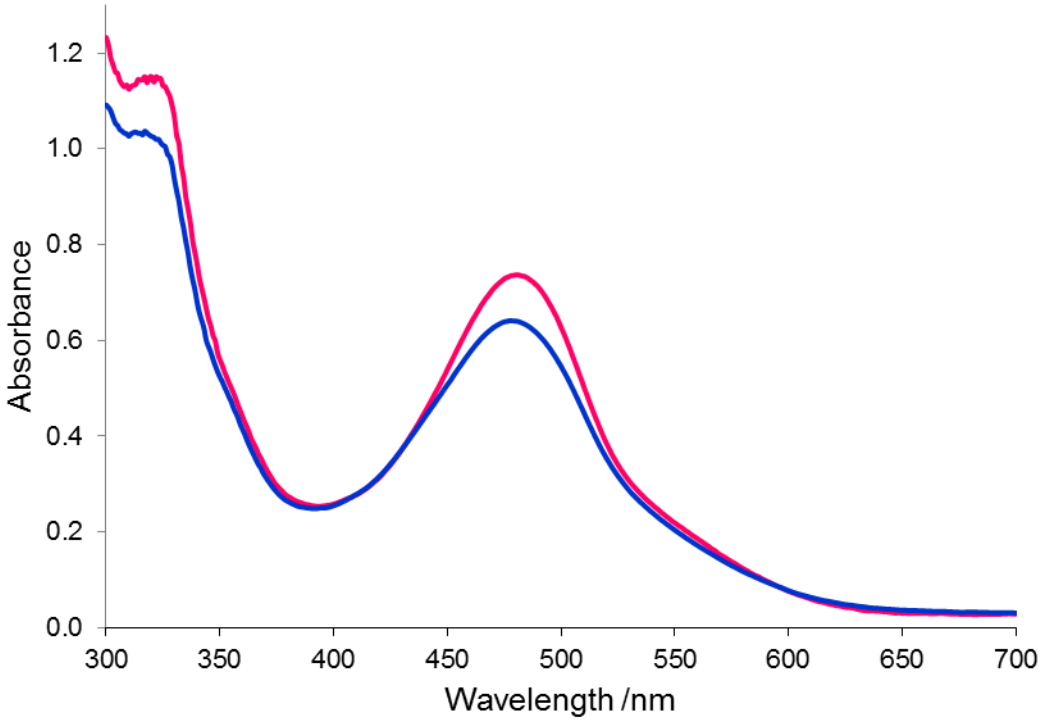

Figure 3.23 UV-vis spectrum of [DC-5-seco-Cbs] at reaction t = 0 minutes (pink) and after 24 hours (blue) from the unsuccessful aquacyano synthesis attempt.

The second synthetic procedure attempted was a modification of a method developed by Palet *et al.*[14] for the removal of axially coordinated cyano groups from dicyanocobalt(III)heptapropylcobyrinate and dicyanocobalt(III)heptamethylcobyrinate. During the procedure, [DC-5-seco-Cbs] was dissolved in methanol (10.0 ml) and transferred to a round bottom flask to which glacial acetic acid was added to achieve a 10% (v/v) acetic acid solution whilst stirring. The solvent was then evaporated *in vacuo* and the UV-vis spectrum recorded to monitor the reaction, after which the residue was re-dissolved in the 10% acetic acid solution. The procedure was repeated typically between 4 – 6 times until the UV-vis spectrum no longer changed, and this approach proved successful. As the conversion proceeded, the principal bands blue shifted from 480 nm to 460 nm, respectively, (Figure 3.24) as the colour changed from red-orange to an orange-brown, after which no further change in the absorption wavelength was observed, indicating a complete conversion of dicyanosecocobester to aquacyanosecocobester. As with $[ACCbs]^+$, the $[AC\text{-}5\text{-}seco\text{-}Cbs]^+$ was then dried on a high-vacuum line. The purity of the product was

References on page 103

assessed by HPLC (Figure 3.25) wherein a single peak with a retention time of 8.32 min was detected.

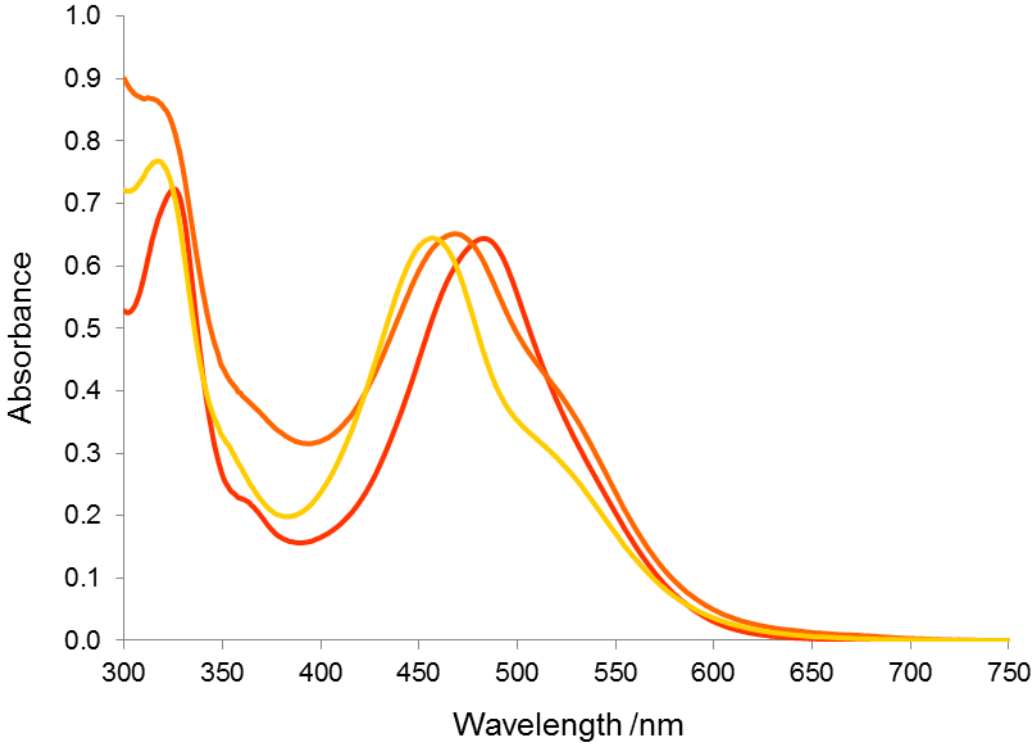

Figure 3.24 UV-vis spectra illustrating the successful conversion of [DC-5-seco-Cbs] to [AC-5-seco-Cbs]$^{+}$ from the start of the reaction (red), half way through the conversion (orange) and at the end of the conversion (yellow) run in methanol.

References on page 103

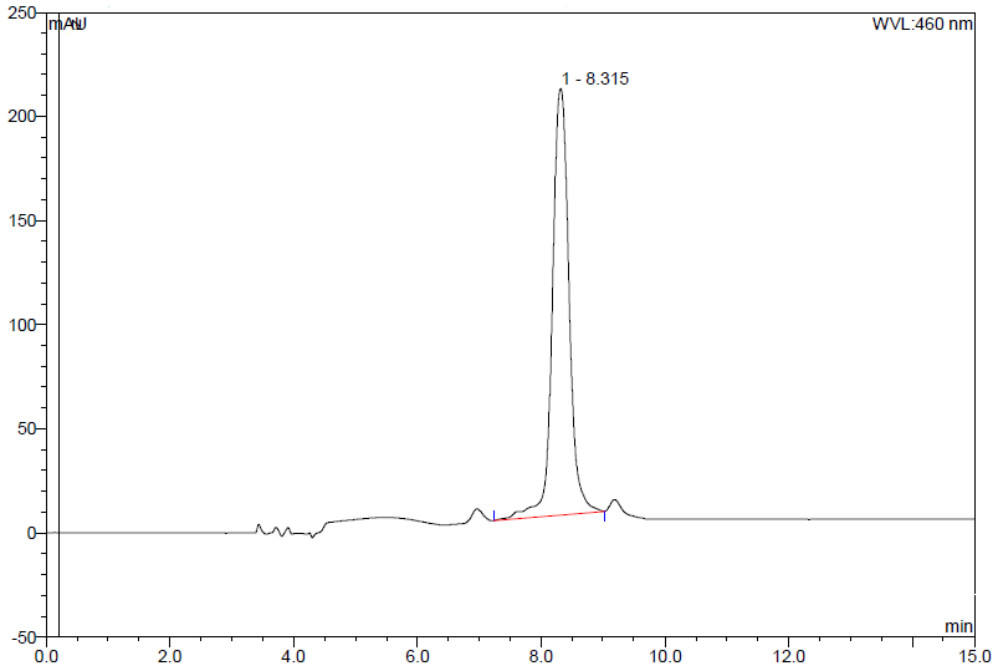

Figure 3.25 HPLC chromatogram of $[AC\text{-}5\text{-}seco\text{-}Cbs]^+$ with a single peak at a retention time of 8.32 minutes, together with two small peaks occurring at 7.8 and 9.2 minutes, corresponding to the spontaneous formation of the diaqua and dicyano species, respectively, in solution.

FTIR and ESI mass spectra were recorded to ensure that the diaqua compound, in which both cyanide ligands have been replaced by a water molecule, had not formed.

The ESI mass spectrum was recorded in the positive mode. The molecular ion peak ($C_{53}H_{75}CoN_5O_{17}$) was detected at 1112.11 at low intensity. Characteristic peaks detected at 1094.38 and 1068.37 correspond to the facile loss of the axial ligands $(M\text{-}H_2O)^+$, $C_{53}H_{73}CoN_5O_{16}$; (calc. 1095.09) and $(M\text{-}H_2O\text{-}CN+H)^+$, $C_{52}H_{73}CoN_4O_{16}$ (calc. 1069.07), respectively, thus confirming that it was indeed the $[AC\text{-}5\text{-}seco\text{-}Cbs]^+$ that was formed. Selected mass spectra can be found in **Appendix D.4**.

The success of the reaction was further confirmed by FTIR (Figure 3.26) in which the peak corresponding to the stretching frequency of cyanide (2091 cm^{-1}) was preserved, albeit at a lower frequency. The FTIR spectrum also proves the correct product has been formed as

References on page 103

the spectrum does not change from the initial [DC-5-seco-Cbs] spectrum with the exception of the cyanide signal. Selected FTIR spectra can be found in **Appendix E.4**.

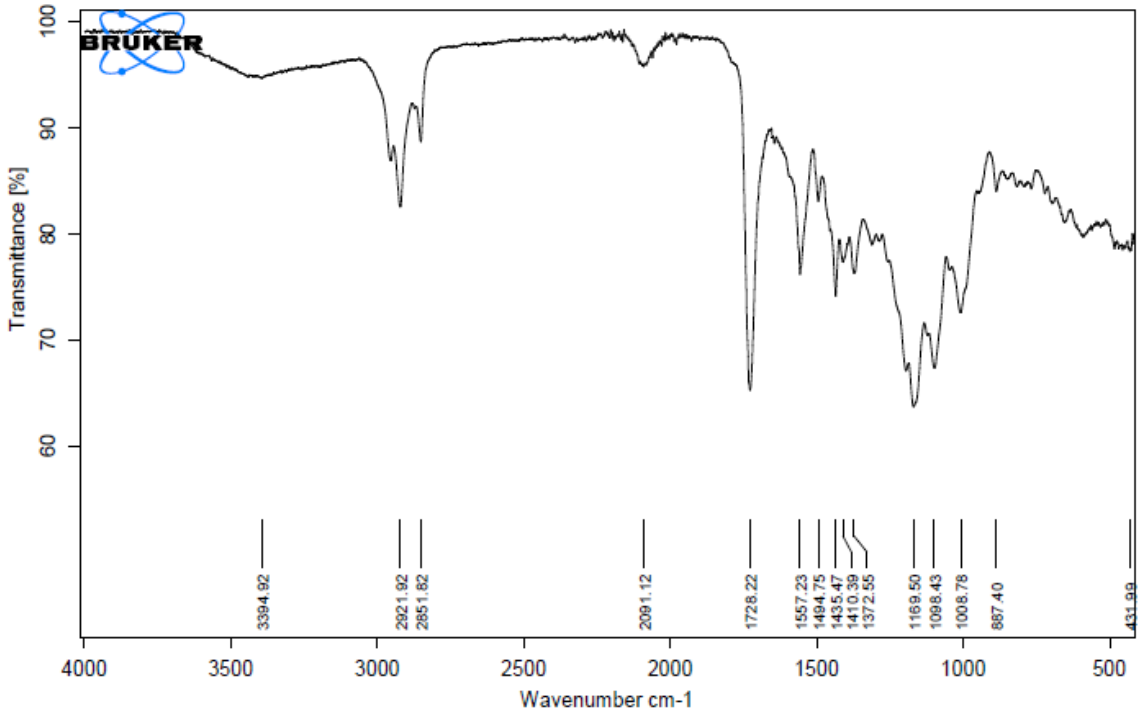

Figure 3.26 The FTIR spectrum of $[AC\text{-}5\text{-}seco\text{-}Cbs]^{+}$ indicating the presence of a cyanide signal at 2091 cm^{-1}.

3.2.3.1 Synthesis and Characterisation of Hexamethyl Coα,Coβ-dicyano-7-de-(carboxymethyl)-7,8-didehydrocob(III)yrinate (Dicyanopyrocobester)

The pyrolysis procedure for the synthesis of dicyanopyrocobester was adapted from a method previously reported by Inhoffen.[15,16] Dicyanocobester (500 mg, 459 µmol) was added to decalin (25.0 ml), stirred and refluxed at 190 ^{o}C for 45 minutes in a dark room under dim red light. [DCCbs] is insoluble in decalin at room temperature, but dissolved upon heating as the colour of the reaction mixture changed from purple to brown. After cooling to room temperature, subsequent extraction into methanolic HCN (25 ml) resulted in a colour change from brown to green. The UV-vis spectrum (Figure 3.27) showed a large hypsochromic shift when compared to [DCCbs], hence indicating the lengthening of the corrin chromophore by the formation of a new double bond between C7 and C8

References on page 103

accompanied by the formal elimination of a methyl acetate, with bands observed at 710, 676, 368 and 329 nm in methanol.[16]

TLC of the crude product revealed a green band (the required product), followed by a purple band ([DCCbs]) and numerous green bands.[15] Purification of dicyanopyrocobester proved to be extremely difficult due to its high sensitivity to both air and light,[17] thus making traditional separation and purification attempts virtually impossible to use. Inhoffen reported successfully purifying dicyanopyrocobester through a combination of preparative thin layer (silica gel 60 and dichloromethane:methanol (+ HCN) (97:3) eluent) and flash column chromatography (silica gel 60 and dichloromethane:methanol (+ HCN) (98:1.5) eluent). However, as the developed plate was left to dry during PTLC, the green bands appeared to turn black. The same was observed during flash column chromatography, as well as in any attempt to dry the product i*n vacuo*.

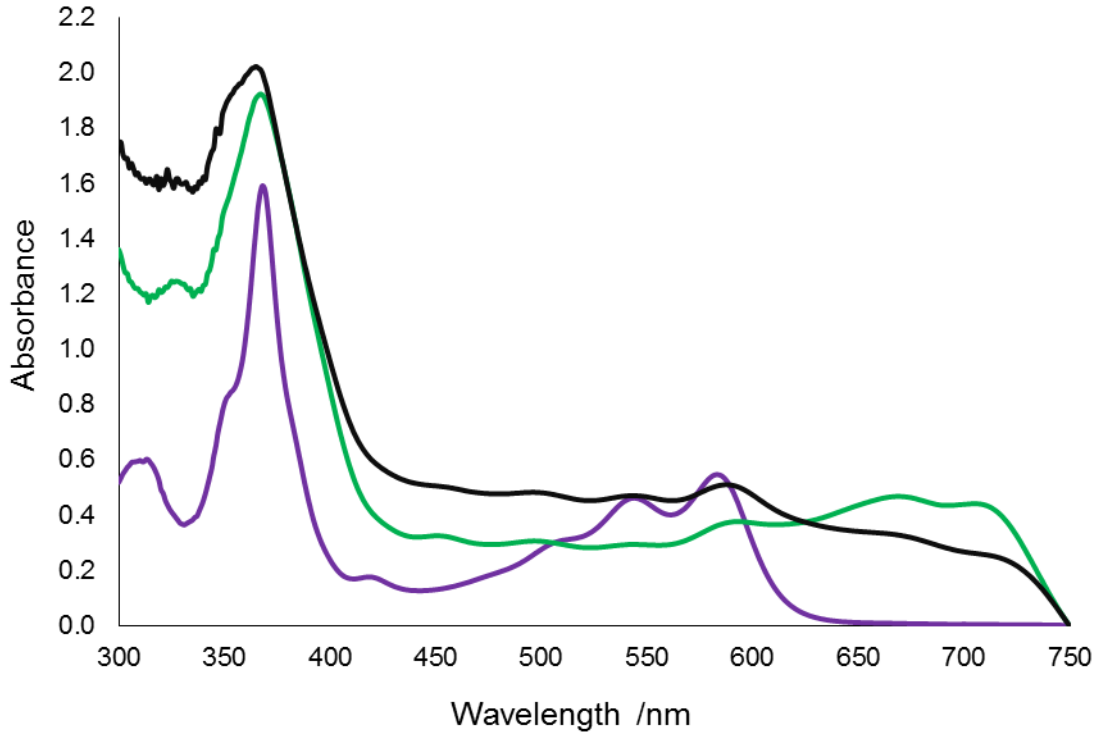

Figure 3.27 UV-vis spectra of [DCCbs] (purple), dicyanopyrocobester (green) and the decomposed product after exposure to air and light (black).

References on page 103

Figure 3.28 PTLC plate for the purification of dicyanopyrocobester in a dichloromethane: methanol (97:3) eluent.

Stability tests were performed to assess the pyrocobester's sensitivity to air and light by exposing some samples to air, some to light and some to both air and light. The formation of a black solution suggested decomposition of the compounds in less than an hour; however the rate of decomposition was enhanced by the presence of light. It was then decided to expose the pyrocobester to glacial acetic acid, which is a key reagent in the conversion to the aquacyano form in the subsequent synthetic step, which resulted in a black solution as well, thus rendering this compound an unfeasible option for solution chemistry work.

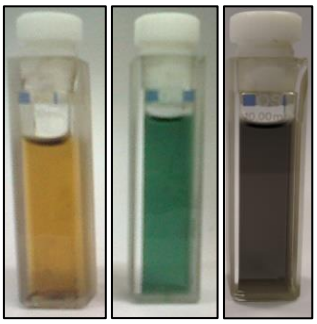

Figure 3.29 A photograph showing the brown coloured solution after completion of the reflux procedure (left), a green solution obtained after the extraction procedure (middle) and a black solution obtained after exposure to air, light and acid (right).

References on page 103

3.3 Conclusions

The main reagent in this study, dicyanocobester was successfully synthesised according to the procedure set out by Werthemann. [DC-5-seco-Cbs] was also successfully synthesised according to the photolysis procedure set out by Kräutler, for which a novel purification method was developed. The isomer, [DC-15-seco-Cbs], could not be purified or isolated without trace amounts of [DCCbs]; consequently no further work was performed on [DC-15-seco-Cbs]. Dicyanopyrocobester, although successfully synthesised, could not be purified due the sensitivity to both air and light as well as a key reagent in the conversion to the aquacyano form. As a result, efforts into developing a purification method suitable for an air and light sensitive compound were not pursued. The dicyano complexes were also successfully converted to the aquacyano forms for further solution chemistry investigations. All synthetic attempts and subsequent chromatography were repeated several times with reproducible yields and consistent purity. All synthesised compounds were characterised by UV-vis spectroscopy, HPLC, TLC, IR, NMR and mass spectrometry.

References on page 103

REFERENCES FOR CHAPTER 3

1. Chemaly, S. M.; Brown, K. L.; Fernandes, M. A.; Munro, O. Q.; Grimmer, C.; Marques, H. M. *Inorg. Chem.* **2011**, 50, 8700-8718.
2. Werthemann, L. PhD, ETH, Zürich, 1968.
3. Markwell, A. J.; Pratt, J. M.; Shaikjee, S. S.; Toerien, J. G. *J. Chem. Soc.; Dalton Trans*. **1987**, 1349-1357.
4. Hamza, M. S. A. *J. Inorg. Biochem*. **1998**, 69, 269-274.
5. Kraemer, T. Zelder, F. *Anal. Methods* **2015**, 7, 9707-9712.
6. Kräutler, B. *Helv. Chim. Acta.* **1982**, 65, 1941-1948.
7. Skoog, D. A.; West, D. M. In *Fundamentals of Analytical Chemistry*; Thomson Learning Inc., Belmont, 1982, pp 482, 680-682.
8. Armarego, W. L. F.; Chai, C. In *Purification of Laboratory Chemicals*; Elsevier, Oxford, 2009, pp 18-27.
9. Schiebel, H. M.; Schulten, H. R. *Mass Spectrom. Rev.* **1986**, 5, 249-311.
10. Hinze, R. P.; Schiebel, H. M.; Laas, H.; Heise, K. P.; Gossauer, A.; Inhoffen, H. H.; Ernst, L.; Schulten, H. R. *Liebigs Ann. Chem*. **1979**, 6, 811-828.
11. Tsubaki, M.; Yoshikawa, S. *Biochemistry* **1993**, 32, 164-173.
12. Boffi, A.; Chiancone, E.; Takahashi, S.; Rousseau, D. L. *Biochemistry* **1997**, 36, 4505-4509.
13. Brown, K. L. In *Chemistry and Biochemistry of B_{12}*; Banerjee, R. Ed.; John Wiley & Sons, Inc., New York, 1999, pp 197-237.
14. Palet, C.; Munoz, M.; Daunert, S.; Bachas, L. G.; Valiente, M. *Anal. Chem.* **1993**, 65, 1533-1536.
15. Ernst, L.; Holze, G.; Inhoffen, H. H. *Liebigs Ann. Chem.* **1981**, 198-201.
16. Ernst, L.; Holze, G. *Liebigs Ann. Chem*. **1982**, 118-120.
17. Kräutler, B.; Stepanek, R.; Holze, G. *Helv. Chim. Acta*, **1983**, 66, 44-49.

CHAPTER 4

ACID DISSOCIATION OF COORDINATED H_2O

4.1 Introduction

Axially coordinated water in similar corrin complexes such as $[ACCbs]^+$ and aquacobalamin (B_{12a}, $[H_2OCbl]^+$) dissociates as illustrated in Equation 4.1.

$$[CN–Co–H_2O]^+ \rightleftharpoons [CN–Co–OH] + H^+$$

[Equation 4.1]

It is imperative to know the value of the dissociation constant to allow for adjustments to be made in both ligand binding and kinetic investigations in order to obtain pH-independent equilibrium and rate constant values. This is especially important when a proton is removed from the axial water group at high pH, resulting in the formation of a hydroxocyanocobester complex which is inert to substitution reactions.[1,2,3]

As has been noted,[1] the determination of the pK_a of $[ACCbs]^+$ is difficult. The pK_a is significantly higher than the pK_a of H_2O in either aquacobalamin, 7.76 (i.e., H_2O *trans* to DMBz nucleotide base);[4] or diaquacobinamide, 5.9 (H_2O *trans* to H_2O)[5], and, estimated at > 11[1] and ca. 10.8,[6] similar to the pK_a of aquahydroxocobinamide, 10.3 (H_2O *trans* to OH^-),[5] or aquacyanocobinamide, 11.0[7,8] (H_2O *trans* to CN^-). The difficulty in the determination of the pK_a arises because of hydrolysis of one or more of the methyl ester side-chains,[9,10] a reaction whose rate increases with pH and with temperature.[1]

In this study, the pK_a's of $[ACCbs]^+$ and $[AC\text{-}5\text{-}seco\text{-}Cbs]^+$ were determined as a function of temperature from the spectroscopic changes accompanying the changes in pH so as to ensure the results were obtained under the same experimental conditions.

References on page 120

4.2 Results and Discussion

4.2.1 pK_a Determination of $[ACCbs]^+$

The titration procedure for the spectrophotometric determination of the acid dissociation constant was described previously (Section 2.4.2).[11,12] The pK_a value was determined by titrating $[ACCbs]^+$ in an aqueous multi-component buffer with negligible volumes of H_2SO_4 and NaOH between pH ca. 5.5 and 12.5, following the reaction by UV-vis spectroscopy with the spectrum recorded between 300 nm and 750 nm at each value of pH.

Figure 4.1 shows the spectral changes associated with the titration of $[ACCbs]^+$ with OH^- at 10 ^oC where the rate of hydrolysis of the side changes is expected to be relatively slow.

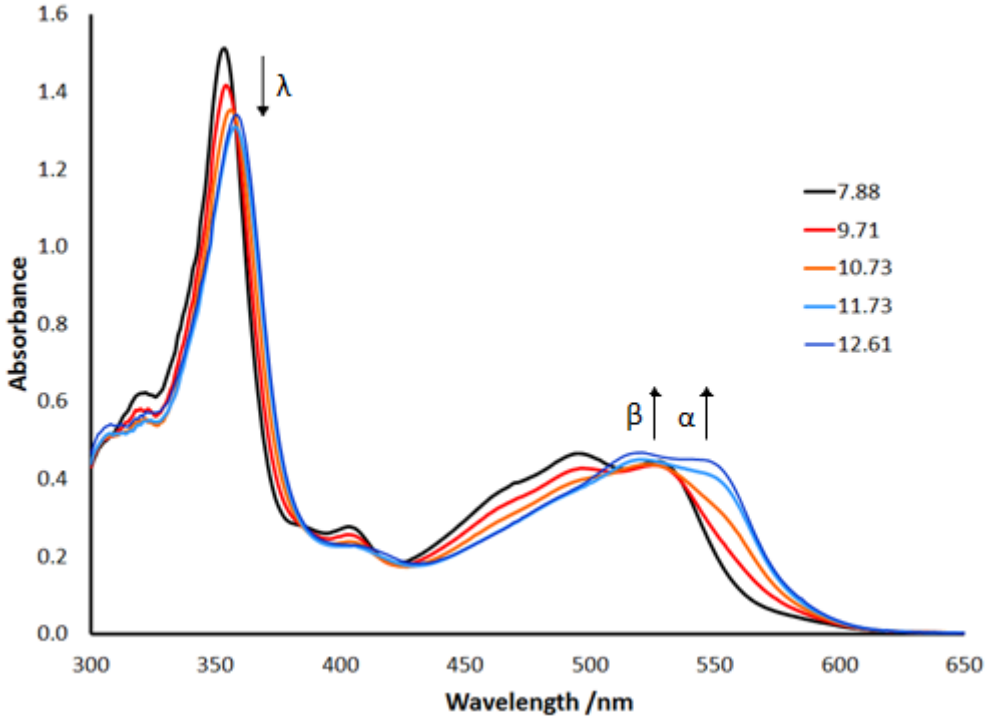

Figure 4.1 Dependence of the UV-vis spectra of $[ACCbs]^+$ on pH at 10 ^oC. The pH value at which each spectrum was recorded is given in the insert to the figure.

As pH is increased, the γ band decreases in intensity and moves to longer wavelengths; the αβ bands also move to the red. These spectral changes are very similar to those seen on deprotonation of Co(III)-bound H_2O in all aqua Co(III) corrins.[4,5,7,8] However, isosbestic points are not well defined in Figure 4.1. Moreover, at pH > ca. 11, the spectra change

References on page 120

slowly with time and the αβ bands move pronouncedly to longer wavelengths. These effects are more marked as temperature is increased and become quite rapid at pH > 10.5 and T > 35 ^{o}C.

Figure 4.2 shows a plot of the change in absorbance as a function of pH at 560 nm. The change in absorbance was fitted to an ionisation isotherm (Equation 2.1) relevant when only one acid/base equilibrium is present.

$$A = \frac{[H^+]A_0 + K_a A_1}{[H^+] + K_a}$$

[Equation 2.1]

In Equation 2.1, A_0 and A_1 are the limiting values of the absorbance at the monitoring wavelength at low and high pH, respectively, and K_a is the equilibrium constant for dissociation of H^+ from the axially coordinated H_2O. The equation was fitted by standard non-linear least squares methods using SigmaPlot[13] where A is the absorbance at the monitoring wavelength, and with A_0, A_1 and K_a as variables in the fitting procedure. Figure 4.3 shows the fit of Equation 2.1 to the absorbance changes at the γ band maximum of $[ACCbs]^+$, 353 nm.

The fits to the experimental data are quite poor with $0.969 < r^2 < 0.989$ which is not surprising given the lack of well-defined isosbestic points. Values of pK_a are heavily dependent on how far along the titration reliable data is obtained and also on monitoring wavelength. Given these constraints to the system, it is not unexpected that the value of the pK_a for ionisation of H_2O as a function of temperature between 10 ^{o}C and 40 ^{o}C shows no trend with temperature and become less and less reliable at the higher temperatures of the temperature range studied.

References on page 120

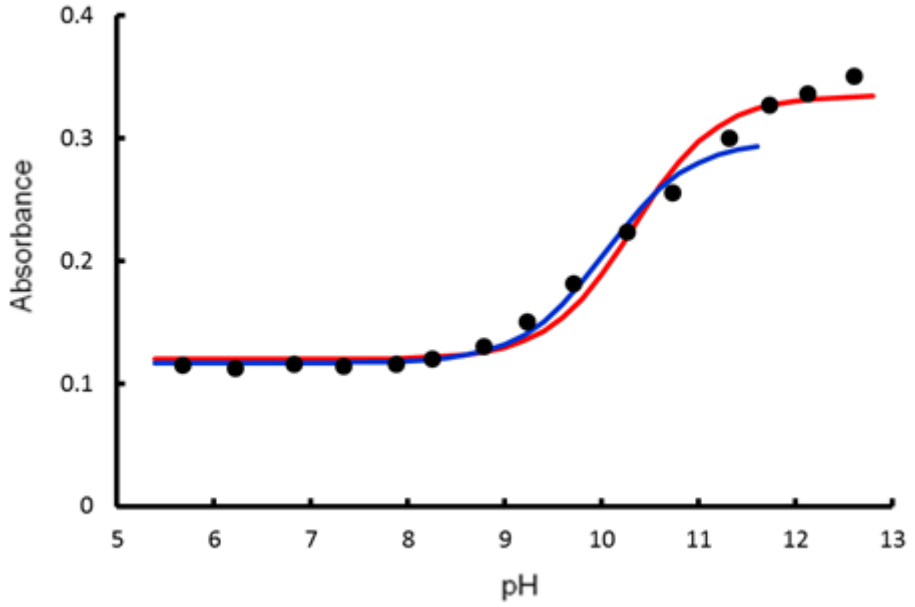

Figure 4.2 Change in absorbance at 560 nm with pH for the titration of $[ACCbs]^+$ with OH^-. The experimental data are given as ●. The solid red line is a fit of Equation 2.1 to all the data and gave pK_a = 10.33(8). The solid blue line is a fit to all data with pH ≤ 11.3 (i.e., omitting the three data points at the higher pH values). This gave pK_a = 10.04(8).

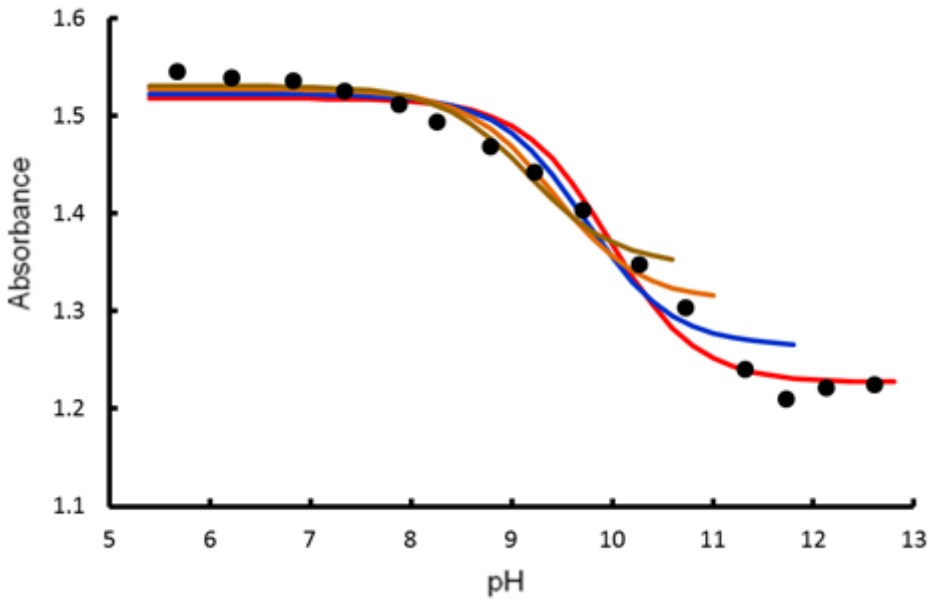

Figure 4.3 Change in absorbance at 353 nm with pH for the titration of $[ACCbs]^+$ with OH^-. The experimental data are given as ●. The red line shows the fit of Equation 2.1 to all data and gave pK_a = 10.0(1). For the blue line (data at pH ≤ 11.3), pK_a = 9.7(1). The orange line (data at pH ≤ 10.7) gave pK_a = 9.4(1), and the brown line (pH ≤ 9.7) gave pK_a = 9.2(1).

References on page 120

The value of the pK_a at each temperature was obtained by fitting Equation 2.1 to between 30 and 40 wavelengths chosen from the 340 – 355 nm, 450 – 470 nm and 520 – 580 nm ranges in the UV-vis spectrum in order to average out the wavelength dependence noted when comparing the results in Figures 4.2 and 4.3. Data were typically confined to pH < 11.2 because of the unreliability of the absorbance readings at higher pH values. The results are summarised in Table 4.1.

Table 4.1 Dependence of the pK_a of coordinated H_2O in aquacyanocobester as a function of temperature.

Temp /^oC	pK_a	Error
10	9.9	0.1
15	10.3	0.2
20	9.5	0.3
25	10.2	0.2
30	9.9	0.3
35	9.1	0.3
40	9.0	0.3

We therefore resorted to averaging the values obtained between 10 ^oC and 30 ^oC (pK_a = 9.8 ± 0.3) for all calculations in this work. We endeavoured where possible to work in pH ranges well removed from this (i.e., where $[ACCbs]^+$ is predominantly in the aqua form) in order to minimise errors that arise from the uncertainty in the value of the pK_a.

4.2.2 pK_a Determination of $[AC\text{-}5\text{-}seco\text{-}Cbs]^+$

Work with aquacyano-5-seco-cobester was easier on the one hand in that hydrolysis of the ester side chains appeared to be significantly slower (i.e, the spectra were more stable at higher pH values and at higher temperatures) but more difficult on the other because cleavage of the corrin and its π conjugated system made the spectroscopic changes

References on page 120

attendant on changes in the coordination of the axial coordination sites of the metal much, much smaller and hence severely impacting the signal-to-noise ratio.

The pK_a of $[AC\text{-}5\text{-}seco\text{-}Cbs]^+$ was determined as with $[ACCbs]^+$. Samples of the spectra obtained during the titration of $[AC\text{-}5\text{-}seco\text{-}Cbs]^+$ with OH^- at 25 ^oC are shown in Figure 4.4. The absorbance changes monitored at between 40 and 50 wavelengths, selected from the 370 – 385 nm, 475 – 500 nm and 580 – 680 nm region were fitted to Equation 2.1, and the pK_a values obtained at these wavelengths were averaged so as to average out the wavelength dependence which was found on determining pK_a (as found with $[ACCbs]^+$). The titrations were performed at four temperatures between 15 ^oC and 40 ^oC. The reproducibility between batches of $[AC\text{-}5\text{-}seco\text{-}Cbs]^+$ was checked by repeating the titration at 25 ^oC on two different batches. Examples of fits obtained at 25 ^oC are shown in Figure 4.5. The data are summarised in Table 4.2.

A plot of ln K_a against T^{-1} for the data in Table 4.2 is shown in Figure 4.6. The best fit straight line was obtained by a weighted linear least squares, with the weighting factor = (relative % error in K)$^{-1}$. Since the slope = $-\Delta H/R$ and intercept = $\Delta S/R$, we found ΔH = – 88 ± 17 kJ mol^{-1} and ΔS = – 434 ± 56 J K^{-1} mol^{-1}. From the values of ΔH and ΔS, pK_a = 7.3 at 25 ^oC for the ionisation of H_2O coordinated to Co(III) in $[AC\text{-}5\text{-}seco\text{-}Cbs]^+$. The thermodynamic parameters were used to determine the percentage of $[AC\text{-}5\text{-}seco\text{-}Cbs]^+$ during titrations with other ligands.

References on page 120

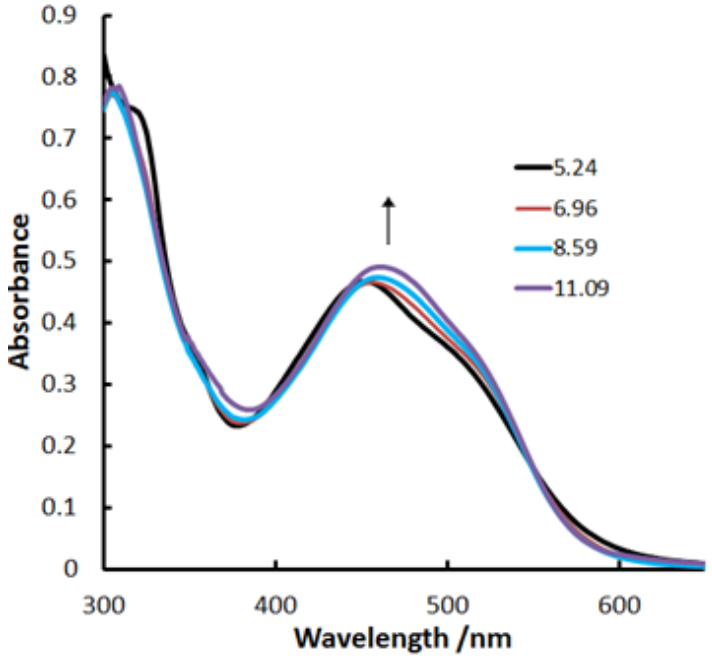

Figure 4.4 Dependence of the UV-vis spectra of [AC-5-seco-Cbs]$^+$ on pH at 25 ^{o}C. The pH value at which each spectrum was recorded is given in the insert to the figure.

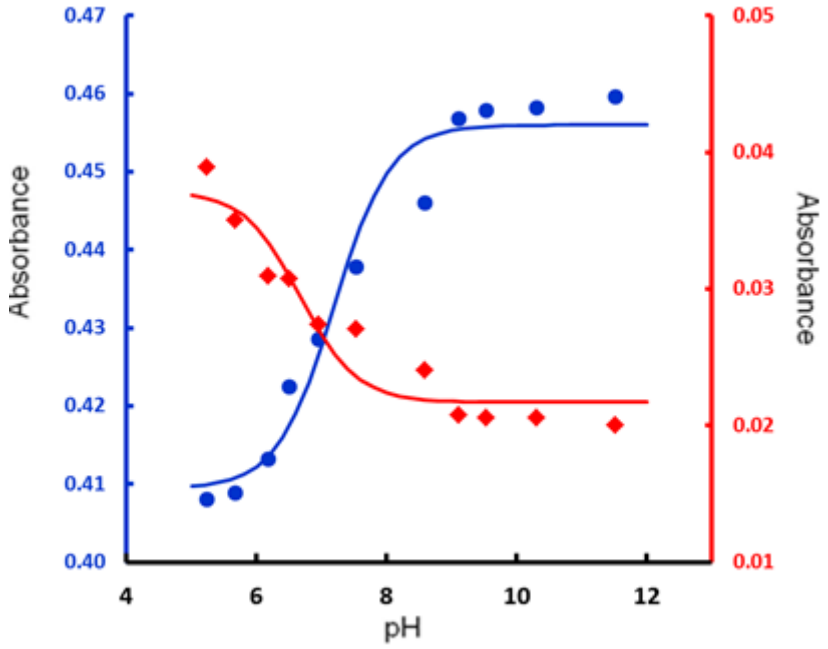

Figure 4.5 Changes in absorbance of 25 ^{o}C on titration of [AC-5-seco-Cbs]$^+$ with OH^- monitored at 480 nm (blue ●, left vertical axis) and 595 nm (red ◆, right vertical axis). The solid lines are fits of the data to Equation 2.1. The data at 480 nm gave pK_a = 7.2(1) while that at 595 nm gave pK_a = 6.7(2).

References on page 120

Table 4.2. pK_a values of [AC-5-seco-Cbs]$^+$ determined as a function of temperature by titration with OH^-.

T (^{o}C)	$1/T$ (K^{-1})	pK_a	Err in pK_a	K_a /10^{-8}	Err in K_a /10^{-9}	1/(Rel% err in K_a)	ln K_a	Upper error in ln K_a	Lower error in ln K_a
15	0.00347	6.91	0.13	12	4	0.02866	-15.91	0.30	0.43
25[a]	0.003354	7.17	0.17	7	3	0.02087	-16.51	0.39	0.65
25[b]	0.003354	7.12	0.08	8	2	0.04944	-16.39	0.18	0.23
30	0.003299	7.59	0.08	2.6	0.5	0.04944	-17.48	0.18	0.23
40	0.003193	8.11	0.14	0.8	0.3	0.02629	-18.67	0.32	0.48

[a,b] From different batches of [AC-5-seco-Cbs]$^+$.

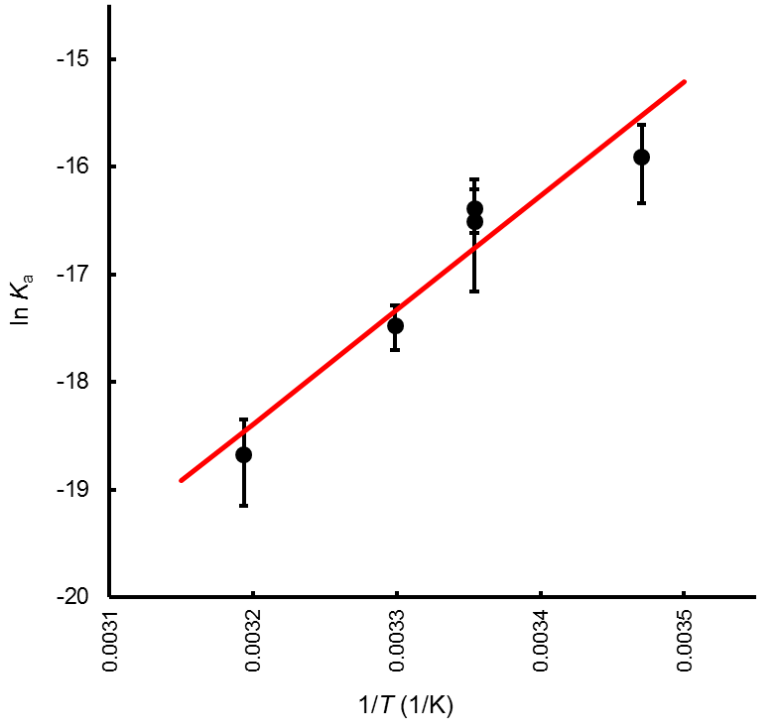

Figure 4.6. Plot of ln K_a against T^{-1} for ionisation of coordinated H_2O in [AC-5-seco-Cbs]$^+$. The best fit line (r^2 = 0.90) was determined by a weighted least squares method and gave a slope of 1.1(2) × 10^4 K and an intercept of – 52 ± 7.

References on page 120

4.2.3 Hydrolysis

A major difficulty encountered in the determination of the acid dissociation constant of [AC-5-seco-Cbs]$^+$ and [ACCbs]$^+$ was the unreliability of data at higher pH values. It is likely that the ester side chains on the periphery of the corrin macrocycle are hydrolysed to carboxylates at high pH.[1,14,15] Carboxylates are significantly more polar than esters. This would alter the polarity of the corrins significantly, and the corrin would behave differently within the same environment. This was investigated with the use of HPLC. It was previously determined that [AC-5-seco-Cbs]$^+$ gave rise to a single peak with a retention time of 7.04 minutes. The MeCN:H_2O (1:1) mobile phase used is very polar, resulting in the secocobester being retained by the less polar stationary phase column. Consequently, if the esters were indeed hydrolysed into carboxylates, the hydrolysed secocobester should elute earlier.

To test this, [AC-5-seco-Cbs]$^+$ was injected onto the column and eluted with the MeCN:H_2O eluent system, resulting in a peak with a retention time of 7.04 minutes (Figure 4.7 (a)). Now, as we assumed hydrolysis was occurring at high pH, the pH of the [AC-5-seco-Cbs]$^+$ solution was increased to pH 13 by diffusing a negligible volume of 8 M NaOH into a vial containing [AC-5-seco-Cbs]$^+$, and a small volume was withdrawn and immediately injected onto the column. The resultant chromatogram (Figure 4.7 (b)) indicated an immediate change on addition of base as the [AC-5-seco-Cbs]$^+$ peak still remained but numerous new peaks were detected between 1.92 and 4.82 minutes, suggesting the start of hydrolysis. The secocobester solution, to which NaOH was added, was then allowed to stand for an hour, after which a chromatogram was run again. The resulting chromatogram (Figure 4.7 (c)) was very different to that of [AC-5-seco-Cbs]$^+$ as the secocobester peak around 7.0 minutes had now completely disappeared and a new peak emerged with a retention time of 2.0 minutes, suggesting most if not all side chains had been completely hydrolysed to carboxylates. After 2 hours of exposure to base, the chromatogram had not undergone any further appreciable change implying hydrolysis was complete within an hour of exposure to base (Figure 4.7 (d)).

It may be concluded that the unreliability of data observed above pH 9.5 during pK_a titrations was indeed due to the hydrolysis of ester side chains demonstrated at pH 13.

References on page 120

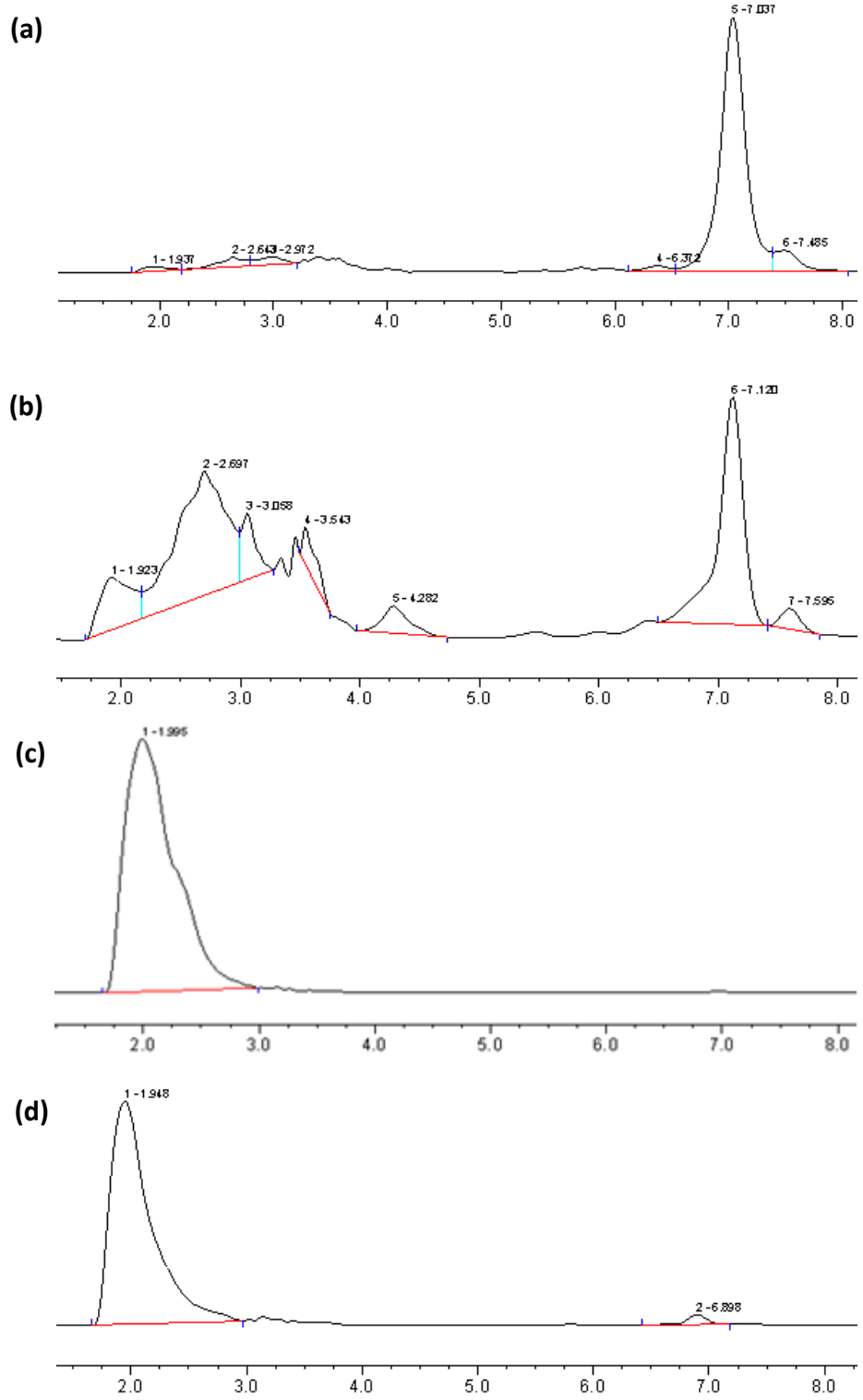

Figure 4.7 HPLC chromatograms of $[AC\text{-}5\text{-}seco\text{-}Cbs]^+$ **(a)**, $[AC\text{-}5\text{-}seco\text{-}Cbs]^+$with base **(b)**, $[AC\text{-}5\text{-}seco\text{-}Cbs]^+$ after 1 hour **(c)** and $[AC\text{-}5\text{-}seco\text{-}Cbs]^+$ after 2 hours **(d)** using a MeCN:H_2O (1:1) mobile phase.

References on page 120

The MeCN:de-ionised water (1:1) isocratic elution method used for these determinations is not ideal for HPLC analysis of $[AC\text{-}5\text{-}seco\text{-}Cbs]^+$ as acetonitrile contains trace amounts of cyanide. Hence the water ligand of $[AC\text{-}5\text{-}seco\text{-}Cbs]^+$ was rapidly displaced by a cyanide ion to revert to the original [DC-5-seco-Cbs], as can be seen in the UV-vis spectrum obtained in the chromatogram (Figure 4.8). It was therefore decided to design a more suitable solvent system for investigations involving the aquacyano forms.

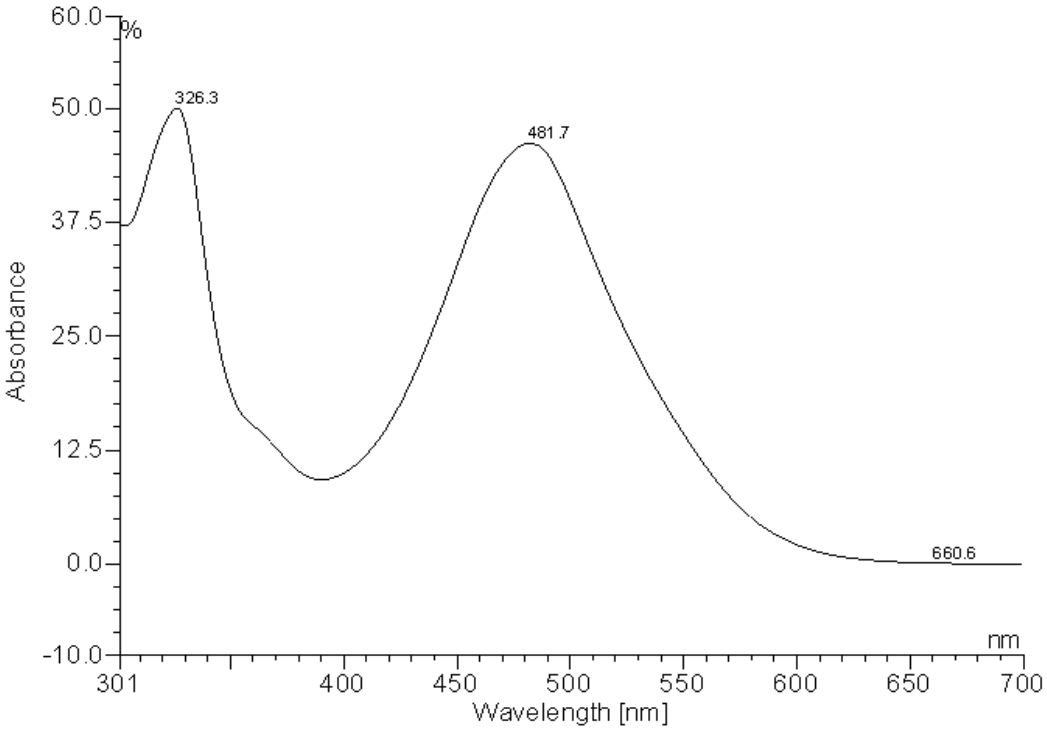

Figure 4.8 UV-vis spectrum obtained from the peak corresponding to [DC-5-seco-Cbs] in the HPLC chromatogram caused by exposing $[AC\text{-}5\text{-}seco\text{-}Cbs]^+$ to acetonitrile.

A literature review of $[ACCbs]^+$ solution chemistry revealed that the use of a methanol-phosphate buffer solvent system provided efficient separation of peaks as well as preserving the aquacyano form.[1] Thus all hydrolysis investigations were then repeated but now using a methanol-phosphate buffer (0.025 M, pH 3.0) multi-step elution program (Chapter 2.3.2) to ensure a more accurate representation of the species present in solution.

$[AC\text{-}5\text{-}seco\text{-}Cbs]^+$ was re-run in the new phosphate buffer-methanol system resulting in a chromatogram (Figure 4.9 (a)) with one major peak (R_t = 8.48 minutes, 82.34%) and two

References on page 120

smaller peaks, one of which is that of [DC-5-seco-Cbs] which had not been converted to the aqua form and the second is that of the diaqua species forming spontaneously in solution. On addition of base (8 M NaOH, pH 13) the chromatogram revealed an instant change with all peaks disappearing and new peaks forming with a retention time between 3.0 – 4.0 minutes and between 5.0 – 7.0 minutes (Figure 4.9 (b)). This suggests hydrolysis is occurring. The peaks occurring between 3.0 – 4.0 minutes indicate significant hydrolysis whereas the peaks occurring between 5.0 – 7.0 minutes appear to be less hydrolysed and disappear with time. After an hour of exposure to base, the chromatogram of [AC-5-seco-Cbs]$^+$ showed peaks with a retention time of around 3.5 minutes, and little else (Figure 4.9 (c)). Since this was not a single, well-defined peak, it suggests that not all the esters have been converted within an hour. On the contrary, the chromatogram of [AC-5-seco-Cbs]$^+$ after 2 hours of exposure to base (Figure 4.9 (d) showed a better defined, sharper peak with a retention time of 3.38 minutes, suggesting hydrolysis was almost complete. The UV-vis spectrum (Figure 4.10) of the secocobester proved the secocobester was present in the aquacyano form throughout investigations.

References on page 120

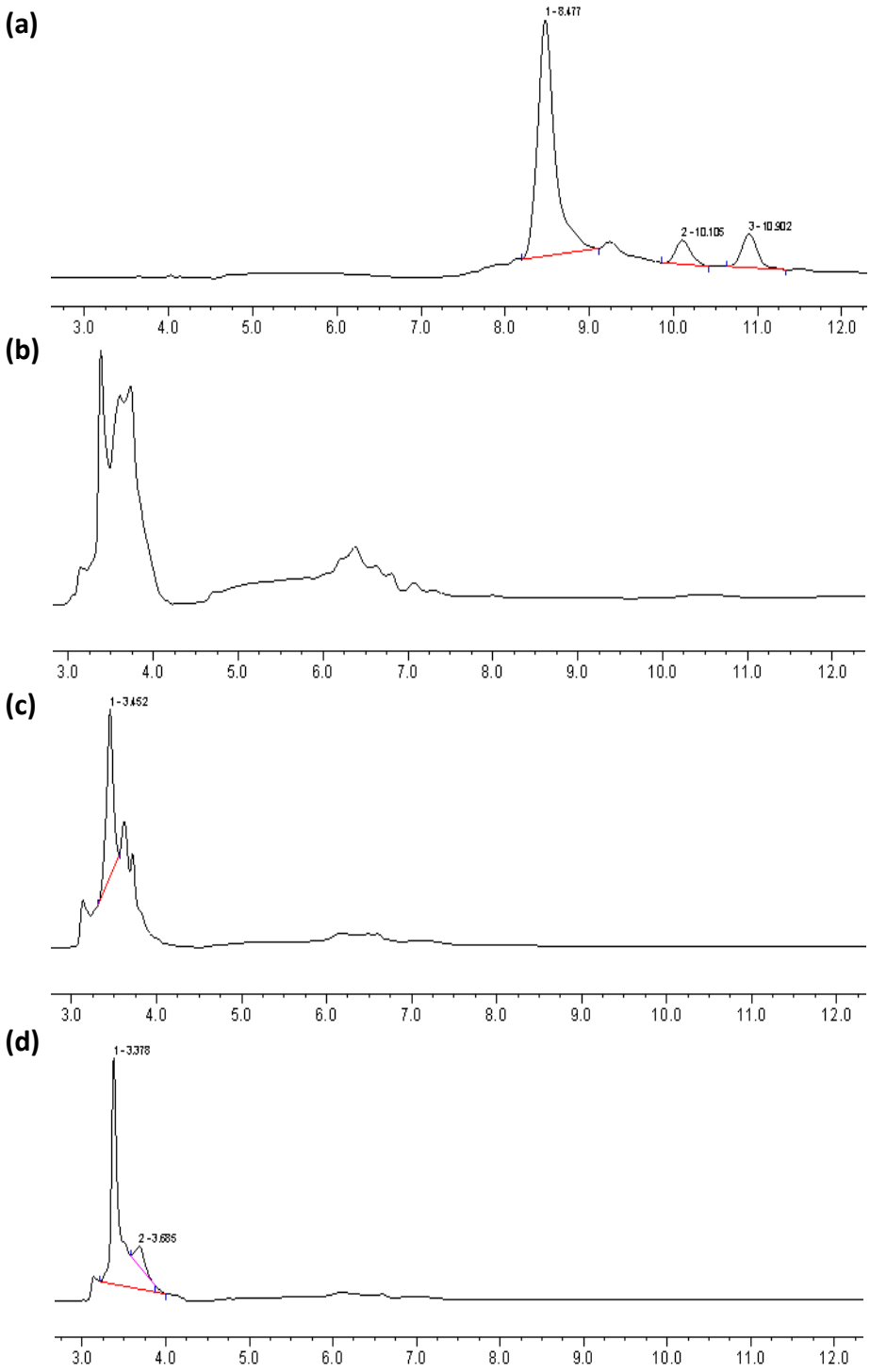

Figure 4.9 HPLC chromatograms of $[AC\text{-}5\text{-}seco\text{-}Cbs]^+$ **(a)**, $[AC\text{-}5\text{-}seco\text{-}Cbs]^+$ with base **(b)**, $[AC\text{-}5\text{-}seco\text{-}Cbs]^+$ after 1 hour **(c)** and $[AC\text{-}5\text{-}seco\text{-}Cbs]^+$ after 2 hours **(d)** using a phosphate-methanol elution system.

References on page 120

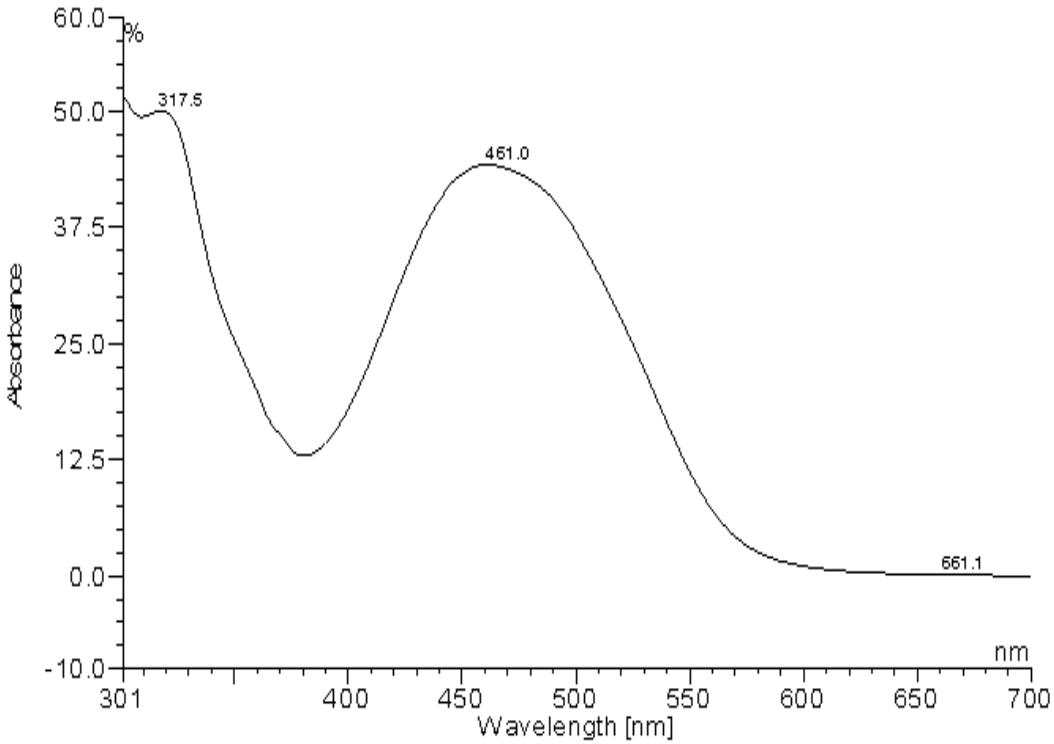

Figure 4.10 UV-vis spectrum obtained from the peak corresponding to [AC-5-seco-Cbs]$^+$ in the HPLC chromatogram.

The susceptibility of [ACCbs]$^+$ to hydrolysis was determined for comparison purposes. Figure 4.11 (a) shows the initial chromatogram of [ACCbs]$^+$ with twin peaks at a retention time of 5.78 minutes (47.0%) and 5.99 minutes (47.6%), respectively, corresponding to the α and β isomers, as well as two contaminant peaks on either side at R_t = 5.58 minutes (1.95%) and 6.4 minutes (3.48%). On addition of base (8M NaOH, pH 13), the resulting chromatogram already revealed the broadening of the peaks, indicating a change in the structure of [ACCbs]$^+$ (Figure 4.11 (b)). After an hour of exposure to base, the chromatogram of [ACCbs]$^+$ had significantly altered. One could no longer detect the peak corresponding to [ACCbs]$^+$; instead a peak with a retention time of 5.77 minutes formed, which, although has a similar retention time as [ACCbs]$^+$, there were many other overlapping peaks, at longer retention times as well (Figure 4.11 (c)). There was no significant change after two hours of exposure to base (Figure 4.11 (d)). Hence, like [AC-5-seco-Cbs]$^+$, [ACCbs]$^+$ undergoes hydrolysis of the ester side chains as reported by Chemaly and Hamza.[1,14,15]

References on page 120

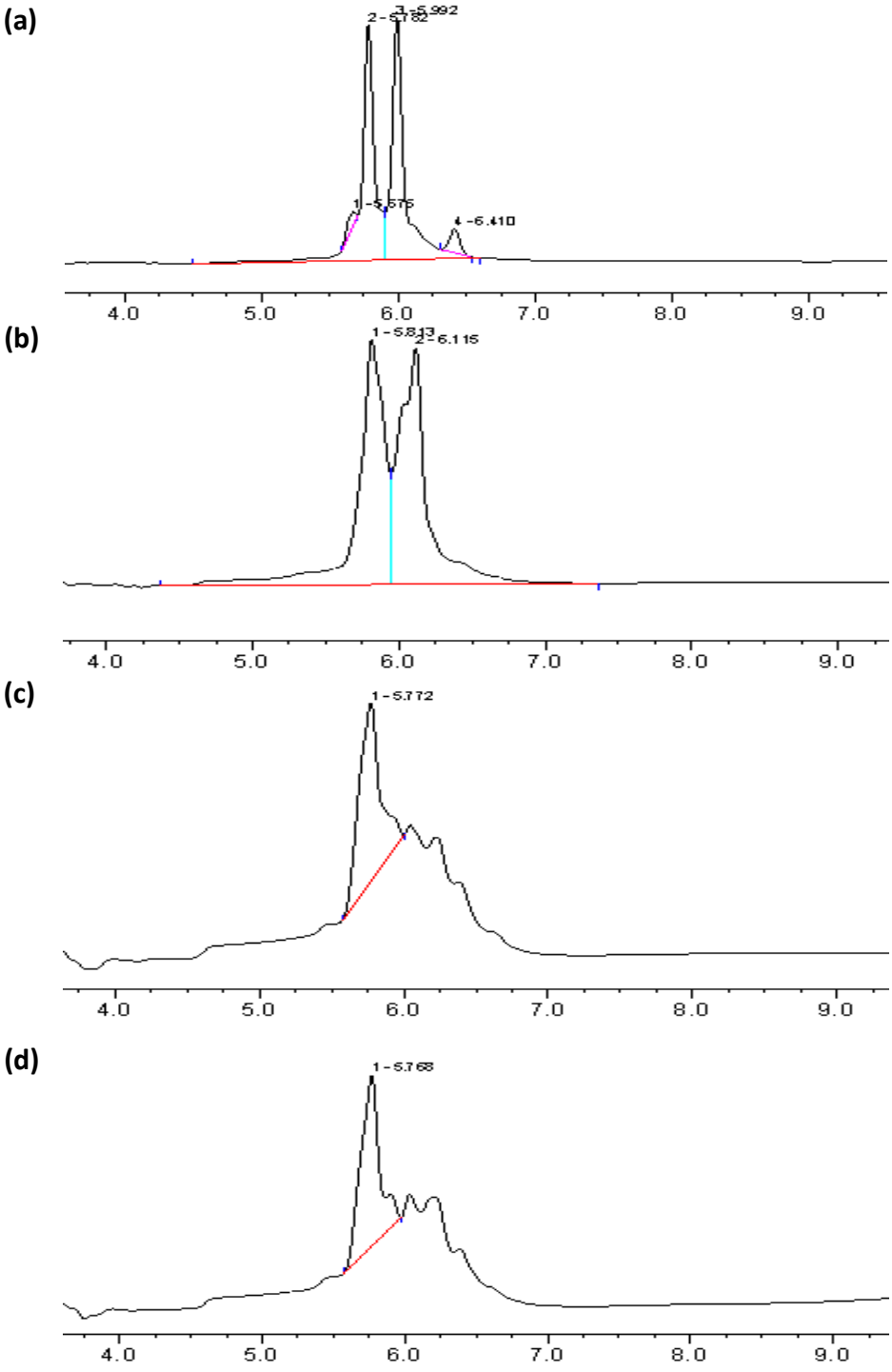

Figure 4.11 HPLC chromatograms of $[ACCbs]^+$ **(a)**, $[ACCbs]^+$ with base **(b)**, $[ACCbs]^+$ after 1 hour **(c)** and $[ACCbs]^+$ after 2 hours **(d)** using a phosphate-methanol elution system.

References on page 120

4.3 Conclusions

The pK_a of coordinated H_2O decreased dramatically from 9.8(3) to 7.3 on cleaving the corrin ring; hence coordinated H_2O in $[AC\text{-}5\text{-}seco\text{-}Cbs]^+$ is considerably more acidic than in $[ACCbs]^+$. Its ionisation is a strongly exothermic process ($\Delta H = -88 \pm 17$ kJ mol^{-1}) moderated by a very negative $\Delta S = -434 \pm 56$ J K^{-1} mol^{-1}. The pK_a of H_2O in $[Co(H_2O)_6]^{3+}$ is 2.9.[16] It is also low in other simple Co(III) complexes, for example, 3.09 in $[Co(nta)(H_2O)(\mu\text{-}OH)(H_2O)(nta)Co]^-$ (nta = nitrilotriacetate);[17] 4.98 in $[Co(tn)_2(H_2O)_2]^{3+}$ (tn = 1,3-diaminopropane);[18] 5.6 in $[Co(cyclen)(H_2O)_2]^{3+}$ (cyclen = 1,4,7,11-tetraazacyclododecane),[19] and with 5 N-donors, in $[Co(NH_3)_5(H_2O)]^{3+}$, 6.22[20] or 6.36.[21] By comparison, the pK_a for the corresponding Co(II) complex, which is much less polarizing, is much higher, as in $[Co(H_2O)_6]^{2+}$, at 9.7.[22]

The deprotonation of coordinated H_2O is a function of the charge density on the metal ion. A comparison of the pK_as of $[ACCbs]^+$ and $[AC\text{-}5\text{-}seco\text{-}Cbs]^+$ shows clearly that Co is much softer, and has a lower charge density in the former than in the latter. This supports our hypothesis that the integral corrin ligand confers on Co at least some measure of softer Co(II)-like character. Cleavage of the corrin restores the metal ion to much more Co(III)-like behaviour.

During the determination of the pK_a value of $[AC\text{-}5\text{-}seco\text{-}Cbs]^+$ and $[ACCbs]^+$, large scatter in data was consistently observed at higher pH values. This was attributed to (and verified by HPLC) the hydrolysis of the ester side chains on the periphery of the corrin macrocycle. Subsequently care was taken to ensure work was done at a pH at which minimal hydrolysis occurred.

References on page 120

REFERENCES FOR CHAPTER 4

1. Chemaly, S. M.; Brown, K. L.; Fernandes, M. A.; Munro, O. Q.; Grimmer, C.; Marques, H. M. *Inorg. Chem*. **2011**, 50, 8700-8718.
2. Chemaly, S. M.; Florczak, M.; Dirr, H.; Marques, H. M. *Inorg. Chem.* **2011**, 50, 8719-8727.
3. Knapton, L. Ph.D. Thesis, University of the Witwatersrand, Johannesburg, 2005.
4. Xia, L.; Cregan, A. G.; Berben, L. A.; Brasch, N. E. *Inorg. Chem.* **2004**, *43*, 6848-6857.
5. Baldwin, D. A.; Betterton, E. A.; Pratt, J. M. *J. Chem. Soc., Dalton Trans.* **1983**, 217-223.
6. Nowakowska, M. *Synthesis and Reactions of a Modified Cobalt Corrin,* MSc; dissertation reserved and converted to PhD thesis, University of the Witwatersrand, Johannesburg, 2014.
7. Offenhartz, B. H.; George, P. *Biochemistry* **1963**, *2*, 142-145.
8. Hayward, G. C.; Hill, H. A. O.; Pratt, J. M.; Vanston, N. J.; Williams, R. J. P. *J. Chem. Soc. A* **1965**, 6485-6493.
9. Kräutler, B.; Caderas, C.; Konrat, R.; Puchberger, M.; Kratky, C. *Helv. Chim. Acta* **1995**, *78*, 581-599.
10. Shimakoshi, H.; Abiru, M.; Izumi, S.; Hisaeda, Y. *Chem. Commun.* **2009**, 6427-6429.
11. Munro, O. Q.; Marques, H. M. *Inorg. Chem*. **1996**, 35, 3752-3767.
12. Sannasy, D. MSc Dissertation, University of the Witwatersrand, Johannesburg, 2006.
13. SigmaPlot, v. 14, Systat Software, San Jose, CA, 2017
14. Hamza, M. S. A. *J. Inorg. Biochem.* **1998**, 69, 269-274.
15. Chemaly, S. M.; Kendall, L.; Nowakowska, M.; Pon, D.; Perry, C. B.; Marques, H. M. *Inorg. Chem*. **2013**, 52, 1077-1083.
16. Sisley, M. J.; Jordan, R. B. *Inorg. Chem.* **2006**, *45*, 10758-10763.
17. Visser, H. G.; Purcell, W.; Basson, S. S. *Trans. Met. Chem.* **2002**, *27*, 461-468.
18. Massoud, S. S.; Milburn, R. M. *Inorg. Chim. Acta* **1988**, *146*, 3-4.
19. Lee, J. H.; Britten, J.; Chin, J. *J. Am. Chem. Soc.* **1993**, *115*, 3618-3622.
20. Splinter, R. C.; Harris, S. J.; Tobias, R. S. *Inorg. Chem.* **1967**, *7*, 897-902.
21. Yajima, F.; Yamasaki, A.; Fujiwara, S. *Inorg. Chem.* **1971**, *10*, 2350-2352.
22. Grzybkowski, W. *Polish J. Environ. Stud.* **2006**, *15*, 655-663.

CHAPTER 5

EQUILIBRIUM CONSTANTS FOR LIGAND COORDINATION

5.1 Introduction

As mentioned in Chapter 1, the chemistry of vitamin B_{12} and its derivatives has attracted much interest over the years. The usually inert Co(III) centre exhibits remarkable lability when coordinated to the corrin macrocycle.[1–27] The axially coordinated water ligand quite rapidly undergoes substitution by a variety of exogenous ligands, L, (Equation 2.2).

$$[CN–Co–H_2O] + L \overset{K}{\rightleftharpoons} [CN–Co–L] + H_2O$$

[Equation 2.2]

Many equilibrium constants (the equilibrium constant for Equation 2.2 expressed as log *K* and also referred to as a stability, binding or formation constant) have been spectrophotometrically determined for the formation of metal-ligand complexes of the corrinoids.[1–27]

A binding constant is a measure (in this case) of the affinity of a metal ion for an exogenous ligand which can provide invaluable insight into the nature of the metal ion, or more specifically, into the macrocyclic influence exerted on the metal (*cis*-influence).

Of importance to this study, Chemaly and co-workers have determined the equilibrium constants for the formation of complexes with $[ACCbs]^+$ **(1)** in which the 13-atom, 14 π-electron system normally associated with cobalt corrins has been retained, as well as with $[ACSYCbs]^+$ **(2)**, in which oxidation at the C5 position resulted in a diminished delocalised system.[2] Equilibrium constants obtained for the complexing of anionic ligands SO_3^{2-}, CN^-, NO_2^-, N_3^-, and $S_2O_3^{2-}$ to $[ACCbs]^+$ and $[ACSYCbs]^+$ are shown in Table 5.1. It was found that interruption of the conjugated system resulted in a less electron-rich and more Co(III)-like ion. Consequently π-donor ligands (N_3^- and $S_2O_3^{2-}$) bound preferentially to the less electron-rich $[ACSYCbs]^+$, whereas π- acceptor ligands (SO_3^{2-}, CN^-, NO_2^-) bound preferentially to the more electron-rich $[ACCbs]^+$.

References on page 170

Determination of equilibrium constants as a function of temperature showed that ligands with a harder donor atom (N in N_3^- and NO_2^-) produce Δ*H* values that are more negative in their reactions with $[ACSYCbs]^+$ than with $[ACCbs]^+$, whereas soft donor atom ligands (C in CN^- and S in SO_3^{2-}) produced more negative Δ*H* values in their reactions with $[ACCbs]^+$. This indicates a preference of the more electron-rich Co(III) in $[ACCbs]^+$ for the softer ligands and the less electron-rich Co(III) in $[ACSYCbs]^+$ for the harder ligands.

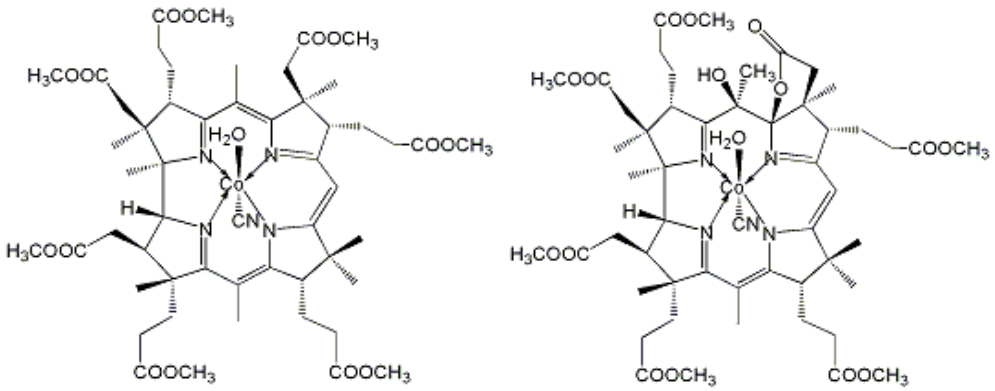

Figure 5.1 The structures of $[ACCbs]^+$ (left) and $[ACSYCbs]^+$ (right).[2,3,18]

Table 5.1 The equilibrium constants (log $K^{25^\circ C}$) for the substitution of water in $[ACCbs]^+$ and $[ACSYCbs]^+$ by various anionic ligands.[3]

	$[ACCbs]^+$			**$[ACSYCbs]^+$**		
Ligand	**Δ*H* / kJ mol^{-1}**	**Δ*S* / J K^{-1} mol^{-1}**	**log K^{25}**	**Δ*H* / kJ mol^{-1}**	**Δ*S* / J K^{-1} mol^{-1}**	**log K^{25}**
SO_3^{2-}	50(3)	265(9)	5.08	59(1)	253(5)	2.88
NO_2^-	–6(9)	33(3)	2.88	–22(4)	–32(2)	2.34
CN^-	–23(2)	81(6)	8.26	–17(1)	80(5)	7.16
N_3^-	–9(7)	18(3)	2.59	–18(7)	–12(2)	2.63
$S_2O_3^{2-}$	21(3)	80(10)	0.5	–	–	0.6(2)[a]

[a] From determination at a single temperature (25 °C).[7]

References on page 170

It would be interesting to assess the effect disrupting the conjugation system by cleavage of the corrin ring as well as the subsequent opening of the macrocyclic cavity would have on the log *K* values of Table 5.1. This is addressed in this Chapter, in which the equilibrium constants for the substitution of the axially coordinated water of $[AC\text{-}5\text{-}seco\text{-}Cbs]^+$ by the aforementioned ligands as a function of temperature will be discussed. The results will be compared to analogous data for $[ACCbs]^+$ and $[ACSYCbs]^+$, to elucidate the effect that modification of the electronic structure of the corrin ring has on the binding properties of the central Co(III) ion, to investigate the importance of the *cis*-influence on these systems. The equilibrium constants for the substitution reactions of $[ACCbs]^+$ were re-determined to ensure reproducibility and to ensure comparable results under the same experimental conditions. As an aside, the coordination of neutral N-donor ligands by $[AC\text{-}5\text{-}seco\text{-}Cbs]^+$ and $[ACCbs]^+$ were briefly studied.

5.2 Results and Discussion

5.2.1 The Dependence of Equilibrium Constants on pH: Binding Studies of Sulfite

The extraordinarily low pK_a value of $[AC\text{-}5\text{-}seco\text{-}Cbs]^+$ (Chapter 4) prompted us to validate the value by determining the pH dependence of the binding constant for the substitution of axially coordinated H_2O by an exogenous ligand. This is because the predominant species found above the pK_a (7.28) will be the hydroxo complex (hydroxocyano-5-secocobester), which, as with other hydroxo complexes of Co(III) macrocycles, are generally inert to substitution and few ligands will compete with OH^- for the metal ion.[3,5,28,29] As such, the observed log *K* values should decrease with increasing pH.

Thus a ligand for which log *K* was relatively high (to compensate for the decreasing value with increasing pH, hence eliminating NO_2^- and N_3^-) and which has a pK_a below that of the operating pH range (which eliminated CN^-) was required. It was therefore decided to use SO_3^{2-} as a probe ligand, which has log *K* = 5.00 and 3.06 for coordination by $[ACCbs]^+$ and $[ACSYCbs]^+$, respectively,[3] and a pK_a (6.95)[30] below the pH range of interest (7 – 9.5).

Aliquots of a stock solution of Na_2SO_3 (1.76 M) at the appropriate pH for the study were added to a solution of $[AC\text{-}5\text{-}seco\text{-}Cbs]^+$ buffered at the same pH. The spectrophotometric

References on page 170

change in absorbance during the titration is shown in Figure 5.2 indicating a red shift upon coordination of sulfite.

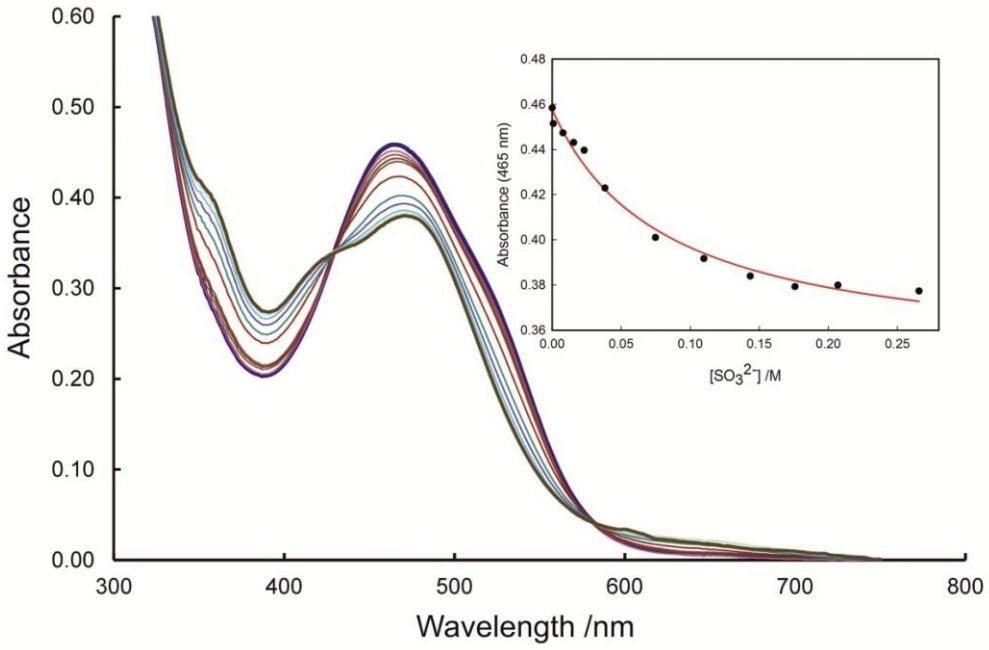

Figure 5.2 Titration of $[AC\text{-}5\text{-}seco\text{-}Cbs]^{+}$ with SO_3^{2-} at pH 8.90, 25 °C. The insert shows a fit of Equation 2.3 to the absorbance changes observed at 465 nm.

The value of log *K* was determined by fitting the absorbance change at every 1 nm between 370 – 410 nm and 450 – 500 nm to a binding isotherm (Equation 2.3).

$$A_z = \frac{A_0 + A_1 K[\mathrm{L}]}{1 + K[\mathrm{L}]}$$

[Equation 2.3]

The log *K* results are given in Table 5.2. Values above pH 9 were unreliable because formation of the sulfite complex was incomplete even at the highest concentrations of SO_3^{2-} used (ca. 0.4 M). As previously mentioned, should the pK_a value of 7.28 be genuine, the equilibrium constants of SO_3^{2-} should show a decreasing log *K* trend as a function of pH. This is based on the assumption that the binding constant for the substitution of the coordinated hydroxyl group is much smaller than that for coordinated water. As seen in Table 5.2, as the pH increased from 7.06 to 8.90, the percentage of the hydroxocyano form

References on page 170

increased significantly. This suggests that under pH 7.0 conditions, when 56.29% of the secocobester is present in the aquacyano form, log *K* should be much higher as there is more of the $[AC\text{-}5\text{-}seco\text{-}Cbs]^+$ species in solution with which to bind the incoming ligand. This is in contrast to pH 9.0 conditions when only 1.64% of the secocobester is present as $[AC\text{-}5\text{-}seco\text{-}Cbs]^+$, resulting in very small log *K* values. Results indicated a definite decrease in log *K* with increasing pH. Correcting for the pK_a of $[AC\text{-}5\text{-}seco\text{-}Cbs]^+$ (Equation 2.6) gives a value that, within experimental error, is virtually independent of pH, thus confirming the reliability of the value of 7.28 at 25 ^oC for the pK_a of $[AC\text{-}5\text{-}seco\text{-}Cbs]^+$.

$$K = K_{(obs)}(1+10^{(pKL - pH)})(1+10^{(pH - pKCo)})$$

[Equation 2.6]

Table 5.2 The pH Dependence of Equilibrium Constants for the Substitution of coordinated H_2O in $[AC\text{-}5\text{-}seco\text{-}Cbs]^+$ (25 ^oC) by SO_3^{2-}.

Ligand	pH	% present as $[AC\text{-}5\text{-}seco\text{-}Cbs]^+$	log K_{obs}	log K [a]
SO_3^{2-}	7.17	56.29	3.45(3)	3.70(3)
	7.73	26.28	3.01(11)	3.58(11)
	8.09	13.41	3.1(2)	3.9(2)
	8.55	5.09	2.47(10)	3.76 (10)
	9.06	1.64	1.81(5)	3.60(5)
Average				3.4(1)[b]

[a]Corrected for the pK_a = 7.28 of $[AC\text{-}5\text{-}seco\text{-}Cbs]^+$ at 25 ^oC.

References on page 170

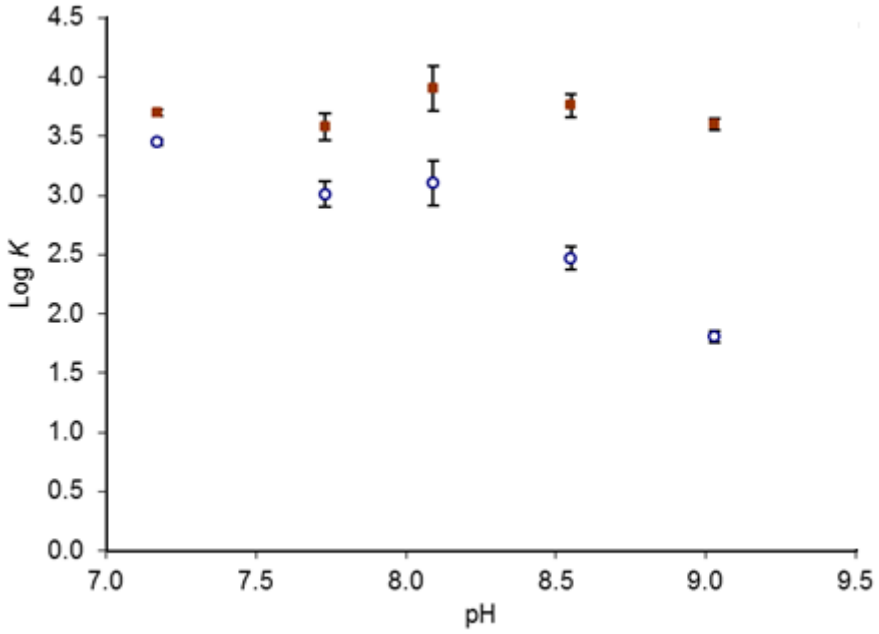

Figure 5.3 A plot illustrating the pH-independence of log *K* values once corrected for the pK_a of [AC-5-seco-Cbs]$^+$ (red) with respect to the pH-dependence of log *K* (blue) for the coordination of SO_3^{2-} to [AC-5-seco-Cbs]$^+$.

Following the validation of the pK_a of [AC-5-seco-Cbs]$^+$ using the probe ligand, SO_3^{2-}, the binding of SO_3^{2-} by [AC-5-seco-Cbs]$^+$ was then studied as a function of temperature. Aliquots of a stock solution of Na_2SO_3 (1.7623 – 1.8099 M, pH 9) were added to a solution of [AC-5- seco-Cbs]$^+$ buffered in CHES (μ = 0.1 M, pH 9). Equilibrium constants for the coordination of sulfite by [AC-5-seco-Cbs]$^+$ were determined by fitting the experimental data obtained at multiple wavelengths on either side of the isosbestic points in the UV-vis spectrum to a binding isotherm as before. The equilibrium constants obtained as a function of temperature are given in Table 5.3. From the thermodynamic parameters obtained in the van't Hoff plot (Figure 5.4), log *K* = 3.87 at 25 ^oC for the coordination of SO_3^{2-} by [AC-5-seco-Cbs]$^+$.

References on page 170

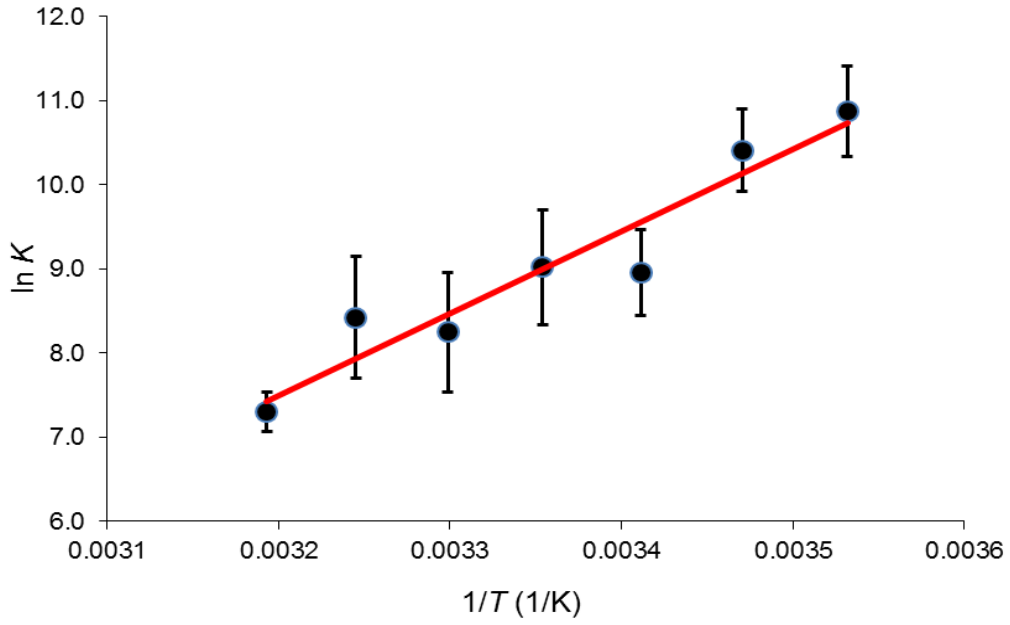

Figure 5.4 Plot of ln *K* against T^{-1} for coordination of SO_3^{2-} by $[AC\text{-}5\text{-}seco\text{-}Cbs]^+$. The straight line in this, and all other van't Hoff plots in this Chapter, is a weighted least squares fit to the experimental data; the weighting was (relative % error)$^{-1}$. From the slope $\Delta H = -83 \pm 10$ kJ mol^{-1} and from the intercept $\Delta S = -205 \pm 33$ J K^{-1} mol^{-1}. $R^2 = 0.945$.

The equilibrium constants for the coordination of SO_3^{2-} by $[ACCbs]^+$ were re-determined in a competition reaction in the presence of 0.20 M N_3^- as the log *K* was expected to be large. Under these conditions, 99% of the cobester solution was present in the form of $[(N_3)(CN)Cbs]^+$.

Aliquots of a stock solution of Na_2SO_3 (0.01984 – 0.0220 M, pH 7) were added to a solution of $[ACCbs]^+$ buffered in MOPS (μ = 0.1 M, pH 7) in the presence of 0.20 M N_3^-. Log *K* values were then determined from the measured log *K* for substitution of N_3^- by SO_3^{2-} and the log *K* for substitution of axially coordinated H_2O by N_3^- (Table 5.3). Log *K* = 6.08 at 25 °C for the coordination of SO_3^{2-} by [azidocyanoCbs].

References on page 170

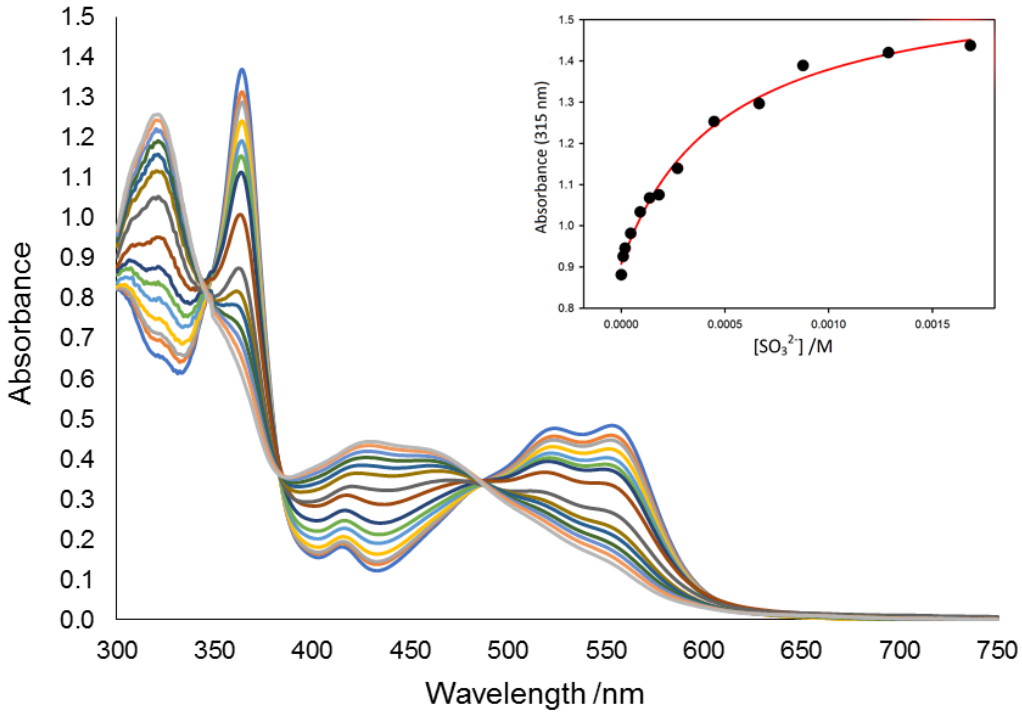

Figure 5.5 The electronic absorption spectrum from the titration of $[ACCbs]^{+}$ in the presence of 0.20 M N_3^- with SO_3^{2-} at pH 7.03, 30 °C. The insert shows a fit of Equation 2.3 to the absorbance changes observed at 315 nm.

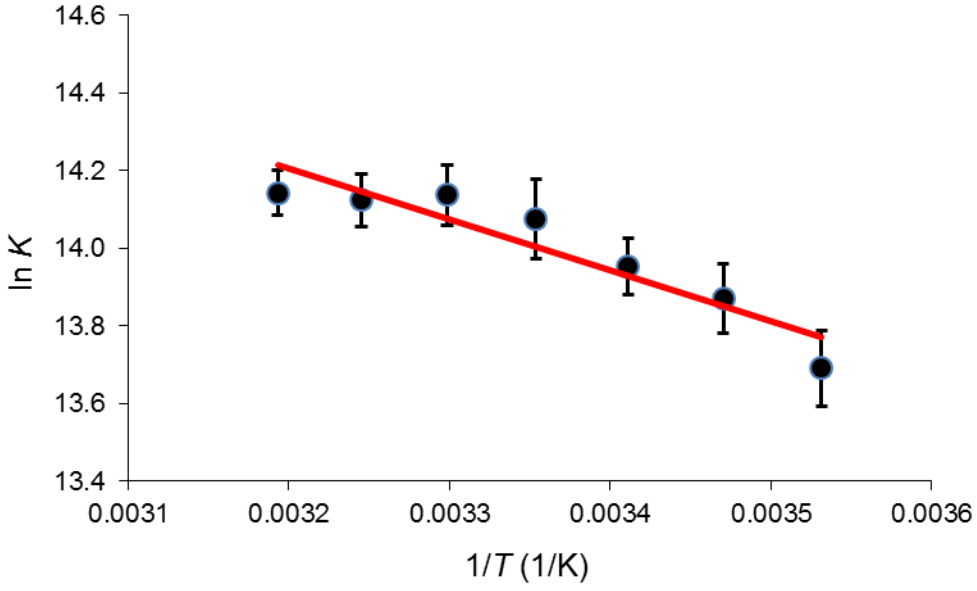

Figure 5.6 Plot of ln K against T^{-1} for coordination of SO_3^{2-} by $[(N_3)(CN)Cbs]$. From the slope $\Delta H = -10 \pm 2$ kJ mol^{-1} and from the intercept $\Delta S = 151 \pm 6$ J K^{-1} mol^{-1}. $R^2 = 0.861$.

References on page 170

5.2.2 Ligand Binding Studies with Cyanide

The ligand binding studies of cyanide with $[AC\text{-}5\text{-}seco\text{-}Cbs]^+$ were conducted by adding aliquots of a freshly prepared stock solution of NaCN (0.494 – 0.505 M, pH 8) to a solution of $[AC\text{-}5\text{-}seco\text{-}Cbs]^+$ buffered in Tris/HCl (μ = 0.1 M, pH 8), after which an absorption spectrum was recorded. With increasing complex formation, the 5-seco-cobester peak underwent a red shift from 462 nm to 480 nm (Figure 5.7).

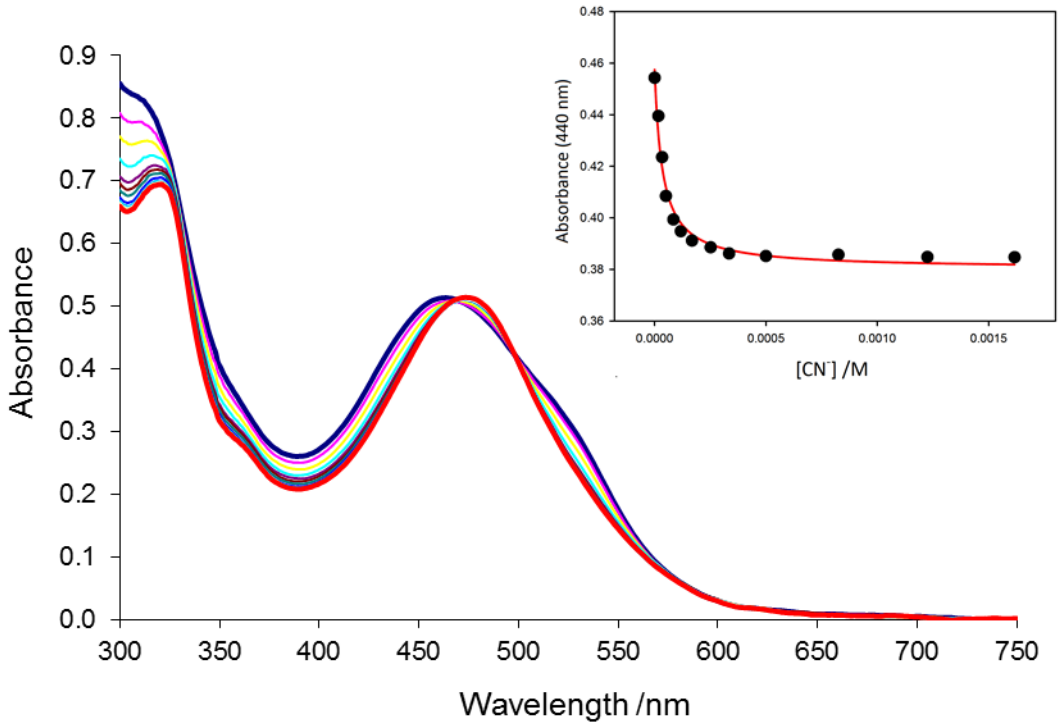

Figure 5.7 The electronic absorption spectrum from the titration of $[AC\text{-}5\text{-}seco\text{-}Cbs]^+$ with CN^- at pH 7.97, 25 °C. The insert shows a fit of Equation 2.5 to the absorbance changes observed at 440 nm.

The effective concentration of CN^- was determined using Equation 5.1 (it is assumed that log *K* for coordination of HCN is negligible compared to that for coordination of CN^-).

$$\text{Fraction of free cyanide anion} = 1/(1 + 10^{(pK\text{aHCN} - pH)})$$

[Equation 5.1]

References on page 170

Equation 2.5 was then fitted to experimental data obtained between 400 – 450 nm, 470 – 490 nm and 525 – 535 nm. It must be noted that the isotherm differs to that used for all other titrations as in this case the log *K* values were expected to be larger than 4 by analogy with observations made for $[ACCbs]^+$ and $[ACSYCbs]^+$ (Chapter 2.4.3).[3] The equilibrium constants obtained as a function of temperature are given in Table 5.3. Log *K* = 5.34 at 25 ˚C for the coordination of CN^- by $[AC\text{-}5\text{-}seco\text{-}Cbs]^+$.

$$A_\lambda = \frac{A_0 + A_1 K [L]_{free}}{1 + K [L]_{free}}$$

[Equation 2.5]

The binding of the smaller, strong field, soft cyanide ligand to Co(III) appears to be very favourable and in fact has the highest equilibrium constants for each macrocycle. Cyanide tends to be a very good ligand for transition metals because of its negative charge, small size and capability of engaging in π-bonding.[31] The favourable binding of cyanide to cobalt coordinated to a corrin macrocycle could be attributed to the synergistic bonding between cobalt and cyanide. Thus the bonding may occur in two ways. Firstly, cyanide can donate electron density to the cobalt ion by means of a σ bond, and secondly, the cobalt ion could donate some electron density to the cyanide ion through π bonding, thus fortifying the Co-CN bond which subsequently results in very high log *K* values.

We then proceeded to determine the ligand stoichiometry from a Hill plot (Equation 5.2).

$$\log\left[\frac{A_0 - A}{A - A_\infty}\right] = n \log(L) + \log K$$

[Equation 5.2]

where *A* corresponds to the absorbance at the monitored wavelength and A_0 and A_∞ correspond to the absorbance of the cobalt complex and cobalt-ligand complex, respectively, and the slope, n, gives ligand stoichiometry. We found that n = 1.06(5). Therefore, only one ligand coordinates at the binding site $[AC\text{-}5\text{-}seco\text{-}Cbs]^+$. This confirms that a single binding site is available on the corrin, as expected from the characterisation of the complex.

References on page 170

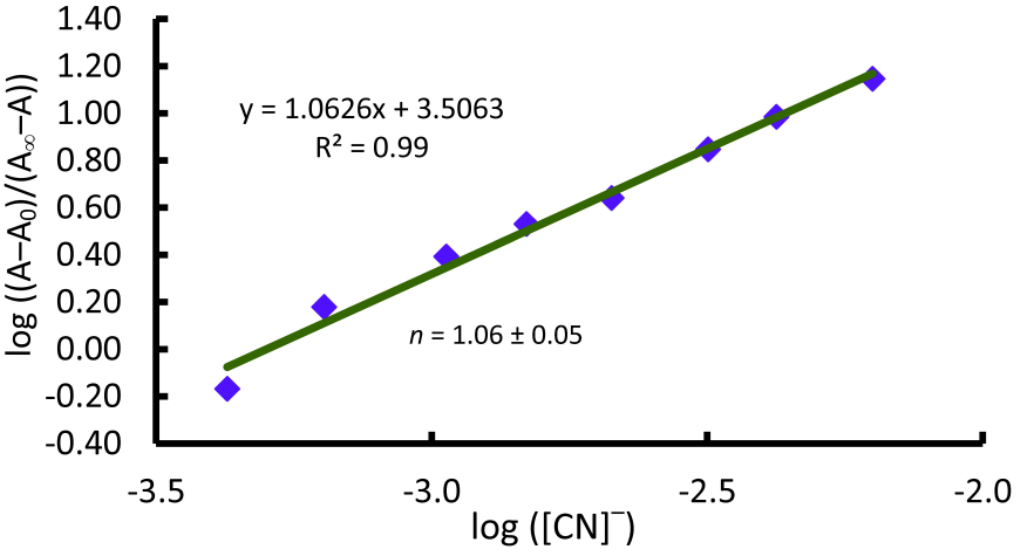

Figure 5.8 A Hill plot for the coordination of CN^- at 25 ^oC to $[AC\text{-}5\text{-}seco\text{-}Cbs]^+$ monitored at 420 nm. The slope gives the ligand stoichiometry, n = 1.06 ± 0.05. There are no further changes observed up to $[CN^-]$ of 0.25 M, affirming the availability of one single replaceable ligand in $[AC\text{-}5\text{-}seco\text{-}Cbs]^+$.

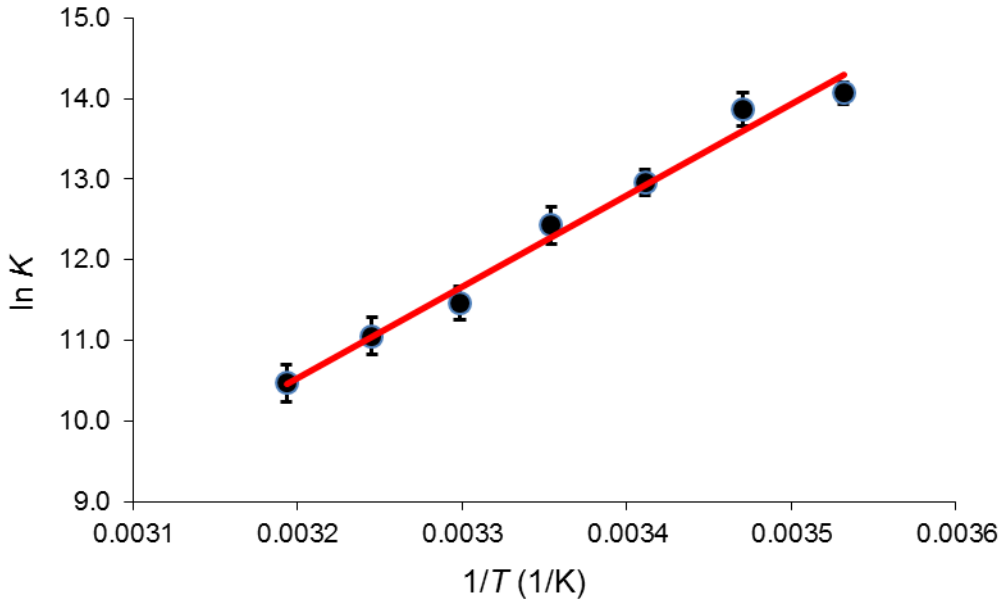

Figure 5.9 Plot of ln K against T^{-1} for coordination of CN^- by $[AC\text{-}5\text{-}seco\text{-}Cbs]^+$. From the slope ΔH = – 93 ± 5 kJ mol^{-1} and from the intercept ΔS = 209 ± 18 J K^{-1} mol^{-1}. R^2 = 0.985.

References on page 170

The equilibrium constants for the coordination of CN^- by $[ACCbs]^+$ were also re-determined in a competition reaction in the presence of 0.20 M N_3^-.

Aliquots of a stock solution of NaCN (0.009569 – 0.01020 M, pH 7) were added to a solution of $[ACCbs]^+$ buffered in MOPS (μ = 0.1 M, pH 7) in the presence of 0.2 M azide. Log *K* values were then first determined from the measured log *K* for substitution of N_3^- by CN^- by fitting Equation 2.5 to experimental data obtained between 325 – 335 nm, 365 – 375 nm, 460 – 470 nm and 580 – 590 nm and then correcting for the log *K* value for the substitution of axially coordinated H_2O by N_3^- (Table 5.3). Log *K* = 9.01 at 25 °C for the coordination of CN^- by [azidocyanoCbs].

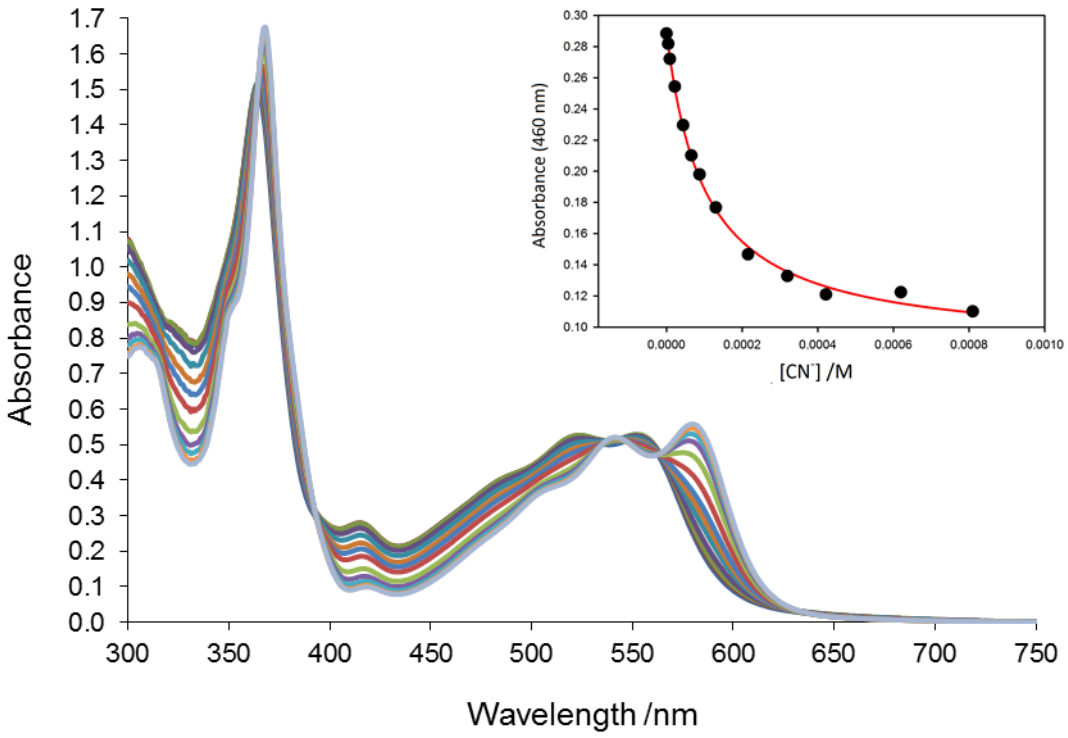

Figure 5.10 The electronic absorption spectrum from the titration of $[ACCbs]^+$ in the presence of 0.2 M N_3^- with CN^- at pH 7.03, 30 °C. The insert shows a fit of Equation 2.5 to the absorbance changes observed at 460 nm.

References on page 170

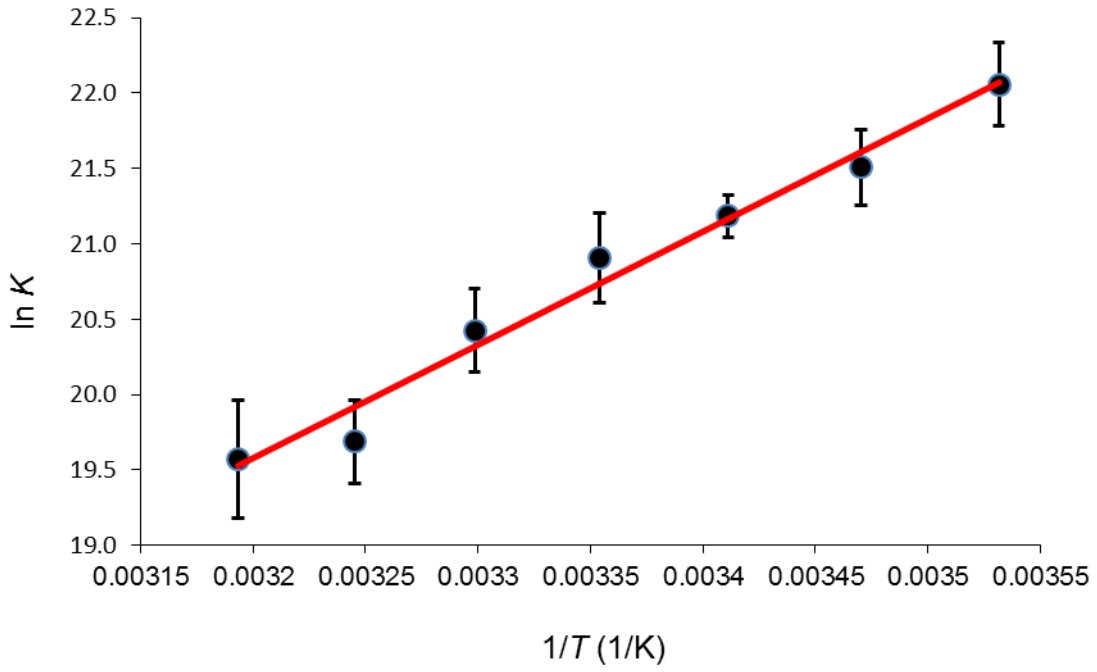

Figure 5.11 Plot of ln *K* against T^{-1} for coordination of CN^- by [(N_3)(CN)Cbs]. From the slope $\Delta H = -63 \pm 4$ kJ mol^{-1} and from the intercept $\Delta S = 38 \pm 14$ J K^{-1} mol^{-1}. $R^2 = 0.979$.

5.2.3 Ligand Binding Studies with Nitrite

The equilibrium constants for the coordination of nitrite to [AC-5-seco-Cbs]$^+$ were determined by adding aliquots of a stock solution of $NaNO_2$ (0.9041 – 0.9393 M, pH 7) to a solution of [AC-5-seco-Cbs]$^+$ buffered in MOPS (μ = 0.1 M, pH 7). Equation 2.3 was fitted to experimental data monitored between 420 – 480 nm. Log *K* = 2.43 at 25 ^oC for the coordination of NO_2^- by [AC-5-seco-Cbs]$^+$.

The equilibrium constants for the coordination of NO_2^- by [ACCbs]$^+$ were also re-determined by adding aliquots of a stock solution of $NaNO_2$ (0.0655 – 0.0838 M, pH 7) to a solution of [ACCbs]$^+$ buffered in MOPS (μ = 0.1 M, pH 7). Equation 2.3 was fitted to experimental data monitored between 450 – 490 nm and 545 – 575 nm. Log *K* = 3.08 at 25 ^oC for the coordination of NO_2^- by [ACCbs]$^+$.

References on page 170

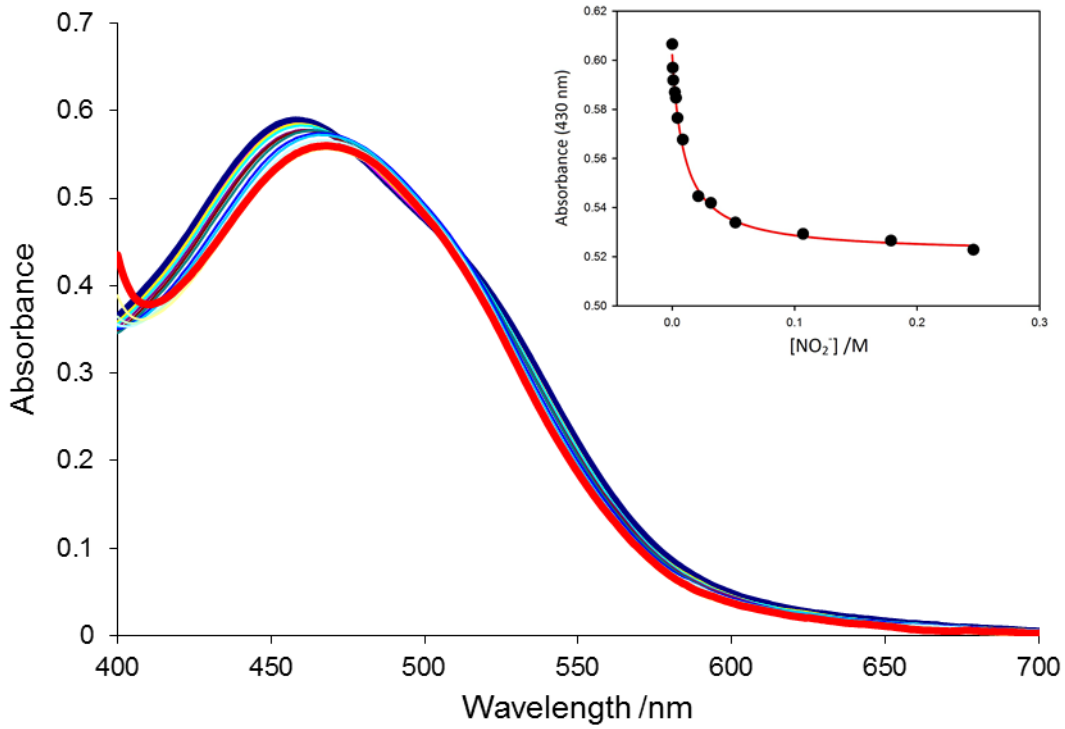

Figure 5.12 The electronic absorption spectrum from the titration of $[AC\text{-}5\text{-}seco\text{-}Cbs]^+$ with NO_2^- at pH 6.98, 25 °C. The insert shows a fit of Equation 2.3 to the absorbance changes observed at 430 nm.

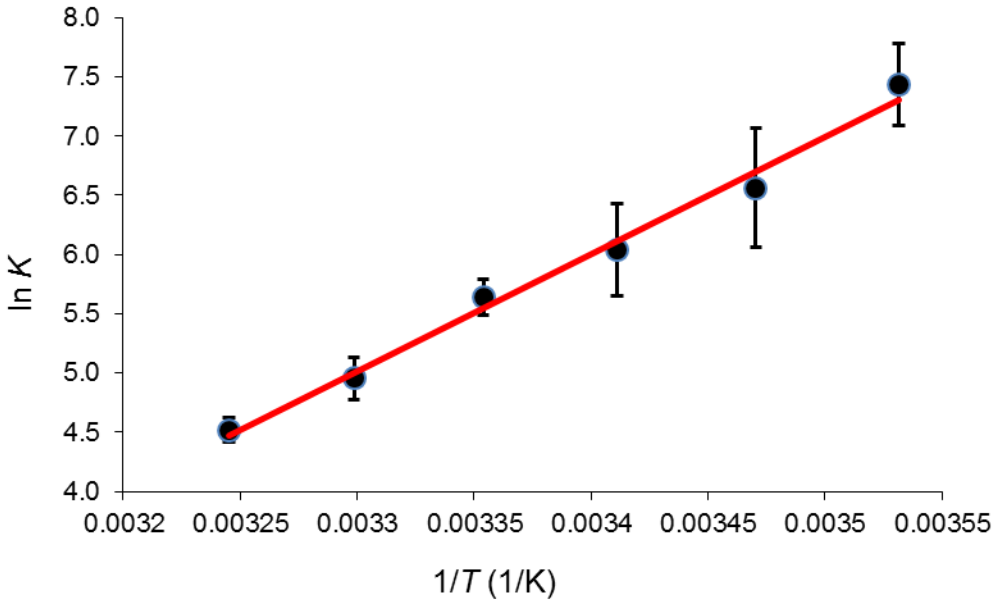

Figure 5.13 Plot of ln K against T^{-1} for coordination of NO_2^- by $[AC\text{-}5\text{-}seco\text{-}Cbs]^+$. From the slope $\Delta H = -82 \pm 3$ kJ mol^{-1} and from the intercept $\Delta S = -229 \pm 11$ J K^{-1} mol^{-1}. $R^2 = 0.993$.

References on page 170

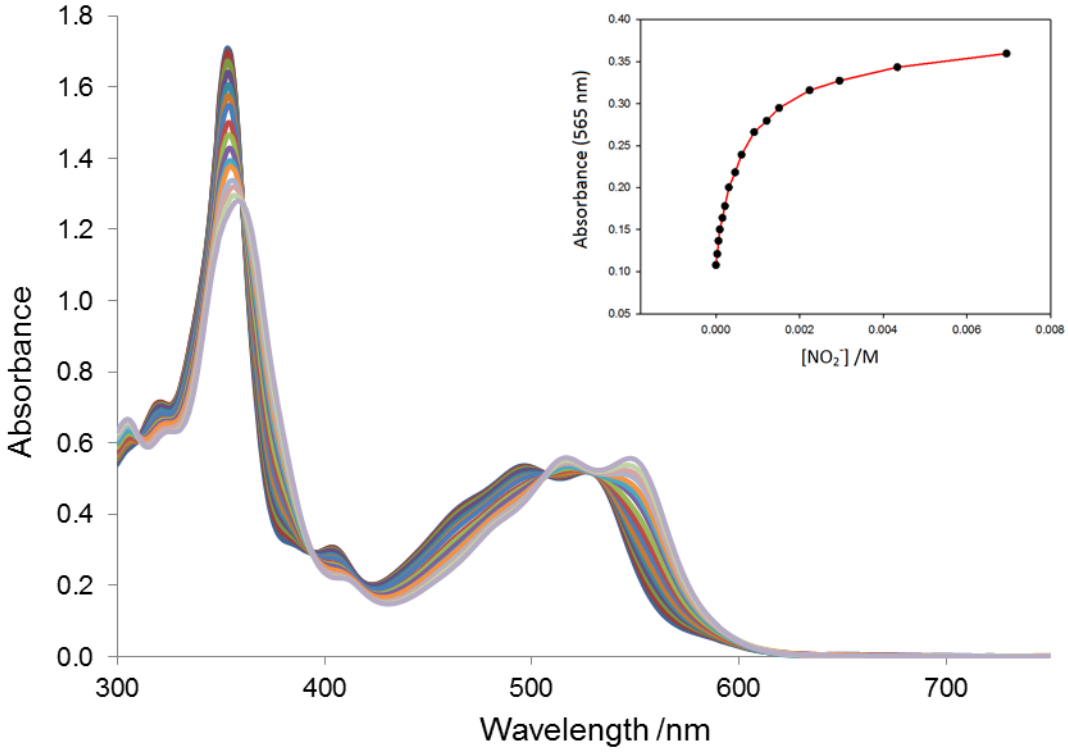

Figure 5.14 The electronic absorption spectrum from the titration of $[ACCbs]^+$ with NO_2^- at pH 7.02, 15 °C. The insert shows a fit of Equation 2.3 to the absorbance changes observed at 565 nm.

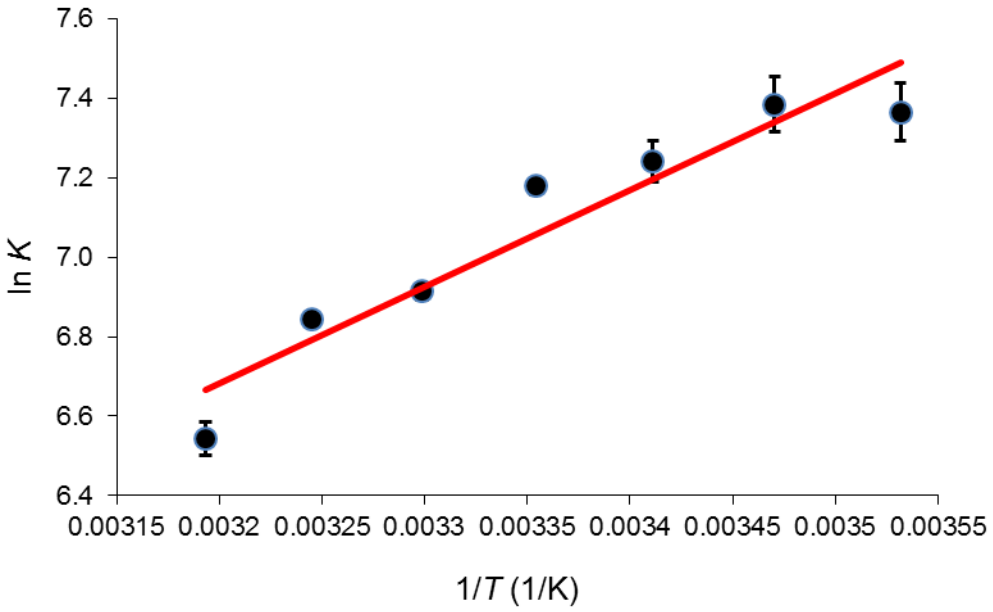

Figure 5.15 Plot of ln K against T^{-1} for coordination of NO_2^- by $[ACCbs]^+$. From the slope $\Delta H = -21 \pm 3$ kJ mol^{-1} and from the intercept $\Delta S = -11 \pm 10$ J K^{-1} mol^{-1}. $R^2 = 0.901$.

References on page 170

5.2.4 Ligand Binding Studies with Azide

Aliquots of stock solution of NaN_3 (0.2090 – 0.2167 M, pH 6) were added to a solution of $[AC\text{-}5\text{-}seco\text{-}Cbs]^+$ buffered with MES (μ = 0.1 M, pH 6). Aliquots of the azide solution were also added to the reference cuvette (buffer) so as to cancel out the effect of azide absorbing in the same wavelength range region as $[AC\text{-}5\text{-}seco\text{-}Cbs]^+$. Equation 2.3 was fitted to absorbance data obtained between 400 – 500 nm. Log *K* was found to be 2.96 at 25 °C.

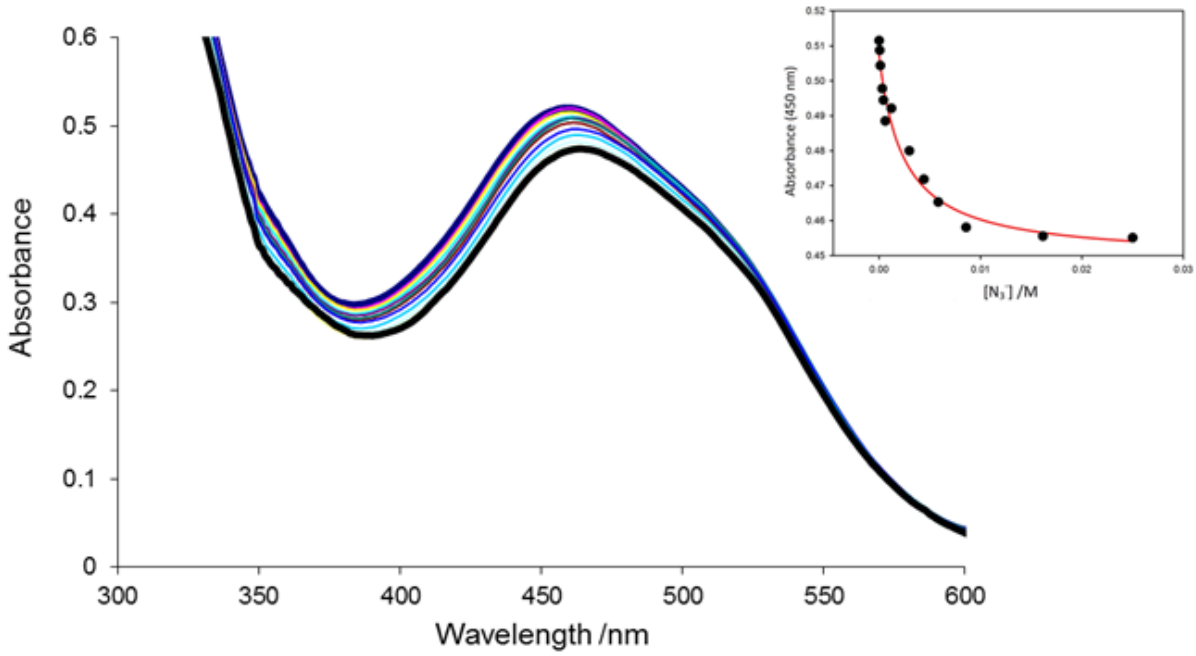

Figure 5.16 The electronic absorption spectrum from the titration of $[AC\text{-}5\text{-}seco\text{-}Cbs]^+$ with N_3^- at pH 6.04, 25 °C. The insert shows a fit of Equation 2.3 to the absorbance changes observed at 450 nm.

We then proceeded to determine the ligand stoichiometry from a Hill plot (Equation 5.2). We found that n = 1.08(7). Therefore, verifying once again that only one ligand coordinates at the binding site $[AC\text{-}5\text{-}seco\text{-}Cbs]^+$.

References on page 170

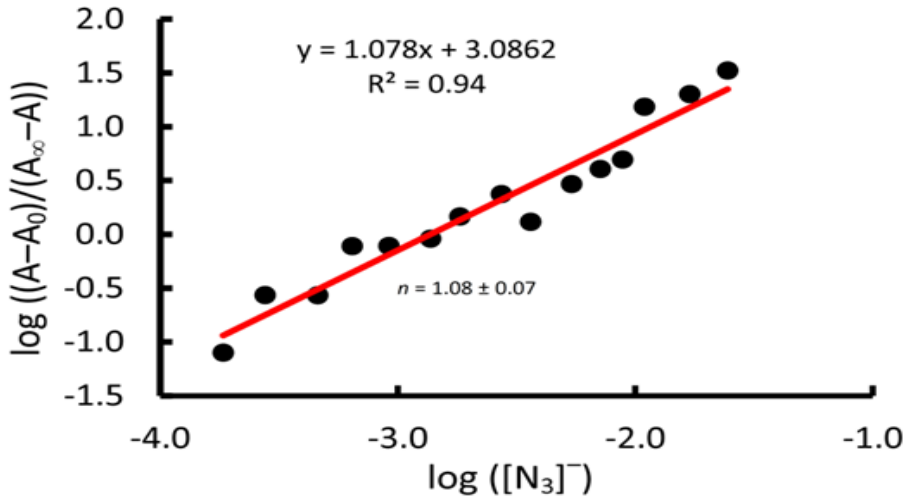

Figure 5.17 A Hill plot for the coordination of N_3^- by [AC-5-seco-Cbs]$^+$ at 420 nm. The slope gives the ligand stoichiometry, n = 1.08 ± 0.07.

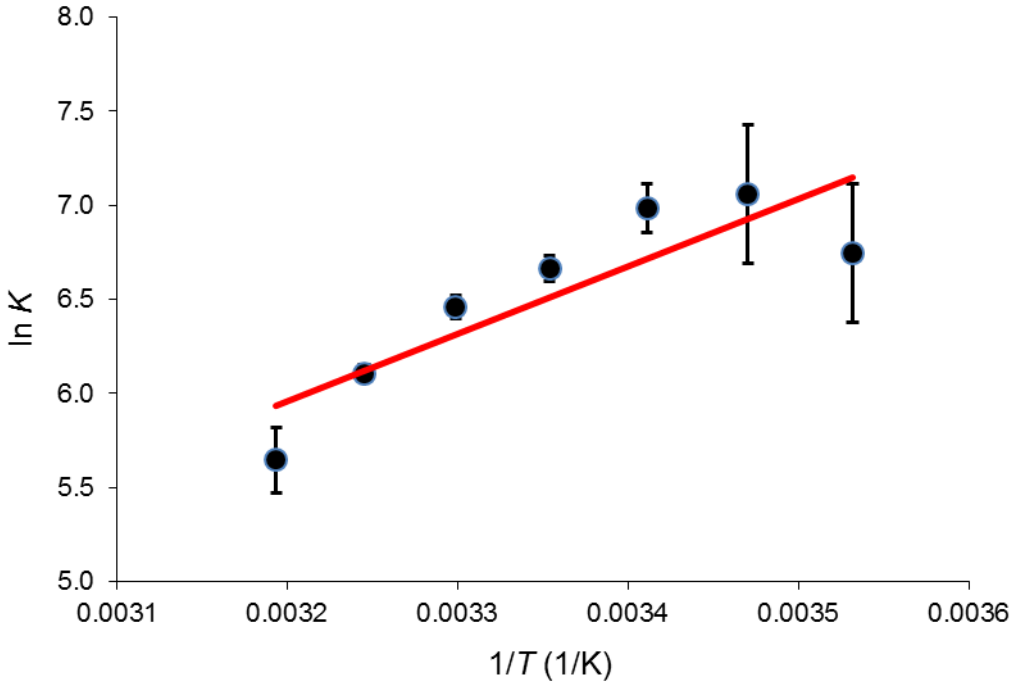

Figure 5.18 Plot of ln K against T^{-1} for coordination of N_3^- by [AC-5-seco-Cbs]$^+$. From the slope ΔH = – 44 ± 5 kJ mol^{-1} and from the intercept ΔS = 91 ± 15 J K^{-1} mol^{-1}. R^2 = 0.957.

References on page 170

The equilibrium constants for the coordination of N_3^- by $[ACCbs]^+$ were also re-determined by adding aliquots of a NaN_3 solution (0.143 – 0.982 M, pH 6) to a solution of $[ACCbs]^+$ buffered in MES (μ = 0.1 M, pH 6). Equation 2.3 was fitted to experimental data monitored between 345 – 375 nm, 455 – 465 nm and 550 – 560 nm. Log *K* = 2.75 at 25 °C for the coordination of N_3^- by $[ACCbs]^+$.

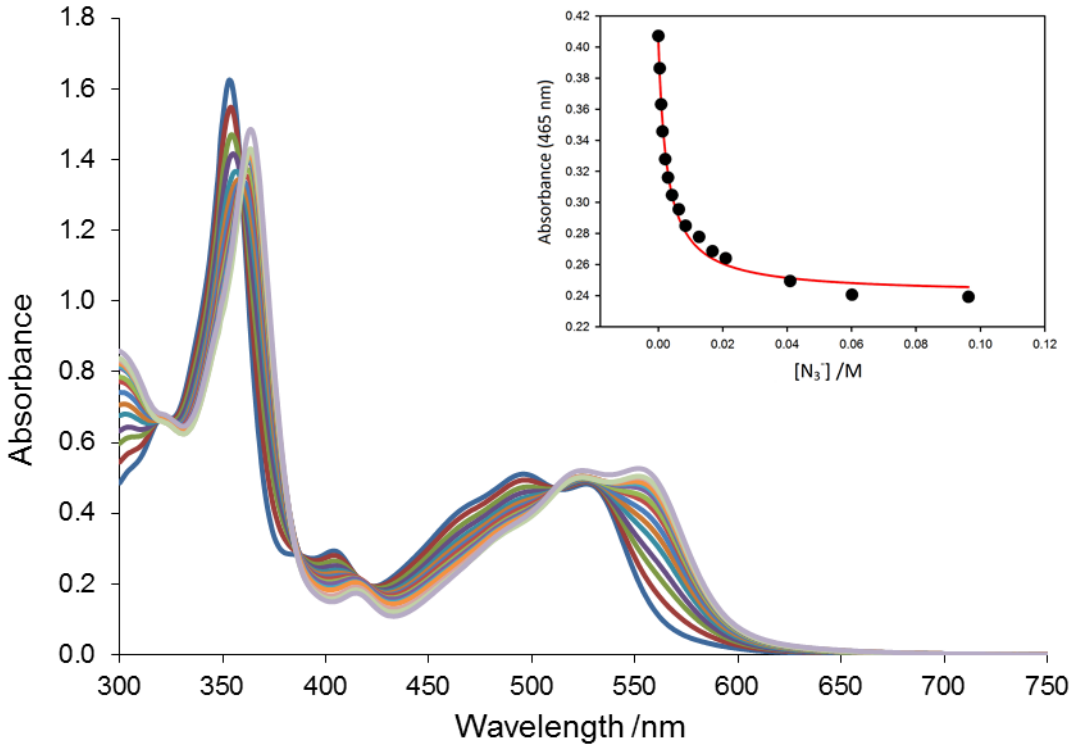

Figure 5.19 The electronic absorption spectrum from the titration of $[ACCbs]^+$ with N_3^- at pH 5.93, 25 °C. The insert shows a fit of Equation 2.3 to the absorbance changes observed at 465 nm.

References on page 170

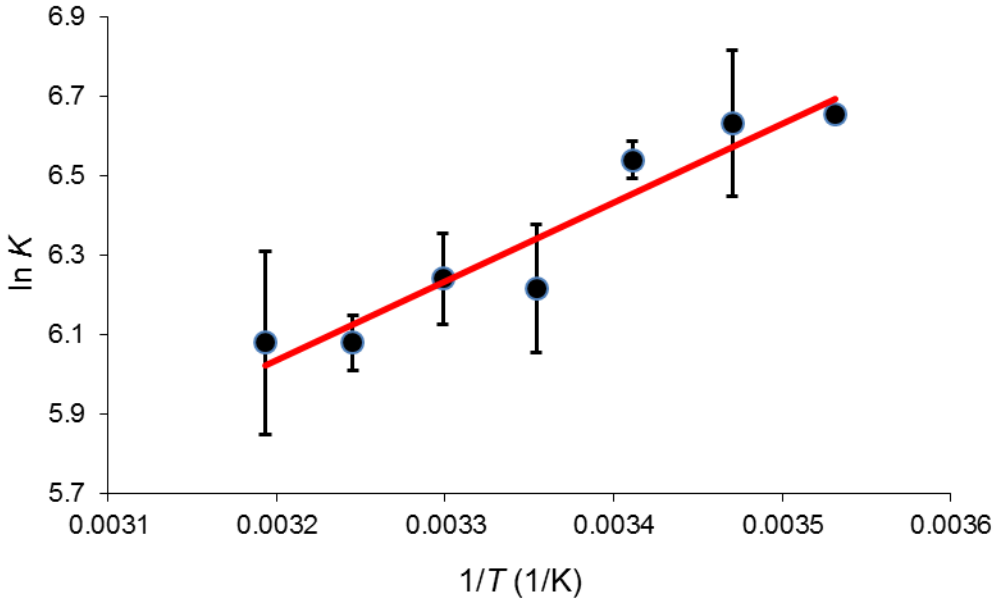

Figure 5.20 Plot of ln *K* against T^{-1} for coordination of N_3^- by $[ACCbs]^+$. From the slope $\Delta H = -16 \pm 2$ kJ mol^{-1} and from the intercept $\Delta S = 0 \pm 6$ J K^{-1} mol^{-1}. $R^2 = 0.933$.

5.2.5 Ligand Binding Studies with Thiosulfate

Aliquots of a stock solution of $Na_2S_2O_3$ (Sigma) solution (1.6653 – 1.6702 M, pH 6) were added to a solution of $[AC\text{-}5\text{-}seco\text{-}Cbs]^+$ buffered with MES (μ = 0.1 M, pH 6). Experimental data were analysed between 370 – 400 nm, 430 – 470 nm and 560 – 590 nm, to which Equation 2.3 was fitted. Log *K* was found to be 1.58 at 25 °C.

This result was very unexpected. Log *K* values available[3] for the coordination of $S_2O_3^{2-}$ to $[ACCbs]^+$ and $[ACSYCbs]^+$ are only 0.51(4) and – 0.21(1), respectively. It was also noted that titrations with $S_2O_3^{2-}$ were particularly problematic. It was then thought that perhaps the $S_2O_3^{2-}$ was contaminated with sulfites which would bind more readily to the cobalt ion, consequently resulting in false, higher log *K* values for the coordination of $S_2O_3^{2-}$. To test this, the titrations were repeated using $S_2O_3^{2-}$ sourced from a different supplier (Saarchem).

Using the same procedure, aliquots of thiosulfate (Saarchem, 1.67 M, pH 6.89) were added to a solution of $[AC\text{-}5\text{-}seco\text{-}Cbs]^+$ and an even higher log *K* value of 2.33(5) was obtained, which did not conclusively eliminate the possibility of sulfite contamination.

References on page 170

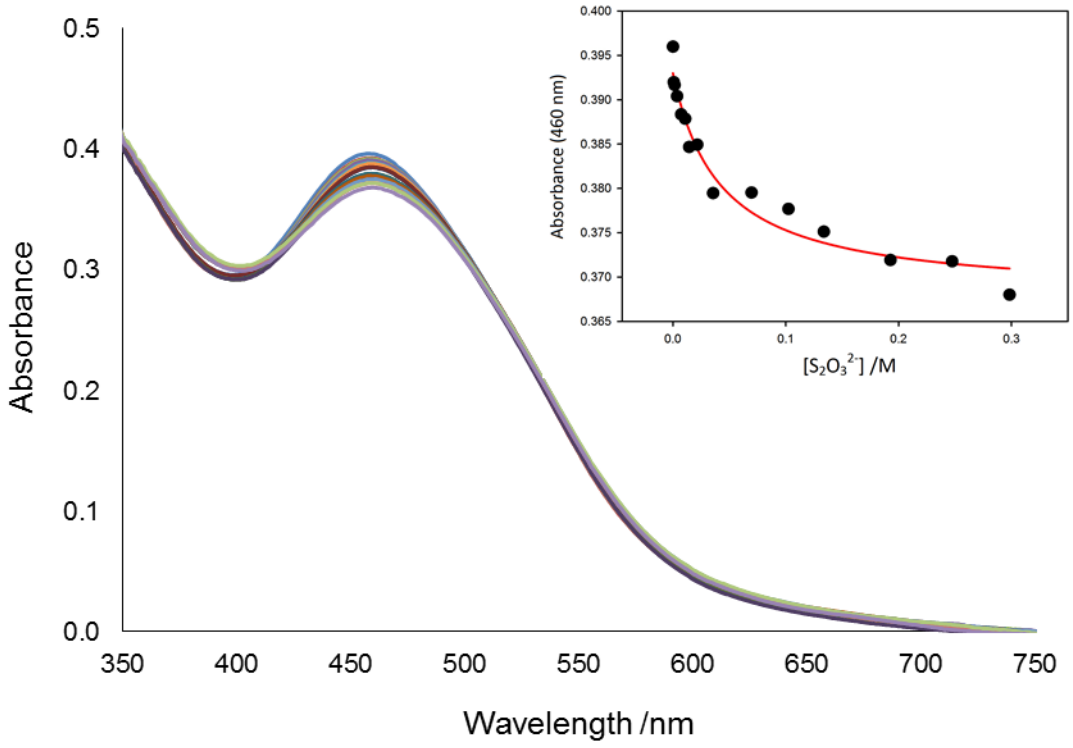

Figure 5.21 The electronic absorption spectrum from the titration of $[AC\text{-}5\text{-}seco\text{-}Cbs]^{+}$ with $S_2O_3^{2-}$ at pH 6.02, 25 °C. The insert shows a fit of Equation 2.3 to the absorbance changes observed at 460 nm.

A literature search showed that the electronic absorption spectrum resulting from the coordination of $S_2O_3^{2-}$ as well as SO_3^{2-} to another corrin complex, aquacobalamin, were well known.[31] Therefore, if the electronic spectrum of $S_2O_3^{2-}$ (Sigma) coordinated to aquacobalamin was recorded, one could simply compare the resulting spectrum to those obtained for coordinated $S_2O_3^{2-}$ and SO_3^{2-} as reported by Pratt,[32] so as to determine whether the change in absorbance observed was as a result of the coordination of $S_2O_3^{2-}$ or SO_3^{2-}.

Consequently, a solution of aquacobalamin was prepared, to which a crystal of $S_2O_3^{2-}$ was added. In the resulting electronic absorption spectrum (Figure 5.22), the γ band absorbed at 368 nm, which is consistent with the observation made by Pratt for the absorbance of a thiosulfate-corrin complex at 367 nm.[32] If a sulfite complex were to have formed, the γ band would have shifted to 346 nm. It can therefore be concluded that the $S_2O_3^{2-}$ sourced from Sigma-Aldrich is contaminant-free.

References on page 170

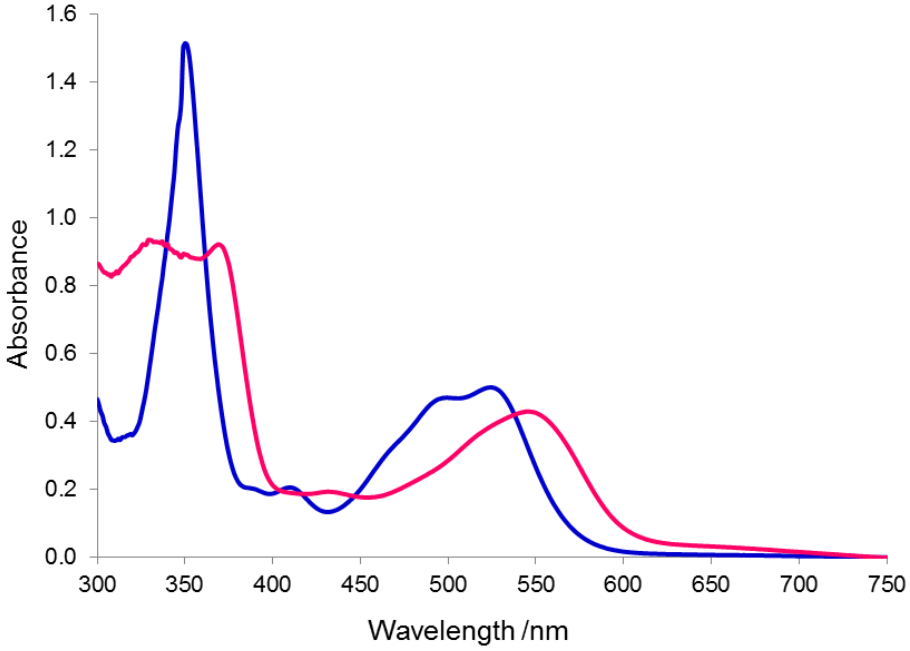

Figure 5.22 The electronic absorption spectrum of aquacobalamin (blue) and the coordinated $S_2O_3^{2-}$ complex (pink).

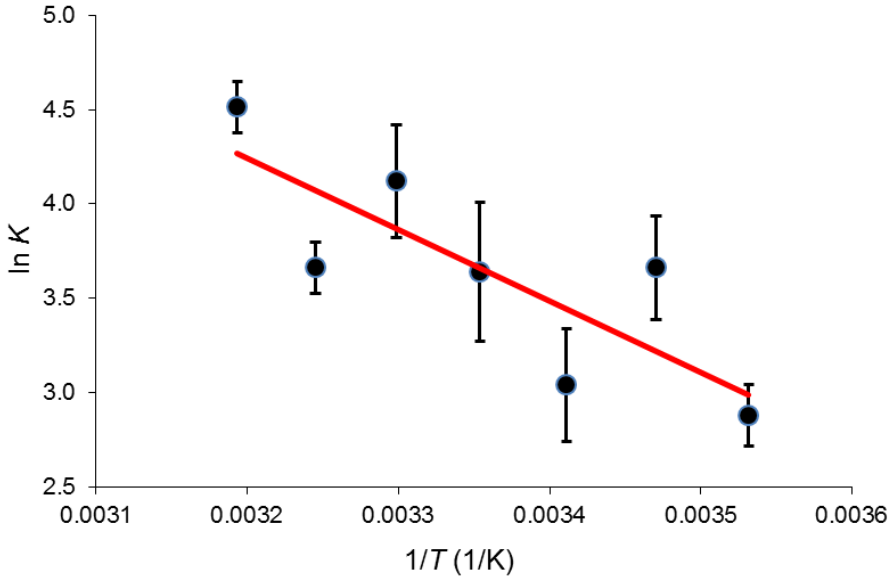

Figure 5.23 Plot of ln K against T^{-1} for coordination of $S_2O_3^{2-}$ by $[AC\text{-}5\text{-}seco\text{-}Cbs]^+$. From the slope ΔH = 32 ± 9 kJ mol^{-1} and from the intercept ΔS = 137 ± 30 J K^{-1} mol^{-1}. R^2 = 0.714.

The equilibrium constants for the coordination of $S_2O_3^{2-}$ by $[ACCbs]^+$ were then re-determined by adding aliquots of a stock $Na_2S_2O_3$ solution (1.7987 – 2.2960 M, pH 6) to a

References on page 170

solution of $[ACCbs]^+$ buffered in MES (μ = 0.1 M, pH 6). Equation 2.3 was fitted to experimental data monitored between 350 – 360 nm, 495 – 505 nm and 575 – 585 nm. Log *K* was found to be 0.68 at 25 °C.

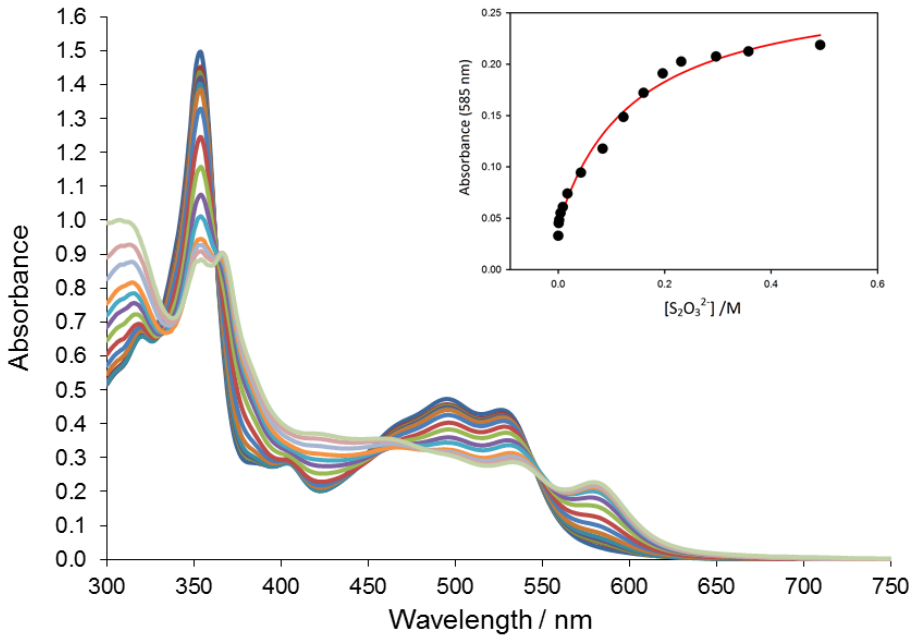

Figure 5.24 The electronic absorption spectrum from the titration of $[ACCbs]^+$ with $S_2O_3^{2-}$ at pH 6.12, 25 °C. The insert shows a fit of Equation 2.3 to the absorbance changes observed at 585 nm.

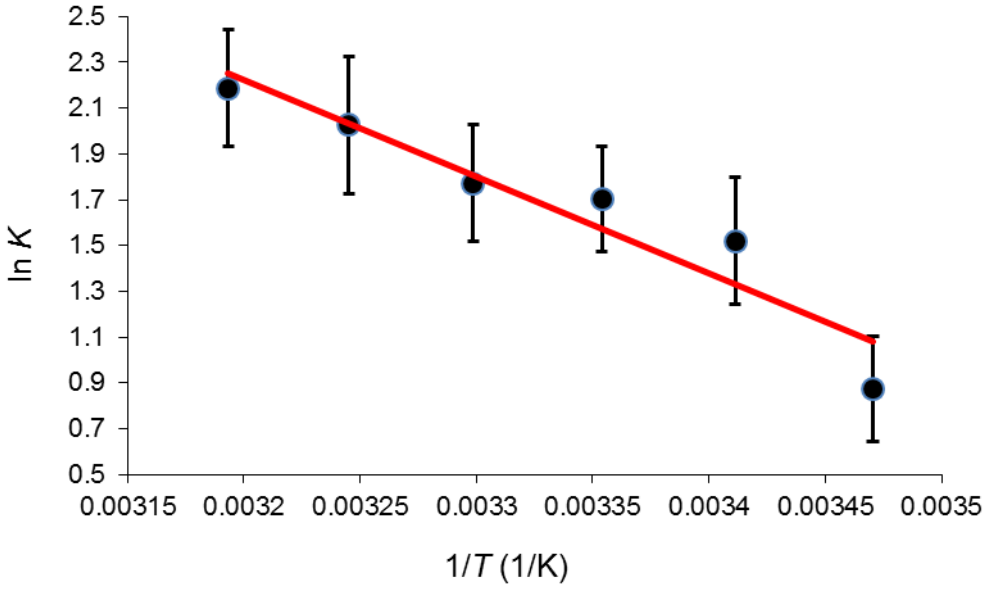

Figure 5.25 Plot of ln *K* against T^{-1} for coordination of $S_2O_3^{2-}$ by $[ACCbs]^+$. From the slope ΔH = 36 ± 6 kJ mol^{-1} and from the intercept ΔS = 134 ± 19 J K^{-1} mol^{-1}. R^2 = 0.907.

References on page 170

5.3 Summary of Results

Table 5.3 Equilibrium constants for the Substitution of Coordinated H_2O in $[ACCbs]^+$, $[AC\text{-}5\text{-}seco\text{-}Cbs]^+$ and $[ACSYCbs]^+$ by Some Anionic Ligands[a].

		$[ACCbs]^+$ [b]				**$[AC\text{-}5\text{-}seco\text{-}Cbs]^+$**				**$[ACSYCbs]^+$ [b]**		
ligand	***T* / °C**	**log *K***	**Δ*H* / kJ mol^{-1}**	**Δ*S* / J K^{-1} mol^{-1}**	**log K^{25}**	**log *K***	**Δ*H* / kJ mol^{-1}**	**Δ*S* / J K^{-1} mol^{-1}**	**log K^{25}**	**Δ*H* / kJ mol^{-1}**	**Δ*S* / J K^{-1} mol^{-1}**	**log K^{25}**
CN^-	10	9.58(12)	–63(4)	–38(14)	9.05	6.11(06)	–93(5)	–209(18)	5.38	*–17(1)*	*80(5)*	*7.16*
	15	9.34(11)	*–23(2)*	*81(6)*	*8.26*	6.02(09)						
	20	9.20(06)				5.63(07)						
	25	9.08(13)				5.40(10)						
	30	8.9(2)				4.98(09)						
	35	8.55(12)				4.80(10)						
	40	8.50(17)				4.55(10)						
SO_3^{2-}	10	5.95(2)	10(2)	151(6)	6.13	4.7(2)	–83(10)	–205(33)	3.83	*59(1)*	*253(5)*	*2.88*
	15	6.02(9)	*50(3)*	*265(9)*	*5.08*	4.5(2)						
	20	6.06(2)				3.9(2)						
	25	6.11(5)				3.8(2)						
	30	6.14(4)				3.6(3)						
	35	6.13(3)				3.7(3)						
	40	6.14(5)				3.2(1)						
NO_2^-	10	3.20(3)	–21(3)	–11(10)	3.11	3.2(2)	–82(3)	–229(11)	2.40	*–22.9(4)*	*–32(2)*	*2.34*
	15	3.21(3)	*–6.6(9)*	*33(3)*	*2.88*	2.9(2)						
	20	3.15(2)				2.6(2)						
	25	3.12(1)				2.45(7)						
	30	3.00(1)				2.15(8)						
	35	2.97(1)				1.96(5)						
	40	2.84(2)				1.2(2)						

References on page 170

	[ACCbs]$^{+}$ [b]					[AC-5-seco-Cbs]$^{+}$				[ACSYCbs]$^{+}$ [b]		
ligand	***T*** **/ °C**	**log *K***	**Δ*H* / kJ mol^{-1}**	**Δ*S* / J K^{-1} mol^{-1}**	**log *K*^{25}**	**log *K***	**Δ*H* / kJ mol^{-1}**	**Δ*S* / J K^{-1} mol^{-1}**	**log *K*^{25}**	**Δ*H* / kJ mol^{-1}**	**Δ*S* / J K^{-1} mol^{-1}**	**log *K*^{25}**
N_3^-	10	2.890(9)	–16(2)	0(6)	2.80		–44(5)	–91(15)	2.96	*–18.6(7)*	*–12(2)*	*2.63*
	15	2.88(8)	*–9.4(7)*	*18(3)*	*2.59*	3.1(2)						
	20	2.84(2)				3.03(6)						
	25	2.70(7)				2.90(3)						
	30	2.71(5)				2.81(3)						
	35	2.64(3)				2.65(2)						
	40	2.64(10)				2.45(8)						
$S_2O_3^{2-}$	10		36(6)	134(19)	0.69	1.25(7)	32(9)	137(30)	1.55			*0.6(2)* [c]
	15	0.38(10)	*21(3)*	*80(10)*	*0.50*	1.59(12)						
	20	0.66(12)				1.32(13)						
	25	0.74(10)				1.6(2)						
	30	0.77(11)				1.79(13)						
	35	0.88(13)				1.59(6)						
	40	0.95(11)				1.96(6)						

[a]Corrected for the effect of pH (Equation 2.6). [b]Values in italics from Chemaly *et al.* [3]. [c] From determination at a single temperature (25 °C).[3]

References on page 170

We hypothesised that the partially delocalised electron cloud and macrocyclic cavity size of the corrin rings are leading factors in the labilising of the central Co(III) ion. We undertook to investigate the effect varying these factors would have on the equilibrium constants for the coordination of various anionic ligands to the cobalt ion.

Log *K* values obtained in this study for the coordination of CN^-, SO_3^{2-}, NO_2^-, N_3^- and $S_2O_3^-$ by $[ACCbs]^+$ were somewhat lower than previously determined. Reasons for the numerical differences are unclear but, the affinity of the metal for the ligands follow the same order previously found (*viz*., log *K* for $CN^- > SO_3^{2-} > NO_2^- > N_3^- > S_2O_3^-$). Although there is a measure of uncertainty in the actual numerical values, the principal aim of this study was to establish a general trend in the binding of anionic ligands; hence the values obtained in this study only were used for the purpose of this discussion.

In a previous report comparing the chemistry of the Co(III) ion in $[ACCbs]^+$ and $[ACSYCbs]^+$,[3] it was found that since $[ACCbs]^+$ retains the 13-atom, 14 π-electron system that is normally associated with cobalt corrins, the corrin ring has an extensive conjugation system affording the metal a highly electron rich equatorial environment. The partially delocalised electron cloud can then transfer electron density onto the Co(III) ion, thus imparting to it a degree of softer Co(II) character. Consequently, $[ACCbs]^+$ binds to ligands with a softer donor atom, such as CN^- and SO_3^{2-} more readily than $[ACSYCbs]^+$. By contrast, $[ACSYCbs]^+$, which has the same macrocyclic cavity size as $[ACCbs]^+$, but with a diminished conjugated system as a result of the oxidation at the C5 position, binds harder ligands (N_3^-) better compared to $[ACCbs]^+$. It was concluded that interruption of the conjugation system resulted in a somewhat harder Co(III) center, and that this, in particular, discriminates against soft ligands.

The log $K^{25^\circ C}$ values for coordination of CN^- (Table 5.3) clearly indicate that $[ACCbs]^+$ (9.05) has a far higher affinity for this ligand than $[ACSYCbs]^+$ (7.16) or $[AC\text{-}5\text{-}seco\text{-}Cbs]^+$ (5.38); however, $[AC\text{-}5\text{-}seco\text{-}Cbs]^+$ has a higher affinity for SO_3^{2-} (3.83) than $[ACSYCbs]^+$ (2.88), both of which are much lower than $[ACCbs]^+$ (6.13). It is concluded that the Co(III) in the presence of an intact corrin equatorial ligand, as in $[ACCbs]^+$, has a significantly higher affinity for the soft ligands CN^- and SO_3^{2-} than Co(III) in a corrin with an interrupted π-conjugated system, as in $[ACSYCbs]^+$ or Co(III) in a corrin which has been cleaved, as in [AC-

References on page 170

5-seco-Cbs]$^+$. However, it is not a simple matter of the nature of the donor atom because the affinity is reversed in the case of $S_2O_3^{2-}$ for which log $K^{25^\circ C}$ for [AC-5-seco-Cbs]$^+$ > [ACCbs]$^+$ ≈ [ACSYCbs]$^+$ and must therefore reflect the electronic property of the ligand as a whole.

Although nitrite is an ambidentate ligand and can bind to the cobalt ion through either the harder oxygen atom or the softer nitrogen atom, the vast majority of six–coordinate Co(III) NO_2^- complexes with four other N-donor ligands, i.e., $[(N_4)LCo^{III}\text{-}(NO_2)]^{n+}$, bind NO_2^- through the nitro (N-bound) rather than the nitrito (O-bound) form. A search of the Cambridge Structural Database[38] produced 317 such nitro compounds, and only 6 nitrito compounds. Furthermore, nitrocobalamin has been crystallized and its structure reported,[33,34] but any reports of nitritocobalamin or allied structures (i.e., any nitrito-corrins, -corroles or -porphyrins) could not be found. It is therefore reasonably confidently concluded that NO_2^- coordinates Co(III) in [ACCbs]$^+$, [ACSYCbs]$^+$ and [AC-5-seco-Cbs]$^+$ through N. [ACCbs]$^+$ has a somewhat larger affinity for this ligand (log $K^{25^\circ C}$ = 3.11) than [ACSYCbs]$^+$ (2.34) or [AC-5-seco-Cbs]$^+$ (2.40). Also worth noting is that nitrite is stabilized by its resonance structure, and the negative charge of the anion is distributed equally between the two oxygen atoms. Thus the electron density of the ligand is less accessible for binding to cobalt, making it a poorer ligand for cobalt cobalt than CN^- or SO_3^{2-} as indicated by the lower log *K* values.

In the case of N_3^-, the electron density is less accessible for binding to the cobalt ion because of the internal stabilisation afforded by the resonance within the ligand; this also makes azide a comparatively poorer ligand for Co(III); the log $K^{25^\circ C}$ values are quite similar for all three Co(III) complexes. The pattern that emerges with [AC-5-seco-Cbs]$^+$ therefore confirms the observations previously noted for [ACCbs]$^+$ and [ACSYCbs]$^+$: interruption of the conjugation of the corrin, or its cleavage, significantly decreases the affinity of Co(III) for the softer ligands CN^-, SO_3^{2-} and, more marginally, NO_2^-, but has little effect on the affinity for a hard ligand such as N_3^-.

Values of log $K^{25^\circ C}$ do not reveal the full picture, however. It was reported elsewhere that there is a compensation effect between values of $\Delta H^\ddagger$ and $\Delta S^\ddagger$ for the kinetics of the ligand substitution reactions of Co(III) corrins, i.e., for a wide range of ligands both activation

References on page 170

parameters tend to decrease monotonically.[12,13, 29, 35-37] The effect is to level out the values of the second order rate constant for substitution of coordinated H_2O by a series of incoming ligands. A similar compensation effect between values of Δ*H* and Δ*S* was also observed in the study of the thermodynamics of the substitution of axially coordinated H_2O in $[ACCbs]^+$ and $[ACSYCbs]^+$ by anionic[3] and by neutral N-donor[18] ligands. That trend is evident again in the results reported here (Figure 5.26). What is striking, and unexpected, are the very negative values for Δ*H* (with the exception of $S_2O_3^{2-}$), offset by Δ*S* values which are also large and negative, for coordination of these anionic ligands by $[AC\text{-}5\text{-}seco\text{-}Cbs]^+$.

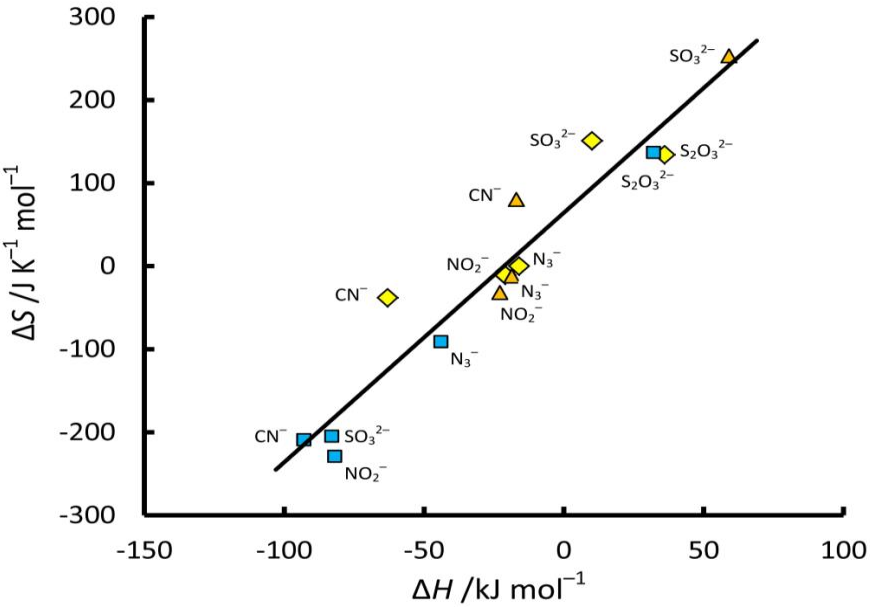

Figure 5.26 The compensation effect between Δ*H* and Δ*S* for coordination of anionic ligands by $[ACCbs]^+$ (◆), $[AC\text{-}5\text{-}seco\text{-}Cbs]^+$ (■) and $[ACSYCbs]^+$ (▲).

The macrocyclic cavity in a corrin is smaller than, for example, in a porphyrin. From a search of the Cambridge Structural Database[38], it was found that the N21–N23 and N22–N24 distances (i.e. the distance between the *trans* N-donors in the corrin macrocycle) are typically 3.8 Å (*n* =128 compounds, 290 observations, 3.616 Å min, 3.975 Å max), which is significantly smaller than the 3.9 Å found for all Co(III) porphyrins (*n* = 242 compounds, 496

References on page 170

observations, 3.789 Å min, 4.313 Å max). The covalent radius of N is 0.68 Å whereas that of Co is 1.33 Å. Thus, the sum of twice the covalent radius of N and Co is 4.0 Å. This highlights that in corrins, the metal ion is compressed compared to, for example, in a porphyrin. This relief of steric compression might be expected to significantly affect the behaviour of Co(III).

$[AC\text{-}5\text{-}seco\text{-}Cbs]^+$ has both the diminished π-electron system of $[ACSYCbs]^+$ and a cleaved macrocyclic ring.[39,40] Despite many attempts, diffraction-quality crystals of dicyano-5-seco-Cbs could not be obtained (the aquacyano derivative is very unlikely to crystallize because of its existence as a mixture of two diastereomers). As a result, DFT modeling was used to assess the effect that cleavage of the corrin has on the structure of the complexes. All DFT and Quantum Theory of Atoms in Molecules (QTAIM) modelling reported in this study was performed by Dr. Pradeep Varadwaj, Dr. Arpita Varadwaj and Prof. Koichi Yamashita at the University of Tokyo.

The BP86 functional is known to reproduce the structures and properties of cobalt corrinoids (such as the Co–C bond dissociation energy of adenosylcobalamin) quite well, especially if dispersion is taken into account.[41-44] This was verified for [DCCbs] by comparing the geometry of the coordination sphere of the metal, and the corrin fold angle (the angle between the mean planes through N21, C4, C5, C6, N22, C9 and C10, and N24, C16, C15, C14, N23, C11 and C10)[74] of the crystal structure of [DCCbs] (CSD refcode CODZAW10)[45] and of [DCSYCbs] (CSD refcode XEHDIZ)[6] with the geometry and fold angle of the DFT structures obtained with a 6-311++G(d,p) basis set and the BP86-D3, B3LYP, PBE0 and PBEPBE functionals. For reasons explained below, the structures were also energy minimized with BP86-D3/6-311G(d,p). The results are summarized in Appendix J.1 and confirm that the BP86-D3 functional best reproduces the XRD structures.

The model of [DCSYCbs] failed to converge using the 6-311++G(d,p) basis set even after several hundred iterations. A smaller basis set, 6-311G(d,p), was therefore used for the modelling. The DFT modelling reproduced the structures of [DCCbs] and [DCSYCbs] reasonably well, including the corrin fold angle. It may appear that the smaller basis set actually reproduces the coordination sphere of [DCCbs] better (average relative percentage

References on page 170

deviation of 0.42%) than the larger basis set (0.56%), but given that the average esd for bond lengths in the crystallographic structure is 0.01 – 0.03 Å, there was no statistically significant difference between the two models, and between the models and the crystallographic structure.

The coordination sphere geometry of [DCSYCbs] is quite well reproduced using BP86-D3/6-311G(d,p), although the Co–N(22) bond length is too long by 0.03 Å. The corrin fold angle of 15.6^{o} is somewhat over-estimated, at 19.6^{o}, in the modelled structure. The bond angles are reproduced to better than 2^{o}. The DFT–minimized structures of the models of [DCCbs], [DCSYCbs] and [DC-5-seco-Cbs] are shown in Figure 5.27 below. Overlays of the XRD structures of [DCCbs] and [DCSYCbs] and the modelled structures are shown in Figure 5.28. A comparison of the coordination geometry of the BP86-D3/6-311G(d,p)-modelled structures of [DCCbs], [DCSYCbs] and [DC-5-seco-Cbs] is given in Table 5.4. Given the good agreement between the DFT and XRD structures of [DCCbs] and [DCSYCbs], there is some confidence in the structure of [DC-5-seco-Cbs].

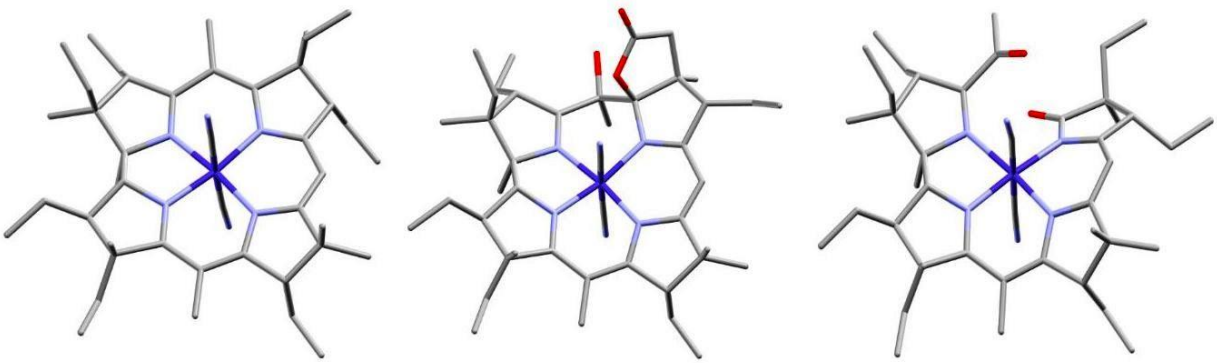

Figure 5.27 DFT predicted (BP86/6-311G(d,p)) models of [DCCbs], [DCSYCbs] and [DC-5-seco-Cbs].

References on page 170

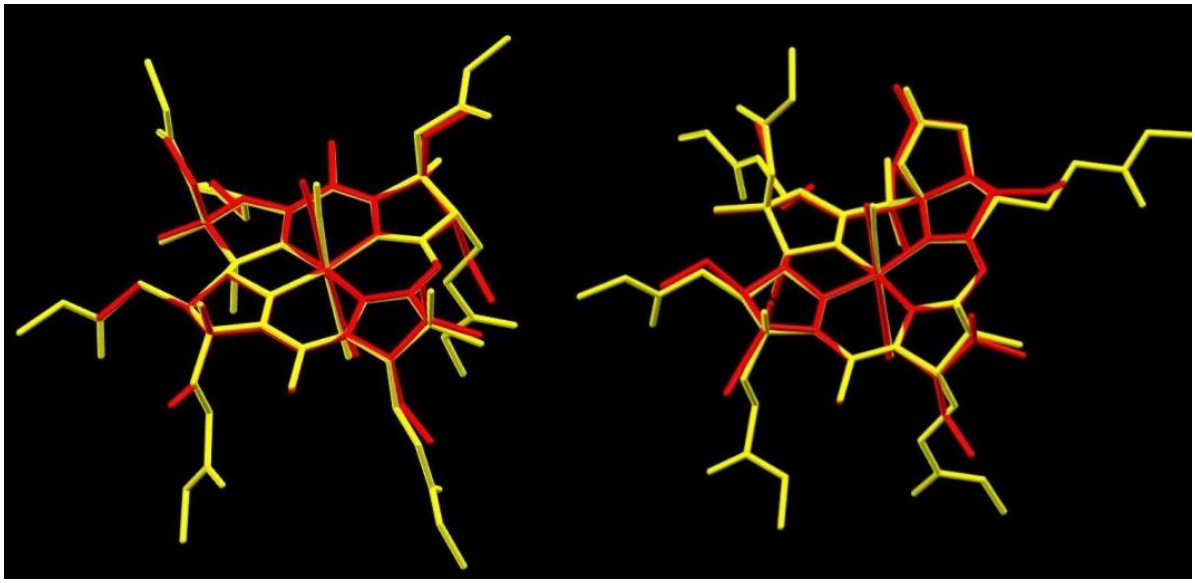

Figure 5.28 An overlay of the XRD structures of [DDCbs] and [DCSYCbs] (yellow) and their BP86/6-311G(d,p) models (red). The overlay is the best fit of the 24 atoms of the corrin core and Co. RMS deviation of [DCCbs] = 0.091 Å, and 0.141 Å for [DCSYCbs].

Table 5.4 Comparison of the coordination sphere geometry of BP86-D3/6-311G(d,p)-modelled structures of [DCCbs], [DCSYCbs] and [DC-5-seco-Cbs].

	[DCCbs]	[DCSYCbs]	[DC-5-seco-Cbs]
Bond /Å			
Co – CN(α)	1.925	1.920	1.917
Co – CN(β)	1.928	1.928	1.928
Co – N(21)	1.890	1.902	1.947
Co – N(22)	1.937	1.943	1.968
Co – N(23)	1.933	1.916	1.924
Co – N(24)	1.891	1.878	1.893
Angle /deg			
CN(α) – Co– CN(β)	176.8	173.3	174.4
N(21)– Co – N(23)	173.4	172.8	169.7
N(22)– Co– N(24)	173.2	168.4	174.5
Corrin fold angle	3.3	19.6	33.0

The cleavage of the corrin does not unduly perturb the coordination sphere of the metal ion and the metal remains essentially octahedral. The Co–N bonds lengths to N(21) and N(22)

References on page 170

increase significantly, while the Co–N(23) and Co–N(24) bond lengths do not change appreciably. The Co–CN bond length to CN coordinated on the α face is shorter by 0.008 Å, but the bond to the β–CN does not change. The very similar bond lengths to CN^- offer an explanation as to why ν_{CN} for [DC-5-seco-Cbs] (2124 cm^{-1}) is very similar to that for [DCCbs] itself (2123 cm^{-1}).

Compared to $[ACCbs]^+$, $[AC\text{-}5\text{-}seco\text{-}Cbs]^+$ has a significantly lower affinity for the CN^-, SO_3^{2-} and NO_2^-, but a higher affinity for N_3^- and $S_2O_3^{2-}$. This is similar to the trend seen between $[ACCbs]^+$ and $[ACSYCbs]^+$. This trend clearly does not correlate with the hardness of the donor atom *per se* (S is the donor in both SO_3^{2-} and $S_2O_3^{2-}$, and N is the donor in both NO_2^- and in N_3^-). There appears to be a correlation with the position of these ligands in the spectrochemical series.[45,46] The order in the spectrochemical series of the ligands under consideration is $N_3^- < S_2O_3^{2-} < \underline{N}O_2^- < SO_3^{2-} < CN^-$. The first two behave as π donors towards metal ions, and the last three, being much higher in the series, as π acceptor ligands. This therefore suggests that as the hardness of the metal increases and its electron density decreases in the order $[ACCbs]^+ > [ACSYCbs]^+ \approx [AC\text{-}5\text{-}seco\text{-}Cbs]^+$, so the thermodynamic stability of its complexes with the π acceptor ligands decreases, i.e., the metal becomes less capable of participating in M→L charge transfer. Conversely, the thermodynamic stability of the complexes with the π donor ligands increases as the metal ion becomes more Co(III)–like, and is more capable of accepting electron density from the ligand.

In order to gain further insight and to test this explanation, DFT modeling with BP86-D3/6-311G(d,p) was used to determine the structures of $[\alpha\text{-}CN^-,\beta\text{-}X\text{-}5\text{-}seco\text{-}Cbs]^{n+}$ and $[\alpha\text{-}X,\beta\text{-}CN^-\text{-}5\text{-}seco\text{-}Cbs]^{n+}$. As with the modeling of [DC-5-seco-Cbs], the ester side chains of the corrin were truncated to ethyl groups. The difficulty that arises is that these complexes almost certainly exist as mixtures of two diastereomers in solution and there seems to be no simple way to determine the relative proportion of the two; they could not be separated using HPLC (they co-elute as a broad band) or TLC (streaking on the plates). Moreover, although the DFT modeling adequately reproduces the structures of [DCCbs] and [DCSYCbs], there is no way of determining the adequacy of the modeling in reproducing the structure of [DC-5-seco-Cbs], let alone its complexes with other ligands. The partial charge q(r) (in units of *e*) on Co and the six donor atoms in its inner coordination sphere are given in Appendix J.2.

References on page 170

The charge on Co and the average charge on, firstly, Co and the six donor atoms of its inner coordination sphere (averaged over the two diastereomers where applicable) and, secondly, on Co and the four corrin N donor atoms, are given in Table 5.5.

Table 5.5. Charges q(r)/*e* on cobalt and the six inner coordination sphere donor atoms in $[(X)(CN)Co(corrin)]^{n+}$ complexes determined from a QTAIM analysis of the wavefunction of their BP86–D3/6–311G(d,p) structures.

X	Corrin	Co	Σ Coord Sphere	Σ(Co & eq N)
CN^-	Cbs	1.125	– 1.645	– 2.919
	SYCbs	1.112	– 1.647	– 2.929
	5-Seco-Cbs	1.118	– 1.564	– 2.858
SO_3^{2-}	Cbs	1.057	0.124	– 2.965
	SYCbs	1.042	0.120	– 2.988
	5-Seco-Cbs	1.052	0.166	– 2.926
NO_2^-	Cbs	1.146	– 1.868	– 2.896
	SYCbs	1.133	– 1.873	– 2.914
	5-Seco-Cbs	1.137	– 1.787	– 2.843
N_3^-	Cbs	1.152	– 2.564	– 2.884
	SYCbs	1.145	– 2.586	– 2.897
	5-Seco-Cbs	1.152	– 2.502	– 2.825
H_2O	Cbs	1.131	– 3.321	– 2.951
	SYCbs	1.126	– 3.359	– 2.971
	5-Seco-Cbs	1.137	– 3.311	– 2.920

There is no trend in the partial charge on Co itself. However, the sum of the partial charges on the metal and the entire coordination sphere, or the metal and the four equatorial donor N atoms, becomes less negative in the 5-seco-Cbs complexes than in either the cobesters themselves or the stable yellow cobesters. This lends support to the notion that cleavage of the corrin has made the metal and its immediate environment more positive (or less negative). However, in the stable yellow cobesters the metal and its environment is *less* positive than in the cobesters, contrary to our expectations and the rationalization used to explain the trends in log *K* values.[3,18] QTAIM charges are generally believed to be

References on page 170

reliable,[47,48] so it appears likely that log *K* values are a function of multiple factors, the charge on the metal and its immediate environment probably being only one of them.

In the absence of a crystal structure, DFT modelling was relied on to provide an indication of the likely geometry around the coordination sphere of the metal ion. A topological analysis of the electron density was used to provide insight into the strength and nature of the chemical bonds. The charge density, ρ_r, at a bond critical point is an indicator of the strength of a chemical bond,[49-53] while the ratio of the potential and kinetic energy densities at the bond critical point, $|V_r|/G_r$, is useful to characterize the nature of a chemical bond.[54] In particular, chemical bonds where $|V_r|/G_r < 1$ are characteristic of predominantly closed shell (ionic) interactions. They are also characterized by small values of ρ_r, a relatively small and positive value of the Laplacian of the electron density, $\nabla^2\rho_r$, and a positive value for the total electronic energy density, H_r ($= V_r + G_r$ [55]) that is close to zero;[56] metal-ligand bonds usually have $H_r < 0$ and close to zero.[54, 55, 57–59] Bonds with $|V_r|/G_r > 2$ are typically covalent interactions; and $1 < |V_r|/G_r, < 2$ is diagnostic of bonds of intermediate character. A full analysis of the coordination sphere of the modelled compounds is given in Appendix J.3. and summarized in Table 5.6.

Table 5.6 Average coordination sphere bond lengths and topological properties of the electron density at bond critical points in $[(X)(CN)Co(corrin)]^{n+}$ complexes determined from a QTAIM analysis of the wavefunction of their BP86-D3/6-311G(d,p) structures.[a]

Corrin	Bond	Bond length (av) /Å	ρ_r (av)	$\nabla^2\rho_r$ (av)	V_r (av)	G_r (av)	H_r (av)	$\lvert V_r\rvert/G_r$ (av)
$[(CN)_2Co(Corrin)]$								
Cbs	Co-CN	1.927	0.116	0.287	– 0.146	0.109	– 0.037	1.335
SYCbs		1.924	0.116	0.289	– 0.147	0.109	– 0.038	1.349
5-Seco-Cbs		1.923	0.116	0.283	– 0.147	0.109	– 0.038	1.349
Cbs	Co-N(corrin)	1.913	0.110	0.449	– 0.166	0.139	– 0.027	1.189
SYCbs		1.910	0.111	0.450	– 0.168	0.140	– 0.028	1.198
5-Seco-Cbs		1.933	0.104	0.431	– 0.155	0.131	– 0.024	1.178
$[(SO_3(CN)Co(corrin)]^-$								
Cbs	Co-SO_3	2.334	0.080	0.107	– 0.067	0.047	– 0.020	1.430

References on page 170

Corrin	Bond	Bond length (av) /Å	ρ_r (av)	$\nabla^2\rho_r$ (av)	V_r (av)	G_r (av)	H_r (av)	$\lvert V_r \rvert / G_r$ (av)
SYCbs		2.401	0.070	0.091	– 0.056	0.039	– 0.017	1.423
5-Seco-Cbs		2.240	0.069	0.098	– 0.057	0.041	– 0.016	1.399
Cbs	Co-CN	1.993	0.099	0.271	– 0.121	0.095	– 0.027	1.284
SYCbs		1.975	0.103	0.280	– 0.128	0.099	– 0.029	1.293
5-Seco-Cbs		1.918	0.109	0.278	– 0.135	0.102	– 0.033	1.319
Cbs	Co-N(corrin)	1.898	0.113	0.486	0.179	– 0.150	0.029	1.191
SYCbs		1.894	0.114	0.488	0.181	– 0.152	0.030	1.194
5-Seco-Cbs		1.929	0.110	0.470	0.171	– 0.144	0.027	1.185
[(NO_2)(CN)Co(corrin)]								
Cbs	Co-NO_2	1.995	0.096	0.352	– 0.126	0.107	– 0.019	1.179
SYCbs		2.018	0.099	0.400	– 0.116	0.100	– 0.017	1.166
5-Seco-Cbs		2.028	0.089	0.321	– 0.112	0.096	– 0.016	1.165
Cbs	Co-CN	1.913	0.120	0.283	– 0.150	0.110	– 0.039	1.358
SYCbs		1.910	0.120	0.285	– 0.151	0.111	– 0.040	1.359
5-Seco-Cbs		1.910	0.120	0.279	– 0.150	0.110	– 0.040	1.365
Cbs	Co-N(corrin)	1.906	0.112	0.462	0.172	– 0.144	0.028	1.195
SYCbs		1.907	0.110	0.442	0.171	– 0.143	0.028	1.195
5-Seco-Cbs		1.941	0.105	0.438	0.158	– 0.134	0.024	1.178
[(N_3)(CN)Co(corrin)]								
Cbs	Co-N_3	2.047	0.078	0.292	– 0.098	0.086	– 0.013	1.146
SYCbs		2.040	0.079	0.301	– 0.100	0.088	– 0.013	1.143
5-Seco-Cbs		2.030	0.082	0.304	– 0.104	0.090	– 0.014	1.153
Cbs	Co-CN	1.878	0.129	0.294	– 0.165	0.119	– 0.045	1.382
SYCbs		1.880	0.128	0.295	– 0.164	0.119	– 0.045	1.380
5-Seco-Cbs		1.884	0.127	0.287	– 0.161	0.116	– 0.045	1.383
Cbs	Co-N(corrin)	1.906	0.112	0.462	0.171	– 0.143	0.028	1.194
SYCbs		1.906	0.112	0.460	0.171	– 0.143	0.028	1.195
5-Seco-Cbs		1.929	0.105	0.439	0.157	– 0.134	0.024	1.177
[(H_2O)(CN)Co(corrin)]$^+$								
Cbs	Co-OH_2	2.180	0.046	0.250	– 0.063	0.063	0.000	0.995
SYCbs		2.169	0.050	0.271	– 0.068	0.068	0.000	0.999
5-Seco-Cbs		2.083	0.061	0.341	– 0.086	0.085	0.000	1.004
Cbs	Co-CN	1.820	0.147	0.268	– 0.189	0.128	– 0.061	1.473
SYCbs		1.825	0.146	0.271	– 0.186	0.127	– 0.059	1.466

References on page 170

Corrin	Bond	Bond length (av) /Å	ρ_r (av)	$\nabla^2\rho_r$ (av)	V_r (av)	G_r (av)	H_r (av)	$\lvert V_r\rvert / G_r$ (av)
5-Seco-Cbs		1.836	0.143	0.270	– 0.181	0.124	– 0.057	1.457
Cbs	Co-N(corrin)	1.902	0.114	0.463	0.174	– 0.145	0.029	1.202
SYCbs		1.904	0.113	0.456	0.173	– 0.143	0.029	1.203
5-Seco-Cbs		1.926	0.107	0.436	0.160	– 0.134	0.025	1.186

[a] The mean values of the charge density (ρ) and its Laplacian ($(\nabla^2\rho)$) at the bond critical points are in au. (1 au of ρ = 6.7483 eÅ^{-3}, and 1 au of $\nabla^2\rho$ = 24.099 eÅ^{-5}). The values of the energy density are in au (1 au = 627.5095 kcal mol^{-1}).

The equatorial Co–N bonds of the cobalt corrins are predominantly ionic bonds with some covalent character ($|V_r|/G_r \approx 1.2$). Cleavage of the corrin ring causes the average equatorial Co–N bond lengths (and in particular the Co–N(21) and Co–N(24) bonds, Appendix J.3) to increase by between 0.02 and 0.04 Å; this weakens them (ρ_r decreases) and marginally decreases their covalent character ($|V_r|/G_r$ decreases). The Co–CN bond length to CN^- coordinated on the lower (α) face of the corrin decreases on going from Cbs to SYCbs to 5-seco-Cbs (1.925 Å to 1.920 Å to 1.917 Å) while the Co–CN_β bond length is invariant. In the aquacyanocobesters the effect is more marked. The average Co–OH_2 bond length (average of the two diastereomers) decreases from 2.180 Å to 2.169 Å to 2.083 Å, while the average Co–CN bond to the *trans* CN^- ligand increases from 1.820 Å to 1.825 Å, to 1.836 Å, i.e., a normal *trans* influence is apparent. The Co–OH_2 bond is a predominantly ionic bond ($|V_r|/G_r \leq 1$), while the Co–CN bond has significant covalent character ($|V_r|/G_r \approx 1.46$).

The trend towards shorter axial bonds as the corrin is changed from Cbs to SYCbs to 5-seco-Cbs that is evident in the dicyano and aquacyano complexes persists more or less in the azidocyano and sulfitocyano complexes. The DFT model of one of the isomers of sulfitocyano-SYCbs, that with SO_3^{2-} coordinated to Co on the β face of the corrin, has a very long Co-S bond, 2.448 Å, cf. 2.353 Å in the α-sulfito isomer. The modelling converged to this structure despite using different starting structures, Figure 5.29. This suggests that sulfitocyano-SYCbs exists predominantly as the α-sulfito isomer. If that is the case, the Co-S bond is marginally longer in sulfitocyano-SYCbs (2.353 Å) than the average Co-S bond length in the Cbs sulfitocyano diastereomers (2.334 Å); it is significantly shorter, average of 2.240 Å, in the sulfitocyano diastereomers of 5-seco-Cbs. The steric factors introduced by

References on page 170

the presence of the lactone in stable yellow cobester may complicate a rationalization of the kinetics and thermodynamics of its ligand substitution reactions; anomalously low log *K* values for coordination of aromatic N-donor ligands were noted, for example.[18]

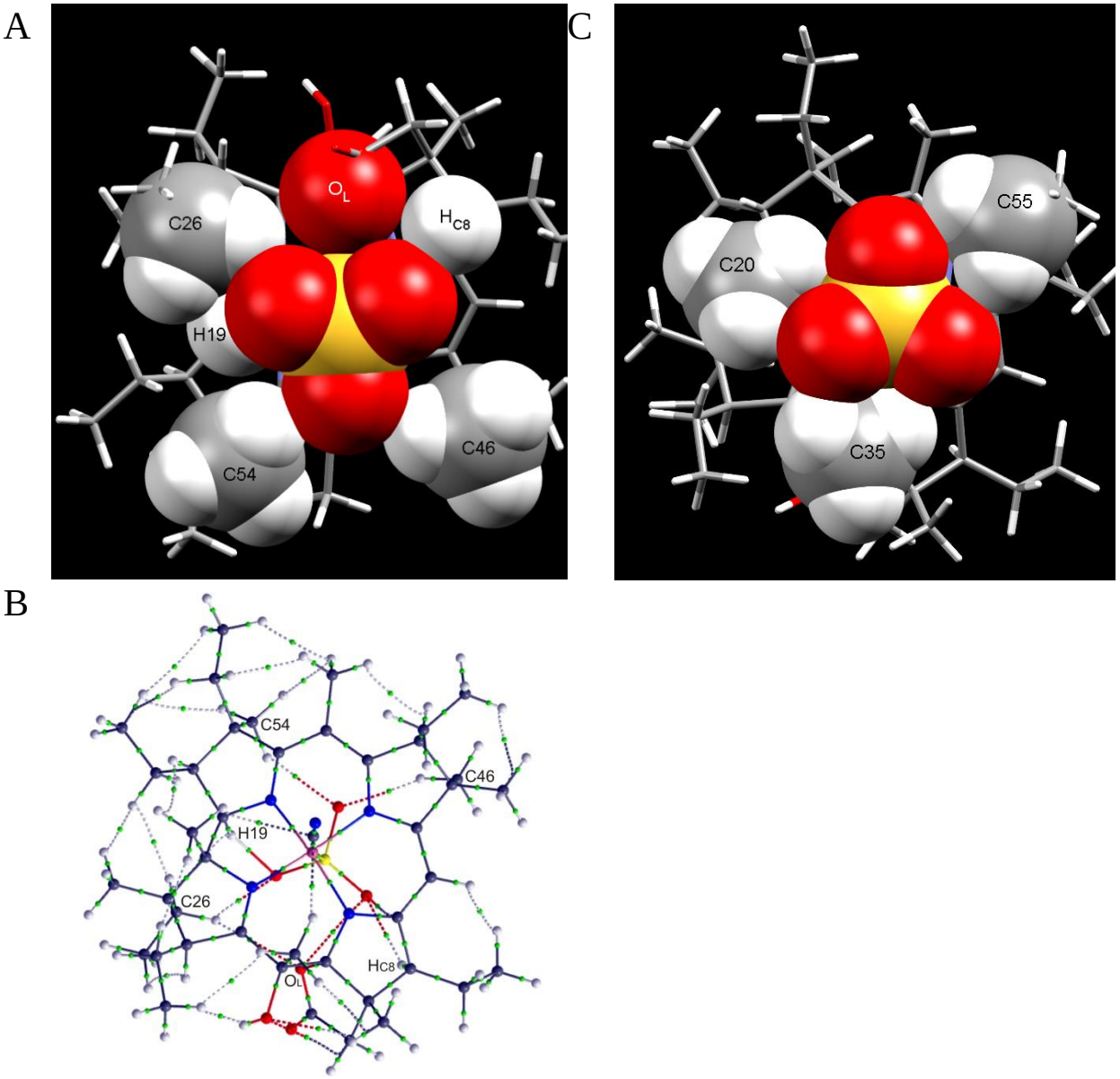

Figure 5.29 **(A)** The SO_3^{2-} ligand in [α-CN,β-SO_3SYCbs]$^+$ comes in close contact with C26 of the *b* side chain, the lactone oxygen O_L on C76, the C8 proton, H19, and the sentinel C46 and C54 methyl groups. This results in a long Co–S bond of 2.448 Å**.** **(B)** The molecular graph shows that bond paths are developed between the SO_3^{2-} O atoms and these groups. **(C)** Steric crowding on the α face is less severe, and the Co–S bond length is 2.353 Å.

References on page 170

The normal *trans* influence is also seen in the azidocyano complexes (Co-CN bond lengths increases as Co–N_3 decreases); the sulfitocyano complexes show an inverse *trans* influence, and Co–N bond length decreases parallel with the overall decrease in the Co-S bond lengths. Strikingly different is the behavior of the axial bond lengths in the nitrocyano complexes. The Co–NO_2 bond lengths *increase* as the corrin is changed from Cbs to SYCbs to 5-seco-Cbs, while the *trans* Co–CN remains virtually unchanged.

As noted, there are exceptions, but two factors clearly influence the values of log *K.* The predominant trend of shorter bonds to the equatorial ligands offers a rationalization why in general Δ*H* values are more negative for substitution of H_2O by an exogenous ligand when the corrin is 5-seco-Cbs than either Cbs or SYCbs (Figure 5.26). The compensation effect between Δ*H* and Δ*S* tends to level out the variation in log *K* values. Secondly, the increase in positive charge on the metal and its immediate coordination environment clearly discriminates against the coordination of the softer ligands, and appears to favour, relatively speaking, the coordination of ligands further along in the spectrochemical series.

References on page 170

5.4 Ligand Binding Studies with Neutral N-Donor Ligands

Although the main focus of this study was to investigate the binding of anionic ligands by $[AC\text{-}5\text{-}seco\text{-}Cbs]^+$, it would be worthwhile to briefly investigate the binding of neutral N-donor ligands by $[AC\text{-}5\text{-}seco\text{-}Cbs]^+$, to assess whether the binding trends observed thus far also extend to neutral ligands. Chemaly and co-workers have previously determined the equilibrium constants for the coordination of neutral N-donor ligands with $[ACCbs]^+$ and $[ACSYCbs]^+$ as a function of temperature (Table 5.7).[18]

Table 5.7 The equilibrium constants (log $K^{25^\circ C}$) for the substitution of water in $[ACCbs]^+$ and $[ACSYCbs]^+$ by various neutral N-donor ligands.[18]

	$[ACCbs]^+$			$[ACSYCbs]^+$		
Ligand	**ΔH / kJ mol^{-1}**	**ΔS / J K^{-1} mol^{-1}**	**log K^{25}**	**ΔH / kJ mol^{-1}**	**ΔS / J K^{-1} mol^{-1}**	**log K^{25}**
NH_3	- 41(1)	-85(2)	2.75	-46(2)	-98(7)	2.94
NH_2EtOH	- 24(2)	-44(7)	1.91	-79(3)	-23(9)	1.52
NH_2EtOMe	- 51(2)	-136(8)	1.84	-53(4)	-145(15)	1.70
N-MeIm	- 23(1)	5(4)	4.29	23(3)	107(11)	1.56
4-MePy	-29(2)	-33(8)	3.36	5(1)	24(2)	0.38

It was argued that the softer aromatic N-donor ligands (N-MeIm and the pyridines) bind more readily to $[ACCbs]^+$, whereas the harder aliphatic N-donor ligands (ammonia, ethanolamine and methoxyethylamine) bound marginally preferentially to $[ACSYCbs]^+$. For the ligand substitution reactions of $[ACCbs]^+$, the binding of all ligands resulted in large and negative ΔH and ΔS values, with the exception of N-MeIm, where ΔS is nearly zero. For ligand substitution reactions of $[ACSYCbs]^+$, the harder aliphatic N-donor ligands (NH_3, NH_2EtOH, NH_2EtOMe) also resulted in large and negative ΔH and ΔS values. In contrast, the softer aromatic N-donor ligands (N-MeIm and 4-MePy) yielded positive ΔH and ΔS values. Thus, based on the affinity of $[ACCbs]^+$ for the softer ligands, the distinction between the softer Co(III) in $[ACCbs]^+$ and the harder Co(III) in $[ACSYCbs]^+$ observed for the binding of anionic ligands was maintained for the neutral N-donor ligands.

References on page 170

The equilibrium constants for the coordination of three probe ligands; N-methylimidazole, 4-methylpyridine and ethanolamine with [AC-5-seco-Cbs]$^+$ were determined in this study. Once again, the equilibrium constants for the substitution reactions of [ACCbs]$^+$ were re-determined in this work to ensure reproducibility and to ensure comparable results under the same experimental conditions.

5.4.1 Ligand Binding Studies with N-Methylimidazole

Aliquots of a stock solution of N-MeIm (0.02946 – 0.03201 M, pH 8) were added to a solution of [AC-5-seco-Cbs]$^+$ buffered in Tris/HCl (μ = 0.1 M, pH 8). Aliquots of the N-MeIm solution were also added to the reference cuvette (buffer) so as to cancel out the effect of the ligand absorbing in the same wavelength range region as [AC-5-seco-Cbs]$^+$. Equation 2.3 was fitted to experimental data monitored between 400 – 410 nm, 440 – 450 nm, 470 – 480 nm and 540 – 550 nm. Log K = 3.35 at 25 ^{o}C for the coordination of N-MeIm by [AC-5-seco-Cbs]$^+$.

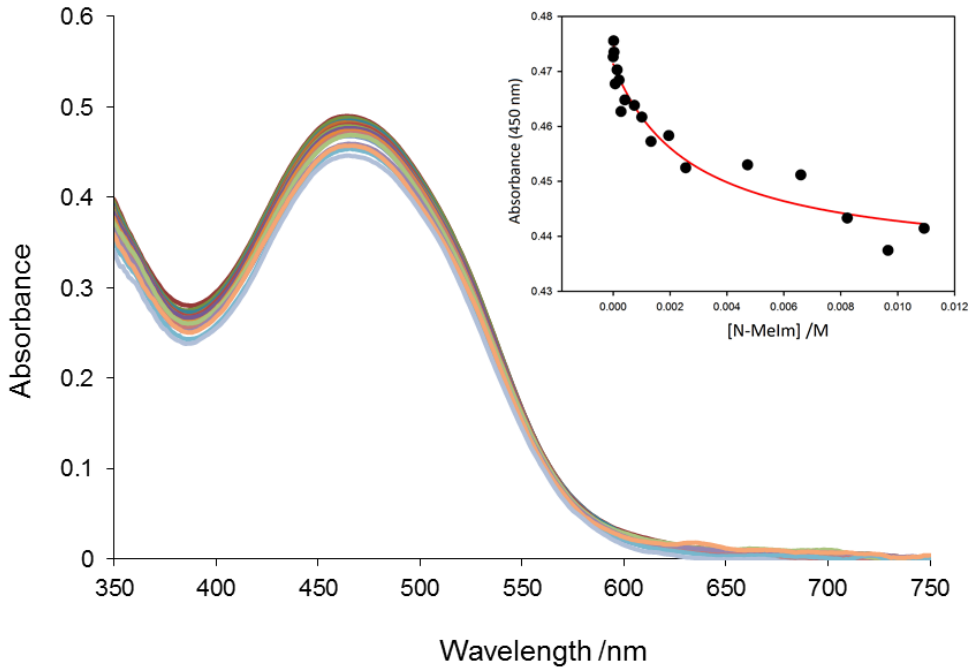

Figure 5.30 The electronic absorption spectrum from the titration of [AC-5-seco-Cbs]$^+$ with N-MeIm at pH 8.01, 40 ^{o}C. The insert shows a fit of Equation 2.3 to the absorbance changes observed at 450 nm.

References on page 170

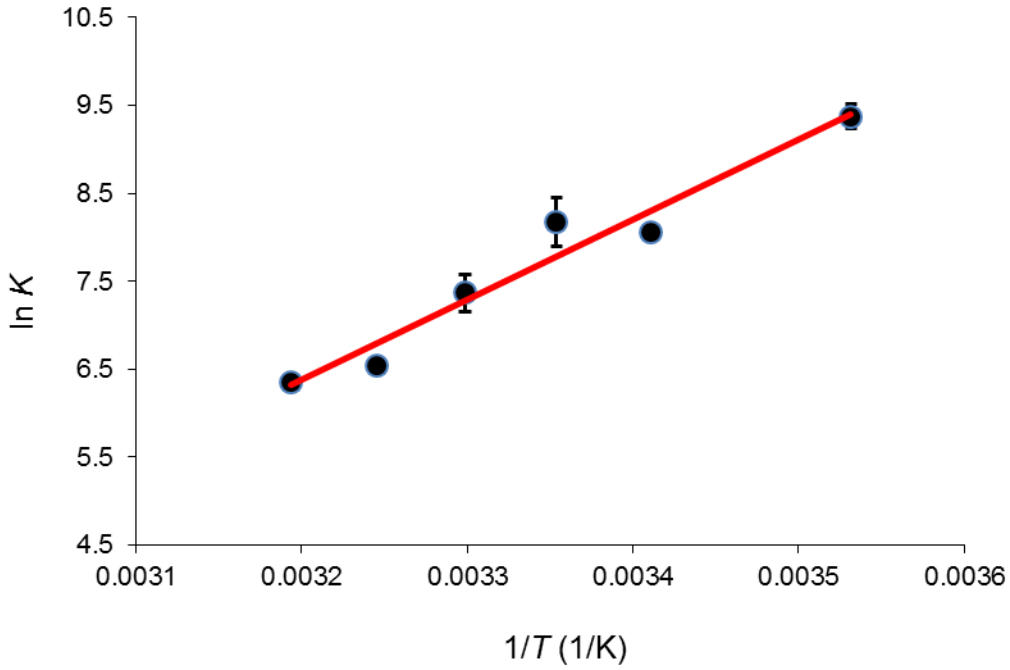

Figure 5.31 Plot of ln K against T^{-1} for coordination of N-MeIm by [AC-5-seco-Cbs]$^{+}$. From the slope ΔH = – 76 ± 7 kJ mol^{-1} and from the intercept ΔS = 192 ± 24 J K^{-1} mol^{-1}. R^2 = 0.967.

The equilibrium constants for the coordination of N-MeIm by [ACCbs]$^{+}$ were also re-determined by adding aliquots of a N-MeIm solution (0.0104 – 0.1166 M, pH 9) to a solution of [ACCbs]$^{+}$ buffered in CHES (μ = 0.1 M, pH 9). Aliquots of the N-MeIm solution were also added to the reference cuvette (buffer) so as to cancel out the effect of the ligand absorbing in the same wavelength range region as [ACCbs]$^{+}$. Equation 2.3 was fitted to experimental data monitored between 330 – 370 nm, 450 – 465 nm and 550 – 565 nm. Log K = 4.08 at 25 ^{o}C for the coordination of N-MeIm by [ACCbs]$^{+}$.

References on page 170

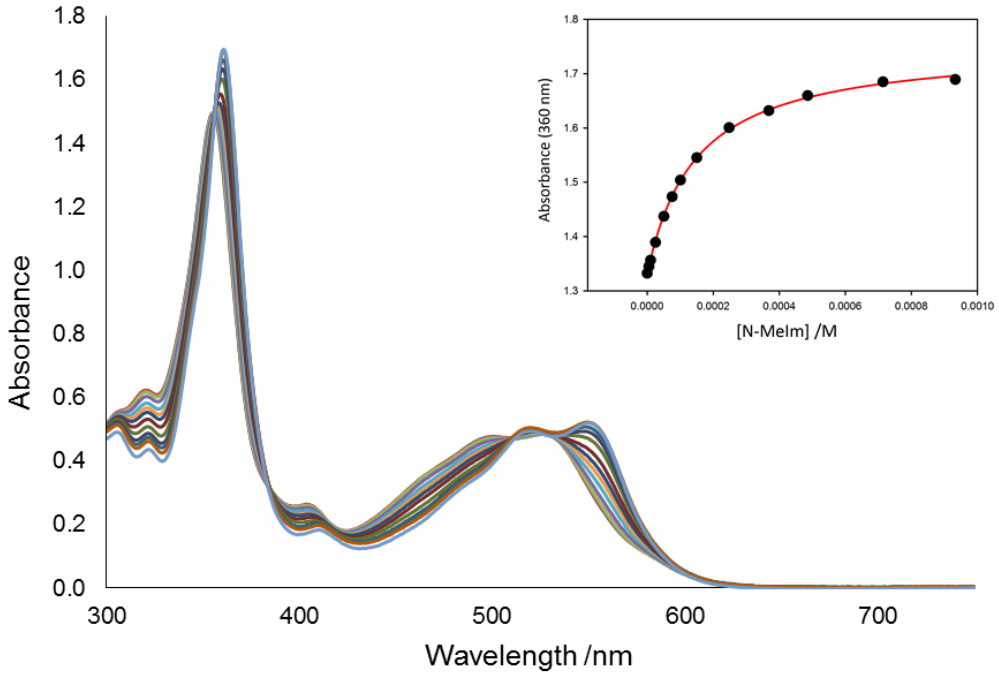

Figure 5.32 The electronic absorption spectrum from the titration of $[ACCbs]^+$ with N-MeIm at pH 9.09, 40 °C. The insert shows a fit of Equation 2.3 to the absorbance changes observed at 360 nm.

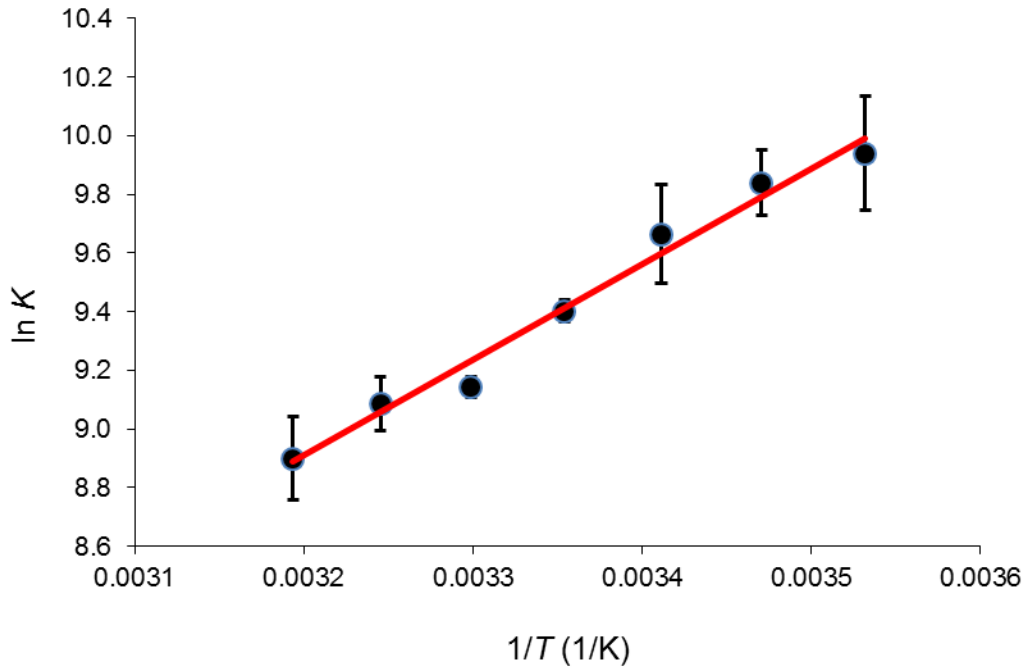

Figure 5.33 Plot of ln K against T^{-1} for coordination of N-MeIm by $[ACCbs]^+$. From the slope $\Delta H = -28 \pm 2$ kJ mol^{-1} and from the intercept $\Delta S = -17 \pm 8$ J K^{-1} mol^{-1}. $R^2 = 0.965$.

References on page 170

5.4.2 Ligand Binding Studies with 4-Methylpyridine

Aliquots of a stock solution of 4-MePy (0.1326 – 0.1394 M, pH 8) were added to a solution of $[AC\text{-}5\text{-}seco\text{-}Cbs]^+$ buffered in Tris/HCl (μ = 0.1 M, pH 8). Aliquots of the 4-MePy solution were also added to the reference cuvette (buffer) so as to cancel out the effect of the ligand absorbing in the same wavelength range region as $[AC\text{-}5\text{-}seco\text{-}Cbs]^+$. Equation 2.3 was fitted to experimental data monitored between 400 – 410 nm, 440 – 450 nm, 480 – 490 nm and 530 – 540 nm. Log *K* was found to be 2.72.

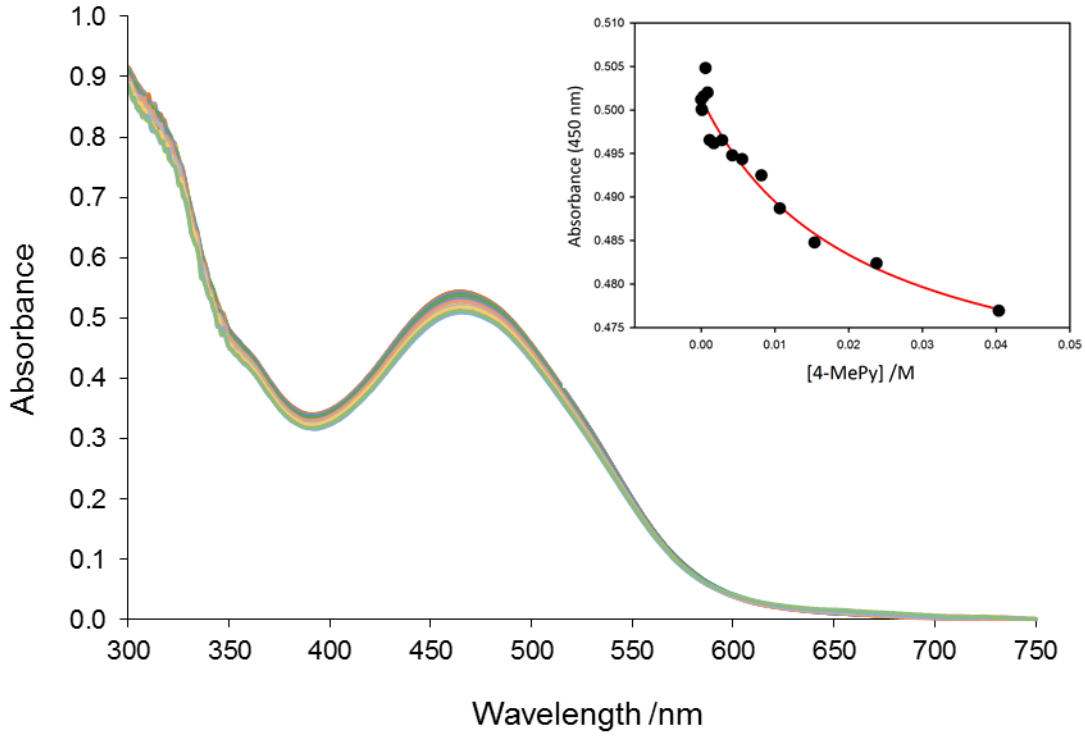

Figure 5.34 The electronic absorption spectrum from the titration of $[AC\text{-}5\text{-}seco\text{-}Cbs]^+$ with 4-MePy at pH 8.10, 15 ^{o}C. The insert shows a fit of Equation 2.3 to the absorbance changes observed at 450 nm.

References on page 170

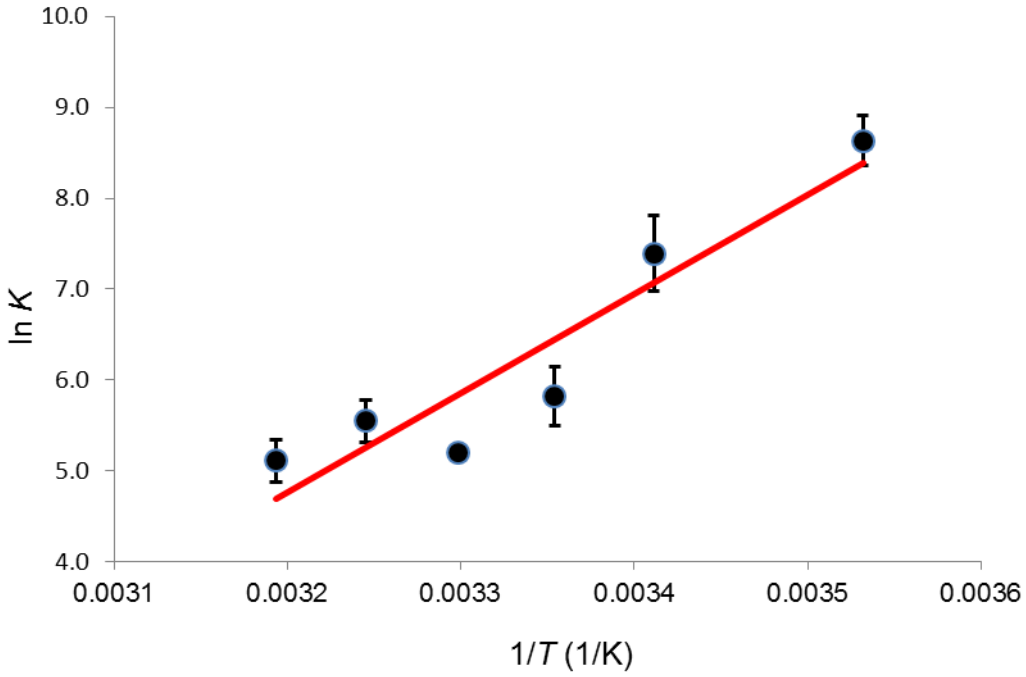

Figure 5.35 Plot of ln *K* against T^{-1} for coordination of 4-MePy by [AC-5-seco-Cbs]$^{+}$. From the slope ΔH = – 92 ± 21 kJ mol^{-1} and from the intercept ΔS = – 257 ± 70 J K^{-1} mol^{-1}. R^2 = 0.825.

The equilibrium constants for the coordination of 4-MePy by [ACCbs]$^{+}$ were also re-determined by adding aliquots of a 4-MePy solution (0.04942 – 0.05107 M, pH 9) to a solution of [ACCbs]$^{+}$ buffered in CHES (μ = 0.1 M, pH 9). Aliquots of the 4-MePy solution were also added to the reference cuvette (buffer) so as to cancel out the effect of the ligand absorbing in the same wavelength range region as [ACCbs]$^{+}$. Equation 2.3 was fitted to experimental data monitored between 340 – 350 nm, 360 – 370 nm, 460 – 470 nm and 550 – 560 nm. Log *K* = 3.38 at 25 ^{o}C for the coordination of 4-MePy by [ACCbs]$^{+}$.

References on page 170

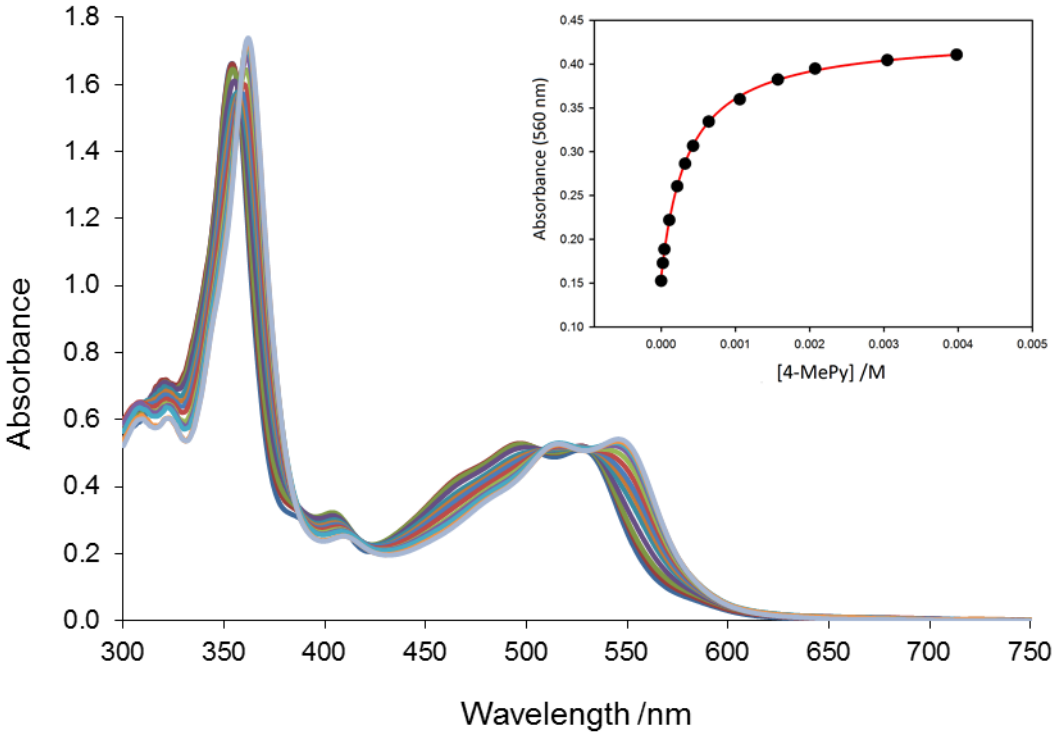

Figure 5.36 The electronic absorption spectrum from the titration of $[ACCbs]^+$ with 4-MePy at pH 9.02, 15 °C. The insert shows a fit of Equation 2.3 to the absorbance changes observed at 560 nm.

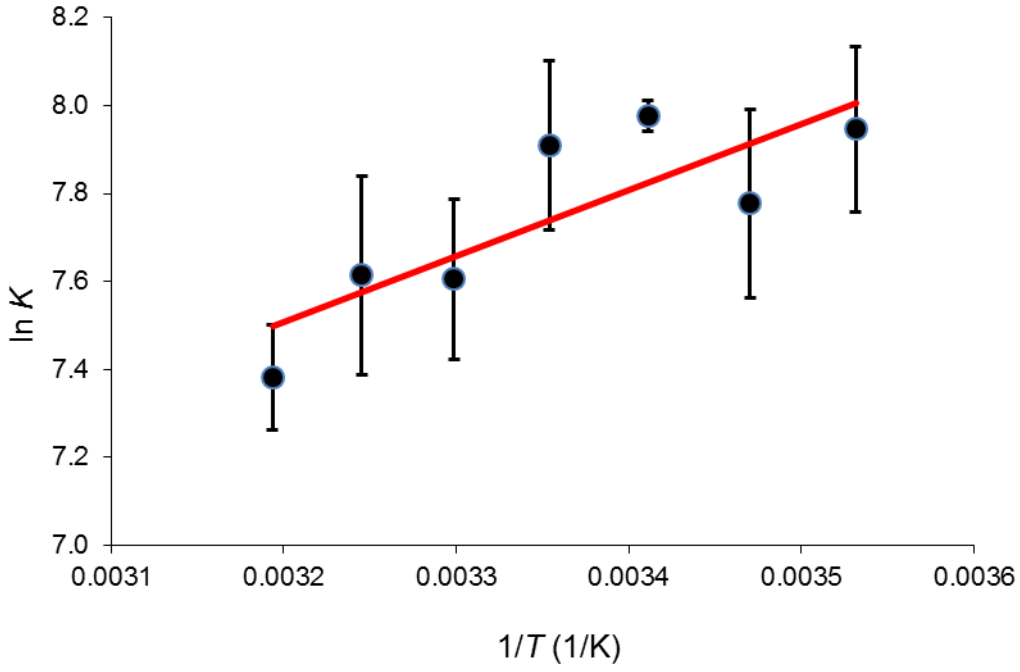

Figure 5.37 Plot of ln K against T^{-1} for coordination of 4-MePy by $[ACCbs]^+$. From the slope $\Delta H = -16 \pm 4$ kJ mol^{-1} and from the intercept $\Delta S = 12 \pm 15$ J K^{-1} mol^{-1}. $R^2 = 0.721$.

References on page 170

5.4.3 Ligand Binding Studies with Ethanolamine

For reasons discussed below, reliable data for the coordination of ethanolamine by [AC-5-seco-Cbs]$^+$ could not be obtained.

The equilibrium constants for the coordination of ethanolamine by [ACCbs]$^+$ were re-determined by adding aliquots of a stock solution of NH_2EtOH (1.7923 – 1.8017 M, pH 9) to a solution of [ACCbs]$^+$ buffered in CHES (μ = 0.1 M, pH 9). Aliquots of the ethanolamine solution were also added to the reference cuvette (buffer) so as to cancel out the effect of the ligand absorbing in the same wavelength range region as [ACCbs]$^+$. Equation 2.3 was fitted to experimental data monitored between 340 – 350 nm, 360 – 370 nm, 460 – 470 nm and 545 – 555 nm. Log *K* = 2.33 at 25 °C for the coordination of NH_2EtOH by [ACCbs]$^+$.

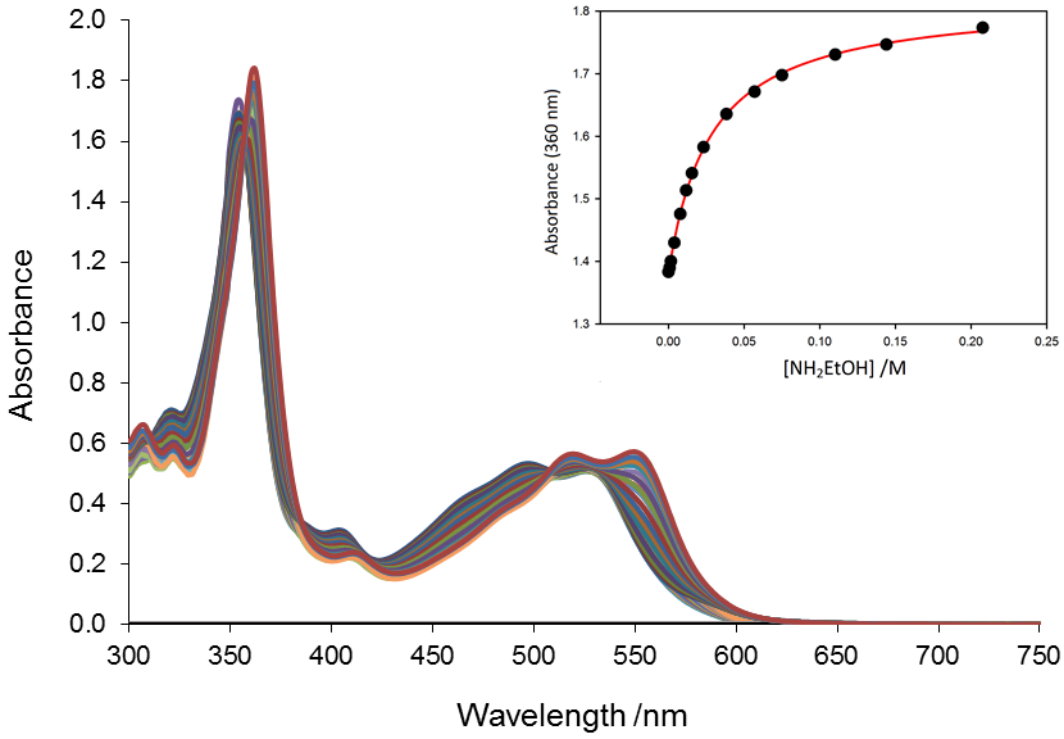

Figure 5.38 The electronic absorption spectrum from the titration of [ACCbs]$^+$ with NH_2EtOH at pH 8.92, 25 °C. The insert shows a fit of Equation 2.3 to the absorbance changes observed at 360 nm.

References on page 170

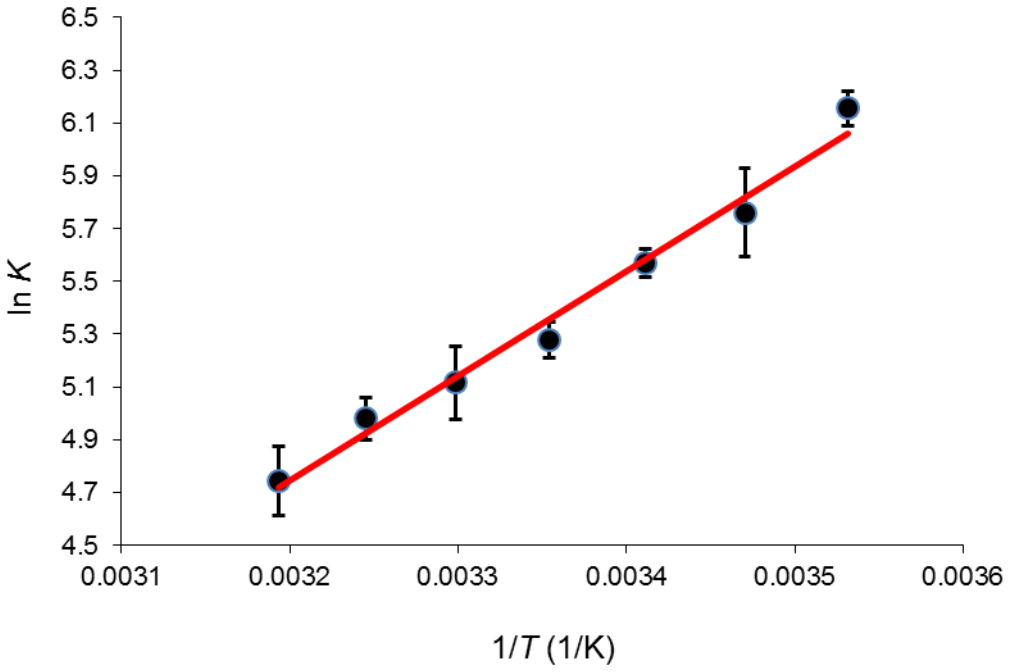

Figure 5.39 Plot of ln *K* against T^{-1} for coordination of NH_2EtOH by $[ACCbs]^+$. From the slope $\Delta H = -34 \pm 2$ kJ mol^{-1} and from the intercept $\Delta S = -68 \pm 7$ J K^{-1} mol^{-1}. $R^2 = 0.984$.

Log *K* values obtained for the coordination of N-MeIm, 4-MePy and NH_2EtOH are in line with the results previously reported (Table 5.8). The affinity of the cobalt for these ligands followed the same trend previously found; N-MeIm > 4-MePy > NH_2EtOH. Thermodynamic parametres indicated that the softer aromatic ligands bind more readily to $[ACCbs]^+$, whereas the binding of the harder aliphatic ligand by $[ACSYCbs]^+$ was more favourable.

The pK_a values of the neutral N-donor ligands studied are generally much higher than the pK_a of $[AC\text{-}5\text{-}seco\text{-}Cbs]^+$, which together with the small spectroscopic changes associated with $[AC\text{-}5\text{-}seco\text{-}Cbs]^+$ make these titrations very difficult, and could not always provide reliable data (as with ethanolamine) as it was very difficult to operate in a pH range that could accommodate the large difference in pK_as.

References on page 170

5.4.4 Summary of Results

Table 5.8 Equilibrium constants for the Substitution of Coordinated H_2O in $[ACCbs]^+$, $[AC\text{-}5\text{-}seco\text{-}Cbs]^+$ and $[ACSYCbs]^+$ by Some Neutral Ligands.

		$[ACCbs]^+$ [a]				$[AC\text{-}5\text{-}seco\text{-}Cbs]^+$				$[ACSYCbs]^+$ [a]		
Ligand	***T*** **/ °C**	**log *K***	**Δ*H* / kJ mol^{-1}**	**Δ*S* / J K^{-1} mol^{-1}**	**log K^{25}**	**log *K***	**Δ*H* / kJ mol^{-1}**	**Δ*S* / J K^{-1} mol^{-1}**	**log K^{25}**	**Δ*H* / kJ mol^{-1}**	**Δ*S* / J K^{-1} mol^{-1}**	**log K^{25}**
N-MeIm	10	4.32(9)	–28(2)	–17(8)	4.08	4.07(6)	–76(7)	–192(24)	3.35	*23(3)*	*107(11)*	*1.56*
	15	4.27(5)	*–23(1)*	*5(4)*	*4.29*	-						
	20	4.20(7)				3.50(4)						
	25	4.08(2)				3.55(12)						
	30	3.97(2)				3.20(9)						
	35	3.95(4)				2.84(3)						
	40	3.87(6)				2.76(6)						
4-MePy	10	3.45(8)	-15(4)	12(15)	3.38	3.75(12)	–92(21)	–257(70)	2.72	*5(1)*	*24(2)*	*0.38*
	15	3.38(9)	*–29(2)*	*-33(8)*	*3.36*	-						
	20	3.46(2)				3.21(18)						
	25	3.44(8)				2.53(14)						
	30	3.30(8)				2.41(10)						
	35	3.31(10)				2.22(10)						
	40	3.21(5)				3.2(1)						
NH_2EtOH	10	2.67(3)	–34(2)	–68(7)	2.33	-	-	-	-	*–79(3)*	*–23(9)*	*1.52*
	15	2.50(7)	*–6.6(9)*	*33(3)*	*2.88*	-						
	20	2.42(2)				-						
	25	2.29(3)				-						
	30	2.22(6)				-						
	35	2.16(4)				-						
	40	2.06(6)				-						

[a] Values in italics from Chemaly *et al.* [18].

References on page 170

The log *K* values for the coordination of neutral ligands by [AC-5-seco-Cbs]$^+$ were surprisingly significantly larger than the corresponding values for [ACSYCbs]$^+$. The neutral ligands are quite bulky, hence the larger equilibrium constants obtained for [AC-5-seco-Cbs]$^+$ could be attributed to the relief of steric constraints afforded by cleaving the corrin ring which subsequently opens up the macrocyclic cavity. In contrast, the additional lactone group in [ACSYCbs]$^+$ increases the steric hindrance around the cobalt, hence inhibiting the binding of larger ligands; resulting in the unsually low log *K* values observed. This rationalisation could be tested by DFT modelling.

5.5 Conclusions

It is concluded that disruption of the conjugation system as well as the size of the macrocyclic cavity, have a very significant impact on the thermodynamic stability of the complexes of the cobalt corrins. This demonstrates how perturbation of the electronic structure of the corrin in the cobalt corrin complexes significantly affects the coordination chemistry of the axial coordination sites.

The environment in which Co(III) finds itself in a corrin macrocycle such as vitamin B_{12} significantly affects its properties. When coordinated to such a macrocycle, the typically inert d^6 Co(III) metal centre exhibits remarkable lability.[1–27,33,60] It is postulated that the partially delocalised electron cloud of the corrin ring transfers electron density to the Co(III) ion, imparting to it a degree of labile Co(II) character.[1,2,15,18,19] This has been tested in previous investigations in which the electronic structure of the corrin was perturbed by oxidation at the C5 position ([ACSYCbs]$^+$);[2,3,18] substitution of the C10–H by electron-withdrawing and electron-donating groups,[20] varying the nature of the axial ligands and altering the macrocyclic cavity size by comparing corrins with porphyrins and corroles. To further test this, the corrin structure was cleaved at the C5 position. This therefore not only interrupts the conjugated π-electron system, but also opens up the macrocyclic cavity. Equilibrium constants (log *K*) were determined for the substitution of axially coordinated water by SO_3^{2-}, CN^-, NO_2^-, N_3^- and $S_2O_3^{2-}$. These results were then used to compare the chemistry of an intact corrin ring, in aquacyanocobester [ACCbs]$^+$, in which the conjugation

References on page 170

system is retained, as well as in aquacyano-stable yellow cobester $[ACSYCbs]^+$, in which the conjugation is disrupted at a single point.

As the metal ion becomes less electron rich and more Co(III)-like ($[ACCbs]^+$ > $[ACSYCbs]^+$ > $[AC\text{-}5\text{-}seco\text{-}Cbs]^+$), the stability of its complexes with π acceptor ligands (CN^-, SO_3^-, NO_2^-) decreases, and the extent of the decrease ($\Delta\log K = \log K_{[ACCbs]+} - \log K_{[AC\text{-}5\text{-}seco\text{-}Cbs]+}$) becomes smaller the further along the ligand is in the spectrochemical series (i.e., the discrimination becomes smaller as the π acceptor ability of the ligand decreases). Conversely, the thermodynamic stability of the complexes with π donor ligands (N_3^- and $S_2O_3^{2-}$) tends to increase at the metal becomes more Co(III)-like, although the effect is smaller. These findings were supported by DFT modelling.

The binding of neutral N-donor ligands (N-MeIm, 4-MePy and NH_2EtOH) was also briefly investigated. The distinction between the softer Co(III) in $[ACCbs]^+$ and the harder Co(III) in $[AC\text{-}5\text{-}seco\text{-}Cbs]^+$ ($[ACCbs]^+$> $[ACSYCbs]^+$ > $[AC\text{-}5\text{-}seco\text{-}Cbs]^+$) observed for the binding of anionic ligands is maintained for the neutral N-donor ligands. Results also indicated the effect of relieving the steric hindrance surrounding the axial coordination site in $[AC\text{-}5\text{-}seco\text{-}Cbs]^+$ on the binding of the larger neutral ligands.

This therefore provides further evidence that some of the unique Co(III) chemistry exploited in nature in the B_{12} systems (Chapter 1) is likely to have its origins in the structure of the equatorial ligands.

References on page 170

REFERENCES FOR CHAPTER 5

1. Brown, K. L.; Cheng, S.; Zou, X.; Zubkowski, J. D.; Valente, E. J.; Knapton, L.; Marques, H. M. *Inorg. Chem*. **1997**, 36, 3666-3675.
2. Chemaly, S. M.; Brown, K. L.; Fernandes, M. A.; Munro, O. Q.; Grimmer, C.; Marques, H. M. *Inorg. Chem.* **2011**, 50, 8700-8718.
3. Chemaly, S. M.; Florczak, M.; Dirr, H.; Marques, H. M. *Inorg. Chem.* **2011**, 50, 8719-8727.
4. Randall, W. C.; Alberty, R. A. *Biochemistry* **1967**, 6, 1520-1525.
5. Reenstra, W. W.; Jencks, W. P. *J. Am. Chem. Soc*. **1979**, 101, 5780-5791.
6. Marques, H. M.; Egan, T. J.; Marsh, J. H.; Mellor, J. R.; Munro, O. Q. *Inorg. Chim. Acta.* **1989**, 166, 249-255.
7. Balt, S.; van Herk, A. M. *Transition Met. Chem*. **1983**, 8, 152-154.
8. Baldwin, D. A.; Betterton, E. A.; Pratt, J. M. *J. Chem. Soc., Dalton Trans.* **1983**, 2217-2222.
9. Marques, H. M.; Brown, K. L.; Jacobsen, D. W. *J. Biol. Chem*. **1988**, 263, 12378-12383.
10. Stochel, G.; van Eldik, R.; Kunkely, H.; Vogler, A. *Inorg. Chem*. **1989**, 28, 4314-4318.
11. Stochel, G.; van Eldik, R*. Inorg. Chem.* **1990**, 29, 2075-2077.
12. Marques, H. M*. J. Chem. Soc., Dalton Trans.* **1991**, 1437-1442.
13. Marques, H. M.; Bradley, J. C.; Campbell, L. A. *J. Chem. Soc., Dalton Trans*. **1992**, 2019-2027.
14. Waddington, M. D.; Finke, R. G. *J. Am. Chem. Soc*. **1993**, 115, 4629-4640.
15. Marques, H. M.; Knapton, L. *J. Chem. Soc., Dalton Trans.* **1997**, 3827-3833.
16. Hamza, M. S. A.; Zou, X.; Brown, K. L.; van Eldik, R. *Inorg. Chem*. **2001**, 40, 5440-5447.
17. Hamza, M. S. A.; Elawady, M. A.; Marques, H. M. *S. Afr. J. Chem*. **2008**, 61, 68-73.
18. Chemaly, S. M.; Kendall, L.; Nowakowska, M.; Pon, D.; Perry, C. B.; Marques, H. M. *Inorg. Chem*. **2013**, 52, 1077-1083.
19. Perry, C. B.; Marques, H. M. *S. Afr. J. Chem.* **2005**, 58, 9-15.
20. Knapton, L. Ph.D. Thesis, University of the Witwatersrand, Johannesburg, 2005.
21. Ghadimi, N.; Perry, C. B.; Govender, P. P.; Marques, H. M. *Inorg. Chim. Acta.* **2016**, 450, 269-278.
22. Ghadimi, N. Ph.D Thesis, University of the Witwatersrand, Johannesburg, 2016.

23. Mathura, S.; Sanassy, D.; de Sousa, A. S.; Perry, C. B.; Navizet, I.; Marques, H. M. *J. Inorg. Biochem*. **2013**, 123, 66-79.
24. Mathura, S. Ph.D Thesis, University of the Witwatersrand, Johannesburg, 2014.
25. Zipp, C. F.; Michael, J. P.; Fernandes, M. A.; Nowakowska, M.; Dirr, H. W.; Marques, H. M. *Inorg. Chem. Comm*. **2015**, 57, 15-17.
26. Zipp, C. F.; Michael, J. P.; Fernandes, M. A.; Mathura, S.; Perry, C. B.; Navizet, I.; Govender, P. P.; Marques, H. M. *Inorg. Chem*. **53**, 4418-4429.
27. Zipp, C. F. Ph.D Thesis, University of the Witwatersrand, Johannesburg, 2014.
28. Marques, H. M.; Baldwin, D. A.; Pratt, J. M. *J. Inorg. Biochem.* **1987,** 29, 77-91.
29. Marques, H. M.; Bradley, J. C.; Brown, K. L.; Brooks, H. *J. Chem. Soc., Dalton Trans.* **1993**, 3475-3478.
30. Martell, A. E.; Smith, R. M.; Motekaites, R. J., NIST Standard Database 46. Criticially Selected Stability Constants of Metal Complexes, V. 8.0, NIST, Gaithersburg, MD, 2004.
31. Firth, R. A.; Hill, H. O. A.; Pratt, J. M.; Thorp, R. G.; Williams, R. J. P. *J. Chem. Soc. A* **1969**, 381-386.
32. Pratt, J. M.; Thorp, R. G. *J. Chem. Soc. A* **1966**, 187-191.
33. Perry, C. B.; Fernandes, M. A.; Brown, K. L; Valente, E. J.; Marques, H. M. *Eur. J. Inorg. Chem.* **2003**, 136, 2095-2107.
34. Garau, G.; Geremia, S.; Marzilli, L. G.; Nardin, G.; Randaccio, L.; Tauzher, G. *Acta Cryst., Sec. B* **2003**, 51-59.
35. Knapton, L.; Marques, H. M. *Dalton Trans.* **2005**, 889-895.
36. Marques, H. M. *S. Afr. J. Chem.* **1991,** 44, 114-117.
37. Marques, H. M.; Bradley, J. C.; Campbell, L. A. *J. Chem. Soc., Dalton Trans.* **1992**, 2019-2027.
38. CSD v. 5.38; Cambridge Crystallographic Data Centre (CCDC): Cambridge, UK, 2016.
39. Hinze, R. P.; Schiebel, H. M.; Laas, H.; Heise, K. P.; Gossauer, A.; Inhoffen, H. H.; Ernst, L.; Schulten, H. R. *Liebigs Ann. Chem.* **1979**, 811-828.
40. Kräutler, B. *Helv. Chim. Acta* **1982,** 65, 1941-1948.
41. Kozlowski, P. M.; Kamachi, T.; Toraya, T.; Yoshikawa, K. *Angew. Chem. Int. Ed. Engl.* **2007,** 46, 980-983.
42. Jensen, K. P.; Ryde, U. *J. Phys. Chem. A* **2003,** 107, 7539-7545.

43. Kepp, K. P. *J. Phys. Chem. A* **2014,** 118, 7104−7117.
44. Kuta, J.; Patchkovskii, S.; Zgierski, M. Z.; Kozlowski, P. M. *J. Comput. Chem.* **2006,** 27, 1429-1437.
45. Lever, A. B. P. *Inorganic Electronic Spectroscopy*. 2 ed.; Elsevier: New York, 1986.
46. Jørgensen, C. K. *Modern Aspects of Ligand Field Theory*. Elsevier: New York, 1971.
47. Bader, R. F. W.; Matta, C. F. *J. Phys. Chem. A* **2004,** 108 8385-8394.
48. Huang, L.; Matta, C.; Massa, L. *Struct. Chem.* **2015,** 26, 1433-1442.
49. Howard, S. T.; Krygowski, T. M. *Can. J. Chem.* **1997,** 75, 1174-1181.
50. O'Brien, S. E.; Popelier, P. L. *Can. J. Chem.* **1999,** 77, 28-36.
51. Espinosa, E.; Souhassou, M.; Lachekar, H.; Lecomte, C. *Acta Cryst. B* **1999,** 55, 563-572.
52. Grabowski, S. J. *J. Phys. Chem. A* **2000,** 105, 5551-5557.
53. Bader, R. F. W.; Matta, C. F.; Cortés-Guzmán, F. *Organometallics* **2004,** 23, 6253-6263.
54. Espinosa, E.; Alkorta, I.; Elguero, J.; Molins, E. *J. Chem. Phys.* **2002,** 117, 5529-5542.
55. Cremer, D.; Kraka, E. *Angew. Chem. Int. Ed. Engl.* **1984,** 23, 627-628.
56. Bone, R. G. A.; Bader, R. F. W. *J. Phys. Chem.* **1996,** 100, 10892-10911.
57. Bobrov, M. F.; Popova, G. V.; Tsirelson, V. G. *Russ. J. Phys. Chem.* **2006,** 80, 584-590.
58. Macchi, P.; Sironi, A. *Coord. Chem. Rev.* **2003,** 238-239, 383-412.
59. Bader, R. F. W.; Matta, C. F. Bonding to titanium. *Inorg. Chem.* **2001,** 40, 5603-5611.
60. Gütlich, P.; Goodwin, H. A. *Top. Curr. Chem.* **2004**, 233, 1-47.

CHAPTER 6

THE KINETICS OF THE LIGAND SUBSTITUTION REACTION OF AQUACYANO-5-SECOCOBESTER WITH CYANIDE

6.1 Introduction

Subsequent to the discovery of vitamin B_{12}, interest in cobalt corrin chemistry has been enormous due to the remarkable lability of a typically inert Co(III) ion observed when encapsulated in a corrin macrocycle.[1-27] This lability is clearly a consequence of the coordination environment and to date many studies have been carried out to investigate the lability of a Co(III) ion towards ligand substitution reactions. For example, in one such study in which an incoming ligand (L) substitutes an axially coordinated water in a corrin, porphyrin, cobaloxime and amine complex (denoted by Co(III)(N_4), where N_4 represents a four nitrogen donor coordinating system), the approximate relative lability ratio was found to be 10^9:10^6:10^4:1 respectively.[1,2,15]

$$[X–Co(III)(N_4)–OH_2] + L \rightleftharpoons [X–Co(III)(N_4)–L] + H_2O$$

[Equation 1.3]

These results indicated that labilisation increases with increasing extent of delocalisation of the π-electron system of the corrin ring ($(NH_3)_4$ < cobaloxime < porphyrin < corrin), and decreasing macrocyclic cavity size (porphyrin < corrin).[2] These observations suggest that the labilisation likely originates as a consequence of a *cis*-effect in which the electron-rich corrin transfers electron density onto the cobalt ion, thereby imparting to it a significant degree of labile Co(II)-like character.[1,2,15,18,19]

In more recent studies relevant to this work, a kinetics study of the substitution of H_2O by CN^- on Co(III) showed that $[ACCbs]^+$ is more labile than $[ACSYCbs]^+$ and the second-order rate constant k^{II} is between 4.6 (at 5 ^oC) and 2.6 (at 35 ^oC) times larger.[3] There is, therefore, a significant increase in the inertness of Co(III) consequent on a decrease in the extent of conjugation of the corrin macrocycle. In another study, the k^{II} values for the reaction of $[AC(10–NH_2)Cbs]^+$, $[ACCbs]^+$ and $[AC(10–NO_2)Cbs]^+$ at 25 ^oC are not strikingly different (2.5×10^4 $M^{-1}s^{-1}$; 8.1×10^4 $M^{-1}s^{-1}$; 1.6×10^3 $M^{-1}s^{-1}$) even in the presence of electron-withdrawing

References on page 188

and electron-donating substituents on the corrin periphery. This is deceptive and is because of a compensation effect between $\Delta H^{\ddagger}$ and $\Delta S^{\ddagger}$ values.[21]

The investigation into the effect of the electronic structure of the corrin ligand on the kinetics of the ligand substitution reactions of Co(III) is extended in this work, by assessing the effect cleavage of the corrin ring has on the lability of Co(III).

The kinetics of the substitution of axially coordinated water in $[AC\text{-}5\text{-}seco\text{-}Cbs]^{+}$ with a probe ligand, cyanide, were studied as a function of temperature. Cyanide was selected as the probe ligand as the affinity of Co(III) in corrins for cyanide is very high, the ligand substitution reactions are relatively fast and there are analogous data for comparison with other cobalt corrins. Knowledge of the rate constant for the substitution of coordinated H_2O by CN^{-} in $[AC\text{-}5\text{-}seco\text{-}Cbs]^{+}$ would greatly enhance our understanding of the kinetic *cis*-effect occurring in corrin complexes, by further assessing the effect of the equatorial ligand on the lability of the $Co–OH_2$ bond. This was achieved by comparing the rate constant for ligand substitution reactions of water bound to cobalt in $[ACCbs]^{+}$ and $[ACSYCbs]^{+}$, which are both Co(III) corrin macrocycles with a CN^{-} and H_2O moiety in the α and β binding sites, respectively.[2,3,18]

It would also be of interest to observe what effect the ligand *trans* to the axial water has on the lability of the $Co(III)–OH_2$ bond in $[AC\text{-}5\text{-}seco\text{-}Cbs]^{+}$, and this was achieved by comparing the rate constants obtained for the substitution of water axially bound to a cobalt ion in vitamin B_{12a} (aquacobalamin) to that of $[AC\text{-}5\text{-}seco\text{-}Cbs]^{+}$. By contrast, aquacobalamin is a Co(III) corrin macrocycle with a water coordinated at the β binding position, but in which a dimethylbenzimidazole base (DMBz) is coordinated at the α binding site.[5,20] Although the kinetics of the reaction between B_{12a} and CN^{-} have been reported,[5] that study was compromised by the workers carrying out the reaction in the presence of chloride (used to adjust ionic strength). Since Cl^{-} does coordinate to Co(III) in B_{12a},[5,20,21] there would inevitably have been a mixture of aquacobalamin and chlorocobalamin in solution, and the reported rate constant would have been an aggregate rate constant for substitution of both H_2O and Cl^{-}.

References on page 188

Hence, the aim of the work in this chapter is to study the kinetics of the substitution of axially coordinated water by probe ligand CN^- as a function of temperature for [AC-5-seco-Cbs]$^+$ and aquacobalamin under pseudo first-order conditions spectrophotometrically. The second-order rate constants were determined from the slopes of plots of the pseudo first-order rate constants against ligand concentration. These results were then compared to similar data available for [ACCbs]$^+$ and [ACSYCbs]$^+$.[3,15]

6.2 Results and Discussion

The second-order rate constant, k^{II}, for the substitution of an axially coordinated water in [AC-5-seco-Cbs]$^+$ by a probe ligand cyanide, (Equation 2.8) were determined by monitoring the spectroscopic changes observed during determination of log *K* for coordination of CN^- by [AC-5-seco-Cbs]$^+$ (Figure 5.7) but now as a function of time.

$$[CN–Co–H_2O] + CN^- \overset{k^{II}}{\rightleftharpoons} [CN–Co–CN] + H_2O$$

[Equation 2.8]

Aliquots of a freshly prepared stock solution of NaCN (0.5 M, pH 10.5) were added to a 50 μM solution of [AC-5-seco-Cbs]$^+$ buffered with CAPS (μ = 0.1 M, pH 10.5) under pseudo first-order conditions (i.e. [CN^-] > 10 × [AC-5-seco-Cbs]$^+$). The reaction was monitored at 400 nm. The absorbance *vs*. time trace showed biphasic kinetics (Figure 6.1). Since the diastereomers of aquacyano complexes (α-cyano, β-aqua and α-aqua, β-cyano isomers) are expected to react at indistinguishable rates,[3] the presence of isomers could not be the reason for the observed biphasic kinetics. However, as found with both [ACCbs]$^+$ and [ACSYCbs]$^+$ in aqueous solution,[3] and more recently in 50% isopropanol with [AC-(10–X)-Cbs]$^+$ in which X, the substituent at the C10 position of the corrin ring, is NH_2, H or NO_2,[21] and unsurprising given that there is HPLC evidence (*vide supra*) that solutions of [AC-5-seco-Cbs]$^+$ contain both [DC-5-seco-Cbs] and [$(H_2O)_2$-5-seco-Cbs]$^{2+}$, the reaction is biphasic.

References on page 188

By analogy with $[ACCbs]^+$ and $[ACSYCbs]^+$, the faster rate is attributed to substitution of axial H_2O by CN^- *trans* to CN^-, and the slower phase to the reaction of the diaqua complex with CN^-, i.e., substitution of H_2O *trans* to H_2O.

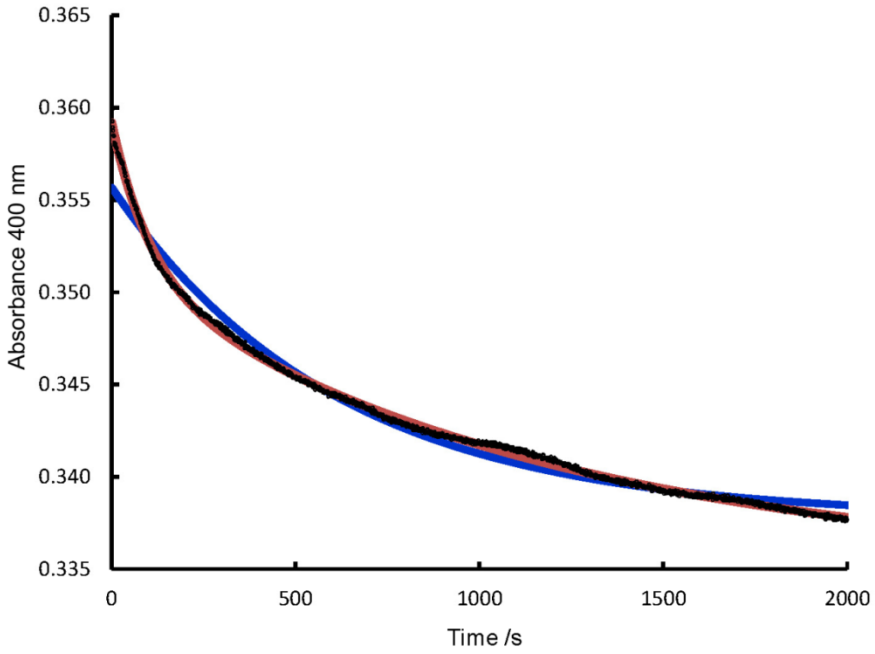

Figure 6.1 ΔA_{400} with time on substitution of H_2O by CN^- in $[AC\text{-}5\text{-}seco\text{-}Cbs]^+$ at 25 °C with $[CN^-]$ = 0.1012 M, pH 10.64. The experimental data are shown as small black dots. The blue line is the best fit line of the data to a single exponential function. It clearly fails to fit the data during the earlier phase of the reaction. The red line is a fit of the experimental data to a double exponential function. The slower phase is attributed to reaction of $[(H_2O)_2\text{-}5\text{-}seco\text{-}Cbs]^{2+}$ with CN^-. For the data shown the best fit was obtained with $A_0 = 0.3592 \pm 3.6 \times 10^{-5}$; $A_1 = 0.3511 \pm 5.1 \times 10^{-5}$; $A_\infty = 0.3349 \pm 6.1 \times 10^{-5}$; $k_f^{obs} = 9.8(1) \times 10^{-3}$ s^{-1} and $k_s^{obs} = 9.0(1) \times 10^{-4}$ s^{-1}. Correcting for the fraction of the inert hydroxosecocobester ($pK_a = 7.28$) gives k_f = 22 s^{-1} and k_s = 2.0 s^{-1}, from which $k_f^{II} = 220$ M^{-1} s^{-1} and $k_s^{II} = 20$ M^{-1} s^{-1}.

Hence, the observed pseudo first-order rate constants (k_l^{obs}) for the coordination of CN^- to $[AC\text{-}5\text{-}seco\text{-}Cbs]^+$ determined between 25 – 40 °C were obtained by fitting a double exponential function (Equation 2.9) to the absorbance *vs*. time data. The concentration of CN^- was varied between 0.2 M and 0.02 M at 25 °C, and between 0.15 M and 0.015 M; at

References on page 188

30 °C, 35 °C and 40 °C. The observed first order rate constants were corrected for the pK_a of [AC-5-seco-Cbs]$^+$ (the hydroxo complexes of Co(III) corrins are inert to substitution) [3,5,28,29] to obtain values of k_i (i = f,s). Since pK_{HCN} = 9.04,[30] at the pH these reactions were conducted, cyanide is > 95% present as CN^-. HCN reacts an order of magnitude slower than CN^- with aquacobalamin (vitamin B_{12a})[5] and its concentration is negligible under our conditions; hence the observed reaction is virtually exclusively due to displacement of H_2O by CN^-. The second order rate constant, k_i^{II} (i = f, s), was then obtained from the slope of a plot of k_i against [CN^-].

$$A_\lambda = A_\infty + (A_0 - A_1)e^{-k_f^{obs}t} + (A_1 - A_\infty)e^{-k_s^{obs}t}$$

[Equation 2.9]

There is considerable uncertainty in the measured rate constants and the values were not very reproducible across the temperature range (25 – 40 °C) and CN^- concentration range (0.2 – 0.015 M), so there is considerable error (up to 50% in some cases) in the values obtained. Figure 6.2 gives an example of a plot of k_i against [CN^-]. It is peculiar that the intercept appears to be statistically different from zero, implying that the reverse rate constant, $k_{f,r}$ (for the dissociation of CN^- from [DC-5-seco-Cbs]), is observable. The ratio of the $k_f^{II}/k_{f,r}$ varies between 10 and 20 across the temperature ranges studied; this is clearly incompatible with a log K > 5 obtained for the formation of [DC-5-seco-Cbs] (Table 5.3).

There also appears to be no meaningful variation on the second order rate constants with temperature (Table 6.1). We conclude therefore that, at best, we can *estimate* that the second-order rate constant, k^{II}, for substitution of H_2O in [AC-5-seco-Cbs]$^+$ by CN^- is between about 20 and 100 $M^{-1}s^{-1}$.

References on page 188

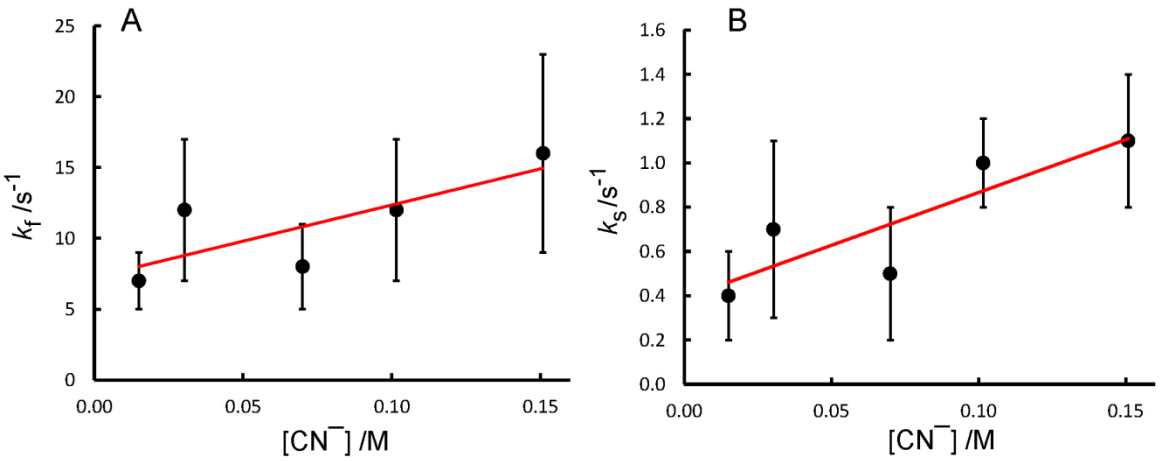

Figure 6.2 Plots of the rate constant for the fast (k_f) and slow (k_s) phases of the reaction of CN^- with $[AC\text{-}5\text{-}seco\text{-}Cbs]^+$ at 30 °C in CAPS buffer, μ = 0.1 M, pH 10.5. For the fast phase, k_f^{II} = 53 ± 23 $M^{-1}s^{-1}$ from the slope, and $k_{f,r}$ = 7.0 ± 0.5 s^{-1} from the intercept. For the slow phase, k_s^{II} = 5 ± 2 $M^{-1}s^{-1}$ and $k_{s,r}$ = 0.4 ± 0.2 s^{-1}.

Notwithstanding this uncertainty in the value of k^{II}, a broad conclusion can be drawn. The value of k^{II}, for the substitution of axially coordinated water by cyanide in $[ACCbs]^+$ and $[ACSYCbs]^+$ in aqueous solution is 4.8(3) × 10^4 $M^{-1}s^{-1}$ and 1.53(2) × 10^4 $M^{-1}s^{-1}$, respectively;[3] in 50% isopropanol, k^{II} for substitution of H_2O in the aquacyano complexes of 10-X-Cbs, where X is the substituent at the C10 position of corrin, is 7.8 × 10^4 $M^{-1}s^{-1}$ for X = H (i.e., for $[ACCbs]^+$ itself); 3.0 × 10^4 $M^{-1}s^{-1}$ for X = NH_2; and 1.7 × 10^3 $M^{-1}s^{-1}$ for X = NO_2.[21] We find here that for $[AC\text{-}5\text{-}seco\text{-}Cbs]^+$, $k^{II} \approx 10^2$ $M^{-1}s^{-1}$. Although interrupting the delocalized system in $[ACSYCbs]^+$ caused a threefold decrease in the rate constants when compared to $[ACCbs]^+$ with its intact corrin, disrupting both the conjugation and cleaving the corrin ring causes the rate constant to drop, probably by over two orders of magnitude. Clearly both the extent of the electron density of the macrocyclic ligand, and the size of the macrocyclic cavity affect the lability of Co(III).

References on page 188

Table 6.1 Rate constants for the substitution of H_2O by CN^- in $[AC\text{-}5\text{-}seco\text{-}Cbs]^+$, μ = 0.1 M (CAPS buffer).

Temp /°C	$[CN^-]$ /M	pH	pK_a ($[AC\text{-}5\text{-}seco\text{-}Cbs]^+$)	k_f^{obs} /× 10^{-2} s^{-1} [a]	k_s^{obs} /× 10^{-3} s^{-1} [a]	k_f /s^{-1} [b]	k_s /s^{-1} [b]	k_f^{II} /$M^{-1}s^{-1}$	$k_{f,r}$ [c] /s^{-1}	k_s^{II} /$M^{-1}s^{-1}$	$k_{s,r}$ [c] /s^{-1}
25	0.0200	10.55	7.28	0.7(2)	0.6(1)	13(4)	1.2(2)	114(38)	15.2(5)	9(3)	1.3(3)
	0.0592	10.55		1.5(6)	1.1(3)	28(11)	2.1(5)				
	0.1012	10.63		1.1(5)	0.9(3)	27(11)	2.1(6)				
	0.1498	10.56		1.9(9)	1.5(4)	35(18)	2.9(9)				
	0.2024	10.65		1.4(7)	1.1(3)	34(16)	2.7(7)				
30	0.0150	10.47	7.53	0.8(2)	0.5(2)	7(2)	0.4(2)	53(23)	7.0(5)	5(2)	0.4(2)
	0.0303	10.52		1.2(5)	0.8(4)	12(5)	0.7(4)				
	0.0700	10.52		0.8(3)	0.5(3)	8(3)	0.5(3)				
	0.1016	10.52		1.2(5)	1.1(2)	12(5)	1.0(2)				
	0.1509	10.54		1.5(7)	1.1(3)	16(7)	1.1(3)				
35	0.0148	10.48	7.78	1.0(2)	0.7(1)	5.2(8)	0.34(5)	68(7)	4(1)	4(1)	0.32(8)
	0.0296	10.47		1.2(4)	0.9(2)	6(2)	0.45(9)				
	0.0707	10.56		1.7(3)	1.4(5)	10(2)	0.8(3)				
	0.0994	10.55		1.8(5)	1.0(3)	11(3)	0.6(2)				
	0.1515	10.56		2.3(1.4)	1.5(8)	14(8)	0.9(5)				
40	0.0148	10.41	8.02	1.1(2)	0.9(1)	2.6(4)	0.21(3)	29(8)	1.9(6)	1.9(5)	0.18(4)
	0.0149	10.37		0.8(1)	0.72(8)	1.9(2)	0.16(2)				
	0.0300	10.41		1.6(3)	1.2(2)	3.8(7)	0.29(4)				
	0.0301	10.41		1.11(8)	0.96(5)	2.7(2)	0.24(1)				
	0.0701	10.39		1.3(3)	1.4(4)	3.0(7)	0.33(9)				
	0.0696	10.45		1.3(1)	1.0(2)	3.4(3)	0.28(6)				
	0.1012	10.45		3(2)	1.3(1)	7(4)	0.35(4)				
	0.1002	10.51		1.9(5)	1.3(3)	6(1)	0.39(8)				
	0.1485	10.41		1.7(4)	1.5(2)	4(1)	0.36(5)				
	0.1515	10.52		2.6(9)	2.3(7)	8(3)	0.7(2)				

[a]Mean and standard deviation of five experiments. [b]Corrected for the fraction of inert hydroxocyano-seco-cobester. No correction was made for the pK_a of HCN.
[c]Apparent reverse rate constants, from the intercept of k_i (i = f,s) against $[CN^-]$.

References on page 188

As an aside, we decided to investigate what effect the nature of the ligand *trans* to the coordinated water would have on the rate of substitution. In the corrins examined thus far ($[ACCbs]^+$, $[ACSYCbs]^+$ and $[AC\text{-}5\text{-}seco\text{-}Cbs]^+$), one of the coordination sites was occupied by a cyanide moiety. It would be intriguing to observe whether the rate of substitution would be affected if the *trans* site was occupied by a ligand other than cyanide, for example the dimethylbenzimidazole base in aquacobalamin.

Reenstra and Jencks previously determined the rate constant for the substitution of axially coordinated water in aquacobalamin under pseudo first-order conditions to be 250 $M^{-1}s^{-1}$.[5] As explained above, this value is suspect because of the presence of chloride in their system, which is a competing ligand for Co(III). Therefore, the kinetics were re-examined under the same conditions employed for $[AC\text{-}5\text{-}seco\text{-}Cbs]^+$ to ensure comparable results.

Aliquots of a freshly prepared cyanide solution (0.5 M, pH 10.5) were added to a solution of aquacobalamin (ca. 30 μM) buffered with CAPS (μ = 0.1 M, pH 10.5) under pseudo first-order conditions. The decrease in absorbance at 362.1 nm with time was observed as a function of cyanide concentration (Figure 6.3). The observed pseudo first-order rate constant (k_l^{obs}) was obtained by fitting a standard exponential to the experimental data obtained for each titration. As before, each rate constant was corrected for the pK_a of aquacobalamin. Six different cyanide solutions with an effective concentration range between 0.03 and 0.15 M were used (Table 6.2).

References on page 188

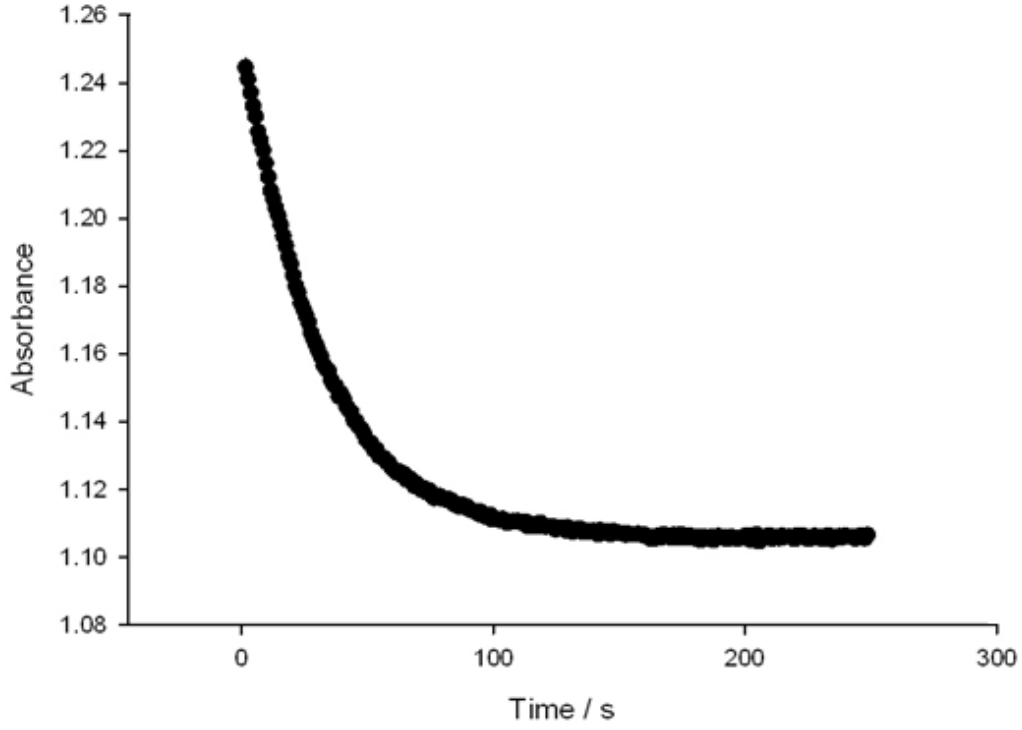

Figure 6.3 Monophasic fit of the absorbance change at 362.1 nm as a function of time for the binding of CN^- (0.15 M) by aquacobalamin (CAPS, μ = 0.1 M, pH 10.5, 25.0 ^oC).

Table 6.2 Rate constants for the substitution of axially coordinated water in aquacobalamin by CN^-.

Cyanide /M	k_l/s^{-1}	Error
0.0289	16.67	2.10
0.0485	21.60	1.45
0.0769	27.00	3.73
0.0965	31.53	3.68
0.1162	31.35	2.17
0.1460	44.26	3.81

References on page 188

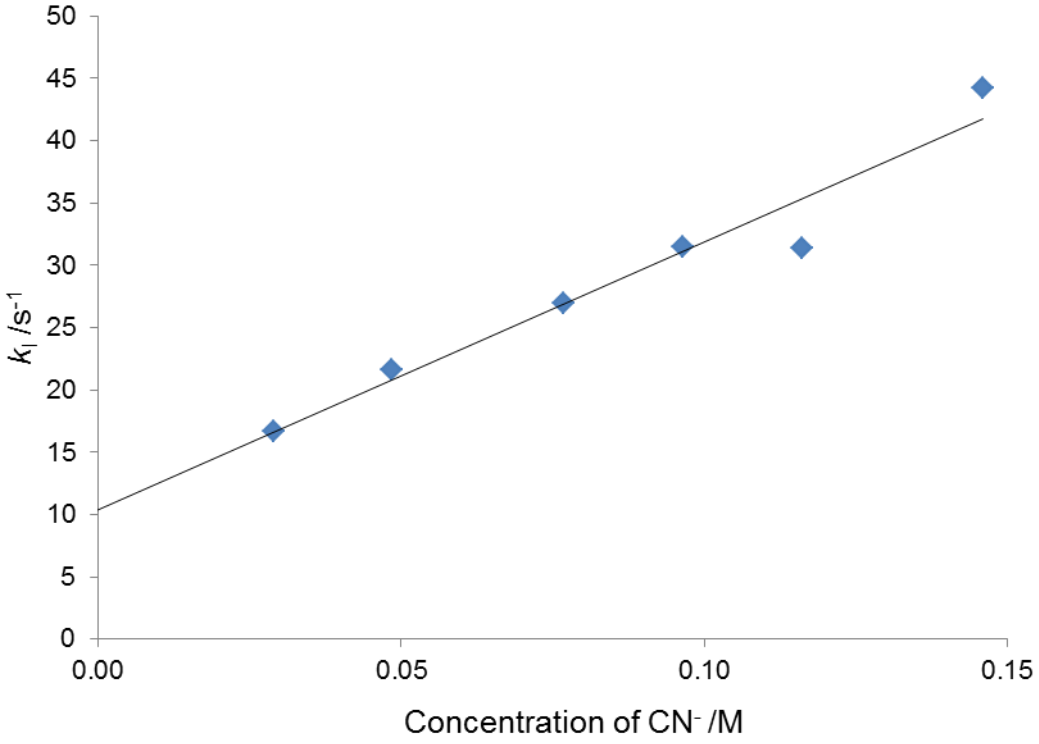

Figure 6.4 A plot of the pH-corrected pseudo first-order rate constants, k_I, versus [CN^-] (CAPS, μ = 0.1 M, pH 10.5, 25.0 °C).

The rate constant was found to be 2.1(2) × 10^2 $M^{-1}s^{-1}$. The plot also revealed that the reaction was reversible. An interesting observation though is that the absorbance decreased with increasing cyanide concentration, however; when the spectra of aquacobalamin and cyanocobalamin were compared, the intensity of the absorbance of cyanocobalamin was greater than that of aquacobalamin at 362.1 nm. The question then arose, why does the absorbance appear to decrease when aquacobalamin is converted to cyanocobalamin? Under high cyanide concentrations, not only does cyanide readily displace coordinated water, but the nucleotide base as well (Equation 6.1). This results in the formation of dicyanocobalamin, which absorbs less intensely at 362.1 nm.

$$[H_2O\text{–}Co(Corr)\text{–}DMBz] + CN^- \rightleftharpoons [CN\text{–}Co(Corr)\text{–}DMBz] + CN^- \rightleftharpoons [CN\text{–}Co(Corr)\text{–}CN]$$

DMBz

[Equation 6.1]

References on page 188

To compensate for this effect, the reactions were repeated but with a much lower concentration of cyanide (0.05 M). The absorbance *vs*. time trace also showed monophasic kinetics (Figure 6.5). The pseudo first-order rate constants were then determined by fitting a standard exponential to the increasing absorbance measurements recorded at 362.1 nm as a function of pH (Table 6.3). Seven different cyanide concentration solutions with an effective concentration range between 0.0008 M and 0.003 M were used. To account for the much lower cyanide concentration, the reaction was monitored for a longer period of time to ensure the reaction reached completion.

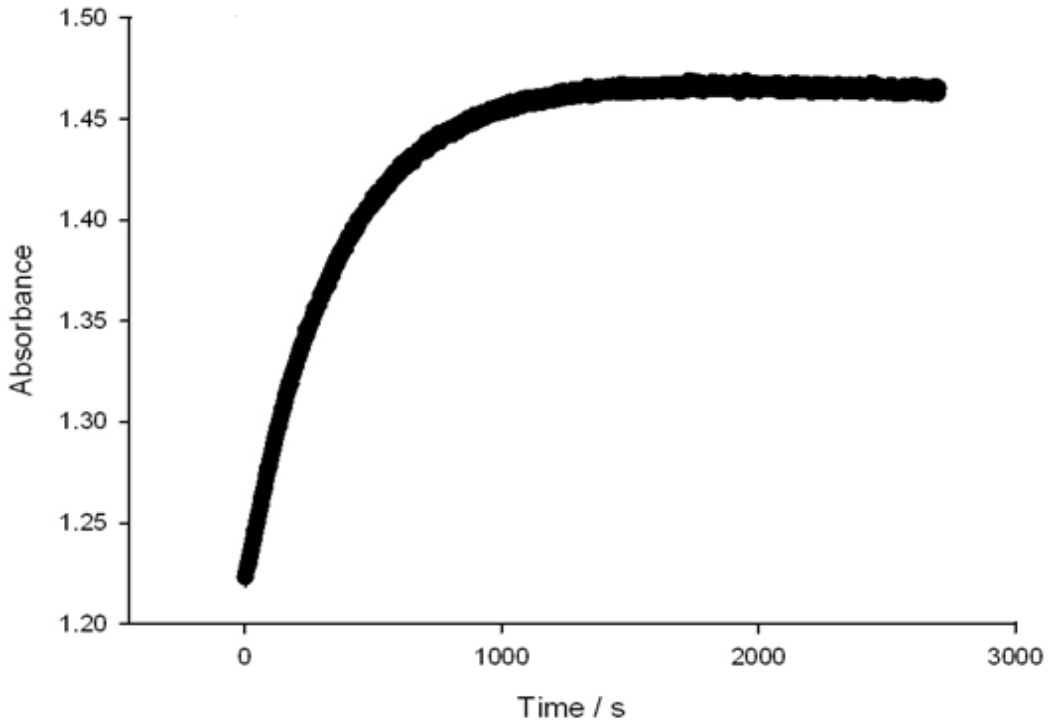

Figure 6.5 Monophasic fit of the absorbance change at 362.1 nm as a function of time for the binding of CN^- (0.0008 M) by aquacobalamin (CAPS, μ = 0.1 M, pH 10.5, 25 ^{o}C).

References on page 188

Table 6.3 Rate constants for the substitution of axially coordinated water in aquacobalamin by CN^-.

Cyanide /M	k_l /s^{-1}	Error
7.93×10^{-4}	0.83	0.14
7.71×10^{-4}	0.73	0.17
7.71×10^{-4}	0.75	0.13
7.71×10^{-4}	0.75	0.18
7.71×10^{-4}	0.78	0.11
8.57×10^{-4}	0.67	0.12
8.57×10^{-4}	0.71	0.13
8.71×10^{-4}	0.68	0.09
8.71×10^{-4}	0.76	0.10
8.71×10^{-4}	0.68	0.14
9.75×10^{-4}	1.09	0.25
9.75×10^{-4}	1.04	0.25
9.75×10^{-4}	0.94	0.28
9.91×10^{-4}	1.01	0.14
9.91×10^{-4}	1.01	0.13
1.96×10^{-3}	1.60	0.27
1.96×10^{-3}	1.82	0.27
1.96×10^{-3}	1.79	0.23
1.90×10^{-3}	1.61	0.51
1.90×10^{-3}	1.86	0.25
2.94×10^{-3}	2.14	0.57
2.94×10^{-3}	2.17	0.48
2.94×10^{-3}	2.28	0.41
2.94×10^{-3}	2.48	0.64
2.94×10^{-3}	2.26	0.53
0.001435	1.76	0.54

References on page 188

Table 6.3 ***(continued)***

Cyanide /M	k_l /s^{-1}	Error
0.001437	1.45	0.50
0.001435	1.43	0.41
0.001435	1.41	0.43
0.001477	1.76	0.66
0.002433	2.20	0.48
0.002425	1.96	0.55
0.002428	2.44	0.46
0.002428	2.04	0.39
0.002449	1.98	0.41

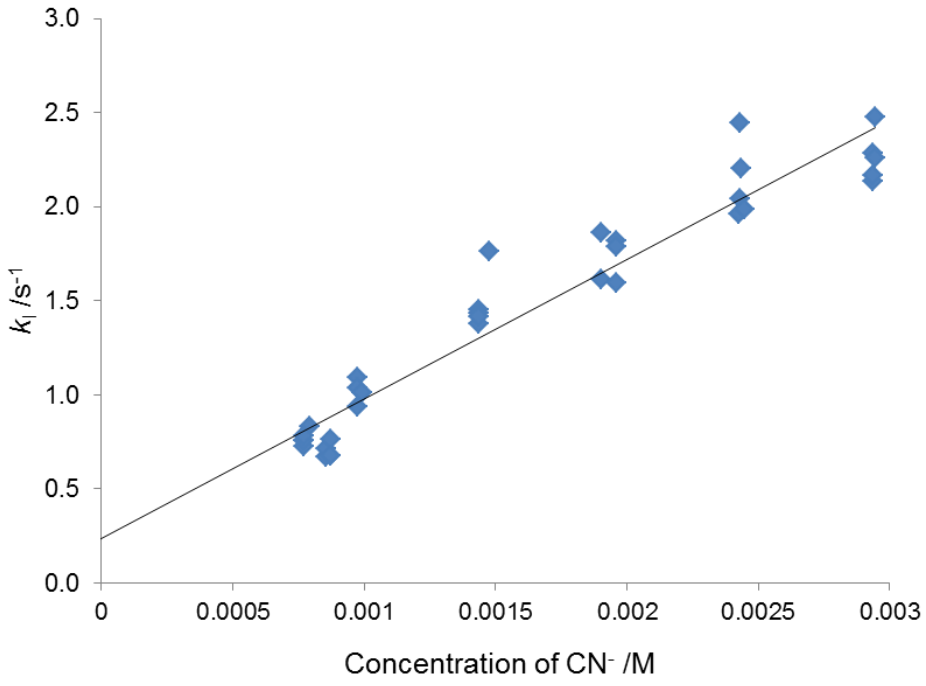

Figure 6.6 A plot of the pH-corrected pseudo first-order rate constant, k_l, versus [CN^-] (CAPS, μ = 0.1 M, pH 10.5, 25.0 °C).

Figure 6.6 reveals that the reaction is also reversible with a rate constant of 0.14(5) $M^{-1}s^{-1}$, and the rate constant for the substitution of axially coordinated water was found to be

References on page 188

787(35) $M^{-1}s^{-1}$. This result is significantly higher than the value determined by Reenstra (250 $M^{-1}s^{-1}$).[5] The lower value obtained earlier 2.1(2) × 10^2 $M^{-1}s^{-1}$ can be attributed to the displacement of the dimethylbenzimidazole base *trans* to cyanide by high concentrations of CN^-.

Aquacobalamin, like $[ACCbs]^+$, has an unperturbed delocalised corrin system. Seeing that the *cis*-effect of the corrin ring is the same, the extraordinary difference in rate constants (787 $M^{-1}s^{-1}$ [5] and 4.8 × $10^4 M^{-1}s^{-1}$,[3] respectively) can only be attributed to the nature of the ligand *trans* to the axially coordinated water. CN^- has a greater *trans* effect than DMBz, i.e.; CN^- bonds more effectively to the metal than DMBz. This then weakens the *trans* Co-OH_2 thus labilising it.

6.3 Conclusions

In this chapter, we evaluated the kinetic *cis*-effect of cobalt corrins in effort to further explore how the corrin macrocycle influences the binding properties of the cobalt ion. This was achieved by studying the rate of substitution of axially coordinated water in a cleaved corrin $[AC\text{-}5\text{-}seco\text{-}Cbs]^+$ by an incoming ligand, cyanide, as a function of temperature.

The substitution of water coordinated to Co(III) by cyanide showed biphasic kinetics. The faster reaction was attributed to substitution of H_2O by CN^- *trans* to CN^-, and the slower phase to reaction of the diaqua complex with CN^-, i.e., substitution of H_2O *trans* to H_2O. We estimate that $k^{II} \approx 10^2$ $M^{-1}s^{-1}$ for the coordination of CN^- by $[AC\text{-}5\text{-}seco\text{-}Cbs]^+$. This is significantly lower than the rate constants obtained for the same reaction involving $[ACCbs]^+$ (4.8(3) × 10^4 $M^{-1}s^{-1}$) and $[ACSYCbs]^+$ (1.53(2) × 10^4 $M^{-1}s^{-1}$).[3] Hence, Co(III) becomes evidently more inert with a decrease in the extent of delocalisation of electron density on the π-electron system of the corrin ring, and, more significantly, its release from the small cavity of the corrin, hence highlighting the significant kinetic *cis*-effect afforded by the equatorial corrin ligand.

For interest, the effect of the ligand *trans* to the axially coordinated water on the lability of the axially coordinated water was determined by comparing the chemistry of $[AC\text{-}5\text{-}seco\text{-}Cbs]^+$ and aquacobalamin, in which a bulky dimethylbenzimidazole base is found in the α

References on page 188

coordination site as opposed to a cyanide moiety as in [AC-5-seco-Cbs]$^{+}$. Results revealed an extraordinary impact with an observed rate constant of only 787 $M^{-1}s^{-1}$ for the substitution of axially coordinated water in aquacobalamin.[5] This suggests the withdrawal of a significant amount of electron density from the centre of the corrin macrocycle, resulting in a more inert cobalt ion. Thus, much like the observed kinetic *cis*-effect, the *trans*-effect also has a tremendous impact on lability in cobalt corrin chemistry.

References on page 188

REFERENCES FOR CHAPTER 6

1. Brown, K. L.; Cheng, S.; Zou, X.; Zubkowski, J. D.; Valente, E. J.; Knapton, L.; Marques, H. M. *Inorg. Chem*. **1997**, 36, 3666-3675.
2. Chemaly, S. M.; Brown, K. L.; Fernandes, M. A.; Munro, O. Q.; Grimmer, C.; Marques, H. M. *Inorg. Chem.* **2011**, 50, 8700-8718.
3. Chemaly, S. M.; Florczak, M.; Dirr, H.; Marques, H. M. *Inorg. Chem.* **2011**, 50, 8719-8727.
4. Randall, W. C.; Alberty, R. A. *Biochemistry* **1967**, 6, 1520-1525.
5. Reenstra, W. W.; Jencks, W. P. *J. Am. Chem. Soc*. **1979**, 101, 5780-5791.
6. Marques, H. M.; Egan, T. J.; Marsh, J. H.; Mellor, J. R.; Munro, O. Q. *Inorg. Chim. Acta.* **1989**, 166, 249-255.
7. Balt, S.; van Herk, A. M. *Transition Met. Chem*. **1983**, 8, 152-154.
8. Baldwin, D. A.; Betterton, E. A.; Pratt, J. M. *J. Chem. Soc., Dalton Trans.* **1983**, 2217-2222.
9. Marques, H. M.; Brown, K. L.; Jacobsen, D. W. *J. Biol. Chem*.**1988**, 263, 12378-12383.
10. Stochel, G.; van Eldik, R.; Kunkely, H.; Vogler, A. *Inorg. Chem*. **1989**, 28, 4314-4318.
11. Stochel, G.; van Eldik, R. *Inorg. Chem.* **1990**, 29, 2075-2077.
12. Marques, H. M. *J. Chem. Soc., Dalton Trans.* **1991**, 1437-1442.
13. Marques, H. M.; Bradley, J. C.; Campbell, L. A. *J. Chem. Soc., Dalton Trans*. **1992**, 2019-2027.
14. Waddington, M. D.; Finke, R. G. *J. Am. Chem. Soc*. **1993**, 115, 4629-4640.
15. Marques, H. M.; Knapton, L. *J. Chem. Soc., Dalton Trans.* **1997**, 3827-3833.
16. Hamza, M. S. A.; Zou, X.; Brown, K. L.; van Eldik, R. *Inorg. Chem*. **2001**, 40, 5440-5447.
17. Hamza, M. S. A.; Elawady, M. A.; Marques, H. M. *S. Afr. J. Chem*. **2008**, 61, 68-73.
18. Chemaly, S. M.; Kendall, L.; Nowakowska, M.; Pon, D.; Perry, C. B.; Marques, H. M. *Inorg. Chem*. **2013**, 52, 1077-1083.
19. Perry, C. B.; Marques, H. M. *S. Afr. J. Chem.* **2005**, 58, 9-15.
20. Knapton, L. Ph.D. Thesis, University of the Witwatersrand, Johannesburg, 2005.
21. Ghadimi, N.; Perry, C. B.; Govender, P. P.; Marques, H. M. *Inorg. Chim. Acta.* **2016**, 450, 269-278.

22. Ghadimi, N. Ph.D Thesis, University of the Witwatersrand, Johannesburg, 2016.
23. Mathura, S.; Sanassy, D.; de Sousa, A. S.; Perry, C. B.; Navizet, I.; Marques, H. M. *J. Inorg. Biochem*. **2013**, 123, 66-79.
24. Mathura, S. Ph.D Thesis, University of the Witwatersrand, Johannesburg, 2014.
25. Zipp, C. F.; Michael, J. P.; Fernandes, M. A.; Nowakowska, M.; Dirr, H. W.; Marques, H. M. *Inorg. Chem. Comm*. **2015**, 57, 15-17.
26. Zipp, C. F.; Michael, J. P.; Fernandes, M. A.; Mathura, S.; Perry, C. B.; Navizet, I.; Govender, P. P.; Marques, H. M. *Inorg. Chem*. **53**, 4418-4429.
27. Zipp, C. F. Ph.D Thesis, University of the Witwatersrand, Johannesburg, 2014.
28. Marques, H. M.; Baldwin, D. A.; Pratt, J. M. *J. Inorg. Biochem.* **1987,** 29, 77-91.
29. Marques, H. M.; Bradley, J. C.; Brown, K. L.; Brooks, H. *J. Chem. Soc., Dalton Trans.* **1993**, 3475-3478.
30. Martell, A. E.; Smith, R. M.; Motekaites, R. J., NIST Standard Database 46. Criticially Selected Stability Constants of Metal Complexes, V. 8.0, NIST, Gaithersburg, MD, 2004.

CHAPTER 7

CONCLUSIONS AND FUTURE WORK

7.1 Conclusions

The main findings and general conclusions of this study are summarised in this Chapter. More detailed summaries are provided at the end of each relevant chapter.

The typically inert Co(III) ion exhibits remarkable lability when coordinated to a corrin macrocycle such as in vitamin B_{12a}.[1-20] It has been suggested that the origin of this labilisation effect originates from a significant kinetic *cis*-effect through the delocalisation of electron density from the relatively electron-rich corrin to Co(III), thus conferring to it a degree of soft, labile Co(II)-like character.[2,3,16,21] Another important feature of the corrin ring is the relatively small macrocyclic cavity (as opposed to, for example, a porphyrin). It appears that Co(III) may be compressed within the corrin macrocycle, which is likely to significantly impact its chemistry. To eludicate what additional effect this may have on the chemistry of Co(III), we prepared a vitamin B_{12} derivative, [DC-5-seco-Cbs], by perturbing the electronic structure of [DCCbs] through a photosensitized oxygenation reaction. Not only does this disrupt the partially conjugated system of a normal corrin ring, but the bond between C5 and C6 has been cleaved such that the equatorial ligand of Co(III) is no longer macrocyclic, thereby relieving the steric constraints surrounding the axial coordination site of Co(III) corrins.

Once synthesised, [DC-5-seco-Cbs] was purified through a combination of column and preparative thin layer chromatography. The secocobester was characterised by UV-vis spectroscopy, HPLC, IR, NMR and mass spectrometry, the results of which were compared to literature to confirm the identity of the secocobester. Despite considerable effort, we were unable to completely purify the [DC-15-seco-Cbs] isomer simultaneously synthesised during the photooxygenation procedure.

[DC-5-seco-Cbs] has a cyanide moiety occupying both axial ligand coordination sites. Cyanide binds very strongly to the cobalt ion, hence before any solution chemistry investigations could be performed, the secocobester had to be converted to the aquacyano

References on page 197

derivative, in which a coordinated water could be readily displaced by an exogenous ligand, as with $[ACCbs]^+$, $[ACSYCbs]^+$ and $[H_2OCbl]^+$. $[AC\text{-}5\text{-}seco\text{-}Cbs]^+$ was successfully synthesised by exposing [DC-5-seco-Cbs] to methanol and glacial acetic acid to remove one of the axial CN^- ligands. $[AC\text{-}5\text{-}seco\text{-}Cbs]^+$ was characterised by UV-vis spectroscopy, HPLC, IR and mass spectrometry. Further evidence that the species prepared was indeed $[AC\text{-}5\text{-}seco\text{-}Cbs]^+$ rather than the diaqua (or aquahydroxo) species was provided by Hill plots obtained during ligand binding studies which showed that $n \approx 1$ (Equation. 7.1), where N_4 represents the four equatorial N donors of the corrin, X is the ligand *trans* to coordinated H_2O, and charges are omitted for convenience.

$$[X\text{–}Co(N_4)\text{–}OH_2] + n\text{L} \rightarrow [X\text{–}Co(N_4)\text{–L}] + H_2O$$

[Equation 7.1]

Since ligand substitutions and the rate of these reactions are pH-dependent due to the formation of the kinetically-inert hydroxocyano species,[1,2,5] the pK_a of $[AC\text{-}5\text{-}seco\text{-}Cbs]^+$ needed to be determined spectrophotometrically as a function of temperature to allow for pH corrections to all equilibrium and rate constant values. From the slope and intercept of a plot of ln K_a against T^{-1}, $\Delta H = -88 \pm 17$ kJ mol^{-1} and $\Delta S = -434 \pm 56$ J K^{-1} mol^{-1}, from which a remarkably low pK_a of 7.28 at 25 ^{o}C was found. We also re-determined the pK_a of $[ACCbs]^+$ under similar experimental conditions as used for $[AC\text{-}5\text{-}seco\text{-}Cbs]^+$ and found the pK_a to be 9.8(3), an average value across the temperature range 10 ^{o}C – 30 ^{o}C, since no trend of the pK_a with T could be established. The pK_a of coordinated H_2O has decreased dramatically from 9.8(3) to 7.3 on cleaving the corrin ring, thus clearly demonstrating the effect of the corrin ring on the charge density and polarizing ability of the cobalt ion.

The equilibrium constants for the substitution of axially coordinated water by a selection of incoming ligands were determined as a function of temperature. The anionic ligands selected for the study were soft donor atom ligands SO_3^{2-}, CN^- and $S_2O_3^{2-}$, as well as hard donor atom ligands NO_2^- and N_3^-. The equilibrium constants for the coordination of these ligands by $[AC\text{-}5\text{-}seco\text{-}Cbs]^+$ were compared to analogous data for $[ACCbs]^+$, a corrin with an intact delocalised system (the values were re-determined in this study), and $[ACSYCbs]^+$, a

References on page 197

corrin with a diminished delocalised π electron system to observe the effect the nature of the corrin ring has on the binding properties of the Co(III) ion.[2]

The results showed that the log *K* values correlate with the position of the ligands in the spectrochemical series. The π donor ligands (N_3^- and $S_2O_3^{2-}$) bound preferentially to the less electron-rich (Co(III)-like) metal ion afforded by the disrupted corrin ring in $[AC\text{-}5\text{-}seco\text{-}Cbs]^+$, whereas the π acceptor ligands (NO_2^-, $SO_3^{2-}$and CN^-) bound preferentially to the more electron-rich metal ion in $[ACCbs]^+$. The study has thus shown that disruption of the delocalised system through the cracking of the corrin ring and the subsequent opening of the macrocyclic cavity inhibits the transfer of electron density to the Co(III) ion, hence curtailing the imparting of a softer Co(II)-like character on the metal. The increase in positive charge on the metal and its immediate coordination environment clearly discriminates against the coordination of the softer ligands, and appears to favour, relatively speaking, the coordination of ligands further along the spectrochemical series. These findings were supported by DFT calculations (BP86-D3/6-311G(d,p)), which showed that (i) cleavage of the corrin does not unduly perturb the coordination sphere of the metal ion and the metal remains essentially octahedral; (ii) the sum of the partial charges on the metal and the entire coordination sphere, or the metal and the four equatorial donor N atoms, is less negative in the 5-seco-Cbs complexes than in the Cbs complexes themselves and supports the supposition that cleavage of the corrin has made the metal and its immediate environment more positive; (iii) that cleavage of the corrin causes the bonds to the equatorial N donors to lengthen, relieving the steric compression on the metal; and (iv) this allows the bonds to the axial ligands to be shorter than in the cobester itself, explaining why Δ*H* values for substitution of H_2O by an incoming ligand and very negative.

We also briefly explored the binding of neutral N-donor ligands (N-MeIm, 4-MePy and NH_2EtOH). The distinction between the softer Co(III) in $[ACCbs]^+$ and the harder Co(III) in $[AC\text{-}5\text{-}seco\text{-}Cbs]^+$ ($[ACCbs]^+$ > $[ACSYCbs]^+$ > $[AC\text{-}5\text{-}seco\text{-}Cbs]^+$) observed for the binding of anionic ligands was maintained for the neutral N-donor ligands. Furthermore, results also indicated that relieving the steric hindrance surrounding the axial coordination site in $[AC\text{-}5\text{-}seco\text{-}Cbs]^+$ did enhance the metal's ability to bind larger neutral ligands.

References on page 197

Kinetics data for the substitution of H_2O *trans* to CN^- by cyanide were obtained under pseudo first-order conditions. The results showed that the substitution of coordinated water proceeded with biphasic kinetics. We suggested that the faster reaction corresponds to the substitution of axially coordinated water by CN^-, whereas the slower reaction corresponds to the substitution of coordinated water in the diaqua species. We estimate that $k^{II} \approx 10^2\ M^{-1}s^{-1}$ for the coordination of CN^- by $[AC\text{-}5\text{-}seco\text{-}Cbs]^+$. This is significantly lower than the rate constants obtained for the same reaction involving $[ACCbs]^+$ ($4.8(3) \times 10^4\ M^{-1}s^{-1}$) and $[ACSYCbs]^+$ ($1.53(2) \times 10^4\ M^{-1}s^{-1}$).[3] This illustrates how diminishing the extent of conjugation of the corrin ligand and relieving the constraints of the macrocyclic cavity significantly increases the inertness of the central Co(III) ion.

For interest, the data were compared to analogous data for aquacobalamin. In this way, the effect of the ligand *trans* to the axially coordinated water on its substitution could be elucidated.[7] The aquacobalamin reactions were repeated to ensure comparable results under the same experimental conditions. It was found that as the *trans* ligand varied from cyanide to a dimethylbenzimidazole (DMBz) base ($[AC\text{-}5\text{-}seco\text{-}Cbs]^+$ to aquacobalamin), the rate constant increased from $k^{II} \approx 10^2\ M^{-1}\ s^{-1}$ to $7.87 \times 10^2\ M^{-1}s^{-1}$. Although CN^- has a larger *trans* effect than DMBz (*cf.* $k^{II} = 4.8(3) \times 10^4\ M^{-1}s^{-1}$ *vs*. $7.87 \times 10^2\ M^{-1}s^{-1}$ for substitution of H_2O by CN^- in $[ACCbs]^+$ (H_2O *trans* to CN^-) and $[H_2OCbl]^+$ (H_2O *trans* to DMBz), respectively, the cracking of the corrin ring and associated opening of the macrocyclic cavity overrides this and results in an even more pronounced inert Co(III) character ($k^{II} \approx 10^2\ M^{-1}s^{-1}$ for $[AC\text{-}5\text{-}seco\text{-}Cbs]^+$.

The results presented in this work indicate how profoundly the identity of the equatorial ligand materially affects the thermodynamic and kinetic properties of the Co(III) ion, and influences the ability of the secocobester to bind exogenous ligands. This also suggests that the origin of this labilising effect is due to both the topology and the electronic structure of the corrin ring.

References on page 197

7.2 Future Work

These findings have contributed significantly to the foundation of research into the *cis*-labilising effect on cobalt corrins, however; a few shortcomings were identified in this work which need to be investigated further in future.

All attempts to crystallise [DC-5-seco-Cbs] failed to produce diffraction quality crystals; hence a more in depth literature search into the crystallisation of related macrocycles needs to be conducted.

As we were unsuccessful in our attempts to purify hexamethyl Coα,Coβ-dicyano-7-de-(carboxymethyl)-7-8-didehydro-cobyrinate ('pyrocobester')[22,23] in which the length of the corrin chromophore has been increased but the macrocyclic cavity remains intact, further work is warranted into developing a suitable method to purify a highly air and light sensitive compound through a combination of column and preparative thin layer chromatography, as well as to develop a method with which to remove an axial cyanide without compromising the corrin ring, as the resulting increased electron density of the corrin ring can provide invaluable insight into the lability of the Co(III) ion.

If this is successful, then hexamethyl Coα,Coβ-dicyano-5,6-dioxo-7-de-(carboxymethyl)-7-8-didehydro-5,6-seco-cobyrinate ('secopyrocobester')[23] will also be synthesised by the photosensitized oxygenation of the pyrocobester to investigate the effect cracking the extended chromophore of the pyrocobester would have on the lability of Co(III) within the system.

As we have now studied the effect of modifying the corrin ring at the C5 position, future endeavours will include expanding the research into the stable yellow cobesters by investigating the properties of the cobalt ion in $[15\text{-ACSYCbs}]^+$ in which the corrin is interrupted at the C15 position.[24] We will also revisit the purification of [DC-15-seco-Cbs] using semi-preparative HPLC. The effect these modifications might have on the properties of the central Co(III) ion will be compared to analogous data to further the understanding of the *cis*-labilising effect of cobalt corrins.

The ligand binding studies for the substitution of axially coordinated water by neutral N-donor ligands in $[\text{AC-5-seco-Cbs}]^+$ was very limited as most neutral N-donor ligands have

References on page 197

much higher pK_a values than [AC-5-seco-Cbs]$^+$; as such, it was difficult to find experimental conditions to allow for sufficient concentrations of both [AC-5-seco-Cbs]$^+$ and the ligands to exist in the unprotonated forms required for binding. Hence, a larger variety of neutral N-donor ligands with lower pK_a values need to be found and investigated. Substituted pyridines and azoles will be investigated.

A different class of compound that might be interesting to explore are the texaphyrins (Figure 7.1).[25] They are penta-aza porphyrin-like compounds. They present the metal with a much larger macrocyclic cavity. Whilst they are well-known to coordinate the lanthanides,[26] their complexes with the later first row divalent cations has been reported.[25] The synthesis of these compounds, largely pioneered by the Sessler group, does not appear unduly difficult. The larger macrocyclic cavity will undoubtedly favour Co(II) over Co(III) because of its larger ionic radius. There are many references (especially in the patent literature) to Co(III) texaphyrins so it should be possible to oxidise the metal to the desired trivalent state.

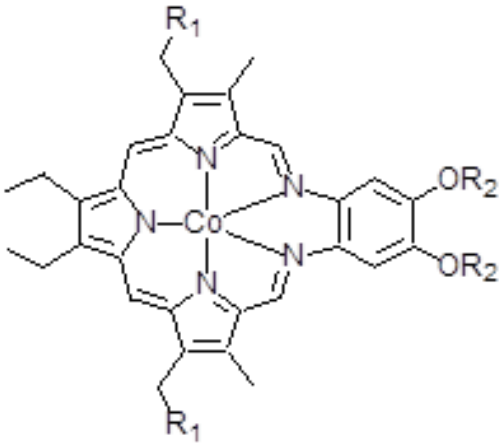

Figure 7.1 Structure of a texaphyrin.

Lastly, this study has revealed the significant effect of relieving the steric constraints of the corrin ring on the activity of Co(III). However, in previous work on [ACSYCbs]$^+$, steric effects imposed by the lactone group have not been taken into account. Subsequently, DFT modelling on the binding of neutral ligands such as the imidazoles and pyridines by

References on page 197

$[ACSYCbs]^+$ is required to verify why the equilibrium constants were so exceptionally low relative to $[AC\text{-}5\text{-}seco\text{-}Cbs]^+$ and $[ACCbs]^+$.

References on page 197

REFERENCES FOR CHAPTER 7

1. Knapton, L. Ph.D. Thesis, University of the Witwatersrand, Johannesburg, 2005.
2. Chemaly, S. M.; Florczak, M.; Dirr, H.; Marques, H. M. *Inorg. Chem.* **2011**, 50, 8719-8727.
3. Brown, K. L.; Cheng, S.; Zou, X.; Zubkowski, J. D.; Valente, E. J.; Knapton, L.; Marques, H. M. *Inorg. Chem*. **1997**, 36, 3666-3675.
4. Marques, H. M.; Egan, T. J.; Marsh, J. H.; Mellor, J. R.; Munro, O. Q. *Inorg. Chim. Acta.* **1989**, 166, 249-255.
5. Chemaly, S. M.; Brown, K. L.; Fernandes, M. A.; Munro, O. Q.; Grimmer, C.; Marques, H. M. *Inorg. Chem*. **2011**, 50, 8700-8718.
6. Randall, W. C.; Alberty, R. A. *Biochemistry* **1967**, 6, 1520-1525.
7. Reenstra, W. W.; Jencks, W. P. *J. Am. Chem. Soc*. **1979**, 101, 5780-5791.
8. Balt, S.; van Herk, A. M. *Transition Met. Chem*. **1983**, 8, 152-154.
9. Baldwin, D. A.; Betterton, E. A.; Pratt, J. M. *J. Chem. Soc., Dalton Trans.* **1983**, 2217-2222.
10. Marques, H. M.; Brown, K. L.; Jacobsen, D. W. *J. Biol. Chem*. **1988**, 263, 12378-12383.
11. Stochel, G.; van Eldik, R.; Kunkely, H.; Vogler, A. *Inorg. Chem*. **1989**, 28, 4314-4318.
12. Stochel, G.; van Eldik, R. *Inorg. Chem.* **1990**, 29, 2075-2077.
13. Marques, H. M. *J. Chem. Soc., Dalton Trans.* **1991**, 1437-1442.
14. Marques, H. M.; Bradley, J. C.; Campbell, L. A. *J. Chem. Soc., Dalton Trans*. **1992**, 2019-2027.
15. Waddington, M. D.; Finke, R. G. *J. Am. Chem. Soc*. **1993**, 115, 4629-4640.
16. Marques, H. M.; Knapton, L. *J. Chem. Soc., Dalton Trans.* **1997**, 3827-3833.
17. Hamza, M. S. A.; Zou, X.; Brown, K. L.; van Eldik, R. *Inorg. Chem*. **2001**, 40, 5440-5447.
18. Hamza, M. S. A.; Elawady, M. A.; Marques, H. M. *S. Afr. J. Chem*. **2008**, 61, 68-73.
19. Chemaly, S. M.; Kendall, L.; Nowakowska, M.; Pon, D.; Perry, C. B.; Marques, H. M. *Inorg. Chem.* **2013**, 52, 1077-1083.
20. Perry, C. B.; Marques, H. M. *S. Afr. J. Chem.* **2005**, 58, 9-15.
21. Perry, C. B.; Fernandes, M. A.; Brown, K. L; Valente, E. J.; Marques, H. M. *Eur. J. Inorg. Chem.* **2003**, 136, 2095-2107.
22. Ernst, L.; Holze, G.; Inhoffen, H. H. *Liebigs Ann. Chem*. **1981**, 198-201.

23. Kräutler, B.; Stepanek, R.; Holze, G. *Helv. Chim. Acta.* **1983**, 66, 44-49.
24. Holze, G.; Gossauer, A.; Ernst, L. *Helv. Chim. Acta*, **1986**, 69, 1567-1570.
25. Hannah, S.; Lynch, V.; Guldi, D. M.; Gerasimchuk, N.; MacDonald, C. L. B.; Magda, D.; Sessler, J. L., *J. Am. Chem. Soc.* **2002,** 124, 8416-8427.
26. Sessler, J. L.; Hemmi, G.; Mody, T. D.; Murai, T.; Burrell, A.; Young, S. W., *Acc. Chem. Res.* **1994,** 27, 43-50.

APPENDICES

APPENDIX A.1

Table A.1 Summary of chemicals used in this study.

Chemical	Supplier	Grade
Acids and Bases		
Ammonia (as 25% NH_4OH)	Saarchem	AR
Glacial acetic acid	N.T. Laboratory Supplies	CP
Hydrochloric acid (32%)	ACE	CP
Phosphoric acid	Sigma-Aldrich	AR
Sodium hydroxide (Pellets)	Merck	CP
Sulfuric acid	Merck	GR
Biological Reagents		
Cyanocobalamin	Sigma-Aldrich	BP
Dicyanocobyrinic acid heptamethyl ester	Sigma-Aldrich	BP
Hydroxocobalamin acetate	Roussel	BP
Fine Chemicals, Reagents and Ligands		
4-Methylpyridine	Sigma-Aldrich	CP
Ethanolamine	Sigma-Aldrich	CP
Methylene blue	Sigma-Aldrich	CP
N-methylimidazole	Sigma-Aldrich	CP
Sodium azide	Riedel-de Haën	CP
Sodium bicarbonate	Sigma-Aldrich	CP
Sodium carbonate	Sigma-Aldrich	CP
Sodium cyanide	Merck	CP
Sodium dichromate	Saarchem	CP
Sodium nitrite	Saarchem	CP
Sodium sulfate	ACE	CP
Sodium sulphite	Saarchem	CR
Sodium thiosulfate	Saarchem	CR

Table A.1 *(continued)*

Solvents and Gases		
Acetone	Promark Chemicals	CP
Acetonitrile	ACE	CP
Acetonitrile	Merck	HPLC
Benzene	SMM Chemicals	CP
Chloroform	ACE	CP
Cyclohexane	ACE	CP
Decalin	Sigma-Aldrich	CP
Deuterated methanol	Sigma-Aldrich	CP
Deuterated chloroform	Sigma-Aldrich	CP
Dichloromethane	ACE	CP
Diethyl ether	ACE	CP
Ethyl acetate	ACE	CP
Hexane	ACE	CP
Methanol	ACE	CP
Methanol	Sigma-Aldrich	HPLC
Methyl acetate	Sigma-Aldrich	CP
Nitrogen (gas)	Afrox	UHP
Oxygen	Afrox	AR
Toluene	Merck	CP
Trichloroethylene	Sigma-Aldrich	CP
Triethylamine	Saarchem	CP
Buffers		
3-(Cyclohexylamino)-propanesulfonic acid (CAPS)	Sigma-Aldrich	AR
Cyclohexylaminoethanesulfonic acid (CHES)	Sigma-Aldrich	AR
3-(N-Morpholino)-ethanesulfonic acid (MES)	Sigma-Aldrich	AR

Table A.1 *(continued)*

3-(N-Morpholino)-propanesulfonic acid (MOPS)	Sigma-Aldrich	AR
Potassium hydrogen phthalate	Saarchem	GR
Sodium hydrogen carbonate	Sigma-Aldrich	CP
Tris(hydroxymethyl)-aminoethane (Tris)	Merck	CP
Metrohm Standard Buffer 4.0	Metrohm	
Metrohm Standard Buffer 7.0	Metrohm	
Metrohm Standard Buffer 9.0	Metrohm	

Key: **AR** = Analytical Reagent **CR** = Chemical Reagent
BP = Biologically Pure **GR** = General Reagent
CP = Chemically Pure **UHP** = Ultra High Pressure
HPLC = High Performance Liquid Chromatography

APPENDIX A.2

Table A.2 Summary of equipment and software used in this study.

Material	Source	Specification
General Equipment and Instrumentation		
Centrifuge	Hettich	Rotofix 32A
Cuvettes	Hellma	Quartz, 1.0 cm, Type 110-QS
Cuvettes	Hellma	Quartz, 1.0 cm, flow cell, Type 175.000-QS
Electrodes	Metrohm	Metrohm LL UnitrodePt 1000
Electrodes	Ohaus	ST310
HPLC	Dionex	Reverse phase system
FTIR	Bruker	Alpha
Mass spectrometer	Bruker	Compact Q-TOF
NMR	Bruker	Avance 500 III Ultra Shield Plus
Rotary evaporator	Labotec	Buchi R-100 Rotavapor
Peristaltic pump		Watson-Marlow 101U
pH meter	Metrohm	Metrohm 780
pH meter	Ohaus	Starter 3100
UV-vis spectrophotometer	CARY	3E, 300 BIO
UV-vis spectrometer	Agilent	Diode array
Vacuum pump	Labotec	KNF Laboport Diaphragm vacuum pump
Water-circulating bath	Thermofisher	HAAKE K10
Separation and Filters		
Aluminium oxide	Sigma-Aldrich	Activated, neutral, Brockmann 1, 58 Å pore size
Aluminium oxide TLC plates	Sigma-Aldrich	PET support, fluorescent indicator 254 nm, 20 × 20 cm, 200 µm thick

Table A.2 *(continued)*

Membrane filters	Pall	PTFE, 47.0 mm, 1.0 μm pore
HPLC guard column	Supelco	C18 reverse phase
Silica Gel 60 (Flash)	Sigma-Aldrich	High purity, 60 Å pore size, particle size 40-63 μm
Silica Gel TLC plates	Sigma-Aldrich	Aluminum support, fluorescent indicator 254 nm, 20 × 20 cm, 200 μm thick
Software		
Material	**Source**	**-**
Chromeleon	Dionex	
Excel	Microsoft	
Compass DataAnalysis	Bruker	
MestReNova	Mestrelab	
OPUS	Bruker	
WinUV	Cary	
SigmaPlot	Systat Software	
UV-visible ChemStation	Agilent	

APPENDIX B.1

CALCULATION FOR MULTI-COMPONENT BUFFER

For a 50.0 ml, 0.1 M multi-component buffer containing 1.0 mM MES, MOPS, Tris, CHES, potassium hydrogen phthalate (KHP) and 0.1 M Na_2SO_4:

Ionic Strength of Na_2SO_4: $\mu = \frac{1}{2}\Sigma c_1 z_1^2 = 0.1$ M

$= (\frac{1}{2}[Na^+].(1)^2) + (\frac{1}{2}[SO_4^{2-}].(-2)^2) = 0.1$ M

$= \frac{1}{2}[Na^+] + 2[SO_4^{2-}] = 0.1$ M

Since $[Na^+] = 2[SO_4^{2-}]$

$\therefore \mu = \frac{1}{2}.2.[SO_4^{2-}] + 2[SO_4^{2-}] = 0.1$ M

$= [SO_4^{2-}] + 2[SO_4^{2-}] = 0.1$ M

$= 3[SO_4^{2-}] = 0.1$ M

$\therefore [SO_4^{2-}] = 0.0333$ M

For Na_2SO_4: $C_1V_1 = C_2V_2$

(0.1)(*x*) = (0.0333)(0.05)

x = 0.01665 L

x = 16.7 ml of a 0.1 M Na_2SO_4 solution

For buffers: $C_1V_1 = C_2V_2$

(0.1)(*x*) = (0.001)(0.05)

x = 0.0005 L

x = 0.5 ml of a 1.0 mM solution of MES, MOPS, Tris, CHES and KHP

Therefore, a 50.0 ml, 0.1 M multi-component buffer solution requires:

- 16.7 ml of 0.1 M Na_2SO_4
- 0.5 ml of 1.0mM MES, MOPS, Tris, CHES and KHP
- 30.8 ml de-ionised water

APPENDIX B.2

DERIVATION OF EQUATIONS FOR THE DETERMINATION OF BINDING CONSTANTS

B.1 The binding isotherm of a system with log *K* < 4

An equilibrium exists between the cobalt corrin (M) and free ligand in solution:

$$M + L \rightleftharpoons ML$$

The equilibrium constant can be defined as:

$$K = \frac{[ML]}{[M][L]}$$

From Beer's Law (where ε is the molar absorptivity constant and b is the path length of the cell) the initial and final absorbances can be defined as:

$$A_0 = \varepsilon_M b[M]_0$$

$$A_1 = \varepsilon_{ML} b[ML]_1$$

At any point during the titration:

$$A = \varepsilon_M b[M] + \varepsilon_{ML} b[ML]$$

$$[ML]_0 = [M] + [ML]$$

$$[ML]_1 = [M]_0 = [M] + [ML]$$

$$A = \varepsilon_M b([M]_0 - [ML]) + \varepsilon_{ML} b[ML]$$

$$A = \varepsilon_M b[M]_0 - \varepsilon_M b[ML] + \varepsilon_{ML} b[ML]$$

$$A - \varepsilon_M b[M]_0 = [ML](\varepsilon_{ML} b - \varepsilon_M b)$$

$$\therefore \quad [ML] = \frac{A - \varepsilon_M b[M]_0}{\varepsilon_{ML} b - \varepsilon_M b} \qquad \textbf{[A.2.1.1]}$$

Similarly:

$$A = \varepsilon_M b[M] + \varepsilon_{ML} b[ML]$$

$$A = \varepsilon_M b[M] + \varepsilon_{ML} b([ML]_1 - [M])$$

$$A = \varepsilon_M b[M] + \varepsilon_{ML} b[ML]_1 - \varepsilon_{ML} b[M])$$

$$A - \varepsilon_{ML}b[ML]_1 = [M](\varepsilon_M b - \varepsilon_{ML}b)$$

$$\therefore \quad [M] = \frac{A - \varepsilon_{ML}b[ML]_1}{(\varepsilon_M b - \varepsilon_{ML}b)}$$

$$\therefore \quad [M] = \frac{A - A_1}{(\varepsilon_M b - \varepsilon_{ML}b)} \qquad \textbf{[A.2.1.2]}$$

Consider the equilibrium constant

$$K = \frac{[ML]}{[M][L]}$$

Substituting in Equations **A.2.1.1** and **A.2.1.2**:

$$K = \frac{A - A_0}{\varepsilon_{ML}b - \varepsilon_M b} \cdot \frac{1}{L} \cdot \frac{\varepsilon_M b - \varepsilon_{ML}b}{A - A_1}$$

$$K = \frac{A - A_0}{\varepsilon_{ML}b - \varepsilon_M b} \cdot \frac{1}{L} \cdot \frac{\varepsilon_{ML}b - \varepsilon_M b}{A_1 - A}$$

$$K = \frac{A - A_0}{A_1 - A} \cdot \frac{1}{L}$$

$$K[L] = \frac{A - A_0}{A_1 - A}$$

$$\therefore \quad K[L] = \frac{A_0 - A}{A - A_1}$$

Assuming that $[L]_0 \approx [L]$ and K is small (< 4)

$$K[L] = \frac{A_0 - A}{A - A_1}$$

$$A_0 - A = K[L](A - A_1)$$

$$A_0 - A = K[L]A - K[L]A_1$$

$$K[L]A + A = K[L]A_1 + A_0$$

$$A(K[L] + 1) = K[L]A_1 + A_0$$

$$\therefore \quad A = \frac{A_0 + A_1K[L]}{1 + K[L]} \qquad \textbf{[A.2.1.3]}$$

B.2 The binding isotherm of a system with log *K* > 4

If K is large, $[L]_{free} \neq [L]_T$. An explicit expression for $[L]_{free}$ must therefore be derived.

$$[L]_{free} = [L]_T - [ML]$$

$$[ML] = [M]_T - [M]$$

$$[M]_T = [ML] + [M]$$

From the equilibrium constant:

$$[M]_T = [ML] \quad \frac{[ML]}{K[L]_{free}}$$

$$[M]_T = [ML] \quad 1 + \frac{1}{K[L]_{free}}$$

$$[M]_T = [ML] \quad 1 + \frac{K[L]_{free}}{K[L]_{free}}$$

$$\therefore \quad [ML] = \frac{[M]_T K[L]_{free}}{1 + K[L]_{free}}$$

$$\therefore \quad [L]_{free} = [L]_T - \frac{[M]_T K[L]_{free}}{1 + K[L]_{free}}$$

$$\therefore \quad [L]_{free}(1 + K[L]_{free}) = [L]_T(1 + K[L]_{free}) - [M]_T K[L]_{free}$$

$$[L]_{free} + K[L]_{free}^2 = [L]_T + K[L]_T[L]_{free} - [M]_T K[L]_{free}$$

$$K[L]_{free}^2 + (1 + K[M]_T - K[L]_T)[L]_{free} - [L]_T = 0$$

This has the form:

$$a_1[L]_{free}^2 + a_2[L]_{free} + a_3 = 0$$

where $a_1 = K$; $a_2 = 1 + K[M]_T - K[L]_T$; $a_3 = -[L]_T$.

$$\therefore \quad [L]_{free} = \frac{-a_2 \pm \sqrt{a_2^2 - 4a_1a_3}}{2a_1}$$

Since $[L]_{free} > 0$

$$\therefore \quad [L]_{free} = \frac{-a_2 + \sqrt{a_2{}^2 - 4a_1a_3}}{2a_1}$$

Substituting into **A.2.1.3**

$$\therefore \quad A = \frac{A_0 + A_1K[L]_{free}}{1 + K[L]_{free}} \qquad \textbf{[A.2.1.4]}$$

APPENDIX C

TLC ANALYSIS

Table C.1 R_f values from the TLC analysis of Method 1 and 2.

	[DCCbs]	Photo-Oxygenation Product
Method 1	0.11	0.17, 0.10
Method 2	0.68	0.69, 0.61

Table C.2 R_f values from the determination of an EtOAc:MeOH:toluene system.

	[DCCbs]	Photo-Oxygenation Product
a	0.65	0.65, 0.54, 0.45, 0.16
b	0.81	0.81, 0.75, 0.45, 0.20
c	0.35	0.46, 0.32, 0.23, 0.15
d	0.31	0.28, 0.19
e	0.19	0.12
f	0.20	0.17, 0.08

Table C.3 R_f values from the determination of an EtOAc:toluene:acetone system on silica.

	[DCCbs]	[DC-15-seco-Cbs]	[DC-5-seco-Cbs]	Middle Fractions
a	0.09	0.09	0.82, 0.06	0.06
b	0.10	0.10	0.84, 0.33, 0.15, 0.08	0.08
c	0.06	0.08	0.07	0.05
d	0.18	0.19	0.87, 0.25, 0.12	0.10, 0.08
e	0.31	0.29	0.94, 0.41, 0.25, 0.18	0.25, 0.15
f	0.40	0.38	0.38, 0.28	0.40, 0.29
g	0.56	0.54	0.93, 0.62, 0.51, 0.41	0.54, 0.41
h	0.71	0.71	0.71, 0.61	0.72, 0.61

Table C.4 R_f values from the determination of an EtOAc:toluene:acetone system of alumina.

	[DCCbs]	[DC-15-seco-Cbs]	[DC-5-seco-Cbs]	Middle Fractions
a	0.20	0.20, 0.15	0.10	0.16, 0.09
b	0.19	0.20, 0.15	0.09	0.12, 0.07
c	0.23	0.21, 0.17	0.18, 0.10	0.18, 0.09
d	0.38	0.38, 0.31	0.30, 0.18	0.30, 0.16
e	0.53	0.46	0.41, 0.22	0.43, 0.21
f	0.67	0.64	0.61, 0.43	0.64, 0.44
g	0.87	0.77	0.74, 0.57	0.73, 0.56
h	0.81	0.79	0.75, 0.58	0.76, 0.60

Table C.5 R_f values from investigations into isocratic solvent systems.

	Alumina		Silica	
	[DCCbs]	[DC-15-seco-Cbs]	[DCCbs]	[DC-15-seco-Cbs]
a	0.45	0.45, 0.37	0.17	0.17
b	0.00	0.00	0.00	0.00
c	0.82	0.84	0.69	0.72
d	0.00	0.00	0.00	0.00
e	0.00	0.00	0.00	0.00
f	0.98	0.95	0.37	0.57
g	0.00	0.00	0.00	0.00

Table C.6 R_f values from the investigations of various combinations of solvents on alumina.

	[DCCbs]	[DC-15-seco-Cbs]	[DC-5-seco-Cbs]	Middle Fractions
a	0.00	0.00	0.00	0.00
b	0.97	0.98	0.99	0.99
c	0.55	0.55, 0.51	0.48, 0.33	0.46, 0.31
d	0.46	0.42, 0.29	0.36, 0.23, 0.13	0.39, 0.22
e	0.00	0.00	0.00	0.00
f	0.00	0.00	0.00	0.00

Table C.7 R_f values from the investigations of various combinations of solvents on silica.

	[DCCbs]	[DC-15-seco-Cbs]	[DC-5-seco-Cbs]	Middle Fractions
a	0.00	0.00	0.00	0.00
b	0.92	0.91, 0.86	0.87, 0.83	0.89
c	0.19	0.20	0.15, 0.11	0.14, 0.11
d	0.18	0.18	0.15, 0.10	0.18, 0.11
e	0.00	0.00	0.00	0.00
f	0.00	0.00	0.00	0.00

Table C.8 R_f values from investigations into a suitable EtOAc:hexane solvent system.

	[DCCbs]	**[DC-15-seco-Cbs]**
a	0.39	0.38, 0.27
b	0.37	0.35, 0.21
c	0.36	0.36, 0.23
d	0.05	0.05
e	0.14	0.13, 0.09
f	0.09	0.09, 0.06
g	0.06	0.06
h	0.00	0.00
i	0.05	0.04
j	0.00	0.00
k	0.00	0.00
l	0.00	0.00

Table C.9 R_f values from the determination of the volume of acetonitrile required for optimum separation in addition to an EtOAc:hexane (10:0.01) solvent system.

	[DCCbs]	**[DC-15-seco-Cbs]**
a	0.41	0.41, 0.32
b	0.46	0.44, 0.34
c	0.28	0.27
d	0.56	0.56, 0.46
e	0.24	0.15
f	0.88	0.88, 0.81
g	0.77	0.77
h	0.92	0.90

Table C.10 R_f values from the determination of the volume of acetonitrile required for optimum separation in addition to an EtOAc:hexane (10:0.1) solvent system.

	[DCCbs]	**[DC-15-seco-Cbs]**
a	0.43	0.42, 0.30
b	0.37	0.37, 0.25
c	0.48	0.47, 0.40
d	0.60	0.57, 0.43
e	0.78	0.76, 0.68
f	0.90	0.88, 0.83
g	0.76	0.73
h	0.95	0.92, 0.89

Table C.11 R_f values from the determination of the volume of acetonitrile required for optimum separation in addition to an EtOAc:hexane (10:0.5) solvent system.

	[DCCbs]	**[DC-15-seco-Cbs]**
a	0.28	0.27, 0.19
b	0.31	0.30, 0.21
c	0.49	0.47, 0.39
d	0.77	0.75, 0.43
e	0.29	0.29, 0.20
f	0.86	0.84, 0.79
g	0.92	0.90, 0.85
h	0.93	0.90

APPENDIX D.1

ESI-MS DATA FOR [DCCbs]

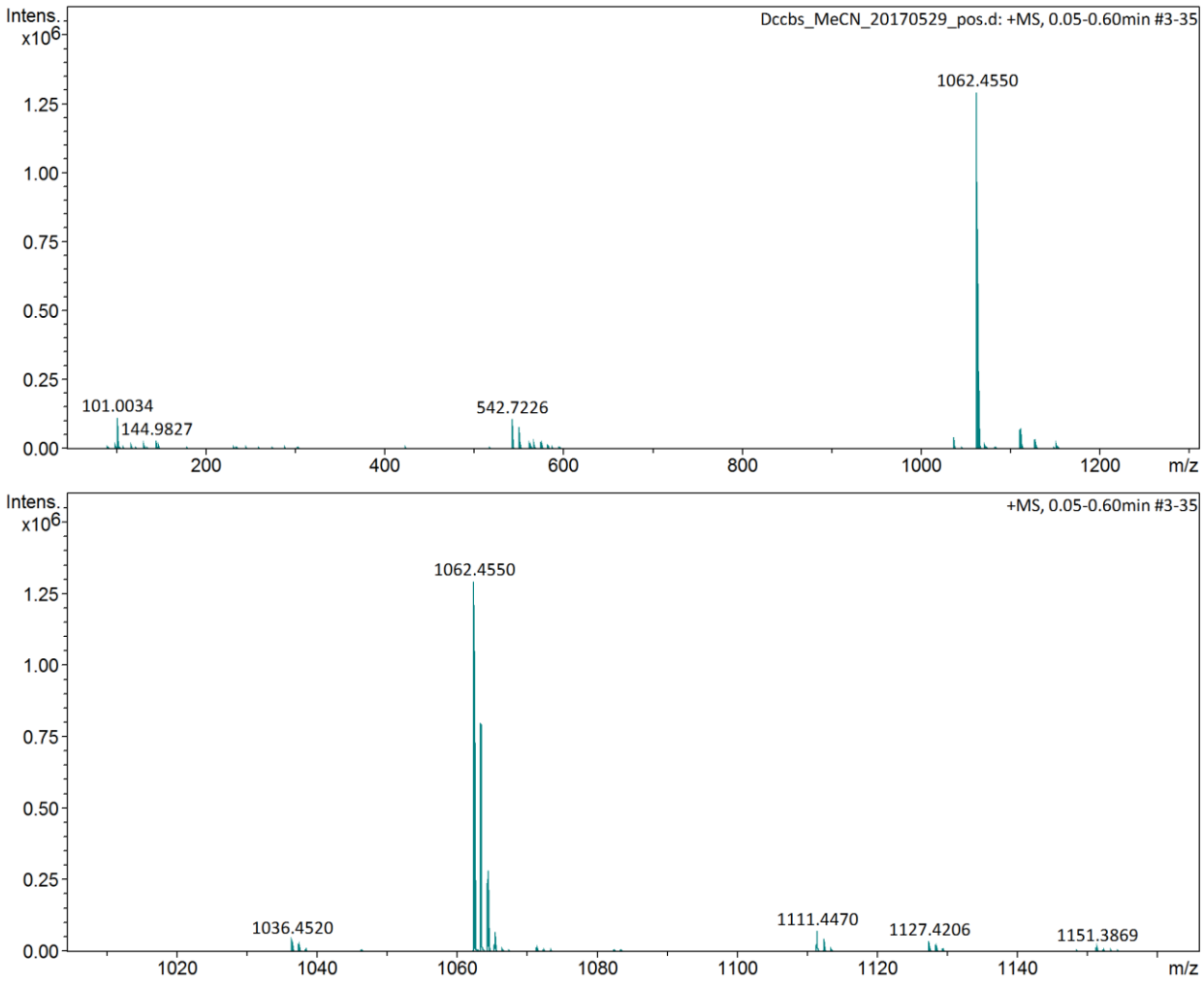

Figure D.1 The positive mode ESI-MS spectrum of [DCCbs].

APPENDIX D.2

ESI-MS DATA FOR $[ACCbs]^+$

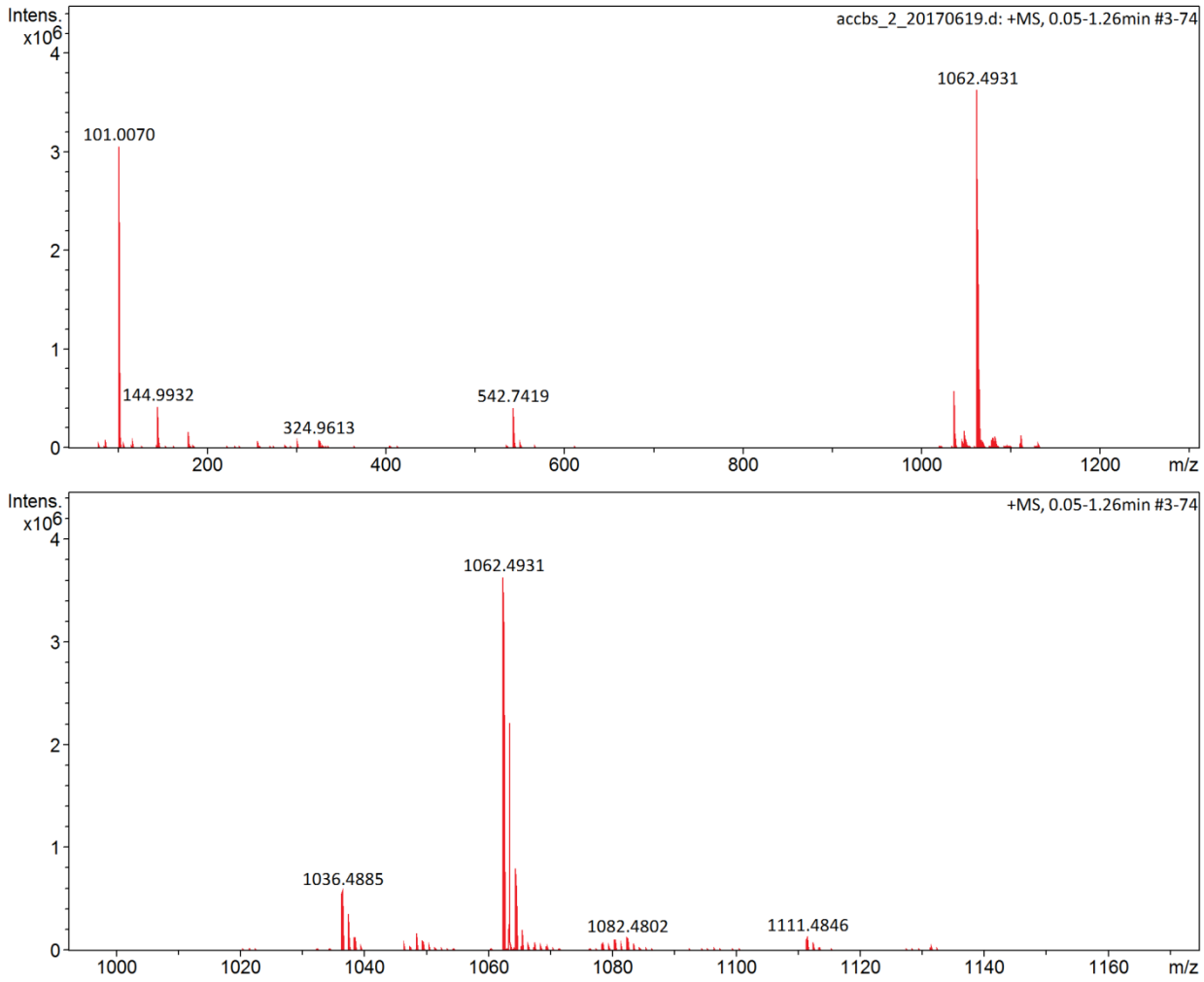

Figure D.2 The positive mode ESI-MS spectrum of $[ACCbs]^+$.

APPENDIX D.3

ESI-MS DATA FOR [DC-5-Seco-Cbs]

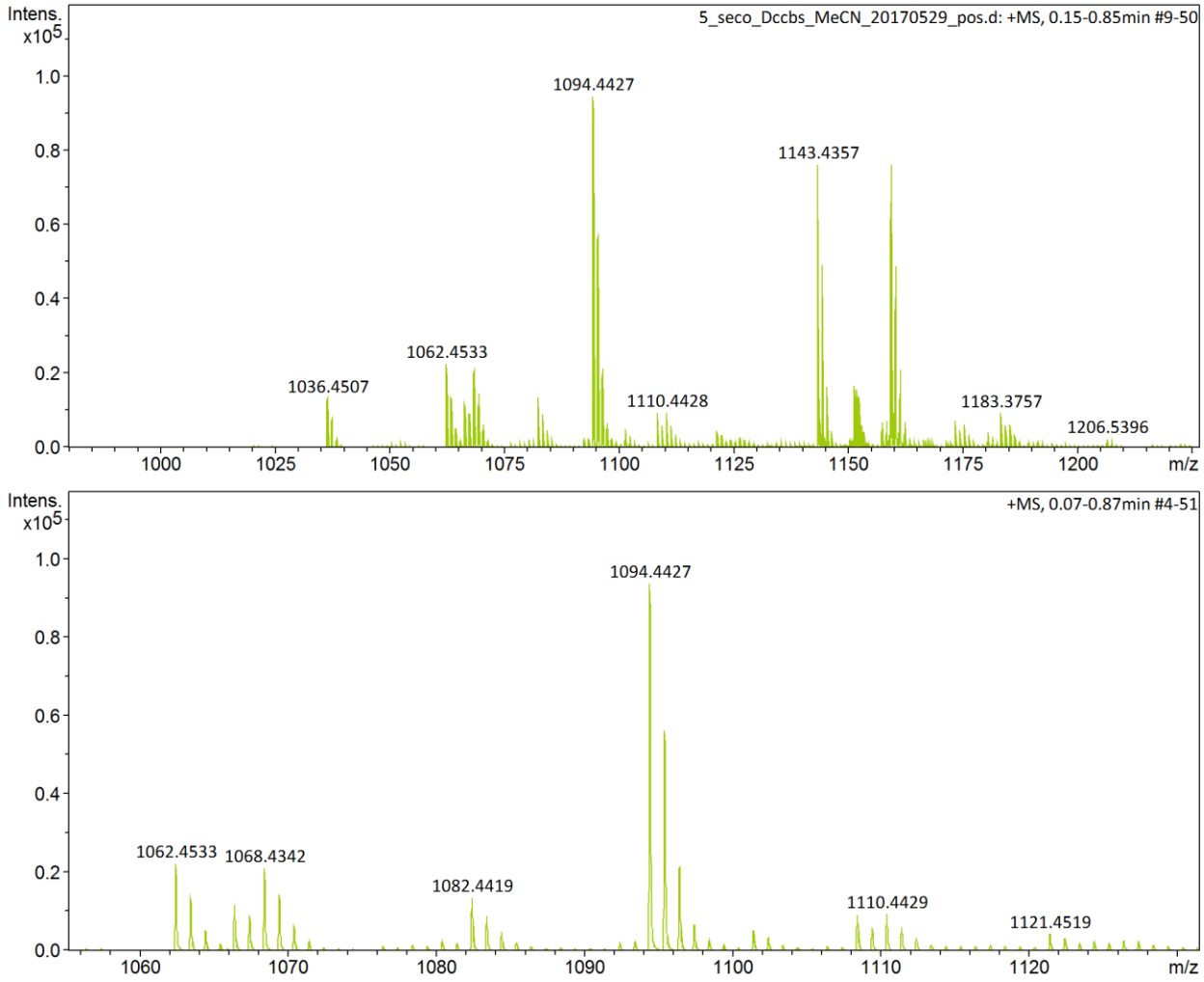

Figure D.3 The positive mode ESI-MS spectrum of [DC-5-seco-Cbs].

APPENDIX D.4

ESI-MS DATA FOR [AC-5-Seco-Cbs]$^{+}$

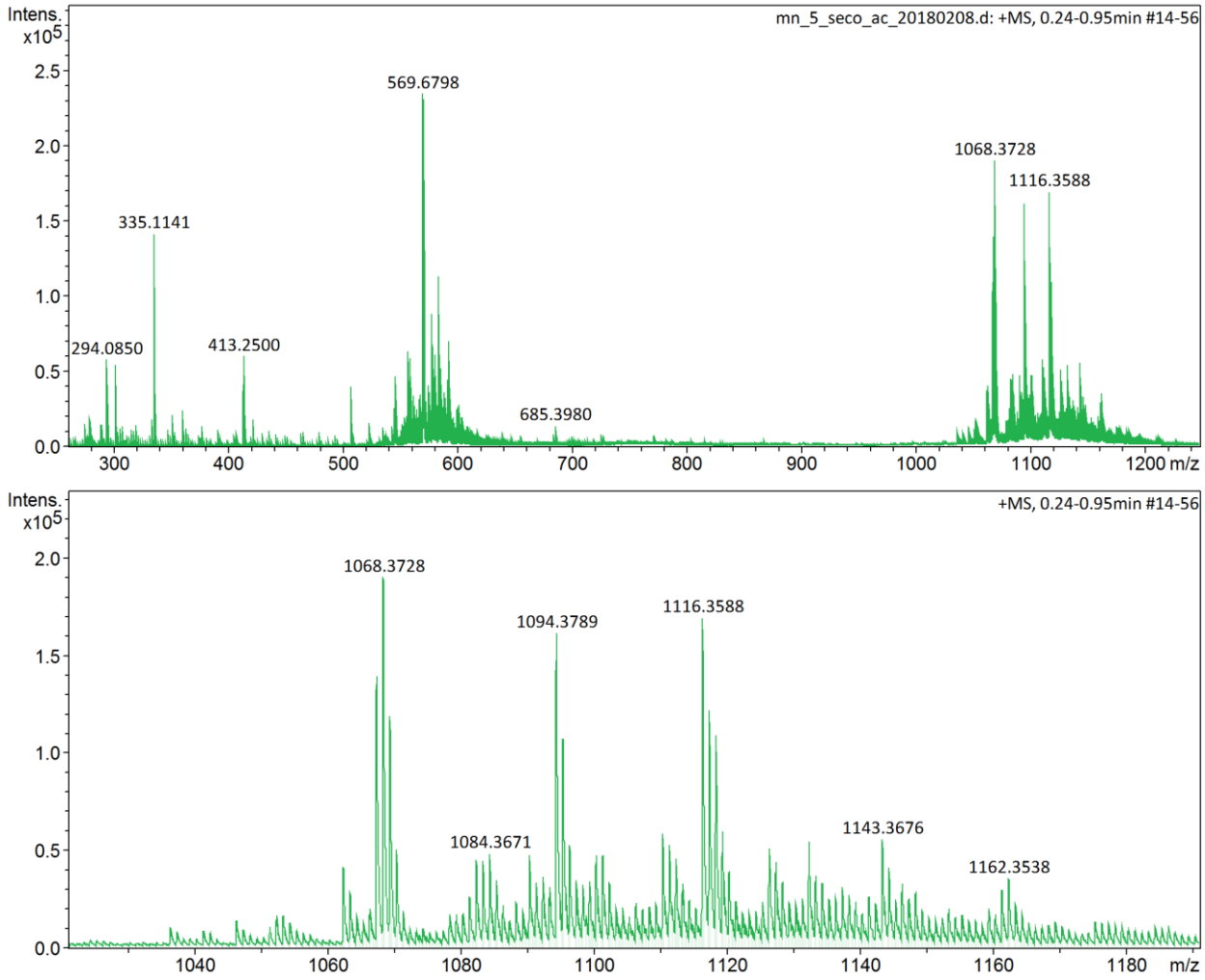

Figure D.4 The positive mode ESI-MS spectrum of [AC-5-seco-Cbs]$^{+}$.

APPENDIX E.1

FTIR SPECTRUM DATA FOR [DCCbs]

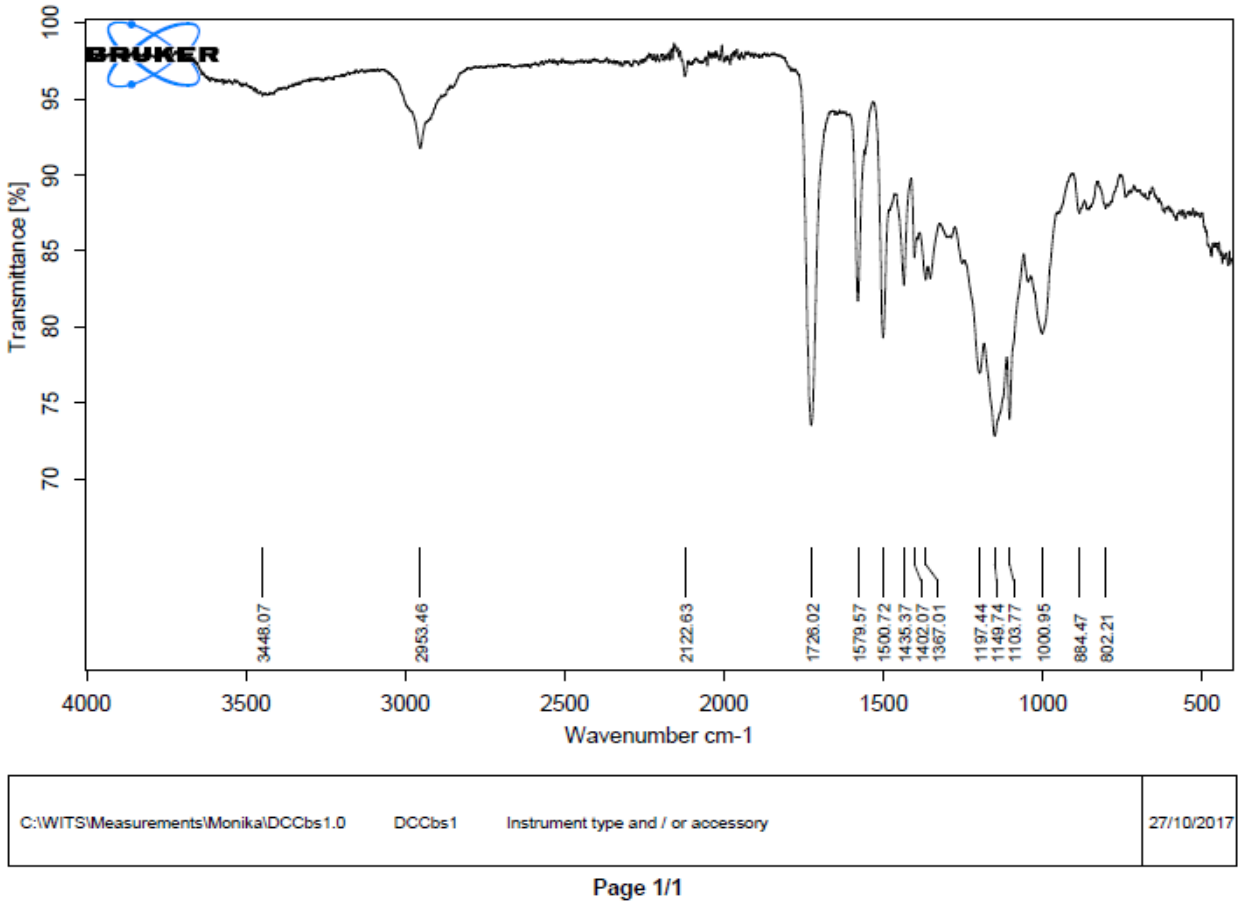

Figure E.1 FTIR spectrum of [DCCbs].

APPENDIX E.2

FTIR SPECTRUM DATA FOR $[ACCbs]^+$

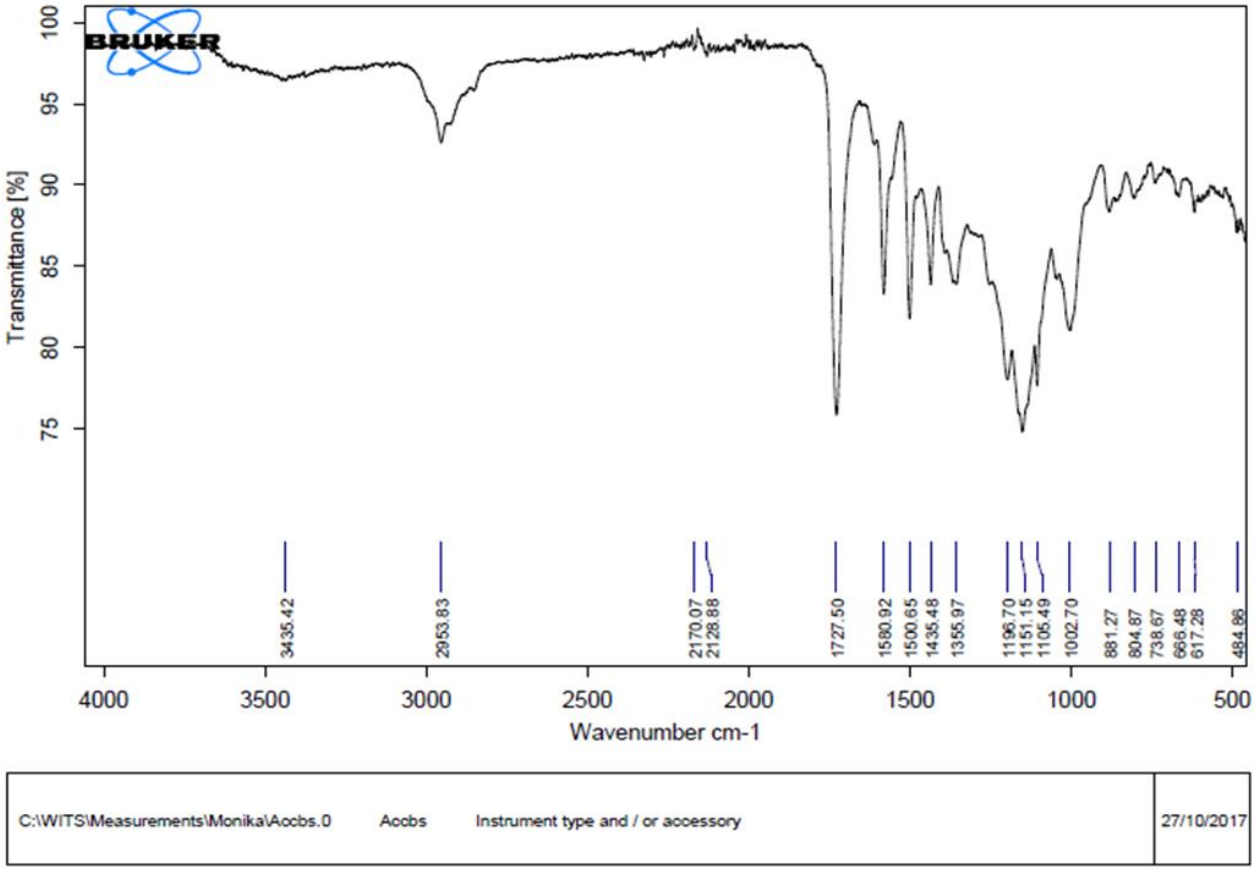

Figure E.2 FTIR spectrum of $[ACCbs]^+$.

APPENDIX E.3

FTIR SPECTRUM DATA FOR [DC-5-Seco-Cbs]

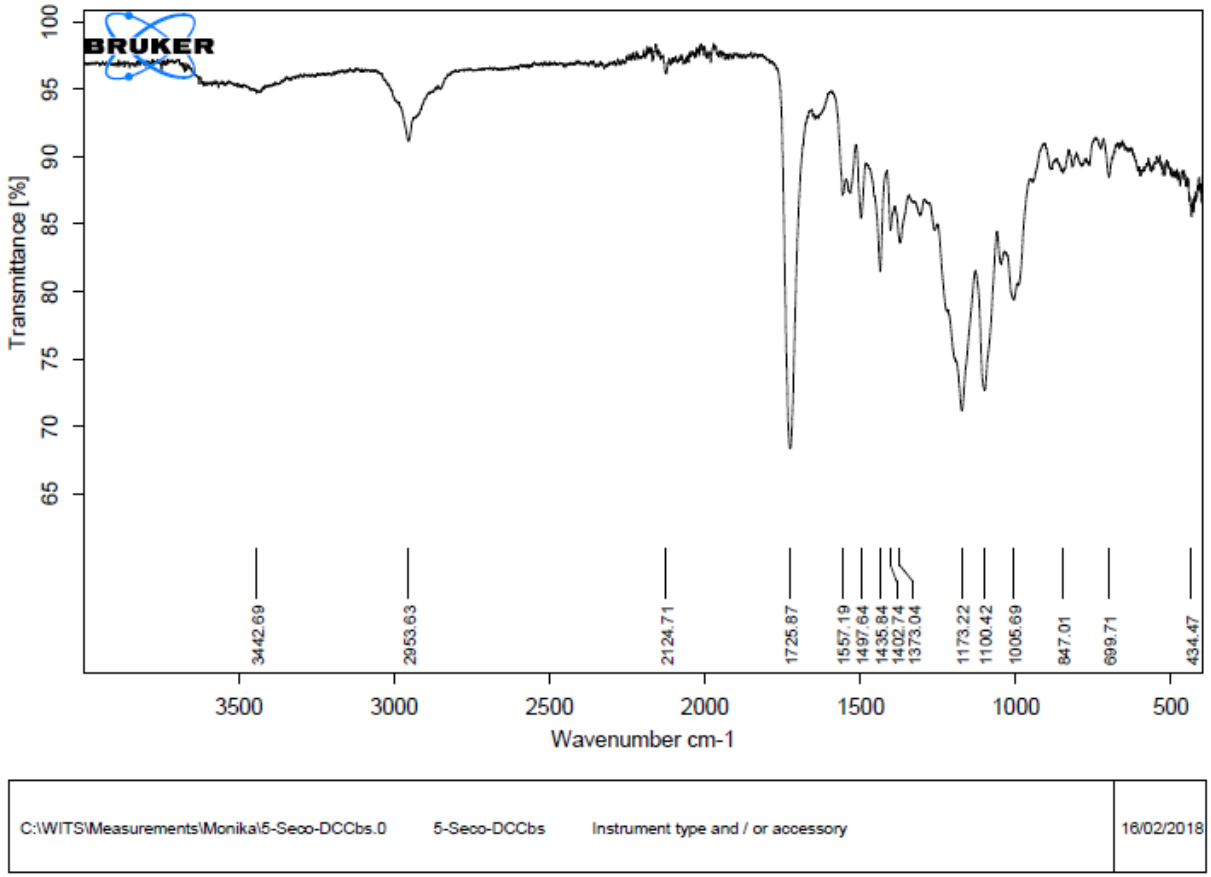

Figure E.3 FTIR spectrum of [DC-5-Seco-Cbs].

Table E.1 Interpretation of the IR spectrum of [DC-5-Seco-Cbs].

Wavenumber /cm^{-1}	**Assignment**
3442.69	O-H stretch; water of crystallisation
2953.63	C-H stretch: aliphatic
2124.71	C≡N stretch
1725.87	C=O stretch: ester
1557.19	C-C stretch: aromatic
1497.64	C-C stretch: aromatic
1435.84	C-H bend: -$COOCH_3$
1402.74	
1373.04	C-H bend: $COOCH_3$/ C-O stretch: ester
1173.22	C-O stretch
1100.42	
1005.69	
847.01	
699.71	
434.47	

APPENDIX E.4

FTIR SPECTRUM DATA FOR [AC-5-Seco-Cbs]$^{+}$

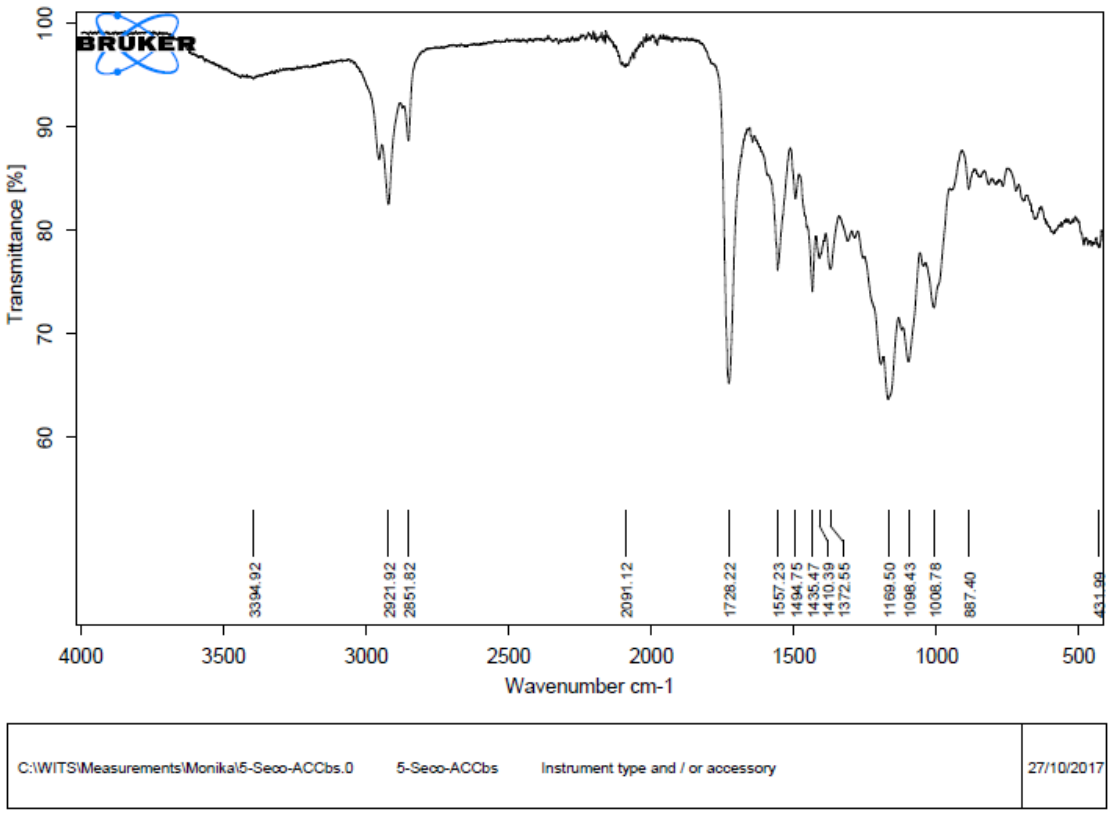

Figure E.4 FTIR spectrum of [AC-5-Seco-Cbs]$^{+}$.

Table E.2 Interpretation of the IR spectrum of $[AC\text{-}5\text{-}Seco\text{-}Cbs]^+$.

Wavenumber /cm^{-1}	Assignment
3394.92	O-H stretch; water of crystallisation
2921.93	C-H stretch: aliphatic
2851.82	C-H stretch: aliphatic
2091.12	C≡N stretch
1728.22	C=O stretch: ester
1557.23	C-C stretch: aromatic
1494.75	C-C stretch: aromatic
1435.47	C-H bend: $-COOCH_3$
1410.39	
1372.55	C-H bend: $-COOCH_3$/ C=O stretch: ester
1169.50	
1098.43	
1008.78	
887.49	
431.95	

APPENDIX F

NMR SPECTROSCOPIC DATA FOR [DC-5-seco-Cbs]

Table F.1 ^{1}H and ^{13}C NMR assignments for [DC-5-seco-Cbs].

Assignment	δ ^{13}C /ppm	δ ^{1}H /ppm	Assignment	δ ^{13}C /ppm	δ ^{1}H /ppm
C53	14.62	2.18	C37	40.06	2.59
C25	16.44	1.24	C37	40.06	2.72
C54	17.49	1.18	C18	40.68	2.91
C36	18.43	0.86	C31	42.11	2.32
C47	18.70	1.20	C31	42.11	
C20	19.06	1.80	C2	47.32	
C41	22.22	1.90	C12	48.39	
C41	22.22		C7	48.54	
C30	24.46	2.01	OCH_3	51.01	3.48
C30	24.46		OCH_3	51.13	
C48	25.15	1.55	C8	51.14	3.27
C48	25.15	1.89	OCH_3	51.30	
C46	27.24	1.07	OCH_3	51.33	3.60
C35	29.06	2.52	OCH_3	51.54	
C56	29.90	2.28	OCH_3	51.81	3.67
C56	29.90	2.62	OCH_3	51.83	
C49	30.10	2.42	C13	53.84	2.99
C60	31.17	2.58	C17	58.81	
C60	31.17	2.71	C3	59.33	3.51
C26	31.96	2.30	C19	75.09	3.70
C26	31.96		C1	87.67	
C55	32.84	1.72	C10	94.04	5.62
C55	32.84	2.38	C15	108.32	
C42	33.17	2.51	Axial CN	131.79	
C42	33.17	2.59	Axial CN	135.43	

Table F.1 *(continued)*

Assignment	δ ^{13}C /ppm	δ ^{1}H /ppm	Assignment	δ ^{13}C /ppm	δ ^{1}H /ppm
C14	161.83		C50	174.09	
C38	171.62		C16	177.28	
C61	172.27		C9	179.19	
C57	172.54		C11	182.03	
C27, C32 or C43	173.48		C6	187.81	
C27, C32 or C43	173.52		C4	188.01	
C27, C32 or C43	173.92		C5	196.9	

Table F.2 Comparison of the ^{13}C NMR resonances of [DC-5-seco-Cbs], [DCCbs] and [DCSYCbs].

	[DC-5-seco-Cbs]	[DCCbs]	[DCSYCbs]
Assignment	**δ ^{13}C /ppm**	**δ ^{13}C /ppm**	**δ ^{13}C /ppm**
C53	14.62	15.75	14.96
C25	16.44	17.39	16.05
C54	17.49	18.36	18.43
C36	18.43	19.81	17.32
C47	18.70	19.81	20.06
C20	19.06	22.71	21.75
C41	22.22	27.34	22.29
C30	24.46	25.79	22.88
C48	25.15	26.74	25.75
C46	27.24	31.29	30.71
C35	29.06	16.17	23.55
C56	29.90	30.63	29.71
C49	30.10	31.78	31.04
C60	31.17	32.25	31.85
C26	31.96	42.38	40.55
C55	32.84	33.32	32.87
C42	33.17	32.03	32.47
C37	40.06	43.19	45.35
C18	40.68	40.64	39.88
C31	42.11	34.37	31.70
C2	47.32	47.21	45.48
C12	48.39	48.04	46.69
C7	48.54	49.95	50.69
OCH_3	51.01	52.10	51.68
OCH_3	51.13	52.10	51.83
C8	51.14	55.62	55.91
OCH_3	51.30	52.30	51.91
OCH_3	51.30	52.30	51.91

Table F.2 *(continued)*

	[DC-5-seco-Cbs]	[DCCbs]	[DCSYCbs]
Assignment	**δ ^{13}C /ppm**	**δ ^{13}C /ppm**	**δ ^{13}C /ppm**
OCH_3	51.33	52.30	52.09
OCH_3	51.54	52.40	52.41
OCH_3	51.81	52.40	52.68
OCH_3	51.83	52.83	
C13	53.84	54.78	53.47
C17	58.81	59.71	58.44
C3	59.33	57.97	58.58
C19	75.09	76.19	76.00
C1	87.67	83.98	84.80
C10	94.04	92.19	85.54
C15	108.32	103.96	100.74
Axial CN	131.79	133.50	129.10
Axial CN	135.43	134.00	134.30
C14	161.83	164.63	164.60
C38	171.62	172.26	171.98
C61	172.27	173.62	172.61
C57	172.54	174.31	173.00
C27, C32 or C43	173.48	173.22	172.14
C27, C32 or C43	173.52	174.39	172.61
C27, C32 or C43	173.92	174.94	172.81
C50	174.09	175.28	174.07
C16	177.28	177.65	174.32
C9	179.19	173.15	176.82
C11	182.03	177.97	175.64
C6	187.81	164.83	111.97
C4	188.01	177.48	191.19
C5	196.89	105.46	79.04

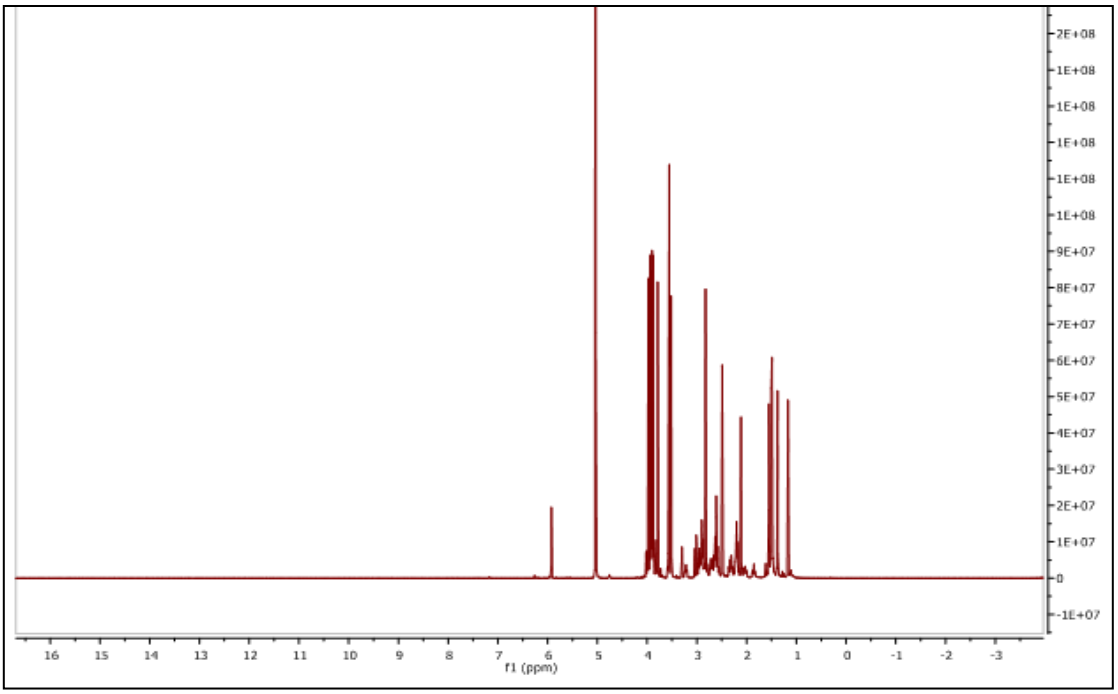

Figure F.1 ^{1}H NMR spectrum of [DC-5-seco-Cbs].

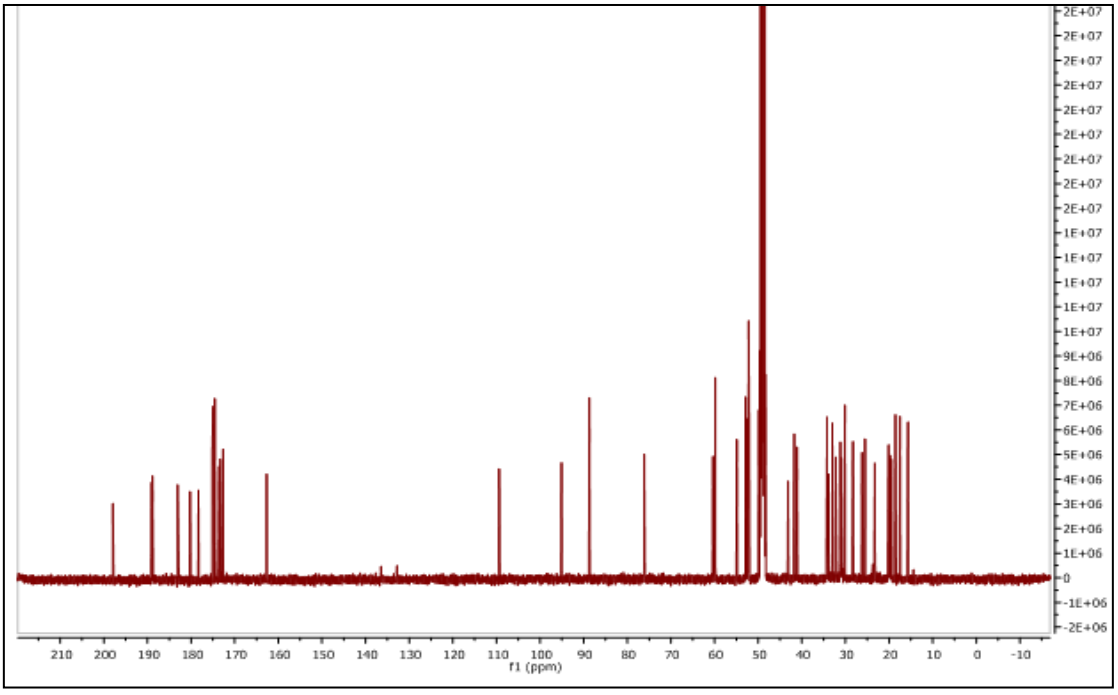

Figure F.2 ^{13}C NMR spectrum of [DC-5-seco-Cbs].

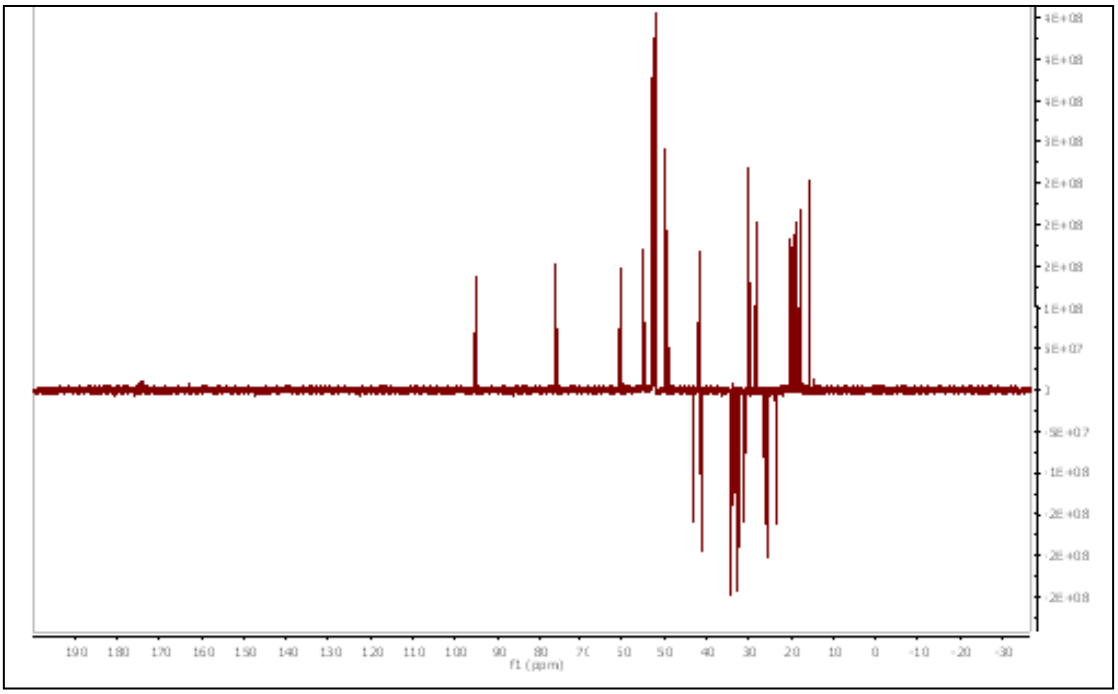

Figure F.3 Dept 135 spectrum of [DC-5-seco-Cbs].

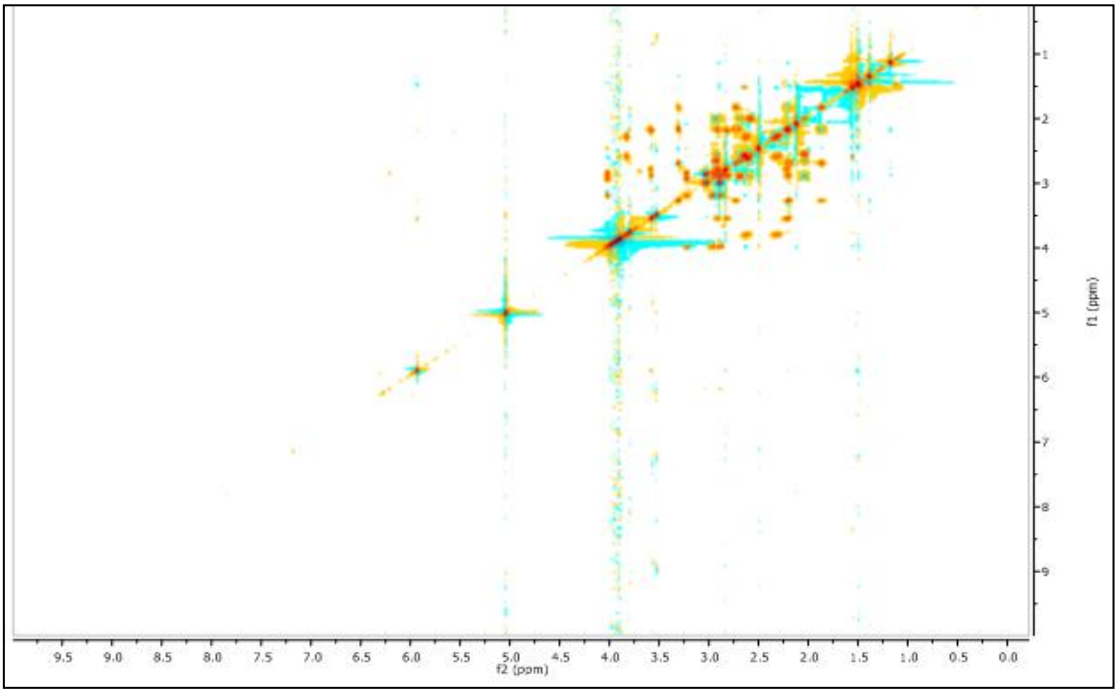

Figure F.4 TOCSY spectrum of [DC-5-seco-Cbs].

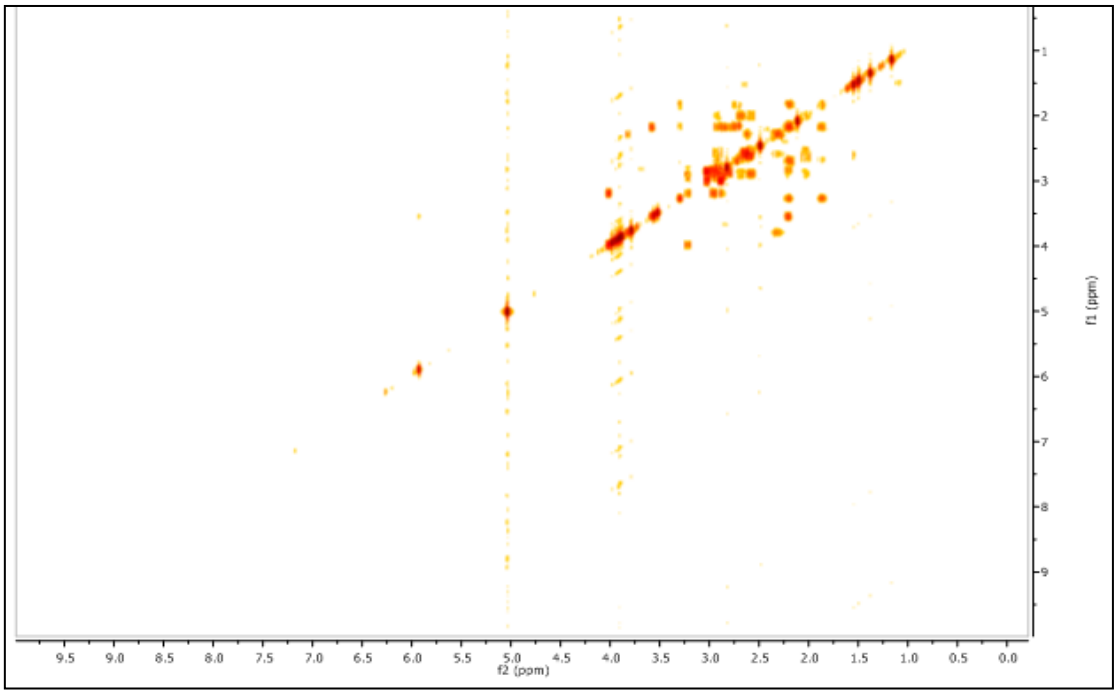

Figure F.5 COSY spectrum of [DC-5-seco-Cbs].

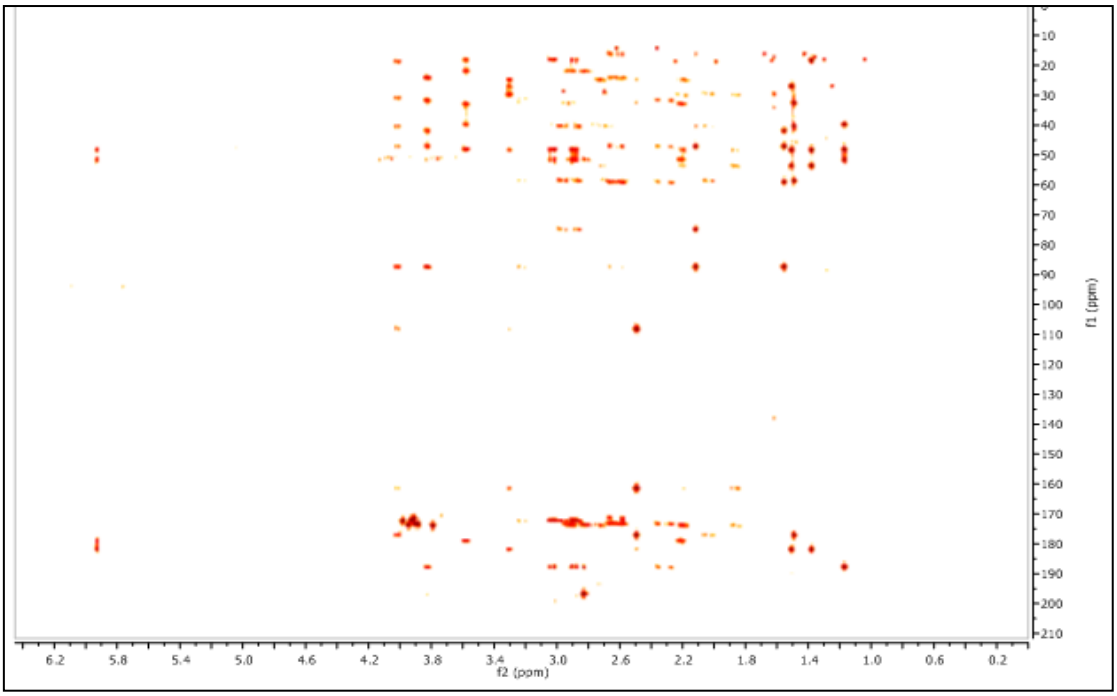

Figure F.6 HMBC spectrum of [DC-5-seco-Cbs].

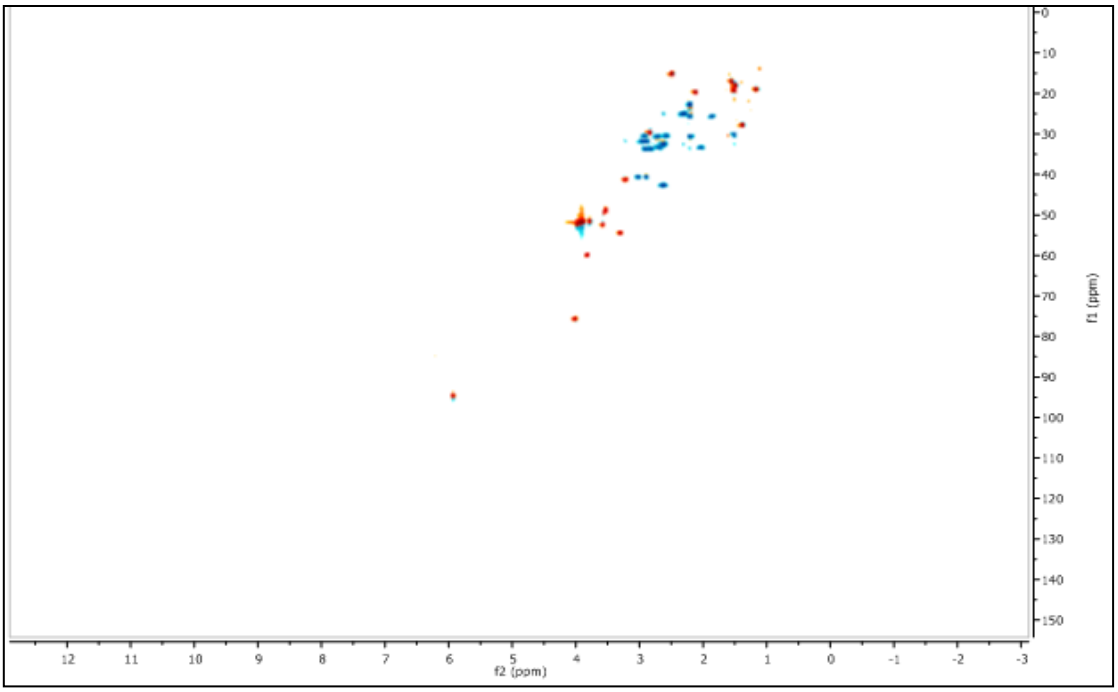

Figure F.7 HSQC spectrum of [DC-5-seco-Cbs].

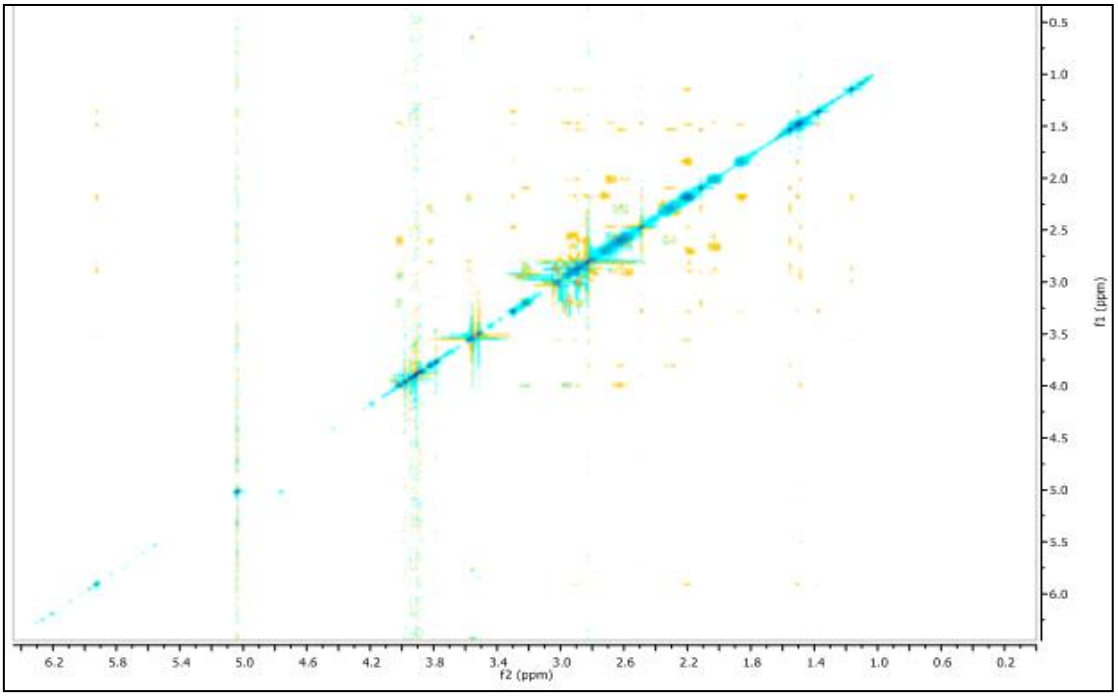

Figure F.8 ROESY spectrum of [DC-5-seco-Cbs].

APPENDIX G

DETERMINATION OF ACID DISSOCIATION CONSTANTS

The change in absorbance of $[AC\text{-}5\text{-}seco\text{-}Cbs]^+$ and $[ACCbs]^+$ in an aqueous multi-component buffer as a result of an increase in pH is illustrated in Figure G.1 and Figure G.3, respectively. The experimental data for pK_a titrations can be found on the accompanying CD. The transposed data used for the determination of the acid dissociation constant and the weighted pK_a values can be found in Table G.1, Table G.2, Table G.3 and Table G.4. pK_a values were determined by fitting the experimental data using non-linear least-squares methods employing a Newton-Raphson procedure to an ionisation isotherm (Equation 2.1, Chapter 2.4.2). The ionisation isotherms are shown in Figure G.2 and Figure G.4.

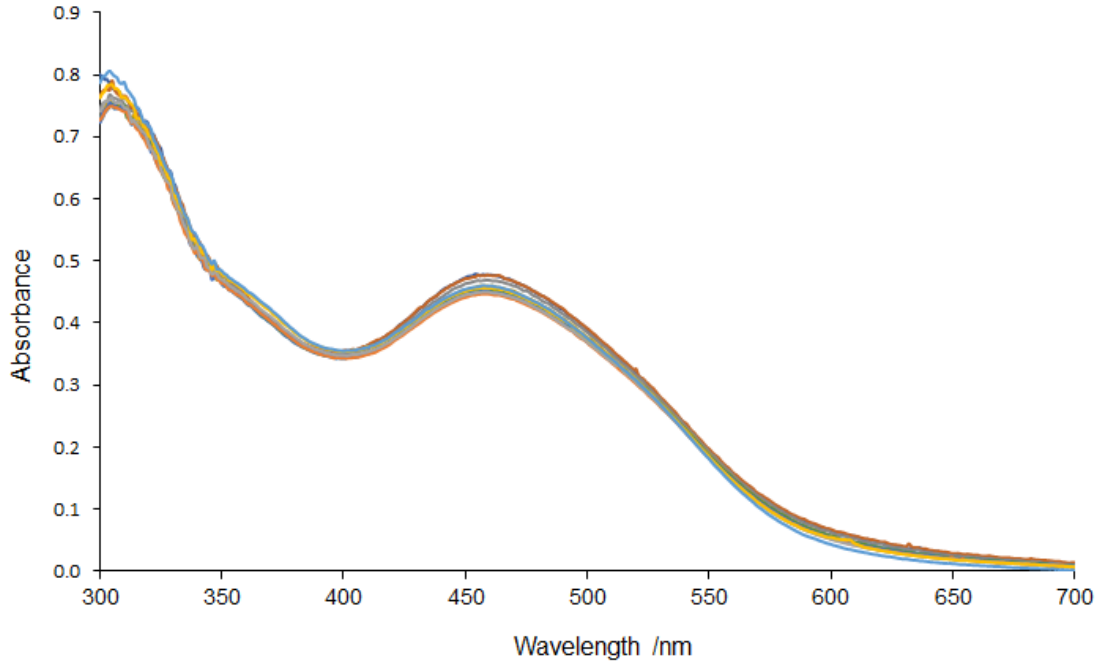

Figure G.1 The effects of pH on the absorbance spectrum of $[AC\text{-}5\text{-}seco\text{-}Cbs]^+$ ranging from pH 5.65 to pH 10.87 at 25.0 ^{o}C in an aqueous solution.

Table G.1 Transposed data for the determination of the pK_a of [AC-5-seco-Cbs]$^+$ at specific wavelengths.

	Absorbance at wavelength /nm										
pH	**470**	**469**	**468**	**467**	**466**	**465**	**464**	**463**	**462**	**461**	**460**
5.65	0.466603	0.46848	0.47089	0.470978	0.471748	0.4737	0.474738	0.475902	0.476942	0.476949	0.477074
6.19	0.467476	0.468188	0.469635	0.470576	0.471937	0.47449	0.47656	0.476375	0.475986	0.476369	0.476435
6.79	0.459406	0.460999	0.46261	0.463488	0.464785	0.466133	0.466587	0.467627	0.468081	0.467891	0.468784
7.37	0.4515	0.452437	0.452377	0.45354	0.455299	0.455892	0.45701	0.457215	0.458735	0.459776	0.459164
7.81	0.446508	0.447243	0.448413	0.449475	0.451196	0.451552	0.452191	0.453079	0.453755	0.455288	0.454442
8.28	0.444765	0.445793	0.446979	0.447869	0.449346	0.450371	0.45126	0.45151	0.452123	0.453355	0.454159
8.68	0.44158	0.442433	0.443735	0.445015	0.446437	0.447188	0.447748	0.44848	0.448154	0.449479	0.449992
9.14	0.438412	0.438796	0.440109	0.441425	0.442824	0.443751	0.444728	0.444586	0.444867	0.445829	0.446462
9.72	0.440587	0.441569	0.443281	0.443804	0.445103	0.446279	0.44693	0.44783	0.448094	0.448578	0.449617
10.34	0.447776	0.448356	0.450042	0.450996	0.453413	0.453312	0.454375	0.45488	0.454949	0.456157	0.456442

Table G.1 *(continued)*

	Absorbance at wavelength /nm										
pH	**590**	**589**	**588**	**587**	**586**	**585**	**584**	**583**	**582**	**581**	**580**
5.65	0.078601	0.08192	0.08285	0.084051	0.085943	0.088149	0.089544	0.092846	0.094609	0.096735	0.098271
6.19	0.081828	0.084193	0.084833	0.086241	0.088381	0.090361	0.091548	0.093886	0.096841	0.098998	0.10074
6.79	0.076112	0.077869	0.079774	0.081567	0.082925	0.085988	0.087799	0.089276	0.09114	0.093191	0.096719
7.37	0.070436	0.072588	0.073189	0.075652	0.077534	0.079882	0.081247	0.083657	0.086435	0.089436	0.090819
7.81	0.070697	0.072568	0.074739	0.075626	0.077385	0.079527	0.081599	0.083836	0.085634	0.087848	0.090546
8.28	0.070386	0.072498	0.07413	0.075554	0.077315	0.080046	0.081972	0.084157	0.086659	0.089174	0.09094
8.68	0.067582	0.069257	0.071258	0.073762	0.075143	0.076854	0.079278	0.081188	0.08311	0.085548	0.087868
9.14	0.065968	0.067605	0.069419	0.072097	0.07347	0.074988	0.077327	0.078894	0.081175	0.083954	0.08561
9.72	0.065144	0.067598	0.068913	0.070717	0.072528	0.075132	0.076567	0.078815	0.081042	0.082839	0.085181
10.34	0.06643	0.067532	0.068916	0.070842	0.073557	0.075144	0.076176	0.078865	0.08084	0.082648	0.085032

Table G.2 The weighted pK_a values and associated errors at the monitored wavelengths.

Wavelength /nm	p*K*a	Error	K_a
460	7.0183	0.0014	9.58738E-08
461	7.0191	0.0014	9.56974E-08
462	7.023	0.0013	9.48418E-08
463	7.0287	0.0014	9.36052E-08
464	7.0367	0.0014	9.18967E-08
465	7.0525	0.0013	8.86135E-08
466	7.0627	0.0014	8.65566E-08
467	7.0719	0.0014	8.47423E-08
468	7.0729	0.0015	8.45474E-08
469	7.1062	0.0013	7.83069E-08
470	7.1087	0.0013	7.78574E-08
580	7.1209	0.0008	7.57007E-08
581	7.121	0.0009	7.56833E-08
582	7.1445	0.0009	7.16968E-08
583	7.1592	0.0008	6.93107E-08
584	7.1658	0.0008	6.82653E-08
585	7.1875	0.0009	6.49382E-08
586	7.1949	0.0009	6.3841E-08
587	7.2193	0.0008	6.03532E-08
588	7.2516	0.0009	5.60273E-08
589	7.2947	0.001	5.07341E-08
590	7.3663	0.001	4.30229E-08
	pK_a	**7.12**	
	Error	**0.08**	

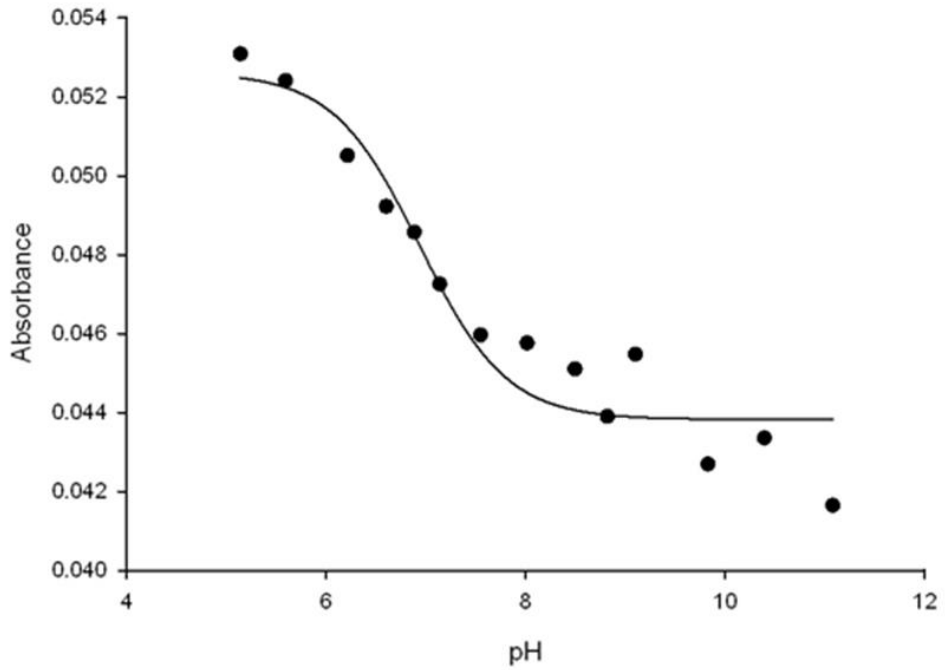

Figure G.2 A plot of the change in absorbance on adding a negligible volume of NaOH to a solution of $[AC\text{-}5\text{-}seco\text{-}Cbs]^+$ at 586 nm, to which a single acid dissociation constant equation has been fitted. The solid circles indicate the experimentally determined absorbance values. The solid line indicates the best fit curve.

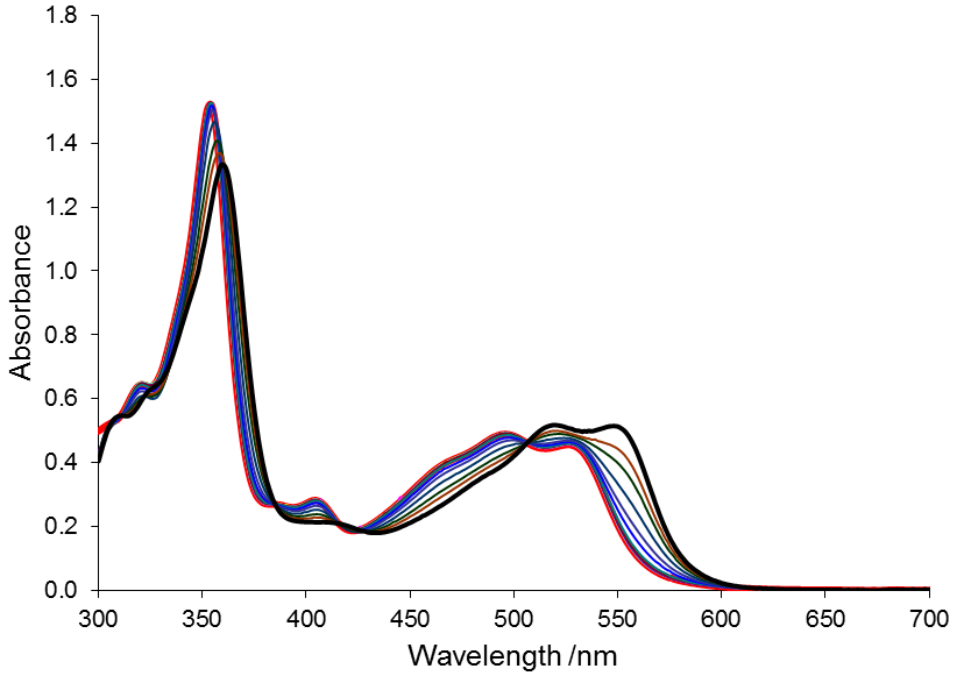

Figure G.3 The effects of pH on the absorbance spectrum of $[ACCbs]^+$ ranging from pH 5.75 to pH 12.64 at 25.0 ^{o}C in an aqueous solution.

Table G.3 Transposed data for the determination of the pK_a of $[ACCbs]^+$ at specific wavelengths.

	Absorbance at wavelength /nm										
pH	**355**	**354**	**353**	**352**	**351**	**350**	**349**	**348**	**347**	**346**	**345**
5.75	1.747389	1.768814	1.767967	1.740288	1.702448	1.648837	1.590008	1.477546	1.420383	1.35866	1.297133
6.19	1.741728	1.764029	1.762007	1.746732	1.703947	1.647629	1.587081	1.488668	1.412731	1.364419	1.291792
6.76	1.740923	1.760117	1.759838	1.732169	1.695071	1.642508	1.581344	1.475749	1.408617	1.34604	1.283377
7.3	1.725224	1.746499	1.747097	1.723451	1.684411	1.640024	1.57914	1.488671	1.428123	1.350319	1.288037
7.86	1.719117	1.737652	1.737015	1.71561	1.679924	1.630844	1.567416	1.458985	1.398137	1.329039	1.280179
8.39	1.70224	1.723224	1.724884	1.699626	1.668033	1.613279	1.556017	1.446882	1.380201	1.332375	1.268057
9.08	1.672806	1.690964	1.692302	1.674057	1.63117	1.592159	1.528632	1.420996	1.367286	1.303741	1.243395
9.64	1.638133	1.655031	1.655054	1.632203	1.589961	1.541399	1.487558	1.391381	1.33549	1.268581	1.216828
10.27	1.579265	1.589645	1.58395	1.557549	1.519113	1.471188	1.421613	1.342685	1.282232	1.229815	1.171833
10.71	1.531876	1.531502	1.519359	1.491382	1.453531	1.408041	1.359828	1.287153	1.229672	1.175362	1.131647
11.29	1.498953	1.485534	1.469639	1.438075	1.398225	1.355515	1.308152	1.233842	1.199258	1.142902	1.108305

Table G.3 *(continued)*

	Absorbance at wavelength /nm										
pH	**470**	**469**	**468**	**467**	**466**	**465**	**464**	**463**	**462**	**461**	**460**
5.75	0.474291	0.471171	0.468024	0.464347	0.460626	0.456666	0.452433	0.44758	0.442331	0.436912	0.431199
6.19	0.472786	0.469702	0.466527	0.462877	0.459134	0.455065	0.450875	0.446037	0.44106	0.435338	0.429589
6.76	0.471011	0.468003	0.464744	0.461148	0.457385	0.453402	0.449177	0.444765	0.439264	0.433529	0.427855
7.3	0.467943	0.464768	0.461572	0.458051	0.454217	0.450205	0.446046	0.441221	0.435916	0.430158	0.424663
7.86	0.46499	0.462029	0.458633	0.454987	0.451377	0.447448	0.443281	0.438377	0.433537	0.427772	0.422049
8.39	0.460802	0.457866	0.454431	0.450932	0.447248	0.443287	0.439239	0.434213	0.429212	0.423799	0.418206
9.08	0.452655	0.449844	0.446389	0.443065	0.439388	0.435325	0.431191	0.426247	0.421334	0.415904	0.410403
9.64	0.441432	0.43863	0.435193	0.431744	0.428178	0.424287	0.420088	0.415303	0.410454	0.405378	0.400074
10.27	0.41937	0.416236	0.412908	0.409327	0.405839	0.402107	0.398001	0.393362	0.388788	0.383797	0.378718
10.71	0.398755	0.395456	0.392022	0.388384	0.384863	0.380724	0.376822	0.372479	0.367984	0.363179	0.3586
11.29	0.380506	0.376896	0.373089	0.369444	0.365516	0.361631	0.357587	0.353255	0.348773	0.344216	0.339729

Table G.3 *(continued)*

	Absorbance at wavelength /nm										
pH	**560**	**559**	**558**	**557**	**556**	**555**	**554**	**553**	**552**	**551**	**550**
5.75	0.130379	0.138932	0.148211	0.15807	0.168542	0.179777	0.191854	0.204519	0.21821	0.231974	0.246553
6.19	0.130514	0.138887	0.148046	0.157816	0.168267	0.179299	0.191472	0.204181	0.217423	0.231307	0.245847
6.76	0.130563	0.13907	0.148233	0.157947	0.168288	0.179298	0.191385	0.20395	0.21719	0.230922	0.245349
7.3	0.130701	0.139174	0.148055	0.157795	0.167916	0.178679	0.190602	0.203153	0.216299	0.229952	0.24417
7.86	0.130705	0.139132	0.148122	0.157588	0.167817	0.178632	0.190419	0.202691	0.215662	0.229343	0.243439
8.39	0.131363	0.139801	0.148417	0.158079	0.167971	0.178746	0.190278	0.20268	0.21545	0.228849	0.242925
9.08	0.136012	0.144265	0.153103	0.162367	0.172431	0.183056	0.194655	0.206204	0.218804	0.231719	0.245078
9.64	0.148859	0.157178	0.165982	0.175387	0.185147	0.195332	0.206349	0.217825	0.229778	0.242143	0.254898
10.27	0.191887	0.201194	0.210639	0.220197	0.2299	0.239686	0.250357	0.260708	0.271418	0.282306	0.293293
10.71	0.241841	0.252371	0.262705	0.272794	0.28281	0.292345	0.302276	0.312075	0.3215	0.330724	0.339928
11.29	0.295769	0.307601	0.319214	0.33172	0.340866	0.350706	0.360361	0.369526	0.378033	0.386006	0.393368

Table G.4 The weighted pK_a values and associated errors at the monitored wavelengths.

Wavelength /nm	pK_a	Error	K_a
345	9.7957	0.0136	1.60066E-10
346	9.8503	0.0094	1.41156E-10
347	9.925	0.0169	1.1885E-10
348	9.9378	0.0145	1.15398E-10
349	9.9679	0.0146	1.07671E-10
350	9.9952	0.0172	1.01111E-10
351	10.009	0.0167	9.7949E-11
352	10.0228	0.0139	9.48855E-11
353	10.0349	0.0173	9.22784E-11
354	10.0406	0.0148	9.10752E-11
355	10.0461	0.0196	8.9929E-11
460	10.0996	0.0058	7.9506E-11
461	10.1125	0.0058	7.71792E-11
462	10.1159	0.0059	7.65773E-11
463	10.1208	0.0059	7.57182E-11
464	10.1294	0.006	7.42335E-11
465	10.1312	0.0059	7.39265E-11
466	10.1343	0.0059	7.34007E-11
467	10.1349	0.0059	7.32993E-11
468	10.1356	0.0059	7.31813E-11
469	10.1395	0.0058	7.2527E-11
470	10.1406	0.0059	7.23436E-11
550	10.6216	0.0007	2.39001E-11
551	10.6269	0.001	2.36102E-11
552	10.6341	0.0012	2.3222E-11

Table G.4 *(continued)*

553	10.6507	0.0018	2.23512E-11
554	10.6513	0.0013	2.23203E-11
554	10.6611	0.0022	2.18223E-11
556	10.6687	0.0026	2.14437E-11
557	10.6804	0.0032	2.08737E-11
558	10.6927	0.0038	2.02908E-11
559	10.7058	0.0044	1.96879E-11
560	10.7202	0.0051	1.90458E-11

pK_a	**10.16**
Error	**0.20**

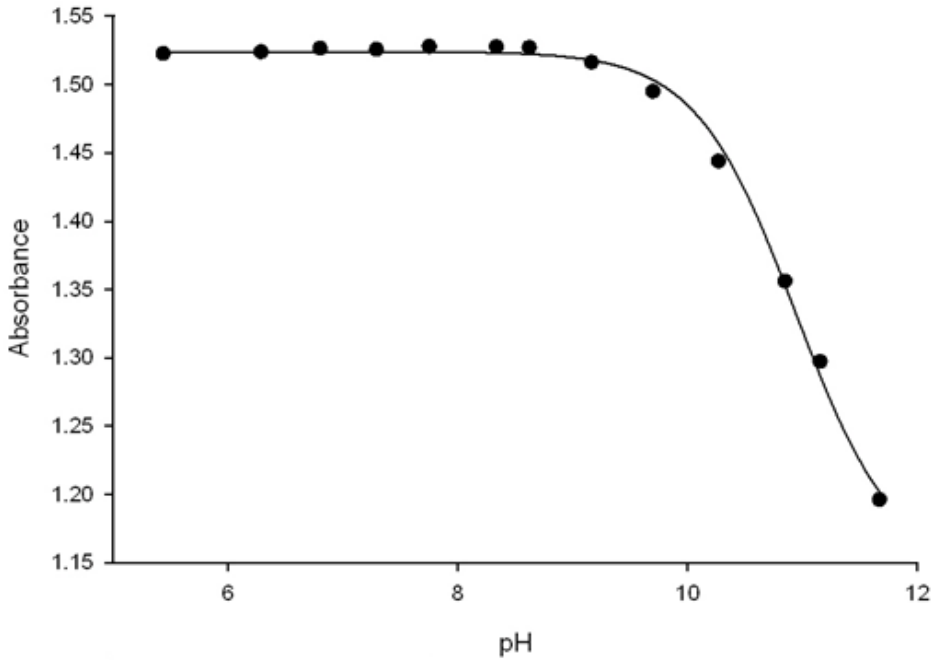

Figure G.4 A plot of the change in absorbance of $[ACCbs]^+$ at 354 nm to which a single acid dissociation constant equation has been fitted. The solid circles indicate the experimentally determined absorbance values. The solid line indicates the best fit curve.

APPENDIX H

DETERMINATION OF EQUILIBRIUM CONSTANTS

The change in absorbance of $[AC\text{-}5\text{-}seco\text{-}Cbs]^+$ associated with the coordination of exogenous ligands is illustrated in Figure H.1. The experimental data for all ligand titrations can be found on the accompanying CD. The transposed data used for the determination of the binding constants can be found in Table H.1 and Table H.2. The binding constants were determined by fitting the data to Equation 2.3 when $K < 4$ (as in this case) or Equation 2.5 when $K > 4$. The final binding constants were then determined from the sum of the weighted K_{obs} values experimentally obtained for each wavelength. pH-independent binding constants, *K,* were determined using Equation 2.6. The associated errors were calculated as the sum of the weighted relative percentage error reciprocals.

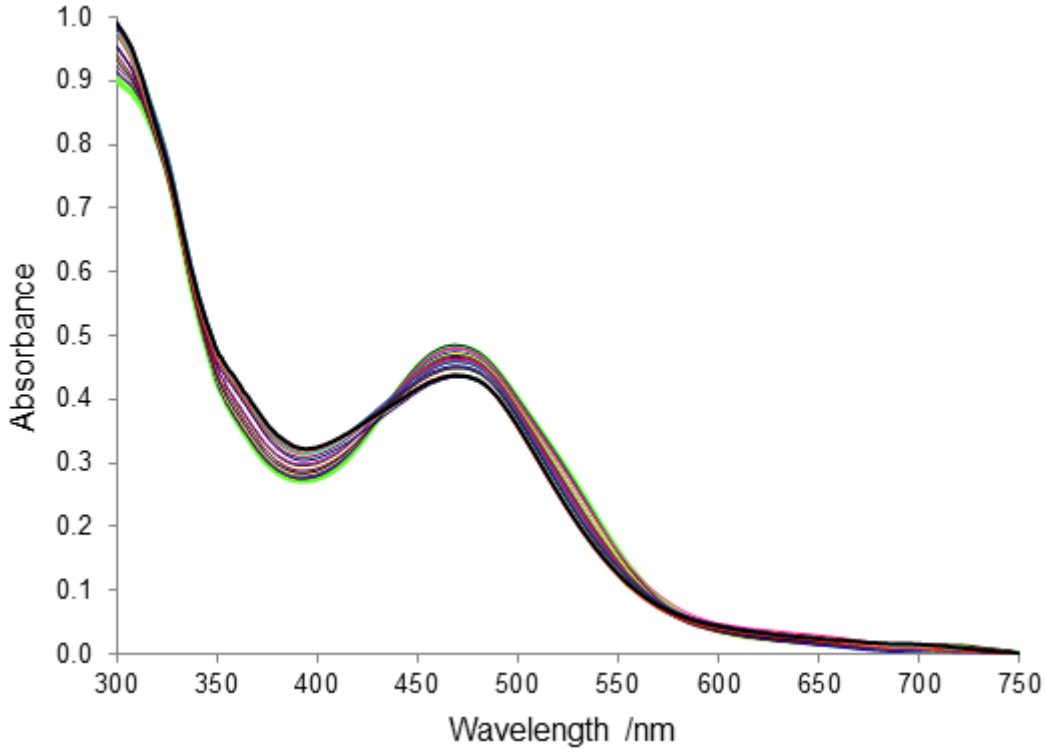

Figure H.1 The electronic absorption spectrum from the coordination of SO_3^{2-} to $[AC\text{-}5\text{-}seco\text{-}Cbs]^+$ (pH 8.86, 25.0 ˚C).

Table H.1 Transposed data for the determination of the equilibriu constant from the coordination of SO_3^{2-} to $[AC\text{-}5\text{-}seco\text{-}Cbs]^+$ at specific wavelengths.

	Absorbance at wavelength /nm										
$[SO_3^{2-}]$ /M	**560**	**559**	**558**	**557**	**556**	**555**	**554**	**553**	**552**	**551**	**550**
0	0.127467	0.131135	0.134957	0.13888	0.142752	0.146671	0.150649	0.154543	0.158792	0.163041	0.167533
0.000767	0.122554	0.12623	0.129983	0.133684	0.137593	0.141543	0.145745	0.150189	0.15427	0.158628	0.16286
0.001533	0.119257	0.122912	0.126547	0.130317	0.134272	0.138189	0.142283	0.146303	0.150511	0.155046	0.159504
0.003828	0.11582	0.119359	0.123051	0.126738	0.130677	0.134487	0.138581	0.142587	0.146699	0.150829	0.155235
0.007639	0.115601	0.119186	0.122759	0.126396	0.130329	0.134001	0.138039	0.141949	0.145923	0.15008	0.154394
0.011434	0.114241	0.117844	0.121413	0.125088	0.128829	0.132657	0.136589	0.140407	0.144467	0.148555	0.152856
0.015212	0.112609	0.116023	0.119681	0.123197	0.127052	0.130807	0.134691	0.138587	0.142729	0.146747	0.151059
0.02272	0.114302	0.11789	0.121446	0.125022	0.128747	0.132421	0.136429	0.140243	0.144233	0.148309	0.152496
0.037545	0.114527	0.118181	0.121503	0.125187	0.128943	0.132571	0.136682	0.140368	0.144308	0.148385	0.152604
0.055725	0.113989	0.117412	0.120979	0.12453	0.128276	0.132073	0.135979	0.139789	0.143646	0.147755	0.151996
0.073526	0.115745	0.119213	0.122701	0.12623	0.129932	0.133681	0.13758	0.141323	0.145208	0.14931	0.153395
0.108038	0.112958	0.116296	0.119842	0.123242	0.126861	0.130408	0.134262	0.137918	0.141558	0.145534	0.149634
0.14117	0.110235	0.11347	0.116762	0.120071	0.123591	0.127191	0.130898	0.134455	0.138208	0.141869	0.146045
0.20361	0.112251	0.115344	0.11859	0.122063	0.125603	0.129087	0.132887	0.136337	0.140039	0.143818	0.147871
0.315111	0.110541	0.113908	0.117002	0.120308	0.123886	0.127409	0.130976	0.134441	0.138236	0.14226	0.146327

Table H.1 *(continued)*

	Absorbance at wavelength /nm									
$[SO_3^{2-}]$ /M	**480**	**479**	**478**	**477**	**476**	**475**	**474**	**473**	**472**	**471**
0	0.427531	0.429468	0.43141	0.43308	0.434868	0.436438	0.438018	0.439552	0.441085	0.442371
0.000767	0.424682	0.426766	0.428737	0.430496	0.432373	0.43393	0.435378	0.436936	0.438309	0.439627
0.001533	0.422623	0.4247	0.426696	0.428482	0.430328	0.432043	0.433551	0.435099	0.436503	0.437936
0.003828	0.417783	0.419577	0.421576	0.423497	0.425334	0.426951	0.42842	0.429976	0.431373	0.432575
0.007639	0.414476	0.41631	0.41826	0.419962	0.421805	0.423437	0.424909	0.42667	0.427903	0.42903
0.011434	0.410898	0.412877	0.414714	0.416641	0.418341	0.419905	0.421353	0.422895	0.424194	0.425443
0.015212	0.408447	0.410143	0.412266	0.413913	0.415731	0.417282	0.418526	0.420172	0.421436	0.422636
0.02272	0.409328	0.411302	0.413148	0.414913	0.416752	0.418355	0.419731	0.421358	0.422714	0.423778
0.037545	0.409357	0.411329	0.413146	0.414909	0.416665	0.418032	0.419507	0.420959	0.422333	0.42347
0.055725	0.407599	0.409409	0.411389	0.412964	0.414614	0.416224	0.417468	0.418943	0.420196	0.421314
0.073526	0.40904	0.410849	0.412707	0.414542	0.416031	0.417576	0.41894	0.42045	0.421586	0.422572
0.108038	0.406715	0.408514	0.410214	0.411774	0.41352	0.41496	0.416234	0.417745	0.41883	0.420028
0.14117	0.401789	0.403431	0.405312	0.406902	0.408612	0.410028	0.411464	0.412789	0.41406	0.415112
0.20361	0.40364	0.4055	0.407349	0.408832	0.410488	0.411876	0.413171	0.414747	0.415645	0.416777
0.315111	0.400299	0.401901	0.40372	0.405223	0.406741	0.408215	0.409477	0.410955	0.412106	0.413144

Table H.1 *(continued)*

	Absorbance at wavelength /nm									
$[SO_3^{2-}]$ /M	**470**	**469**	**468**	**467**	**466**	**465**	**464**	**463**	**462**	**461**
0	0.443711	0.444679	0.445566	0.446566	0.447251	0.448056	0.448632	0.449065	0.449154	0.449651
0.000767	0.440733	0.441689	0.442998	0.44363	0.444438	0.445223	0.445673	0.446302	0.44644	0.446834
0.001533	0.439061	0.440307	0.4413	0.442257	0.443049	0.443828	0.444288	0.444588	0.444819	0.44519
0.003828	0.433792	0.434857	0.435854	0.436789	0.437508	0.438316	0.438974	0.439487	0.439863	0.44011
0.007639	0.430335	0.431173	0.43232	0.433184	0.433968	0.434856	0.435346	0.435929	0.436062	0.436432
0.011434	0.426609	0.427598	0.428604	0.42945	0.430214	0.431071	0.431553	0.431901	0.432389	0.432593
0.015212	0.42366	0.424659	0.425675	0.426303	0.427237	0.428012	0.428541	0.428932	0.429124	0.429519
0.02272	0.424893	0.425689	0.426884	0.427672	0.428239	0.428921	0.429606	0.429913	0.430158	0.430601
0.037545	0.42448	0.425382	0.426532	0.427324	0.42803	0.428715	0.429228	0.429565	0.429947	0.430067
0.055725	0.422438	0.423291	0.424217	0.424976	0.425741	0.426265	0.426935	0.427257	0.427479	0.427977
0.073526	0.423587	0.424617	0.425436	0.426226	0.426726	0.427375	0.427828	0.428279	0.428573	0.428742
0.108038	0.421165	0.422131	0.423117	0.423919	0.424532	0.425294	0.425963	0.426414	0.426469	0.426919
0.14117	0.416206	0.41706	0.418147	0.418834	0.419574	0.420291	0.420868	0.421358	0.421693	0.422156
0.20361	0.417856	0.418781	0.419777	0.42066	0.421349	0.422296	0.422891	0.4234	0.423904	0.424301
0.315111	0.414177	0.415035	0.415999	0.416919	0.417698	0.418306	0.419052	0.419749	0.419911	0.420407

Table H.1 *(continued)*

	Absorbance at wavelength /nm									
$[SO_3^{2-}]$ /M	**460**	**459**	**458**	**457**	**456**	**455**	**454**	**453**	**452**	**451**
0	0.44958	0.449568	0.4496	0.449051	0.448602	0.44802	0.447429	0.44655	0.445542	0.444291
0.000767	0.446742	0.446778	0.446736	0.446331	0.44575	0.445215	0.44455	0.443823	0.442744	0.441706
0.001533	0.445171	0.445228	0.445304	0.444885	0.444339	0.443881	0.443133	0.442572	0.441377	0.440289
0.003828	0.440175	0.440236	0.440293	0.439959	0.439431	0.43887	0.43821	0.437465	0.436105	0.435105
0.007639	0.43655	0.436516	0.436574	0.436443	0.436052	0.435367	0.43479	0.434157	0.432987	0.431814
0.011434	0.432631	0.432518	0.432618	0.432474	0.431899	0.431449	0.430823	0.429956	0.428945	0.427933
0.015212	0.429608	0.429551	0.429613	0.429286	0.428894	0.428509	0.427384	0.426773	0.425862	0.425053
0.02272	0.430516	0.430707	0.430631	0.430293	0.429997	0.429408	0.428946	0.428303	0.427173	0.42611
0.037545	0.430095	0.430183	0.430285	0.429912	0.429462	0.429068	0.428597	0.427618	0.426699	0.425883
0.055725	0.427801	0.427847	0.42785	0.427537	0.42707	0.426809	0.426026	0.425169	0.424153	0.423369
0.073526	0.428599	0.42866	0.428584	0.428241	0.427837	0.427403	0.426858	0.42585	0.424877	0.423916
0.108038	0.426857	0.427061	0.427169	0.426846	0.426535	0.426196	0.425352	0.424837	0.42417	0.423272
0.14117	0.422158	0.422571	0.422869	0.422578	0.422538	0.421969	0.421509	0.421261	0.420709	0.420106
0.20361	0.424589	0.42472	0.425048	0.424892	0.424896	0.42433	0.424161	0.423842	0.423539	0.423039
0.315111	0.420515	0.420815	0.421063	0.420859	0.420905	0.420782	0.420056	0.419818	0.419437	0.418999

Table H.1 *(continued)*

	Absorbance at wavelength /nm									
$[SO_3^{2-}]$ /M	**450**	**449**	**448**	**447**	**446**	**445**	**444**	**443**	**442**	**441**
0	0.44302	0.441605	0.440109	0.438329	0.4362	0.434484	0.432529	0.430541	0.427903	0.426068
0.000767	0.440255	0.438827	0.4375	0.435594	0.433609	0.431482	0.429407	0.427479	0.425216	0.423394
0.001533	0.439215	0.43776	0.436306	0.43416	0.432023	0.430368	0.428356	0.426372	0.424115	0.422408
0.003828	0.434002	0.432887	0.431608	0.42977	0.42775	0.426209	0.424484	0.422452	0.42031	0.418492
0.007639	0.430543	0.429525	0.428084	0.426547	0.424741	0.423128	0.421294	0.419539	0.417475	0.415864
0.011434	0.426764	0.425766	0.424468	0.422819	0.42104	0.419545	0.417848	0.416057	0.41421	0.412729
0.015212	0.423859	0.422676	0.421645	0.420081	0.418067	0.416863	0.415184	0.413556	0.411696	0.410231
0.02272	0.425109	0.424006	0.422752	0.421211	0.419575	0.418272	0.416811	0.415124	0.413292	0.411963
0.037545	0.424789	0.423589	0.422621	0.421274	0.419557	0.418039	0.416469	0.415133	0.413367	0.412071
0.055725	0.422315	0.42123	0.419905	0.418635	0.417001	0.415803	0.414368	0.412807	0.41104	0.409855
0.073526	0.422966	0.42191	0.420864	0.419587	0.41783	0.416603	0.415133	0.413903	0.412093	0.410889
0.108038	0.422444	0.421498	0.420556	0.419192	0.417834	0.416758	0.415469	0.413987	0.412576	0.411647
0.14117	0.419441	0.418729	0.418092	0.416972	0.415546	0.414826	0.413924	0.412884	0.411492	0.410708
0.20361	0.422548	0.421679	0.420971	0.420035	0.418966	0.418261	0.417197	0.41654	0.415241	0.414447
0.315111	0.418432	0.417759	0.417058	0.416062	0.415037	0.414267	0.413477	0.412654	0.411526	0.411143

Table H.2 The weighted *K* values and associated errors at the monitored wavelengths.

Wavelength /nm	*K*	Corrected for pH
441	130.042	159.1705
442	131.4191	154.5808
443	131.4223	155.3368
444	131.437	148.6139
445	131.9313	149.2833
446	133.2741	152.0391
447	134.0576	150.1337
448	134.1172	148.7504
449	134.3773	145.4556
450	134.6897	144.4503
451	135.0988	141.6403
452	135.1793	142.0648
453	135.441	141.3051
454	136.7642	129.4220
455	137.9597	128.8361
456	138.7287	128.0988
457	140.9832	128.4044
458	141.1346	128.8013
459	141.3326	127.5304
460	144.228	129.5458
461	144.4749	130.0000
462	146.5499	129.3440
463	148.2788	129.8718
464	150.5481	128.7035

Table H.2 *(continued)*

Wavelength /nm	*K*	Corrected for pH
465	155.1853	129.0390
466	155.3802	136.4636
467	158.3965	136.7477
468	159.7096	135.0652
469	169.3875	134.4318
470	175.636	131.7164
471	185.0918	129.0265
472	186.627	127.0454
473	196.3988	126.0234
474	210.3456	126.3207
475	225.3831	146.4578
476	240.8261	143.9998
477	261.6344	142.8805
478	292.5625	141.4087
479	307.0501	139.1598
480	344.2844	137.9498
550	375.3147	141.9324
551	130.042	145.4860
552	131.4191	144.7486
553	131.4223	147.5794
554	131.437	150.0553
555	131.9313	151.0693

K = 6759.492412
Error = 2403.863695

pH = 8.86
pK_a=7.28

Fraction Aqua = 0.02562858

Log *K*	**3.83**
Error	**0.13**

APPENDIX I

DETERMINATION OF RATE CONSTANTS

The change in absorbance of $[AC\text{-}5\text{-}seco\text{-}Cbs]^+$ associated with the coordination of cyanide with time monitored at 400 nm is illustrated in Figure I.1 and the corresponding data to determine the rate constant is found in Table I.1. The experimental data for all kinetics reactions, determination of rate constants and regression analysis can be found on the accompanying CD. Rate constants were determined by fitting a double exponential equation (Equation 2.9) (as in this example) or single exponential equation (Equation 2.10) using non-linear least-squares methods employing a Newton-Raphson procedure to the experimental data.

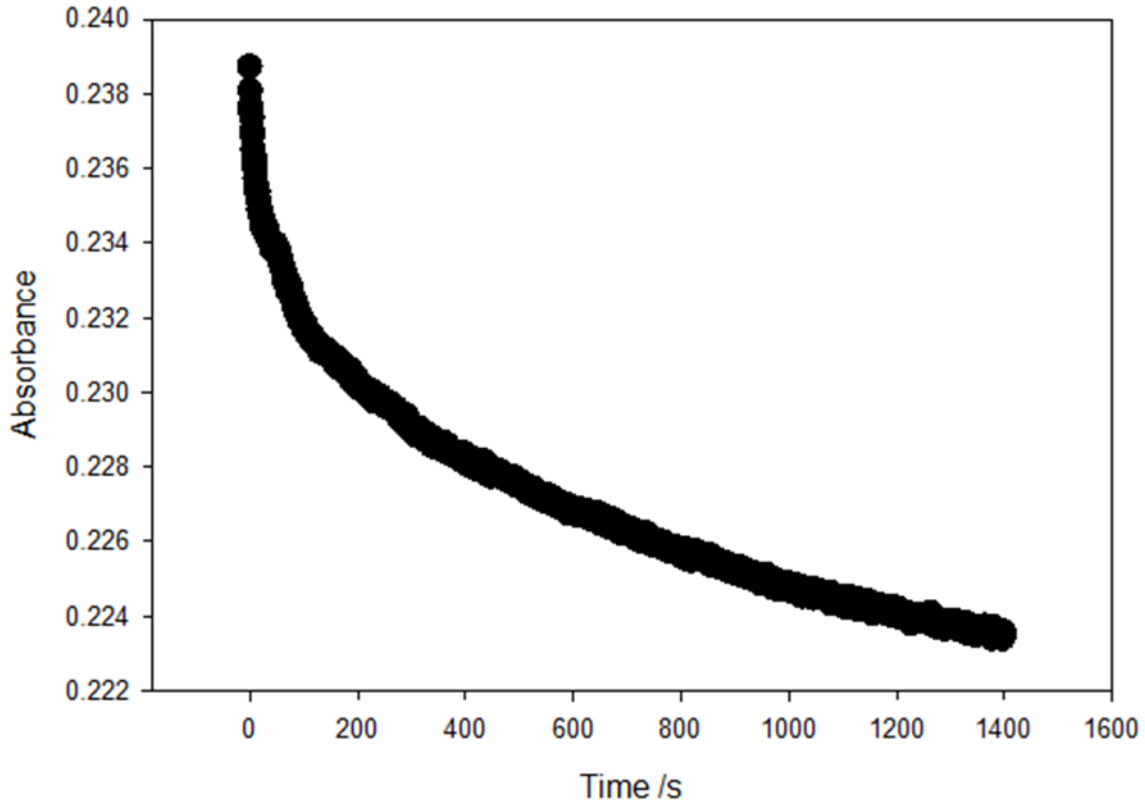

Figure I.1 Biphasic fit of the absorbance change at 400 nm as a function of time for the binding of CN^- (0.20 M) by $[AC\text{-}5\text{-}seco\text{-}Cbs]^+$ (CAPS, μ = 0.1 M, pH 10.5, 25.0 ^oC).

Table I.1 Data for the determination of the rate constant for the coordination of CN^- to $[AC\text{-}5\text{-}seco\text{-}Cbs]^+$.

k1	0.0122	k2	0.0012
	0.0042		0.0008
	0.0224		0.0016
	0.0198		0.0012
	0.0126		0.0009
Mean	1.42E-02		1.14E-03
Std dev	7.16E-03		3.13E-04
H+	2.13796E-11		
Ave H+	2.22317E-11		
Ave pH	10.65302819		
pKa 5SecoACCbs	7.28		
pKa CN-	8.944		
pH of expt	10.65302819		
Fraction ACbs aqua	0.000423436		
Fraction CN-	0.980832449		
k1 corrected	**33.63**	**k2 corrected**	**2.69**
std dev	**16.91**		**0.74**

APPENDIX J

DFT DATA

Table J.1. Comparison on the coordination sphere geometry of [DCCbs] and [DCSYCbs] determined by DFT methods and X-ray diffraction structures.

DCCbs	BP86-D3/6-311G(d,p)	BP86-D3/6-311++G(d,p)	B3LYP/6-311++G(d,p)	PBE0 6-311++G(d,p)	PBEPBE 6-311++G(d,p)	XRD data	BP86-D3/6-311G(d,p)		BP86-D3/6-311++G(d,p)		B3LYP/6-311++G(d,p)		PBE0 6-311++G(d,p)		PBEPBE 6-311++G(d,p)	
Bond	*r* /Å	*r* /Å	*r* /Å	*r* /Å	*r* /Å	**CODZAW10[e]**	Δ[a]	Rel%Δ[b]	Δ	Rel%Δ	Δ	Rel%Δ	Δ	Rel%Δ	Δ	Rel%Δ
Co-CN(□□[c]	1.925	1.933	1.956	1.938	1.935	1.925	0.000	0.00%	-0.008	0.42%	-0.031	1.61%	-0.013	0.68%	-0.010	0.52%
Co-CN(β)[d]	1.928	1.936	1.961	1.934	1.938	1.924	-0.004	0.21%	-0.012	0.62%	-0.037	1.92%	-0.010	0.52%	-0.014	0.73%
Co-N(21)	1.890	1.894	1.912	1.892	1.899	1.893	0.003	0.16%	-0.001	0.05%	-0.019	1.00%	0.001	0.05%	-0.006	0.32%
Co-N(22)	1.937	1.942	1.953	1.924	1.947	1.920	-0.017	0.89%	-0.022	1.15%	-0.033	1.72%	-0.004	0.21%	-0.027	1.41%
Co-N(23)	1.933	1.935	1.943	1.933	1.937	1.932	-0.001	0.05%	-0.003	0.16%	-0.011	0.57%	-0.001	0.05%	-0.005	0.26%
Co-N(24)	1.891	1.895	1.912	1.892	1.900	1.914	0.023	1.20%	0.019	0.99%	0.002	0.10%	0.022	1.15%	0.014	0.73%
Average Deviation coord sphere								0.42%		0.56%		1.15%		0.44%		0.66%
Angle	/deg	/deg	/deg	/deg	/deg		Δ	Rel%Δ	Δ	Rel%Δ	Δ	Rel%Δ	Δ	Rel%Δ	Δ	Rel%Δ
CN(□□-Co-CN(β)	176.8	177.0	177.1	177.5	177.0	175.0	-1.8	1.03%	-2.000	1.14%	-2.100	1.20%	-2.500	1.43%	-2.000	1.14%
N(21)-Co-N23	173.4	173.2	173.2	172.9	173.2	173.4	0.0	0.00%	0.200	0.12%	0.200	0.12%	0.500	0.29%	0.200	0.12%
N(22)-Co-N24	173.2	173.1	172.9	173.2	172.9	172.4	-0.8	0.46%	-0.700	0.41%	-0.500	0.29%	-0.800	0.46%	-0.500	0.29%
Average Deviation coord sphere								0.50%		0.55%		0.54%		0.73%		0.52%
Corrin fold angle	3.3	3.1	5.0	3.9	3.9	5.2										

Continued on next page

DCSYCbs	BP86-D3/6-311G(d,p)	BP86-D3/6-311++G(d,p)	B3LYP/6-311++G(d,p)	PBE0 6-311++G(d,p)	PBEPBE 6-311++G(d,p)	XRD data	BP86-D3/6-311G(d,p)		BP86-D3/6-311++G(d,p)		B3LYP/6-311++G(d,p)		PBE0 6-311++G(d,p)		PBEPBE 6-311++G(d,p)	
Bond	*r* /Å		*r* /Å	*r* /Å	*r* /Å	**XEHDIZ**[f]	Δ[a]	Rel%Δ[b]			Δ	Rel%Δ	Δ	Rel%Δ	Δ	Rel%Δ
Co-CN(□□[c]	1.920		1.952	1.934	1.930	1.918	-0.002	0.10%			-0.034	1.77%	-0.016	0.83%	-0.012	0.63%
Co-CN(β)[d]	1.928		1.956	1.935	1.934	1.930	0.002	0.10%			-0.026	1.35%	-0.005	0.26%	-0.004	0.21%
Co-N(21)	1.902		1.931	1.916	1.910	1.901	-0.001	0.05%			-0.030	1.58%	-0.015	0.79%	-0.009	0.47%
Co-N(22)	1.943		1.957	1.943	1.948	1.931	-0.012	0.62%			-0.026	1.35%	-0.012	0.62%	-0.017	0.88%
Co-N(23)	1.916		1.921	1.907	1.920	1.883	-0.033	1.75%			-0.038	2.02%	-0.024	1.27%	-0.037	1.96%
Co-N(24)	1.878		1.895	1.882	1.883	1.879	0.001	0.05%			-0.016	0.85%	-0.003	0.16%	-0.004	0.21%
Average Deviation coord sphere								0.45%				1.49%		0.66%		0.73%
Angle	/deg	/deg	/deg	/deg	/deg		Δ	Rel%Δ	Δ	Rel%Δ	Δ	Rel%Δ	Δ	Rel%Δ	Δ	Rel%Δ
CN(□□-Co-CN(β)	173.3		174.4	174.6	173.4	173.0	-0.3	0.17%			-1.400	0.81%	-1.600	0.92%	-0.400	0.23%
N(21)-Co-N23	172.8		172.8	172.6	172.7	173.4	0.6	0.35%			0.600	0.35%	0.800	0.46%	0.700	0.40%
N(22)-Co-N24	168.4		169.2	169.4	168.7	169.9	1.5	0.88%			0.700	0.41%	0.500	0.29%	1.200	0.71%
Average Deviation coord sphere								0.47%				0.52%		0.56%		0.45%
Corrin fold angle	19.6		17.4	21.7	22.7	15.6										

[a]Δ is is the difference in the parameter between the XRD structure and the DFT structure. [b]The difference Δ expressed as an absolute percentage relative deviation. [c]Co–CN bond length to cyanide coordinated in the α coordination site. [d]Co–CN bond length to cyanide coordinated in the β coordination site. [e]Markwell, A.J.; Pratt, J.M.; Shaikjee, M.S.; Toerien, J.G. *J. Chem. Soc., Dalton Trans.* **1987**, 1349-1357. The average σ(C–C bonds) is 0.01–0.03 Å. [f]Chemaly, S. M.; Brown, K. L.; Fernandes, M. A.; Munro, O. Q.; Grimmer, C.; Marques, H. M. *Inorg. Chem.* **2011,** *50*, 8700-8718. The average σ(C–C bonds) is 0.006–0.010 Å.

Table J.2. Charges q(r)/*e* on cobalt and the six inner coordination sphere donor atoms in $[(X)(CN)Co(corrin)]^{n+}$ complexes determined from a QTAIM analysis of the wavefunction of their BP86-D3/6-311G(d,p) structures.

X	Corrin										
CN^-			**Co**	**N21**	**N22**	**N23**	**N24**	**C(α)**	**C(β)**	**Σ Coord Sphere[a]**	**Σ(Co & eq N)[b]**
	Cbs		1.125	-0.993	-1.022	-1.028	-1.001	0.636	0.638	-1.645	-2.919
	SYCbs		1.112	-1.002	-1.003	-1.034	-1.002	0.632	0.650	-1.647	-2.929
	5-Seco-Cbs		1.118	-0.950	-0.998	-1.027	-1.001	0.643	0.652	-1.564	-2.858
SO_3^{2-}			**Co**	**N21**	**N22**	**N23**	**N24**	**C**	**S**	**Av Σ Coord Sphere[c]**	**Av Σ(Co & eq N)[d]**
	Cbs	Alpha sulfito	1.057	-0.981	-1.021	-1.027	-0.993	0.619	2.477	0.124	-2.965
		Beta sulfito	1.057	-0.987	-1.014	-1.024	-0.996	0.616	2.464		
	SYCbs	Alpha sulfito	1.044	-0.987	-0.996	-1.040	-0.991	0.638	2.479	0.120	-2.988
		Beta sulfito	1.040	-0.991	-1.011	-1.032	-1.012	0.620	2.479		
	5-Seco-Cbs	Alpha sulfito	1.050	-0.947	-0.994	-1.031	-0.993	0.657	2.467	0.166	-2.926
		Beta sulfito	1.054	-0.963	-1.002	-1.035	-0.991	0.647	2.412		
NO_2^-			**Co**	**N21**	**N22**	**N23**	**N24**	**C**	**N**	**Av Σ Coord Sphere[c]**	**Av Σ(Co & eq N)[d]**
	Cbs	Alpha nitro	1.146	-0.994	-1.017	-1.029	-1.000	0.644	0.381	-1.868	-2.896
		Beta nitro	1.146	-0.995	-1.022	-1.026	-1.001	0.645	0.387		
	SYCbs	Alpha nitro	1.134	-1.009	-0.996	-1.039	-0.996	0.656	0.381	-1.873	-2.914
		Beta nitro	1.131	-1.003	-1.012	-1.030	-1.008	0.645	0.400		
	5-Seco-Cbs	Alpha nitro	1.133	-0.955	-1.000	-1.030	-1.001	0.666	0.392	-1.787	-2.843
		Beta nitro	1.141	-0.952	-0.995	-1.029	-0.997	0.648	0.405		
N_3^-			**Co**	**N21**	**N22**	**N23**	**N24**	**C**	**N**	**Av Σ Coord Sphere[c]**	**Av Σ(Co & eq N)[d]**
	Cbs	Alpha azido	1.152	-0.987	-1.013	-1.029	-1.006	0.660	-0.328	-2.564	-2.884
		Beta azido	1.151	-0.990	-1.024	-1.026	-0.995	0.657	-0.350		
	SYCbs	Alpha azido	1.145	-1.003	-0.997	-1.032	-1.008	0.670	-0.351	-2.586	-2.897
		Beta azido	1.144	-1.001	-1.011	-1.033	-0.998	0.652	-0.348		
	5-Seco-Cbs	Alpha azido	1.151	-0.952	-1.004	-1.031	-0.997	0.672	-0.329	-2.502	-2.825
		Beta azido	1.152	-0.947	-1.000	-1.027	-0.994	0.658	-0.356		

X	Corrin									
H_2O			Co	N21	N22	N23	N24	C	O	Av Σ Coord Sphere[c]	Av Σ(Co & eq N)[d]
	Cbs	Alpha aqua	1.131	-1.009	-1.019	-1.035	-1.017	0.685	-1.059	-3.321	-2.951
		Beta aqua	1.130	-1.014	-1.022	-1.027	-1.020	0.687	-1.052		
	SYCbs	Alpha aqua	1.121	-1.026	-1.003	-1.044	-1.021	0.695	-1.061	-3.359	-2.971
		Beta aqua	1.130	-1.028	-1.021	-1.041	-1.008	0.679	-1.090		
	5-Seco-Cbs	Alpha aqua	1.131	-1.009	-1.019	-1.035	-1.017	0.685	-1.059	-3.311	-2.920
		Beta aqua	1.142	-0.979	-1.016	-1.024	-1.013	0.68	-1.089		

[a]Sum of the QTAIM charges on Co and the six donor atoms of its inner coordination sphere. [b]Sum of the QTAIM charges on Co and the four equatorial donor atoms of the corrin. [c]As for Footnote a, averaged over the two diastereomers. [d]As for Footnote b, averaged over the two diastereomers.

Table J.3. The coordination geometry and analysis of the topological properties of the electron density of the bonds in the coordination sphere of $[(X)(CN)Co(5\text{-seco-Cbs})]^{n+}$ determined from the BP86-D3/6-311G(d,p) structures

$[(CN)_2Co(Corrin)]$															
Bond	Corrin	Bond length /Å	ρ	$\nabla^2\rho_r$	V_r	G_r	H_r	$\lvert V_r\rvert/G_r$		Bond length (av) /Å	ρ_r (av)	$\nabla^2\rho_r$ (av)	$\lvert V_r\rvert/G_r$ (av)	V_r (av)	G_r (av)	H_r (av)
Co-CN(a)	Cbs	1.925	0.116	0.286	-0.146	0.109	-0.037	1.339	Co-CN	1.927	0.116	0.287	1.335	-0.146	0.109	-0.037
	SYCbs	1.920	0.116	0.296	-0.149	0.111	-0.038	1.342		1.924	0.116	0.289	1.349	-0.147	0.109	-0.038
	5SecoCbs	1.917	0.118	0.285	-0.149	0.110	-0.039	1.355		1.923	0.116	0.283	1.349	-0.147	0.109	-0.038
Co-CN(b)	Cbs	1.928	0.115	0.288	-0.145	0.109	-0.036	1.330								
	SYCbs	1.928	0.115	0.281	-0.145	0.107	-0.038	1.355								
	5SecoCbs	1.928	0.115	0.282	-0.145	0.108	-0.037	1.343								
Co-N21	Cbs	1.890	0.117	0.469	-0.179	0.148	-0.031	1.209	Co-N(corrin)	1.913	0.110	0.449	1.189	-0.166	0.139	-0.027
	SYCbs	1.902	0.111	0.485	-0.175	0.148	-0.027	1.182		1.91	0.111	0.450	1.198	-0.168	0.140	-0.028
	5SecoCbs	1.947	0.099	0.436	-0.149	0.129	-0.020	1.155		1.933	0.104	0.431	1.178	-0.155	0.131	-0.024
Co-N22	Cbs	1.937	0.103	0.428	-0.152	0.130	-0.022	1.169								
	SYCbs	1.943	0.102	0.413	-0.148	0.125	-0.023	1.184								
	5SecoCbs	1.968	0.095	0.399	-0.136	0.118	-0.018	1.153								
Co-N23	Cbs	1.933	0.104	0.431	-0.154	0.131	-0.023	1.176								
	SYCbs	1.916	0.110	0.434	-0.162	0.135	-0.027	1.200								
	5SecoCbs	1.924	0.107	0.427	-0.156	0.131	-0.025	1.191								
Co-N24	Cbs	1.891	0.116	0.467	-0.178	0.148	-0.030	1.203								
	SYCbs	1.878	0.121	0.470	-0.185	0.151	-0.034	1.225								
	5SecoCbs	1.893	0.116	0.464	-0.177	0.146	-0.031	1.212								

Co-SO_3	Cbs	α–SO_3	2.333	0.080	0.106	-0.067	0.047	-0.020	1.433	Co-SO_3	2.334	0.080	0.107	1.430	-0.067	0.047	-0.020
		β–SO_3	2.334	0.080	0.108	-0.067	0.047	-0.020	1.428								
	SYCbs	α–SO_3	2.353	0.076	0.104	-0.063	0.045	-0.019	1.417		2.401	0.070	0.091	1.423	-0.056	0.039	-0.017
		β–SO_3	2.448	0.064	0.077	-0.049	0.034	-0.015	1.429								
	5SecoCbs	α–SO_3	2.240	0.067	0.086	-0.053	0.037	-0.016	1.422		2.24	0.069	0.098	1.399	-0.057	0.041	-0.016
		β–SO_3	2.240	0.071	0.110	-0.061	0.044	-0.017	1.376								
Co-CN	Cbs	α–SO_3	2.000	0.097	0.269	-0.119	0.093	-0.026	1.279	Co-CN	1.993	0.099	0.271	1.284	-0.121	0.095	-0.027
		β–SO_3	1.986	0.100	0.273	-0.124	0.096	-0.028	1.289								
	SYCbs	α–SO_3	1.987	0.100	0.270	-0.123	0.095	-0.028	1.293		1.975	0.103	0.280	1.293	-0.128	0.099	-0.029
		β–SO_3	1.962	0.105	0.290	-0.133	0.103	-0.030	1.293								
	5SecoCbs	α–SO_3	1.906	0.106	0.273	-0.131	0.099	-0.031	1.314		1.918	0.109	0.278	1.319	-0.135	0.102	-0.033
		β–SO_3	1.929	0.112	0.284	-0.139	0.105	-0.034	1.325								
Co-N21	Cbs	α–SO_3	1.873	0.120	0.512	-0.195	0.161	-0.034	1.208	Co-N(corrin)	1.898	0.113	0.486	1.191	0.179	-0.150	0.029
		β–SO_3	1.875	0.120	0.511	-0.194	0.161	-0.033	1.205								
	SYCbs	α–SO_3	1.870	0.120	0.539	-0.200	0.167	-0.033	1.195		1.894	0.114	0.488	1.194	0.181	-0.152	0.030
		β–SO_3	1.888	0.113	0.525	-0.187	0.159	-0.028	1.176								
	5SecoCbs	α–SO_3	1.962	0.110	0.495	-0.176	0.150	-0.026	1.175		1.929	0.110	0.470	1.185	0.171	-0.144	0.027
		β–SO_3	1.946	0.111	0.485	-0.176	0.149	-0.027	1.184								
Co-N22	Cbs	α–SO_3	1.924	0.106	0.462	-0.163	0.139	-0.024	1.172								
		β–SO_3	1.923	0.106	0.461	-0.163	0.139	-0.024	1.173								
	SYCbs	α–SO_3	1.930	0.104	0.443	-0.157	0.134	-0.023	1.173								
		β–SO_3	1.924	0.106	0.449	-0.161	0.137	-0.025	1.180								
	5SecoCbs	α–SO_3	1.945	0.092	0.394	-0.132	0.115	-0.017	1.144								
		β–SO_3	1.968	0.104	0.445	-0.158	0.134	-0.023	1.173								
Co-N23	Cbs	α–SO_3	1.920	0.107	0.463	-0.165	0.141	-0.025	1.176								
		β–SO_3	1.913	0.109	0.469	-0.169	0.143	-0.026	1.181								
	SYCbs	α–SO_3	1.913	0.109	0.463	-0.169	0.142	-0.027	1.186								
		β–SO_3	1.901	0.113	0.467	-0.174	0.145	-0.029	1.196								

	5SecoCbs	α–SO_3	1.909	0.110	0.459	-0.168	0.141	-0.027	1.188								
		β–SO_3	1.924	0.109	0.457	-0.166	0.140	-0.026	1.185								
Co-N24	Cbs	α–SO_3	1.875	0.119	0.510	-0.193	0.160	-0.033	1.204								
		β–SO_3	1.877	0.119	0.504	-0.191	0.159	-0.033	1.207								
	SYCbs	α–SO_3	1.856	0.126	0.514	-0.204	0.166	-0.038	1.227								
		β–SO_3	1.868	0.123	0.505	-0.197	0.162	-0.036	1.219								
	5SecoCbs	α–SO_3	1.883	0.121	0.504	-0.194	0.160	-0.034	1.213								
		β–SO_3	1.893	0.124	0.518	-0.202	0.166	-0.036	1.219								
Co-NO_2	Cbs	α-NO_2	1.990	0.097	0.355	-0.129	0.109	-0.020	1.183	Co-NO_2	1.995	0.096	0.352	1.179	-0.126	0.107	-0.019
		β–NO_2	2.000	0.094	0.349	-0.124	0.106	-0.018	1.174								
	SYCbs	α-NO_2	1.998	0.110	0.488	-0.125	0.107	-0.018	1.171		2.018	0.099	0.400	1.166	-0.116	0.100	-0.017
		β–NO_2	2.038	0.087	0.312	-0.108	0.093	-0.015	1.162								
	5SecoCbs	α-NO_2	2.047	0.085	0.306	-0.104	0.090	-0.014	1.155		2.028	0.089	0.321	1.165	-0.112	0.096	-0.016
		β–NO_2	2.008	0.093	0.337	-0.120	0.102	-0.018	1.175								
Co-CN	Cbs	α-NO_2	1.914	0.119	0.285	-0.150	0.110	-0.039	1.355	Co-CN	1.913	0.120	0.283	1.358	-0.150	0.110	-0.039
		β–NO_2	1.911	0.120	0.282	-0.150	0.110	-0.040	1.360								
	SYCbs	α-NO_2	1.913	0.120	0.278	-0.149	0.109	-0.040	1.364		1.91	0.120	0.285	1.359	-0.151	0.111	-0.040
		β–NO_2	1.906	0.120	0.291	-0.152	0.113	-0.040	1.354								
	5SecoCbs	α-NO_2	1.906	0.121	0.281	-0.152	0.111	-0.041	1.367		1.91	0.120	0.279	1.365	-0.150	0.110	-0.040
		β–NO_2	1.914	0.119	0.277	-0.148	0.109	-0.040	1.363								
Co-N21	Cbs	α-NO_2	1.882	0.119	0.483	-0.186	0.154	-0.033	1.214	Co-N(corrin)	1.906	0.112	0.462	1.195	0.172	-0.144	0.028
		β–NO_2	1.884	0.118	0.482	-0.185	0.153	-0.032	1.211								
	SYCbs	α-NO_2	1.904	0.104	0.428	-0.175	0.149	-0.027	1.179		1.907	0.110	0.442	1.195	0.171	-0.143	0.028
		β–NO_2	1.906	0.110	0.486	-0.174	0.148	-0.026	1.178								
	5SecoCbs	α-NO_2	1.962	0.095	0.422	-0.142	0.124	-0.018	1.147		1.941	0.105	0.438	1.178	0.158	-0.134	0.024
		β–NO_2	1.938	0.102	0.448	-0.155	0.133	-0.021	1.160								
Co-N22	Cbs	α-NO_2	1.928	0.105	0.445	-0.159	0.135	-0.024	1.178								
		β–NO_2	1.928	0.107	0.446	-0.159	0.135	-0.024	1.180								
	SYCbs	α-NO_2	1.933	0.112	0.446	-0.155	0.131	-0.024	1.182								
		β–NO_2	1.934	0.104	0.427	-0.154	0.131	-0.024	1.182								

	5SecoCbs	α-NO_2	1.946	0.101	0.424	-0.149	0.127	-0.021	1.167								
		β–NO_2	1.980	0.093	0.389	-0.131	0.114	-0.017	1.150								
Co-N23	Cbs	α-NO_2	1.926	0.106	0.447	-0.160	0.136	-0.024	1.179								
		β–NO_2	1.924	0.117	0.477	-0.161	0.136	-0.025	1.182								
	SYCbs	α-NO_2	1.909	0.123	0.483	-0.168	0.140	-0.028	1.202								
		β–NO_2	1.918	0.109	0.436	-0.162	0.136	-0.027	1.195								
	5SecoCbs	α-NO_2	1.909	0.111	0.444	-0.166	0.138	-0.027	1.197								
		β–NO_2	1.926	0.107	0.432	-0.157	0.133	-0.025	1.186								
Co-N24	Cbs	α-NO_2	1.887	0.117	0.476	-0.182	0.151	-0.032	1.209								
		β–NO_2	1.888	0.106	0.442	-0.182	0.151	-0.031	1.208								
	SYCbs	α-NO_2	1.872	0.094	0.353	-0.192	0.156	-0.035	1.227								
		β–NO_2	1.881	0.120	0.476	-0.186	0.152	-0.033	1.219								
	5SecoCbs	α-NO_2	1.883	0.118	0.482	-0.185	0.153	-0.032	1.212								
		β–NO_2	1.983	0.115	0.467	-0.177	0.147	-0.030	1.206								
Co-N_3	Cbs	α-N_3	2.045	0.078	0.295	-0.098	0.086	-0.012	1.143	Co-N_3	2.047	0.078	0.292	1.146	-0.098	0.086	-0.013
		β–N_3	2.048	0.078	0.289	-0.098	0.085	-0.013	1.149								
	SYCbs	α-N_3	2.037	0.079	0.307	-0.102	0.089	-0.013	1.140		2.04	0.079	0.301	1.143	-0.100	0.088	-0.013
		β–N_3	2.043	0.079	0.295	-0.099	0.087	-0.013	1.147								
	5SecoCbs	α-N_3	2.035	0.081	0.299	-0.102	0.088	-0.014	1.153		2.03	0.082	0.304	1.153	-0.104	0.090	-0.014
		β–N_3	2.024	0.082	0.310	-0.105	0.092	-0.014	1.152								
Co-CN	Cbs	α-N_3	1.877	0.129	0.296	-0.165	0.120	-0.046	1.382	Co-CN	1.878	0.129	0.294	1.382	-0.165	0.119	-0.045
		β–N_3	1.879	0.128	0.293	-0.164	0.119	-0.045	1.382								
	SYCbs	α-N_3	1.881	0.128	0.287	-0.163	0.117	-0.045	1.387		1.88	0.128	0.295	1.380	-0.164	0.119	-0.045
		β–N_3	1.878	0.128	0.302	-0.166	0.121	-0.045	1.373								
	5SecoCbs	α-N_3	1.884	0.127	0.285	-0.161	0.116	-0.045	1.385		1.884	0.127	0.287	1.383	-0.161	0.116	-0.045
		β–N_3	1.884	0.127	0.289	-0.161	0.117	-0.045	1.382								
Co-N21	Cbs	α-N_3	1.885	0.118	0.479	-0.184	0.152	-0.032	1.210	Co-N(corrin)	1.906	0.112	0.462	1.194	0.171	-0.143	0.028
		β–N_3	1.884	0.118	0.481	-0.184	0.152	-0.032	1.210								
	SYCbs	α-N_3	1.903	0.111	0.488	-0.176	0.149	-0.027	1.179		1.906	0.112	0.460	1.195	0.171	-0.143	0.028
		β–N_3	1.904	0.110	0.488	-0.175	0.148	-0.026	1.178								

	5SecoCbs	α-N_3	1.944	0.100	0.445	-0.152	0.131	-0.020	1.154		1.929	0.105	0.439	1.177	0.157	-0.134	0.024
		β–N_3	1.948	0.099	0.436	-0.148	0.129	-0.020	1.152								
Co-N22	Cbs	α-N_3	1.936	0.103	0.436	-0.154	0.132	-0.023	1.171								
		β–N_3	1.930	0.105	0.441	-0.157	0.134	-0.023	1.175								
	SYCbs	α-N_3	1.938	0.103	0.425	-0.152	0.129	-0.023	1.178								
		β–N_3	1.937	0.103	0.424	-0.152	0.129	-0.023	1.178								
	5SecoCbs	α-N_3	1.960	0.097	0.407	-0.141	0.121	-0.019	1.159								
		β–N_3	1.973	0.094	0.399	-0.135	0.117	-0.018	1.149								
Co-N23	Cbs	α-N_3	1.923	0.107	0.446	-0.161	0.136	-0.025	1.181								
		β–N_3	1.925	0.106	0.446	-0.160	0.136	-0.024	1.180								
	SYCbs	α-N_3	1.905	0.112	0.447	-0.169	0.140	-0.028	1.202								
		β–N_3	1.914	0.110	0.441	-0.164	0.137	-0.027	1.196								
	5SecoCbs	α-N_3	1.914	0.110	0.441	-0.163	0.137	-0.026	1.193								
		β–N_3	1.920	0.108	0.435	-0.159	0.134	-0.025	1.190								
Co-N24	Cbs	α-N_3	1.882	0.119	0.483	-0.186	0.153	-0.033	1.212								
		β–N_3	1.883	0.118	0.480	-0.184	0.152	-0.032	1.211								
	SYCbs	α-N_3	1.869	0.123	0.490	-0.194	0.158	-0.036	1.226								
		β–N_3	1.875	0.122	0.474	-0.188	0.153	-0.035	1.227								
	5SecoCbs	α-N_3	1.887	0.117	0.473	-0.181	0.150	-0.032	1.210								
		β–N_3	1.888	0.117	0.474	-0.180	0.150	-0.031	1.207								
Co-OH_2	Cbs	α-H_2O	2.174	0.046	0.250	-0.064	0.064	0.000	0.994	Co-OH2	2.18	0.046	0.250	0.995	-0.063	0.063	0.000
		β–H_2O	2.186	0.046	0.250	-0.062	0.062	0.000	0.997								
	SYCbs	α-H_2O	2.183	0.049	0.269	-0.067	0.067	0.000	0.996		2.169	0.050	0.271	0.999	-0.068	0.068	0.000
		β–H_2O	2.155	0.051	0.273	-0.069	0.068	0.000	1.003								
	5SecoCbs	α-H_2O	2.086	0.060	0.337	-0.085	0.085	0.000	1.004		2.083	0.061	0.341	1.004	-0.086	0.085	0.000
		β–H_2O	2.080	0.061	0.344	-0.087	0.086	0.000	1.004								
Co-CN	Cbs	α-H_2O	1.819	0.147	0.268	-0.189	0.129	-0.061	1.471	Co-CN	1.82	0.147	0.268	1.473	-0.189	0.128	-0.061
		β–H_2O	1.820	0.147	0.268	-0.188	0.128	-0.061	1.475								
	SYCbs	α-H_2O	1.828	0.145	0.265	-0.184	0.125	-0.059	1.470		1.825	0.146	0.271	1.466	-0.186	0.127	-0.059
		β–H_2O	1.822	0.146	0.277	-0.188	0.129	-0.059	1.462								

	5SecoCbs	α-H_2O	1.838	0.142	0.271	-0.180	0.124	-0.056	1.454		1.836	0.143	0.270	1.457	-0.181	0.124	-0.057
		β–H_2O	1.834	0.143	0.268	-0.182	0.124	-0.057	1.460								
Co-N21	Cbs	α-H_2O	1.881	0.121	0.486	-0.186	0.153	-0.033	1.218	Co-N(corrin))	1.902	0.114	0.463	1.202	0.174	-0.145	0.029
		β–H_2O	1.877	0.121	0.486	-0.190	0.156	-0.034	1.219								
	SYCbs	α-H_2O	1.914	0.109	0.465	-0.169	0.143	-0.026	1.183		1.904	0.113	0.456	1.203	0.173	-0.143	0.029
		β–H_2O	1.907	0.111	0.475	-0.174	0.146	-0.028	1.188								
	5SecoCbs	α-H_2O	1.957	0.097	0.428	-0.145	0.126	-0.019	1.151		1.926	0.107	0.436	1.186	0.160	-0.134	0.025
		β–H_2O	1.951	0.099	0.430	-0.148	0.128	-0.020	1.157								
Co-N22	Cbs	α-H_2O	1.925	0.107	0.444	-0.160	0.136	-0.025	1.183								
		β–H_2O	1.923	0.107	0.444	-0.161	0.136	-0.025	1.185								
	SYCbs	α-H_2O	1.925	0.107	0.434	-0.159	0.134	-0.025	1.190								
		β–H_2O	1.933	0.105	0.426	-0.155	0.131	-0.024	1.185								
	5SecoCbs	α-H_2O	1.951	0.100	0.414	-0.146	0.125	-0.021	1.169								
		β–H_2O	1.967	0.096	0.399	-0.138	0.119	-0.019	1.161								
Co-N23	Cbs	α-H_2O	1.921	0.109	0.449	-0.163	0.138	-0.026	1.186								
		β–H_2O	1.917	0.109	0.449	-0.165	0.139	-0.026	1.190								
	SYCbs	α-H_2O	1.895	0.116	0.462	-0.177	0.146	-0.031	1.210								
		β–H_2O	1.910	0.111	0.441	-0.166	0.138	-0.028	1.203								
	5SecoCbs	α-H_2O	1.906	0.112	0.446	-0.168	0.140	-0.028	1.202								
		β–H_2O	1.903	0.114	0.437	-0.168	0.139	-0.029	1.211								
Co-N24	Cbs	α-H_2O	1.884	0.118	0.474	-0.185	0.152	-0.033	1.216								
		β–H_2O	1.885	0.118	0.474	-0.184	0.151	-0.033	1.216								
	SYCbs	α-H_2O	1.876	0.122	0.477	-0.189	0.154	-0.035	1.227								
		β–H_2O	1.869	0.124	0.471	-0.191	0.155	-0.037	1.238								
	5SecoCbs	α-H_2O	1.878	0.121	0.474	-0.188	0.153	-0.035	1.226								
		β–H_2O	1.891	0.117	0.461	-0.178	0.147	-0.031	1.214								

APPENDIX K

PUBLICATION

Probing the Nature of the Co(III) Ion in Corrins: the Reactions of Aquacyano-5-seco-Cobyrinic Acid Heptamethyl Ester with Anionic Ligands

Monika Nowakowska[a], Susan M. Chemaly[a], Amanda Rousseau,[a] Penny P. Govender[b], Pradeep R. Varadwaj[c,d], Arpita Varadwaj[c,d], Koichi Yamashita,[c,d] and Helder M. Marques[a]*

[a]Molecular Sciences Institute, School of Chemistry, University of the Witwatersrand, P.O. Wits, Johannesburg, 2050 South Africa; [b]Department of Applied Chemistry, University of Johannesburg, South Africa; [c]Department of Chemical Systems Engineering, School of Engineering, The University of Tokyo 7-3-1, Hongo, Bunkyo-ku, Japan 113-8656; and [d]CREST-JST, 7 Gobancho, Chiyoda-ku, Tokyo, Japan 102-0076

ABSTRACT:

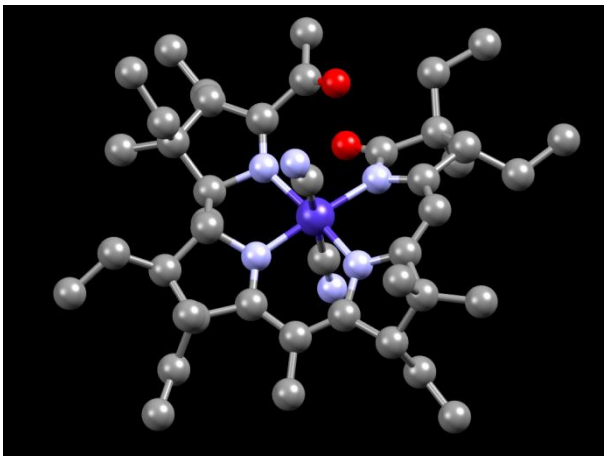

The substitution of H_2O in aquacyano-5,6-dioxo-5,6-seco-heptamethylcob(III)yrinate, (aquacyano-5-seco-cobester, $[AC\text{-}5\text{-}seco\text{-}Cbs]^+$), in which the C5–C6 bond of the corrin ring of this vitamin B_{12} derivative is cleaved, by a variety of anionic ligands is reported. The pK_a for ionization of coordinated water decreases from 9.8 ± 0.3 in aquacyanocobyrinic acid heptamethyl ester (aquacyanocobester, $[ACCbs]^+$) to 7.28 at 25 °C (ΔH = –88 ± 17 kJ mol^{-1} and ΔS = –434 ± 56 J K^{-1} mol^{-1}) in $[AC\text{-}5\text{-}seco\text{-}Cbs]^+$. The p$K_a$, confirmed by determining the pH-dependence of coordination of SO_3^{2-} by $[AC\text{-}5\text{-}seco\text{-}Cbs]^+$, shows Co(III) in this complex behaves much more like Co(III) in simple hexacoordinate complexes than in intact cobalt corrins. A comparison of log K values for coordination of CN^-, SO_2^{2-}, NO_2^-, N_3^- and $S_2O_3^{2-}$ by $[ACCbs]^+$ and $[AC\text{-}5\text{-}seco\text{-}Cbs]^+$ demonstrates that cleavage of the corrin ring significantly decreases the affinity of Co(III) for the softer ligands CN^-, SO_3^{2-} and, more marginally, NO_2^-. However, $[AC\text{-}5\text{-}seco\text{-}Cbs]^+$ has a higher affinity for N_3^- and $S_2O_3^{2-}$ than $[ACCbs]^+$. These trends correlate with the position of the ligands in the spectrochemical series ($N_3^- < S_2O_3^{2-} < NO_2^- < SO_3^{2-} < CN^-$); the first two behave as π donors towards metal ions, and the last three as π acceptors. Cleavage of the corrin, with a concomitant increase in hardness of the metal, decreases it affinity for π acceptors while the

thermodynamic stability of its complexes with π donors increases as the metal ion becomes more Co(III)-like, and more capable of accepting electron density from the ligand. The temperature-dependence of log *K* values show very negative values for Δ*H* offset by Δ*S* values which are also large and negative. In the absence of crystal structures, DFT methods (BP86-D3/6-311G(d,p)) were used to assess the structural consequences of cleavage of the corrin. The topological properties of the electron density were assessed using QTAIM. The cleavage of the corrin does not unduly perturb the coordination sphere of the metal ion and the metal remains essentially octahedral. The sum of the partial charges on the metal and the entire coordination sphere, or the metal and the four equatorial donor N atoms, is less negative in the 5-seco-Cbs complexes than in the Cbs themselves and supports the supposition that cleavage of the corrin has made the metal and its immediate environment more positive. Cleavage of the corrin causes the bond lengths to the equatorial N donors to increase and allows the bonds to the axial ligands usually to be shorter, offering a rationalization for the observed very negative Δ*H* values for substitution of H_2O by an exogenous ligand. The rate of substitution of H_2O by CN^- in $[AC\text{-}5\text{-}seco\text{-}Cbs]^+$ is some two orders of magnitude slower than that of the substitution of H_2O by CN^- in $[ACCbs]^+$. Cleavage of the corrin has therefore significantly decreased the lability of Co(III). This study demonstrates how perturbation of the electronic structure of the corrin in cobalt corrin complexes significantly affects the coordination chemistry of the axial coordination sites and points to the importance of cis effects in the chemistry of the cobalt corrinoids.

■ INTRODUCTION

We have been interested for some time in exploring the nature of Co(III) in the cobalt corrins (derivatives of vitamin B_{12}) to arrive at a better understanding why this normally inert low spin d^6 metal ion is unusually labile in these systems.[1-13] We have suggested that the lability arises from the delocalization of electron density from the relatively electron-rich corrin equatorial ligand to Co(III), making the metal softer and conferring on it at least some measure of labile Co(II) character. The problem of the meaning of the formal oxidation state of a metal ion in a complex where the ligands have a delocalized electronic structure has been recognized for many years.[14-16] If cobalt in the corrins does indeed have some Co(II) character by virtue of its coordination by corrin, then perturbing the electronic and topological structure of the corrin should affect its chemistry.

It is well-established that there is electronic communication between the axial coordination sites of the cobalt corrins and the equatorial corrin ligand. For example, the UV-vis spectra of these compounds, which are dominated by transitions between predominantly corrin-based orbitals,[17, 18] are heavily dependent on the identity of the axial ligands;[5, 19] the bond length between C10 and Cl in $[X–(10\text{-}Cl)Cbls]^{n+}$ (Cbl = cobalamin) where the C10 H has been replaced by Cl (see Figure 1 for the standard numbering of the corrins), depends on the polarizability of the axial ligand X ($Me^- > CN^- > H_2O$); and the presence of a strongly electron withdrawing group at C10, as in $[H_2O–(10\text{-}NO)Cbl]^+$, deactivates the towards displacement of the axial H_2O ligand.[2]

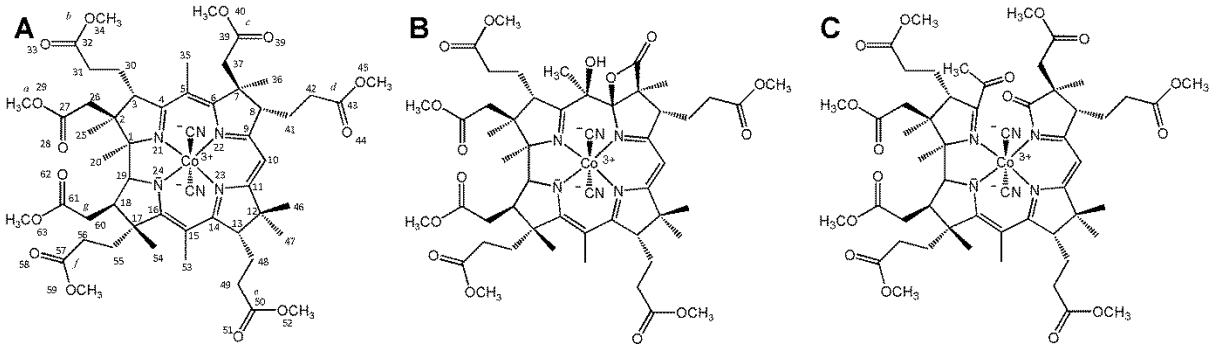

Figure 1. The structure of (A) dicyanocobester ([DCCbs]), (B) dicyano stable yellow cobester ([DCSYCbs]), with interrupted conjugation at C5 and the *c* side chain condensed to a lactone at C6, (C) dicyano-5-seco-cobester ([DC-5-seco-Cbs]), in which the corrin ring has been cleaved at C5. In this standard view of the cobalt corrins, the upper coordination site is referred to as the β coordination site, and the lower site as the α coordination site. Loss of one CN^- ligand and its replacement by H_2O leads to a mixture of (usually) inter-converting aquacyano cobester ($[ACCbs]^+$) diastereomers in each case; for example, $[\alpha\text{-}CN,\beta\text{-}H_2O\text{-}ACCbs]^+$ and $[\alpha\text{-}H_2O,\beta\text{-}CN\text{-}ACCbs]^+$

We have prepared and fully characterized a derivative of the heptamethyl ester of cobyrinic acid, (5*R*,6*R*)-Co*α*,Co*β*-dicyano-5,6-dihydro-5-hydroxy-hepta-methylcob(III)yrinate-*c*,6-lactone, referred to as a stable yellow cobester, [DCSYCbs], (see Figure 1), from the corresponding dicyanocobyrinic acid heptamethyl ester, Co*α*,Co*β*-dicyano-heptamethylcob(III)yrinate ([DCCbs], Figure 1), in which the 13 atom, 14 π-e^- delocalized system of normal corrins is interrupted by oxidation of the C5 carbon.[6] The spectroscopic evidence (and in particular ^{59}Co NMR and the stretching frequency ν_{CN} of the CN ligands) indicated that interrupting the conjugation of the equatorial ligand resulted in a harder Co(III) center. Determination of equilibrium constants (log *K*) for the substitution of coordinated H_2O in $[ACCbs]^+$ and $[ACSYCbs]^+$ by ligands with softer (C in CN^-, S in SO_3^{2-}) and harder (N in NO_2^- and N_3^-) donor atoms as a function of temperature showed that the ligands with a harder donor atom produce Δ*H* values that are more negative in their reactions with $[ACSYCbs]^+$ than with $[ACCbs]^+$, but if the donor atom is softer then Δ*H* is less positive, or more negative, for reactions with $[ACCbs]^+$ than with $[ACSYCbs]^+$.[7]

In a similar study, we compared the coordination of a variety of ligands including the anions N_3^-, NO_2^-, SCN^-, SO_3^{2-} and CN^- by $[ACCbs]^+$ and its derivatives aquacyano(10–nitro)cobester, $[AC(10–NO_2)Cbs]^+$, and aquacyano(10–amino)cobester, $[AC(10–NH_2)Cbs]^+$ in which the H at C10 of corrin is replaced by electron-withdrawing NO_2 and electron-donating NH_2, respectively.[13] We found that $[AC(10–NH_2)Cbs]^+$ and $[ACCbs]^+$ have a similar affinity for virtually all the ligands but $[AC(10–NO_2)Cbs]^+$ has a lower affinity for the softer anions CN^- and SO_3^{2-} and a much higher affinity for the harder anions SCN^-, N_3^- and NO_2^-.

A kinetics study of the substitution of H_2O by CN^- on Co(III) demonstrated that $[ACCbs]^+$ is more labile than $[ACSYCbs]^+$ and the second-order rate constant k_{II} is between 4.6 (at 5 °C) and 2.6 (at 35 °C) times larger.[7] There is therefore a significant increase in the inertness of Co(III) consequent on a decrease in the extent of conjugation of the corrin macrocycle. Whilst k_{II} values for the reaction of $[AC(10–NH_2)Cbs]^+$, $[ACCbs]^+$ and $[AC(10–NO_2)Cbs]^+$ and at 25°C are not strikingly different (2.5×10^4 M^{-1} s^{-1}; 8.1×10^4 M^{-1} s^{-1}; 1.6×10^3 M^{-1} s^{-1}) this is because of masking by a compensation effect between $\Delta H^‡$ and $\Delta S^‡$ values.[13] Were all three reactions to have the same value of $\Delta S^‡$, the rate constants would have varied in the ratio 10^9:10^6:1 as the C10 substituent changed from NH_2 through H to NO_2.

One of the features of the corrin ligand is its rather small macrocyclic cavity. From a search of the Cambridge Structural Database[20] we find that the average diagonal N–N distance

across the cavity in all Co(III) corrins is 3.79(4) Å (*n* =128 compounds, 290 observations, 3.616 Å min, 3.975 Å max), significantly smaller than the 3.92(4) Å found for all Co(III) porphyrins (*n* = 242 compounds, 496 observations, 3.789 Å min, 4.313 Å max). This suggests that Co(III) is compressed in a corrin macrocycle and this is likely to significantly impact its chemistry.[21]

To evaluate what additional effect this might have on the chemistry of its axial coordination sites we have therefore prepared Co*α*,Co*β*-dicyano-5,6-dioxo-5,6-seco-heptamethylcob(III)yrinate, Figure 1C, [DC-5-seco-Cbs]) as originally reported by Inhoffen[22] and subsequently by Kräutler.[23] Not only is the conjugated pathway of a normal corrin disrupted, but the C5–C6 bond has been cleaved and the equatorial ligand of Co(III) is no longer a macrocycle. We report equilibrium constants (as log *K* values) for substitution of H_2O in the aquacyano derivative, $[AC\text{-}5\text{-}seco\text{-}Cbs]^+$, by five anionic ligands, CN^-, SO_3^{2-}, NO_2^-, N_3^- and $S_2O_3^-$; the re-determined log *K* values for coordination of these ligands by $[ACCbs]^+$; and compare the kinetics of the substitution of H_2O by CN^- in $[AC\text{-}5\text{-}seco\text{-}Cbs]^+$ and $[ACCbs]^+$.

■ EXPERIMENTAL

Materials and methods. De-ionised water was produced by a Millipore DirectQ UV3 system and further purified using a Millipore MilliQ unit (18 MΩcm). All reagents used in this study were commercially available from Merck, Sigma-Aldrich or Saarchem and used without further purification. The measurement of pH was performed using either a Metrohm 780 pH meter with a Metrohm LL UnitrodePt 1000 glass electrode or an Ohaus Starter 3100 pH meter with an Ohaus ST310 electrode. Metrohm Ion analysis standard buffer solutions (pH 4.0, 7.0 and 9.0) were used to calibrate the electrode using a 3 buffer calibration an hour prior to use, at a temperature specific to the experiment being performed using a water-circulating bath.

UV-vis spectra were recorded in 1.00 cm pathlength quartz cuvettes on a Cary 300 BIO UV-vis spectrophotometer, fitted with a Cary Dual Cell Peltier system set at the appropriate temperature. Curve-fitting using standard non-linear least squares methods was performed with SigmaPlot.[24] The substitution of H_2O in $[AC\text{-}5\text{-}seco\text{-}Cbs]^+$ proceeded sufficiently slowly for the reaction kinetics to be measured using a conventional UV-vis spectrophotometer.

HPLC analyses were performed using a reverse phase C18 column (Supelco Analytical 5 µm, 250.0 × 4.6 mm) and a Supelco guard column using a Dionex UltiMate 3000 pump and a photodiode array detector with Chromeleon Chromatographic Management System software.[25] Isocratic elution was with 1:1 acetonitrile:water. Gradient elution (25 mM ammonium phosphate, pH 3; MeOH) was performed at a flow rate of 1 mL min^{-1} from 98% buffer linearly to 35% buffer over 3 minutes, maintained to t = 8 min, then back linearly to 98% buffer by t = 13 min, and maintained to t = 15 min.

Electrospray ionization (ESI) mass spectra were recorded on a Waters Synapt G2 Mass spectrometer. The sample was prepared in acetonitrile and exposed to an ESI source with a cone voltage of 15 V. Infrared spectra were recorded on a Bruker Tensor 27 spectrophotometer fitted with a diamond anvil cell. One-dimensional ^{1}H and ^{13}C, two-dimensional proton homonuclear (COSY, TOCSY, and ROESY) and two-dimensional heteronuclear (^{1}H–^{13}C) (HSQC, HMBC) nuclear magnetic resonance measurements were recorded on a Bruker Avance 500 III Ultra Shield Plus spectrometer operating at 500 MHz equipped with a 5.0 mm PABBO broadband probe. All NMR data was collected at 25.0 °C in 5.0 mm NMR tubes on 20.0 mg samples dissolved in 600.0 µl CD_3OD (99.8% deuteration). Chemical shifts on the δ scale (parts per million (ppm)) are reported relative to the signal obtained from deuterated methanol taken at δ 49.00 ppm for ^{13}C NMR or at δ 3.31 ppm for ^{1}H NMR.

Synthesis of Coα,Coβ-dicyano-5,6-dioxo-5,6-seco-heptamethylcob(III)yrinate ([DC-5-seco-Cbs]). The synthesis of [DC-5-seco-Cbs] from [DCCbs] by photo-oxygenolysis was adapted from the procedure reported by Kräutler.[23] Dicyanocobyrinic acid heptamethyl ester (dicyanocobester, [DCCbs], Sigma-Aldrich; 354 mg, 324 µmol) and methylene blue (0.33 mg, 1.02 µmol) were dissolved in deuterated methanol (CH_3OD) (9.3 ml). This solution was placed in a 45 × 5 × 40 mm rectangular glass photolysis cell fitted with two 8 mm diameter ground glass joints. These were fitted with rubber septa and inlet and outlet needles that allowed for a slow, steady stream of oxygen to bubble through the solution. The photolysis cell was immersed in a glass-walled water bath maintained at 15.0 °C which itself was immersed into a double-walled cylinder with a 3 mm gap between its walls. Into this cavity was placed a 0.5 M sodium dichromate solution to filter out radiation with $\lambda < 550$ nm. The cell was then illuminated with a 15 V, 150 W halogen lamp placed 5 cm away from the cell. The progress of the reaction was monitored by recording the UV-vis spectrum of aliquots withdrawn at 45 minute intervals against a reference solution of methylene blue in deuterated

methanol. After 135 minutes of irradiation, the photolysis was discontinued, the contents were transferred to a round bottom flask and the solvent was evaporated using a rotary evaporator set at 40˚C.

Isolation of [DC-5-seco-Cbs] from the [DCCbs] starting material, and [DC-15-seco-Cbs], which is also produced in the reaction, was partially achieved by flash chromatography on a 28.0 × 2.0 cm silica gel column (30.0 g) containing sodium cyanide (0.75 g) using EtOAc:MeOH:toluene (10:0.25:0.25) as eluent. This was followed by preparative thin layer chromatography (PTLC) on 200 × 200 mm, 2000 μm silica plates (Merck) using methyl acetate:benzene (4:1) as mobile phase. Separated bands were scraped off using a sharp blade and recovered from the silica by extraction with dichloromethane:methanol (10:1). The extractant was shaken with 20 mL aliquots of a $NaHCO_3$ solution containing 20 mg NaCN, the organic layer was separated, dried, and the solvent evaporated. [DC-5-seco-Cbs] was dissolved in a solution of dichloromethane (0.5 ml) and benzene (1.0 ml) and precipitated by adding the solution to cyclohexane (25.0 ml). The precipitate was centrifuged (4000 rpm, 10 min) and dried on a high-vacuum line.

Synthesis of aquacyano-5-seco-cobester ([AC-5-seco-Cbs]$^+$). The removal of one of the CN^- ligands from [DC-5-seco-Cbs] to produce [AC-5-seco-Cbs]$^+$ was by a modification of a procedure developed by Palet *et al*.[26] for the removal of axially coordinated cyanide from dicyanoheptapropylcobyrinate and dicyanocobalt(III)heptamethylcobyrinate. [DC-5-seco-Cbs] was dissolved in methanol (10.0 ml) and transferred to a round bottom flask to which glacial acetic acid was added to give a 10% (v/v) acetic acid solution while stirring. The solvent was then evaporated using a rotary evaporator at 40 ˚C. The residue was re-dissolved in the 10% methanol-acetic acid solution and the procedure was repeated typically between 4 and 6 times until there was no further change in the UV-vis spectrum. The product, [AC-5-seco-Cbs]$^+$, was dried on a high-vacuum line.

Acid dissociation constant of [AC-5-seco-Cbs]$^+$ was determined spectrophotometrically using a method previously described.[27] The compound was dissolved in methanol (100.0 μl) and diffused into an aqueous multi-component buffer (35 mL) consisting of 1 mM solutions of potassium hydrogen phthalate (KHP), 2-(*N*-morpholino)ethanesulfonic acid (MES), 3-(*N*-morpholino)propanesulfonic acid (MOPS), 2-amino-2-hydroxymethyl-propane-1,3-diol (TRIS)/HCl and 2-(cyclohexylamino)ethanesulfonic acid (CHES) together with Na_2SO_4 to adjust the total ionic strength of the buffer system to 0.1 M. The solution was transferred to a stirred 50 mL

jacketed glass cell connected to a water-circulating bath set to the appropriate temperature. The pH of the sample was adjusted from pH 5.0 to 11.5 by diffusing negligible volumes of 8 M NaOH with a drawn-out capillary tube. The sample was circulated through a 1 cm flow cell (Hellma) housed in the compartment of a Cary 3E UV-vis spectrophotometer using a Watson-Marlow 101U peristaltic pump. The spectrum was recorded at intervals of approximately 0.5 pH units. The changes in the absorbance spectrum as a function of pH at multiple wavelengths on either side of the observed isosbestic points were fitted to eqn. 1 as objective function with A_0, A_1 and K_a as variables, where A_λ is the absorbance measurement at the monitored wavelength, λ; A_0 and A_1 are the initial and final absorbance measurements respectively at the monitored wavelength; and K_a is the equilibrium constant for ionization of coordinated H_2O. The acid dissociation constant, reported as pK_a, was found from a weighted average of the results obtained at the wavelengths monitored.

$$A_\lambda = \left(\frac{A_0 10^{-pH} + A_1 10^{-K_a}}{10^{-pH} + 10^{-K_a}} \right) \quad (1)$$

Ligand substitution reactions: equilibrium constants. Values of equilibrium constants (as log K values, eqn. 2, where N_4 represents the corrin) for the substitution of axially coordinated water in $[AC\text{-}5\text{-}seco\text{-}Cbs]^+$ by L = CN^-, SO_3^{2-}, NO_2^-, $S_2O_3^{2-}$ and N_3^-, eqn. 2, were determined spectrophotometrically.

$$[CN\text{–}Co(N_4)\text{–}OH_2] + L \quad \overset{K}{\rightleftharpoons} \quad [CN\text{–}Co(N_4)\text{–}L] + H_2O \quad (2)$$

The spectrophotometric titrations were performed by adding between 10 and 20 aliquots of a stock solution of the relevant ligand to a buffered solution (μ = 0.1 M, Na_2SO_4) of $[ACCbs]^+$ or $[AC\text{-}5\text{-}seco\text{-}Cbs]^+$ (2.3 mL) contained in a 1.00 cm pathlength quartz cuvette housed in the thermostatted cell block of the spectrophotometer. The spectrum was recorded between 800 and 300 nm and corrected for dilution. Titrations of $[ACCbs]^+$ with N_3^- and $S_2O_3^{2-}$ were performed at pH 6 (MES); titrations with NO_2^-, CN^- and SO_3^{2-} at pH 7 (MOPS). Titrations of $[AC\text{-}5\text{-}seco\text{-}Cbs]^+$ with N_3^- and $S_2O_3^{2-}$ were performed at pH 6 (MES); with NO_2^- and SO_3^{2-} at pH 7 (MOPS); and with CN^- and SO_3^{2-} at pH 9 (CHES). Ligand stock solutions were prepared by dissolving the ligand in the appropriate buffer, and the pH was adjusted to the required pH by the addition of NaOH or H_2SO_4.

Aquacyano derivatives of cobalt corrins exist as inter-converting mixtures of *α*-cyano, *β*-aqua and *α*-aqua, *β*-cyano diastereomers through formation of dicyano and diaqua intermediates.[7, 9, 28-30] The isomers are expected to have a very similar equilibrium constant for the substitution of axially coordinated water by an exogenous ligand, L,[7] but there will be a wavelength dependence of log *K*, dependent on the relative extinction coefficients of the diastereomers at the monitoring wavelengths.[31] To average out this effect, log *K* was determined at every 1 nm in ranges on either side of the isosbestic points which exhibited a large change in absorbance. Typically between 30 and 60 wavelengths were monitored and the data analyzed.

When log *K* is relatively small (log *K* < 4), it is reasonable to assume that the free ligand concentration is approximately the total concentration of ligand added, i.e., $[L]_{free} \approx [L]_{total}$, and the absorbance data at each monitored wavelength were fitted to a simple binding isotherm (eqn. 3) where A_0 and A_1 are the absorbance values corresponding to 0 and 100% cobalt-ligand complex formation respectively at the monitoring wavelength.

$$A_\lambda = \frac{A_0 + A_1 K[L]}{1 + K[L]} \tag{3}$$

If log *K* > 4 the assumption that $[L]_{free} \approx [L]_{total}$ is clearly invalid, as a significant fraction of the total ligand added will be complexed to the metal ion. It is therefore necessary to replace [L] in eqn. 3 with an explicit expression for $[L]_{free}$ (eqn. 4) where $[M]_{total}$ is the metal ion concentraion.[32]

$$[L]_{free} = \frac{-a_2 \pm \sqrt{a_2^2 - 4a_1a_3}}{2a_1}$$
$$a_1 = K; \quad a_2 = 1 + K[M]_{total} - K[L]_{total}; \quad a_3 = -[L]_{total} \tag{4}$$

Assuming that log *K* for substitution of OH^- is insignificantly small compared to that for substitution of H_2O (as is generally found in Co(III) corrin and porphyrin complexes[4, 7, 9, 10, 33-36], and verified here by determining log *K* as a function of pH for coordination of SO_3^{2-} (see below), the observed log *K* values were corrected for the pK_a of [AC-5-seco-Cbs]$^+$, pK_{Co}, to obtain pH-independent log *K* values using eqn. 5; this equation also has a correction for the

protonation of the ligand, pK_L, assuming that the affinity of Co(III) for the protonated ligand is insignificantly low. Values of pK_L were obtained from Martell and Smith.[37]

$$K = K_{obs}\left(1+10^{pH-pK_{Co}}\right)\left(1+10^{pK_L-pH}\right) \quad (5)$$

Although values of log K for coordination of CN^-, SO_3^{2-}, NO_2^-, N_3^- and $S_2O_3^{2-}$ by $[ACCbs]^+$ are available,[7] these were determined again to verify their reproducibility and to ensure that the values were obtained under the same experimental conditions as the values determined for [AC-5-seco-Cbs]$^+$. An identical procedure as described above for [AC-5-seco-Cbs]$^+$ was used for $[ACCbs]^+$, except for titrations with CN^- and SO_3^{2-}; in these cases log K values were determined by competition with N_3^- under conditions where formation of $[(N_3)(CN)ACCbs]$ was > 99%. Log K values were then determined from the measured log K for substitution of N_3^- by CN^- or SO_3^{2-}, and log K for substitution of H_2O by N_3^-.

Ligand substitution reactions: kinetics. The kinetics for the substitution of H_2O by CN^- were investigated using 50 μM solutions of [AC-5-seco-Cbs]$^+$ in 0.1 M CAPS, pH 10.5 to which was added an aliquot of a solution of KCN in the same buffer. The reaction was monitored at 400 nm. Since the absorbance *vs.* time trace was clearly biphasic (see below) the data were fitted to a double exponential function (eqn. 6). In Eq. 6, k_f^{obs} and k_s^{obs} are the pseudo first-order rate constants for the faster and slower phases, respectively, A_∞ is the absorbance at the end of the reaction, $|A_0 - A_1|$ the absorbance change associated with the faster phase and $|A_1 - A_\infty|$ that associated with the slower phase.

$$A_\lambda = A_\infty + (A_0 - A_1)e^{-k_f^{obs}t} + (A_1 - A_\infty)e^{-k_s^{obs}t} \quad (6)$$

The observed first order rate constants were corrected for the pK_a of [AC-5-seco-Cbs]$^+$ (the hydroxo complexes of Co(III) corrins are inert to substitution[7, 38-40]) to obtain values of k_i (i = f,s). Since pK_{HCN} = 9.04,[37] cyanide is > 95% present as CN^-. HCN reacts an order of magnitude slower than CN^- with aquacobalamin (vitamin B_{12a})[38, 41] and its concentration is negligible under our conditions; hence the observed reaction is virtually exclusively due to displacement of H_2O by CN^-. The second order rate constant, k_i^{II} (i = f, s), was then obtained from the slope of a plot of k_i against $[CN^-]$. We have already reported the kinetics for the reaction of $[ACCbs]^+$ with CN^- determined under identical conditions.[7]

DFT calculations. Density functional theory (DFT) calculations were performed using the BP86 functional[41, 42] with a 6-311G(d,p) basis set applied to all atoms as implemented in the Gaussian 09[43] suite of programs. An empirical correction was incorporated to this functional to account for the D3 version of Grimme's dispersion with the original D3 damping function.[44] [DCCbs] was modelled starting from its crystal structure[45] but all corrin side chains were truncated to ethyl groups for computational efficiency. The starting point for the model of [DC-5-seco-Cbs] was the energy-minimized structure of [DCCbs], which was edited to incorporate the oxidation at C5 and C6, and the cleavage of the C5–C6 bond. This was then initially energy-minimized using a 3-21G basis set before changing the basis set to 6-311G(d,p). All geometry optimizations were followed by a frequency calculation to ensure that the structures were completely minimized to a stable ground state. The topological properties of the electron density of the modelled structures were explored by generating wavefunction files with Gaussian 09 and analysed using Bader's Quantum Theory of Atoms in Molecules (QTAIM)[46, 47] as implemented in AIMAll.[48]

■ RESULTS

Synthesis and characterization of [DC-5-seco-Cbs]. As the oxygenation of [DCCbs] proceeded (complete in 135 min under our reaction conditions), the intensity of the α, β and γ bands of [DCCbs] decreased and a broad band at 480 nm with a shoulder at 540 nm emerged. The reaction mixture is likely to consist of unreacted starting material, [DC-5-seco-Cbs] and the isomer, [DC-15-seco-Cbs], where cleavage occurs between C14 and C15.[23] This was confirmed by TLC (silica, EtOAc:MeOH:toluene 10:0.25:0.25 v/v: R_f = 0.31, [DCCbs], purple; 0.25, [DC-15-seco-Cbs], red; and 0.19, [DC-15-seco-Cbs], orange-red; baseline, orange-yellow). After photo-oxidation, the contents of the photolysis cell were placed on a rotary evaporator and all solvent was evaporated (40 °C). The residue was columned (see Experimental) on silica gel. Three broad bands (purple, red, orange-red) emerged. TLC showed that the purple band consisted mostly of unreacted [DCCbs]; the red fractions contained mostly [DC-15-seco-Cbs]; and the orange fraction mostly [DC-5-seco-Cbs]. HPLC (isocratic elution, see above) was used to confirm the TLC analyses at regular intervals; [DC-5-seco-Cbs] elutes at 6.8 min, [DCCbs] at 7.9 min, and what is assumed to be [DC-15-seco-Cbs][23] at 9.0 min. The final purification of the fractions containing predominantly [DC-5-seco-Cbs] was by PTLC (see Experimental). HPLC analysis showed a >98% purity with a small trace (<1%) [DCCbs]. The yield was 42%. Using a similar

procedure, we were unable to completely purify [DC-15-seco-Cbs] (>20% contamination by [DCCbs]).

The UV-vis spectrum of [DC-5-seco-Cbs] (Figure S1 of the Supporting Information) shows the γ band at 326 nm, a shoulder at 365 nm and a broad band at 481 nm with a shoulder at 550 nm. The spectrum is identical to that reported by Kräutler.[23]

The molecular ion peak (*m*/z = 1120.45; 1120.65 calc.) was detected as a low intensity peak in the positive mode ESI spectrum. The most prominent peak was a fragment which showed loss of one CN^- ligand (*m*/*z* = 1094.4, $[M–CN]^+$, calc. 1095.1); $[M+Na]^+$ was observed at 1143.4 (6%, calc. 1144.1); $[M–2CN+H]^+$ at 1068.4 (8%, calc. 1070.1); $[M–CN+H]^{2+}$ at 545.4 (18%, calc. 548.1); and $[M–2CN]^{2+}$ at 535.4 (10%, calc. 534.6). In the negative mode ESI mass spectrum $[M–H]^-$ occurred at 1119.4 (calc. 1120.1).

We found ν_{CN} at 2124 cm^{-1} (*cf.* 2123 and 2138 cm^{-1} for [DCCbs] and [DCSYCbs], respectively[6]). Cyanide is an unusual ligand in that the frequency of the stretch *increases* on coordination to the cobalt ion, compared to free cyanide ligand (2078 or 2080 cm^{-1}).[6] We interpreted the difference in ν_{CN} between [DCCbs] and [DCSYbs] as being due to a stronger *cis* interaction between cobalt and the corrin macrocycle in the former because of its more extensive π-electron density. As a result, the frequency of coordinated cyanide shifts to a lower frequency, and is closer to the stretching frequency of free cyanide. If this interpretation is correct, the value of 2124 cm^{-1} for [DC-5seco-Cbs] is surprising.

The ^1H and ^{13}C NMR assignments were made using the strategy described by Brown[49] and which we applied to assigning the NMR spectra of [DCCbs] and [DCSYCbs].[6] The data are listed in Tables S1 and S2 of the Supporting Information and agree well with the data reported by Inhoffen.[22] The signals corresponding to the axial cyanide ligands were detected at 131.79 and 135.43 ppm. By analogy with our assignments of [DCSYCbs], the signal at 131.79 ppm is tentatively attributed to the *β* cyanide and that at 135.43 ppm to the *α* cyanide. As expected, there are major changes in the ^{13}C resonances of C4, C5, C6 and C35 (see Figure 1 for numbering) of [DC-5-seco-Cbs] compared to those of [DCSYCbs] and especially those of [DCCbs], associated with the oxidation of C5 and C6.

Characterization of [AC-5-seco-Cbs]$^+$. The loss of one of the cyanide ligands from [DC-5-seco-Cbs] produces what is assumed to be a mixture of the two diastereomers [*α*-CN,*β*-H_2O-5-seco-Cbs]$^+$ and [*α*-H_2O,*β*-CN-5-seco-Cbs]$^+$, in quantitative yield. The two principal transitions in the UV-vis spectrum are blue-shifted (Figure S2 of the Supporting Information). Addition of KCN restores the spectrum of [DC-5-seco-Cbs]. HPLC (gradient elution, see Experimental) shows a rather broad major peak with a retention time of 8.32 min

(assumed to be the unresolved diastereomers), a minor peak with a retention time of 9.2 min due to [DC-5-seco-Cbs] and a poorly resolved, minor broad peak with a retention time of *c.* 7.8 min attributed to $[(H_2O)_2$-5-seco-Cbs$]^{2+}$. The presence of [DC-5-seco-Cbs] and $[(H_2O)_2$-5-seco-Cbs$]^{2+}$ is probably due to the interconversion of the two diastereomers of [AC-5-seco-Cbs]$^{2+}$ via intermediacy of [DC-5-seco-Cbs] and $[(H_2O)_2$-5-seco-Cbs$]^{2+}$.

The ν_{CN} is found at 2087 cm^{-1}, quite close to the free cyanide value of 2078 or 2080 cm^{-1},[6] and suggesting a rather ionic Co–CN bond. DFT calculations support this (see below). The molecular ion peak was detected at *m/z* = 1112 in the positive mode ESI spectrum. Peaks due to $(M–H_2O)^+$ (1094.4) and $(M–H_2O–CN+H)^+$ (1068.3) confirm that the procedure employed resulted in the loss of a single $CN^–$ ligand. There is further proof for this. [AC-5-seco-Cbs]$^+$ is capable of binding one ligand (see below); for example, Hill plots shows that it binds 1.06 ± 0.05 $CN^–$ and 1.08 ± 0.08 $N_3^–$. After binding of one $CN^–$, a process that is typically complete when $[CN^–] \leq 50$ mM, there were no further significant spectroscopic changes up to $[CN^–] = 0.25$ M, confirming the availability of a single exchangeable ligand in [AC-5-seco-Cbs]$^+$.

The pK_a of [AC-5-seco-Cbs]$^+$ and [ACCbs]$^+$. There are small absorbance changes in the spectrum of [AC-5-seco-Cbs]$^+$ with pH (Figure S3 of the Supporting Information). As the pH increases the position of the visible band undergoes a red shift from 452 nm to 462 nm and increases marginally in intensity with isosbestic points at 340, 398 and 550 nm. The absorbance changes at one nm intervals between 370 and 380 nm, between 460 and 500 nm, and between 580 and 600 nm were fitted to eqn. 1. The fits were quite poor (Figure S4 of the Supporting Information) because of the small absorbance changes, and because, especially at pH > 10, the absorbance readings were not stable. We attribute this to hydrolysis of the ester side chains, as found for [ACCbs]$^+$.

The pK_a was determined by taking a weighted average of the results for all the wavelengths monitored, with the weighting taken as the reciprocal of the relative percentage error. The titrations were performed at four temperatures between 15 ^oC and 40 ^oC. The reproducibility between batches of [AC-5-seco-Cbs]$^+$ was checked by repeating the titration at 25 ^oC on two different batches.

Table 1. pK_a values of [AC-5-seco-Cbs]$^+$ determined as a function of temperature by titration with $OH^–$

T **(oC)**	**pK_a**	**Err in pK_a**
15	6.91	0.13
25[a]	7.17	0.17
25[b]	7.12	0.08
30	7.59	0.08
40	8.11	0.14

[a,b] From different batches of [AC-5-seco-Cbs]$^+$

The results are summarized in Table 1.

A plot of ln K_a against T^{-1} for the data in Table 1 is shown in Figure S5 of the Supporting Information. From the slope and intercept, respectively, we found ΔH = –88 ± 17 kJ mol^{-1} and ΔS = –434 ± 56 J K^{-1} mol^{-1}; hence pK_a = 7.28 at 25 ^{o}C for ionization of H_2O coordinated to Co(III) in [AC-5-seco-Cbs]$^+$. The thermodynamic parameters were used to determine the fraction of [AC-5-seco-Cbs]$^+$ during titrations with other ligands. The pK_a is significantly lower than a value of c. 11 we estimated previously for both [ACCbs]$^+$ and [ACSYCbs]$^+$.[6]

Using HPLC we found that changing the pH of a solution of [AC-5-seco-Cbs]$^+$ to pH 13 at room temperature with NaOH results in formation of a range of products that elute very quickly from the column (retention times from 1.9 to 4.2, *cf.* 8.3 min for [AC-5-seco-Cbs]$^+$). The area of the peak due to [AC-5-seco-Cbs]$^+$ decreases by about 50% after 1 hour under these conditions, and virtually disappears to be replaced by a single peak with a retention time of 1.9 min after 2 hours. This strongly suggests that the ester side chains of [AC-seco-Cbs]$^+$ (like those of both [DCCbs] and [DCSYCbs]) are prone to hydrolysis, and helps to explain the unstable absorbance readings observed during the determination of the pK_a. Nevertheless, it is certain that the pK_a for coordinated H_2O in [AC-5-seco-Cbs]$^+$ is significantly lower than that in [ACCbs]$^+$ and [ACSYCbs]$^+$

We re-determined the pK_a of [ACCbs]$^+$ under the same conditions as used for [AC-5-seco-Cbs]$^+$ (25 ^{o}C; 1 mM solutions of KHP, MES, MOPS, TRIS and CHES; μ = 0.1 M, Na_2SO_4). As previously reported,[6] the determination of the pK_a of [ACCbs]$^+$ is difficult. It is significantly higher than the pK_a of H_2O in either aquacobalamin (B_{12a}, [H_2OCbl]$^+$), 7.76 (i.e., H_2O trans to dmbzm),[50] or diaquacobinamide, 5.9 (H_2O trans to H_2O)[51], and, estimated at >11[6] or ca. 10.8,[52] similar to the pK_a of aquahydroxocobinamide, 10.3 (H_2O trans to OH^-),[51] and aquacyanocobinamide, 11.0[53, 54] (H_2O trans to CN^-). The difficulty arises because of hydrolysis of one or more of the methyl ester side-chains,[55, 56] a reaction whose rate increases with pH and with temperature.[6] Figure S6 of the Supporting Information shows the spectral changes associated with the titration of [ACCbs]$^+$ with OH^- at 10 ^{o}C where the rate of hydrolysis of the side changes is expected to be relatively slow. As pH increases, the γ band decreases in intensity and moves to longer wavelengths; the $\alpha\beta$ bands also move to the red. These spectral changes are very similar to those seen on deprotonation of Co(III)-bound H_2O in all aquaCo(III) corrins.[50, 51, 53, 54] However, isosbestic points are not well defined. Moreover at pH > ca. 11, the spectra change gradually with time and the $\alpha\beta$ bands move pronouncedly to longer wavelength. These effects are more marked as temperature is increased and become quite rapid at pH > 10.5 and T > 35 ^{o}C.

Figures S7a and S7b show plots of the change in absorbance of $[ACCbs]^+$ as a function of pH at 560 nm. The fits to the experimental data are quite poor with $0.969 < r^2 < 0.989$ which is not surprising given the lack of well-defined isosbestic points. The value of the pK_a is heavily dependent on how far along the titration reliable data are obtained and also on the monitoring wavelength.

The value of the pK_a of $[ACCbs]^+$ at each temperature was obtained by fitting Eq.1 to between 30 and 40 wavelengths chosen from the 340–355, 450–470 and 520–580 nm ranges in the spectrum in order to average out the wavelength dependence noted when comparing the results in Figures S7a and S7b. Data used for fitting were typically confined to pH < 11.2 because of the unreliability of the absorbance readings at higher pH values. Given these constraints, it is not surprising that the value of the pK_a for ionization of H_2O as a function of temperature between 10 ^oC and 40 ^oC shows no trend with temperature and become less and less reliable at the higher temperatures on the temperature range studied (Table 2). We resorted to averaging the values obtained between 10 ^oC and 30 ^oC (pK_a = 9.8 ± 0.3) for all calculations in this work. We endeavored where possible to work in pH ranges well removed from this (i.e., where $[ACCbs]^+$ is predominantly in the aqua form) in order to minimize errors that arise from the uncertainty in the value of the pK_a.

Table 2. Dependence of the pK_a of coordinated H_2O in $[ACCbs]^+$ as a function of temperature

Temp /^oC	pK_a	Error
10	9.9	0.1
15	10.3	0.2
20	9.5	0.3
25	10.2	0.2
30	9.9	0.3
35	9.1	0.3
40	9.0	0.3

The dependence of an equilibrium constant on pH. The surprisingly low value of the pK_a of $[AC\text{-}5\text{-}seco\text{-}Cbs]^+$ prompted us to verify it by determining the pH dependence of the equilibrium constant for the substitution of H_2O by an exogenous ligand. The hydroxo complexes of Co(III) macrocycles are generally inert to substitution and few ligands will compete with OH^- for the metal ion;[7, 38-40] hence log *K* (eqn. 2) should decrease with increasing pH. Thus, a ligand is required for which log *K* is relatively high as the value will fall with increasing pH, making it difficult to obtain reliable results (this eliminated NO_2^- and N_3^-) and the pK_a of the ligand itself must be below the pH range of interest (which eliminated CN^-); we therefore settled on SO_3^{2-} which has log *K* = 5.00 and 3.06 for coordination by $[ACCbs]^+$ and $[ACSYCbs]^+$, respectively,[7] and a pK_a (6.95[37]) reasonably below the pH range of interest (7 – 9.5). In this regard, both NO_2^- and N_3^- would have been preferable (pK_a =

3.04 and 4.6, respectively) but log *K* values were an order of magnitude lower than for SO_3^{2-} (see below).

The value of log *K* was determined by fitting eqn. 3 to the absorbance changes at every 1 nm between 370-410 nm and 450-500 nm of titration of a solution of [AC-5-seco-Cbs]$^+$ at the appropriate pH with a stock solution of Na_2SO_3 at the same pH. Figure 2 shows the spectroscopic changes observed during a titration at pH 8.90.

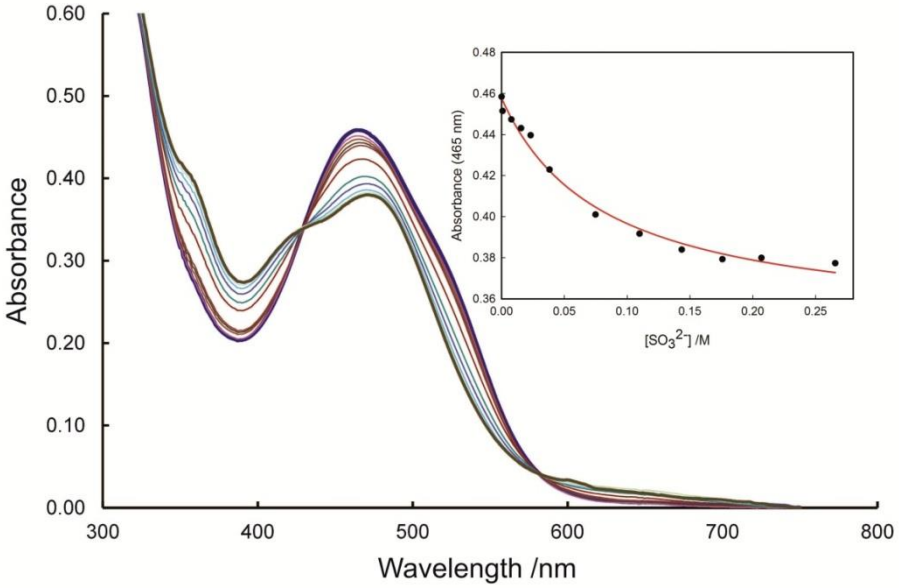

Figure 2. Titration of [AC-5-seco-Cbs]$^+$ with SO_3^{2-} at pH 8.90, 25 ^{o}C. The insert shows a fit of eqn. 3 to the absorbance changes observed at 465 nm.

The results are given in Table 3. Values above pH 9 were unreliable because formation of the product was incomplete even the highest concentrations of SO_3^{2-} used (ca. 0.4 M). The values of log *K* decrease with increasing pH. Correcting for the pK_a of [AC-5-seco-Cbs]$^+$ (eqn. 5) gives a value that, within experimental error, is independent of pH, confirming the reliability of the value of 7.28 at 25 ^{o}C for the pK_a of [AC-5-seco-Cbs]$^+$.

Table 3. The pH Dependence of Equilibrium Constants for the Substitution of Coordinated H_2O in [AC-5-seco-Cbs]$^+$ (25 ^{o}C) by SO_3^{2-}

Ligand	pH	log K_{obs}	log K [a]
SO_3^{2-}	7.17	3.45(3)	3.70(3)
	7.73	3.01(11)	3.58(11)
	8.09	3.1(2)	3.9(2)
	8.55	2.47(10)	3.76 (10)
	9.06	1.81(5)	3.60(5)
Average			3.4(1)[b]

[a]Corrected for the pK_a = 7.28 of [AC-5-seco-

Equilibrium constants. The value of log *K* was determined as a function of temperature (usually between 10 ^{o}C and 40 ^{o}C, but in some cases reliable values could not be obtained at

10 ^{o}C) at a single pH, and a pH-independent value obtained by applying eqn. 5. The data were fitted to eqn. 3, except for CN^- displacement of azide from azidocyanocobester, which was fitted to eqn. 4. Values of ΔH and ΔS were obtained from the slope and intercept, respectively of a plot of ln K against T^{-1}. Examples are shown in Figures S8A and S8B of the Supporting Information for the coordination of CN^- by $[ACCbs]^+$ and $[AC\text{-}5\text{-}seco\text{-}Cbs]^+$, respectively. Equilibrium constants and values of ΔH and ΔS obtained are summarized in Table 4, as are values previously obtained for $[ACCbs]^+$ and $[ACSYCbs]^+$.

Kinetics of substitution of H_2O by CN^-. To assess the effect cleavage of the corrin ring has on the lability of Co(III), the kinetics of the substitution of H_2O in $[AC\text{-}5\text{-}secon\text{-}Cbs]^+$ by CN^- were determined between 25 ^{o}C and 40 ^{o}C under pseudo first order conditions ($[CN^-]$ was varied between 0.2 M and 0.02 M at 25 ^{o}C and between 0.15 M and 0.015 M at 30 ^{o}C, 35 ^{o}C and 40 ^{o}C; corrin concentration ≈ 50 μM). The spectroscopic changes monitored, but now as a function of time, were those observed during the determination of log K for coordination of CN^- by $[AC\text{-}5\text{-}seco\text{-}Cbs]^+$ (Figure S9A).

As found with both $[ACCbs]^+$ and $[ACSYCbs]^+$ in aqueous solution,[7] and more recently in 50% isopropanol with $[AC\text{-}(10\text{-}X)Cbs]^+$ in which X, the substituent at the C10 position of corrin, is NH_2, H or NO_2,[13] and unsurprising given that there is HPLC evidence (see above) that solutions of $[AC\text{-}5\text{-}seco\text{-}Cbs]^+$ contain both [DC-5-seco-Cbs] and $[(H_2O)\text{-}5\text{-}seco\text{-}cobester]^{2+}$, the reaction is biphasic (see Figure S10 of the Supporting Information for an example).

By analogy with $[ACCbs]^{2+}$ and $[ACSYCbs]^+$, the faster phase is attributed to substitution of H_2O by CN^- *trans* to CN^-, and the slower phase to reaction of the diaqua complex with CN^-, i.e., substitution of H_2O *trans* to H_2O, which is inevitably present in solution due to interchange between the two diastereomers (see above). The complete results are given in Table S3 of the Supporting Information. The rate constants were not very reproducible across the temperature range (25 ^{o}C – 40 ^{o}C) and cyanide concentration range (0.2 M – 0.015 M) so there is a considerable error (up to 50% in several cases) in the values obtained. Figure S11 of the Supporting Information gives an example of a plot of k_i against $[CN^-]$. It is peculiar that the intercept appears to be statistically different from zero, implying that the reverse rate constant, $k_{f,r}$ (for the dissociation of CN^- from [DCN-5-seco-Cbs]), is observable. The ratio of the $k_f^{II}/k_{f,r}$ varies between 10 and 20 across the temperature ranges studied; this is clearly incompatible with a log $K > 5$ (Table 4).

Table 4. Equilibrium Constants for the Substitution of Coordinated H_2O in $[ACCbs]^+$ and $[AC\text{-}5\text{-}seco\text{-}Cbs]^+$ by Some Anionic Ligands[a]

	$[ACCbs]^+$ [b]					$[AC\text{-}5\text{-}seco\text{-}Cbs]^+$				$[ACSYCbs]^+$ [b]		
ligand	T / °C	log K	ΔH / kJ mol^{-1}	ΔS / J K^{-1} mol^{-1}	log K^{25}	log K	ΔH / kJ mol^{-1}	ΔS / J K^{-1} mol^{-1}	log K^{25}	ΔH / kJ mol^{-1}	ΔS / J K^{-1} mol^{-1}	log K^{25}
CN^-	10	9.58(12)	–63(4)	–38(14)	9.05	6.11(06)	–93(5)	–209(18)	5.38	*–17(1)*	*80(5)*	*7.16*
	15	9.34(11)	*–23(2)*	*81(6)*	*8.26*	6.02(09)						
	20	9.20(06)				5.63(07)						
	25	9.08(13)				5.40(10)						
	30	8.9(2)				4.98(09)						
	35	8.55(12)				4.80(10)						
	40	8.50(17)				4.55(10)						
SO_3^{2-}	10	5.95(2)	10(2)	151(6)	6.13	4.7(2)	–83(10)	–205(33)	3.83	*59(1)*	*253(5)*	*2.88*
	15	6.02(9)	*50(3)*	*265(9)*	*5.08*	4.5(2)						
	20	6.06(2)				3.9(2)						
	25	6.11(5)				3.8(2)						
	30	6.14(4)				3.6(3)						
	35	6.13(3)				3.7(3)						
	40	6.14(5)				3.2(1)						
NO_2^-	10	3.20(3)	–21(3)	–11(10)	3.11	3.2(2)	–82(3)	–229(11)	2.40	*–22.9(4)*	*–32(2)*	*2.34*
	15	3.21(3)	*–6.6(9)*	*33(3)*	*2.88*	2.9(2)						
	20	3.15(2)				2.6(2)						
	25	3.12(1)				2.45(7)						
	30	3.00(1)				2.15(8)						
	35	2.97(1)				1.96(5)						
	40	2.84(2)				1.2(2)						
N_3^-	10	2.890(9)	–16(2)	0(6)	2.80		–44(5)	–91(15)	2.96	*–18.6(7)*	*–12(2)*	*2.63*
	15	2.88(8)	*–9.4(7)*	*18(3)*	*2.59*	3.1(2)						
	20	2.84(2)				3.03(6)						
	25	2.70(7)				2.90(3)						
	30	2.71(5)				2.81(3)						
	35	2.64(3)				2.65(2)						
	40	2.64(10)				2.45(8)						

	[ACCbs]$^{+}$ [b]					[AC-5-seco-Cbs]$^{+}$				[ACSYCbs]$^{+}$ [b]		
ligand	T / °C	log K	ΔH / kJ mol^{-1}	ΔS / J K^{-1} mol^{-1}	log K^{25}	log K	ΔH / kJ mol^{-1}	ΔS / J K^{-1} mol^{-1}	log K^{25}	ΔH / kJ mol^{-1}	ΔS / J K^{-1} mol^{-1}	log K^{25}
$S_2O_3^{2-}$	10		36(6)	134(19)	0.69	1.25(7)	32(9)	137(30)	1.55			*0.6(2)* [d]
	15	0.38(10)	*21(3)*	*80(10)*	*0.50*	1.59(12)						
	20	0.66(12)				1.32(13)						
	25	0.74(10)				1.6(2)						
	30	0.77(11)				1.79(13)						
	35	0.88(13)				1.59(6)						
	40	0.95(11)				1.96(6)						

[a]Corrected for the effect of pH (Eq. 5). [b]Values in italics from Chemaly *et al.* [7]. [d] From determination at a single temperature (25 °C).[7]

■ DISCUSSION

Co(III) corrinoids have a very high affinity for CN^-; for example, log *K* for coordination of CN^- by aquacobalamin (i.e., replacement of H_2O trans to 5,6-dimethylbenzimidazole) is 14.1[57], log *K* = 8 for coordination by aquacyanocobinamide[54] and 9.05 by $[ACCbs]^+$ (this work, H_2O trans to CN^- in both cases). Up to $[CN^-]$ = 0.25 M, $[AC\text{-}5\text{-}seco\text{-}Cbs]^+$ solutions show evidence of coordinating a single CN^-, and Hill plots for all ligands studied present with a ligand stoichiometry ≈ 1 (Figures S9 and S12 of the Supporting Information are examples). This helps to confirm the MS data that the compound with which we are dealing is indeed the aquacyano complex (and not the diaqua or aquahydroxo complex) and that the procedure used for removing one CN^- ligand does not in fact remove both.

We have suggested that the π electron system of the corrin and its small macrocyclic cavity are factors that are at least partially responsible for modifying the chemistry of Co(III) in the cobalt corrins.[1-13] This is clearly demonstrated by the effect cleavage of the corrin has on the pK_a of coordinated H_2O in $[AC\text{-}5\text{-}seco\text{-}Cbs]^+$ which has decreased from 9.8(3) to 7.28 on cleaving the corrin ring; coordinated H_2O in $[AC\text{-}5\text{-}seco\text{-}Cbs]^+$ is considerably more acidic than in $[ACCbs]^+$. Its ionization is a strongly exothermic process (ΔH = –88 ± 17 kJ mol^{-1}) moderated somewhat by a very negative ΔS = –434 ± 56 J K^{-1} mol^{-1}. The pK_a of H_2O in $[Co(H_2O)_6]^{3+}$ is 2.9.[58] It is also low in other simple Co(III) complexes, for example, 3.09 in $[Co(nta)(H_2O)(\mu\text{-}OH)(H_2O)(nta)Co]^-$ (nta = nitrilotriacetate);[59] 4.98 in $[Co(tn)_2(H_2O)_2]^{3+}$ (tn = 1,3-diaminopropane);[60] 5.6 in $[Co(cyclen)(H_2O)_2]^{3+}$ (cyclen = 1,4,7,11-tetraazacyclododecane),[61] and, with 5 N-donors in $[Co(NH_3)_5(H_2O)]^{3+}$, 6.22[62] or 6.36.[63] By comparison, the pK_a for a simple Co(II) complex, as in $[Co(H_2O)_6]^{2+}$, is much higher, at 9.7.[64] The deprotonation of H_2O coordinated to a metal ion is a function of the charge density on, and hence polarizing power of, the metal ion; Co(II) is of course far less polarizing than Co(III). A comparison of the pK_as of $[ACCbs]^+$ and $[AC\text{-}5\text{-}seco\text{-}Cbs]^+$ shows clearly that Co is much less polarizing and has a lower charge density in the former than in the latter. This suggests that the an integral corrin ligand confers on Co at least some measure of softer, Co(II)-like character; cleavage of the corrin restores the metal ion to much more Co(III)-like behavior.

Table 4 shows that log *K* values obtained in this study for coordination of CN^-, SO_3^{2-}, NO_2^-, N_3^- and $S_2O_3^-$ by $[ACCbs]^{2+}$ are somewhat lower than previously determined. The affinity of the metal for the ligands follow the same order previously found (*viz*., log *K* for $CN^- > SO_3^{2-} > NO_2^- > N_3^- > S_2O_3^-$) but reasons for the numerical differences are unclear. For the

purposes of discussion, we shall rely on the values obtained in this study, but there is a clear measure of uncertainty in the actual numerical value. However, this does not affect the broad trend, the establishment of which was the principal aim of this study.

In a previous report in which we compared the chemistry of Co(III) in $[ACCbs]^+$ and $[ACSYCbs]^+$,[7] we found that $[ACCbs]^+$ binds ligands with a softer donor atom, such as CN^- and SO_3^{2-}, more readily than $[ACSYCbs]^+$. By contrast, $[ACSYCbs]^+$ binds harder ligands (N_3^-) better, although the differences are small (Table 4). We concluded that interruption of the conjugation system results in a somewhat harder Co(III) center, and that this, in particular, discriminates against soft ligands. The log $K^{25^\circ C}$ values for coordination of CN^- clearly indicate that $[ACCbs]^+$ (9.05) has a far higher affinity for this ligand than $[ACSYCbs]^+$ (7.16) or $[AC\text{-}5\text{-}seco\text{-}Cbs]^+$ (5.38); however, $[AC\text{-}5\text{-}seco\text{-}Cbs]^+$ has a higher affinity for SO_3^{2-} (3.83) than $[ACSYCbs]^+$ (2.88), both much lower than $[ACCbs]^+$ (6.13). We can confidently conclude that Co(III) in the presence of an integral corrin equatorial ligand has a significantly higher affinity for the soft ligands CN^- and SO_3^{2-} than Co(III) in a corrin with an interrupted π conjugated system or Co(III) in a corrin which has been cleaved. This cannot be a simple matter of the nature of the donor atom because the affinity is reversed in the case of $S_2O_3^{2-}$ for which log $K^{25^\circ C}$ for $[AC\text{-}5\text{-}seco\text{-}Cbs]^+ > [ACCbs]^+ \approx [ACSYCbs]^+$ and must reflect the electronic property of the ligand as a whole.

Although NO_2^- is an ambident nucleophile, the vast majority of six-coordinate Co(III) NO_2^- complexes with four other N-donor ligands, i.e., $[L\text{–}Co^{III}(N_4)\text{–}(NO_2)]^{n+}$, have the ligand bonded in the nitro (N-bound) rather than the nitrito (O-bound) form. A search of the CSD produced 317 such nitro compounds, and only 6 nitrito compounds. Nitrocobalamin has been crystallized and its structure reported,[3, 65] and we are unaware of any reports of nitritocobalamin or allied structures (i.e., any nitrito-corrins, -corroles or -porphyrins). We can therefore conclude reasonably confidently that NO_2^- coordinates Co(III) in $[ACCbs]^+$, $[ACSYCbs]^+$ and $[AC\text{-}5\text{-}seco\text{-}Cbs]^+$ through N. $[ACCbs]^+$ has a somewhat larger affinity for this ligand (log $K^{25^\circ C} = 3.11$) than $[ACSYCbs]^+$ (2.63) or $[AC\text{-}5\text{-}seco\text{-}Cbs]^+$ (2.40). In the case of N_3^-, log $K^{25^\circ C}$ values are quite similar for all three Co(III) complexes. The pattern that emerges with $[AC\text{-}5\text{-}seco\text{-}Cbs]^+$ therefore confirms what we observed in our comparison of $[ACCbs]^+$ and $[ACSYCbs]^+$: interruption of the conjugation of the corrin, or its cleavage, significantly decreases the affinity of Co(III) for the softer ligands CN^-, SO_3^{2-} and, more marginally, NO_2^-.

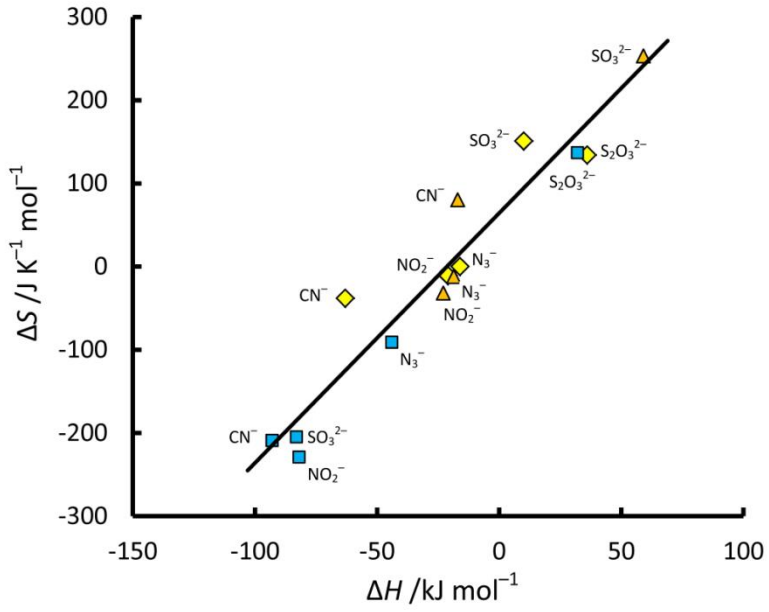

Figure 3. The compensation effect between Δ*H* and Δ*S* for coordination of anionic ligands by [ACCbs]$^+$ (◆), [AC-5-seco-Cbs]$^+$ (■) and [ACSYCbs]$^+$ (▲).

Values of log $K^{25^\circ C}$ do not reveal the full picture, however. We have pointed out elsewhere that there is a compensation effect between values of $\Delta H^{\ddagger}$ and $\Delta S^{\ddagger}$ for the kinetics of the ligand substitution reactions of Co(III) corrins, i.e., for wide range of ligands both activation parameters tend to decrease monotonically.[4, 40, 66-69] The effect is to level out the values of the second order rate constant for substitution of coordinated H_2O by a series of incoming ligands. We noted a similar compensation effect between values of Δ*H* and Δ*S* when we studied the thermodynamics of the substitution of coordinated H_2O in [ACCbs]$^+$ and [ACSYCbs]$^+$ by anionic[7] and by neutral[9] ligands. That trend is evident again in the results reported here (Figure 3). What is striking, and unexpected, are the very negative values for Δ*H* (with the exception of $S_2O_3^{2-}$), offset by Δ*S* values which are also large and negative, for coordination of these anionic ligands by [AC-5-seco-Cbs].

The macrocyclic cavity in corrin is smaller than, for example, in a porphyrin (see Introduction). If this is significant, then relief of steric compression might affect the behavior of Co(III). [AC-5-seco-Cbs]$^+$ has both the diminished π electron system of [ACSYCbs]$^+$ and a cleaved macrocyclic.[22, 23] Despite many attempts we have been unable to produce diffraction-quality crystals of [DC-5-seco-Cbs] (the aquacyano derivative is very unlikely to crystalize because of its existence as a mixture of two diastereomers). We therefore have had to rely on DFT modeling to assess the effect that cleavage of the corrin has on the structure of the complexes.

The BP86 functional is known to reproduce the structures and properties of cobalt corrinoids (such as the Co–C bond dissociation energy of adenosylcobalamin) quite well, especially if

dispersion is taken into account.[70-73] We verified this for [DCCbs] by comparing the geometry of the coordination sphere of the metal, and the corrin fold angle ((the angle between the mean planes through N21, C4, C5, C6, N22, C9 and C10, and N24, C16, C15, C14, N23, C11 and C10[74]) of the crystal structure of [DCCbs] (CSD refcode CODZAW10[45]) and of [DCSYCbs] (CSD refcode XEHDIZ[6]) with the geometry and fold angle of the DFT structures obtained with a 6-311++G(d,p) basis set and the BP86-D3, B3LYP, PBE0 and PBEPBE functionals. For reasons explained below, we also energy minimized the structures with BP86-D3/6-311G(d,p). The results are summarized in Table S4 of the Supporting Information, and confirm that the BP86-D3 functional best reproduces the XRD structures.

The model of [DCSYCbs] failed to converge using the 6-311++G(d,p) basis set even after several hundred iterations. We therefore resorted to using a smaller basis set, 6-311G(d,p) for the modelling. The DFT modelling reproduces the structures reasonably well, including the corrin fold angle. The smaller basis set actually reproduces the coordination sphere of [DCCbs] better (average relative percentage deviation of 0.42%) than the larger basis set (0.56%), but given that the average esd for bond lengths in the crystallographic structure is 0.01–0.03 Å, there is no statistically significant difference between the two models, and between the models and the crystallographic structure.

The coordination sphere geometry of [DCSYCbs] is quite well reproduced using BP86-D3/6-311G(d,p), although the Co–N(22) bond length is too long by 0.03 Å. The corrin fold angle of 15.6^{o} is somewhat over-estimated, at 19.6^{o}, in the modelled structure. The bond angles are reproduced to better than 2^{o}. The DFT-minimized structures of the models of [DCCbs], [DCSYCbs] and [DC-5-seco-Cbs] are shown in Figure S13 of the Supporting Information. An overlay of the XRD structures of [DCCbs] and [DCSYCbs] is shown in Figure S14.

Given the good agreement between the DFT and XRD structures of [DCCbs] and [DCSYCbs], we have some confidence in the structure of [DC-5-seco-Cbs], shown in Figure 4. A comparison of the coordination geometry of the BP86-D3/6-311G(d,p)-modelled structures of [DCCbs], [DCSYCbs] and [DC-5-seco-Cbs] is given in Table 5.

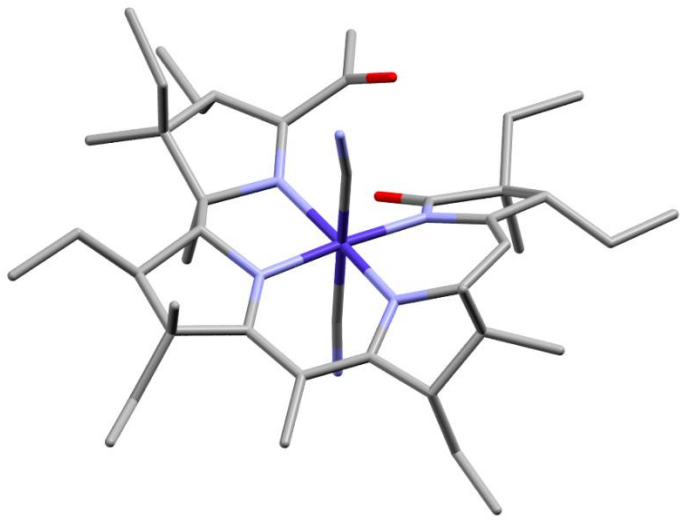

Figure 4. Predicted structure (BP86-D3/6-311G(d,p) of dicyano-5-seco-cobester. All ester side chains have been truncated to ethyl groups for the modelling.

The cleavage of the corrin does not unduly perturb the coordination sphere of the metal ion and the metal remains essentially octahedral. The Co–N bonds lengths to N(21) and N(22) increase significantly, while the Co–N(23) and Co–N(24) bond lengths do not change appreciably. The Co–CN bond length to CN coordinated on the α face is shorter by 0.008 Å, but the bond to the β-CN does not change. The very similar bond lengths to CN^- offer an explanation why ν_{CN} for [DC-5-seco-Cbs] (2124 cm^{-1}) is very similar to that for [DCCbs] itself (2123 cm^{-1}).

Table 5. Comparison of the coordination sphere geometry of BP86-D3/6-311G(d,p)-modelled structures of [DCCbs], [DCSYCbs] and [DC-5-seco-Cbs]

	DCCbs	**DCSYCbs**	**DC-5-seco-Cbs**
Bond /Å			
Co-CN(α)	1.925	1.920	1.917
Co-CN(β)	1.928	1.928	1.928
Co-N(21)	1.890	1.902	1.947
Co-N(22)	1.937	1.943	1.968
Co-N(23)	1.933	1.916	1.924
Co-N(24)	1.891	1.878	1.893
Angle /deg			
CN(α)-Co-CN(β)	176.8	173.3	174.4
N(21)-Co-N(23)	173.4	172.8	169.7
N(22)-Co-N(24)	173.2	168.4	174.5
Corrin fold angle	3.3	19.6	33.0

Compared to $[ACCbs]^+$, $[AC\text{-}5\text{-}seco\text{-}Cbs]^+$ has a significantly lower affinity for the CN^-, SO_3^{2-} and NO_2^-, but a higher affinity for N_3^- and $S_2O_3^{2-}$. This is similar to the trend seen between $[ACCbs]^+$ and $[ACSYCbs]^+$.

This trend clearly does not correlate with the hardness of the donor atom *per se* (S is the donor in both SO_3^{2-} and $S_2O_3^{2-}$, and N is the donor in both NO_2^- and in N_3^-). There appears to be a correlation with the position of these ligands in the spectrochemical series.[75, 76] For the ligands under discussion, the order in the spectrochemical series is $N_3^- < S_2O_3^{2-} < NO_2^- < SO_3^{2-} < CN^-$. The first two behave as π donors towards metal ions, and the last three, being much higher in the series, as π acceptor ligands. This therefore suggests that as the hardness of the metal increases and its electron density decreases in the order $[ACCbs]^+ > [ACSYCbs]^+ \approx [AC\text{-}5\text{-}seco\text{-}Cbs]^+$, so the thermodynamic stability of its complexes with the π acceptor ligands decreases; the metal becomes less capable of participating in M→L charge transfer. Conversely, the thermodynamic stability of the complexes with the π donor ligands increases as the metal ion becomes more Co(III)-like, and is more capable of accepting electron density from the ligand.

In order to gain further insight and to test this explanation, we used DFT modeling with BP86-D3/6-311G(d,p) to determine structures of $[\alpha\text{-}CN^-,\beta\text{-}X\text{-}5\text{-}seco\text{-}Cbs]^{n+}$ and $[\alpha\text{-}X,\beta\text{-}CN^-\text{-}5\text{-}seco\text{-}Cbs]^{n+}$ (X = H_2O, CN^-, SO_3^{2-}, NO_2^- and N_3^-). As with the modeling of [DC-5-seco-Cbs], the ester side chains of the corrin were truncated to ethyl groups for computational efficiency.

The difficulty that arises is that these complexes almost certainly exist as mixtures of two diastereomers in solution and there seems to be no simple way to determine their relative proportion; we have been unable to separate them using HPLC (they co-elute as a broad band) or TLC (streaking on the plates). Moreover, although the DFT modeling adequately reproduces the structures of [DCCbs] and [DCSYCbs], we have no way of determining the adequacy of the modeling in reproducing the structure of [DC-5-seco-Cbs], let alone its complexes with other ligands.

The partial charge q(r) (in units of *e*) on Co and the six donor atoms in its inner coordination sphere are given in Table S5 of the Supporting Information. The charge on Co and the average charge on, firstly, Co and the six donor atoms of its inner coordination sphere (averaged over the two diastereomers where applicable) and, secondly, on Co and the four corrin N donor atoms, are given in Table 6.

Table 6. Charges q(r)/*e* on cobalt and the six inner coordination sphere donor atoms in $[(X)(CN)Co(corrin)]^{n+}$ complexes determined from a QTAIM analysis of the wavefunction of their BP86-D3/6-311G(d,p) structures.[a]

X	Corrin	Co	Σ Coord Sphere	Σ(Co & eq N)
CN^-	Cbs	1.125	-1.645	-2.919
	SYCbs	1.112	-1.647	-2.929
	5-Seco-Cbs	1.118	-1.564	-2.858
SO_3^{2-}	Cbs	1.057	0.124	-2.965
	SYCbs	1.042	0.120	-2.988
	5-Seco-Cbs	1.052	0.166	-2.926
NO_2^-	Cbs	1.146	-1.868	-2.896
	SYCbs	1.133	-1.873	-2.914
	5-Seco-Cbs	1.137	-1.787	-2.843
N_3^-	Cbs	1.152	-2.564	-2.884
	SYCbs	1.145	-2.586	-2.897
	5-Seco-Cbs	1.152	-2.502	-2.825
H_2O	Cbs	1.131	-3.321	-2.951
	SYCbs	1.126	-3.359	-2.971
	5-Seco-Cbs	1.137	-3.311	-2.920

[a]See Table S5 for details.

There is no trend in the partial charge on Co itself. However, the sum of the partial charges on the metal and the entire coordination sphere, or the metal and the four equatorial donor N atoms, becomes less negative in the 5-seco-Cbs complexes than in either the Cbs themselves or the SYCbs. This lends support to the notion that cleavage of the corrin has made the metal and its immediate environment more positive (or less negative). However, in SYCbs the metal and its environment is *less* positive than in the Cbs, contrary to our expectations and the rationalization we used to explain the trends in log *K* values.[7, 9] QTAIM charges are believed to be reliable,[77, 78] so it appears likely that log *K* values are a function of multiple factors, the charge on the metal and its immediate environment probably being only one of them.

In the absence of a crystal structure, we have relied on DFT modelling to provide an indication of the likely geometry around the coordination sphere of the metal ion. We have used a topological analysis of the electron density to provide insight into the strength and nature of the chemical bonds. The charge density, ρ_r, at a bond critical point is an indicator of the strength of a chemical bond,[79-83] while the ratio of the potential and kinetic energy

densities at the bond critical point, $|V_r|/G_r$, is useful to characterize the nature of a chemical bond.[84] In particular, chemical bonds where $|V_r|/G_r < 1$ are characteristic of predominantly closed shell (ionic) interactions. They are also characterized by small values of ρ_r, a relatively small and positive value of the Laplacian of the electron density, $\nabla^2\rho_r$, and a positive value for the total electronic energy density, H_r (= V_r + G_r) that is close to zero;[85] metal–ligand bonds usually have $H_r < 0$ and close to zero.[84-88] Bonds with $|V_r|/G_r > 2$ are typically covalent interactions; and $1 < |V_r|/G_r, < 2$ is diagnostic of bonds of intermediate character. A full analysis of the coordination sphere of the modelled compounds is given in Table S6 of the Supporting Information, and summarized in Table 7.

Table 7. Average coordination sphere bond lengths and topological properties of the electron density at bond critical points in $[(X)(CN)Co(corrin)]^{n+}$ complexes determined from a QTAIM analysis of the wavefunction of their BP86-D3/6-311G(d,p) structures.[a]

Corrin	Bond	Bond length (av) /Å	ρ_r (av)	$\nabla^2\rho_r$ (av)	V_r (av)	G_r (av)	H_r (av)	$\lvert V_r\rvert/G_r$ (av)
$[(CN)_2Co(Corrin)]$								
Cbs	Co–CN	1.927	0.116	0.287	-0.146	0.109	-0.037	1.335
SYCbs		1.924	0.116	0.289	-0.147	0.109	-0.038	1.349
5SecoCbs		1.923	0.116	0.283	-0.147	0.109	-0.038	1.349
Cbs	Co–N(corrin)	1.913	0.110	0.449	-0.166	0.139	-0.027	1.189
SYCbs		1.910	0.111	0.450	-0.168	0.140	-0.028	1.198
5SecoCbs		1.933	0.104	0.431	-0.155	0.131	-0.024	1.178
$[(SO_3(CN)Co(corrin)]^-$								
Cbs	$Co–SO_3$	2.334	0.080	0.107	-0.067	0.047	-0.020	1.430
SYCbs		2.401	0.070	0.091	-0.056	0.039	-0.017	1.423
5SecoCbs		2.240	0.069	0.098	-0.057	0.041	-0.016	1.399
Cbs	Co–CN	1.993	0.099	0.271	-0.121	0.095	-0.027	1.284
SYCbs		1.975	0.103	0.280	-0.128	0.099	-0.029	1.293
5SecoCbs		1.918	0.109	0.278	-0.135	0.102	-0.033	1.319
Cbs	Co–N(corrin)	1.898	0.113	0.486	0.179	-0.150	0.029	1.191
SYCbs		1.894	0.114	0.488	0.181	-0.152	0.030	1.194
5SecoCbs		1.929	0.110	0.470	0.171	-0.144	0.027	1.185
$[(NO_2)(CN)Co(corrin)]$								
Cbs	$Co–NO_2$	1.995	0.096	0.352	-0.126	0.107	-0.019	1.179
SYCbs		2.018	0.099	0.400	-0.116	0.100	-0.017	1.166
5SecoCbs		2.028	0.089	0.321	-0.112	0.096	-0.016	1.165
Cbs	Co–CN	1.913	0.120	0.283	-0.150	0.110	-0.039	1.358
SYCbs		1.910	0.120	0.285	-0.151	0.111	-0.040	1.359
5SecoCbs		1.910	0.120	0.279	-0.150	0.110	-0.040	1.365
Cbs	Co–N(corrin)	1.906	0.112	0.462	0.172	-0.144	0.028	1.195

Corrin	Bond	Bond length (av) /Å	ρ_r (av)	$\nabla^2\rho_r$ (av)	V_r (av)	G_r (av)	H_r (av)	$\lvert V_r\rvert/G_r$ (av)
SYCbs		1.907	0.110	0.442	0.171	-0.143	0.028	1.195
5SecoCbs		1.941	0.105	0.438	0.158	-0.134	0.024	1.178
[(N_3)(CN)Co(corrin)]								
Cbs	Co–N_3	2.047	0.078	0.292	-0.098	0.086	-0.013	1.146
SYCbs		2.040	0.079	0.301	-0.100	0.088	-0.013	1.143
5SecoCbs		2.030	0.082	0.304	-0.104	0.090	-0.014	1.153
Cbs	Co–CN	1.878	0.129	0.294	-0.165	0.119	-0.045	1.382
SYCbs		1.880	0.128	0.295	-0.164	0.119	-0.045	1.380
5SecoCbs		1.884	0.127	0.287	-0.161	0.116	-0.045	1.383
Cbs	Co–N(corrin)	1.906	0.112	0.462	0.171	-0.143	0.028	1.194
SYCbs		1.906	0.112	0.460	0.171	-0.143	0.028	1.195
5SecoCbs		1.929	0.105	0.439	0.157	-0.134	0.024	1.177
[(H_2O)(CN)Co(corrin)]$^+$								
Cbs	Co-OH_2	2.180	0.046	0.250	-0.063	0.063	0.000	0.995
SYCbs		2.169	0.050	0.271	-0.068	0.068	0.000	0.999
5SecoCbs		2.083	0.061	0.341	-0.086	0.085	0.000	1.004
Cbs	Co–CN	1.820	0.147	0.268	-0.189	0.128	-0.061	1.473
SYCbs		1.825	0.146	0.271	-0.186	0.127	-0.059	1.466
5SecoCbs		1.836	0.143	0.270	-0.181	0.124	-0.057	1.457
Cbs	Co–N(corrin)	1.902	0.114	0.463	0.174	-0.145	0.029	1.202
SYCbs		1.904	0.113	0.456	0.173	-0.143	0.029	1.203
5SecoCbs		1.926	0.107	0.436	0.160	-0.134	0.025	1.186

[a] The mean values of the charge density (ρ) and its Laplacian ($\nabla^2\rho$) at the bond critical points are in au. (1 au of ρ = 6.7483 eÅ^{-3}, and 1 au of $\nabla^2\rho$ = 24.099 eÅ^{-5}). The values of the energy density are in au (1 au = 627.5095 kcal mol^{-1}).

The equatorial Co–N bonds of the cobalt corrins are predominantly ionic bonds with some covalent character ($|V_r|/G_r \approx 1.2$). Cleavage of the corrin ring causes the average equatorial Co–N bond lengths (and in particular the Co–N(21) and Co–N(24) bonds, Table S6) to increase by between 0.02 and 0.04 Å; this weakens them (ρ_r decreases) and marginally decreases their covalent character ($|V_r|/G_r$ decreases).

The Co–CN bond length to CN^- coordinated on the lower (α) face of the corrin decreases on going from Cbs to SYCbs to 5-seco-Cbs (1.925 Å to 1.920 Å to 1.917 Å; Table S6) while the Co–CN_β bond length is invariant. In the aquacyanocobesters the effect is more marked. The average Co–OH_2 bond length (average of the two diastereomers) decreases from 2.180 Å to 2.169 Å to 2.083 Å, while the average Co–CN bond to the trans CN^- ligand increases from 1.820 Å to 1.825 Å, to 1.836 Å, i.e., a normal trans influence is apparent. The Co–OH_2 bond

is a predominantly ionic bond ($|V_r|/G_r \leq 1$), while the Co–CN bond has significant covalent character ($|V_r|/G_r \approx 1.46$).

The trend towards shorter axial bonds as the corrin is changed from Cbs to SYCbs to 5-seco-Cbs that is evident in the dicyano and aquacyano complexes persists more or less in the azidocyano and sulfitocyano complexes. The DFT model of one of the isomers of sulfitocyano-SYCbs, that with SO_3^{2-} coordinated to Co on the β face of the corrin, has a very long Co–S bond, 2.448 Å, cf. 2.353 Å in the *α*-sulfito isomer. The structure converged to this despite using different starting structures, Figure S15. This suggests that sulfitocyano-SYCbs exists predominantly as the *α*-sulfito isomer. If that is the case, the Co–S bond is marginally longer in sulfitocyano-SYCbs (2.353 Å) than the average Co–S bond length in the Cbs sulfitocyano diastereomers (2.334 Å); it is significantly shorter, average of 2.240 Å, in the sulfitocyano diastereomers of 5-seco-Cbs. The steric factors introduced by the presence of the lactone in SYCbs may complicate a rationalization of the kinetics and thermodynamics of its ligand substitution reactions (see caption to Figure S15); we noted anomalously low log *K* values for coordination of aromatic N-donor ligands, for example.[9]

A normal trans influence is also seen in the azidocyano complexes (Co–CN bond lengths increases as $Co–N_3$ decreases); the sulfitocyano complexes show an inverse trans influence, and Co–CN bond length decreases parallel with the overall decrease in the Co–S bond lengths. An inverse trans influence has been shown to be the consequence of the interplay between steric effects and electronic factors in cobalt corrin complexes and in probably see here for the sulfite complexes because of the steric interaction between it and the corrin ring substituents.[89] Strikingly different is the behavior of the axial bond lengths in the nitrocyano complexes. The $Co–NO_2$ bond lengths *increase* as the corrin is changed from Cbs to SYCbs to 5-seco-Cbs, while the trans Co–CN remains virtually unchanged.

As noted, there are exceptions, but two factors clearly influence the values of log *K*. The predominant trend of shorter bonds to the axial ligands offers a rationalization why in general Δ*H* values are more negative for substitution of H_2O by an exogenous ligand when the corrin is 5-seco-Cbs than either Cbs or SYCbs (Figure 3). The compensation effect between Δ*H* and Δ*S* tends to level out the variation in log *K* values. Secondly, the increase in positive charge on the metal and its immediate coordination environment clearly discriminates against the coordination of the π acceptor ligands, and appears to favor, relatively speaking, the coordination of ligands low down in the spectrochemical series.

As mentioned in the Results section, there is considerable uncertainty in the rate constants measured for the substitution of H_2O in $[AC\text{-}5\text{-}seco\text{-}Cbs]^+$ by CN^-. Firstly, the

reproducibility is poor (see Figure S11) and there appears to be no meaningful variation on the second order rate constants with temperature (Table S3). We conclude therefore that, at best, we *estimate* that the second order rate constant, k^{II}, for substitution of H_2O in [AC-5-seco-Cbs]$^+$ by CN^- is between about 20 and 100 M^{-1} s^{-1} (Table S3) or c. 10^2 M^{-1} s^{-1}.
Notwithstanding this uncertainty in the value of k^{II}, a broad conclusion can be drawn. The value of k^{II}, for the substitution of axially coordinated water in [ACCbs]$^{2+}$ and [ACSYCbs]$^+$ in aqueous solution is 4.8(3) × 10^4 M^{-1} $s^{-1}$and 1.53(2) × 10^4 M^{-1} s^{-1}, respectively;[7] in 50% isopropanol, k^{II} for substitution of H_2O in the aquacyano complexes of 10-X-Cbs, where X is the substituent at the C10 position of corrin, is 7.8 × 10^4 M^{-1} s^{-1} for X = H (i.e., for [ACCbs]$^+$ itself); 3.0 × 10^4 M^{-1} s^{-1} for X = NH_2; and 1.7 × 10^3 M^{-1} s^{-1} for X = NO_2.[13] We here find that for [AC-5-seco-Cbs]$^+$, k^{II}, ≈ 10^2 M^{-1} s^{-1}. Although interrupting the delocalized system in [ACSYCbs]$^+$ caused a threefold decrease in the rate constants when compared to [ACCbs]$^+$ with its intact corrin, disrupting both the conjugation and cleaving the corrin ring causes the rate constant to drop, probably by over two orders of magnitude. Clearly both the extent of the electron density of the macrocyclic ligand, and the size of the macrocyclic cavity affect the lability of Co(III),a s the metal becomes more Co(III)-like in its behavior. This demonstrates how perturbation of the electronic structure of the corrin in the cobalt corrin complexes significantly affects the coordination chemistry of the axial coordination sites, provides further insight into the origins of the unique chemistry of Co(III) in the cobalt corrins, and emphasizes the importance of cis effects in the chemistry of these compounds.

■ AUTHOR INFORMATION

Corresponding Author
*E-mail: Helder.Marques@ wits.ac.za (H.M.M.).

■ ACKNOWLEDGMENT

The financial assistance of the Department of Science and Technology and the National Research Foundation, Pretoria, through the South African Research Chairs Initiative, and the University of Witwatersrand, Johannesburg, is gratefully acknowledged. AV, PRV and KY thank Institute of Molecular Science, Okazaki, Japan for supercomputing facilities received

for all calculations, and thank CREST project for generous funding (Grant No. JPMJCR12C4).

■ REFERENCES

1. Brown, K. L.; Cheng, S.; Zou, X.; Zubkowski, J. D.; Valente, E. J.; Knapton, L.; Marques, H. M. Cis Effects in the Cobalt Corrins. 1. Crystal Structures of 10-Chloroaquacobalamin Perchlorate, 10-Chlorocyanocobalamin, and 10-Chloromethylcobalamin. *Inorg. Chem.* **1997,** 36, 3666-3675.

2. Marques, H. M.; Knapton, L.; Zou, X.; Brown, K. L. Probing the nature of the Co(III) ion in cobalamins: deactivation of the metal towards ligand substitution in 10-nitrosoaquacobalamin, and the kinetics of the ligand substitution reactions of iodocobalamin. *J. Chem. Soc., Dalton Trans.* **2002**, 3195-3200.

3. Perry, C. B.; Fernandes, M. A.; Brown, K. L.; Zou, X.; Valente, E. J.; Marques, H. M. Probing the Nature of the Co^{III} Ion in Cobalamins Spectroscopic and Structural Investigations of the Reactions of Aquacobalamin (Vitamin B_{12a}) with Ambident Nucleophiles. *Eur. J. Inorg. Chem.* **2003**, 2095-2107.

4. Knapton, L.; Marques, H. M. Probing the nature of the Co(III) ion in cobalamins: a comparison of the reaction of aquacobalamin (vitamin B-12a) and aqua-10-chlorocobalamin with some anionic and N-donor ligands. *Dalton Trans.* **2005**, 889-895.

5. Perry, C. B.; Marques, H. M. Probing the cis and trans Influence in Cobalamin Chemistry by Electronic Spectroscopy. *S. Afr. J. Chem.* **2005,** 58, 9-15.

6. Chemaly, S. M.; Brown, K. L.; Fernandes, M. A.; Munro, O. Q.; Grimmer, C.; Marques, H. M. Probing the Nature of the Co^{III} Ion in Corrins: The Structural and Electronic Properties of Dicyano- and Aquacyanocobyrinic Acid Heptamethyl Ester and a Stable Yellow Dicyano- and Aquacyanocobyrinic Acid Heptamethyl Ester. *Inorg. Chem.* **2011,** 50, 8700-8718.

7. Chemaly, S. M.; Florczak, M.; Dirr, H.; Marques, H. M. Probing the Nature of the Co^{III} Ion in Corrins: A Comparison of the Thermodynamics and Kinetics of the Ligand Substitution Reactions of

Aquacyanocobyrinic Acid Heptamethyl Ester and Stable Yellow Aquacyanocobyrinic Acid Heptamethyl Ester. *Inorg. Chem.* **2011,** 50, 8719-8727.

8. Govender, P. P.; Navizet, I.; Perry, C. B.; Marques, H. M. The cis influence of the corrin in vitamin B_{12} models. *Chem. Phys. Lett.* **2012,** 550, 150-155.

9. Chemaly, S. M.; Kendall, L.; Nowakowska, M.; Pon, D.; Perry, C. B.; Marques, H. M. Probing the Nature of the Co(III) Ion in Corrins: Comparison of Reactions of Aquacyanocobyrinic Acid Heptamethyl Ester and Aquacyano-Stable Yellow Cobyrinic Acid Hexamethyl Ester with Neutral N‑Donor Ligands. *Inorg. Chem.* **2013,** 52, 1077-1083.

10. Mathura, S.; Sannasy, D.; de Sousa, A. S.; Perry, C. B.; Navizet, I.; Marques, H. M. The preparation of N-acetyl-Co(III)-microperoxidase-8 (NAcCoMP8) and its ligand substitution reactions: A comparison with aquacobalamin (vitamin B_{12a}). *J. Inorg. Biochem.* **2013,** 123, 66-79.

11. Govender, P. P.; Navizet, I.; Perry, C. B.; Marques, H. M. DFT Studies of Trans and Cis Influences in the Homolysis of the Co–C Bond in Models of the Alkylcobalamins. *J. Phys. Chem. A* **2013,** 117, 3057-3068.

12. Ghadimi, N.; Perry, C. B.; Fernandes, M.; Govender, P. P.; Marques, H. M. Probing the nature of the Co(III) ion in cobalamins: The reactions of aquacobalamin (vitamin B_{12a}),

aqua-10-chlorocobalamin and aqua-10-bromocobalamin with anionic and neutral ligands. *Inorg. Chim. Acta* **2015,** 436, 29-38.

13. Ghadimi, N.; Perry, C. B.; Govender, P. P.; Marques, H. M. Probing the nature of the Co(III) ion in cobalamins: The ligand substitution reactions of aquacyanocobester, aquacyano(10-nitro)cobester and aquacyano(10-amino)cobester. *Inorg. Chim. Acta* **2016,** 450, 269-278.

14. Williams, R.; Billig, E.; Waters, J. H.; Gray, H. B. The Toluenedithiolate and Maleonitriledithiolate Square-Matrix Systems. *J. Am. Chem. Soc.* **1966,** 88, 43–50.

15. Röhrscheid, F.; Balch, A. L.; Holm, R. H. Potential Electron Transfer Complexes of the [M-O_4] Type: Synthesis and Properties of Complexes Derived from Pyrocatechol and Tetrachloropyrocatechol. *Inorg. Chem.* **1966,** 5, 1542–1551.

16. Fleischer, E. B.; Jacobs, S.; Mestichelli, L. The Kinetics of the Reaction of Cobalt (III) and Iron (III) Hematoporphyrin with Cyanide and Thiocyanate. Evidence for a Dissociative Mechanism. *J. Am. Chem. Soc,* **1967,** 90, 2527-2531.

17. Andruniow, T.; Kozlowski, P. M.; Zgierski, M. Z. Theoretical analysis of electronic absorption spectra of vitamin B_{12} models. *J. Chem. Phys.* **2001,** 115, 7522-7533.

18. Navizet, I.; Perry, C. B.; Govender, P. P.; Marques, H. M. cis Influence in Models of Cobalt Corrins by DFT and TD-DFT Studies. *J. Phys. Chem. B.* **2012,** 116, 8836-8846.

19. Pratt, J. M. In *Chemistry and Biochemistry of B_{12}*; Banerjee, R., Ed.; John Wiley & Sons: New York, 1999; pp 113-164.

20. (CSD), C. S. D. v. 5.38; Cambridge Crystallographic Data Centre (CCDC): Cambridge, UK, 2016.

21. Boeyens, J. C. A. Ionization radii of compressed atoms *J. Chem. Soc., Faraday Trans.* **1994,** 90, 3377-3381

22. Hinze, R.-P.; Schiebel, H. M.; Laas, H.; Heise, K.-P.; Gossauer, A.; Inhoffen, H. H.; Ernst; Schulten, H.-R. Beiträge zur Kenntnis des chromophoren Systems der Corrine, IV. Über die partielle, reversible Ringöffnung am Dicyano-cobyrin-säure-heptamethylester mit intermediärer reversibler Entfernung des Cobalts. *Liebigs Ann. Chem.* **1979**, 811-828.

23. Kräutler, B. The Photooxygenation of Heptamethyl Co*α*,Co*β*-Dicyanocobyrinate. *Helv. Chim. Acta* **1982,** 65, 1941-1948.

24. *SigmaPlot*, v. 14; Systat Software: San Jose, CA, 2017.

25. *Chromeleon*, v. v. 6.8; Dionex Corporation: Sunnyvale, CA, 2010.

26. Palet, C.; Munoz, M.; Daunert, S.; Bachas, L. G.; Valiente, M. Vitamin B12 derivatives as anion carriers in transport through supported liquid membranes and correlation with their behavior in ion-selective electrodes. *Anal. Chem.* **1993,** 65, 1533-1536.

27. Munro, O. Q.; Marques, H. M. Heme−Peptide Models for Hemoproteins. 1. Solution Chemistry of N-Acetylmicroperoxidase-8. *Inorg. Chem.* **1996,** 35, 3752-3767.

28. Friedrich, W. Über einige Eigenschaften der Cyano-Aquo-Corrinoide. *Z. Naturforsch. B* **1966,** 21, 595-596.

29. Friedrich, W.; Bieganowski, R. Über die Bildung von Cyanocobalamin aus Aquocobalamin und Cyano-aquo-Corrinoiden. *Z. Naturforsch. B* **1967,** 22, 741-747.

30. Friedrich, W.; Ohlms, H.; Sandeck, W.; Bieganowski, R. Über die ab-Isomerie der Cyano-aquo-corrinoide. *Z. Naturforsch. B* **1967,** 22, 839-850.

31. Johnson, G. D.; Bowen, R. E. Computation of Association Constants from Spectrophotometric Data. II. Multiple Equilibria. *J. Am. Chem. Soc.* **1965,** 87, 1655-1660.

32. Marques, H. M.; Munro, O. Q.; Crawcour, M. L. Coordination of N-donor ligands by hematohemin. *Inorg. Chim. Acta* **1992,** 196, 221-229.

33. Marques, H. M.; Marsh, J. H.; Mellor, J. R.; Munro, O. Q. The coordination of imidazole and its derivatives by aquocobalamin. *Inorg. Chim. Acta* **1990,** 170, 259-269.

34. Marques, H. M. Proximal charge effects on coordination of histamine by aquocyanocobinamide. *Inorg. Chim. Acta* **1990,** 174, 271-273.

35. Marques, H. M.; Bradley, J. C.; Brown, K. L.; Brooks, H. Placing hydroxide in the thermodynamic trans influence order of the cobalt corrinoids: equilibrium constants for the reaction of some ligands with aquahydroxocobinamide. *Inorg. Chim. Acta* **1993,** 209, 161-169.

36. Perry, C. B.; Shin, N.; Fernandes, M. A.; Marques, H. M. Phenylvinylcobalamin: an alkenylcobalamin featuring a ligand with a large trans influence. *Dalton Trans.* **2013,** 42, 7555-7561.

37. Martell, A. E.; Smith, R. M.; Motekaites, R. J., NIST Standard Database 46. Criticially Selected Stability Constants of Metal Complexes, V. 8.0, NIST, Gaithersburg, MD, 2004.

38. Reenstra, W. W.; Jencks, W. P. Reactions of cyanide with cobalamins. *J. Am. Chem. Soc.* **1979,** 101, 5780-5791.

39. Marques, H. M.; Baldwin, D. A.; Pratt, J. M. Hemes and hemoproteins; 3; The reaction of microperoxidase-8 with cyanide: comparison with aquocobalamin and hemoproteins. *J. Inorg. Biochem.* **1987,** 29, 77-91.

40. Marques, H. M.; Bradley, J. C.; Brown, K. L.; Brooks, H. The Ligand-substitution Reactions of Aquahydroxocobinamide proceed through a Dissociative Interchange Mechanism. *J. Chem. Soc., Dalton Trans.* **1993**, 3475-3478.

41. Perdew, J. P. Density-functional approximation for the correlation energy of the inhomogeneous electron gas. *Phys. Rev. B* **1986,** 33, 8822-8824.

42. Becke, A. D. Density-functional exchange-energy approximation with correct asymptotic behavior. *Phys. Rev. A* **1988,** 38, 3098-3100.

43. Frisch, M. J. T., G. W.; Schlegel, H. B.; Scuseria, G. E.; Robb, M. A.; Cheeseman, J. R.; Scalmani, G.; Barone, V.; Mennucci, B.; Petersson, G. A.; Nakatsuji, H.; Caricato, M.; Li, X.; Hratchian, H. P.; Izmaylov, A. F.; Bloino, J.; Zheng, G.; Sonnenberg, J. L.; Hada, M.; Ehara, M.; Toyota, K.; Fukuda, R.; Hasegawa, J.; Ishida, M.; Nakajima, T.; Honda, Y.; Kitao, O.; Nakai, H.; Vreven, T.; Montgomery, J., J. A.; Peralta, J. E.; Ogliaro, F.; Bearpark, M.; Heyd, J. J.; Brothers, E.; Kudin, K. N.; Staroverov, V. N.; Kobayashi, R.; Normand, J.; Raghavachari, K.; Rendell, A.; Burant, J. C.; Iyengar, S. S.; Tomasi, J.; Cossi, M.; Rega, N.; Millam, N. J.; Klene, M.; Knox, J. E.; Cross, J. B.; Bakken, V.; Adamo, C.; Jaramillo, J.; Gomperts, R.; Stratmann, R. E.; Yazyev, O.; Austin, A. J.; Cammi, R.; Pomelli, C.; Ochterski, J. W.; Martin, R. L.; Morokuma, K.; Zakrzewski, V. G.; Voth, G. A.; Salvador, P.; Dannenberg, J. J.; Dapprich, S.; Daniels, A. D.; Farkas, Ö.; Foresman, J. B.; Ortiz, J. V.; Cioslowski, J.; Fox, D. J. *Gaussian 09; Revision C.01*, v. Gaussian, Inc: Wallingford C, 2009.

44. Grimme, S.; Antony, J.; Ehrlich, S.; Krieg, H. A consistent and accurate ab initio parametrization of density functional dispersion correction (DFT-D) for the 94 elements H-Pu. *J. Chem. Phys.* **2010,** 132, 154104-154119.

45. Markwell, A. J.; Pratt, J. M.; Shaikjee, S. S.; Toerien, J. G. The chemistry of vitamin B_{12}. Part 28. Crystal structure of dicyanocobyrinic acid heptamethyl ester and its interaction with alcohols: the effects of hydrogen bonding to co-ordinated cyanide *J. Chem. Soc., Dalton Trans.* **1987**, 1349-1357.

46. Bader, R. F. W. Atoms in molecules. *Acc. Chem. Res.* **1985,** 18, 9-15.

47. Bader, R. F. *Atoms in Molecules: A Quantum Theory*. Oxford University Press: Oxford, 1990.

48. Keith, T. A. *AIMAll (version 17.01.25)*, v. TK Gristmill Software, http://aim.tkgristmill.com: Overland Park, KS, 2016.

49. Brown, K. L. In *Chemistry and Biochemistry of B_{12}*; Banerjee, R., Ed.; John Wiley & Sons, Inc.: New York, 1999; pp 197-237.

50. Xia, L.; Cregan, A. G.; Berben, L. A.; Brasch, N. E. Studies on the formation of glutathionylcobalamin: Any free intracellular aquacobalamin is likely to be rapidly and irreversibly converted to glutathionylcobalamin. *Inorg. Chem.* **2004,** 43 (21), 6848-6857.

51. Baldwin, D. A.; Betterton, E. A.; Pratt, J. M. The Chemistry of Vitamin B_{12} Part 20. Diaquocobinamide : pK Values and Evidence for Conformational Isomers. *J. Chem. Soc., Dalton Trans.* **1983**, 217-223.

52. Nowakowska, M. Synthesis and Reactions of a Modified Cobalt Corrin. MSc; dissertation reserved and converted to PhD thesis, University of the Witwatersrand, Johannesburg, 2014.

53. Offenhartz, B. H.; George, P. The Ionization of Vitamin B_{12} Factor B. *Biochemistry* **1963,** 2, 142-145.

54. Hayward, G. C.; Hill, H. A. O.; Pratt, J. M.; Vanston, N. J.; Williams, R. J. P. The Chemistry of Vitamin B_{12}. Part 1V. l. The Thermodynamic trans-effect. *J. Chem. Soc. A* **1965**, 6485-6493.

55. Kräutler, B.; Caderas, C.; Konrat, R.; Puchberger, M.; Kratky, C. Lipophilic Functionalized Cobyrinic-Acid Derivatives. Part 1. Cobester α-monoacids (α, α, α, β, β, β-hexamethyl α-hydrogen Coα, Coβ-dicyanocobyrinates). *Helv. Chim. Acta* **1995,** 78, 581-599.

56. Shimakoshi, H.; Abiru, M.; Izumi, S.; Hisaeda, Y. Green molecular transformation by a B_{12}–TiO_2 hybrid catalyst as an alternative to tributyltin hydride. *Chem. Commun.* **2009**, 6427-6429.

57. Lexa, D.; Saveant, J. M.; Zickler, J. Electrochemistry of Vitamin B_{12}. 5. Cyanocobalamins. *J. Am. Chem. Soc.* **1980,** 102, 2654-2663.

58. Sisley, M. J.; Jordan, R. B. First hydrolysis constants of hexaaquacobalt (III) and-manganese (III): Longstanding issues resolved. *Inorg. Chem.* **2006,** 45, 10758-10763.

59. Visser, H. G.; Purcell, W.; Basson, S. S. Kinetic study of the protonations and substitutions of different cobalt(III)–nta complexes. *Trans. Met. Chem.* **2002,** 27, 461-468.

60. Massoud, S. S.; Milburn, R. M. Determination of the acid dissociation constants of coordinated water in cis-$[Cotn_2(H_2O)_2]^{3+}$ ion. *Inorg. Chim. Acta* **1988,** 146, 3-4.

61. Lee, J. H.; Britten, J.; Chin, J. Kinetics and mechanism of a cobalt(III) complex catalyzed hydration of nitriles. *J. Am. Chem. Soc.* **1993,** 115, 3618-3622.

62. Splinter, R. C.; Harris, S. J.; Tobias, R. S. The Solvent Isotope Effect on the Dissociation of the Aquopentaamminecobalt(III) Ion. *Inorg. Chem.* **1967,** 7, 897-902.

63. Yajima, F.; Yamasaki, A.; Fujiwara, S. Cobalt-59 Nuclear Magnetic Resonance Study of Acid Dissociation Equilibria in Aquopentaamminecobalt(II1) Perchlorate and cis- and trans-Aquoamminebis(ethylenediamine) cobalt(III) Bromide. *Inorg. Chem.* **1971,** 10, 2350-2352.

64. Grzybkowski, W. Nature and Properties of Metal Cations in Aqueous Solutions. *Polish J. Environ. Stud.* **2006,** 15, 655-663.

65. Garau, G.; Geremia, S.; Marzilli, L. G.; Nardin, G.; Randaccio, L.; Tauzher, G. Crystal chemistry and binding of NO_2, SCN and SeCN to Co in cobalamins. *Acta Cryst., Sec. B* **2003**, 51-59.

66. Marques, H. M. Ligand substitution reactions of aquocobalamin. Reactions with primary amines *J. Chem. Soc., Dalton Trans.* **1991**, 1437-1442.

67. Marques, H. M. Compensation Effects in Ligand-Substitution Reactions of Aquacobalamin. *S. Afr. J. Chem.* **1991,** 44, 114-117.

68. Marques, H. M.; Bradley, J. C.; Campbell, L. A. Ligand substitution reactions of aquacobalamin: evidence for a dissociative interchange mechanism *J. Chem. Soc., Dalton Trans.* **1992**, 2019-2027.

69. Knapton, L.; Marques, H. M. The effect of solvent on the ligand substitution reactions of aquacobalamin (vitamin B-12a). *S. Afr. J. Chem.* **2006,** 59, 43-47.

70. Kozlowski, P. M.; Kamachi, T.; Toraya, T.; Yoshikawa, K. Does Cob(II)alamin Act as a Conductor in Coenzyme B_{12} Dependent Mutases? *Angew. Chem. Int. Ed. Engl.* **2007,** 46, 980-983.

71. Jensen, K. P.; Ryde, U. Theoretical prediction of the Co−C bond strength in cobalamins. *J. Phys. Chem. A* **2003,** 107, 7539-7545.

72. Kepp, K. P. Co−C Dissociation of Adenosylcobalamin (Coenzyme B_{12}): Role of Dispersion, Induction Effects, Solvent Polarity, and Relativistic and Thermal Corrections. *J. Phys. Chem. A* **2014,** 118, 7104−7117.

73. Kuta, J.; Patchkovskii, S.; Zgierski, M. Z.; Kozlowski, P. M. Performance of DFT in modeling electronic and structural properties of cobalamins. *J. Comput. Chem.* **2006,** 27, 1429-1437.

74. Glusker, J. P. In *B_{12}*; Dolphin, D., Ed.; Wiley-Interscience: New York, 1982; Vol. 1, pp 23-107.

75. Lever, A. B. P. *Inorganic Electronic Spectroscopy*. 2 ed.; Elsevier: New York, 1986.

76. Jørgensen, C. K. *Modern Aspects of Ligand Field Theory*. Elsevier: New York, 1971.

77. Bader, R. F. W.; Matta, C. F. Atomic Charges Are Measurable Quantum Expectation Values: A Rebuttal of Criticisms of QTAIM Charges. *J. Phys. Chem. A* **2004,** 108 8385-8394.

78. Huang, L.; Matta, C.; Massa, L. The kernel energy method (KEM) delivers fast and accurate QTAIM electrostatic charge for atoms in large molecules. *Struct. Chem.* **2015,** 26, 1433-1442.

79. Howard, S. T.; Krygowski, T. M. Benzenoid hydrocarbon aromaticity in terms of charge density descriptors. *Can. J. Chem.* **1997,** 75, 1174-1181.

80. O'Brien, S. E.; Popelier, P. L. Quantum molecular similarity. Part 2: The relation between properties in BCP space and bond length. *Can. J. Chem.* **1999,** 77, 28-36.

81. Espinosa, E.; Souhassou, M.; Lachekar, H.; Lecomte, C. Topological analysis of the electron density in hydrogen bonds. *Acta Cryst. B* **1999,** 55, 563-572.

82. Grabowski, S. J. High-Level Ab Initio Calculations of Dihydrogen-Bonded Complexes. *J. Phys. Chem. A* **2000,** 105, 5551-5557.

83. Bader, R. F. W.; Matta, C. F.; Cortés-Guzmán, F. Where to draw the line in defining a molecular structure. *Organometallics* **2004,** 23, 6253-6263.

84. Espinosa, E.; Alkorta, I.; Elguero, J.; Molins, E. From weak to strong interactions: A comprehensive analysis of the topological and energetic properties of the electron density distribution involving X–H...F–Y systems. *J. Chem. Phys.* **2002,** 117, 5529-5542.

85. Cramer, D.; Kraka, E. The enhancing effects of molecule X (X= PH2Cl, SHCl, ClCl) on chalcogen–chalcogen interactions in cyclic trimers Y⋯ Y⋯ X (Y= SHCl, SeHCl). *Angew. Chem. Int. Ed. Engl.* **1984,** 23, 627-628.

86. Bobrov, M. F.; Popova, G. V.; Tsirelson, V. G. A topological analysis of electron density and chemical bonding in cyclophosphazenes $P_nN_nX_{2n}$ (X = H, F, Cl; n = 2, 3, 4). *Russ. J. Phys. Chem.* **2006,** 80, 584-590.

87. Macchi, P.; Sironi, A. Chemical bonding in transition metal carbonyl clusters: complementary analysis of theoretical and experimental electron densities. *Coord. Chem. Rev.* **2003,** 238-239, 383-412.

88. Bader, R. F. W.; Matta, C. F. Bonding to titanium. *Inorg. Chem.* **2001,** 40, 5603-5611.

89. Kuta, J.; Wuerges, J.; Randaccio, L.; Kozlowski, P. M. Axial Bonding in Alkylcobalamins: DFT Analysis of the Inverse Versus Normal Trans Influence. *J. Phys. Chem. A* **2009,** 113, 11604-11612.

Probing the Nature of the Co(III) Ion in Corrins: the Reactions of Aquacyano-5-seco-Cobyrinic Acid Heptamethyl Ester with Anionic Ligands

Monika Nowakowska[a], Susan M. Chemaly[a], Amanda Rousseau,[a] Penny P. Govender[b], Pradeep R. Varadwaj[c,d], Arpita Varadwaj[c,d], Koichi Yamashita,[c,d] and Helder M. Marques[a]*

[a]Molecular Sciences Institute, School of Chemistry, University of the Witwatersrand, P.O. Wits, Johannesburg, 2050 South Africa, [b]Department of Applied Chemistry, University of Johannesburg, 2050 South Africa, [c]Department of Chemical System Engineering, School of Engineering, The University of Tokyo 7-3-1, Hongo, Bunkyo-ku, Japan 113-8656, and [d]CREST-JST, 7 Gobancho, Chiyoda-ku, Tokyo, Japan 102-0076

SUPPLEMENTARY INFORMATION

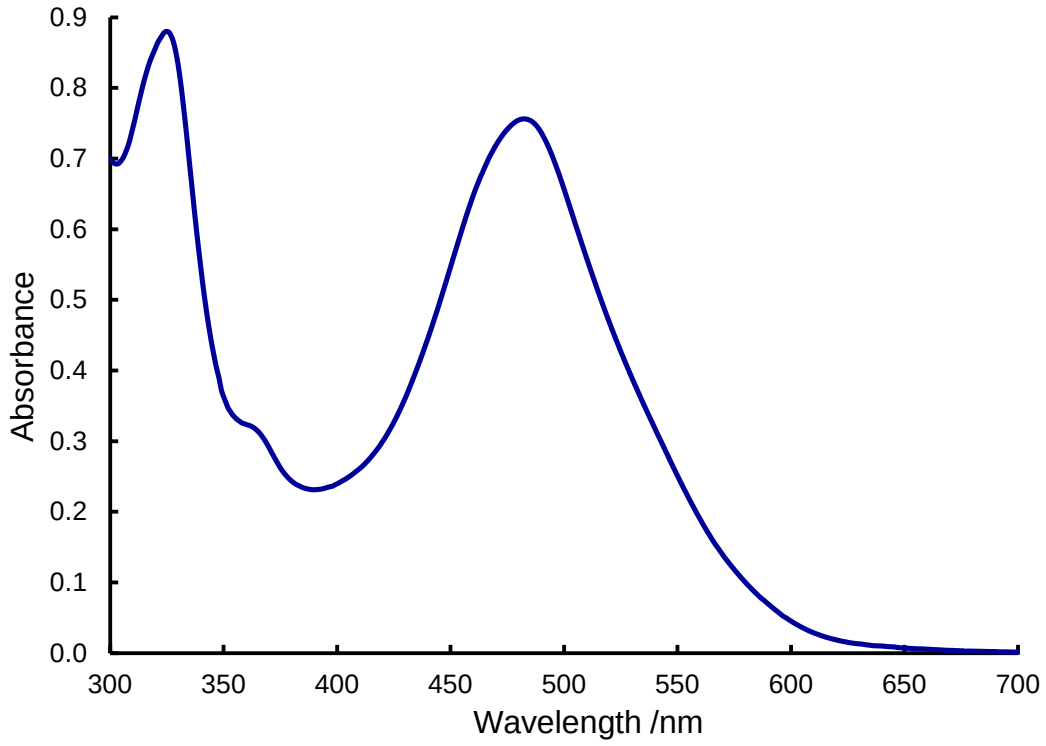

Figure S1. UV-vis spectrum of [DC-5-seco-Cbs] (20 μM) in neutral aqueous solution.

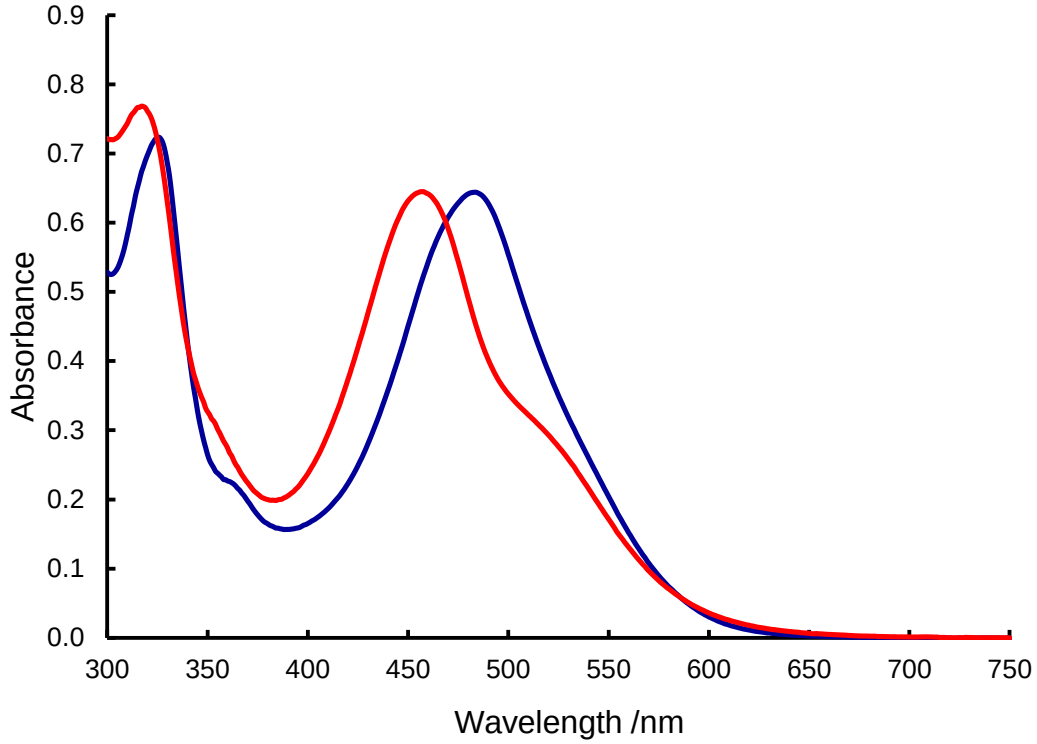

Figure S2. Conversion of [DC-5-seco-Cbs] (blue) to $[AC\text{-}5\text{-}seco\text{-}Cbs]^+$ (red).

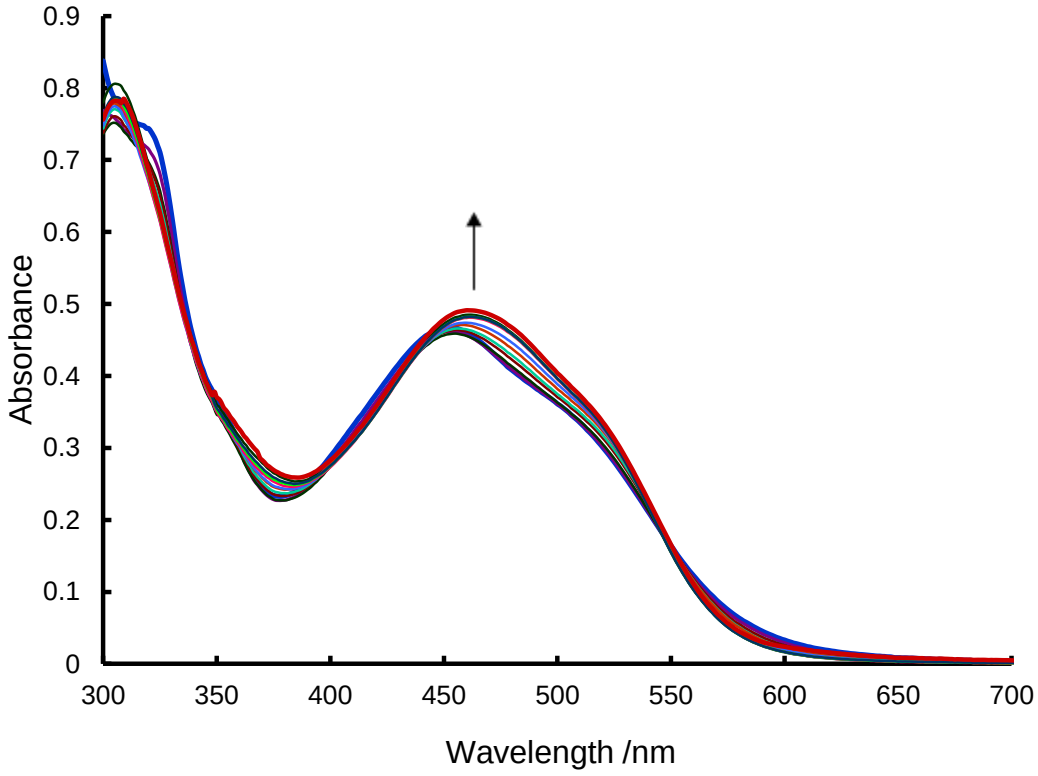

Figure S3. The effects of pH on the absorbance spectrum of $[AC\text{-}5\text{-}seco\text{-}Cbs]^+$ ranging from pH 5.2 (blue) to pH 11.5 (black) at 25.0 ºC in aqueous solution.

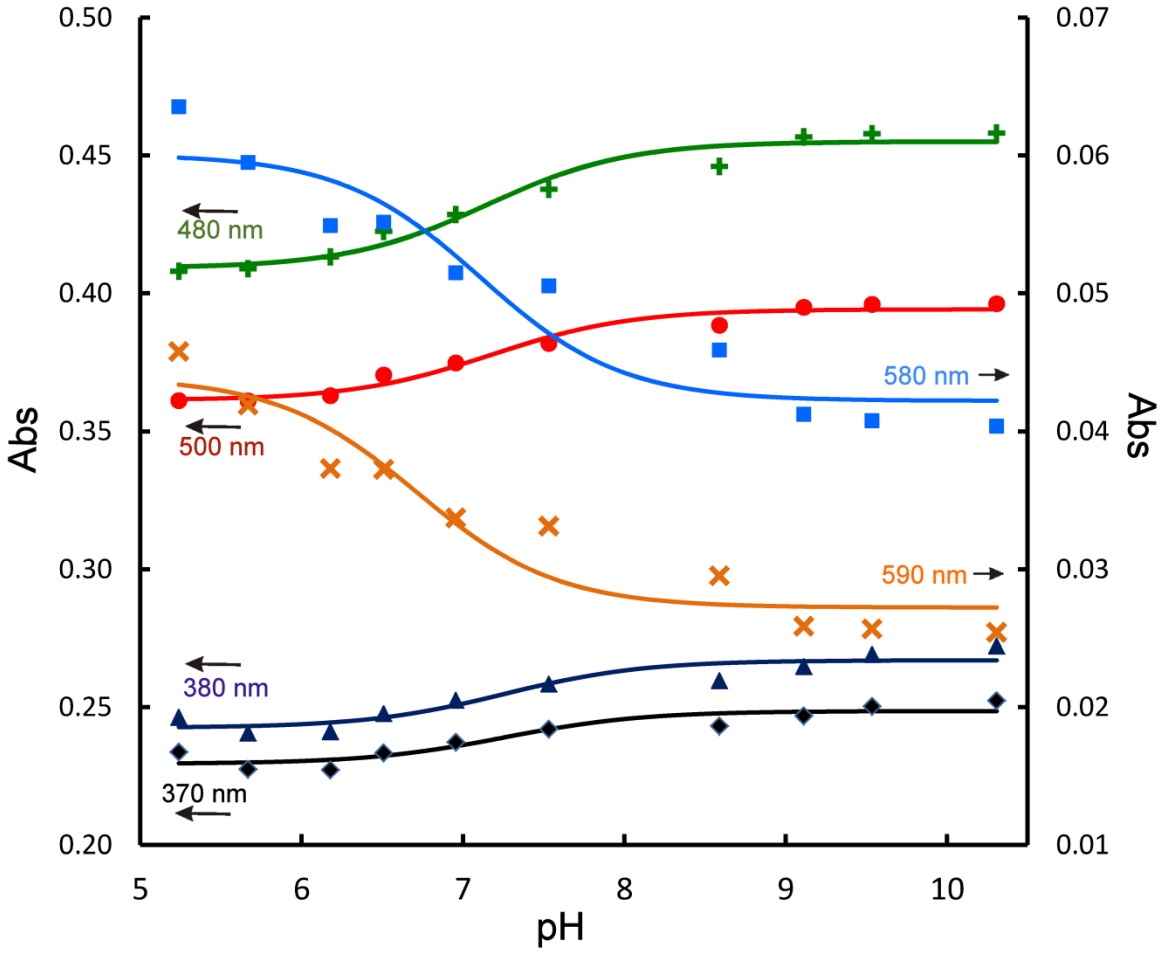

Figure S4. Fit of the change in absorbance of $[AC\text{-}5\text{-}seco\text{-}Cbs]^+$ as a function of pH at 25 ^oC.

Figure S5. Plot of ln K_a against T^{-1} for ionization of coordinated H_2O in $[AC\text{-}5\text{-}seco\text{-}Cbs]^+$. The best fit line ($r^2 = 0.90$) was determined by a weighted least squares method and gave a slope of $1.06 \times 10^4 \pm 2.0 \times 10^3$ and an intercept of -52 ± 7.

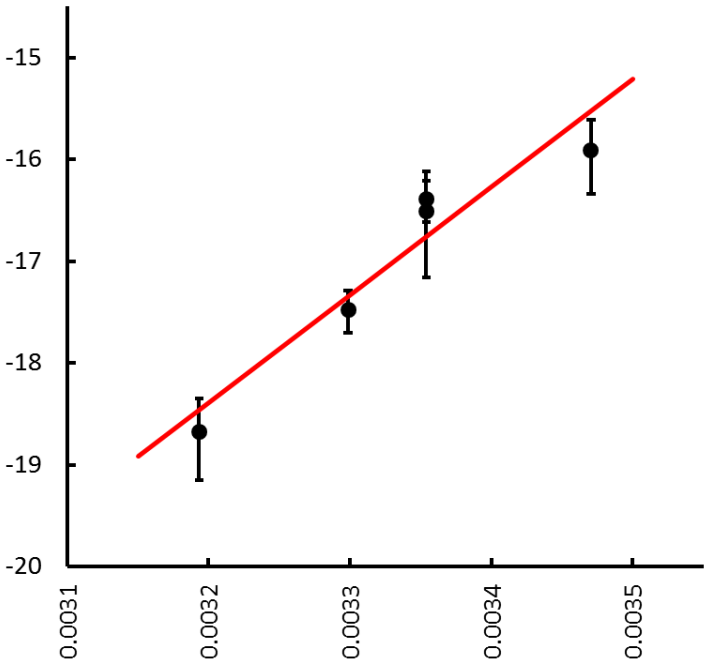

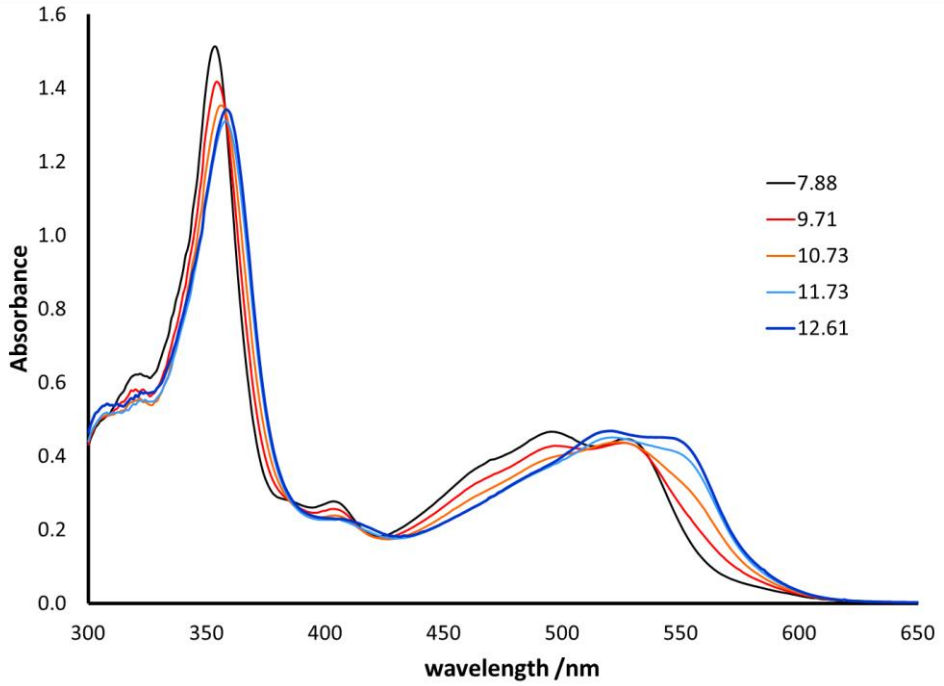

Figure S6. Dependence of the uv-vis spectra of $[ACCbs]^+$ on pH at 10 ^oC. The pH value at which each spectrum was recorded is given in the insert to the figure.

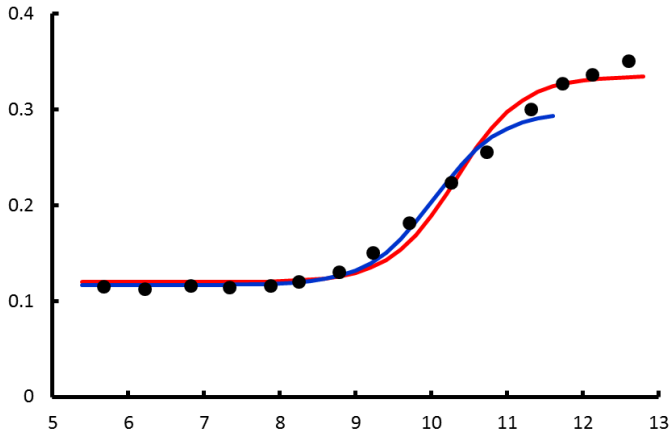

Figure S7a. Change in absorbance at 560 nm with pH for the titration of $[ACCbs]^+$ with OH^-. The experimental data are given as ●. The solid red line is a fit of Eq. 1 to all the data and gave pK_a = 10.33(8). The solid blue line is a fit to all data with pH ≤ 11.3 (i.e., omitting the three data points at the higher pH values). This gave pK_a = 10.04(8).

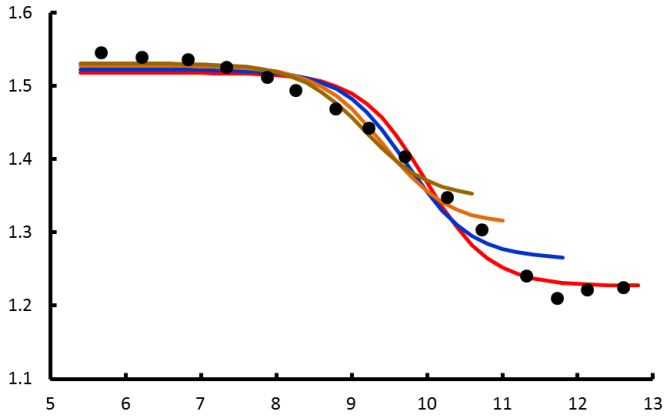

Figure S7b. As for Figure S7a but with absorbance monitored at 353 nm. The red line was fitted to all data and gave pK_a = 10.0(1). For the blue line (data at pH ≤ 11.3), pK_a = 9.7(1). The orange line (data at pH ≤ 10.7) gave pK_a = 9.4(1), and the brown line (pH ≤ 9.2(1).

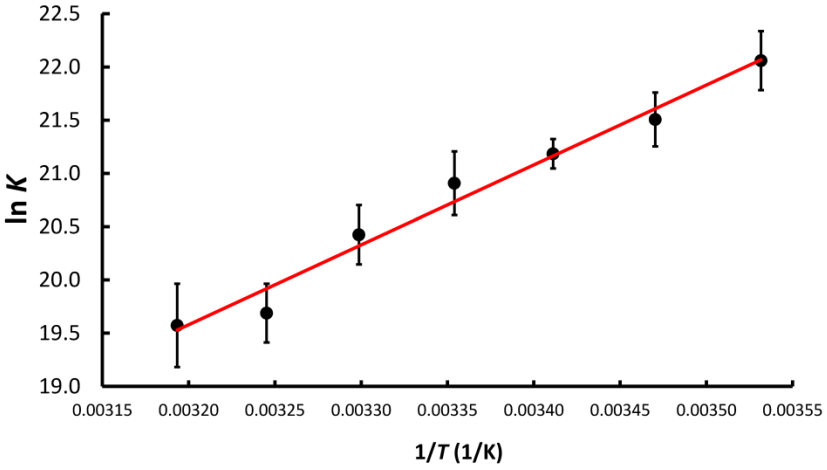

Figure S8A. Plot of ln K against $T^{-1}$for coordination of CN^- by ACCbs determined from a competition titration with N_3^-. From the slope ΔH = –63 ± 4 kJ mol^{-1} and from the intercept ΔS = –38 ± 14 J K^{-1} mol^{-1}. R^2 = 0.979.

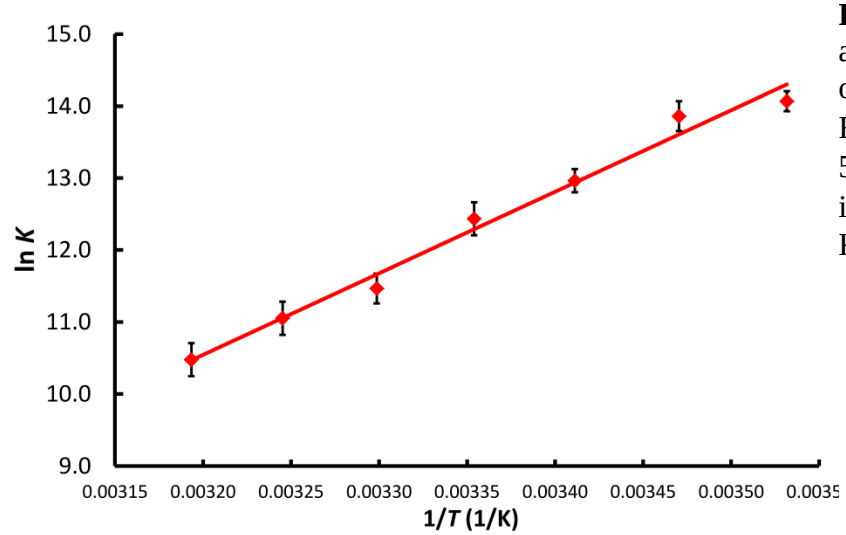

Figure S8B. Plot of ln K against $T^{-1}$for coordination of CN^- by AC-5-seco-Cbs. From the slope ΔH = –93 ± 5 kJ mol^{-1} and from the intercept ΔS = –209 ±18 J K^{-1} mol^{-1}. R^2 = 0.985.

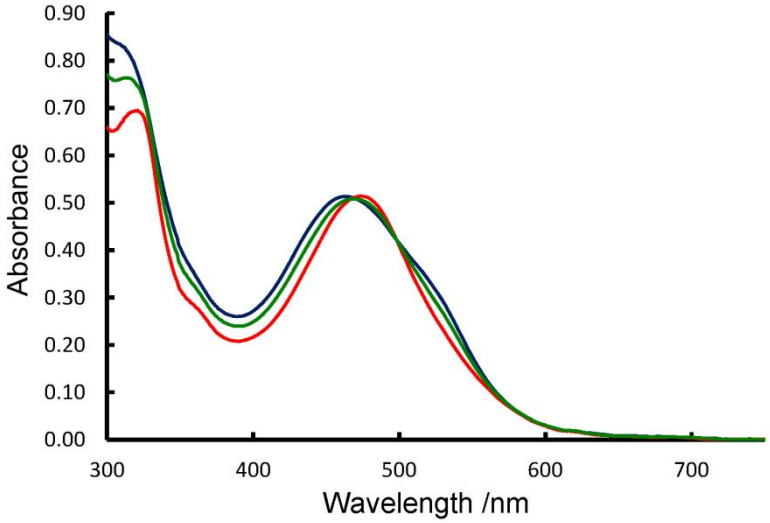

Figure S9A. Spectroscopic changes accompanying the displacement of H_2O in $[AC\text{-}5\text{-}seco\text{-}Cbs]^+$ by CN^- at 25 ^oC, pH 8. $[CN^-]$ = = 0 (blue); 40 μM (green); 20 mM (red).

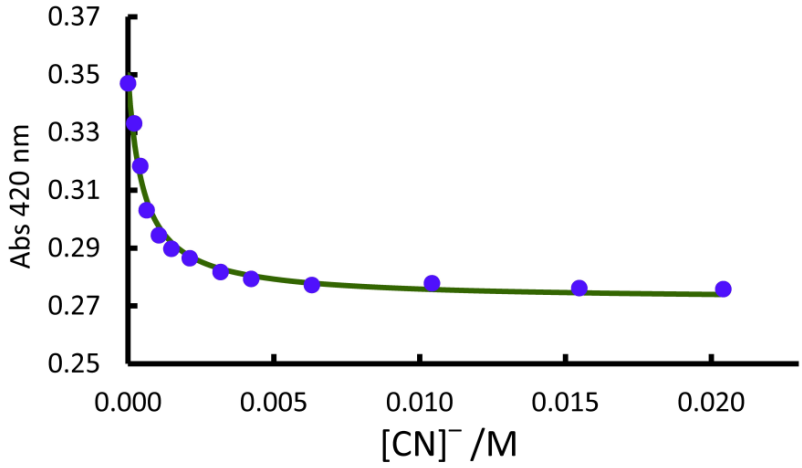

Figure S9B. Fit of Eq. 3 of the text to the absorbance change at 420 nm accompanying the coordination of CN^- by AC-5-seco-Cbs at 25 ^oC, pH 7.97. The best fit line gave A_0 = 0.350 ± 0.003, A_∞ = 0.272 ± 0.002 and K_{obs} = 1.95 × 10^3 ± 2.7 × 10^2.

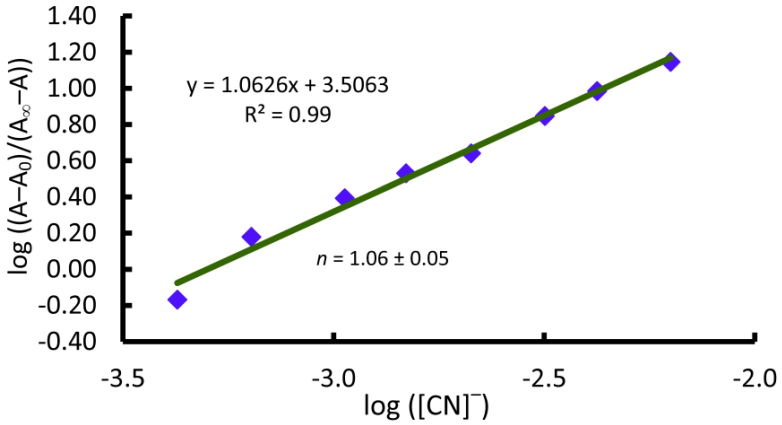

Figure S9C. Hill plot of the 420 nm data of Fig. S8A for coordination of CN^- by AC-5-seco-Cbs. The slope gives the ligand stoichiometry, n = 1.06 ± 0.05. There are no further changes observed up to $[CN^-]$ of 0.25 M, affirming the availability of one single replaceable ligand on the Co(III) corrinoid.

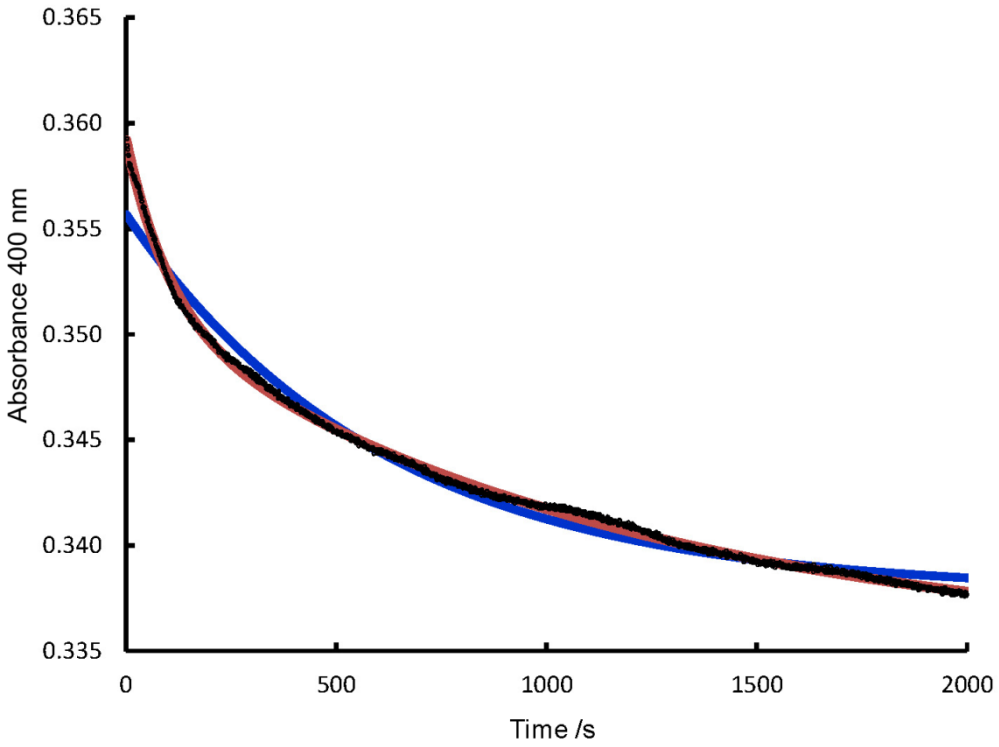

Figure S10. ΔA_{400} with time on substitution of H_2O by CN^- in $[AC\text{-}5\text{-}seco\text{-}Cbs]^+$ at 25 ^oC with $[CN^-]$ = 0.1012 M, pH 10.64. The experimental data are shown as small black dots. The blue line is the best fit line of the data to a single exponential function. It clearly fails to fit the data during the earlier phase of the reaction. The red line is a fit of the experimental data to a double exponential function. The slower phase is attributed to reaction of diaqua-5-seco-Cbs with CN^-. For the data shown the best fit was obtained with $A_0 = 0.3592 \pm 3.6 \times 10^{-5}$; $A_1 = 0.3511 \pm 5.1 \times 10^{-5}$; $A_\infty = 0.3349 \pm 6.1 \times 10^{-5}$; $k_f^{obs} = 9.8(1) \times 10^{-3}$ s^{-1} and $k_s^{obs} = 9.0(1) \times 10^{-4}$ s^{-1}. Correcting for the fraction of the inert hydroxocobester gives $k_f = 22$ s^{-1} and $k_s = 2.0$ s^{-1}, from which $k_f^{II} = 220$ M^{-1} s^{-1} and $k_s^{II} = 20$ M^{-1} s^{-1}.

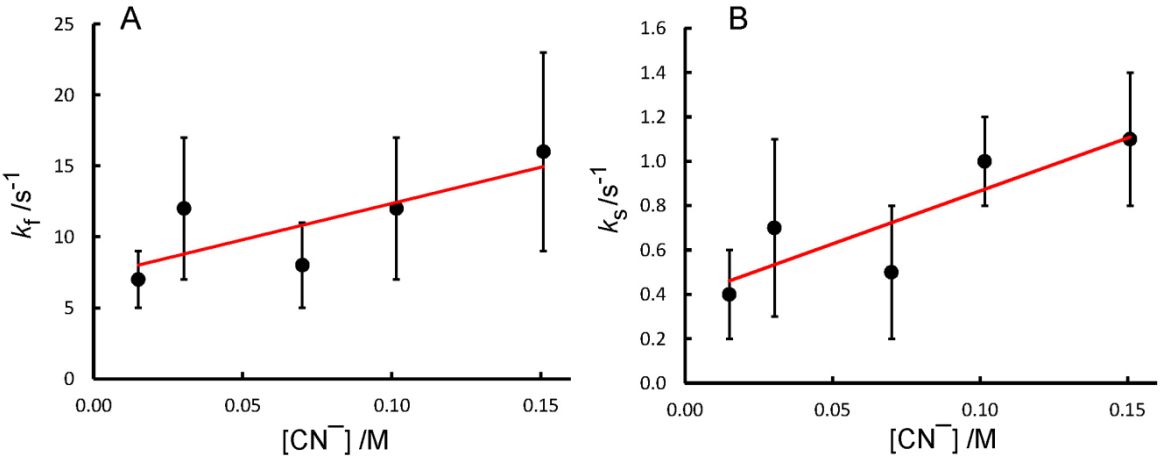

Figure S11. Plots of the rate constant for the fast (k_f) and slow (k_s) phases of the reaction of CN^- with $[AC\text{-}5\text{-}seco\text{-}Cbs]^+$ at 30 °C in CAPS buffer, μ = 0.1 M, pH 10.5. For the fast phase, $k_f^{II} = 53 \pm 23\ M^{-1}\ s^{-1}$ from the slope, and $k_{f,r} = 7.0 \pm 0.5\ s^{-1}$ from the intercept. For the slow phase, $k_s^{II} = 5 \pm 2\ M^{-1}\ s^{-1}$ and $k_{s,r} = 0.4 \pm 0.2\ s^{-1}$.

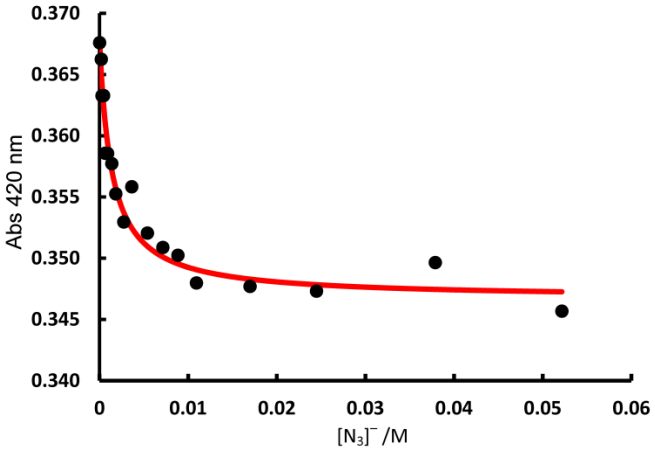

Figure S12A. Fit of Eq. 3 of the text to the absorbance change at 420 nm accompanying the coordination of N_3^- by AC-5-seco-Cbs at 25 ^oC, pH 6.00. The best fit line gave A_0 = 0.368 ± 0.001, A_∞ = 0.347 ± 0.001 and K_{obs} = 7.3 × 10^2 ± 1.5 × 10^2.

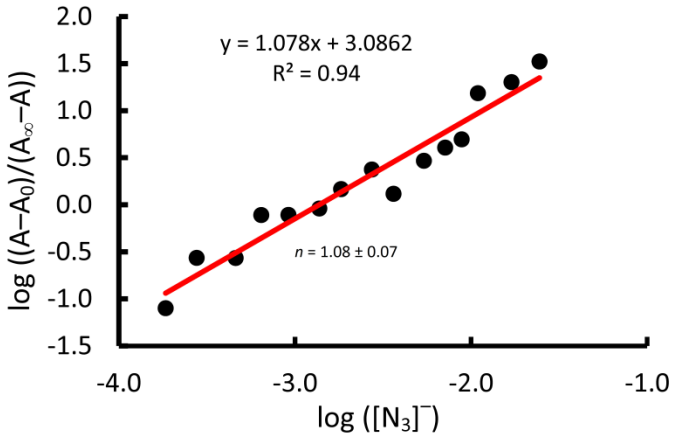

Figure S12B. Hill plot of the 420 nm data of Fig. S9A for coordination of N_3^- by AC-5-seco-Cbs. The slope gives the ligand stoichiometry, n = 1.08 ± 0.07.

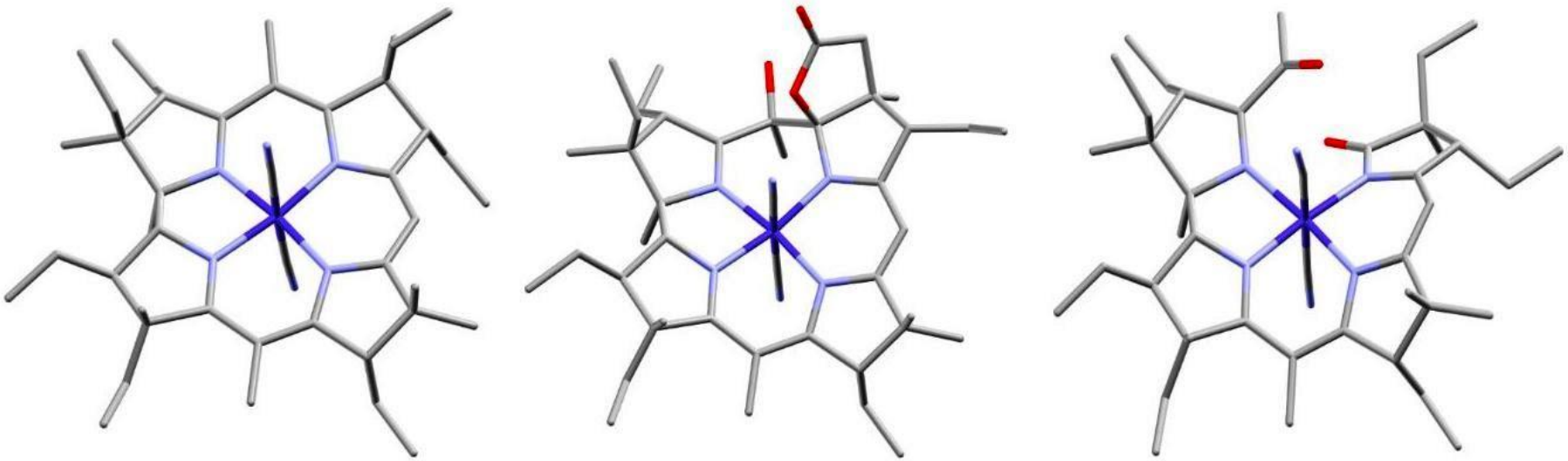

Figure S13. DFT (BP86-D3/6-311G(d,p)) models of DCCbs, DCSYCbs and DC-5-seco-Cbs

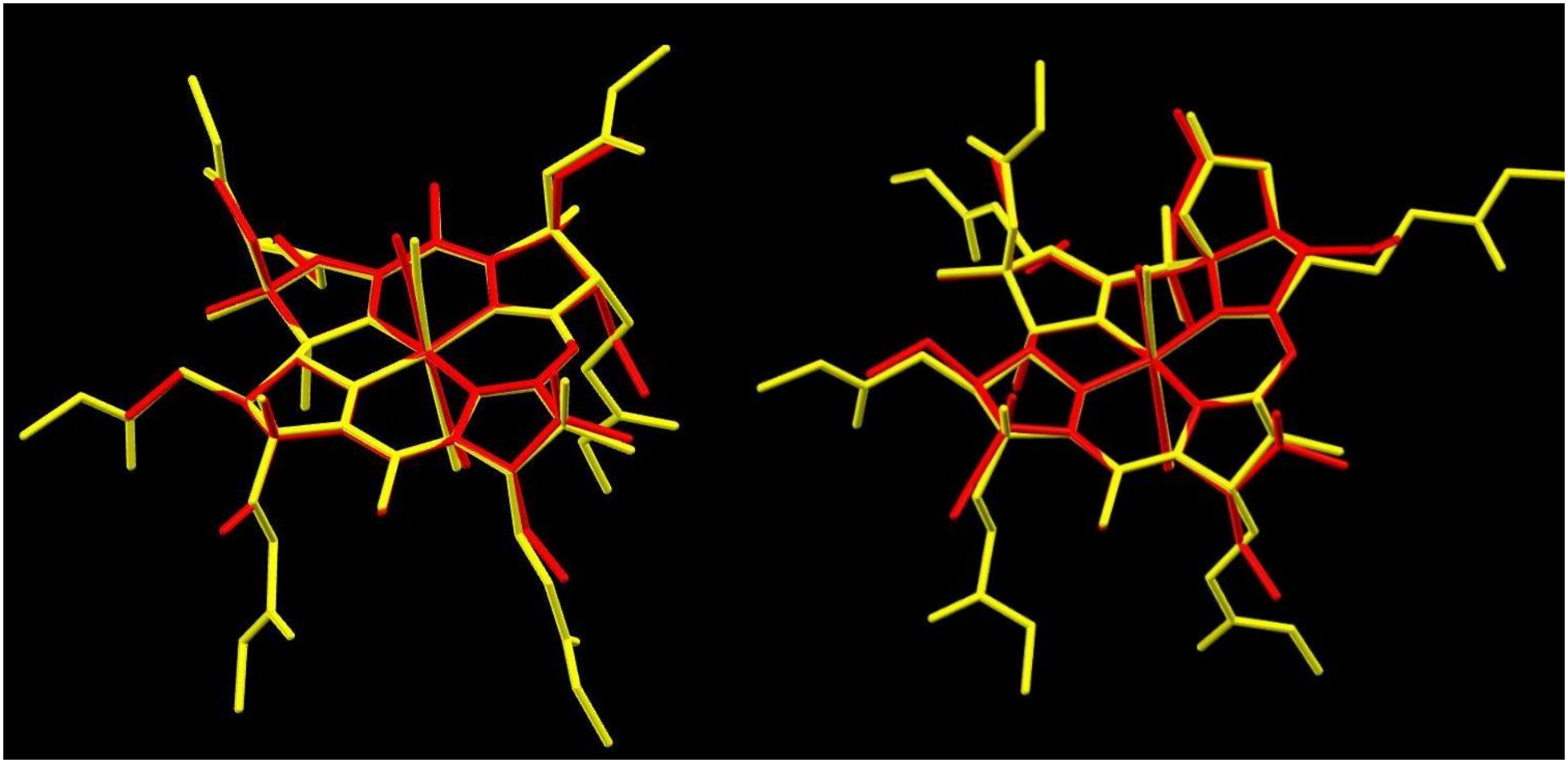

Figure S14. Overlay of the XRD structures of DDCbs and DCSYCbs (yellow) and their BP86-D3/6-311G(d,p)) models (red). The overlay is the best fit of the 24 atoms of the corrin core and Co. RMS deviation of DCCbs = 0.091 Å, and 0.141 Å for DCSYCbs.

A

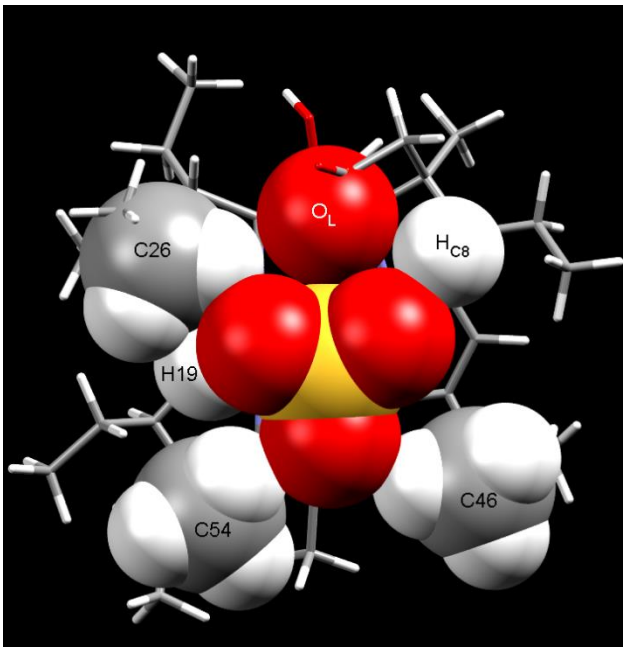

C

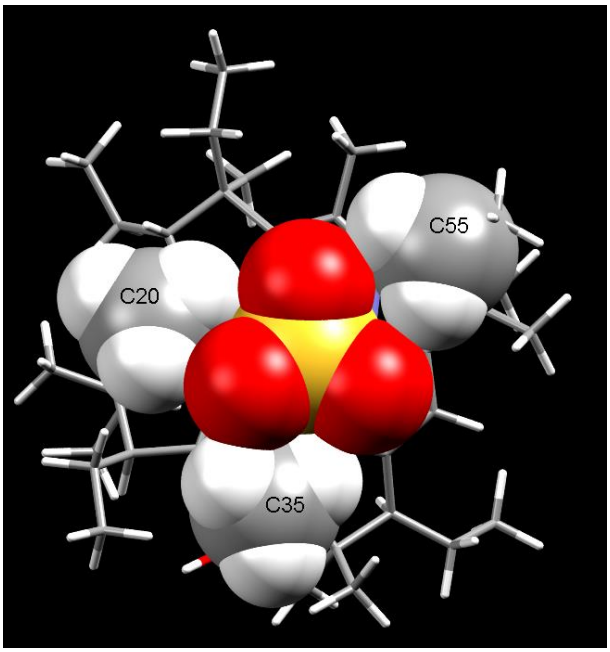

B

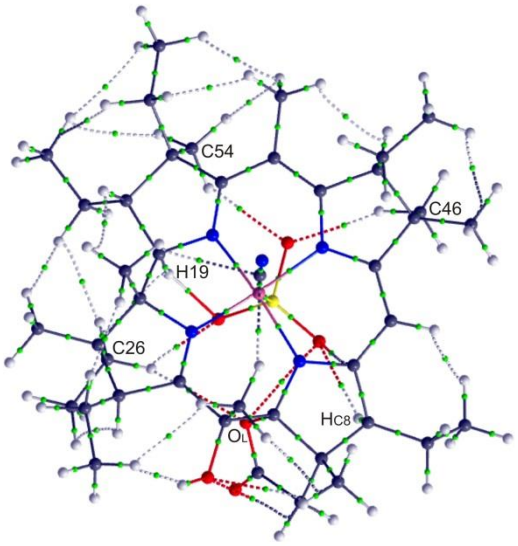

Figure S15. **(A)** The SO_3^{2-} ligand in [α-CN,β-SO_3SYCbs]$^+$ comes in close contact with C26 of the *b* side chain, the lactone oxygen O_L on C76, the C8 proton, H19, and the sentinel C46 and C54 methyl groups. This results in a long Co−S bond of 2.448 Å**.** **(B)** The molecular graph shows that bond paths are developed between the SO_3^{2-} O atoms and these groups. **(C)** Steric crowding on the α face is less severe, and the Co–S bond length is 2.353 Å.

Table S1. ^{1}H and ^{13}C NMR Assignments for [DC-5-seco-Cbs].[a]

Assignment	δ ^{13}C /ppm	δ ^{1}H /ppm	Assignment	δ ^{13}C /ppm	δ ^{1}H /ppm
C53	14.62	2.18	C37	40.06	2.59
C25	16.44	1.24	C37	40.06	2.72
C54	17.49	1.18	C18	40.68	2.91
C36	18.43	0.86	C31	42.11	2.32
C47	18.7	1.2	C31	42.11	
C20	19.06	1.8	C2	47.32	
C41	22.22	1.9	C12	48.39	
C41	22.22		C7	48.54	
C30	24.46	2.01	OCH_3	51.01	3.48
C30	24.46		OCH_3	51.13	
C48	25.15	1.55	C8	51.14	3.27
C48	25.15	1.89	OCH_3	51.3	
C46	27.24	1.07	OCH_3	51.33	3.6
C35	29.06	2.52	OCH_3	51.54	
C56	29.9	2.28	OCH_3	51.81	3.67
C56	29.9	2.62	OCH_3	51.83	
C49	30.1	2.42	C13	53.84	2.99
C60	31.17	2.58	C17	58.81	
C60	31.17	2.71	C3	59.33	3.51
C26	31.96	2.3	C19	75.09	3.7
C26	31.96		C1	87.67	
C55	32.84	1.72	C10	94.04	5.62
C55	32.84	2.38	C15	108.32	
C42	33.17	2.51	Axial CN	131.79	
C42	33.17	2.59	Axial CN	135.43	
C14	161.83		C50	174.09	
C38	171.62		C16	177.28	
C61	172.27		C9	179.19	
C57	172.54		C11	182.03	
C27, C32 or C43	173.48		C6	187.81	
C27, C32 or C43	173.52		C4	188.01	
C27, C32 or C43	173.92		C5	196.9	

[a]As with DCSYCbs (Chemaly, S. M.; Brown, K. L.; Fernandes, M. A.; Munro, O. Q.; Grimmer, C.; Marques, H. M. *Inorg. Chem.* **2011**, *50*, 8700-8718) we were unable to assign the specific ester side chain resonances.

Table S2. ^{13}C NMR Assignments for DC-5-seco-Cbs and a Comparison with the Assignments for DCCbs and DCSYCbs.[a]

	DC-5-seco-Cbs	DCCbs	Δ[b]	DCSYCbs	Δ[c]
Assignment	**δ ^{13}C / ppm**	**δ ^{13}C / ppm**	**δ ^{13}C / ppm**	**δ ^{13}C / ppm**	**δ ^{13}C / ppm**
C53	14.62	15.75	*1.13*	14.96	*0.34*
C25	16.44	17.39	*0.95*	16.05	*-0.39*
C54	17.49	18.36	*0.87*	18.43	*0.94*
C36	18.43	19.81	*1.38*	17.32	*-1.11*
C47	18.70	19.81	*1.11*	20.06	*1.36*
C20	19.06	22.71	*3.65*	21.75	*2.69*
C41	22.22	27.34	*5.12*	22.29	*0.07*
C30	24.46	25.79	*1.33*	22.88	*-1.58*
C48	25.15	26.74	*1.59*	25.75	*0.60*
C46	27.24	31.29	*4.05*	30.71	*3.47*
C35	29.06	16.17	*-12.89*	23.55	*-5.51*
C56	29.90	30.63	*0.73*	29.71	*-0.19*
C49	30.10	31.78	*1.68*	31.04	*0.94*
C60	31.17	32.25	*1.08*	31.85	*0.68*
C26	31.96	42.38	*10.42*	40.55	*8.59*
C55	32.84	33.32	*0.48*	32.87	*0.03*
C42	33.17	32.03	*-1.14*	32.47	*-0.70*
C37	40.06	43.19	*3.13*	45.35	*5.29*
C18	40.68	40.64	*-0.04*	39.88	*-0.80*
C31	42.11	34.37	*-7.74*	31.70	*-10.41*
C2	47.32	47.21	*-0.11*	45.48	*-1.84*
C12	48.39	48.04	*-0.35*	46.69	*-1.70*
C7	48.54	49.95	*1.41*	50.69	*2.15*
OCH_3	51.01	52.10	*1.09*	51.68	*0.67*
OCH_3	51.13	52.10	*0.97*	51.83	*0.70*
C8	51.14	55.62	*4.48*	55.91	*4.77*
OCH_3	51.30	52.30	*1.00*	51.91	*0.61*
OCH_3	51.33	52.30	*0.97*	52.09	*0.76*
OCH_3	51.54	52.40	*0.86*	52.41	*0.87*
OCH_3	51.81	52.40	*0.59*	52.68	*0.87*
OCH_3	51.83	52.83	*1.00*		
C13	53.84	54.78	*0.94*	53.47	*-0.37*
C17	58.81	59.71	*0.90*	58.44	*-0.37*
C3	59.33	57.97	*-1.36*	58.58	*-0.75*
C19	75.09	76.19	*1.10*	76.00	*0.91*
C1	87.67	83.98	*-3.69*	84.80	*-2.87*
C10	94.04	92.19	*-1.85*	85.54	*-8.50*
C15	108.32	103.96	*-4.36*	100.74	*-7.58*

Assignment	DC-5-seco-Cbs δ ^{13}C / ppm	DCCbs δ ^{13}C / ppm	Δ^b δ ^{13}C / ppm	DCSYCbs δ ^{13}C / ppm	Δ^c δ ^{13}C / ppm
axial CN	131.79	133.50	*1.71*	100.74	*-31.05*
axial CN	135.43	134.00	*-1.43*	134.30	*-1.13*
C14	161.83	164.63	*2.80*	164.60	*2.77*
C38	171.62	172.26	*0.64*	171.98	*0.36*
C61	172.27	173.62	*1.35*	172.61	*0.34*
C57	172.54	174.31	*1.77*	173.00	*0.46*
C27, C32 or C43	173.48	173.22	*-0.26*	172.14	*-1.34*
C27, C32 or C43	173.52	174.39	*0.87*	172.61	*-0.91*
C27, C32 or C43	173.92	174.94	*1.02*	172.81	*-1.11*
C50	174.09	175.28	*1.19*	174.07	*-0.02*
C16	177.28	177.65	*0.37*	174.32	*-2.96*
C9	179.19	173.15	*-6.04*	176.82	*-2.37*
C11	182.03	177.97	*-4.06*	175.64	*-6.39*
C6	187.81	164.83	*-22.98*	111.97	*-75.84*
C4	188.01	177.48	*-10.53*	191.19	*3.18*
C5	196.89	105.46	*-91.43*	79.04	*-117.85*

[a]Assignments for DCCbs and DCSYCbs from Chemaly, S. M.; Brown, K. L.; Fernandes, M. A.; Munro, O. Q.; Grimmer, C.; Marques, H. M. *Inorg. Chem.* **2011**, *50*, 8700-8718.

[b]$\Delta = \delta\ ^{13}C_{DCCbs} - \delta\ ^{13}C_{DC\text{-}5\text{-}seco\text{-}Cbs}$

[c]$\Delta = \delta\ ^{13}C_{DCSYCbs} - \delta\ ^{13}C_{DC\text{-}5\text{-}seco\text{-}Cbs}$

Table S3. Rate constants for the substitution of H_2O by CN^- in $[AC\text{-}5\text{-}seco\text{-}Cbs]^+$, μ = 0.1 M (CHAPS buffer)

Temp /°C	$[CN^-]$ /M	pH	pK_a ($[AC\text{-}5\text{-}seco\text{-}Cbs]^+$)	k_f^{obs} /$\times 10^{-2}$ s^{-1} [a]	k_s^{obs} /$\times 10^{-3}$ s^{-1} [a]	k_f /s^{-1} [b]	k_s /s^{-1} [b]	k_f^{II} /$M^{-1}s^{-1}$	$k_{f,r}$ [c] /s^{-1}	k_s^{II} /$M^{-1}s^{-1}$	$k_{s,r}$ [c] /s^{-1}
25	0.0200	10.55	7.28	0.7(2)	0.6(1)	13(4)	1.2(2)	114(38)	15.2(5)	9(3)	1.3(3)
	0.0592	10.55		1.5(6)	1.1(3)	28(11)	2.1(5)				
	0.1012	10.63		1.1(5)	0.9(3)	27(11)	2.1(6)				
	0.1498	10.56		1.9(9)	1.5(4)	35(18)	2.9(9)				
	0.2024	10.65		1.4(7)	1.1(3)	34(16)	2.7(7)				
30	0.0150	10.47	7.53	0.8(2)	0.5(2)	7(2)	0.4(2)	53(23)	7.0(5)	5(2)	0.4(2)
	0.0303	10.52		1.2(5)	0.8(4)	12(5)	0.7(4)				
	0.0700	10.52		0.8(3)	0.5(3)	8(3)	0.5(3)				
	0.1016	10.52		1.2(5)	1.1(2)	12(5)	1.0(2)				
	0.1509	10.54		1.5(7)	1.1(3)	16(7)	1.1(3)				
35	0.0148	10.48	7.78	1.0(2)	0.7(1)	5.2(8)	0.34(5)	68(7)	4(1)	4(1)	0.32(8)
	0.0296	10.47		1.2(4)	0.9(2)	6(2)	0.45(9)				
	0.0707	10.56		1.7(3)	1.4(5)	10(2)	0.8(3)				
	0.0994	10.55		1.8(5)	1.0(3)	11(3)	0.6(2)				
	0.1515	10.56		2.3(1.4)	1.5(8)	14(8)	0.9(5)				
40	0.0148	10.41	8.02	1.1(2)	0.9(1)	2.6(4)	0.21(3)	29(8)	1.9(6)	1.9(5)	0.18(4)
	0.0149	10.37		0.8(1)	0.72(8)	1.9(2)	0.16(2)				
	0.0300	10.41		1.6(3)	1.2(2)	3.8(7)	0.29(4)				
	0.0301	10.41		1.11(8)	0.96(5)	2.7(2)	0.24(1)				
	0.0701	10.39		1.3(3)	1.4(4)	3.0(7)	0.33(9)				
	0.0696	10.45		1.3(1)	1.0(2)	3.4(3)	0.28(6)				
	0.1012	10.45		3(2)	1.3(1)	7(4)	0.35(4)				
	0.1002	10.51		1.9(5)	1.3(3)	6(1)	0.39(8)				
	0.1485	10.41		1.7(4)	1.5(2)	4(1)	0.36(5)				
	0.1515	10.52		2.6(9)	2.3(7)	8(3)	0.7(2)				

[a]Mean and standard deviation of five experiments. [b]Corrected for the fraction of inert hydroxocyano-seco-cobester. No correction was made for the pK_a of HCN. Both HCN and CN^- are known to react with $[H_2OCbl]^+$ but the reaction with CN^- is an order of magnitude faster (Reenstra, W. W.; Jencks, W. P*J. Am. Chem. Soc.* **1979,** 101, 5780-5791; Marques, H. M.; Brown, K. L.; Jacobsen, D. W. *J. Biol. Chem.* **1988,** 263, 12378-12383). At the pH of these experiments cyanide is >95% present as CN^-. Apparent reverse rate constants, from the intercept of k_i (i = f,s) against $[CN^-]$.

Table S4. Comparison on the coordination sphere geometry of DCCbs and DCSYCbs determined by DFT methods and X-ray diffraction structures.

DCCbs	BP86-D3/6-311G(d,p)	BP86-D3/6-311++G(d,p)	B3LYP/6-311++G(d,p)	PBE0 6-311++G(d,p)	PBEPBE 6-311++G(d,p)	XRD data	BP86-D3/6-311G(d,p)		BP86-D3/6-311++G(d,p)		B3LYP/6-311++G(d,p)		PBE0 6-311++G(d,p)		PBEPBE 6-311++G(d,p)	
Bond	*r* /Å	*r* /Å	*r* /Å	*r* /Å	*r* /Å	**CODZAW10[e]**	Δ[a]	Rel%Δ[b]	Δ	Rel%Δ	Δ	Rel%Δ	Δ	Rel%Δ	Δ	Rel%Δ
Co-CN(α)[c]	1.925	1.933	1.956	1.938	1.935	1.925	0.000	0.00%	-0.008	0.42%	-0.031	1.61%	-0.013	0.68%	-0.010	0.52%
Co-CN(β)[d]	1.928	1.936	1.961	1.934	1.938	1.924	-0.004	0.21%	-0.012	0.62%	-0.037	1.92%	-0.010	0.52%	-0.014	0.73%
Co-N(21)	1.890	1.894	1.912	1.892	1.899	1.893	0.003	0.16%	-0.001	0.05%	-0.019	1.00%	0.001	0.05%	-0.006	0.32%
Co-N(22)	1.937	1.942	1.953	1.924	1.947	1.920	-0.017	0.89%	-0.022	1.15%	-0.033	1.72%	-0.004	0.21%	-0.027	1.41%
Co-N(23)	1.933	1.935	1.943	1.933	1.937	1.932	-0.001	0.05%	-0.003	0.16%	-0.011	0.57%	-0.001	0.05%	-0.005	0.26%
Co-N(24)	1.891	1.895	1.912	1.892	1.900	1.914	0.023	1.20%	0.019	0.99%	0.002	0.10%	0.022	1.15%	0.014	0.73%
Average Deviation coord sphere								0.42%		0.56%		1.15%		0.44%		0.66%
Angle	/deg	/deg	/deg	/deg	/deg		Δ	Rel%Δ	Δ	Rel%Δ	Δ	Rel%Δ	Δ	Rel%Δ	Δ	Rel%Δ
CN(α)-Co-CN(β)	176.8	177.0	177.1	177.5	177.0	175.0	-1.8	1.03%	-2.000	1.14%	-2.100	1.20%	-2.500	1.43%	-2.000	1.14%
N(21)-Co-N23	173.4	173.2	173.2	172.9	173.2	173.4	0.0	0.00%	0.200	0.12%	0.200	0.12%	0.500	0.29%	0.200	0.12%
N(22)-Co-N24	173.2	173.1	172.9	173.2	172.9	172.4	-0.8	0.46%	-0.700	0.41%	-0.500	0.29%	-0.800	0.46%	-0.500	0.29%
Average Deviation coord sphere								0.50%		0.55%		0.54%		0.73%		0.52%
Corrin fold angle	3.3	3.1	5.0	3.9	3.9	5.2										

Continued on next page

DCSYCbs	BP86-D3/6-311G(d,p)	BP86-D3/6-311++G(d,p)	B3LYP/6-311++G(d,p)	PBE0 6-311++G(d,p)	PBEPBE 6-311++G(d,p)	XRD data	BP86-D3/6-311G(d,p)		BP86-D3/6-311++G(d,p)		B3LYP/6-311++G(d,p)		PBE0 6-311++G(d,p)		PBEPBE 6-311++G(d,p)	
Bond	*r* /Å		*r* /Å	*r* /Å	*r* /Å	XEHDIZ[f]	Δ[a]	Rel%Δ[b]			Δ	Rel%Δ	Δ	Rel%Δ	Δ	Rel%Δ
Co-CN(α)[c]	1.920		1.952	1.934	1.930	1.918	-0.002	0.10%			-0.034	1.77%	-0.016	0.83%	-0.012	0.63%
Co-CN(β)[d]	1.928		1.956	1.935	1.934	1.930	0.002	0.10%			-0.026	1.35%	-0.005	0.26%	-0.004	0.21%
Co-N(21)	1.902		1.931	1.916	1.910	1.901	-0.001	0.05%			-0.030	1.58%	-0.015	0.79%	-0.009	0.47%
Co-N(22)	1.943		1.957	1.943	1.948	1.931	-0.012	0.62%			-0.026	1.35%	-0.012	0.62%	-0.017	0.88%
Co-N(23)	1.916		1.921	1.907	1.920	1.883	-0.033	1.75%			-0.038	2.02%	-0.024	1.27%	-0.037	1.96%
Co-N(24)	1.878		1.895	1.882	1.883	1.879	0.001	0.05%			-0.016	0.85%	-0.003	0.16%	-0.004	0.21%
Average Deviation coord sphere								0.45%				1.49%		0.66%		0.73%
Angle	/deg	/deg	/deg	/deg	/deg		Δ	Rel%Δ	Δ	Rel%Δ	Δ	Rel%Δ	Δ	Rel%Δ	Δ	Rel%Δ
CN(α)-Co-CN(β)	173.3		174.4	174.6	173.4	173.0	-0.3	0.17%			-1.400	0.81%	-1.600	0.92%	-0.400	0.23%
N(21)-Co-N23	172.8		172.8	172.6	172.7	173.4	0.6	0.35%			0.600	0.35%	0.800	0.46%	0.700	0.40%
N(22)-Co-N24	168.4		169.2	169.4	168.7	169.9	1.5	0.88%			0.700	0.41%	0.500	0.29%	1.200	0.71%
Average Deviation coord sphere								0.47%				0.52%		0.56%		0.45%
Corrin fold angle	19.6		17.4	21.7	22.7	15.6										

[a]Δ is is the difference in the parameter between the XRD structure and the DFT structure. [b]The difference Δ expressed as an absolute percentage relative deviation. [c]Co–CN bond length to cyanide coordinated in the α coordination site. [d]Co–CN bond length to cyanide coordinated in the β coordination site. [e]Markwell, A.J.; Pratt, J.M.; Shaikjee, M.S.; Toerien, J.G. *J. Chem. Soc., Dalton Trans.* **1987**, 1349-1357. The average σ(C–C bonds) is 0.01–0.03 Å. [f]Chemaly, S. M.; Brown, K. L.; Fernandes, M. A.; Munro, O. Q.; Grimmer, C.; Marques, H. M. *Inorg. Chem.* **2011,** *50*, 8700-8718. The average σ(C–C bonds) is 0.006–0.010 Å.

Table S5. Charges q(r)/*e* on cobalt and the six inner coordination sphere donor atoms in [(X)(CN)Co(corrin)]$^{n+}$ complexes determined from a QTAIM analysis of the wavefunction of their BP86-D3/6-311G(d,p) structures.

X	**Corrin**									
CN^-			**Co**	**N21**	**N22**	**N23**	**N24**	**C(α)**	**C(β)**	**Σ Coord Sphere[a]**	**Σ(Co & eq N)[b]**
	Cbs		1.125	-0.993	-1.022	-1.028	-1.001	0.636	0.638	-1.645	-2.919
	SYCbs		1.112	-1.002	-1.003	-1.034	-1.002	0.632	0.650	-1.647	-2.929
	5-Seco-Cbs		1.118	-0.950	-0.998	-1.027	-1.001	0.643	0.652	-1.564	-2.858
SO_3^{2-}			**Co**	**N21**	**N22**	**N23**	**N24**	**C**	**S**	**Av Σ Coord Sphere[c]**	**Av Σ(Co & eq N)[d]**
	Cbs	Alpha sulfito	1.057	-0.981	-1.021	-1.027	-0.993	0.619	2.477	0.124	-2.965
		Beta sulfito	1.057	-0.987	-1.014	-1.024	-0.996	0.616	2.464		
	SYCbs	Alpha sulfito	1.044	-0.987	-0.996	-1.040	-0.991	0.638	2.479	0.120	-2.988
		Beta sulfito	1.040	-0.991	-1.011	-1.032	-1.012	0.620	2.479		
	5-Seco-Cbs	Alpha sulfito	1.050	-0.947	-0.994	-1.031	-0.993	0.657	2.467	0.166	-2.926
		Beta sulfito	1.054	-0.963	-1.002	-1.035	-0.991	0.647	2.412		
NO_2^-			**Co**	**N21**	**N22**	**N23**	**N24**	**C**	**N**	**Av Σ Coord Sphere[c]**	**Av Σ(Co & eq N)[d]**
	Cbs	Alpha nitro	1.146	-0.994	-1.017	-1.029	-1.000	0.644	0.381	-1.868	-2.896
		Beta nitro	1.146	-0.995	-1.022	-1.026	-1.001	0.645	0.387		
	SYCbs	Alpha nitro	1.134	-1.009	-0.996	-1.039	-0.996	0.656	0.381	-1.873	-2.914
		Beta nitro	1.131	-1.003	-1.012	-1.030	-1.008	0.645	0.400		
	5-Seco-Cbs	Alpha nitro	1.133	-0.955	-1.000	-1.030	-1.001	0.666	0.392	-1.787	-2.843
		Beta nitro	1.141	-0.952	-0.995	-1.029	-0.997	0.648	0.405		
N_3^-			**Co**	**N21**	**N22**	**N23**	**N24**	**C**	**N**	**Av Σ Coord Sphere[c]**	**Av Σ(Co & eq N)[d]**
	Cbs	Alpha azido	1.152	-0.987	-1.013	-1.029	-1.006	0.660	-0.328	-2.564	-2.884
		Beta azido	1.151	-0.990	-1.024	-1.026	-0.995	0.657	-0.350		
	SYCbs	Alpha azido	1.145	-1.003	-0.997	-1.032	-1.008	0.670	-0.351	-2.586	-2.897
		Beta azido	1.144	-1.001	-1.011	-1.033	-0.998	0.652	-0.348		
	5-Seco-Cbs	Alpha azido	1.151	-0.952	-1.004	-1.031	-0.997	0.672	-0.329	-2.502	-2.825
		Beta azido	1.152	-0.947	-1.000	-1.027	-0.994	0.658	-0.356		

X	Corrin										
H_2O			Co	N21	N22	N23	N24	C	O	Av Σ Coord Sphere[c]	Av Σ(Co & eq N)[d]
	Cbs	Alpha aqua	1.131	-1.009	-1.019	-1.035	-1.017	0.685	-1.059	-3.321	-2.951
		Beta aqua	1.130	-1.014	-1.022	-1.027	-1.020	0.687	-1.052		
	SYCbs	Alpha aqua	1.121	-1.026	-1.003	-1.044	-1.021	0.695	-1.061	-3.359	-2.971
		Beta aqua	1.130	-1.028	-1.021	-1.041	-1.008	0.679	-1.090		
	5-Seco-Cbs	Alpha aqua	1.131	-1.009	-1.019	-1.035	-1.017	0.685	-1.059	-3.311	-2.920
		Beta aqua	1.142	-0.979	-1.016	-1.024	-1.013	0.68	-1.089		

[a]Sum of the QTAIM charges on Co and the six donor atoms of its inner coordination sphere. [b]Sum of the QTAIM charges on Co and the four equatorial donor atoms of the corrin. [c]As for Footnote a, averaged over the two diastereomers. [d]As for Footnote b, averaged over the two diastereomers.

Table S6. The coordination geometry and analysis of the topological properties of the electron density of the bonds in the coordination sphere of $[(X)(CN)Co(5\text{-seco-Cbs})]^{n+}$ determined from the BP86-D3/6-311G(d,p) structures

$[(CN)_2Co(Corrin)]$																	
Bond	Corrin		Bond length /Å	ρ	$\nabla^2\rho_r$	V_r	G_r	H_r	$\lvert V_r\rvert/G_r$		Bond length (av) /Å	ρ_r (av)	$\nabla^2\rho_r$ (av)	$\lvert V_r\rvert/G_r$ (av)	V_r (av)	G_r (av)	H_r (av)
Co-CN(a)	Cbs		1.925	0.116	0.286	-0.146	0.109	-0.037	1.339	Co-CN	1.927	0.116	0.287	1.335	-0.146	0.109	-0.037
	SYCbs		1.920	0.116	0.296	-0.149	0.111	-0.038	1.342		1.924	0.116	0.289	1.349	-0.147	0.109	-0.038
	5SecoCbs		1.917	0.118	0.285	-0.149	0.110	-0.039	1.355		1.923	0.116	0.283	1.349	-0.147	0.109	-0.038
Co-CN(b)	Cbs		1.928	0.115	0.288	-0.145	0.109	-0.036	1.330								
	SYCbs		1.928	0.115	0.281	-0.145	0.107	-0.038	1.355								
	5SecoCbs		1.928	0.115	0.282	-0.145	0.108	-0.037	1.343								
Co-N21	Cbs		1.890	0.117	0.469	-0.179	0.148	-0.031	1.209	Co-N(corrin)	1.913	0.110	0.449	1.189	-0.166	0.139	-0.027
	SYCbs		1.902	0.111	0.485	-0.175	0.148	-0.027	1.182		1.91	0.111	0.450	1.198	-0.168	0.140	-0.028
	5SecoCbs		1.947	0.099	0.436	-0.149	0.129	-0.020	1.155		1.933	0.104	0.431	1.178	-0.155	0.131	-0.024
Co-N22	Cbs		1.937	0.103	0.428	-0.152	0.130	-0.022	1.169								
	SYCbs		1.943	0.102	0.413	-0.148	0.125	-0.023	1.184								
	5SecoCbs		1.968	0.095	0.399	-0.136	0.118	-0.018	1.153								
Co-N23	Cbs		1.933	0.104	0.431	-0.154	0.131	-0.023	1.176								
	SYCbs		1.916	0.110	0.434	-0.162	0.135	-0.027	1.200								
	5SecoCbs		1.924	0.107	0.427	-0.156	0.131	-0.025	1.191								
Co-N24	Cbs		1.891	0.116	0.467	-0.178	0.148	-0.030	1.203								
	SYCbs		1.878	0.121	0.470	-0.185	0.151	-0.034	1.225								
	5SecoCbs		1.893	0.116	0.464	-0.177	0.146	-0.031	1.212								
$[(SO3(CN)Co(corrin)]^-$																	
Bond	Corrin		Bond length /Å	ρ	$\nabla^2\rho_r$	V_r	G_r	H_r	$\lvert V_r\rvert/G_r$		Bond length (av) /Å	ρ_r (av)	$\nabla^2\rho_r$ (av)	$\lvert V_r\rvert/G_r$ (av)	V_r (av)	G_r (av)	H_r (av)
Co-SO_3	Cbs	α–SO_3	2.333	0.080	0.106	-0.067	0.047	-0.020	1.433	Co-SO_3	2.334	0.080	0.107	1.430	-0.067	0.047	-0.020
		β–SO_3	2.334	0.080	0.108	-0.067	0.047	-0.020	1.428								
	SYCbs	α–SO_3	2.353	0.076	0.104	-0.063	0.045	-0.019	1.417		2.401	0.070	0.091	1.423	-0.056	0.039	-0.017
		β–SO_3	2.448	0.064	0.077	-0.049	0.034	-0.015	1.429								
	5SecoCbs	α–SO_3	2.240	0.067	0.086	-0.053	0.037	-0.016	1.422		2.24	0.069	0.098	1.399	-0.057	0.041	-0.016
		β–SO_3	2.240	0.071	0.110	-0.061	0.044	-0.017	1.376								
Co-CN	Cbs	α–SO_3	2.000	0.097	0.269	-0.119	0.093	-0.026	1.279	Co-CN	1.993	0.099	0.271	1.284	-0.121	0.095	-0.027
		β–SO_3	1.986	0.100	0.273	-0.124	0.096	-0.028	1.289								
	SYCbs	α–SO_3	1.987	0.100	0.270	-0.123	0.095	-0.028	1.293		1.975	0.103	0.280	1.293	-0.128	0.099	-0.029
		β–SO_3	1.962	0.105	0.290	-0.133	0.103	-0.030	1.293								
	5SecoCbs	α–SO_3	1.906	0.106	0.273	-0.131	0.099	-0.031	1.314		1.918	0.109	0.278	1.319	-0.135	0.102	-0.033
		β–SO_3	1.929	0.112	0.284	-0.139	0.105	-0.034	1.325								
Co-N21	Cbs	α–SO_3	1.873	0.120	0.512	-0.195	0.161	-0.034	1.208	Co-N(corrin)	1.898	0.113	0.486	1.191	0.179	-0.150	0.029
		β–SO_3	1.875	0.120	0.511	-0.194	0.161	-0.033	1.205								
	SYCbs	α–SO_3	1.870	0.120	0.539	-0.200	0.167	-0.033	1.195		1.894	0.114	0.488	1.194	0.181	-0.152	0.030
		β–SO_3	1.888	0.113	0.525	-0.187	0.159	-0.028	1.176								

	5SecoCbs	α–SO_3	1.962	0.110	0.495	-0.176	0.150	-0.026	1.175		1.929	0.110	0.470	1.185	0.171	-0.144	0.027
		β–SO_3	1.946	0.111	0.485	-0.176	0.149	-0.027	1.184								
Co-N22	Cbs	α–SO_3	1.924	0.106	0.462	-0.163	0.139	-0.024	1.172								
		β–SO_3	1.923	0.106	0.461	-0.163	0.139	-0.024	1.173								
	SYCbs	α–SO_3	1.930	0.104	0.443	-0.157	0.134	-0.023	1.173								
		β–SO_3	1.924	0.106	0.449	-0.161	0.137	-0.025	1.180								
	5SecoCbs	α–SO_3	1.945	0.092	0.394	-0.132	0.115	-0.017	1.144								
		β–SO_3	1.968	0.104	0.445	-0.158	0.134	-0.023	1.173								
Co-N23	Cbs	α–SO_3	1.920	0.107	0.463	-0.165	0.141	-0.025	1.176								
		β–SO_3	1.913	0.109	0.469	-0.169	0.143	-0.026	1.181								
	SYCbs	α–SO_3	1.913	0.109	0.463	-0.169	0.142	-0.027	1.186								
		β–SO_3	1.901	0.113	0.467	-0.174	0.145	-0.029	1.196								
	5SecoCbs	α–SO_3	1.909	0.110	0.459	-0.168	0.141	-0.027	1.188								
		β–SO_3	1.924	0.109	0.457	-0.166	0.140	-0.026	1.185								
Co-N24	Cbs	α–SO_3	1.875	0.119	0.510	-0.193	0.160	-0.033	1.204								
		β–SO_3	1.877	0.119	0.504	-0.191	0.159	-0.033	1.207								
	SYCbs	α–SO_3	1.856	0.126	0.514	-0.204	0.166	-0.038	1.227								
		β–SO_3	1.868	0.123	0.505	-0.197	0.162	-0.036	1.219								
	5SecoCbs	α–SO_3	1.883	0.121	0.504	-0.194	0.160	-0.034	1.213								
		β–SO_3	1.893	0.124	0.518	-0.202	0.166	-0.036	1.219								

[(NO_2)(CN)Co(corrin)]																	
Bond	Corrin		Bond length /Å	ρ	$\nabla^2\rho_r$	V_r	G_r	H_r	$\lvert V_r\rvert/G_r$		Bond length (av) /Å	ρ_r (av)	$\nabla^2\rho_r$ (av)	$\lvert V_r\rvert/G_r$ (av)	V_r (av)	G_r (av)	H_r (av)
Co-NO_2	Cbs	α-NO_2	1.990	0.097	0.355	-0.129	0.109	-0.020	1.183	Co-NO_2	1.995	0.096	0.352	1.179	-0.126	0.107	-0.019
		β–NO_2	2.000	0.094	0.349	-0.124	0.106	-0.018	1.174								
	SYCbs	α-NO_2	1.998	0.110	0.488	-0.125	0.107	-0.018	1.171		2.018	0.099	0.400	1.166	-0.116	0.100	-0.017
		β–NO_2	2.038	0.087	0.312	-0.108	0.093	-0.015	1.162								
	5SecoCbs	α-NO_2	2.047	0.085	0.306	-0.104	0.090	-0.014	1.155		2.028	0.089	0.321	1.165	-0.112	0.096	-0.016
		β–NO_2	2.008	0.093	0.337	-0.120	0.102	-0.018	1.175								
Co-CN	Cbs	α-NO_2	1.914	0.119	0.285	-0.150	0.110	-0.039	1.355	Co-CN	1.913	0.120	0.283	1.358	-0.150	0.110	-0.039
		β–NO_2	1.911	0.120	0.282	-0.150	0.110	-0.040	1.360								
	SYCbs	α-NO_2	1.913	0.120	0.278	-0.149	0.109	-0.040	1.364		1.91	0.120	0.285	1.359	-0.151	0.111	-0.040
		β–NO_2	1.906	0.120	0.291	-0.152	0.113	-0.040	1.354								
	5SecoCbs	α-NO_2	1.906	0.121	0.281	-0.152	0.111	-0.041	1.367		1.91	0.120	0.279	1.365	-0.150	0.110	-0.040
		β–NO_2	1.914	0.119	0.277	-0.148	0.109	-0.040	1.363								
Co-N21	Cbs	α-NO_2	1.882	0.119	0.483	-0.186	0.154	-0.033	1.214	Co-N(corrin)	1.906	0.112	0.462	1.195	0.172	-0.144	0.028
		β–NO_2	1.884	0.118	0.482	-0.185	0.153	-0.032	1.211								
	SYCbs	α-NO_2	1.904	0.104	0.428	-0.175	0.149	-0.027	1.179		1.907	0.110	0.442	1.195	0.171	-0.143	0.028
		β–NO_2	1.906	0.110	0.486	-0.174	0.148	-0.026	1.178								
	5SecoCbs	α-NO_2	1.962	0.095	0.422	-0.142	0.124	-0.018	1.147		1.941	0.105	0.438	1.178	0.158	-0.134	0.024
		β–NO_2	1.938	0.102	0.448	-0.155	0.133	-0.021	1.160								
Co-N22	Cbs	α-NO_2	1.928	0.105	0.445	-0.159	0.135	-0.024	1.178								
		β–NO_2	1.928	0.107	0.446	-0.159	0.135	-0.024	1.180								

	SYCbs	α-NO_2	1.933	0.112	0.446	-0.155	0.131	-0.024	1.182
		β–NO_2	1.934	0.104	0.427	-0.154	0.131	-0.024	1.182
	5SecoCbs	α-NO_2	1.946	0.101	0.424	-0.149	0.127	-0.021	1.167
		β–NO_2	1.980	0.093	0.389	-0.131	0.114	-0.017	1.150
Co-N23	Cbs	α-NO_2	1.926	0.106	0.447	-0.160	0.136	-0.024	1.179
		β–NO_2	1.924	0.117	0.477	-0.161	0.136	-0.025	1.182
	SYCbs	α-NO_2	1.909	0.123	0.483	-0.168	0.140	-0.028	1.202
		β–NO_2	1.918	0.109	0.436	-0.162	0.136	-0.027	1.195
	5SecoCbs	α-NO_2	1.909	0.111	0.444	-0.166	0.138	-0.027	1.197
		β–NO_2	1.926	0.107	0.432	-0.157	0.133	-0.025	1.186
Co-N24	Cbs	α-NO_2	1.887	0.117	0.476	-0.182	0.151	-0.032	1.209
		β–NO_2	1.888	0.106	0.442	-0.182	0.151	-0.031	1.208
	SYCbs	α-NO_2	1.872	0.094	0.353	-0.192	0.156	-0.035	1.227
		β–NO_2	1.881	0.120	0.476	-0.186	0.152	-0.033	1.219
	5SecoCbs	α-NO_2	1.883	0.118	0.482	-0.185	0.153	-0.032	1.212
		β–NO_2	1.983	0.115	0.467	-0.177	0.147	-0.030	1.206

[(N_3)(CN)Co(corrin)]

Bond	Corrin		Bond length /Å	ρ	$\nabla^2\rho_r$	V_r	G_r	H_r	$\lvert V_r\rvert/G_r$		Bond length (av) /Å	ρ_r (av)	$\nabla^2\rho_r$ (av)	$\lvert V_r\rvert/G_r$ (av)	V_r (av)	G_r (av)	H_r (av)
Co-N_3	Cbs	α-N_3	2.045	0.078	0.295	-0.098	0.086	-0.012	1.143	Co-N_3	2.047	0.078	0.292	1.146	-0.098	0.086	-0.013
		β–N_3	2.048	0.078	0.289	-0.098	0.085	-0.013	1.149								
	SYCbs	α-N_3	2.037	0.079	0.307	-0.102	0.089	-0.013	1.140		2.04	0.079	0.301	1.143	-0.100	0.088	-0.013
		β–N_3	2.043	0.079	0.295	-0.099	0.087	-0.013	1.147								
	5SecoCbs	α-N_3	2.035	0.081	0.299	-0.102	0.088	-0.014	1.153		2.03	0.082	0.304	1.153	-0.104	0.090	-0.014
		β–N_3	2.024	0.082	0.310	-0.105	0.092	-0.014	1.152								
Co-CN	Cbs	α-N_3	1.877	0.129	0.296	-0.165	0.120	-0.046	1.382	Co-CN	1.878	0.129	0.294	1.382	-0.165	0.119	-0.045
		β–N_3	1.879	0.128	0.293	-0.164	0.119	-0.045	1.382								
	SYCbs	α-N_3	1.881	0.128	0.287	-0.163	0.117	-0.045	1.387		1.88	0.128	0.295	1.380	-0.164	0.119	-0.045
		β–N_3	1.878	0.128	0.302	-0.166	0.121	-0.045	1.373								
	5SecoCbs	α-N_3	1.884	0.127	0.285	-0.161	0.116	-0.045	1.385		1.884	0.127	0.287	1.383	-0.161	0.116	-0.045
		β–N_3	1.884	0.127	0.289	-0.161	0.117	-0.045	1.382								
Co-N21	Cbs	α-N_3	1.885	0.118	0.479	-0.184	0.152	-0.032	1.210	Co-N(corrin)	1.906	0.112	0.462	1.194	0.171	-0.143	0.028
		β–N_3	1.884	0.118	0.481	-0.184	0.152	-0.032	1.210								
	SYCbs	α-N_3	1.903	0.111	0.488	-0.176	0.149	-0.027	1.179		1.906	0.112	0.460	1.195	0.171	-0.143	0.028
		β–N_3	1.904	0.110	0.488	-0.175	0.148	-0.026	1.178								
	5SecoCbs	α-N_3	1.944	0.100	0.445	-0.152	0.131	-0.020	1.154		1.929	0.105	0.439	1.177	0.157	-0.134	0.024
		β–N_3	1.948	0.099	0.436	-0.148	0.129	-0.020	1.152								
Co-N22	Cbs	α-N_3	1.936	0.103	0.436	-0.154	0.132	-0.023	1.171								
		β–N_3	1.930	0.105	0.441	-0.157	0.134	-0.023	1.175								
	SYCbs	α-N_3	1.938	0.103	0.425	-0.152	0.129	-0.023	1.178								
		β–N_3	1.937	0.103	0.424	-0.152	0.129	-0.023	1.178								
	5SecoCbs	α-N_3	1.960	0.097	0.407	-0.141	0.121	-0.019	1.159								
		β–N_3	1.973	0.094	0.399	-0.135	0.117	-0.018	1.149								

Co-N23	Cbs	α-N_3	1.923	0.107	0.446	-0.161	0.136	-0.025	1.181
		β–N_3	1.925	0.106	0.446	-0.160	0.136	-0.024	1.180
	SYCbs	α-N_3	1.905	0.112	0.447	-0.169	0.140	-0.028	1.202
		β–N_3	1.914	0.110	0.441	-0.164	0.137	-0.027	1.196
	5SecoCbs	α-N_3	1.914	0.110	0.441	-0.163	0.137	-0.026	1.193
		β–N_3	1.920	0.108	0.435	-0.159	0.134	-0.025	1.190
Co-N24	Cbs	α-N_3	1.882	0.119	0.483	-0.186	0.153	-0.033	1.212
		β–N_3	1.883	0.118	0.480	-0.184	0.152	-0.032	1.211
	SYCbs	α-N_3	1.869	0.123	0.490	-0.194	0.158	-0.036	1.226
		β–N_3	1.875	0.122	0.474	-0.188	0.153	-0.035	1.227
	5SecoCbs	α-N_3	1.887	0.117	0.473	-0.181	0.150	-0.032	1.210
		β–N_3	1.888	0.117	0.474	-0.180	0.150	-0.031	1.207

$[(H_2O)(CN)Co(corrin)]^+$

Bond	Corrin		Bond length /Å	ρ	$\nabla^2\rho_r$	V_r	G_r	H_r	$\lvert V_r\rvert/G_r$		Bond length (av) /Å	ρ_r (av)	$\nabla^2\rho_r$ (av)	$\lvert V_r\rvert/G_r$ (av)	V_r (av)	G_r (av)	H_r (av)
Co-OH_2	Cbs	α-H_2O	2.174	0.046	0.250	-0.064	0.064	0.000	0.994	Co-OH2	2.18	0.046	0.250	0.995	-0.063	0.063	0.000
		β–H_2O	2.186	0.046	0.250	-0.062	0.062	0.000	0.997								
	SYCbs	α-H_2O	2.183	0.049	0.269	-0.067	0.067	0.000	0.996		2.169	0.050	0.271	0.999	-0.068	0.068	0.000
		β–H_2O	2.155	0.051	0.273	-0.069	0.068	0.000	1.003								
	5SecoCbs	α-H_2O	2.086	0.060	0.337	-0.085	0.085	0.000	1.004		2.083	0.061	0.341	1.004	-0.086	0.085	0.000
		β–H_2O	2.080	0.061	0.344	-0.087	0.086	0.000	1.004								
Co-CN	Cbs	α-H_2O	1.819	0.147	0.268	-0.189	0.129	-0.061	1.471	Co-CN	1.82	0.147	0.268	1.473	-0.189	0.128	-0.061
		β–H_2O	1.820	0.147	0.268	-0.188	0.128	-0.061	1.475								
	SYCbs	α-H_2O	1.828	0.145	0.265	-0.184	0.125	-0.059	1.470		1.825	0.146	0.271	1.466	-0.186	0.127	-0.059
		β–H_2O	1.822	0.146	0.277	-0.188	0.129	-0.059	1.462								
	5SecoCbs	α-H_2O	1.838	0.142	0.271	-0.180	0.124	-0.056	1.454		1.836	0.143	0.270	1.457	-0.181	0.124	-0.057
		β–H_2O	1.834	0.143	0.268	-0.182	0.124	-0.057	1.460								
Co-N21	Cbs	α-H_2O	1.881	0.121	0.486	-0.186	0.153	-0.033	1.218	Co-N(corrin))	1.902	0.114	0.463	1.202	0.174	-0.145	0.029
		β–H_2O	1.877	0.121	0.486	-0.190	0.156	-0.034	1.219								
	SYCbs	α-H_2O	1.914	0.109	0.465	-0.169	0.143	-0.026	1.183		1.904	0.113	0.456	1.203	0.173	-0.143	0.029
		β–H_2O	1.907	0.111	0.475	-0.174	0.146	-0.028	1.188								
	5SecoCbs	α-H_2O	1.957	0.097	0.428	-0.145	0.126	-0.019	1.151		1.926	0.107	0.436	1.186	0.160	-0.134	0.025
		β–H_2O	1.951	0.099	0.430	-0.148	0.128	-0.020	1.157								
Co-N22	Cbs	α-H_2O	1.925	0.107	0.444	-0.160	0.136	-0.025	1.183								
		β–H_2O	1.923	0.107	0.444	-0.161	0.136	-0.025	1.185								
	SYCbs	α-H_2O	1.925	0.107	0.434	-0.159	0.134	-0.025	1.190								
		β–H_2O	1.933	0.105	0.426	-0.155	0.131	-0.024	1.185								
	5SecoCbs	α-H_2O	1.951	0.100	0.414	-0.146	0.125	-0.021	1.169								
		β–H_2O	1.967	0.096	0.399	-0.138	0.119	-0.019	1.161								
Co-N23	Cbs	α-H_2O	1.921	0.109	0.449	-0.163	0.138	-0.026	1.186								
		β–H_2O	1.917	0.109	0.449	-0.165	0.139	-0.026	1.190								
	SYCbs	α-H_2O	1.895	0.116	0.462	-0.177	0.146	-0.031	1.210								
		β–H_2O	1.910	0.111	0.441	-0.166	0.138	-0.028	1.203								

	5SecoCbs	α-H_2O	1.906	0.112	0.446	-0.168	0.140	-0.028	1.202
		β–H_2O	1.903	0.114	0.437	-0.168	0.139	-0.029	1.211
Co-N24	Cbs	α-H_2O	1.884	0.118	0.474	-0.185	0.152	-0.033	1.216
		β–H_2O	1.885	0.118	0.474	-0.184	0.151	-0.033	1.216
	SYCbs	α-H_2O	1.876	0.122	0.477	-0.189	0.154	-0.035	1.227
		β–H_2O	1.869	0.124	0.471	-0.191	0.155	-0.037	1.238
	5SecoCbs	α-H_2O	1.878	0.121	0.474	-0.188	0.153	-0.035	1.226
		β–H_2O	1.891	0.117	0.461	-0.178	0.147	-0.031	1.214